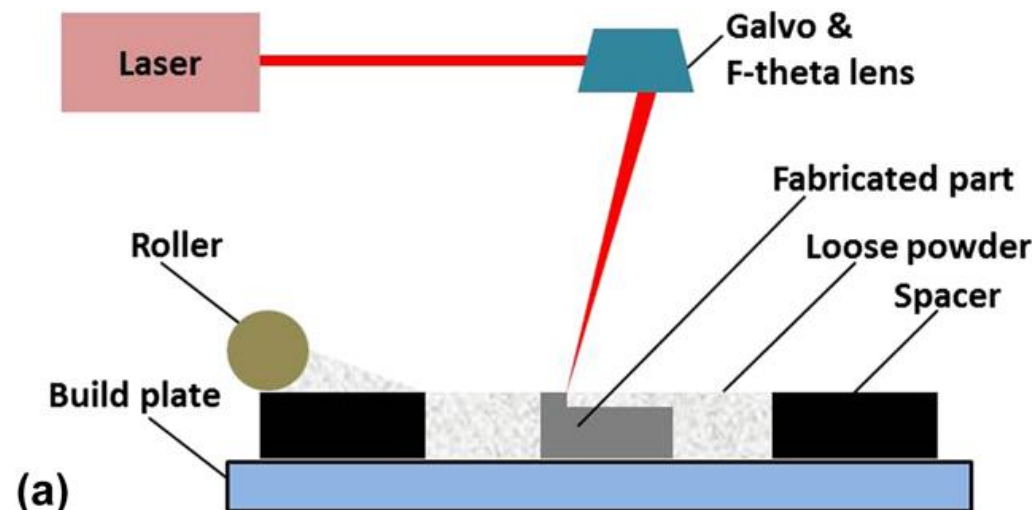


# Thermoelectric (TE) technologies and devices

- Emerging fabrication techniques based on printing: laser printing

Laser additive manufacturing of powdered bismuth telluride, *J. Mater. Res.* 33 (2018) 4031–4039.



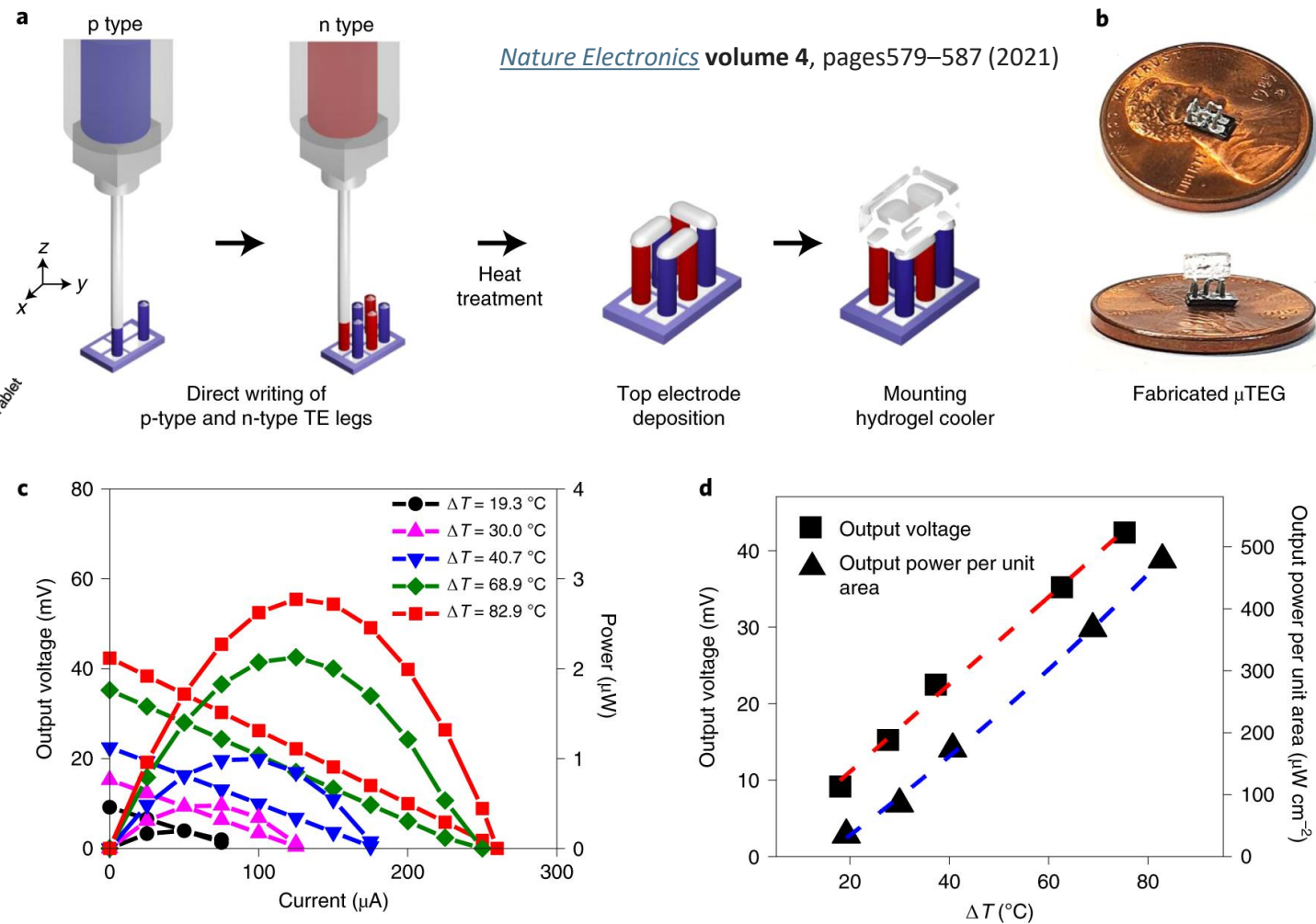
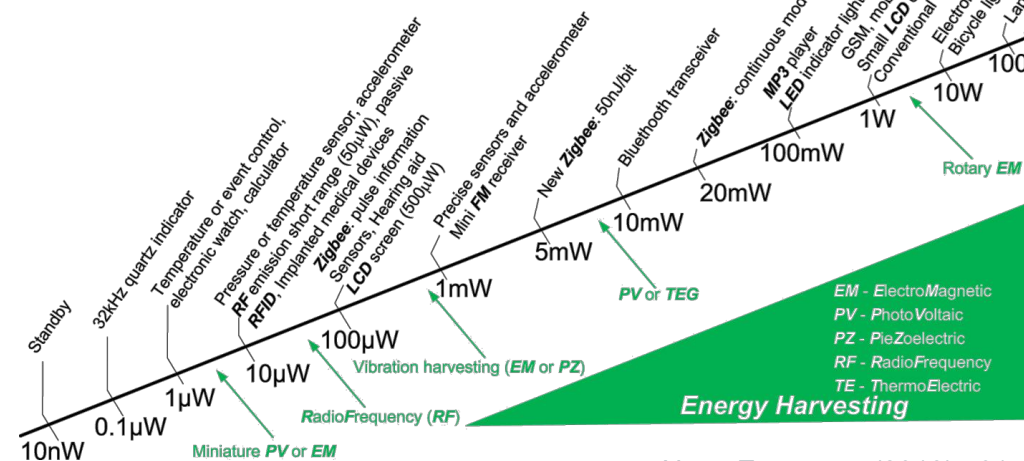
$\text{Bi}_2\text{Te}_3$  –based, moderate  $zT < 0.15$



# Thermoelectric (TE) technologies and devices

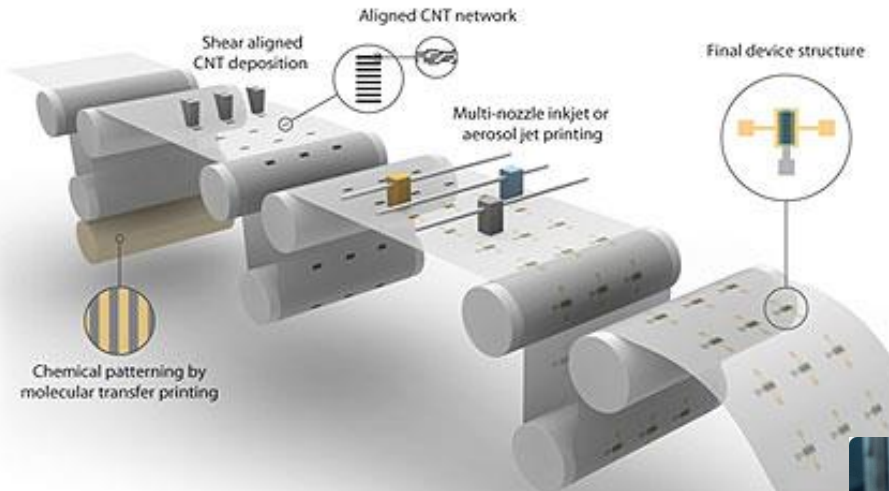
- Emerging fabrication techniques based on printing: microextrusion or direct ink writing (DIW).

Micro devices based on  $\text{Bi}_2\text{Te}_3$  can be printed offering few 100s of micro watts per  $\text{cm}^2$  for  $\Delta T$  of 10's K.



# Thermoelectric (TE) technologies and devices

- **Flexible and printed thermoelectrics** for wearables are mostly based on organic materials that can be printed from liquid phase.

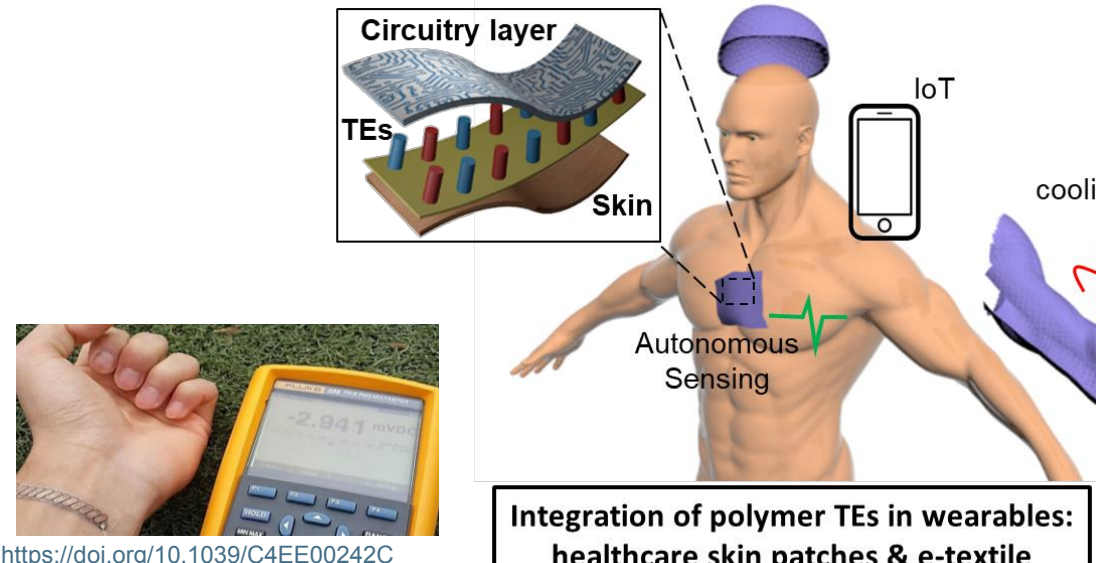
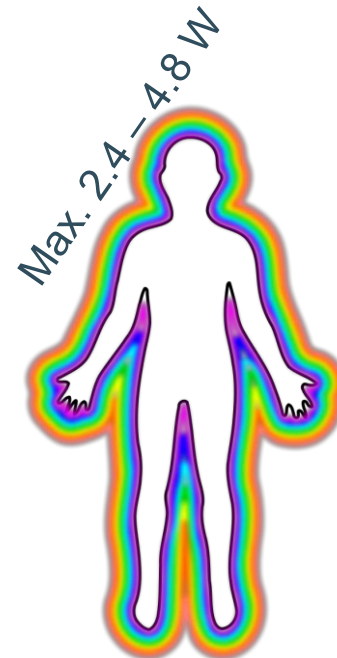


<http://muri-printed-electronics.umn.edu/>



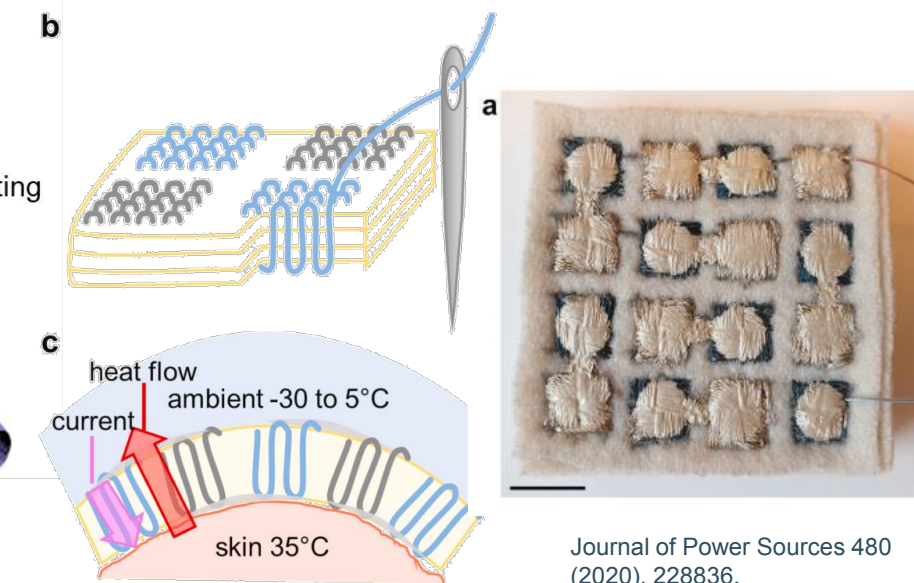
# Thermoelectric (TE) technologies and devices

- Flexible and printed thermoelectrics for wearables: energy harvesters



<https://doi.org/10.1039/C4EE00242C>

Integration of polymer TEs in wearables:  
healthcare skin patches & e-textile



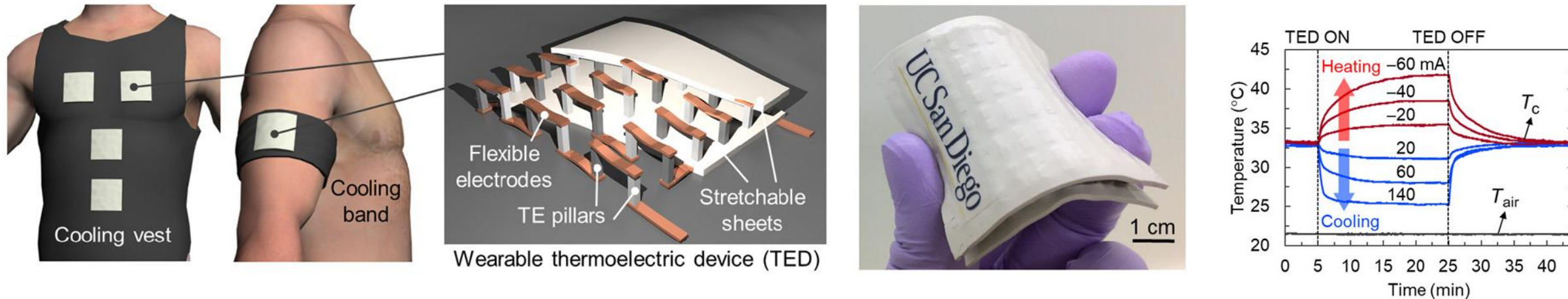
Journal of Power Sources 480  
(2020), 228836.

T. Starner, J.A. Paradiso, Human Generated Power for Mobile Electronics, *Low-Power Electronics Design*, Boca Raton (2004), pp. 1-35

# Thermoelectric (TE) technologies and devices

- Flexible and printed thermoelectrics for wearables: Flexible coolers for body thermal regulation

Hong et al., Sci. Adv. 2019;5 : eaaw0536 17



Flexible thermoelectric device (TED) based on rigid  $\text{Bi}_2\text{Te}_3$  rigid pillars that can deliver more than 10°C cooling effect with a high coefficient of performance (COP > 1.5).

# Materials Physics and Technology for Nanoelectronics



**Clement Merckling**

clement.merckling@kuleuven.be

imec & KU Leuven (MTM)

Kapeldreef 75, B-3001 Leuven



**Francisco Molina-Lopez**

francisco.molinalopez@kuleuven.be

MTM Functional Materials

Kasteelpark Arenberg 44, B-3001 Leuven

# Materials Physics and Technology for Nanoelectronics

## Magnetic materials



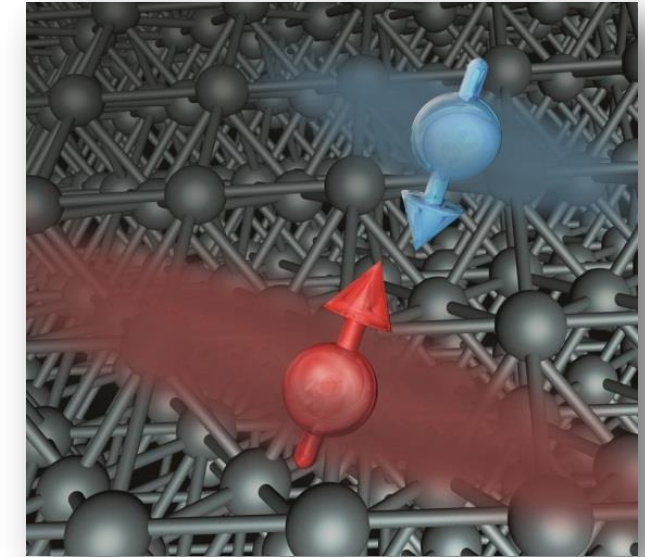
**Clement Merckling**  
[clement.merckling@kuleuven.be](mailto:clement.merckling@kuleuven.be)  
imec & KU Leuven (MTM)  
Kapeldreef 75, B-3001 Leuven



**Francisco Molina Lopez**  
[francisco.molinalopez@kuleuven.be](mailto:francisco.molinalopez@kuleuven.be)  
MTM Functional Materials  
Kasteelpark Arenberg 44, B-3001 Leuven

# Outline

- Magnetism
- Magnetic materials
- Magnetic anisotropy & domains
- Spin transport
- Giant magnetoresistance
- Spin polarized devices
  - Hard Disk Drive (HDD) based on GMR
  - Magnetic Tunnel Junction (MTJ) and Magnetic RAM (MRAM)
  - Spin Transfer Torque (STT) and STT MRAM



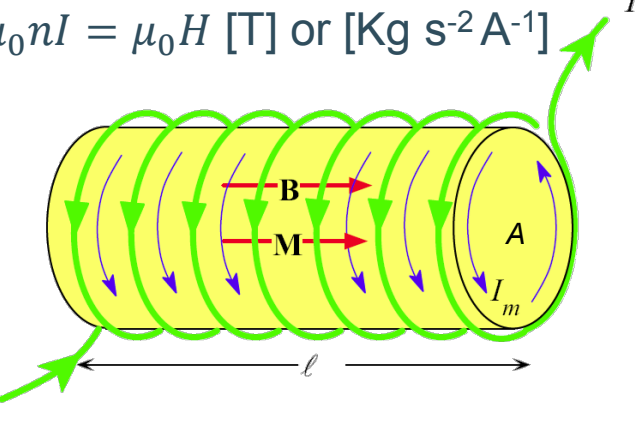
# Magnetism



# Magnetism

- All conductors respond to changing magnetic fields, because via Faraday's law of induction, changing magnetic fields induce electrical fields. In contrast most materials have little response to steady magnetic fields, they are essentially nonmagnetic. The few materials that are magnetic are very important for memories.
- The **inductors** can be seen as the magnetic equivalent of capacitors. While capacitors store their energy in an electric field, inductors can store energy in a **magnetic field**.
- The simplest form of an inductor consists of a coiled conductor.

- An empty inductor is characterized as follows:
  - Magnetic field inside coil:

$$B = \mu_0 n I = \mu_0 H \text{ [T] or [Kg s}^{-2}\text{A}^{-1}\text{]}$$


with  $\mu_0$  being the magnetic permeability in [H/m] (*Henries per meter*) or [ $N/A^2$ ],  $n$  is the number of turns of the coil per length [ $m^{-1}$ ], and  $I$  is the electrical current in the coil in [A].

- The **inductance**  $L = \mu_0 n^2 A l$  incorporates the dimensions of the inductor. The units for  $L$  is [H].

# Magnetism

- Inserting a magnetic material within the coils of the inductor increases its inductance, and its stored energy, by the factor  $\mu_r$ , the **relative permeability**. The magnetic field has now two parts, a contribution from the **current** through the coil (an applied field) and a contribution from the **material**:

$$B = \mu_0 nI + \mu_0 M = \mu_0 H + \mu_0 M = \mu_0 \mu_r H$$

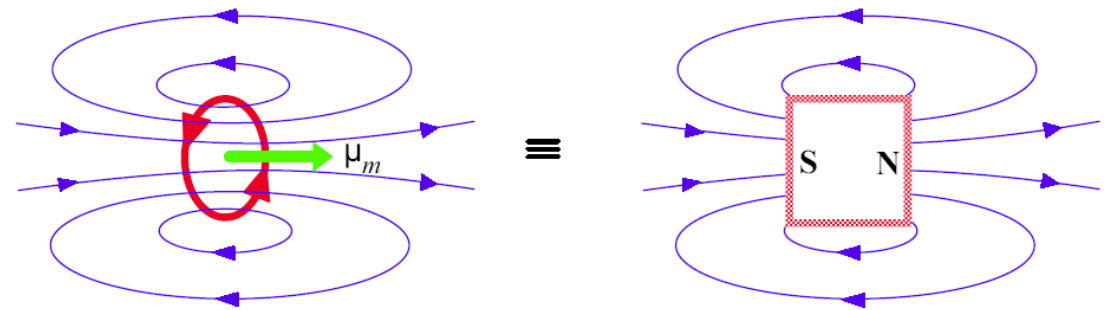
- $B$  represents the **total magnetic field** (or magnetic induction),  $H$  is the **magnetizing field** (or magnetic field strength) [A/m] and  $M$  is the **magnetization** [A/m] due to the material and equals the net magnetic dipole moment per unit volume.
- The relative permeability  $\mu_r$  of the material represents the ratio of the total field in the material to the applied field:
$$\mu_r = \frac{B}{\mu_0 H} = 1 + \frac{M}{H} = 1 + \chi_m$$
- where  $\chi_m$  is the (unitless) **magnetic susceptibility**.

# Magnetism

- Magnetic susceptibility  $\chi_m$  is thus a dimensionless proportionality constant that indicates the **degree of magnetization** of a material in response to an applied magnetic field. The susceptibility indicates whether a material is attracted ( $>0$ ) into or repelled ( $<0$ ) out of a magnetic field, which in turn has implications for practical applications.
- The magnetic susceptibility  $\chi_m$  of most solids is close to 0 and typically falls between  $-10^{-5}$  and  $+10^{-3}$ , meaning  $\mu_r$  is close to 1.
- Materials with small positive magnetic susceptibilities are called **paramagnetic**, and those with small negative magnetic susceptibilities are called **diamagnetic**. For most practical purposes, they can be considered **non-magnetic**.
- A few materials have magnetic susceptibilities of many thousands and their magnetization can vary non-linearly with applied field, that is  $M$  can vary **non-linearly** with  $H$ .

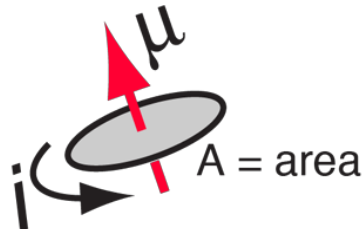
# Magnetic dipoles

- Although electric and magnetic fields, as described by Maxwell's equations, are formally very similar, there is a striking asymmetry between electricity and magnetism in nature, associated with the apparent non-existence of elementary magnetic charges (*i.e.* magnetic monopoles) and magnetic current.
- There are, however, what appear to be **magnetic dipoles**, analogous to electric dipoles.
- A magnetic dipole is a system which when placed in an external magnetic field, experiences a **torque** that tries to rotate the system so as to align its axis parallel to the magnetic field.
- The most familiar example of a magnetic dipole is a bar magnet. The external magnetic field produced by a circular loop of current is identical to that produced by a point magnetic dipole, so the current loop is also a dipole.



# Magnetic dipoles

- The magnetic dipole is characterized by its **magnetic dipole moment**. Let's for example look into the magnetic dipole moment of a current carrying coil (magnetic dipole) of area  $A$ .



- A magnetic moment is created defined by a vector  $\mu = IA$ , where  $I$  is the current through the coil and  $A$  is the area enclosed by the current coil.
- The torque is given by:  $\vec{T} = \vec{\mu} \times \vec{B}$ . This torque tends to line up the magnetic moment with the magnetic field  $B$ , so this represents its lowest energy configuration  $E = -\vec{\mu} \cdot \vec{B}$ .

- The magnetic effect in magnetic materials are due to atomic magnetic dipoles in the materials. The sources that contribute to atomic magnetic moments are:

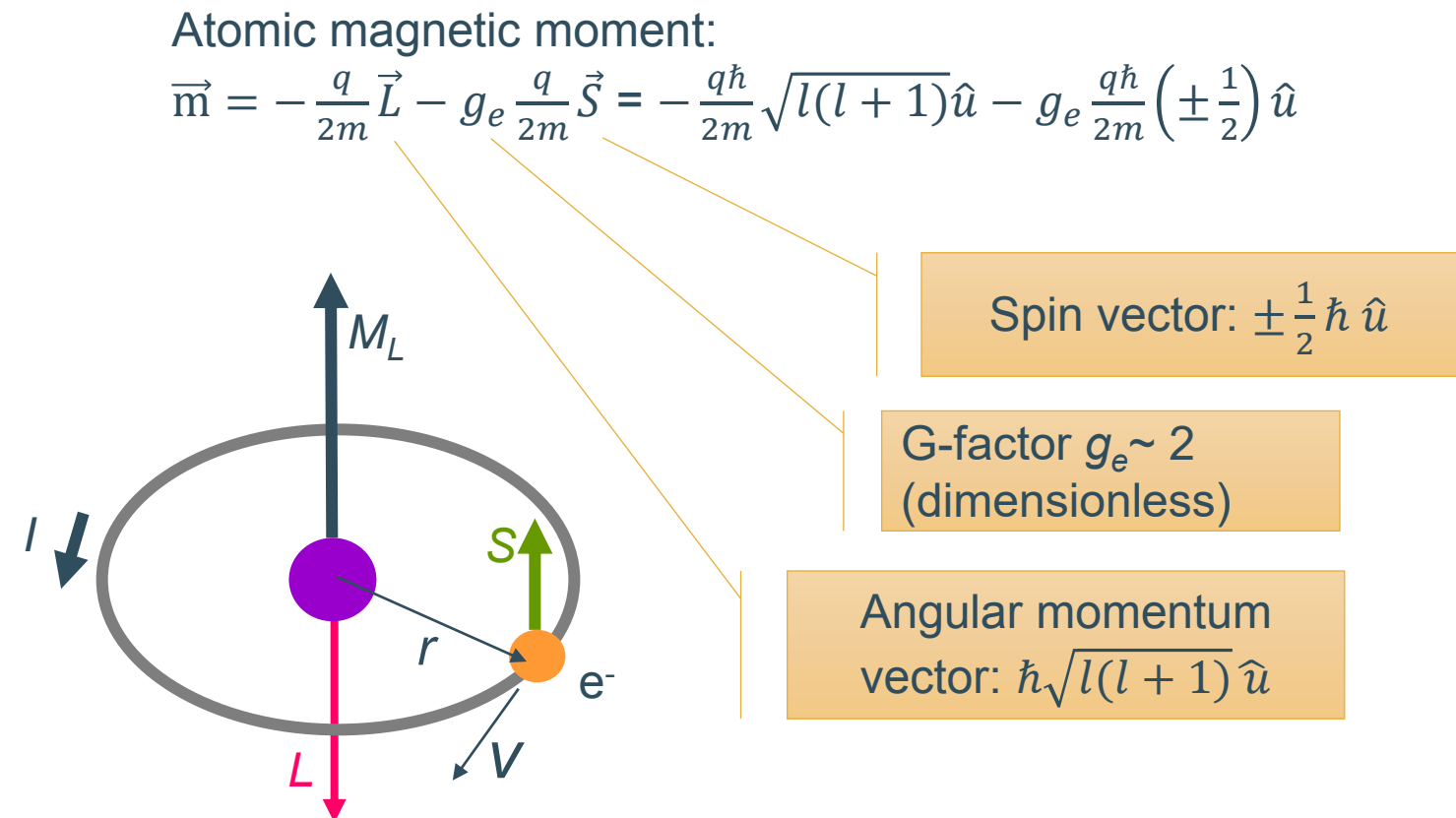
- The electrons “orbiting” around the nucleus in an atom behave like a current loop and have a magnetic dipole moment associated with it, called the **orbital magnetic moment**.
- The magnetic moment due to spin of an electron, i.e. due to spin angular momentum, is called the **spin magnetic moment**.
- In addition, there can be a small contribution from the nucleus called **nuclear magnetic moment**. This effect is usually not significant.

# Magnetic moment

- The total magnetic moment of an electron is given by the sum of the orbital magnetic moment and the spin magnetic moment.
- The **Bohr magneton** is a physical constant and the natural unit for expressing the magnetic moment of an electron caused by its orbital or spin angular momentum.

Bohr magneton:

$$\mu_B = \frac{q\hbar}{2m} = 9.28 \times 10^{-24} [\text{A m}^2] \text{ or } [\text{J T}^{-1}]$$



# Orbital magnetic dipole moments (extra)

- Consider an electron moving with velocity ( $v$ ) in a circular Bohr orbit of radius  $r$ . It produces a current:

$$i = -\frac{q}{T} = -\frac{q\omega}{2\pi}$$

where  $T$  is the orbital period of the electron.

- The current loop produces a magnetic field, with a moment  $\mu_l$ :

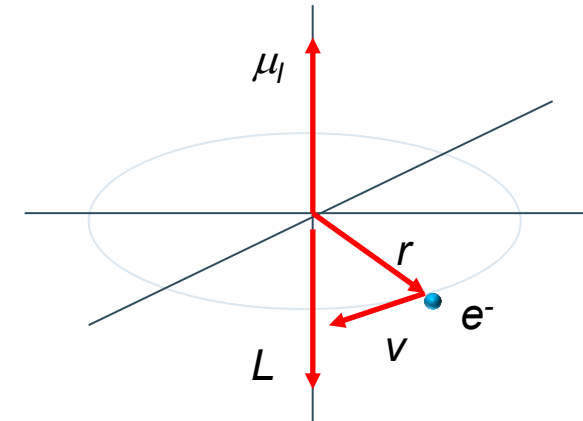
$$\mu_l = iA = -\frac{q\omega}{2\pi}\pi r^2 = -\frac{1}{2}q\omega r^2$$

- The magnitude of orbital angular momentum is  $L = mvr = m\omega r^2$ .
- Combining with previous equation yields:

$$\mu_l = -\frac{q}{2m}L \text{ (see previous slide)}$$

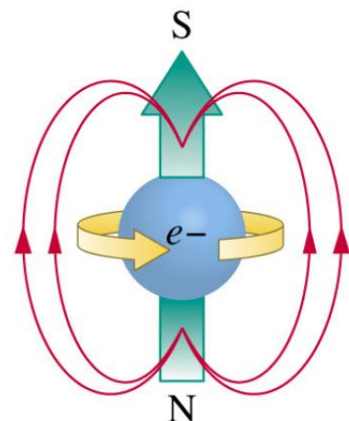
- Electron in external magnetic field  $\vec{B}$  along the axis  $z$ :  $\vec{B}$  creates a torque that aligns  $\vec{\mu}_l$  with  $\vec{B}$ . Quantum theory postulates that the projection of  $L$  on an axis (let's assume  $z$ ) is  $L_z = m_l\hbar$ . The minimum magnetic moment corresponds to  $L_z = \hbar$ , and :

$$\mu_B = \frac{q}{2m}\hbar = 9.27 \times 10^{-24} \text{ Am}^2 \quad (\text{Bohr magneton})$$

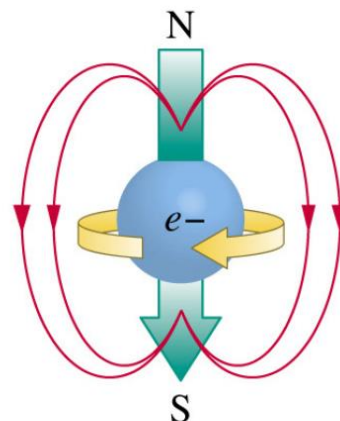


# Electron spin

- As well as mass and charge, an electron has another intrinsic property, i.e. spin angular momentum, or simply **spin**.
  - In quantum mechanics, spin is a fundamental property of atomic nuclei and elementary particles and is an important intrinsic **degree of freedom**.
  - Although as the name indicates spin was originally thought of particles spinning around their own axis, it had been shown by Dirac that electron spin arises naturally within relativistic quantum mechanics.
  - The component of **electron spin** measured along any direction can only take on the values:
- $\hbar s_z$  with  $s_z = \pm \frac{1}{2}$
- Namely, in a classical picture, electron spin can only point to **up or down** along a magnetic field which can be vividly illustrated by a small magnet with its north pole pointing to up or down as shown in the figure.



$$s_z = +\frac{1}{2}$$



$$s_z = -\frac{1}{2}$$

*Classical illustration of electron spin as a small magnet with north pole pointing to up or down.*

# Magnetic materials



# Hund's rule

- In order to understand the magnetic properties of materials, we have to take a deeper look into the **electrons spin distribution**. Each electron state may be occupied by two electrons, one with spin up and one with spin down. The electron spin distribution is determined by **Hund's rule**.

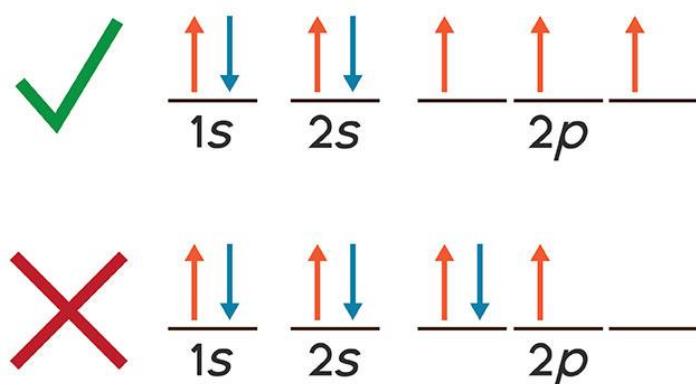


Illustration of Hund's rule in Nitrogen (7 electrons)

- This rule states that when there is orbital degeneracy, the electrons will be arranged to **maximize the total spin**. This means that each electron added to a set of degenerate levels will have the **same parallel spin** as the electron which preceded it. Hund's rule can cause a significant spin imbalance in some materials.
- The physical origin of this rule is Pauli's exclusion principle (two electrons with the same spin can never be found at precisely the same place), and the **repulsive Coulomb interaction energy** (if electrons are far from each other, the overall system energy is lower). The two effects above makes systems with the same spin energetically favorable.
- The difference in energy between the parallel and anti-parallel alignments is the **exchange energy**.

# Magnetic materials

- In case of equal number of electrons with spin up and spin down, the material is **diamagnetic** and the net spin magnetism is zero.
- Many materials behave **paramagnetic**, *i.e.* the electron spins on each atom do not completely cancel; each atom has a net spin and a net magnetic dipole moment ( $\chi_m$  slightly positive).
- Paramagnetic materials remain typically very weakly magnetic because the **individual atomic magnets are uncoupled and point in random directions**. If an external magnetic field is applied, the individual magnets attempt to align with the magnetic field. The energy  $E$  of an atomic dipole of strength  $p_m$  in a field  $H$  is given by:

$$E = -\mu_0 p_m H$$

- At room temperature and usual magnetic fields, the energy of an individual atomic dipole is small compared to  $k_B T$ , and this leads to only a tiny paramagnetic susceptibility.
- The relative permeability  $\mu_r$  of most paramagnetic materials is therefore approximately one, except at very high fields and very low temperatures

# Magnetic materials

- The interesting applications of magnetic materials tend to come not from paramagnetism or diamagnetism, but from arrangements such as **ferromagnetism** where the magnetic moments **remain aligned** even in the absence of an external magnetic field.
- Ferro* is the Latin word for *iron* (this is the reason behind the atomic symbol of iron - Fe), which displays strong magnetic properties.
- In order to understand ferromagnetism we need to consider not just interactions between individual magnetic moments and the external field, but also **interactions between the magnetic moments**.

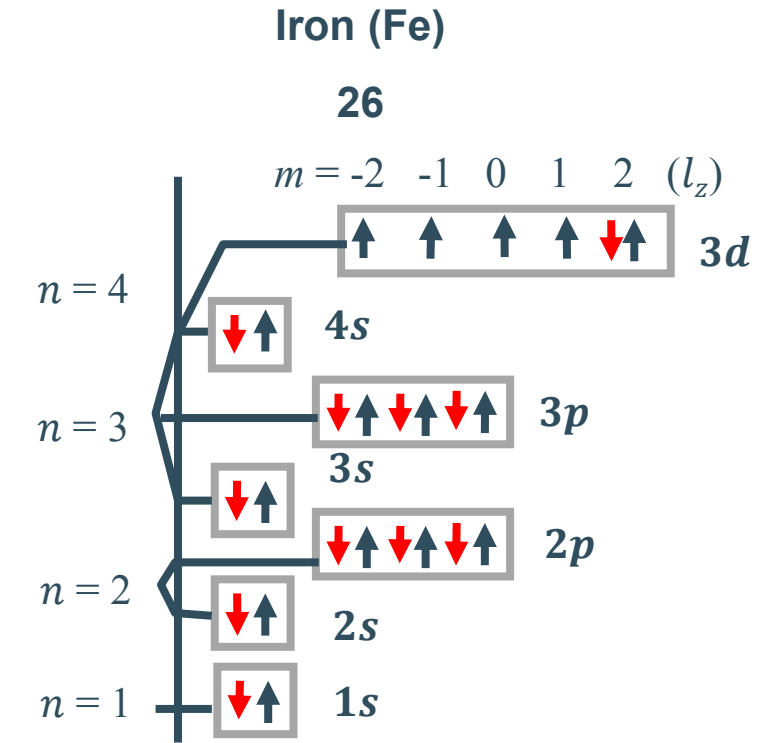


Illustration of Hund's rule for Fe. Notice the spin imbalance in the  $3d$  orbital.

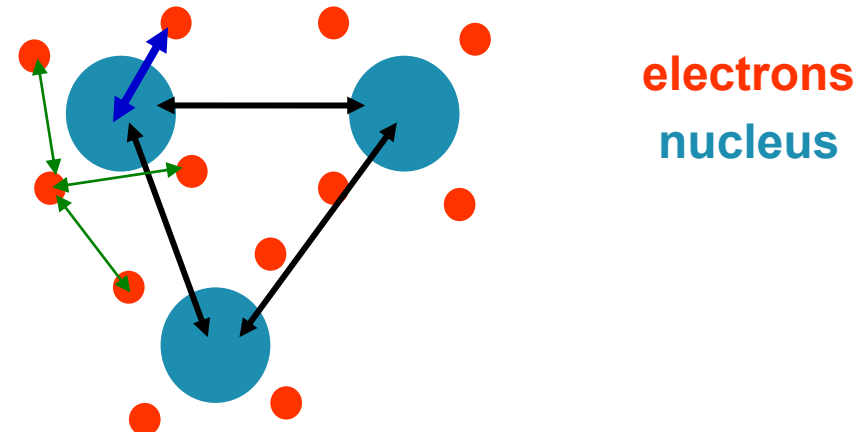
# Magnetic materials

- The periodic arrangement of the spins in these materials results from an electrostatic coupling between the electrons and nucleus of the neighboring atoms, called the **exchange coupling (or energy)**  $U_{ex}$ :

$$U_{ex} = -2J_{ex}\vec{S}_i\vec{S}_j$$

where  $\vec{S}_i$  and  $\vec{S}_j$  are the **spin vectors** on atoms  $i$  and  $j$ , and  $J_{ex}$  is the **exchange integral**, which is related to the overlapping of the electronic orbitals  $i$  and  $j$ .

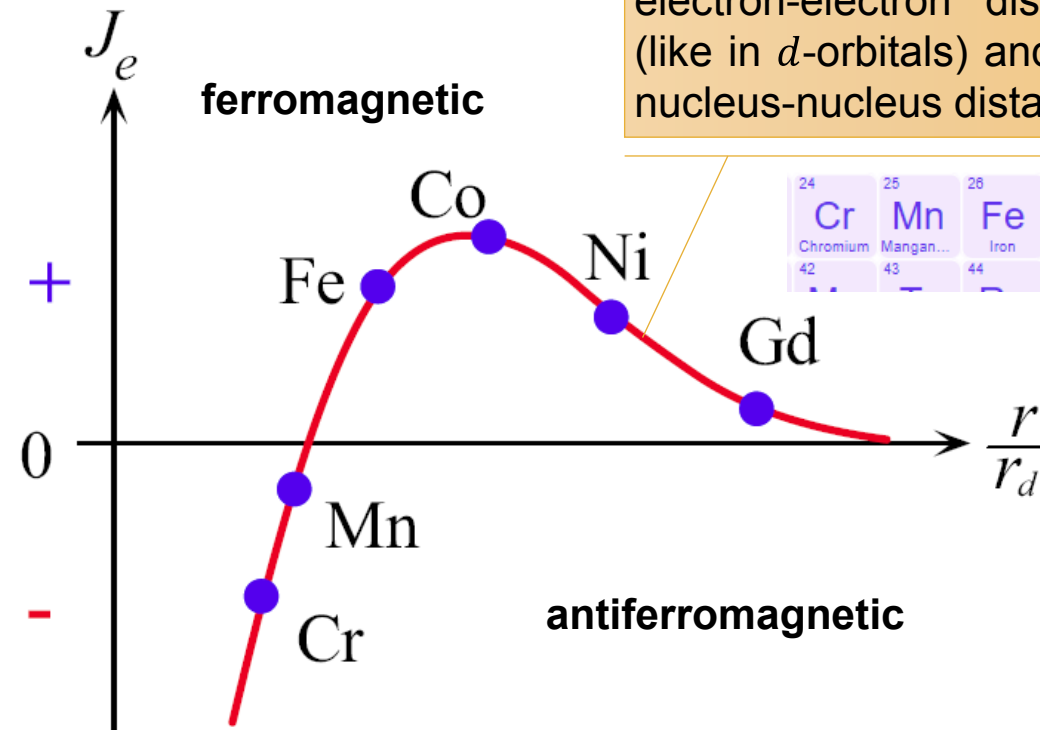
- The exchange integral  $J_{ex}$  is related to the “electron – electron” and “electron – nucleus” interactions of neighboring atoms.



- The exchange interaction is the **source of ferromagnetism**.
- It turns out that  $J_{ex}$  can be *positive* (parallel alignment favored; **ferromagnetism**) or *negative* (anti-parallel alignment favored; **anti-ferromagnetism**).

# Magnetic materials

- If the exchange integral  $J_{ex}$  is **positive**, the exchange coupling is minimal (negative) for parallel spins  $i$  and  $j$ , and the material is **ferromagnetic**
- If the exchange integral  $J_{ex}$  is **negative**, the exchange coupling is minimal for anti-parallel spins  $i$  and  $j$ , and the material is **antiferromagnetic**.



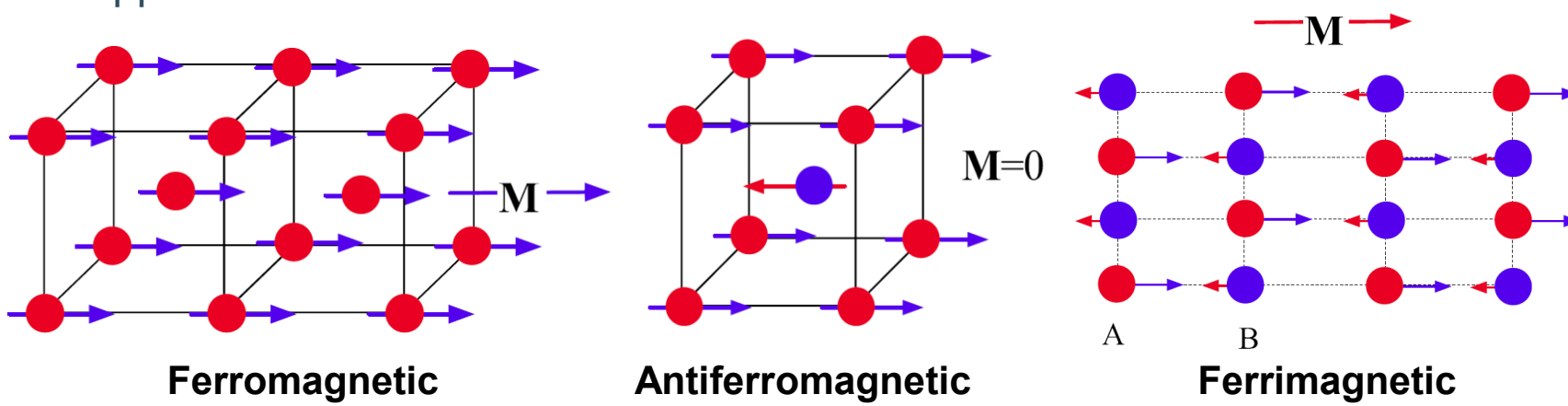
$J_{ex}$  positive for small electron-electron distances (like in  $d$ -orbitals) and large nucleus-nucleus distances.

24	25	26	27	28	29
Cr	Mn	Fe	Co	Ni	Cu
Chromium	Mangan...	Iron	Cobalt	Nickel	Copp

The exchange integral as a function of  $r/r_d$ , where  $r$  is the interatomic distance and  $r_d$  the radius of the  $d$ -orbit (or the average  $d$ -subshell radius). Cr to Ni are transition metals. For Gd, the x-axis is  $r/r_f$  where  $r_f$  is the radius of the  $f$ -orbit.

# Magnetic materials

- In a magnetized region of a **ferromagnetic** material such as iron all the magnetic moments are spontaneously aligned in the same direction. There is a strong magnetization vector  $M$  even in the absence of an applied field.



- In the **antiferromagnetic** BCC crystal (Cr) the magnetic moment of the center atom is cancelled by the magnetic moments of the corner atoms (an eighth of the corner atom belongs to the unit cell).
- In a **ferrimagnetic** crystal. All  $A$ -atoms have their spins aligned in one direction and all  $B$ -atoms have their spins aligned in the opposite direction. As the magnetic moment of an  $A$ -atom is greater than that of a  $B$ -atom, there is net magnetization,  $M$ , in the crystal.

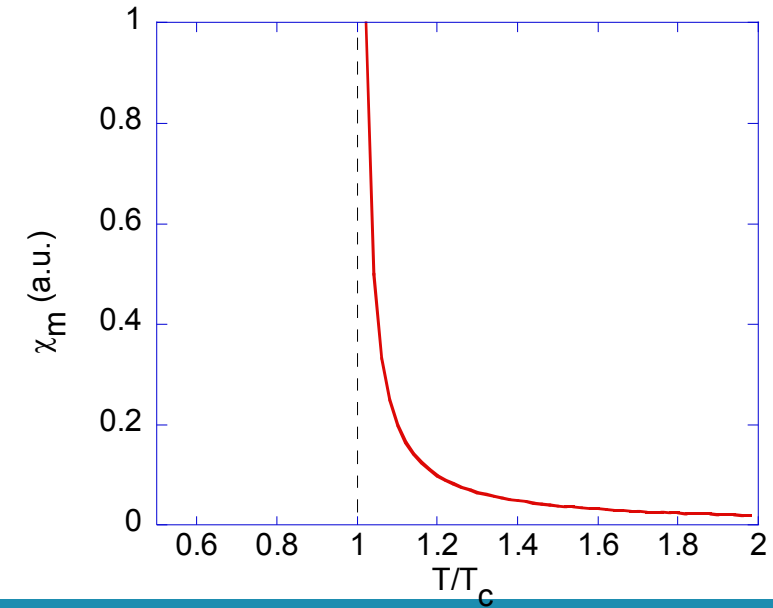
# Ferromagnetic-paramagnetic phase transition

- Ferromagnetic materials exhibit a long-range ordering phenomenon at the atomic level which causes the unpaired electron spins to line up parallel with each other in a region called a **domain**.
- All ferromagnets have a **maximum temperature** where the ferromagnetic property disappears as a result of thermal agitation. This temperature is called the **Curie temperature  $T_c$** . At  $T_c$ , thermal disorder induces a transition from the ordered ferromagnetic phase to a disordered paramagnetic phase.
- The magnetic susceptibility  $\chi_m$  presents a discontinuity at the Curie temperature.

Material	Spontaneous magnetization $M$ (G)	$T_c$ (K)
Fe	1707	1043
Co	1400	1388
Ni	485	627
CrO <sub>2</sub>	515	386

$$\chi_m = \frac{C}{T - T_c}$$

(with  $C$  the **Curie constant**.)



# Magnetic anisotropy & domains

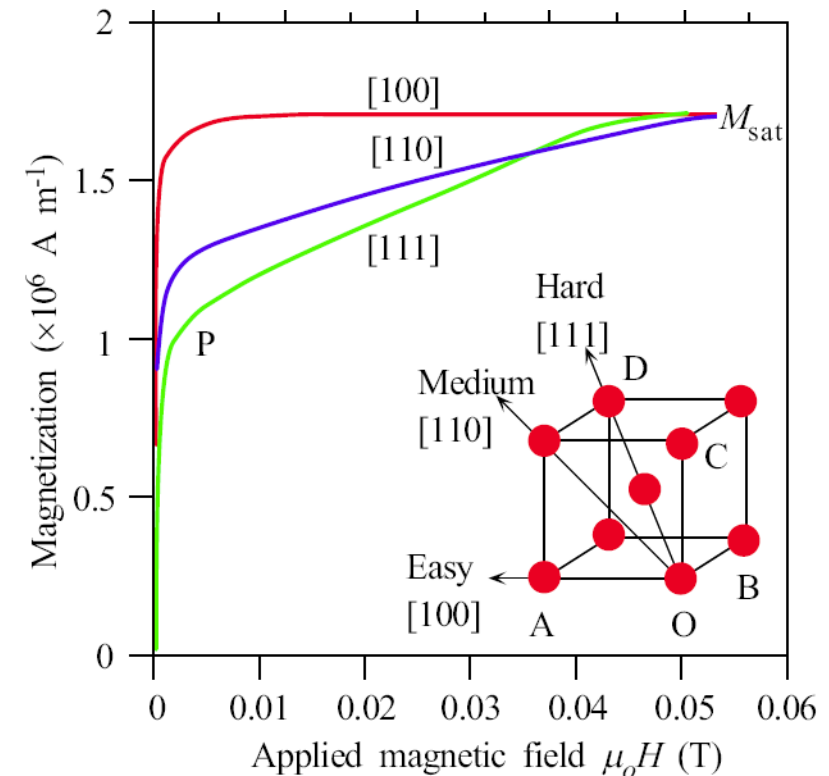


# Magnetic anisotropy

- Most ferromagnetic materials present a **magnetic anisotropy**, i.e. they are preferentially magnetized in a particular direction, called their **easy axis**.
- If  $\varphi$  is the angle between the magnetization  $M$  and the direction of the easy axis, the **anisotropic energy  $U_{an}$**  (energy per volume) is given by:

$$U_{an} = K \sin^2 \varphi$$

with  $K$  the anisotropy constant, which is dependent on material.

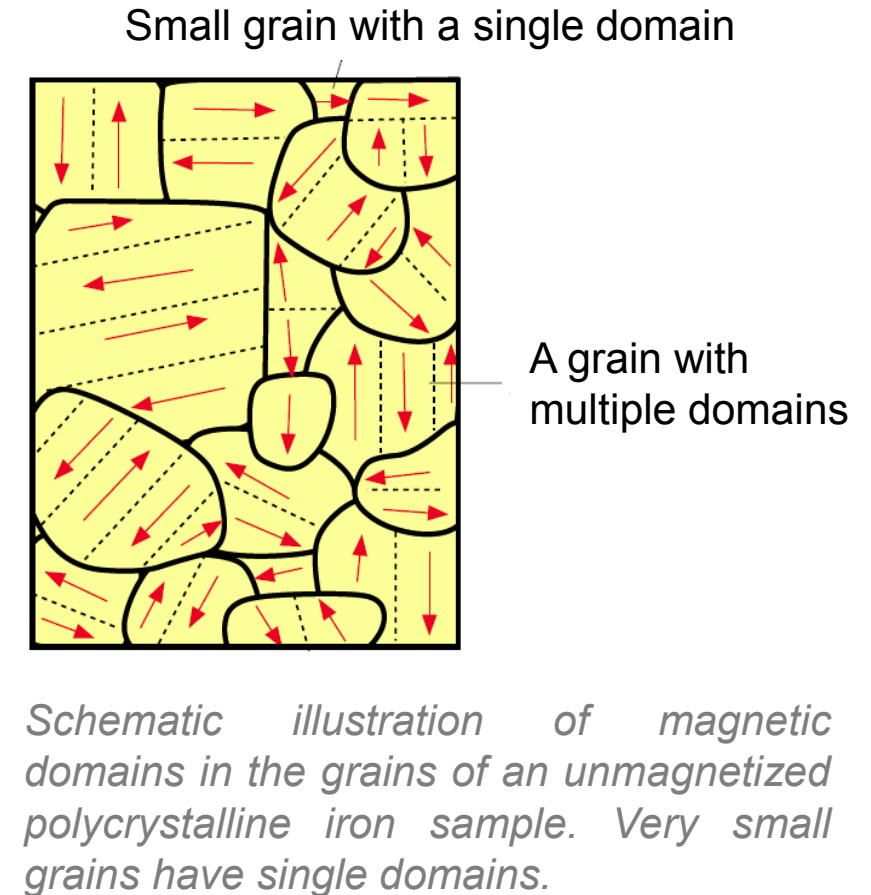


*Magneto-crystalline anisotropy in a single iron crystal.  $M$  versus  $H$  depends on the crystal direction and is easiest along [100] and hardest along [111].*

# Magnetic domains

- At the **atomic scale**, spins of ferromagnetic materials are aligned and parallel. However, at the **macroscopic scale**, not all the spins are necessarily aligned, due to the formation of **magnetic domains**, which all have different orientations for the magnetization  $\vec{M}$ .
- Inside each domain, the magnetization is uniform. However, the relative orientation of  $\vec{M}$  varies from domain to domain.
- When an external magnetic field  $\vec{H}$  is applied to the material, all the domains **tend to orient  $\vec{M}$  parallel to  $\vec{H}$** , to reduce the energy (per volume) of the system:

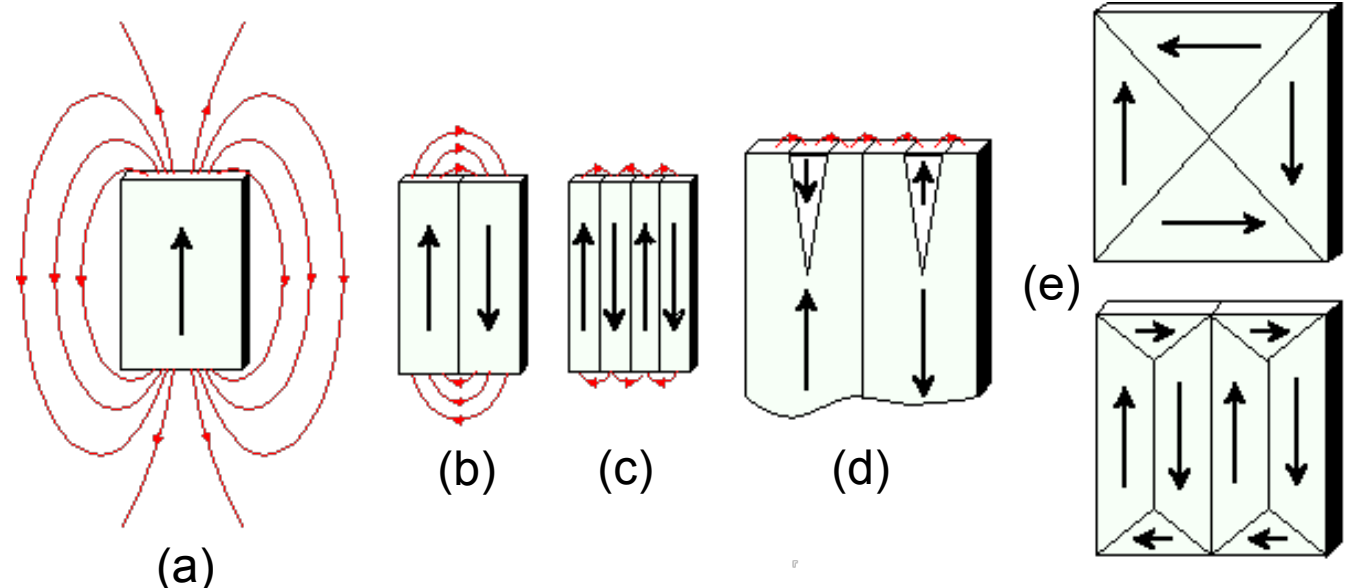
$$E_H = -\mu_0 \vec{M} \cdot \vec{H} = -\mu_0 M H \cos(\theta) [\text{J/m}^3]$$



# Magnetic domains

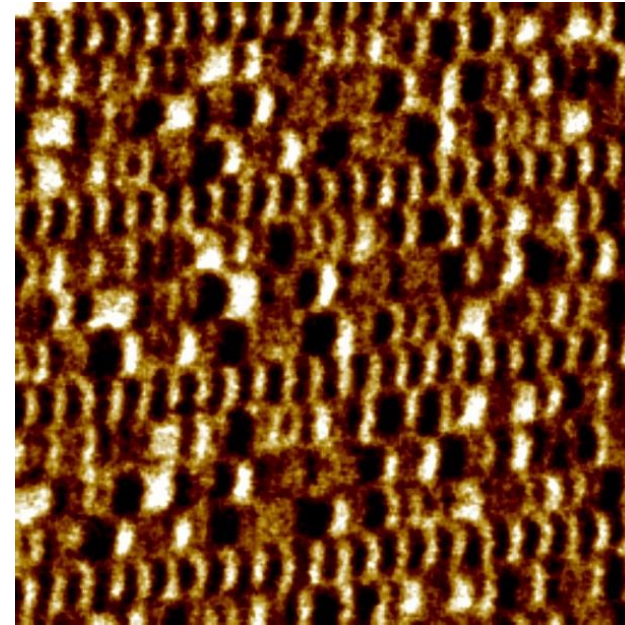
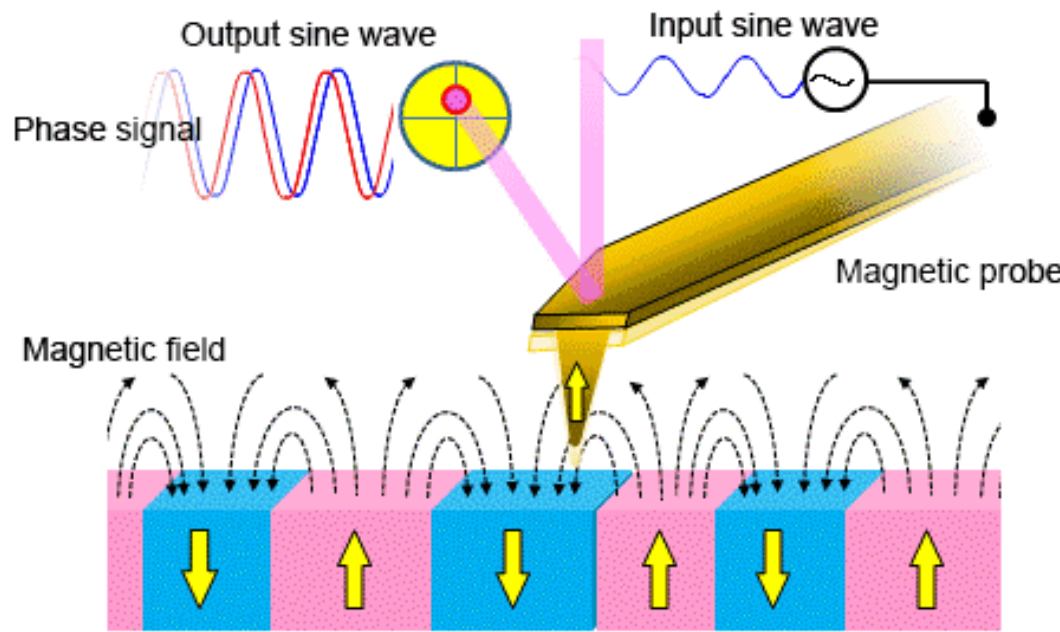
- The formation of domains does have some **energetic cost**. The exchange interaction in a ferromagnet aligns spins because that reduces the total energy of the system. At a **domain wall** (the boundary between two domains), where the perfect ferromagnetic alignment gets disrupted, the local energy should in principle be higher.
- However, the increase in exchange energy is balanced by a **net savings in stray field energy**.

*Illustration of stray magnetic field from a sample with a uniaxial anisotropy with (a) single magnetized domain, (b) two and (c) four domains. (d) Reverse spike domains which can form in a uniaxial domain structure. (e) Flux closure domains which prevent any stray flux from emerging from the sample.*

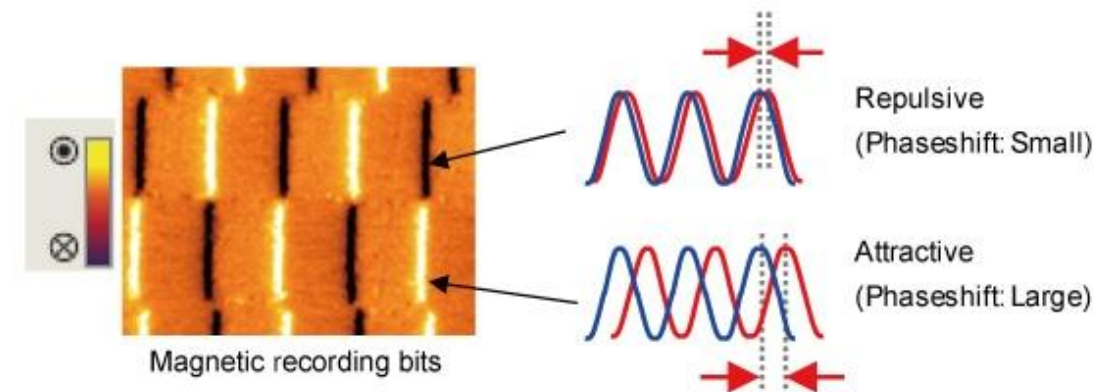


# Magnetic domains

- Magnetic domains can be measured by MFM (magnetic force microscopy).



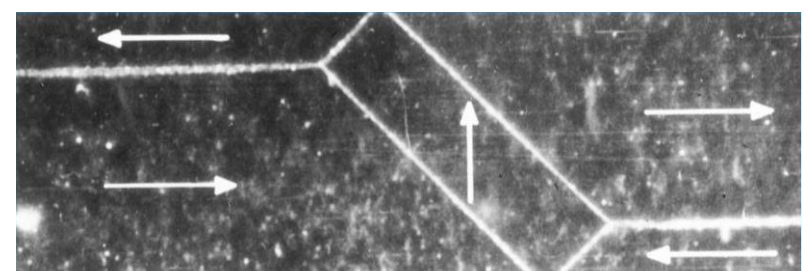
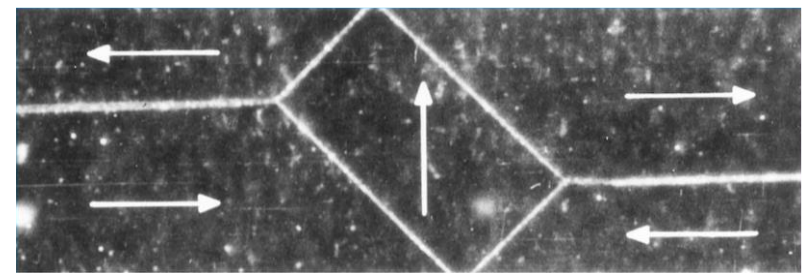
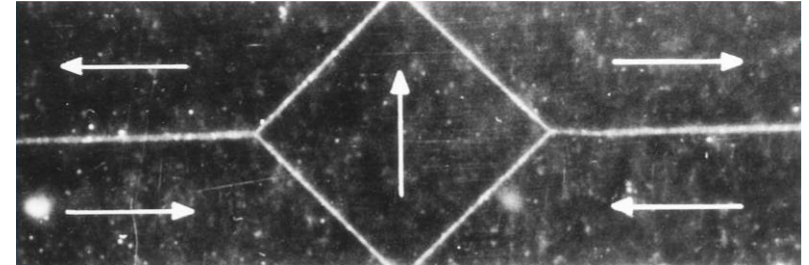
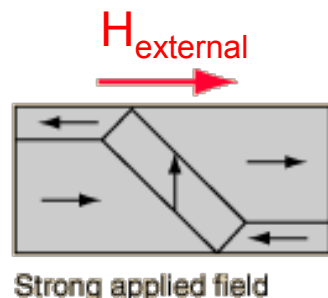
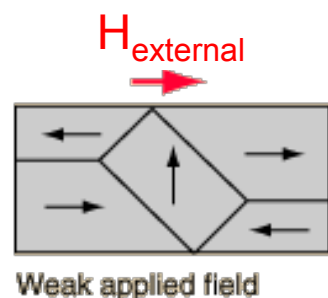
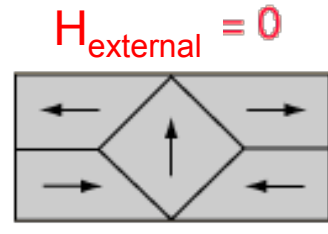
<http://www.parkafm.co.kr/index.php/kr/medias/resources/afm-images>



<https://www.hitachi-hightech.com/global/products/science/tech/em/spm/descriptions/electro/mfm.html>

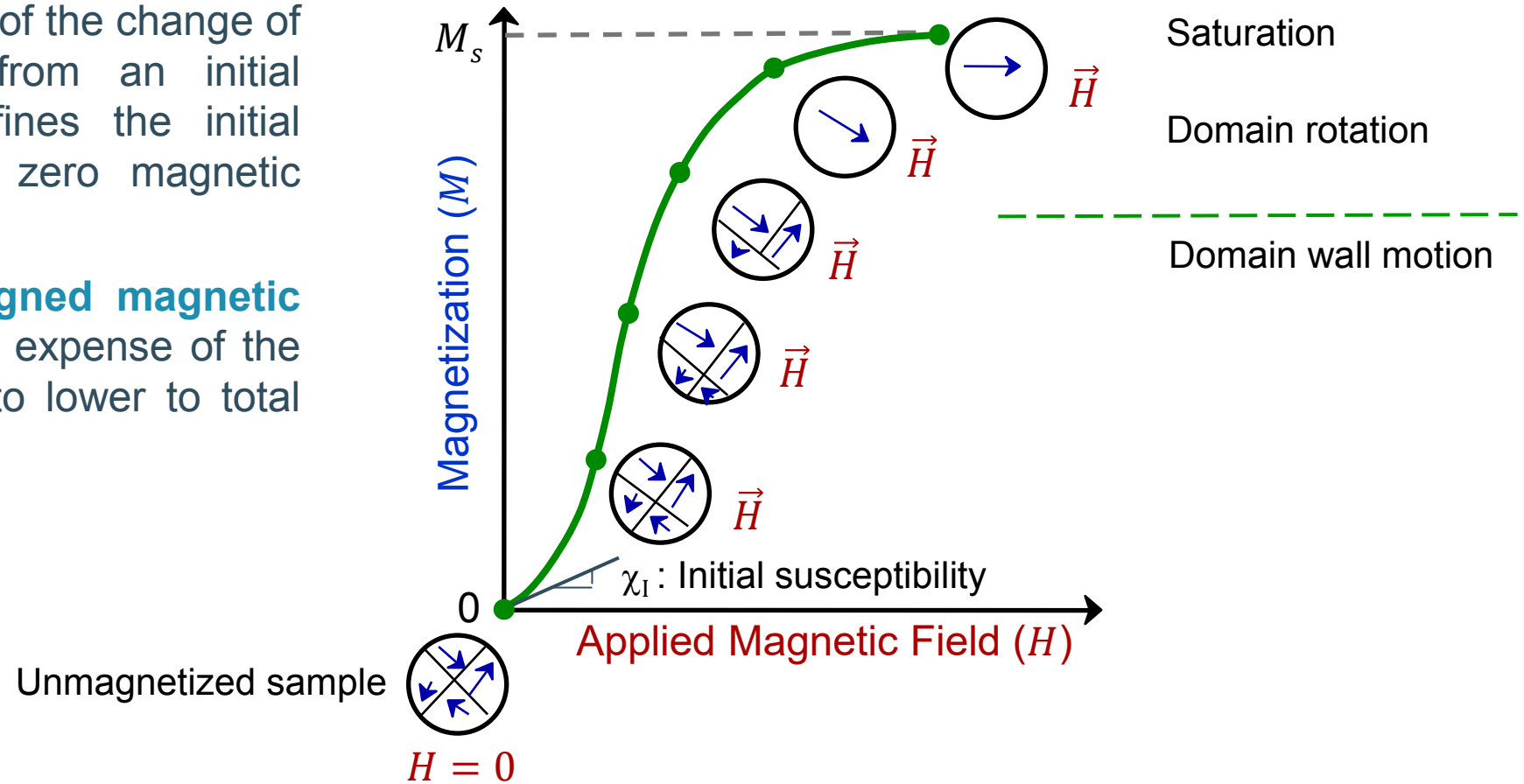
# Magnetic domains

- These pictures illustrate the change of magnetic domains from unmagnetized (at zero field) state to magnetized (under field) state.



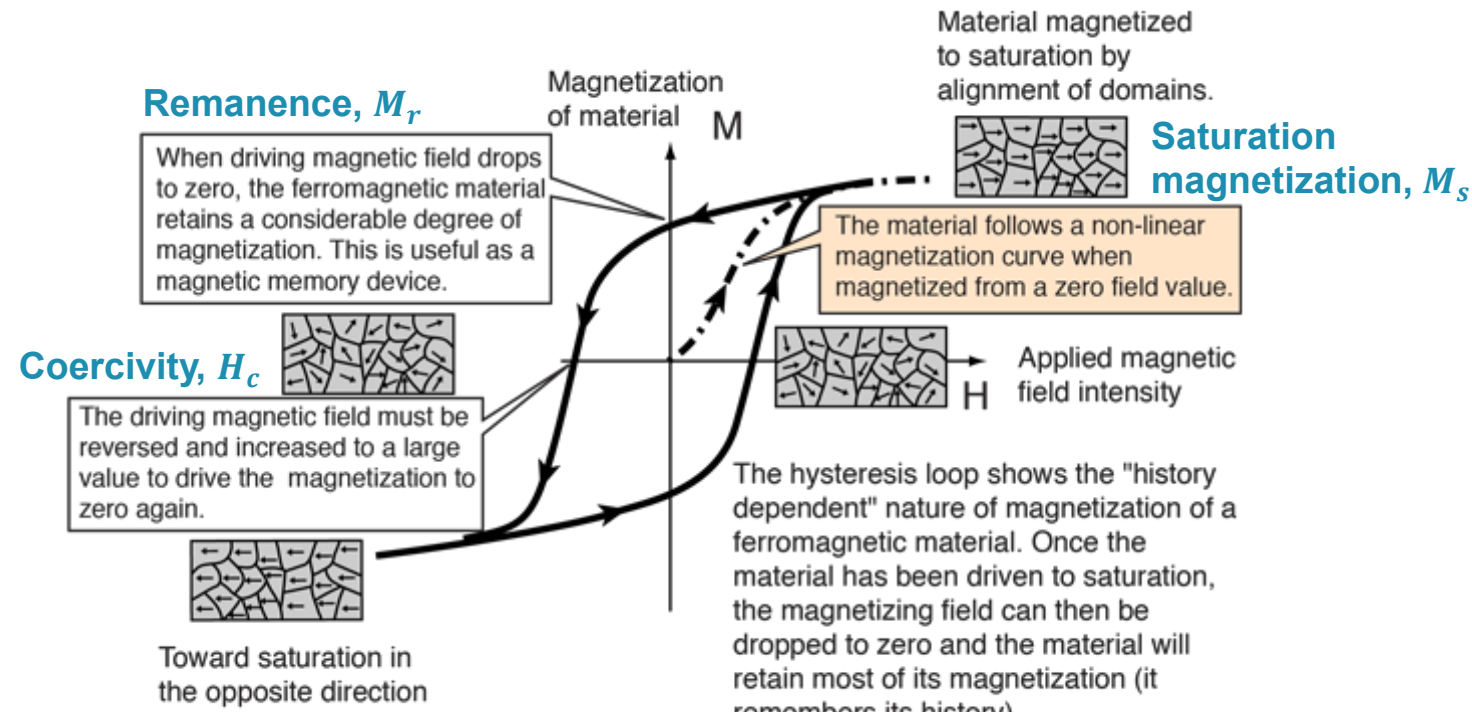
# Magnetic domains

- Schematic illustration of the change of magnetic domains from an initial condition (which defines the initial susceptibility  $\chi_I$ ) at zero magnetic field to **saturation**.
- Domains with an **aligned magnetic moment grow** at the expense of the poorly aligned ones to lower total energy.



# Magnetic hysteresis

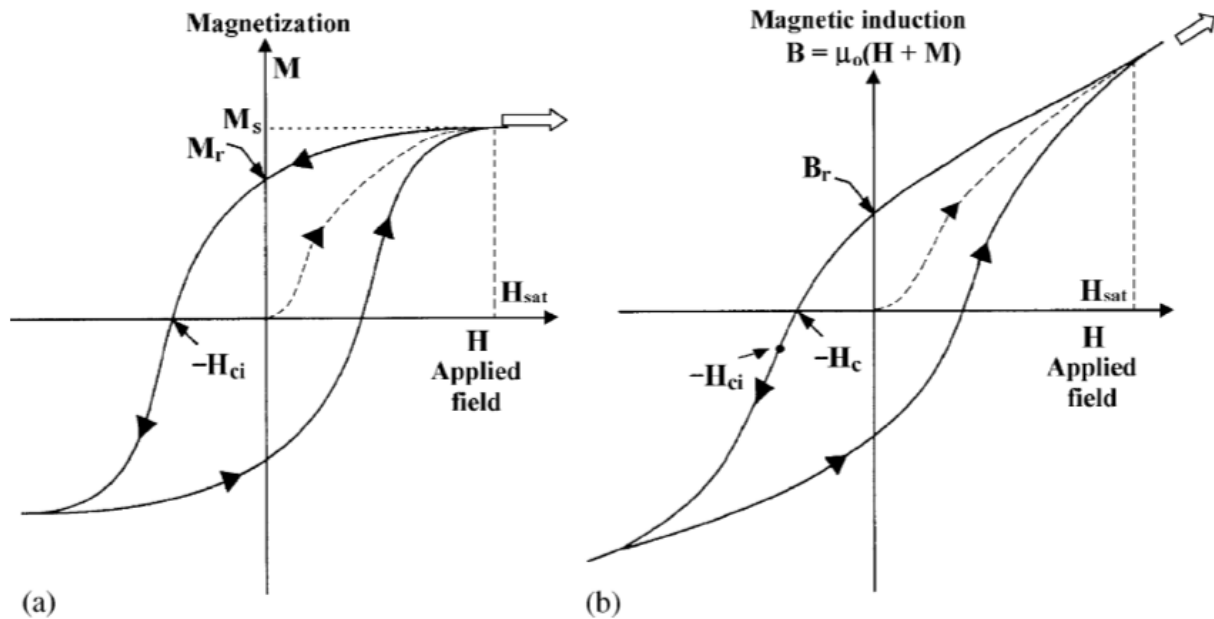
- When a ferromagnetic material is magnetized in one direction, it will not relax back to zero magnetization when the imposed magnetizing field is removed.
- It must be driven back to zero by a field in the opposite direction. If an alternating magnetic field is applied to the material, its magnetization will trace out a loop called a **hysteresis loop**. This is related to the existence of magnetic domains in the material.
- Once the magnetic domains are reoriented, it takes some energy to turn them back again.



<http://hyperphysics.phy-astr.gsu.edu/hbase/Solids/hyst.html>

# Magnetic hysteresis

- It is customary to plot the magnetization  $M$  as a function of the magnetic field strength  $H$ , since  $H$  is a measure of the externally applied field which drives the magnetization.
- There is a distinction between the two notions of '**coercivity**' referred to the  $B(H)$  curve and the  $M(H)$  curve, which turns out to be often confused in textbooks and scientific literature



*Hysteresis curves for a ferromagnetic material: (a)  $M$  vs.  $H$ :  $M_r$  is the remnant magnetization at  $H = 0$ ;  $H_{ci}$  is the intrinsic coercivity, i.e. the reverse field that reduces  $M$  to zero;  $M_s$  is the saturation magnetization; (b)  $B$  vs.  $H$ :  $B_r$  is the remanent induction (or 'remanence') at  $H = 0$ ;  $H_c$  is the coercivity, i.e. the reverse field required to reduce  $B$  to zero.*

H.W.F. Sung and C. Rudowicz, *Magnetism and Magnetic Materials* 260, 250–260 (2003)

# Short note on S.I. versus c.g.s. units

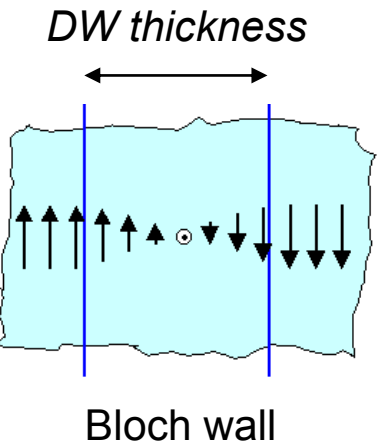
Many people think there is one system called “*The Metric System*”, but actually there are two systems:

- One is the “Système International” or S.I. system, which is the “real” (upper-case) Metric System, which uses Metres, Kilograms and Seconds for length, mass and time. For this reason it is sometimes called the **MKS system**.
- The “other” (lower-case) metric system uses centimeters, grams and seconds. It is most often called the **c.g.s. system**, and sometimes it is called the Gaussian system or the electrostatic system. There are other traditional differences in the two systems when measuring charge and electric and magnetic fields, for example.
- The S.I. unit for magnetic field is the **Tesla, or T**. It comes from the cross-product equation for magnetic force on a moving particle:  $F = qv \times B$ . The magnetic field,  $B$ , must be in units of force per charge per velocity. So  $1 T = 1 \text{ Ns/(Cm)}$ .
- In c.g.s. units, the equation for magnetic force looks different. Instead of  $qv \times B$ , it is  $(qv/c) \times B$ . You have to divide by the speed of light,  $c$ . The unit for magnetic field,  $B$ , is called the **Gauss, G**, where  $1 G = 1 \text{ dyne/esu}$  (esu = statcoulomb) The Earth’s magnetic field at the surface is about  $1/2 G$ , which makes it a very popular unit.
- Tesla’s are bigger than Gauss:  **$1 T = 10^4 G$** .

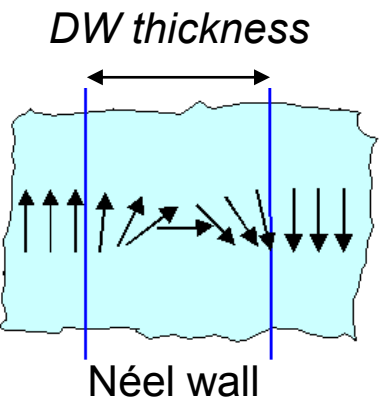
<https://www.physics.utoronto.ca/~jharlow/teaching/Units.htm>

# Domain walls

- Because of the strength of the exchange interaction, which wants to align neighboring spins, **abrupt changes in magnetization direction** (on the atomic scale) costs a lot of **extra energy**. As a result, the local magnetization spreads the change in direction out **over some distance**, i.e. the domain wall **thickness**.
- There are different kinds of domain walls that are possible:



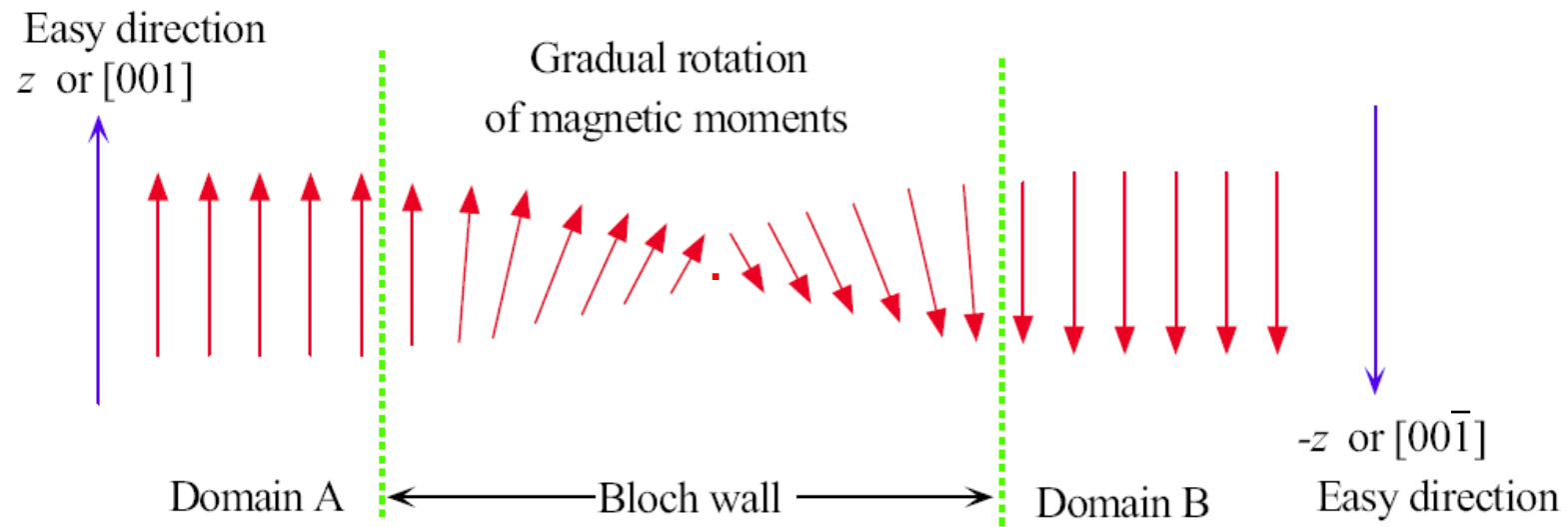
Bloch wall



Néel wall

# Ferromagnetic domains

- Let's take a closer look into the formation of a **Bloch wall** with a  $180^\circ$  change in the easy axis between two domains.



*In a Bloch wall the neighboring spin magnetic moments rotate gradually, and it takes several hundred atomic spacings to rotate the magnetic moment by  $180^\circ$ .*

- The spins in the material will **gradually rotate** to the opposite magnetization direction. The domain wall will **adjust** its thickness to **minimize the total energy**.
- This total energy is the **sum of the exchange energy** and the **anisotropy energy**.

# Ferromagnetic domains

- The exchange coupling tends to minimize the angle between two adjacent spins, in order to minimize the **exchange energy**:

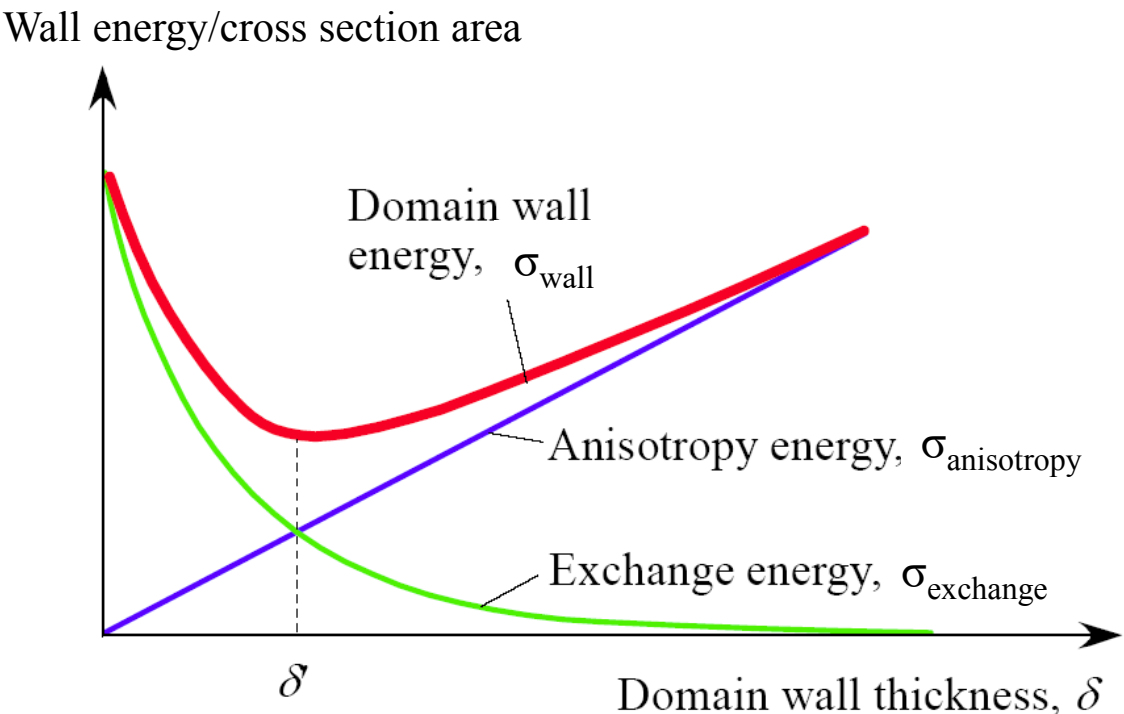
$$U_{ex} = -2J_{ex}\vec{S}_i\vec{S}_j = -2J_{ex}S_iS_j \cos\varphi$$

As a result, the extension of the region between 2 domains (i.e. the domain wall width) would tend to be very large due to this contribution.

- The **anisotropy energy** (per volume) tends to reduce the angle between the magnetization and the easy axis:

$$U_{an} = K \sin^2 \varphi$$

In the transition region, the spins are usually not parallel to the easy axis, such that this contribution tends to minimize the domain wall width.



*Schematic illustration of the potential energy per surface area generated by the anisotropy energy and the exchange energy as a function of the thickness of the domain wall.*

# Ferromagnetic domains

- Consider a change of spin orientation by an angle of  $180^\circ$  between two domains.
- For an infinitesimal change in angle between two adjacent spins, the exchange energy between the two spins reads:

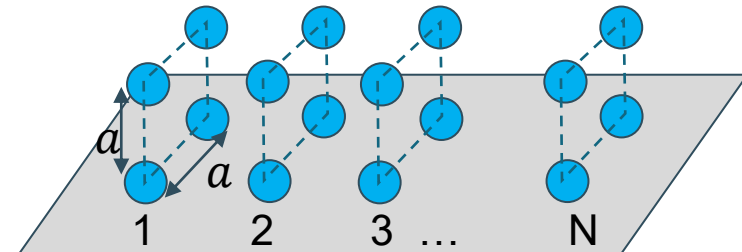
$$\Delta U_{ex} \approx J_{ex} S^2 \varphi^2 \text{ (see details in next slide)}$$

If the total change in angle ( $180^\circ$ ) takes place over  $N$  atoms, then the smallest change is  $\varphi = \pi/N$ . The total exchange energy over these  $N$  atoms then reads:

$$N\Delta U_{ex} \approx J_{ex} S^2 \frac{\pi^2}{N} \text{ (see details in next slide)}$$

- If the lattice constant of the material is  $a$ , then the energy per cross-sectional surface area of the domain wall, due to the exchange coupling is:

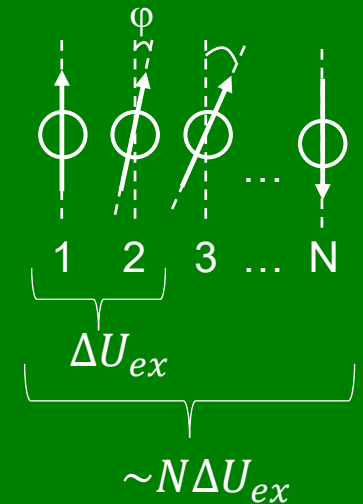
$$\sigma_{ex} \approx J_{ex} S^2 \frac{\pi^2}{Na^2}$$



# Ferromagnetic domains (extra)

- $U_{ex} = -2J_{ex}\vec{S}_i\vec{S}_j = -2J_{ex}S_iS_j \cos\varphi$   $\begin{cases} \text{if } \vec{S}_i \parallel \vec{S}_j \rightarrow U_{ex,0} = -2J_{ex}S^2 \overset{1}{\underset{1-\frac{\varphi^2}{2}}{\cos 0}} \Rightarrow \vec{S}_i \uparrow \uparrow \vec{S}_j \\ \text{if } \vec{S}_i \nparallel \vec{S}_j \rightarrow U_{ex,1} = -2J_{ex}S^2 \overset{\cos\varphi}{\underset{1-\frac{\varphi^2}{2}}{\cos\varphi}} \Rightarrow \vec{S}_i \uparrow \nearrow \vec{S}_j \end{cases}$   $\varphi$  is very small:  $\lim_{\varphi \rightarrow 0} \cos\varphi \approx 1 - \frac{\varphi^2}{2}$  (Taylor series)
- $\Delta U_{ex} = U_{ex,1} - U_{ex,0} = -2J_{ex}S^2 \left(1 - \frac{\varphi^2}{2} - 1\right) = J_{ex}S^2\varphi^2$
- The total spin flip ( $\varphi_{\text{total}} = \pi$ ) occurs over  $N$  atoms. Then  $\varphi = \pi/N$  and  $\Delta U_{ex} = J_{ex}S^2 \frac{\pi^2}{N^2}$
- The total energy to flip the spin is then:

$$N\Delta U_{ex} = J_{ex}S^2 \frac{\pi^2}{N}$$



# Ferromagnetic domains

- Over the domain wall, the maximum variation of the anisotropy surface energy (the energy per cross-sectional surface area of the domain wall) equals:

$$\sigma_{an} \approx KNa$$

where  $Na$  is the width of the domain (remember that  $U_{an}$  was energy per volume).

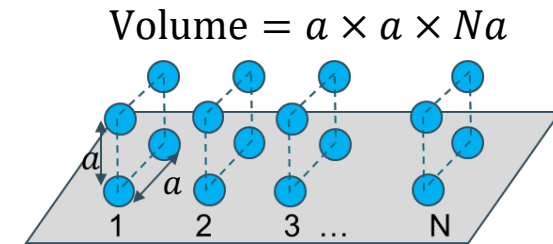
- The total surface energy is then:

$$\sigma \approx J_{ex}S^2 \frac{\pi^2}{Na^2} + KNa$$

- This energy is minimal when:

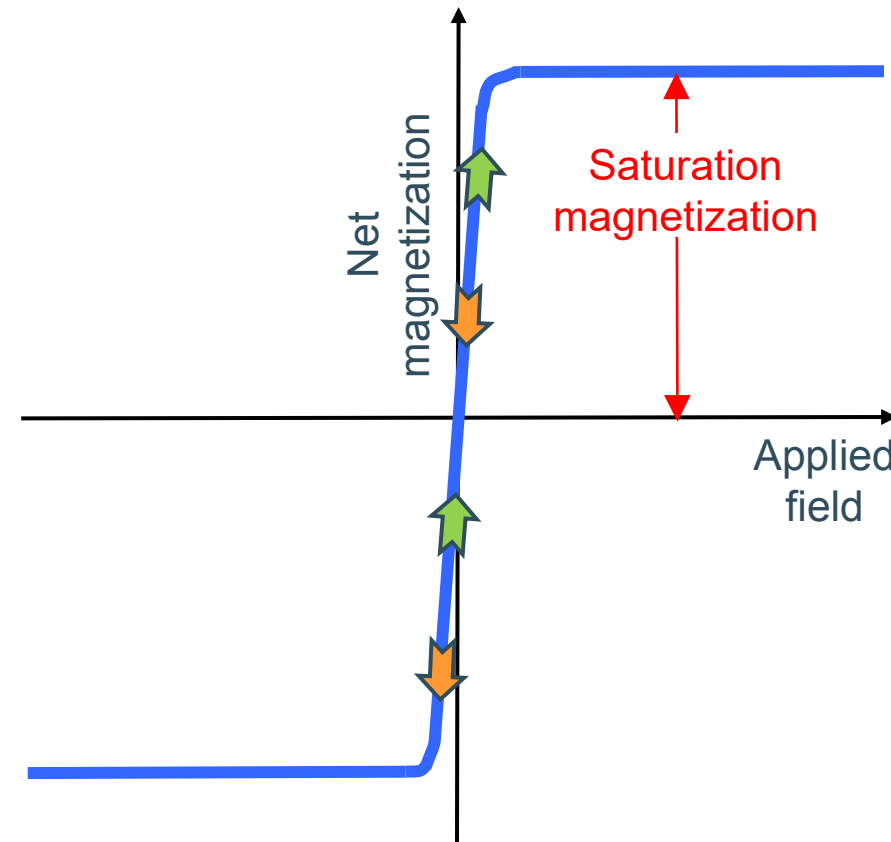
$$\frac{\partial\sigma}{\partial N} = 0 \Rightarrow \frac{-\pi^2 J_{ex} S^2}{N^2 a^2} + Ka = 0 \Rightarrow \delta = Na = \sqrt{\frac{\pi^2 J_{ex} S^2}{Ka}} , \text{ with } \delta \text{ the domain wall width.}$$

- This means that the domain wall width depends strongly on the **anisotropy constant  $K$**  of the material (it can change over few orders of magnitude). Materials with a **large** anisotropy constant  $K$  material typically have domain walls in the order of  $\sim 10$  nm. Materials with a **small**  $K$  value have much wider domain walls that can range from  $\sim 1$  to  $10$   $\mu\text{m}$ .



# Soft and hard magnets

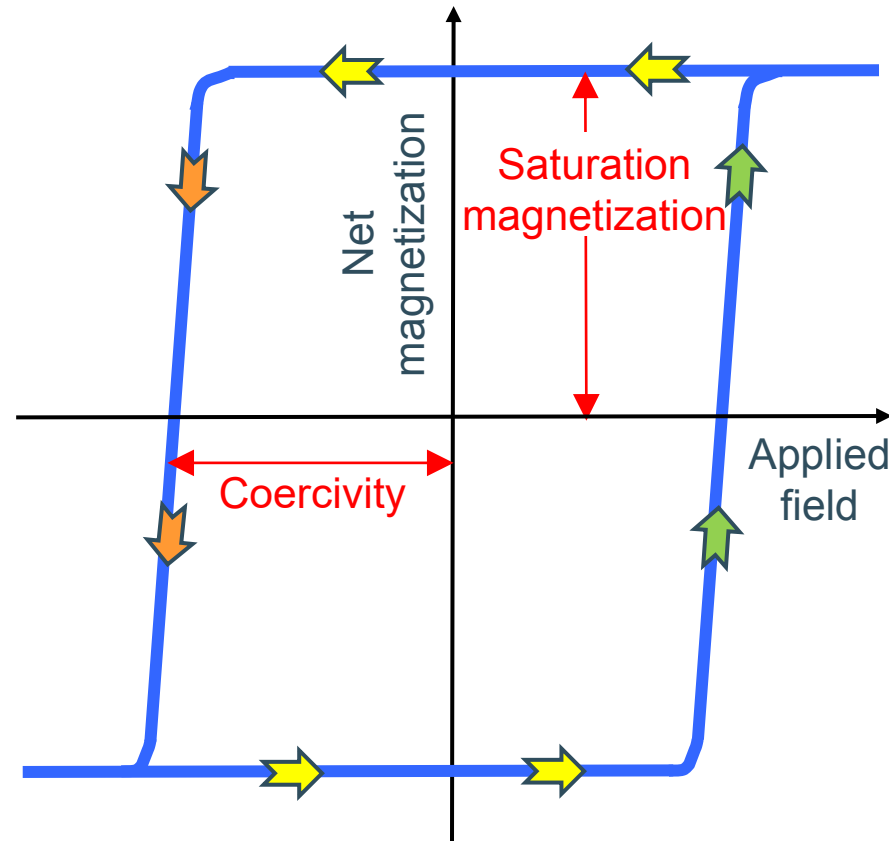
- Two type of ferromagnetic materials are distinguished, based on their response relative to an external magnetic field:



- In **soft magnetic materials**, the magnetization of the different domains can be easily switched by the applied magnetic field. This leads to the **absence of hysteresis** on the magnetization vs magnetic field curve.
- These materials can **change** their state of magnetization many times each second, and are used for AC applications (transformers, recording heads).

# Soft and hard magnets

- Two type of ferromagnetic materials are distinguished, based on their response relative to an external magnetic field:



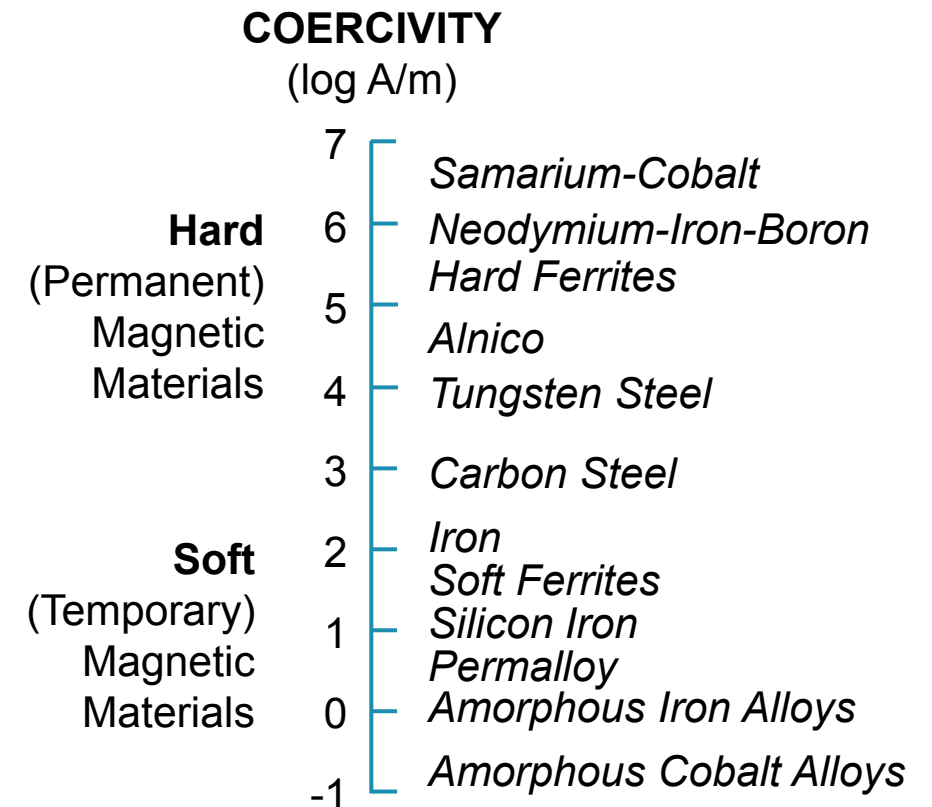
- In **hard magnetic materials**, the magnetization of the different domains cannot be switched easily, leading to a **hysteresis** on the field curve that shows the magnetization versus the magnetic field.
- These materials **maintain** their magnetization state over time and are used as permanent magnet and magnetic memory devices.

# Soft and hard magnets

- A magnetic material is **soft or hard**, depending whether **domain-wall motion** (switching of magnetization between different domains) is **easy or difficult**. This depends much on the microstructure of the material.
- Inhomogeneous materials, with many grain boundaries (poly-crystalline phases), present local variation of the surface energy  $\gamma$  of domain walls, which makes domain wall motion more difficult. Defects can act as ‘pinning’ sites and **impede the domain wall motion**, especially if the domain walls are narrow, i.e. if  $K$  is high.
- Therefore, hard magnets are typically inhomogeneous high- $K$  materials (the anisotropy constant).

# Soft and hard magnets

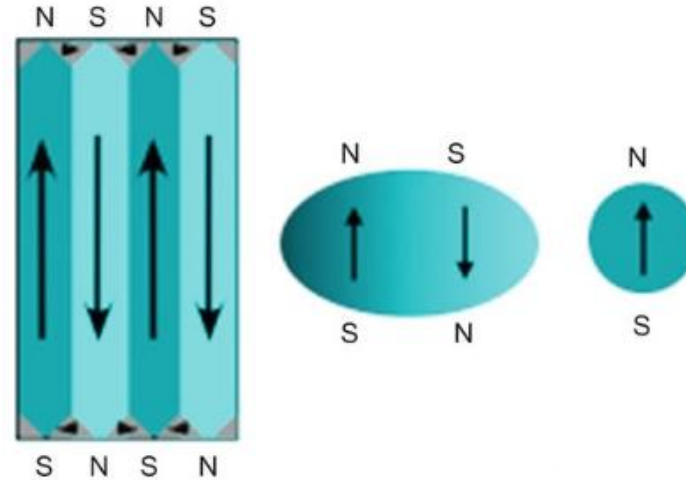
- Homogeneous **low- $K$  materials**, with only few **grain boundaries** and structural defects, have large domain walls with lower surface energy, leading to much **easier motion** of spins at the boundaries between different domains
- Soft magnets are usually homogeneous low- $K$  materials.
- Magnetic materials with a broad range of coercivities are available.
- The **coercivity** is an extrinsic property and, therefore, is sensitive to the micro-structure of the material.



Range of coercivities (note log scale) available for various magnetic materials.

# Magnetic domains: size effect

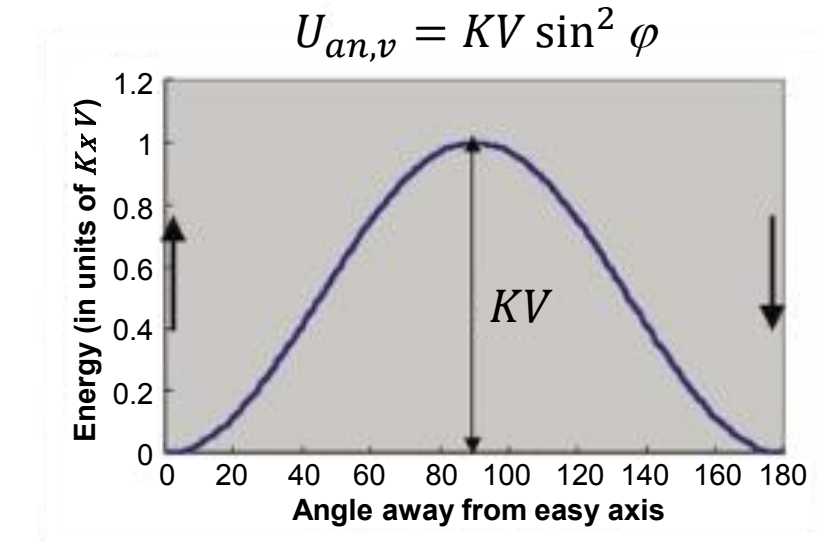
- The average **size** of the magnetic domains is a function of the system energy.
- As the volume of a piece of magnetic material is reduced the number of domains decreases.



- It is clear that when the volume drops below a certain critical value, it becomes energetically unfavorable to include a domain wall and the **uniformly magnetized state** becomes the **lowest energy** configuration. Thus, a piece of magnetic material below the **critical size** stays permanently magnetized at close to its saturation magnetization.

# Magnetic domains: size effect

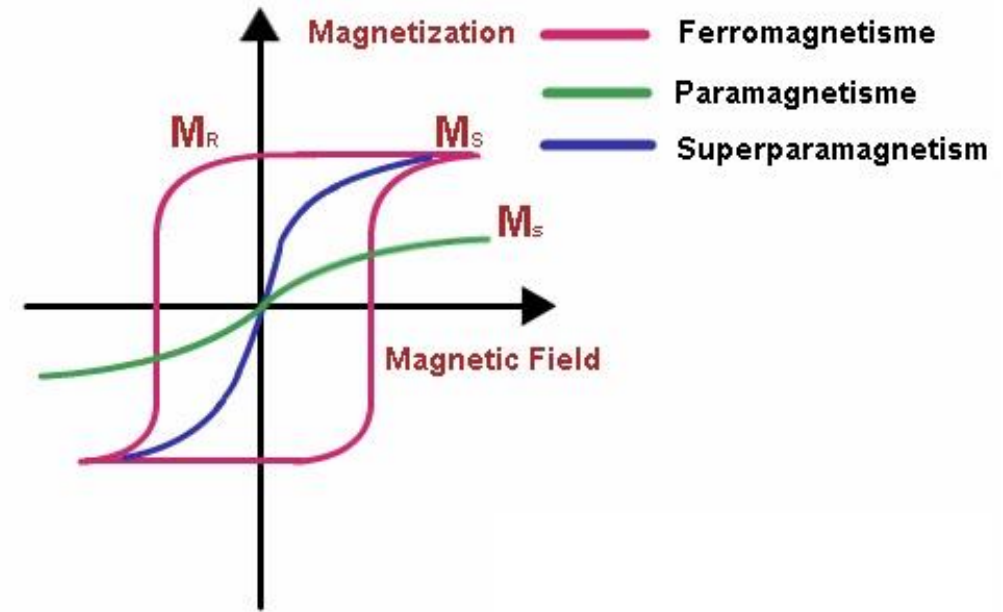
- Consider a particle with a uniaxial anisotropy whose anisotropy energy is given by  $U_{an,v} = KV \sin^2 \varphi$ , where  $K$  is the anisotropy energy density (in  $\text{J.m}^{-3}$ ),  $V$  is the particle volume and  $\varphi$  is the angle between the magnetization vector and the easy axis.
- The system therefore has **two minimal energy** states separated by an **energy barrier** of height  $KV$ .
- As the volume decreases at a specific temperature, there comes another critical diameter at which the magnetization of the nanoparticle is unstable against **thermal fluctuations**, that is,  $KV \sim k_B T$  and the time averaged magnetization goes to zero.
- Thus for a given particle size, there is a temperature that marks the transition from a permanent static moment to one that is fluctuating in a nanoparticle.



*Dependence of anisotropy energy on magnetization direction in a nanoparticle with a uniaxial anisotropy.*

# Superparamagnetism

- This means that in sufficiently small nanoparticles, magnetization can **randomly flip direction**, especially at high temperature. The nanoparticles are said to be in the **superparamagnetic state**.
- Normally, any ferromagnetic or ferri-magnetic material undergoes a transition to a paramagnetic state above its Curie temperature. Superparamagnetism is different from this transition since it occurs **below the Curie temperature** of the material and the magnetization is high.
- In the "macro-spin approximation" it is assumed that under this condition the magnetization of the nanoparticles can be considered as a single **giant magnetic moment**, which is the sum of all the individual magnetic moments carried by the atoms of the nanoparticle.



*Under the influence of a magnetic field paramagnetic materials are slightly magnetized, but when the magnetic field is removed this magnetization goes to zero. On the contrary, ferromagnetic materials present a strong saturation magnetization and a remanent magnetization ( $M_R$ ) in the absence of the magnetic field. Superparamagnetic materials share properties of ferromagnetism and paramagnetism.*

# Superparamagnetism

- Due to the magnetic anisotropy of the nanoparticle, the magnetic moment has usually only **two stable orientations** antiparallel to each other, separated by an **energy barrier**  $KV$ . At finite temperature, there is a finite probability for the magnetization to flip and reverse its direction. The mean time between two flips is called the **Néel relaxation time**  $\tau_N$  and is given by the Néel-Arrhenius equation:

$$\tau_N = \tau_0 \exp\left(\frac{KV}{k_B T}\right)$$

with  $\tau_N$  the average time it takes for the nanoparticle's magnetization to randomly flip as a result of thermal fluctuations,  $\tau_0$  the attempt period (characteristic of the material),  $K$  is the nanoparticle's magnetic anisotropy energy density and  $V$  its volume.  $KV$  is therefore the energy barrier associated with the magnetization moving from its initial easy axis direction, through a "hard plane", to the other easy axis direction.  $k_B$  is the Boltzmann constant and  $T$  the temperature.

- The Néel relaxation time is an exponential function of the **grain volume**, which explains why the flipping probability becomes rapidly **negligible for bulk materials or large nanoparticles**.

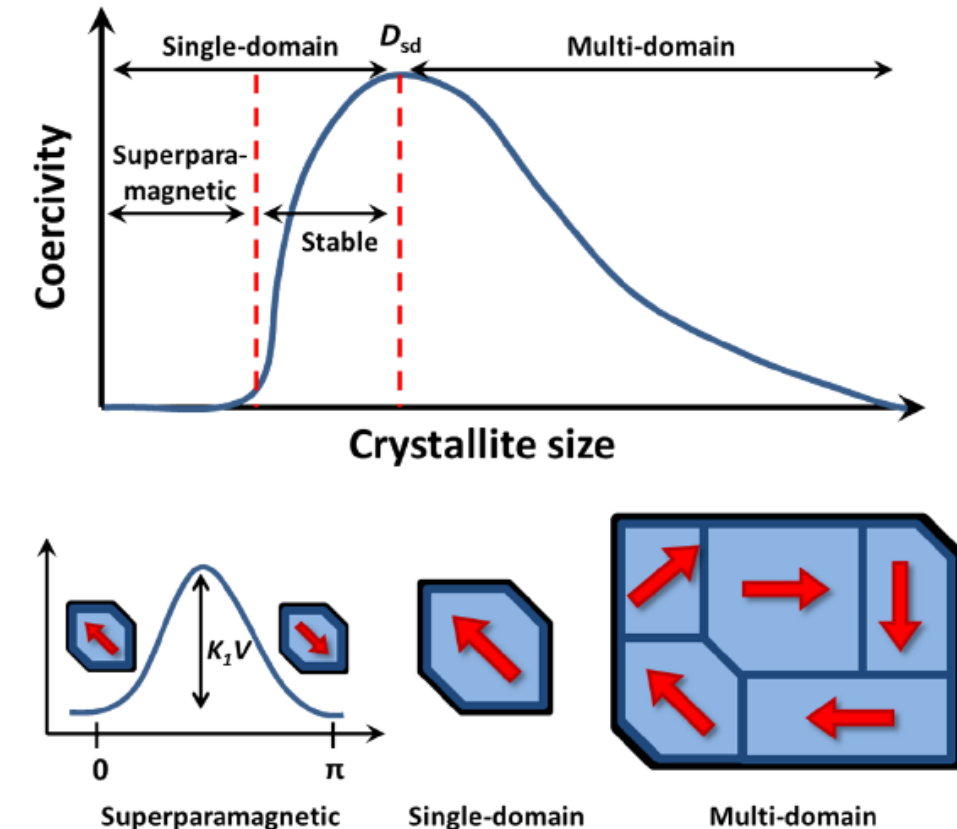
# Superparamagnetism

- Let us imagine that the magnetization of a single magnetic nanoparticle is measured and let us define  $\tau_m$  as the measurement time.
  - If  $\tau_m \gg \tau_N$ , the **nanoparticle magnetization** will flip several times during the measurement and the measured magnetization will **average to zero**.
  - If  $\tau_m \ll \tau_N$ , the magnetization will not flip during the measurement and the measured magnetization will be what the instantaneous magnetization was at the beginning of the measurement.
- In the former case, the nanoparticle will appear to be in the **superparamagnetic** state whereas in the latter case it will appear to be “blocked” in its initial state.
- The state of the nanoparticle (superparamagnetic or blocked) depends on the measurement time. A transition occurs when  $\tau_m = \tau_N$ . Typical in experiments, the measurement time is kept constant and the temperature is varied. Under these conditions the transition between the superparamagnetic and the blocked state is observed at a specific temperature for which  $\tau_m = \tau_N(T)$  is satisfied. This temperature is called the **blocking temperature**, given by:

$$T_B = \frac{KV}{k_B \ln \left( \frac{\tau_m}{\tau_0} \right)}$$

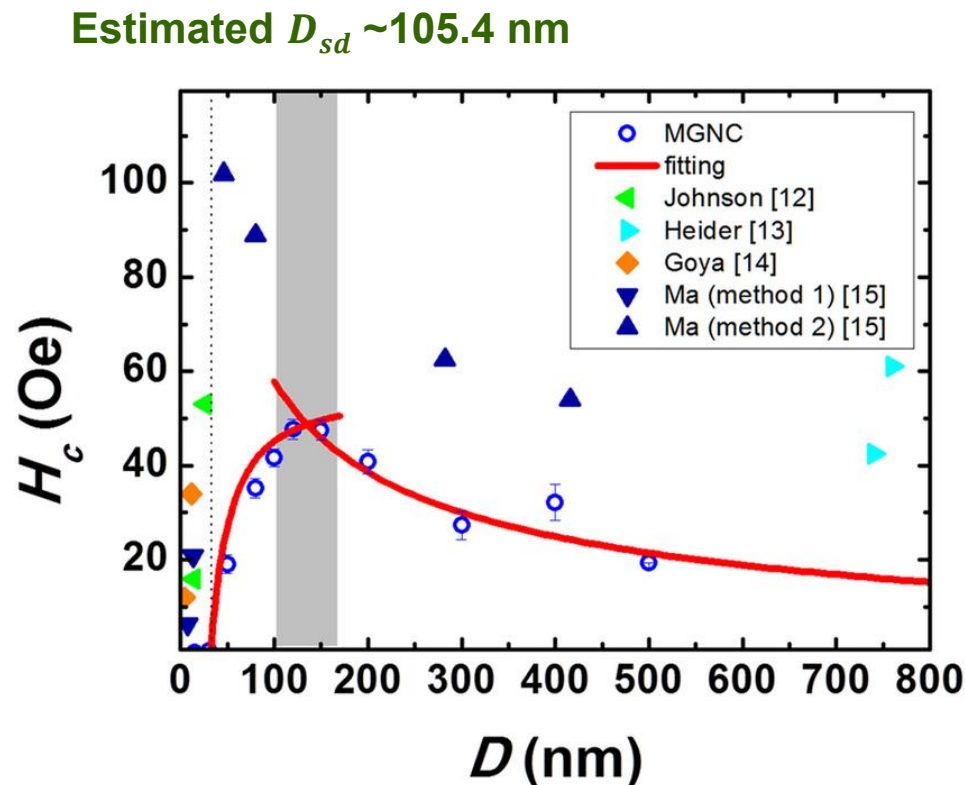
# Size effect on coercivity

- Unlike saturation magnetization, which is, in principle, size-independent, the coercivity is very sensitive to the **size variation**. With decreasing particle size the coercivity of a particle gradually increases to a **maximum value** at a particular size and then rapidly decreases to zero as the particle size further decreases
- Larger crystallites divide into magnetic domains separated by domains walls, which lowers the coercivity of the materials. The highest coercivity is achieved at the **critical magnetic single-domain size** ( $D_{sd}$ ). The decrease of coercivity below  $D_{sd}$  is due to an increased thermal contribution, which randomizes the magnetization. When the particle size decreases further, the coercivity becomes zero, reaching a superparamagnetic state. Unlike the transition from ferromagnetic to ordinary paramagnetic properties in bulk magnets, the ferromagnetic-to-superparamagnetic **transition** in fine particles is solely due to the size effect.

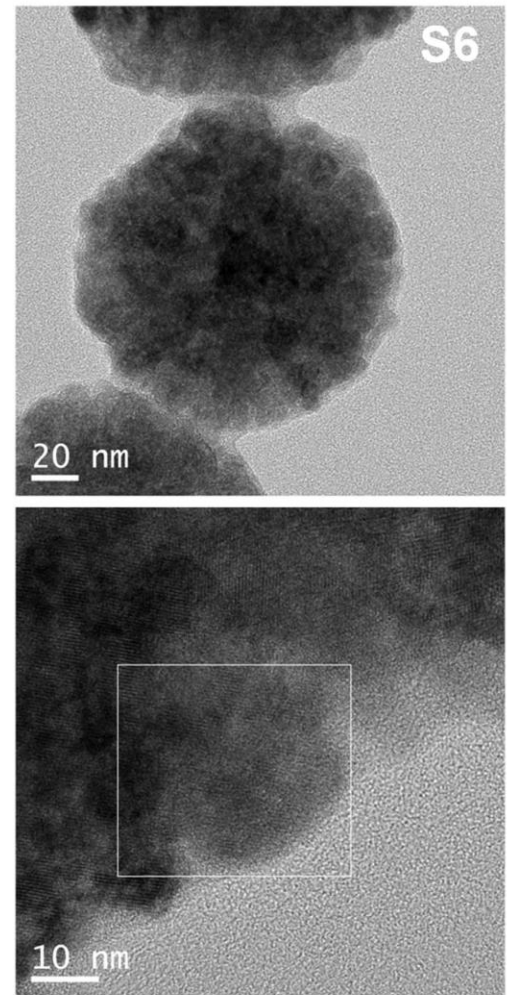
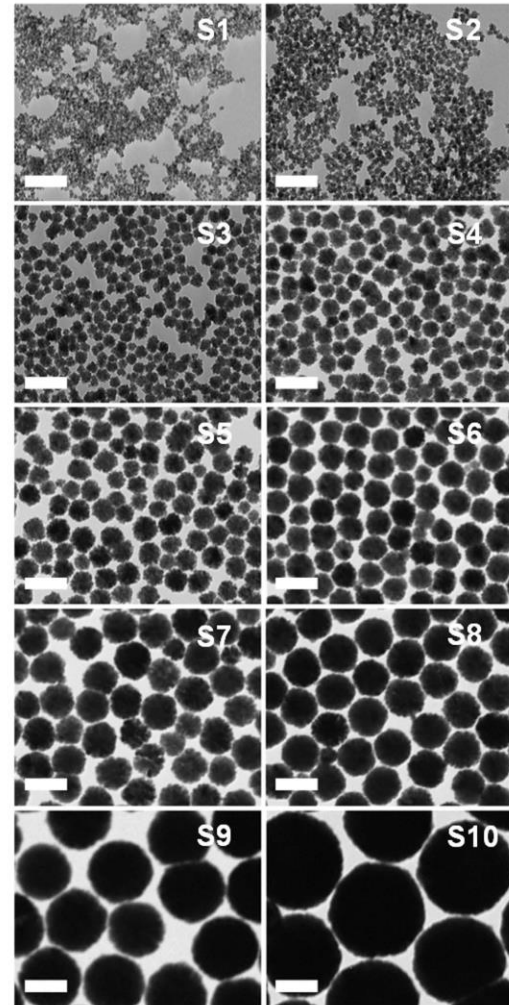


# Size effect on coercivity

- The size effect on coercivity was experimentally verified on the polyol synthesis of magnetite ( $\text{Fe}_3\text{O}_4$ ) nano-particles by adjusting the chemistry.



Scale bars are 200 nm.



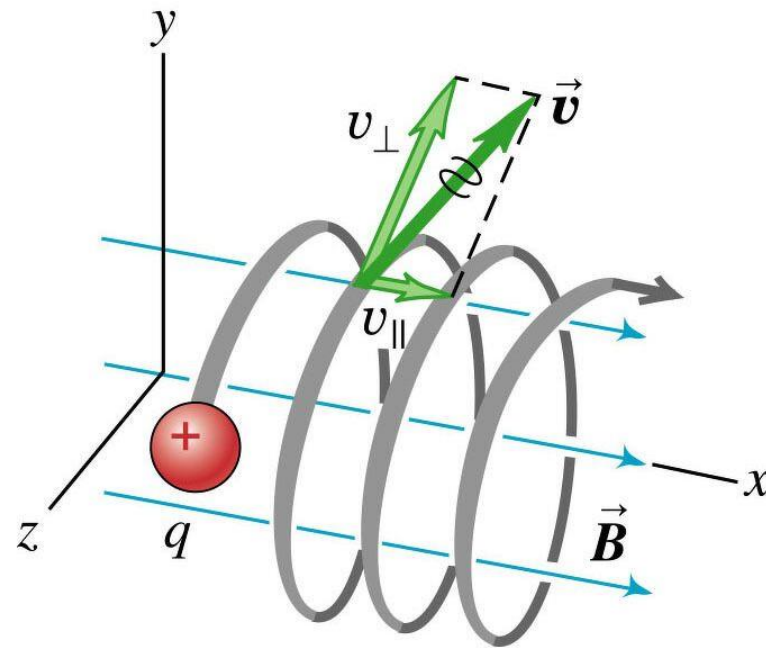
J. S. Lee et al., Sci. Rep. 5, 12135 (2015)

# Spin transport



# Magnetism and electrical resistivity

- The **magnetoresistance** phenomena is the tendency of a material to change the value of its electrical resistance in an externally-applied magnetic field.



## Ordinary Magneto Resistance (OMR)

- The Lorentz force  $\vec{F}$  due to magnetic field modifies the trajectory of electrons :

$$\vec{F} = -q\vec{v} \times \vec{B}$$

- The Ordinary Magneto Resistance (Lord Kelvin, 1856) results in small changes of the bulk resistivity, typically only  $\Delta R / R < 5\%$ .

- The scalar resistivity is given by:

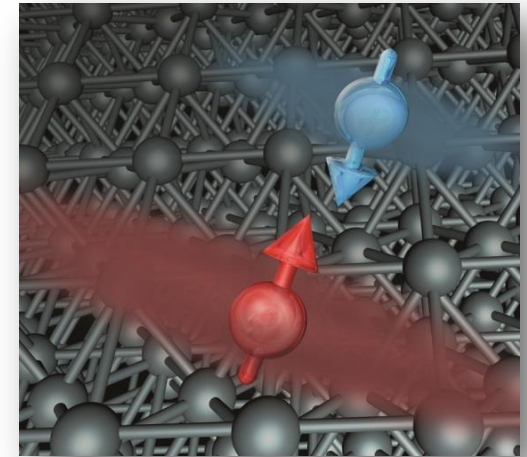
$$\rho_{xx} = \frac{1 + (\mu B)^2}{\sigma_0}$$

where  $B$  is the magnetic field and  $\mu$  the electron mobility.

- Since this effect is rather small, it is not very useful for practical applications.

# Spin polarized transport

Much more interesting applications can be obtained by using **spin-polarized currents**. Spin-polarized transport will occur naturally in any material for which there is an **imbalance of the spin populations** at the Fermi level. This imbalance commonly occurs in **ferromagnetic metals**.

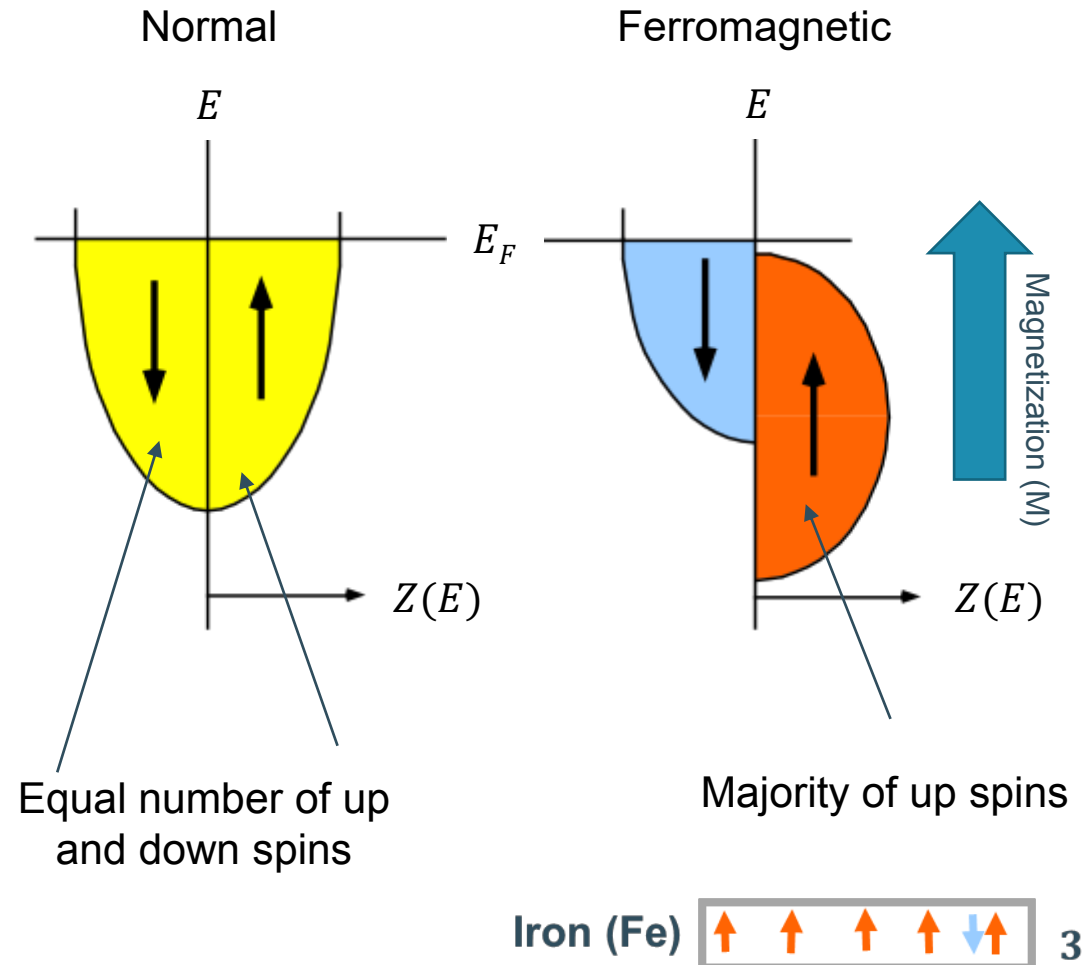


## Mott model

- In the Mott model it is proposed that the electrical conductivity in metals can be described in terms of two largely **independent conducting channels**, corresponding to the **up-spin** and **down-spin** electrons, and electrical conduction occurs in parallel for the two channels.
- In non-magnetic conductors the scattering rate does not depend on the electron spin. However, in ferromagnetic metals the **scattering rates** of the up-spin and down-spin electrons **are different**. Mostly it is assumed that the **scattering is strong for electrons with spin anti-parallel** to the magnetization direction and **weak for electrons with spin parallel** to the magnetization direction (in a bulk material).

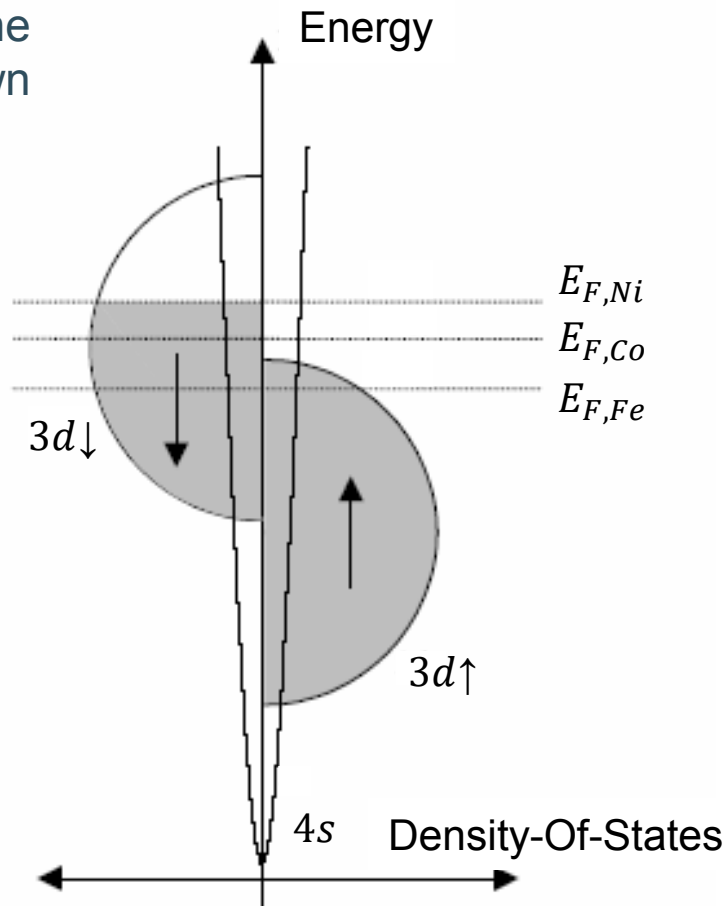
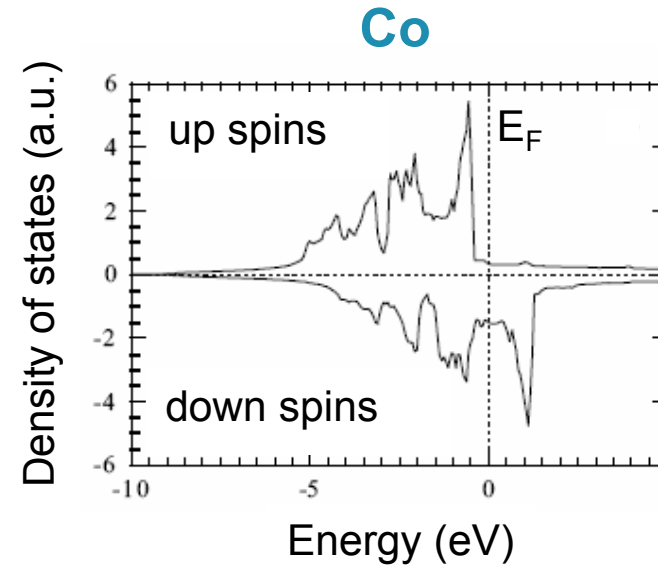
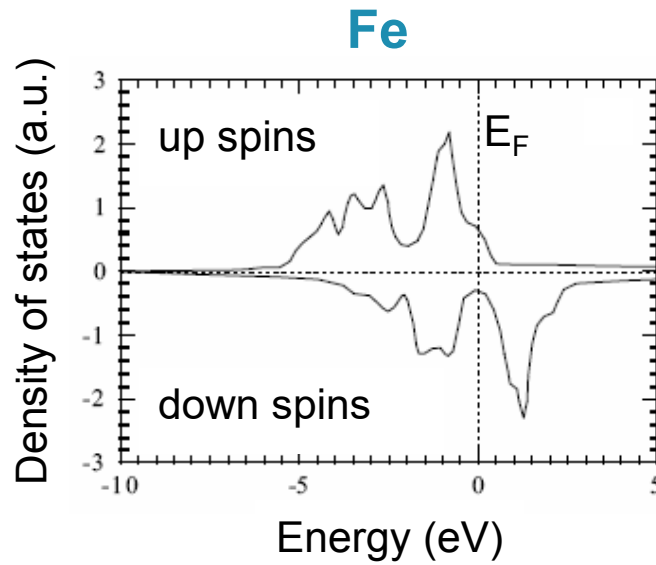
# Band structure of magnetic materials

- The density of states  $Z(E)$  as a function of energy  $E$  is then usually presented as in the right figure.
  - Non-magnetic materials show an **equal number** of up and down spins in the DOS.
  - Ferromagnetic materials have a **majority** of electrons in one spin state (up-state by convention).
- In this schematic diagram, it is seen that for the ferromagnetic material the available majority spin states (up-state) are **completely filled** at the Fermi level, while this is **not the case** for the **minority** spin states (down-state).
- This is a direct consequence of the **spin imbalance** present in these materials due to **Hund's rule**.



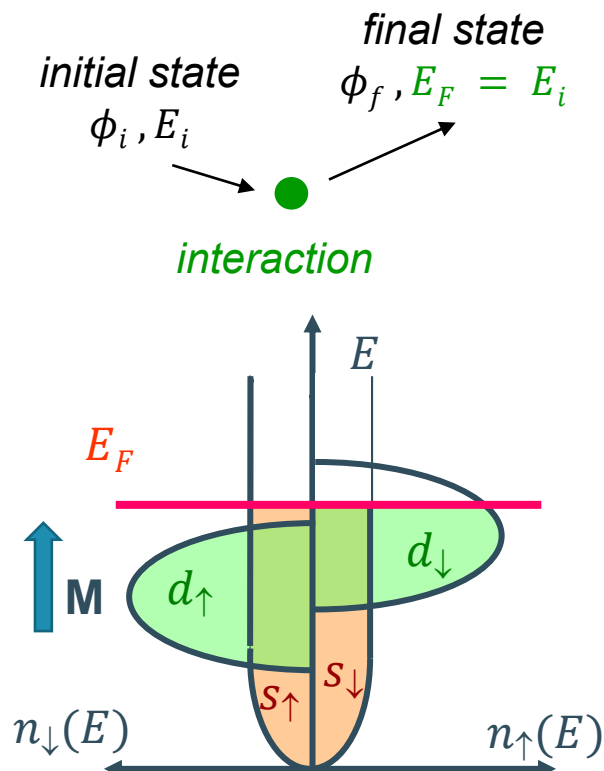
# Band structure of magnetic materials

- In general, in ferromagnetic materials there is an **asymmetry** present near the Fermi level where the Density-Of-States (DOS) of the “d” orbital is larger for down spins with respect to up spins. (The “s” orbital is symmetric).
- For Ni, Co and Fe these differences in the **3d orbitals** can be easily observed.
- There is a different band structures for up spin and down spin electrons .



# Spin dependent transport in the diffusion limit

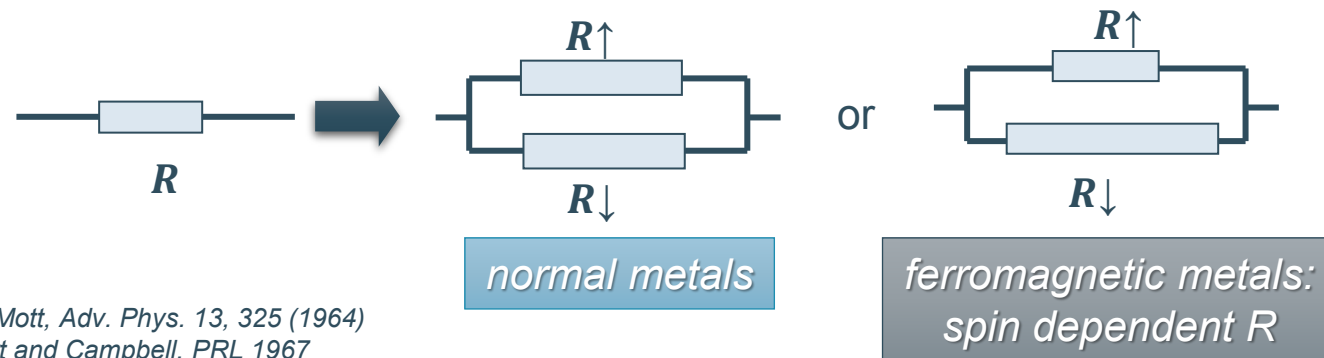
- Fermi "golden rule": **density of scattering probability**  $\propto$  **density of final states**
- This rule states that the scattering probability relates to the density of final states to which the electron can scatter. As a result, in ferromagnetic materials the scattering probability depends on the spin of the electron.
- Ferromagnetic metals (e.g. Fe, Co, Ni and their alloys)
  - "s" and "d" electrons close to the Fermi energy contribute to the electrical conduction but "s" electrons have higher mobility. Therefore, they are the main responsible for the electrical transport.
  - The main scattering effect is the "sd" exchange interaction (i.e. a spin-up "s" electron scatters and occupies a spin-up "d" orbital).
  - The strong difference in density of 3d states at  $E_F$  for spin  $\uparrow$  and spin  $\downarrow$  results in strongly different spin dependent scattering rates. Many empty 3d states for spin  $\downarrow$  imply a large probability of scattering.
  - The change in mean free path translates into changes in the resistivity, such as: mean free paths:  $\lambda_{\downarrow} \ll \lambda_{\uparrow} \rightarrow$  conductivities:  $\sigma_{\downarrow} \ll \sigma_{\uparrow}$



# Spin polarized transport

## Mott model

- This translates into a **different bulk resistivity** for spin-up and spin-down electrons, dependent on the magnetization of the material.
- We assume that the probability of spin-flip scattering is very low.

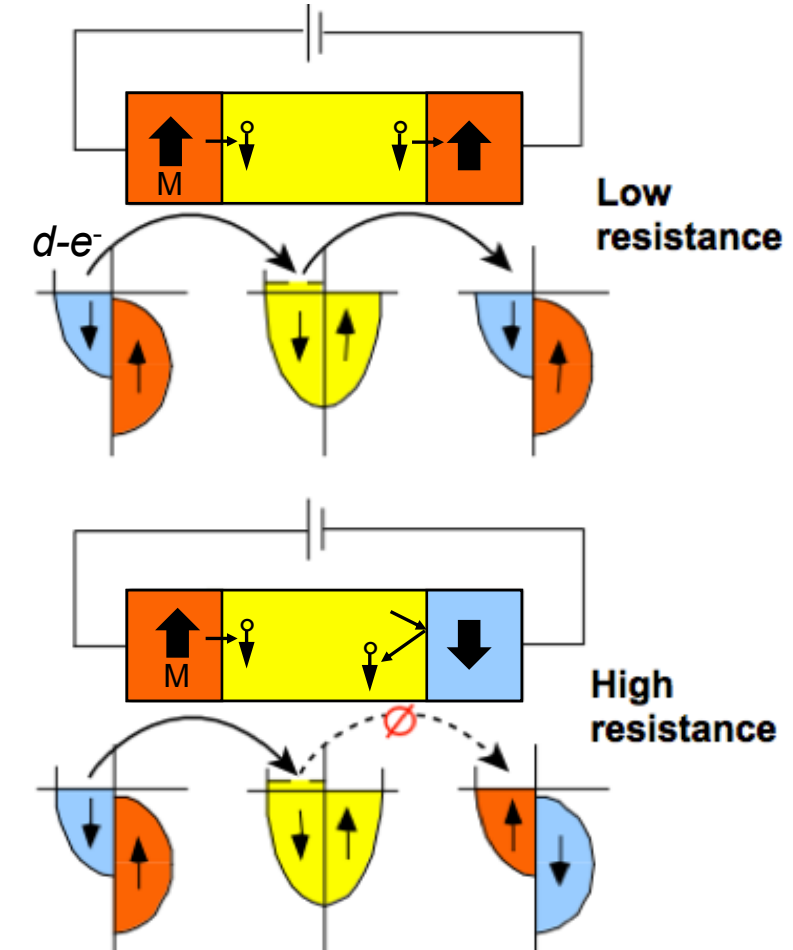


# Giant magnetoresistance



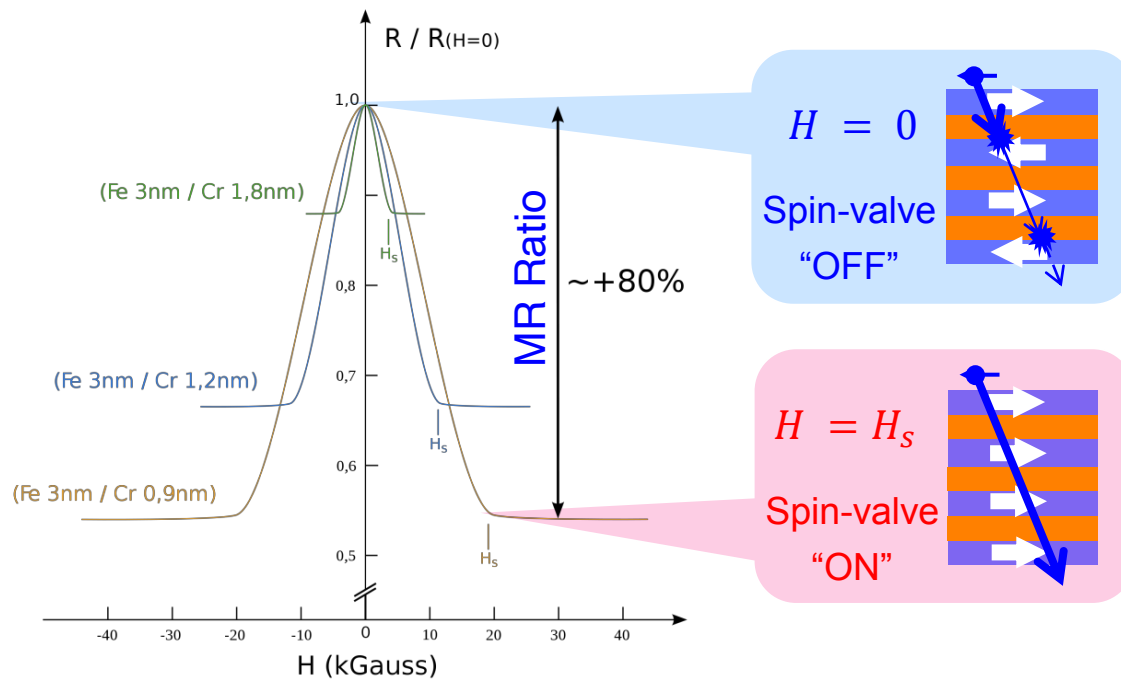
# Spin polarized devices

- The figure illustrates the basic action in a simple spin-polarized device, where it is assumed that the d-electrons are traveling from a ferromagnetic metal, through a normal metal, and into a second ferromagnetic metal.
- In the case where the magnetizations (or, equivalently, the magnetic moments) of the two ferromagnetic metals are in an aligned state, the electrons with the correct spin can freely move from one layer to the next and the resistance is low. When the layers are in the anti-aligned state the carrier movement is blocked at one interface and the measured resistance will be higher.
- In the geometry shown in the figure the current is perpendicular to the plane formed by the interface of the different materials (so-called **current-perpendicular-to-plane** or *CPP* geometry). Actual devices are generally not fabricated in this way, but in the **current-in-plane** (*CIP*) geometry



# Giant magnetoresistance (GMR)

- The CIP geometry makes use of the giant magnetoresistance (GMR) effect in thin magnetic multilayers.



- Like other magnetoresistive effects, GMR is the change in electrical resistance in response to an applied magnetic field. It was discovered that the application of a magnetic field to a Fe/Cr multilayer resulted in a significant reduction of the electrical resistance of the multilayer.
- The change in the resistance of the multilayer arises when the applied field aligns the magnetic moments of the successive ferromagnetic layers. In the absence of the magnetic field the magnetizations of the ferromagnetic layers are antiparallel. Applying the magnetic field, which aligns the magnetic moments and saturates the magnetization of the multilayer, leads to a drop in the electrical resistance of the multilayer.
- This effect was found to be much larger than either ordinary or anisotropic magnetoresistance and was, therefore, called “giant magnetoresistance” or GMR.

# Giant magnetoresistance (GMR)

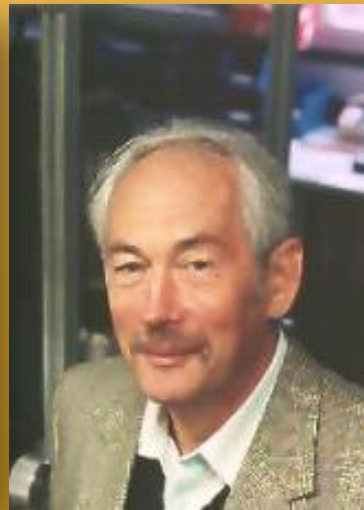
- A very simple resistor model is useful as a starting point for understanding the origin of the current-in-the-plane (CIP) GMR. In this model each metallic bilayer is treated as an independent resistor.
  - If all the magnetic layers are aligned (spin-valve “ON”), there is no strong interface scattering. Hence the whole stack acts as a bulk material (surface scattering is not important) and the resistance measured in the stack is the standard resistance: the GMR is zero.
  - If the magnetic layers are antiparallel (spin-valve “OFF”) thickness of each film is smaller than the **mean free path** of the electrons ( $\lambda$ ), the electrons may scatter strongly at the interface and the resistance of each film is defined by such scattering:

$$\frac{\rho_{\text{thin film}}}{\rho_{\text{bulk crystal}}} = 1 + \frac{3\lambda}{8D} (1 - P) \text{ which is valid for } \frac{\lambda}{D} > 0.3, P = 0 - 1 \text{ (Slides # 46, Chapter 3)}$$

(Then, if the magnetization of each film is the same, the interface scattering is minimized. The material would be equivalent to have a thick conductive film with thickness  $D \gg \lambda$  and the resistance measured for the stack is low. On the other hand, if the magnetization of each magnetic film is opposed to the neighboring films, the material behaves as a stack of thin films with thickness  $D < \lambda$ , in which surface scattering is much higher. Therefore, GMR can be observed.)

# Giant magnetoresistance (GMR)

- This spin polarization effect led to the discovery of the GMR.



Physics Nobel Prize  
2007

1988: GMR discovered simultaneously  
by A. Fert *et al.* (Orsay) and P.  
Grünberg *et al.* (Jülich)

# Spin polarized devices

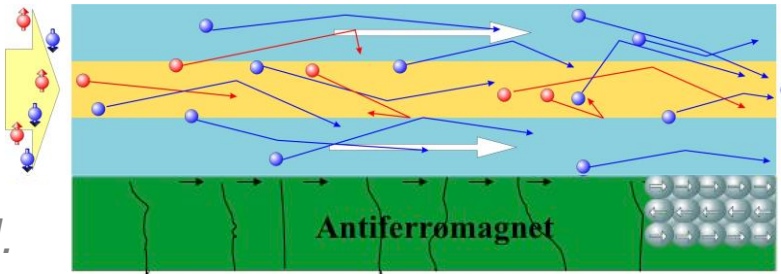


# Hard Disk Drive (HDD) based on GMR

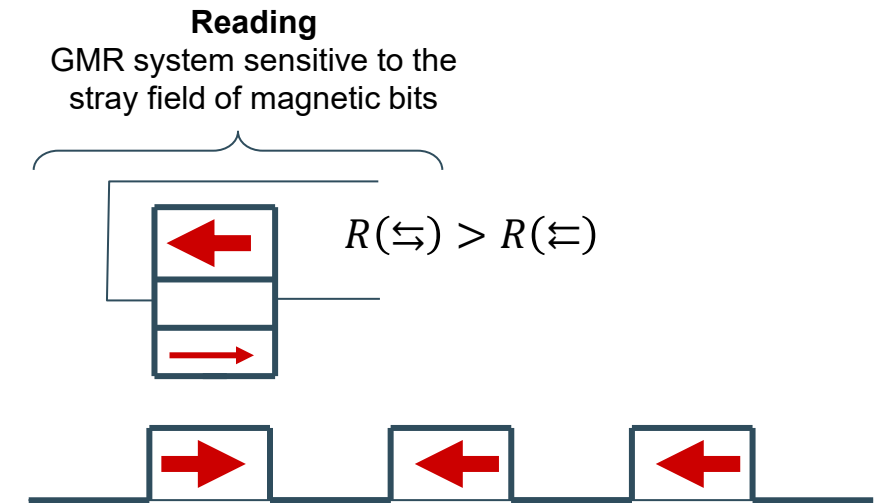
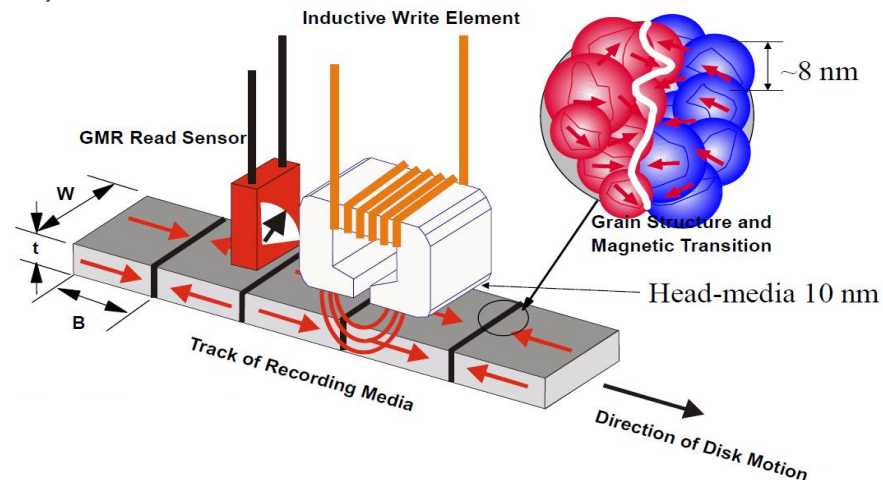
# Spin polarized devices

- GMR: To make a technologically useful device, a “pinning” layer is added to make it harder to change the magnetization of one layer than the other.

*The pinning layer can be a simple layer of an antiferromagnetic material.*



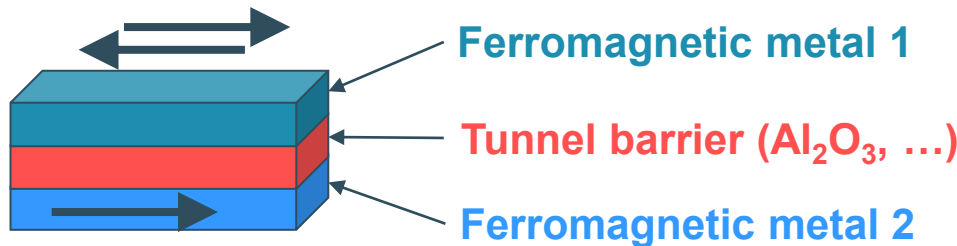
- This structure can be used e.g. to make GMR read heads which have found widespread application in hard disk drives (HDD).



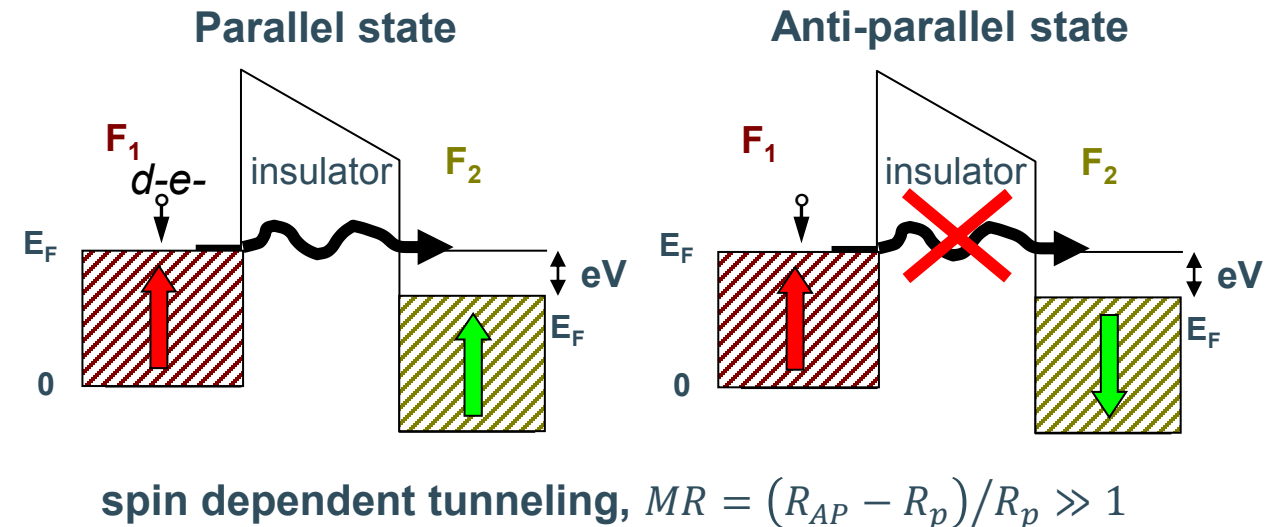
# Magnetic Tunnel Junction (MTJ) and Magnetic RAM (MRAM)

# The Magnetic Tunnel Junction

- A very important structure in spin electronics is the **magnetic tunnel junction** (MTJ).
- It is a magnetic storage and switching device in which two magnetic layers are separated by an insulating barrier (e.g. aluminum oxide, typically 1-2 nanometers thick) allowing an electronic current whose magnitude depends on the orientation of both magnetic layers to tunnel through the barrier when subject to an electric bias.



- The electron spin is not affected by the tunneling.
- The tunneling probability is dependent on the spin.



Claude Chappert, CNRS, France

# The Magnetic Tunnel Junction

- If the magnetic moments of the two ferromagnetic layers are parallel (top figure), spins states with down orientation can be injected from the cathode (M1), and occupy empty down spin states in the anode (M2), leading to a large tunneling current, since:

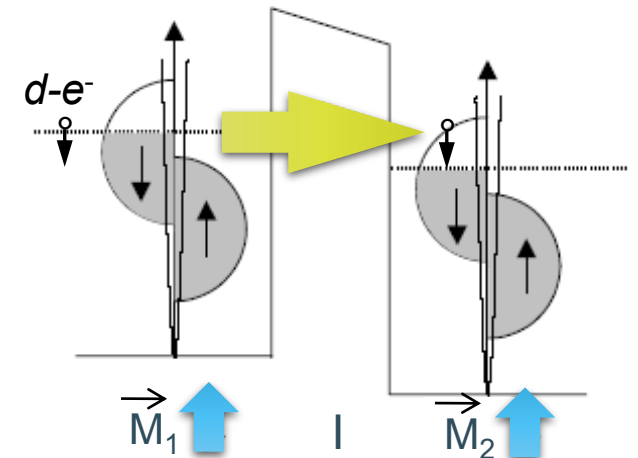
$$J_{\text{tunnel}} \propto T(E, V) f(E_{F,M1}) [1 - f(E_{F,M2})]$$

Tunneling probability

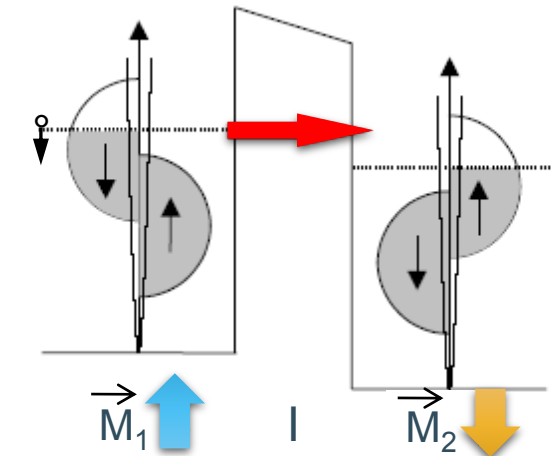
States in M1

Empty states in M2

- The tunneling probability  $T$  depends on the barrier height and thickness of the layer.
- On the other hand, if the magnetic moments of the two ferromagnetic layers are anti-parallel (bottom figure), there are no empty states with down spins available at the anode (M2), and the tunneling current is much reduced.



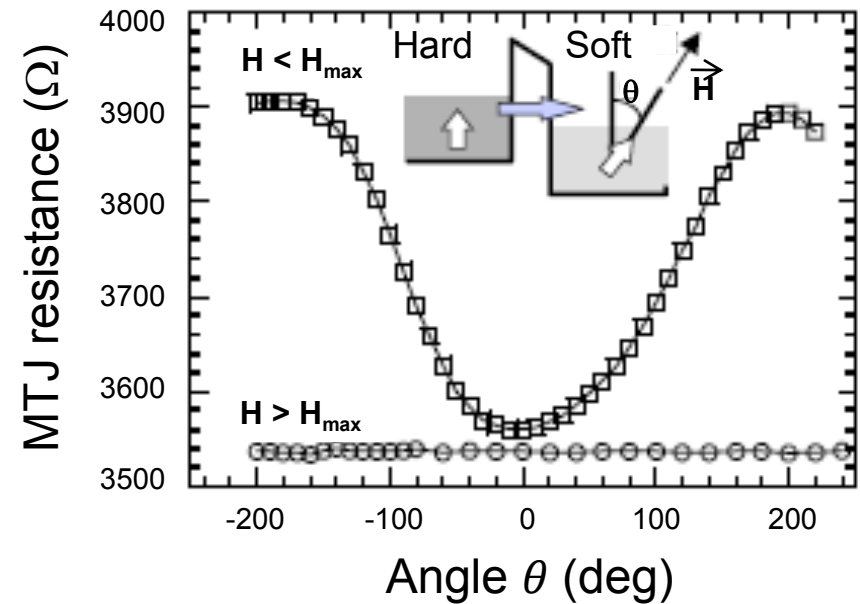
Parallel configuration



Anti-parallel configuration

# The Magnetic Tunnel Junction

- Since such *M1 / Insulator / M2* structure allow the injection of electrons with a specific spin orientation, they are also called “*spin valves*”.
- The resistance of the magnetic tunnel junction can be modulated by changing the orientation of the magnetization of one electrode, with respect to the other, as illustrated in the figure for a  $\text{CoFe}/\text{Al}_2\text{O}_3/\text{Co}$  structure, where the resistance is shown as a function of the angle  $\theta$  between the applied magnetic field and the direction along the magnetization of the CoFe magnetic layer.



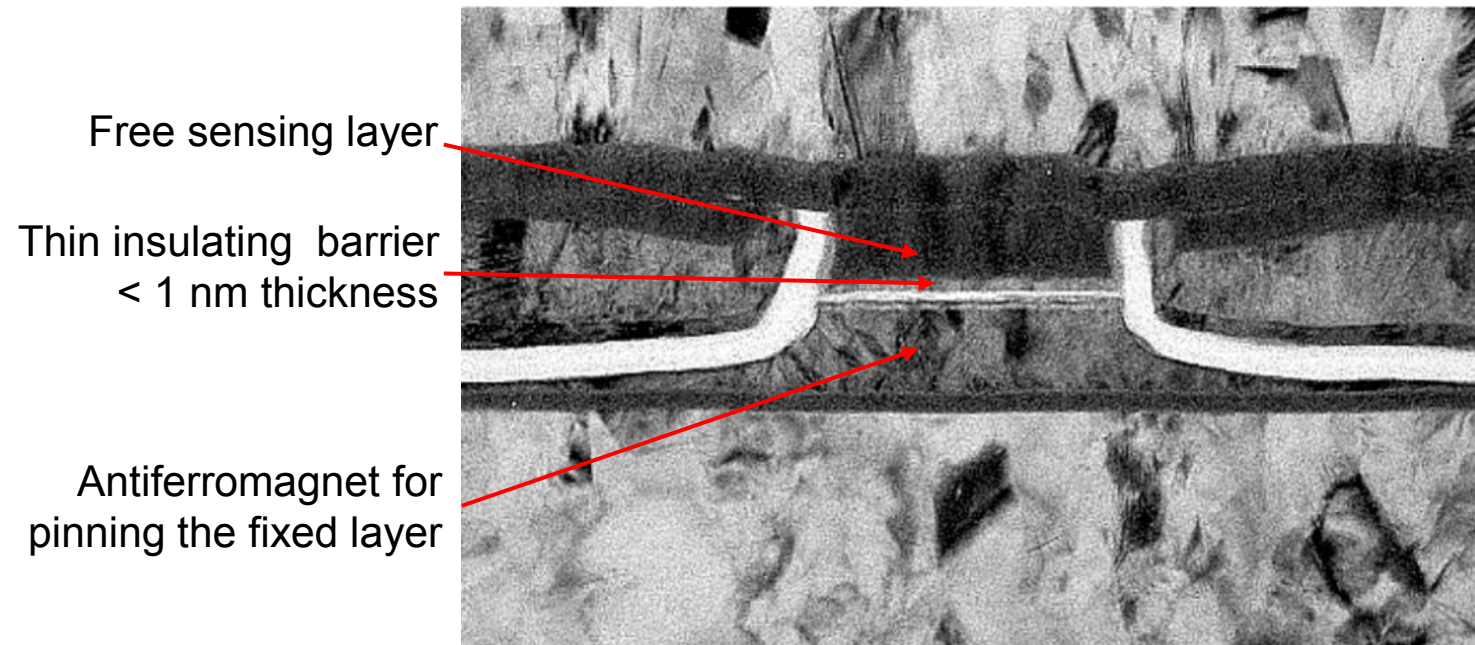
*Resistance of the magnetic  $\text{CoFe}/\text{Al}_2\text{O}_3/\text{Co}$  magnetic tunnel junction as a function of the angle of the applied field for fields below and above the critical value. The resistance varies  $\sim 10\%$  between high and low values.*

# The Magnetic Tunnel Junction

- In the CoFe/Al<sub>2</sub>O<sub>3</sub>/Co structure, the CoFe (M1) layer is a hard-magnetic material, such that it keeps the orientation of its magnetization under the applied magnetic field, for  $H < H_{max}$ .
- The Co layer (M2) is a soft magnet, such that the orientation of its magnetization can be changed under the application of the magnetic field. When  $\theta = 0$ , the magnetizations in M1 and M2 are parallel, and the resistance is low. When  $\theta \sim 180^\circ$ , magnetizations in M1 and M2 are anti-parallel, and the resistance is large.
- When  $H > H_{max}$ , the magnetization of M1 and M2 follows the orientation of  $H$ , and they are always parallel, explaining the low resistance observed in this case.

# The Magnetic Tunnel Junction

- MTJs are used in the write/read head of hard disk drives. As they are more sensitive than write/read heads based on GMR, they allow for a higher information density on the hard disk.

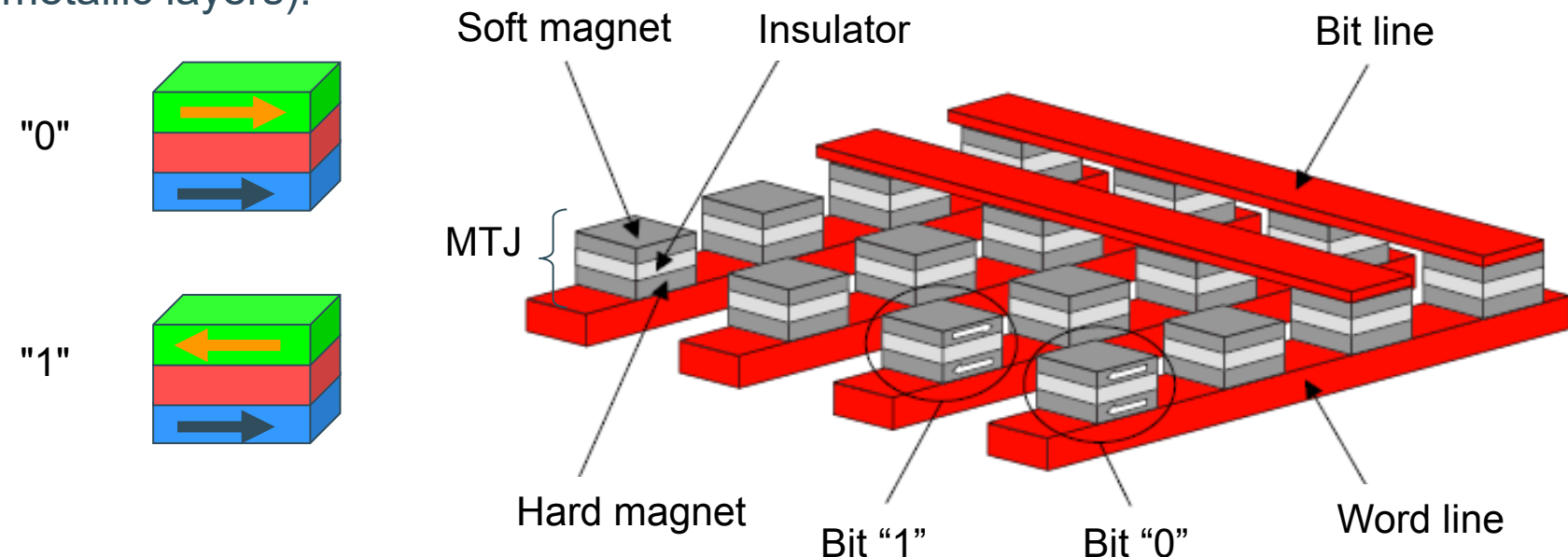


S. Mao, 2005 (Seagate)

- For the tunnel layer typically amorphous oxides such  $\text{TiO}_2$  or  $\text{Al}_2\text{O}_3$  were initially used. Later on, epitaxial tunnel oxides ( $\text{MgO}$ ) were introduced, enhancing significantly the resistance contrast.

# The Magnetic RAM (MRAM)

- Magnetic non-volatile memories can be fabricated by using the spin valve effect. The typical structure of a MRAM (Magnetic Random Access Memory) consists of a series of MTJs, connected by bit lines and a word lines (metallic layers).

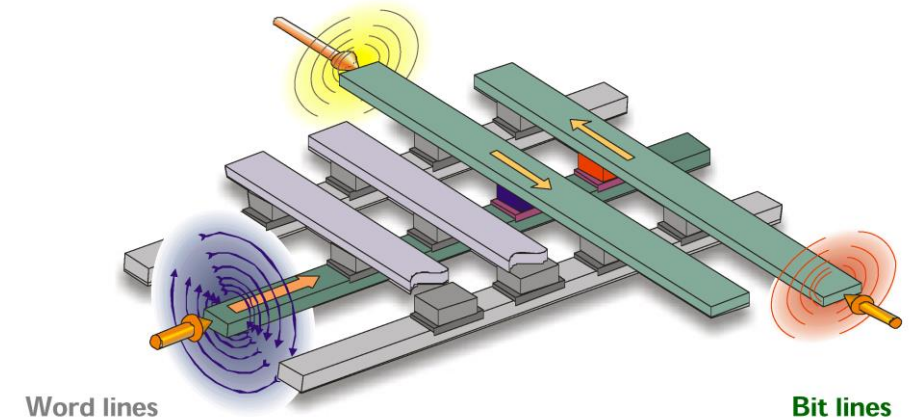


- Principle:
  - store binary information on arrays of magnetic tunnel junctions connected by conducting lines, that serve to address each cell individually for reading and writing
  - writing by sending current pulses in conducting lines

# The Magnetic RAM (MRAM)

- To write the bits of the MRAM, a high current is injected in the *bit* and *word* lines. These currents induce magnetic fields (Ampere's law) that add to each other, leading to a sufficiently high magnetic field to orient the magnetization of the soft magnetic layer in the magnetic tunnel junction.
- The magnetization of the soft magnet compared to the reference layer results in “*low*” or “*high*” values for the resistances of these junctions that can be associated with “1” and “0”.

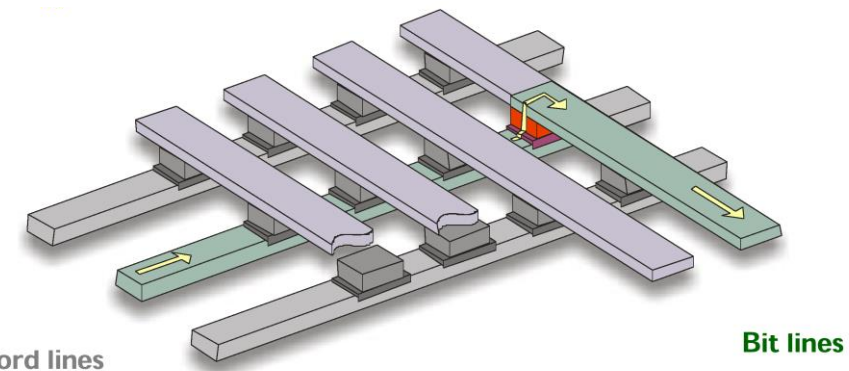
Writing



Word lines

Bit lines

Reading

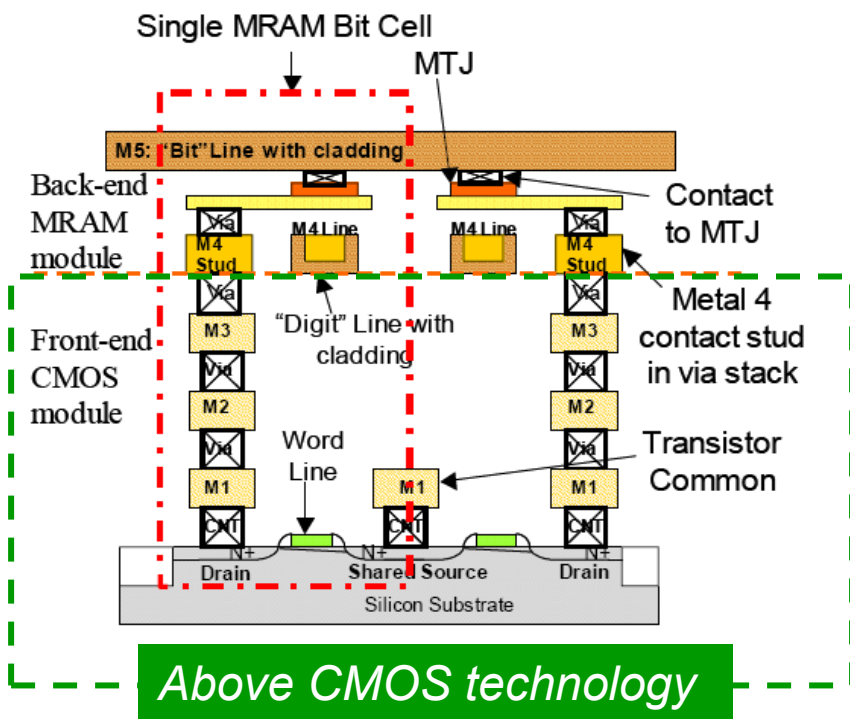


Word lines

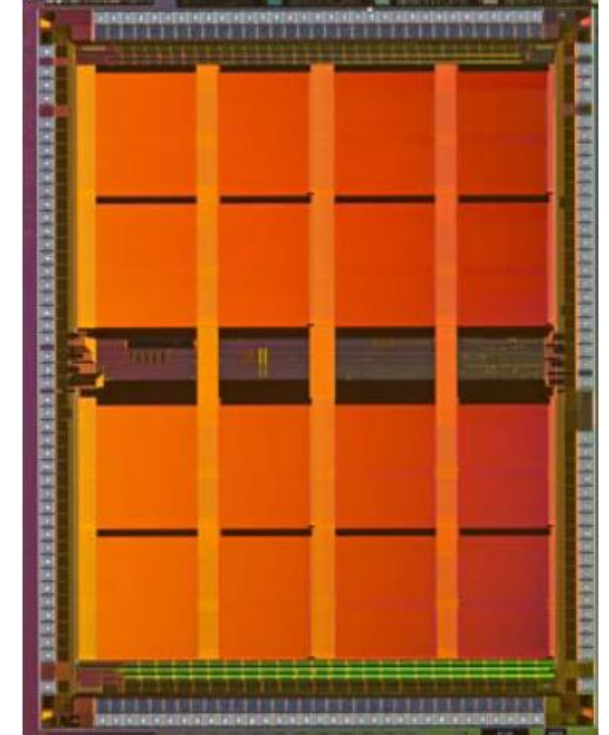
Bit lines

# The Magnetic RAM (MRAM)

- These memories initially received a lot of attention for specific applications as they are very robust and can be made on top of CMOS circuits. However, due to various issues the technology never became a main-stream product.



MRAM made by Freescale. Named "Product of the Year" [Electronics Products Magazine, Jan. 2007]

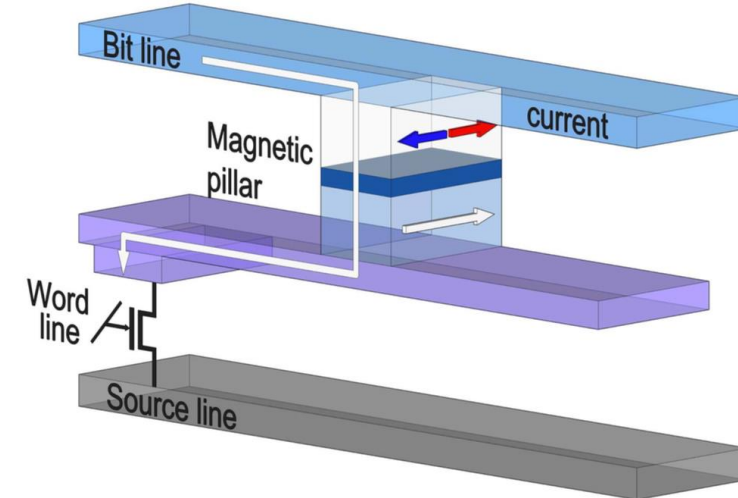
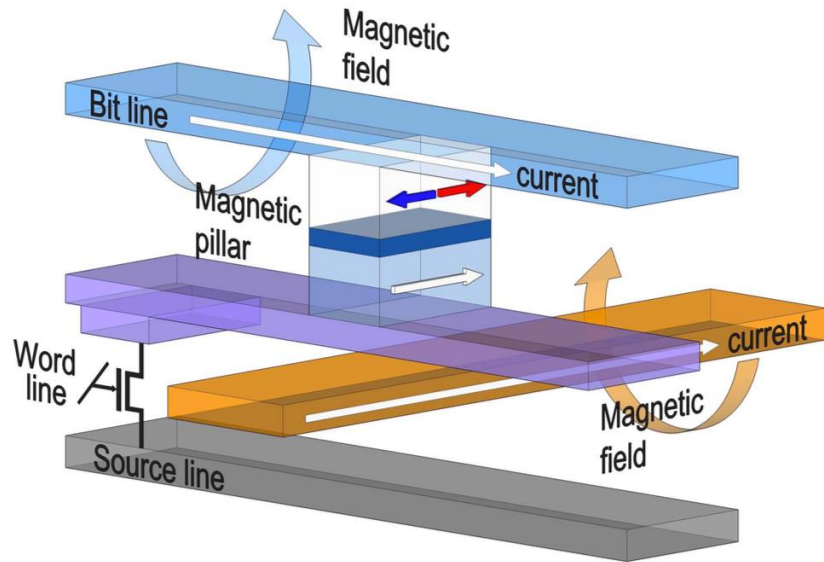


4 Mbit standalone memory  
Toggle switching → reliability,  
speed (30ns), cyclability

# Spin Transfer Torque (STT) and STT MRAM

# From MRAM to ‘spin transfer’ STT-MRAM

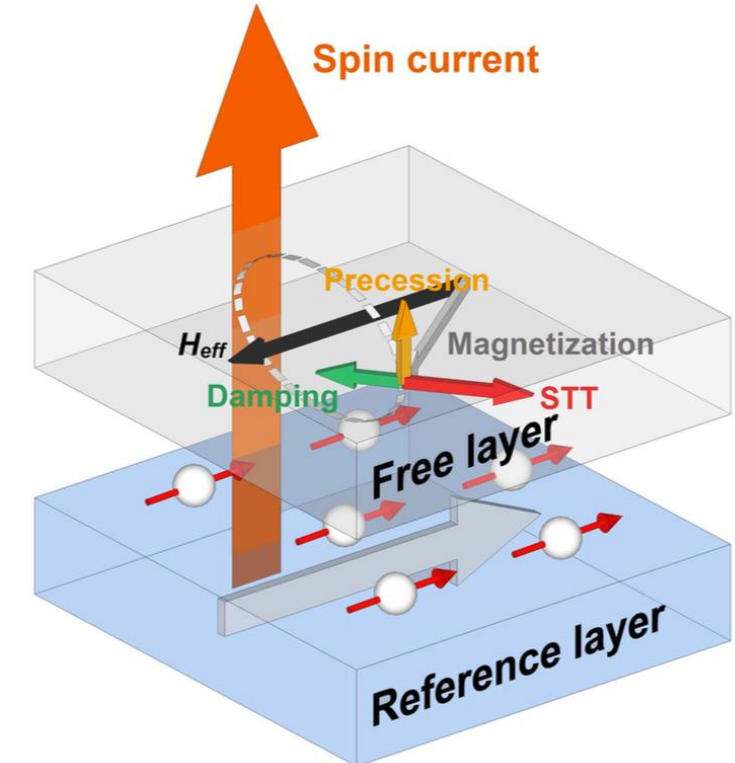
- In conventional field-induced MRAM the write operation is carried out by the current flowing through the wires. The currents generate magnetic fields around the wires. Switching occurs in the cell only, if the magnetic fields from both currents are present at the magnetic pillar.
- In the Spin Torque Transfer Magnetic RAM (STT-MRAM) the switching is obtained by passing a spin polarized current through the tunnel junction. The spin transfer torque effect is used to switch the magnetization of the free layer.



A.Makarov et al, Semiconductor Science and Technology, 31 (2016) 113006

# From MRAM to ‘spin transfer’ STT-MRAM

- **Spin Transfer Torque (STT)** opened a new way of manipulating magnetization dynamics by using spin polarized currents instead of magnetic fields.
- In general, when electrons pass through the thick/hard fixed magnetic layer, the spins of the electrons become aligned with the magnetization of this layer.
- When these spin- polarized electrons enter the free layer (thinner/softer), their spin orientations are getting aligned with the magnetization of the free layer within a transition layer of a few Ångströms. But at the same time, those electrons exert a torque on the magnetization of the free layer by action-reaction, which can cause magnetization switching, if the torque is large enough to overcome the damping.
- Smaller torque values result in magnetization precession around the effective magnetic field.



*Schematic illustration of the spin-transfer torque effect.*

A.Makarov et al, Semiconductor Science and Technology, 31 (2016) 113006

# Spin Transfer Torque (STT)

- In 1935, Landau and Lifshitz have proposed an equation describing the damped motion of the magnetization in a ferromagnet, known as the Landau-Lifshitz (LL) equation. This equation could be used only in a case of small damping. In 1955, Gilbert proposed a modification to the equation which describes the strong damping in the thin films.
- A macro-spin model treats a nanomagnet with the assumption that its internal magnetic degrees of freedom are frozen, so that the dynamics of macro-spin can be phenomenologically described by the Landau-Lifshitz-Gilbert (LLG) equation:

$$\frac{d\vec{M}}{dt} = -\gamma\mu_0(\vec{M} \times \vec{H}_{eff}) - \frac{\alpha\gamma\mu_0}{M_s}\vec{M} \times (\vec{M} \times \vec{H}_{eff})$$

where  $\gamma$  is the gyromagnetic ratio [rad s<sup>-1</sup> T<sup>-1</sup>],  $\alpha$  the dimensionless damping coefficient,  $M_s$  is the saturation magnetization.

- The LLG describes the MRAM switching by magnetic field. In order to be able to describe a switching in STT-MRAM, an additional spin transfer torque (STT) term must be added at the end yielding the Landau-Lifshitz-Gilbert-Slonczewski equation:

$$\frac{d\vec{M}}{dt} = -\gamma\mu_0(\vec{M} \times \vec{H}_{eff}) - \frac{\alpha\gamma\mu_0}{M_s}\vec{M} \times (\vec{M} \times \vec{H}_{eff}) - \beta\vec{M} \times (\vec{M} \times J\hat{m}_f)$$

$\beta$  the coefficient for the STT which depends on both the spin polarization and the geometric configuration between the incoming spin and the local moments in the free layer, and  $J$  the current density. The spin transfer torque counteracts the damping.

# Spin Transfer Torque (STT)

- Landau-Lifshitz-Gilbert-Slonczewski equation:

$$\frac{d\vec{M}}{dt} = -\gamma\mu_0(\vec{M} \times \vec{H}_{eff}) - \frac{\alpha\gamma\mu_0}{M_s}\vec{M} \times (\vec{M} \times \vec{H}_{eff}) - \beta\vec{M} \times (\vec{M} \times \hat{J}m_f)$$

Effective damping

Spin evolution      Excitation term: precessional torque      Intrinsic damping      STT term

The diagram illustrates the precession of a magnetization vector  $\vec{M}$  around an effective field  $\vec{H}_{eff}$ . The initial state is shown as a red arrow labeled  $m_f$ , and the final state is a black arrow labeled  $M$ . A blue dashed line represents the trajectory of the magnetization vector during precession. A pink arrow labeled "Damping" indicates the effect of intrinsic damping. A blue arrow labeled "Spin Torque" indicates the effect of the STT term. The angle between the initial and final magnetization vectors is labeled  $\theta$ .

The figure shows two sets of diagrams illustrating the precession of a magnetization vector  $\vec{M}$  around an effective field  $\vec{H}_{eff}$  for different current densities  $J$ . The left set of diagrams, labeled  $J = J_c$ , shows a full circular precession trajectory. The right set of diagrams, labeled  $J > J_c$ , shows a partial circular precession trajectory. In both cases, the initial magnetization vector  $\vec{M}$  is shown as a black arrow, and the final magnetization vector  $\vec{m}_f$  is shown as a red arrow. The angle between them is labeled  $\theta$ . The precession is driven by the effective field  $\vec{H}_{eff}$  (blue arrow) and the spin torque (green arrow). The damping is indicated by a red arrow labeled "Damping". The STT is indicated by a blue arrow labeled "STT".

Precession of the spin in switching state for  $J = J_c$  and  $J \gg J_c$ . The blue line shows the trajectory, and the bold arrows show the initial and final states of magnetization. The dotted arrows show an intermediate state of magnetization.

# Spin Transfer Torque (STT)

For switching of the free layer to occur, a critical current is needed to make the spin torque larger than the damping force.

- When  $J$  is small and the spin torque term less than the damping term, the dynamics damp out into an equilibrium state.
- When the spin torque is large enough that it overcomes the intrinsic damping (i.e. larger than the critical current), the effective damping coefficient becomes negative. In this case the deviation from the equilibrium state is amplified and the magnetic moments are switched, which can be detected by a resistance change in the magnetic sandwiched structure, e.g. MTJs or spin-valves.
- When  $J$  and  $H$  satisfy certain conditions, persistent precession of the magnetization can be obtained at a frequency of several GHz. When the precession occurs, the angle between the magnetic moments in the free layer and the pinned layer changes rapidly. Due to the magnetoresistance effect, it gives rise to a resistance change at high frequency; therefore a DC current/voltage induced microwave emission can be observed in the device.

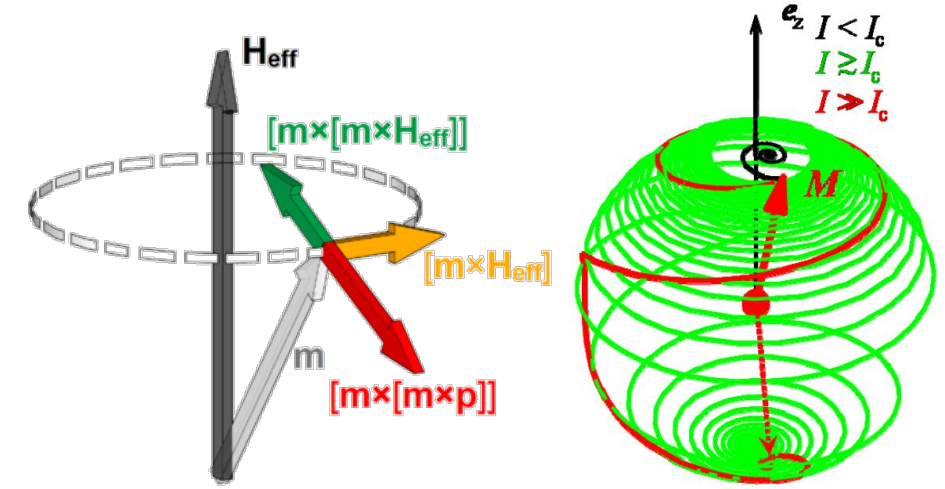
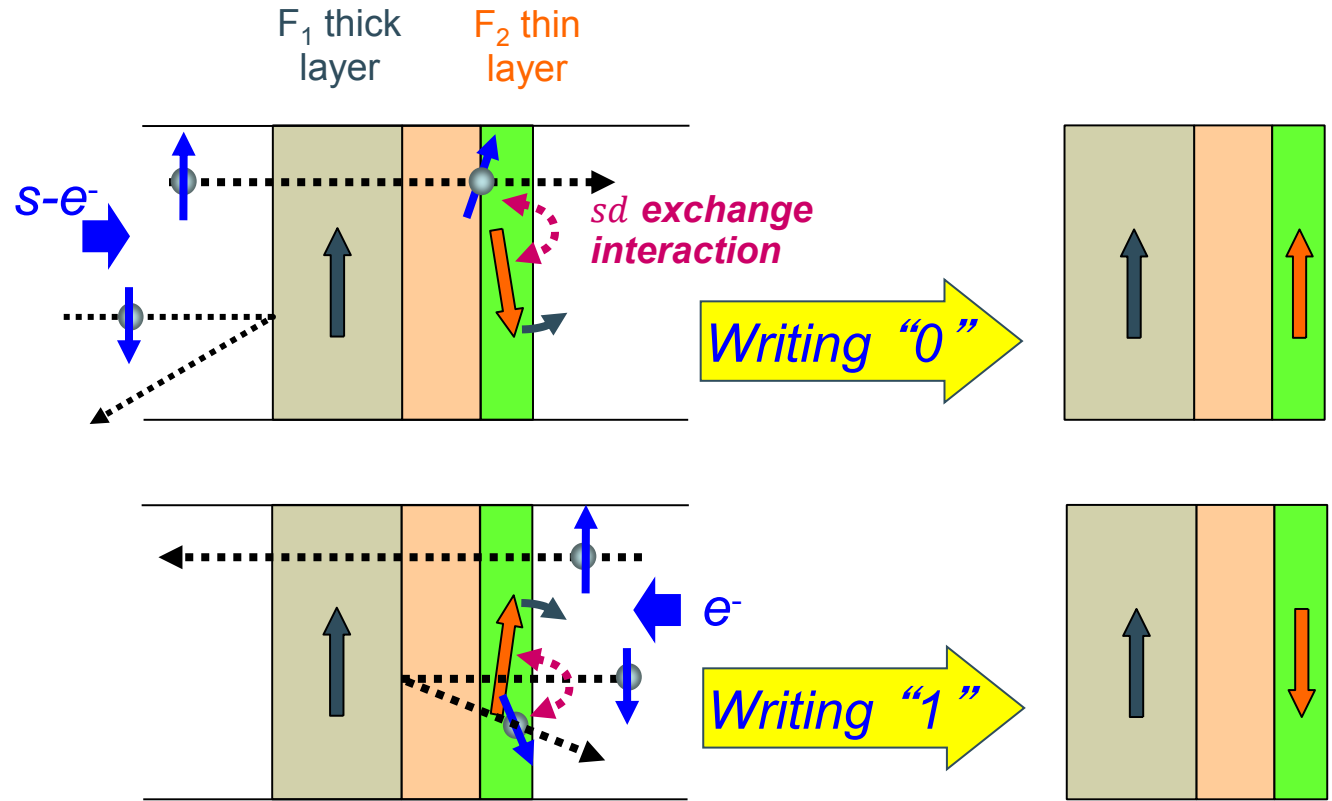


Illustration of the Landau-Lifshitz-Gilbert-Slonczewski equation for a structure with one reference layer and dynamics of the magnetic moments in the free layer (FL) when the damping term is larger, comparable, or smaller than the spin-torque term with various magnitudes of spin polarized current.

# Spin Transfer Torque (STT)

- In this way the spin transfer torque can be used to write a '0' or a '1' into the magnetic memory just by changing the direction of the current flow.



J. C. Slonczewski, JMMM 159, L1 (1996)

Figure illustrating the writing of a '0' or '1' by a bipolar current density  $J_c^+$  and  $J_c^-$

# Magnetic energies for storage

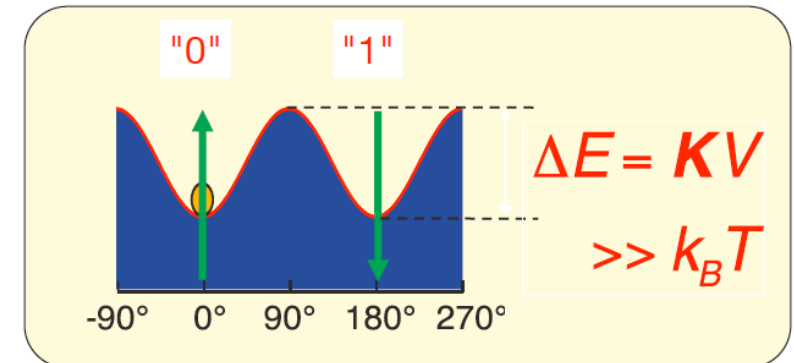
- In order to be useful for non-volatile memory applications, a high thermal (bit) stability is required.
- The stability of the magnetic memory is determined by the magnetic anisotropy energy of the system.
- The volume must be large enough to keep magnetic energy larger than thermal energy. There is a limit in the scaling!!

## **Magnetic anisotropy energy**

total energy changes  
with the orientation of  $\mathbf{M}$



magnetic storage of  
the information



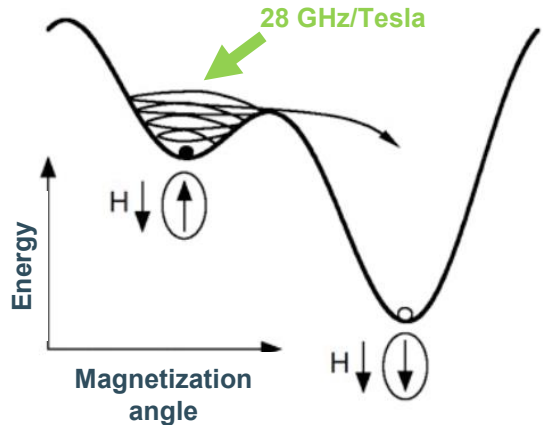
After Thibaut Devolder

# Magnetic energies for storage

- The flipping of magnetization between the two stable states is thermally activated (follows a precession movement). The attempt frequency is function of the material properties and device shape.

- The mean time between two flips is called the Néel relaxation time:

$$\tau = \tau_0 \exp(KV/k_B T)$$



- where attempt time,  $\tau_0 \sim 1 \text{ ns}$

- The long-term stability of the magnetic storage is limited by the spontaneous reversal of the magnetization due to thermal activation.

- To guarantee bit stability for 10 years ( $= 3 \times 10^8 \text{ s}$ ):

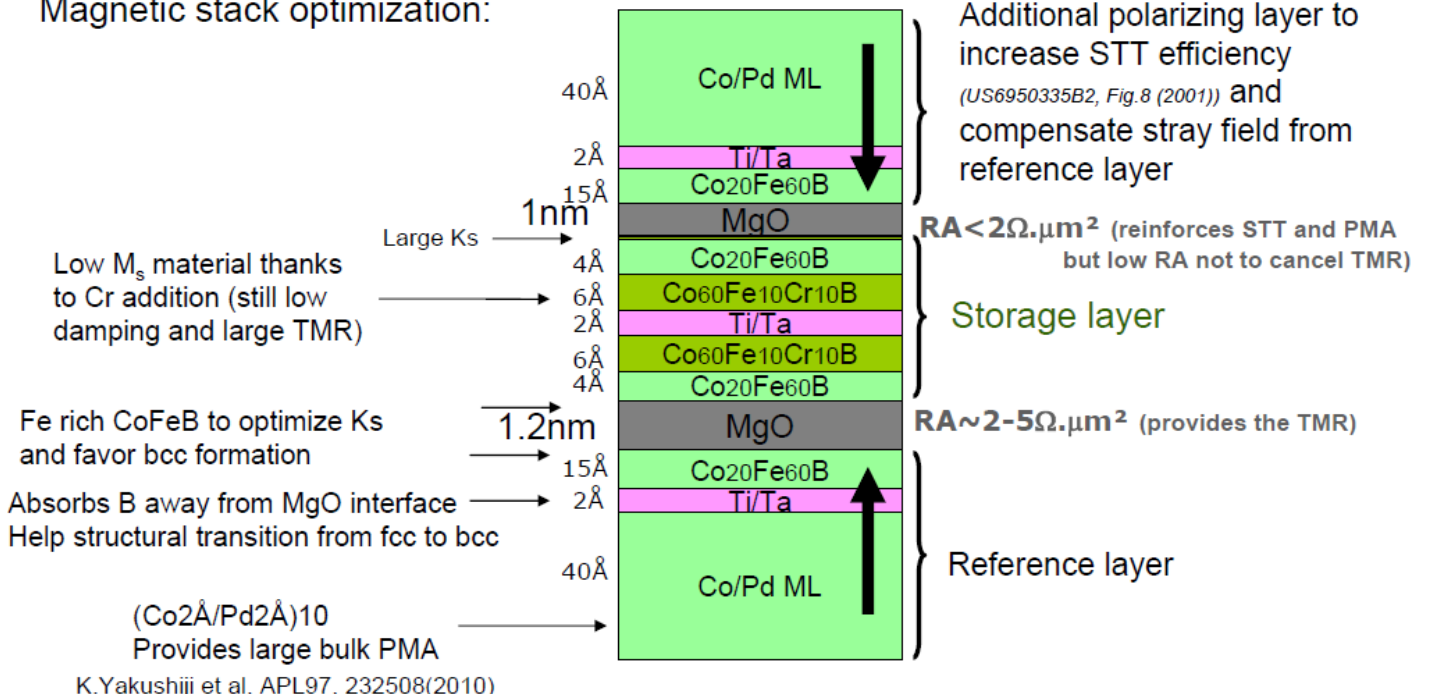
- with error rate ( $1 - P = 10^{-6}$ )  $\Rightarrow KV/k_B T = 54$
      - with error rate ( $1 - P = 10^{-9}$ )  $\Rightarrow KV/k_B T = 68$

- The implication of this is that when one wants to increase the recording density, the bit volume density decreases and material with a higher  $K$  are needed to maintain the stability. On the other hand, increasing  $K$  will increase the energy needed to write the memory. Innovative materials systems will be needed to allow scaling.

# Material stack for p-STT MRAM

- MTJs for STT-MRAMs consist of complex multi-stacks of very thin layers.
- Scalability down to 10nm is expected with currently available materials, making them suitable candidates for fast high-density non-volatile memories.

Magnetic stack optimization:



How small such a stack can be while insuring a 10 year retention?

$$\Delta E = K_{eff}V = [(K_{s1} + K_{s2}) - 2\pi M_s^2 t] \pi R^2 = 70 K_B T \quad \text{with } (K_{s1} + K_{s2}) = 2.9 \text{ erg/cm}^2 \quad \text{and } M_s = 600 \text{ emu/cm}^3$$

⇒ Min diameter = 10 nm still keeping  $\Delta > 70$

Bernard Dieny, CEA, France, IEDM 2011

# Status STT- MRAM



Reverse Engineering ▾

Market Analysis ▾

IP Services ▾

Abc



March 30, 2021



Embedded & Emerging Memory

## World's First 1 Gb 28 nm STT-MRAM Product - by Everspin

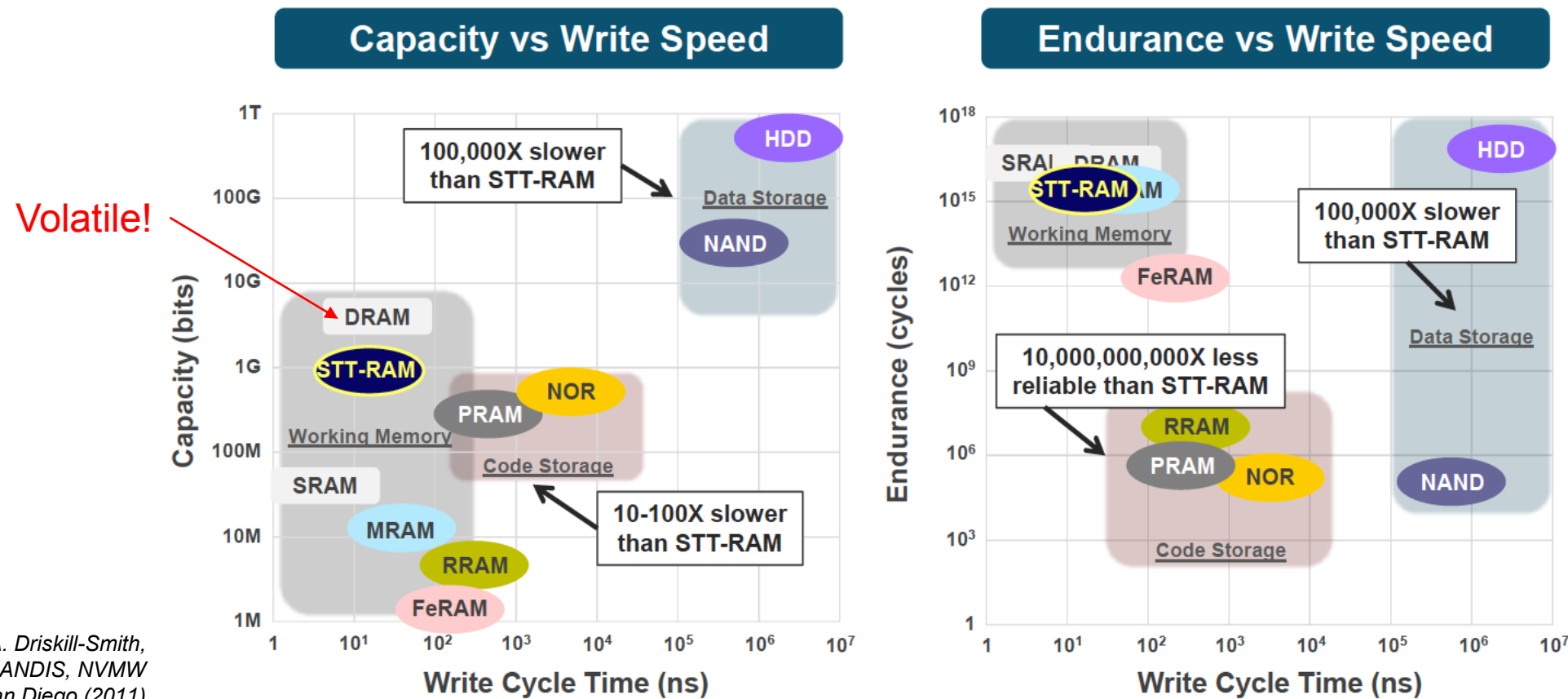
Everspin's new 1-Gigabit (Gb) Spin Torque Transfer Magneto-resistive Random Access Memory (STT-MRAM) device with a 28 nm process is the world's first 1 Gb STT-MRAM product. This 4<sup>th</sup> generation MRAM technology release is a standalone market leader. Its only industry peers, Intel and Micron XPoint Memory, are developing MRAM, ReRAM, and FeRAM memory devices for embedded non-volatile memory (eNVM), rather than discrete emerging memory chips.

According to [Everspin](#), their leading STT-MRAM memory products are being developed for "infrastructure and data center providers to increase the reliability and performance of systems where high-performance data persistence is critical by delivering protection against power loss without the use of supercapacitors or batteries."

Everspin and GlobalFoundries (GF) have been partners since their 40 nm MRAM development and fabrication

# STT-MRAM technology advantages

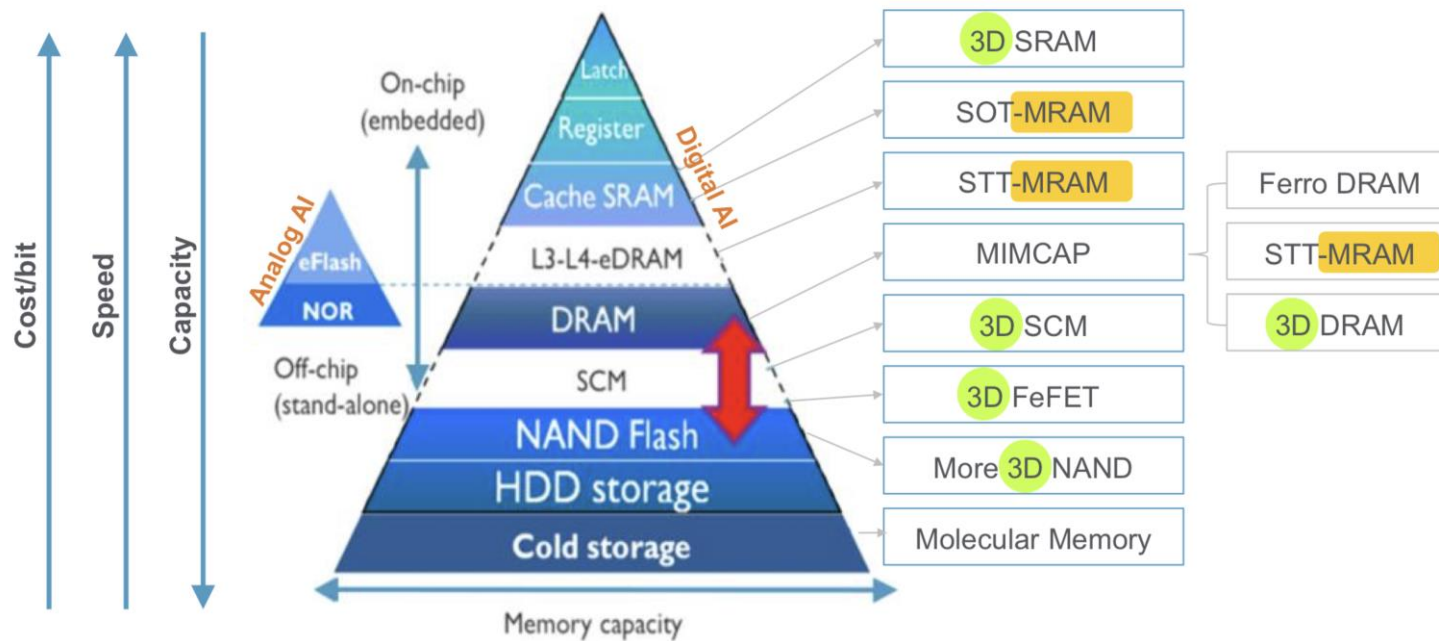
- STT-RAM has the capacity of and speed of working memory (DRAM, SRAM), plus it is non-volatile and has low power consumption.



A. Driskill-Smith,  
GRANDIS, NVMW  
San Diego (2011)

# MRAM application

- Today's systems integrate processors, graphics, as well as memory and storage, often referred to as the memory/storage hierarchy. In the first tier of today's hierarchy, SRAM is integrated into the processor for fast data access. DRAM, the next tier, is separate and used for main memory. Disk drives and NAND-based solid-state storage drives (SSDs) are used for storage.



*"DRAM and NAND are struggling to keep up with the bandwidth and/or power requirements in systems. DRAM is cheap, but it consumes power. DRAM is also volatile, meaning it loses data when the power is shut off in systems. NAND, meanwhile, is cheap and non-volatile (it retains data when the system is shut down). But NAND and disk drives are slow."*

*So for years, the industry has been searching for a "universal memory" that has the same attributes as DRAM and flash and could replace them. The contenders are MRAM, PCM and ReRAM. The new memories make some bold claims. For example, STT-MRAM features the speed of SRAM and the non-volatility of flash with unlimited endurance. Compared to NAND, ReRAM is faster and bit-alterable. And so on.*

*Current and future generations of memories are worth watching. To date, they haven't disrupted the landscape. But they are making a dent against the incumbents in the ever-changing memory market."*

*Emerging memories for pervasive data and compute source*

# Materials Physics and Technology for Nanoelectronics



**Clement Merckling**

clement.merckling@kuleuven.be

imec & KU Leuven (MTM)

Kapeldreef 75, B-3001 Leuven



**Francisco Molina Lopez**

francisco.molinalopez@kuleuven.be

MTM Functional Materials

Kasteelpark Arenberg 44, B-3001 Leuven

# Materials Physics and Technology for Nanoelectronics

## Organic electronics

KU LEUVEN

imec

KU LEUVEN

MATERIAALKUNDE

**Clement Merckling**

clement.merckling@imec.be

IMEC IV, room 2.36

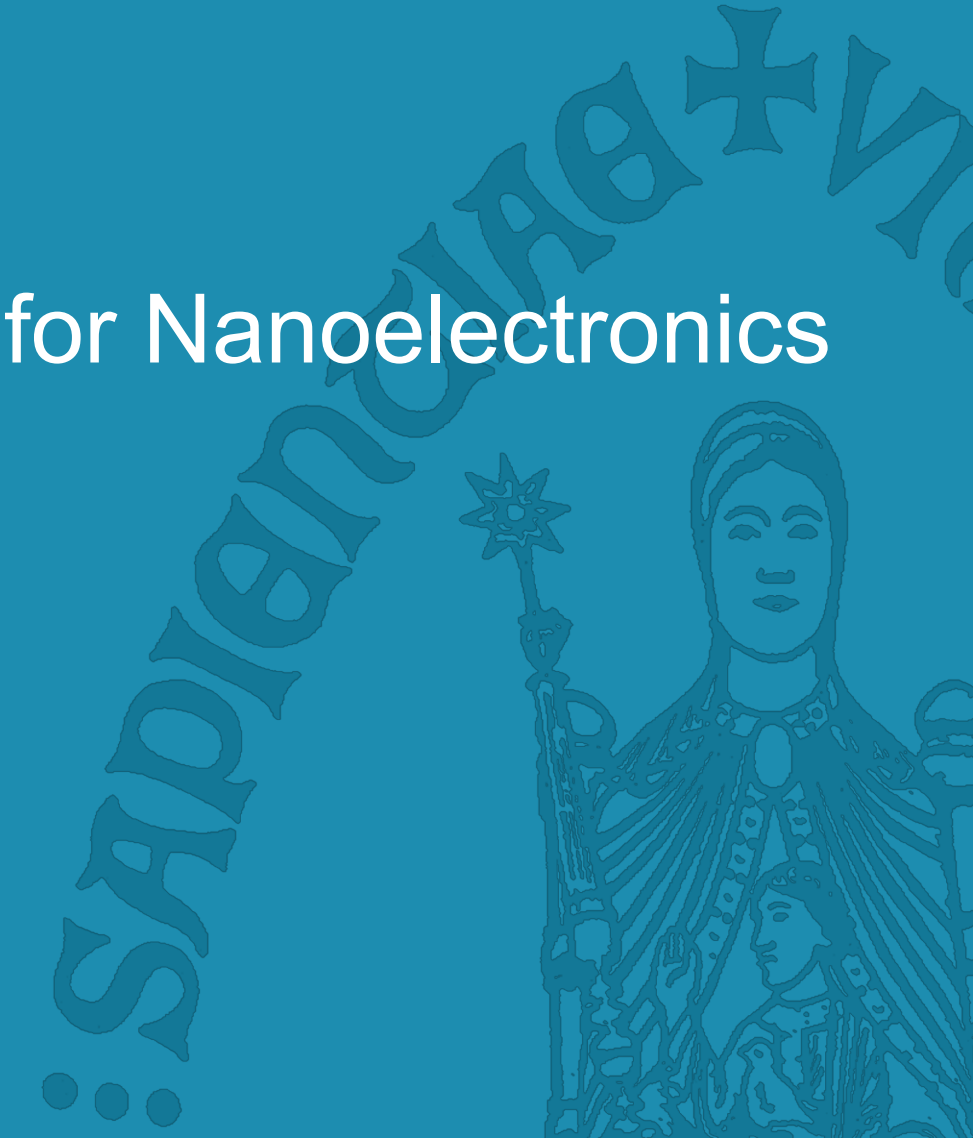
Kapeldreef 75, B-3001 Leuven

**Francisco Molina-Lopez**

francisco.molinalopez@kuleuven.be

Dept. Materials Engineering, room 01.51

Kasteelpark Arenberg 44, B-3001 Leuven



# Outline

- Hybridization
- Electronic structure of conjugated molecules
- Transport in organic electronic materials
- Applications of organic electronic materials



# Hybridization

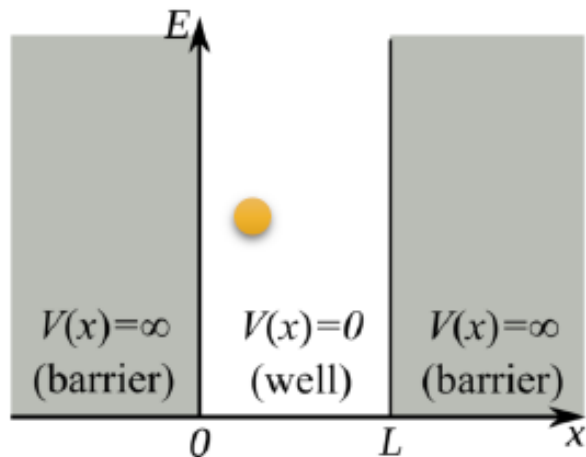


# Hybridization

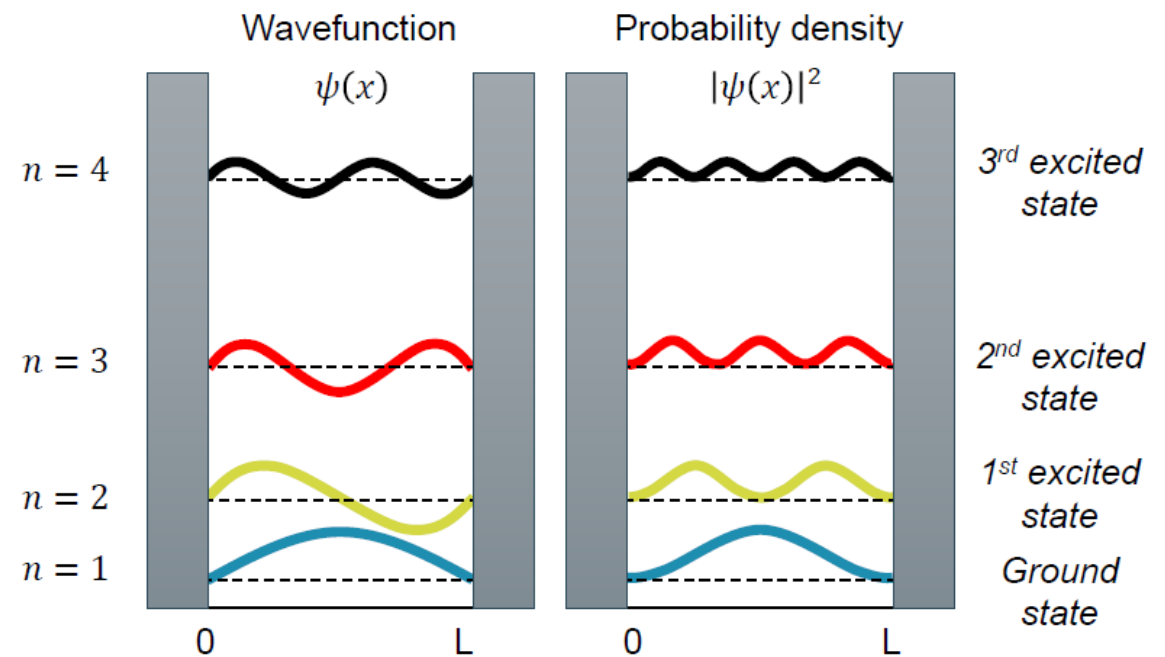
- Atomic orbitals (review from Chapter 2: Solids)

- The **Schrödinger** equation provided the **wavefunction**,  $\Psi(\vec{r}, t)$ , of an electron in an atom, the **probability** of finding it at certain place,  $|\Psi|^2$ , and its quantized **energy**,  $E$ .

Example for 1D potential well (time-independent Schrödinger equation):



$$-\frac{\hbar^2}{2m} \nabla^2 \psi + V\psi = E\psi$$

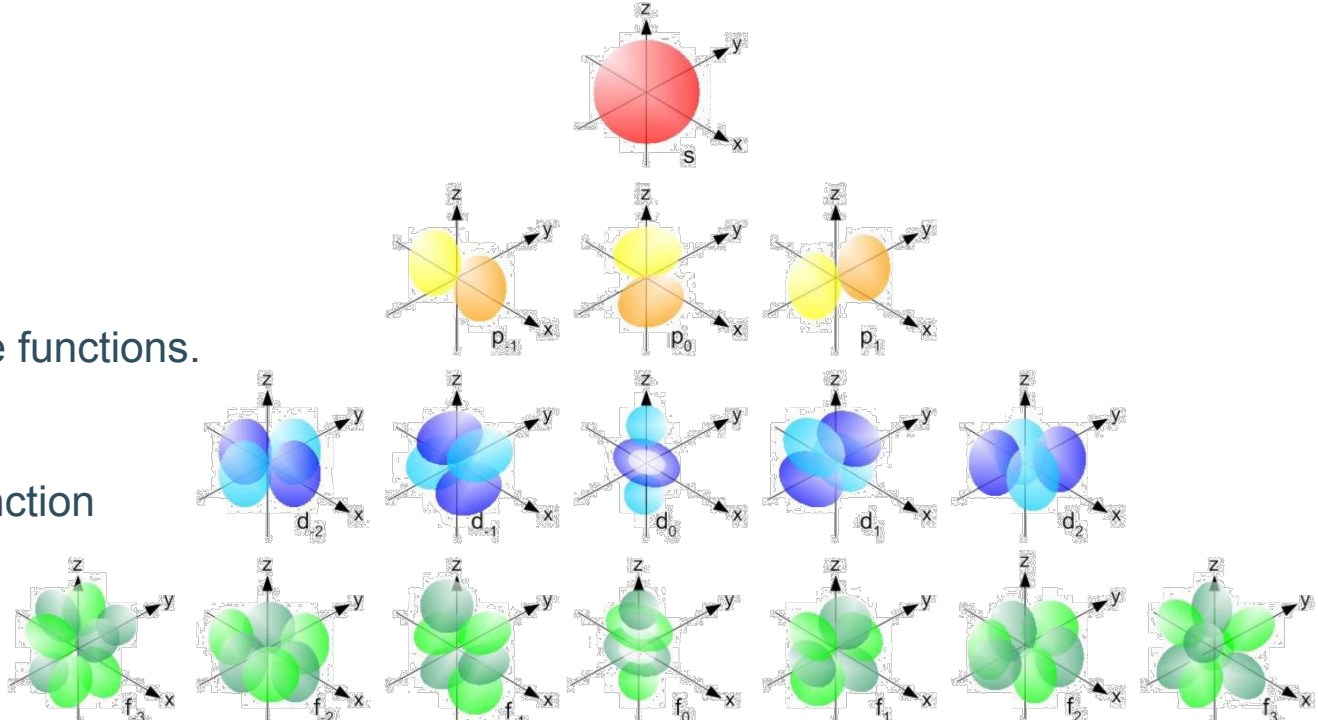


# Hybridization

- Atomic orbitals (review from Chapter 2: Solids)
  - The probability density function  $|\Psi|^2$  in 3D led to the definition of the **atomic orbitals (AO's)** (or zones in the atom where the chances to find electrons are high)

Overview of atomic orbitals shapes of  $s$ ,  $p$ ,  $d$  and  $f$  wave functions.

The color of orbitals represent the phase of the wavefunction (positive or negative amplitude).



# Hybridization

- Molecular orbitals (review from Chapter 2: Solids)

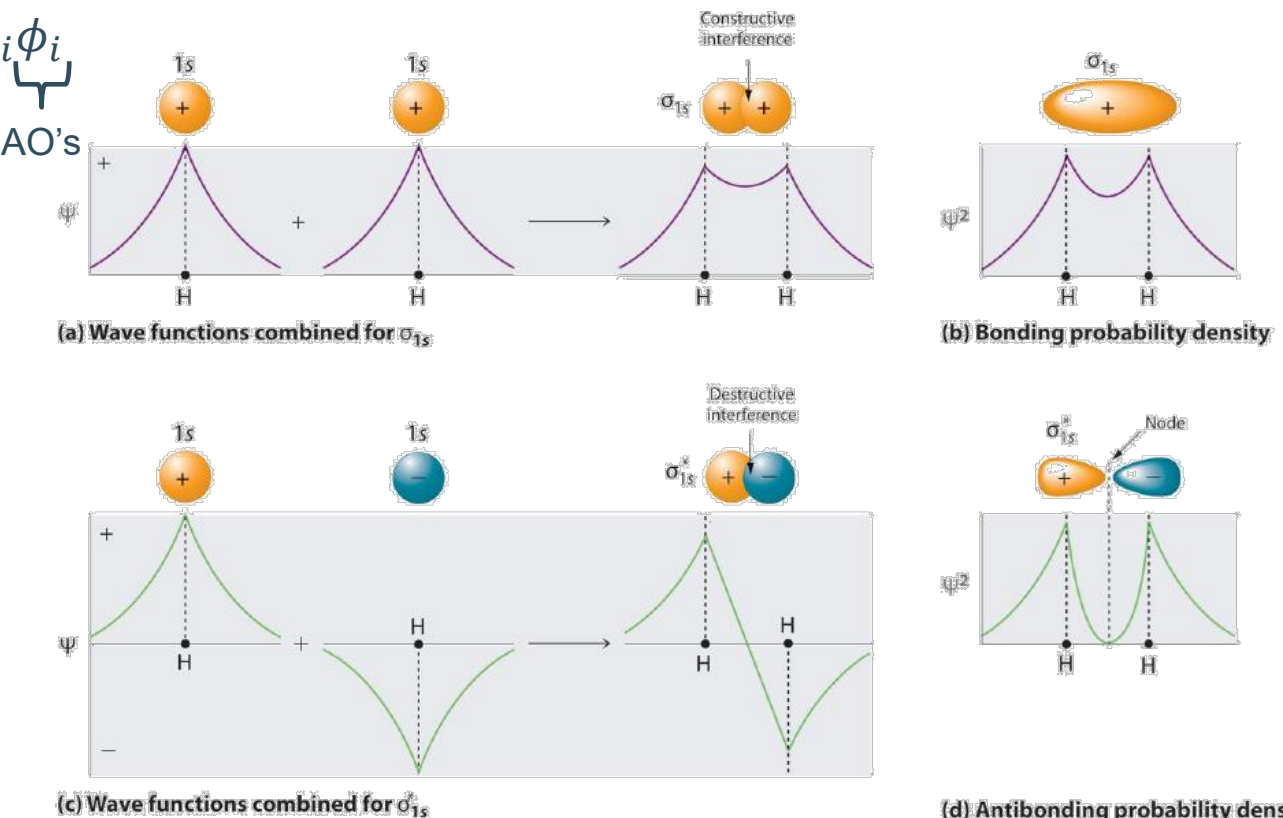
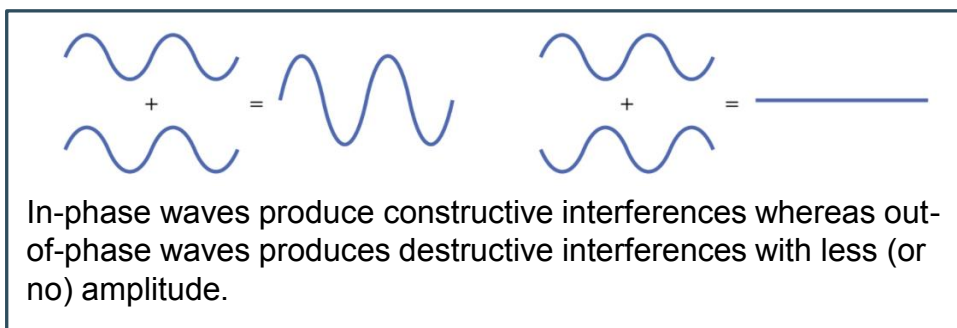
- The solution of the Schrödinger eq. to define molecular orbitals (MO) come from the **linear combination of AO's (LCAO)**:

$$\Psi = \sum u_i \phi_i$$

Example H<sub>2</sub>:

(a), (b) Wavefunctions  $\Psi$  of two H 1s AO and formation of a bonding  $\sigma_{1s}$  MO, probability density  $|\Psi|^2$  of finding the electron in between the two H nuclei is high.

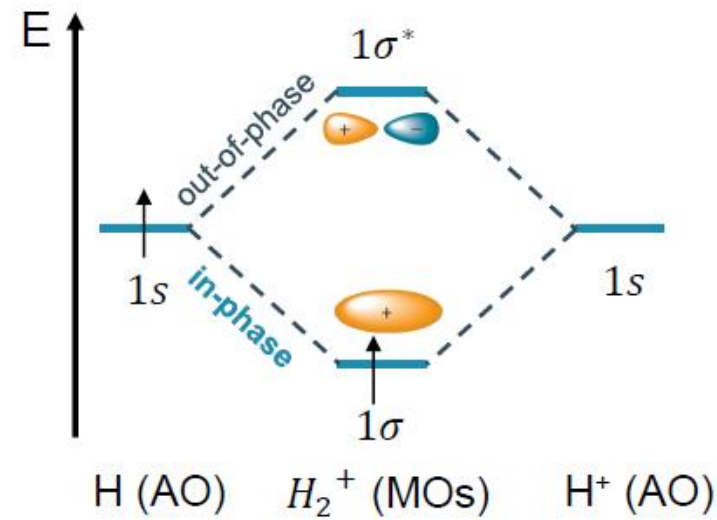
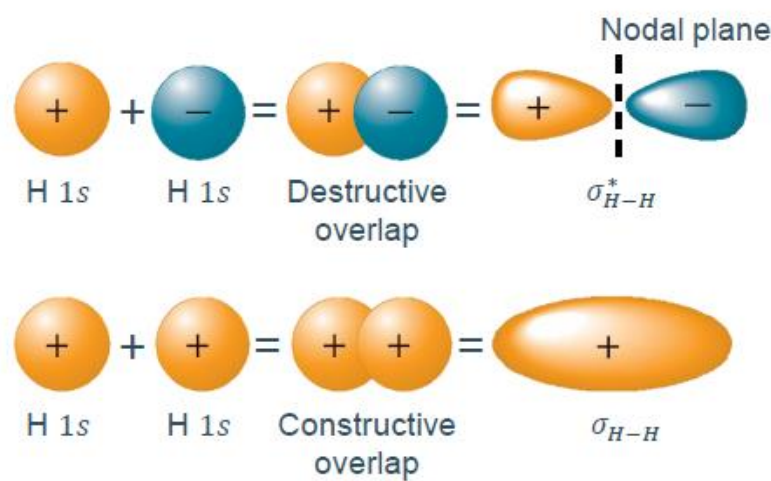
(c), (d) Formation of an antibonding  $\sigma_{1s}^*$  MO, and probability density  $|\Psi|^2$  illustrating the node corresponding to zero electron probability density between the nuclei.



# Hybridization

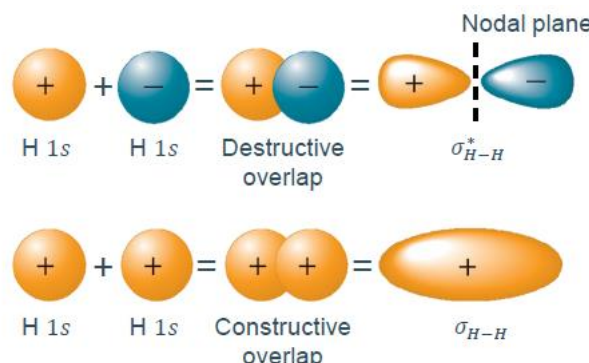
- Molecular orbitals (review from Chapter 2: Solids)
  - The MO's present different **energy** states that depends on whether the **wavefunction** of the electrons from the bonding atoms are **in-phase** or **out-of-phase**

Example of H<sub>2</sub>:

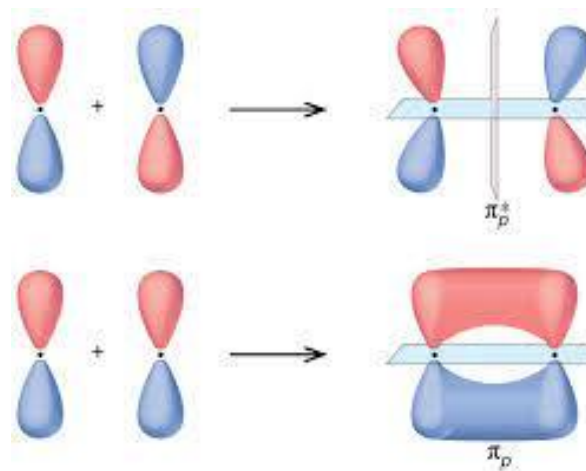


# Hybridization

- Hybridization: Issue of LCAO
  - In the LCAO approach, MO's were built **only from one AO** from each atom.



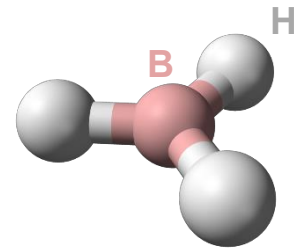
Schematic shapes of bonding and anti-bonding MO's formed by 1s-1s overlap



Schematic shapes of bonding and anti-bonding MO's formed by  $p-p$  overlap

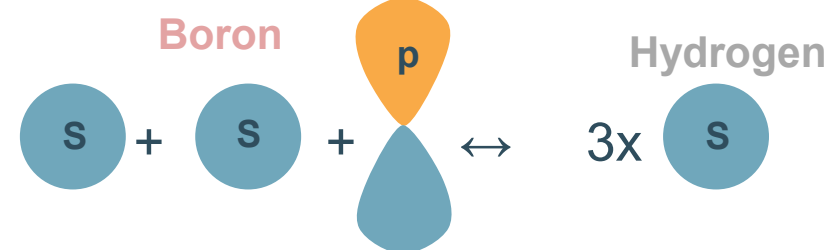
Does this approach correspond to reality?

# Hybridization

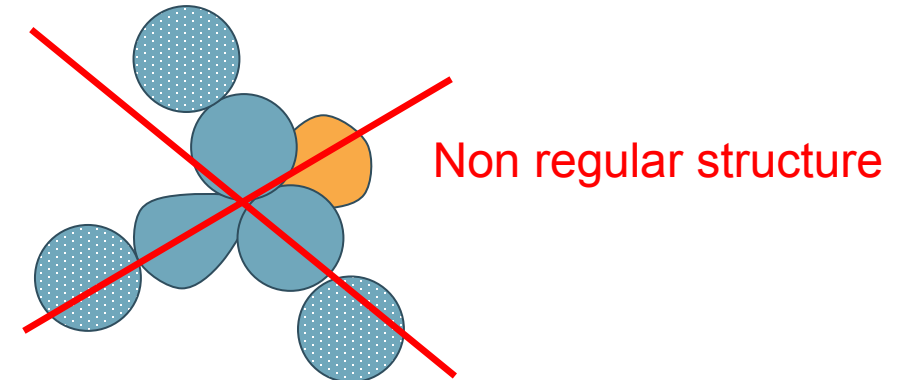
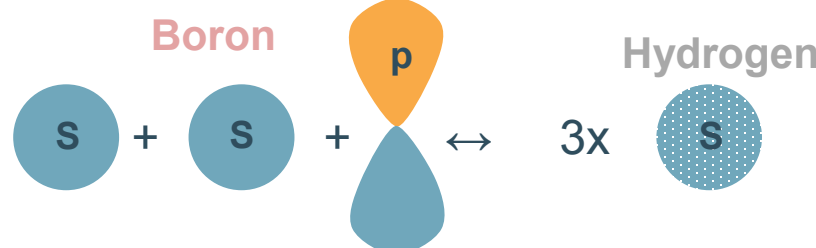


- Hybridization: Issue of LCAO
  - Consider borane (boron trihydride,  $\text{BH}_3$ ):

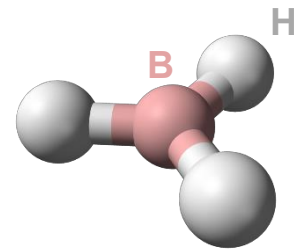
The electronic ground state of B is  $1s^2 2s^2 2p^1$ :



If we assume the MO's being formed from the 3 orbital above, the symmetry of  $\text{BH}_3$  can not be explained!



# Hybridization

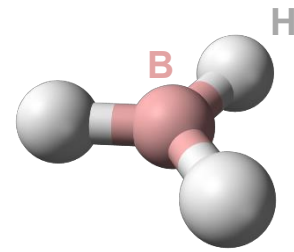


- Hybridization: Issue of LCAO
  - Consider borane (boron trihydride,  $\text{BH}_3$ ):

Greater accuracy can be obtained by using trial wave functions incorporating two or more AOs from individual atoms (forming **hybrid AOs**) as this can lead to MOs of lower energy through increased overlap.

**“Hybridization”** is a mathematical process which is useful in modifying electron densities to allow bonding geometries and electron densities in more complex molecules to be described. The driving force is looking the lowest net potential energy.

# Hybridization



- Hybridization: Explains structure of molecules

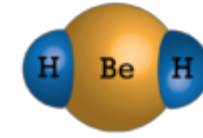
- Consider borane (boron trihydride,  $\text{BH}_3$ ):

Using **hybridization** we can construct three equivalent hybrid AOs for B that explains the regular structure of  $\text{BH}_3$ :



These hybrid AOs extend far from the B nucleus in directions at  $120^\circ$  to each other. The energy cost of creating the hybrid AOs is more than offset by the increased overlap and more negative bond integrals, thereby producing a more stable  $\text{BH}_3$  molecule. Such hybrids are called  **$sp^2$  or trigonal hybrids**.

# Hybridization



- Hybridization: Energy implications
  - Consider, for example, beryllium dihydride ( $\text{BeH}_2$ ):

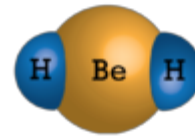


This is known to be a linear molecule (H-Be-H) with an angle of  $180^\circ$  between the two Be-H bonds. MOs to describe the Be-H bonds must be built from the 1s AOs of hydrogen.

The ground state of Be atoms is:  $1s^2 2s^2$

... but constructing MOs for the two Be-H bonds using only 2s AOs of Be yields results for the bond strength and bond length that disagree strongly with experiment.

# Hybridization



- Hybridization: Energy implications

- Consider, for example, beryllium dihydride ( $\text{BeH}_2$ ):

Suppose we instead construct our MOs for  $\text{BeH}_2$  with the following hybrid AOs that also contain  $2p$  AOs (which have energies only slightly higher than the  $2s$  AOs):

$$\phi_1 = \frac{\phi_{2s} + \phi_{2p_x}}{\sqrt{2}} \text{ and } \phi_2 = \frac{\phi_{2s} - \phi_{2p_x}}{\sqrt{2}}$$

(We have chosen  $p_x$  because we define the molecular axis as the  $x$ -axis. The  $\sqrt{2}$  normalizes the functions).

Because the  $2p$  orbitals have a slightly higher energy than the  $2s$  orbitals, these hybrid AOs have a slightly higher energy than pure  $2s$  AOs. But these hybrids extend much farther from the nucleus. This produces more overlap with the  $1s$  orbitals, resulting in a bond integral  $H_{12}$  that is more negative, resulting in a lower total energy (stronger bond).

- The expected energy value is:

$$\langle E \rangle = \frac{\int \psi^* H \psi dV}{\int \psi^* \psi dV} = \frac{\int (u_1 \phi_1^* + u_2 \phi_2^*) H (u_1 \phi_1 + u_2 \phi_2) dV}{\int (u_1 \phi_1^* + u_2 \phi_2^*)(u_1 \phi_1 + u_2 \phi_2) dV} = \frac{2u_1^2 H_{11} + 2u_1 u_2 H_{12}}{u_1^2 + u_2^2}$$

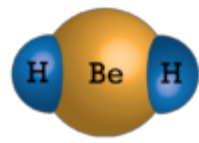
with  $H_{12} = \int \phi_1^* H \phi_2 dV = \int \phi_2^* H \phi_1 dV = H_{21}$

$$H_{11} = \int \phi_1^* H \phi_1 dV = \int \phi_2^* H \phi_2 dV = H_{22}$$

Chapter 2: solids

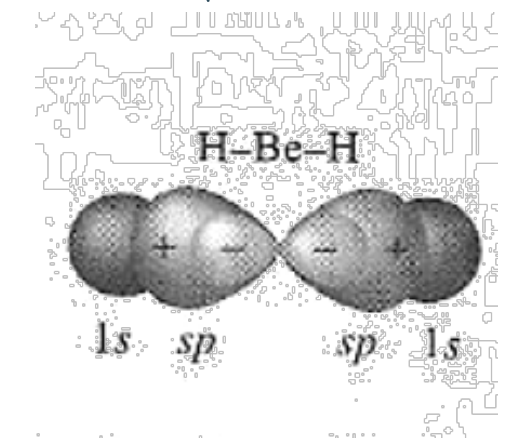
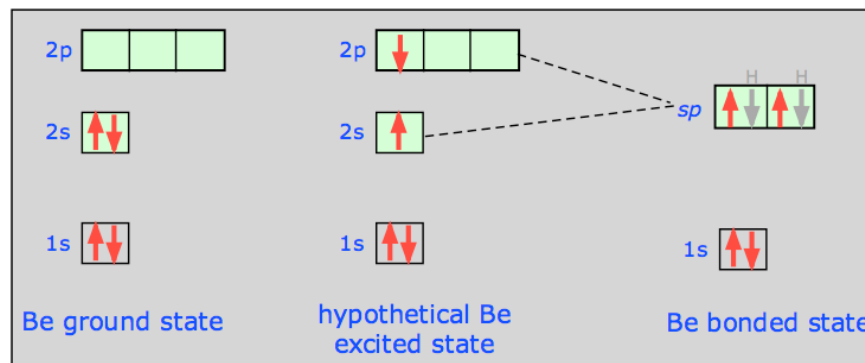
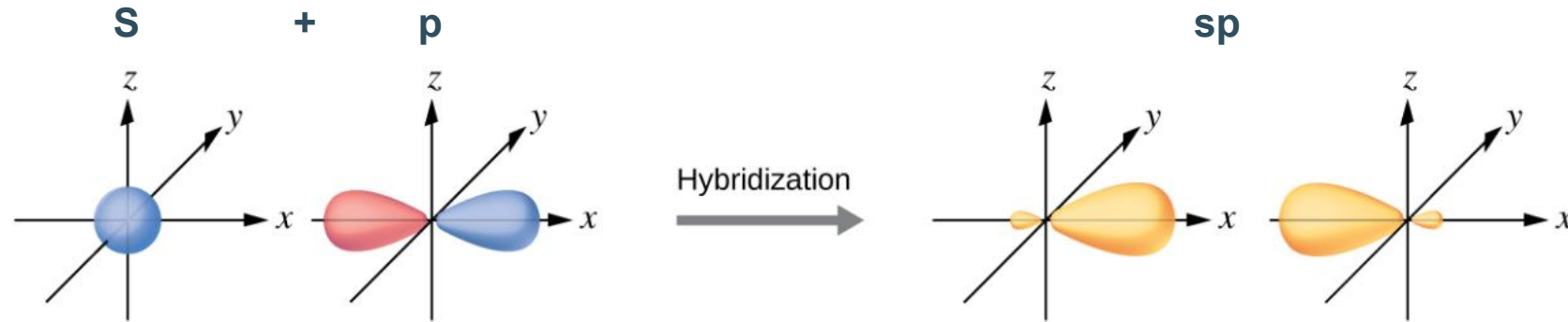
$H_{12} = H_{21}$  is called the *Bond (or resonance) integrals* and  $H_{11} = H_{22}$  the *Coulomb integrals*

# Hybridization



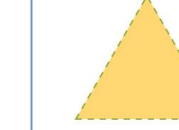
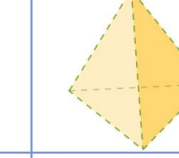
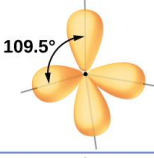
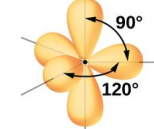
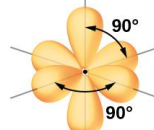
- Hybridization: Energy implications

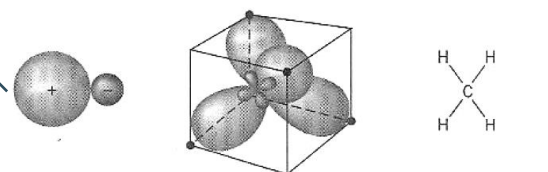
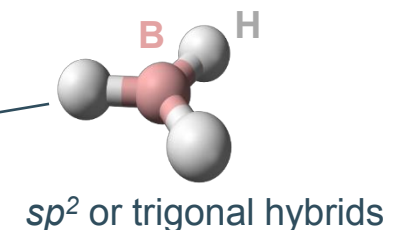
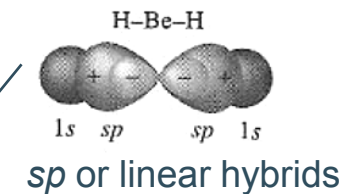
- Consider, for example, beryllium dihydride ( $\text{BeH}_2$ ):  $\phi_1 = \frac{\phi_{2s} + \phi_{2p_x}}{\sqrt{2}}$  and  $\phi_2 = \frac{\phi_{2s} - \phi_{2p_x}}{\sqrt{2}}$



# Hybridization

- Hybridization: summary

Regions of Electron Density	Arrangement	Hybridization	
2	-----	linear	$sp$ 
3		trigonal planar	$sp^2$ 
4		tetrahedral	$sp^3$ 
5		trigonal bipyramidal	$sp^3d$ 
6		octahedral	$sp^3d^2$ 



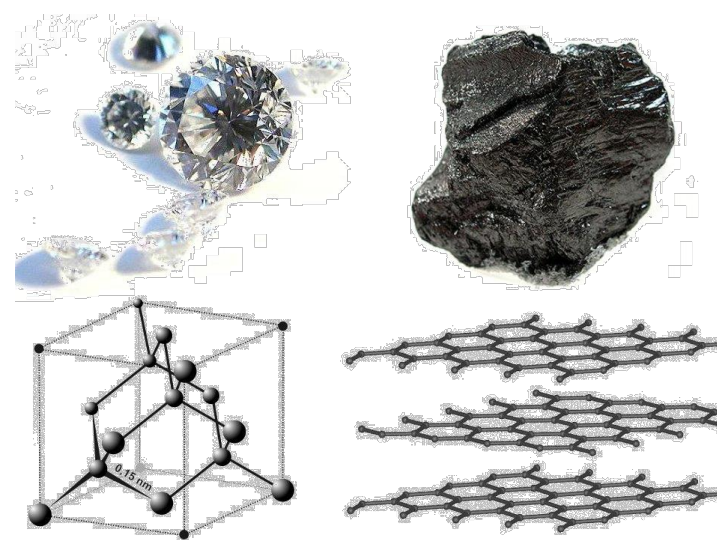
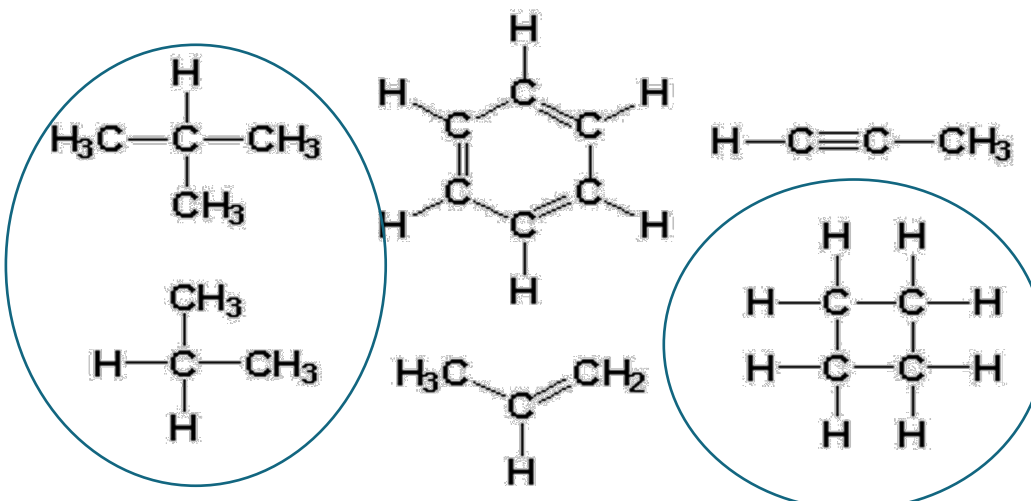
Local symmetries associated with hybrids containing s, p and d AOs.

# Hybridization

- Hybridization: The versatile bonding of Carbon

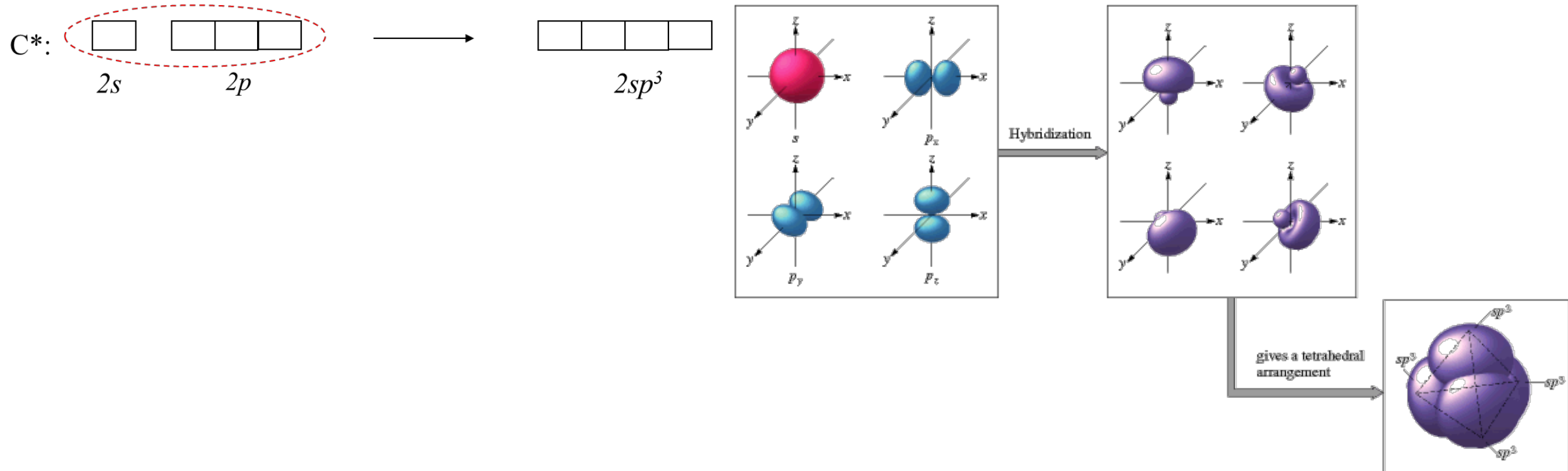
- The four valence electrons of carbon ( $Z = 6$ ), combined with various degrees of hybridization, give carbon a great versatility in bonding. This versatility is responsible for the richness of organic chemistry.

- In many molecules, carbon uses  $sp^3$  hybridization to form bonds with four other atoms. Such molecules are said to be saturated.



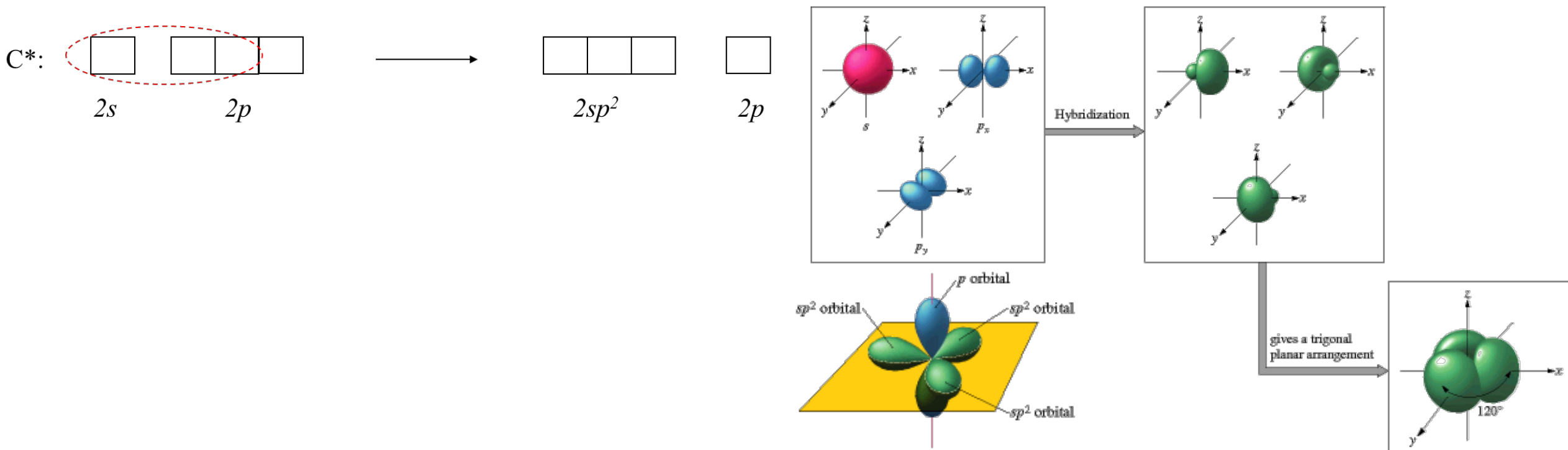
# Hybridization

- Carbon hybridization:
  - $sp^3$  hybridization → linear combination of a  $s$  and 3  $p$  orbitals.



# Hybridization

- Carbon hybridization:
  - $sp^2$  hybridization → linear combination of a s and 2 p orbitals.



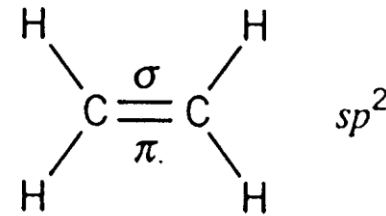
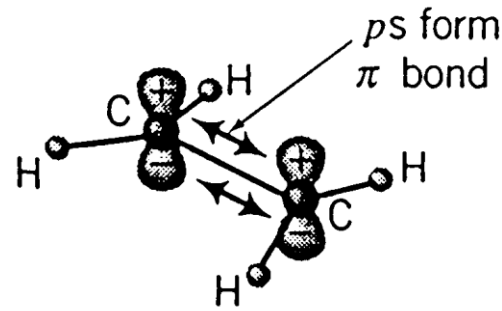
# Hybridization

- Carbon hybridization:

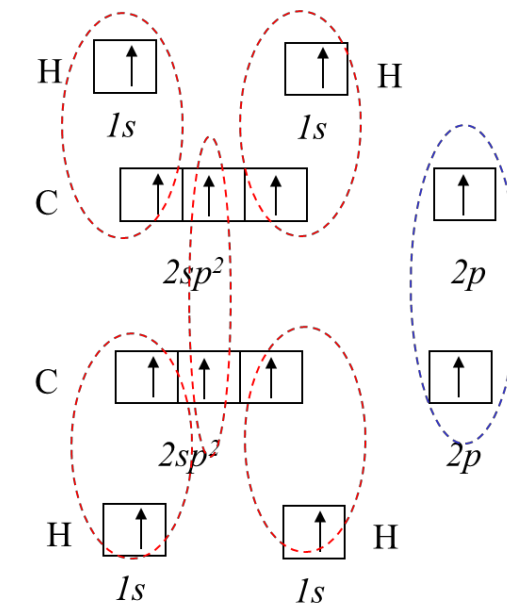
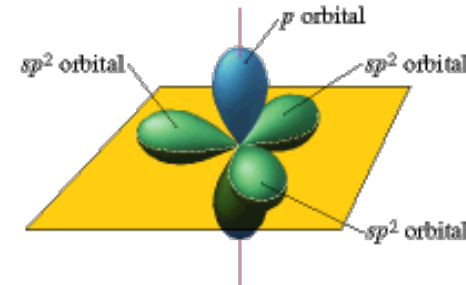
- $sp^2$  hybridization → Example for ethylene.

This molecule is planar, and each carbon has only three neighbors, with two C-H bonds and one C-C bond. The one  $2p$  AO on each carbon, extending out of the molecular plane, **forms a  $\pi$  bond** with the corresponding  $2p$  AO on the other carbon. The C-C bond is therefore a **double bond**, consisting of one  $\sigma$  bond ( $sp^2-sp^2$ ) and one  $\pi$  bond ( $p-p$ ).

Formation of 5  $\sigma$  bonds and 1  $\pi$  bond, with a double C=C bond (bond length: 1.34 Å)

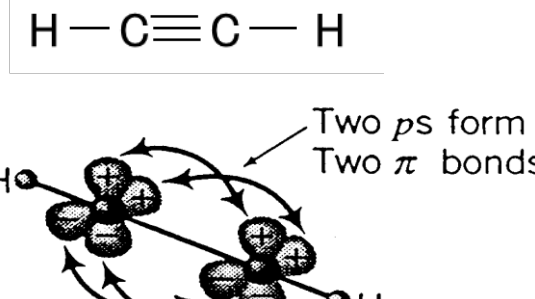
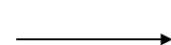
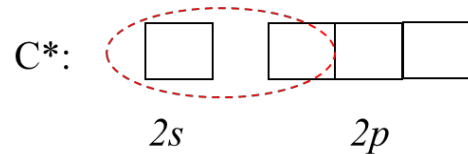


Ethylene, a planar molecule with a double C-C bond.

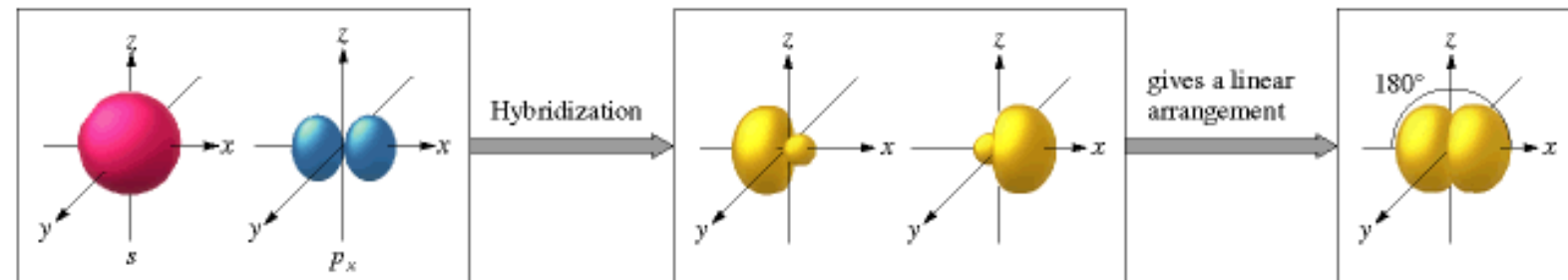


# Hybridization

- Carbon hybridization:
  - $sp$  hybridization → linear combination of a  $s$  and a  $p$  orbital.



Acetylene, a linear molecule with a triple C-C bond.



# Electronic structure of conjugated molecules



# Electronic structure of conjugated molecules

- Conjugated molecules:

- Those with connected  $p$  orbitals with delocalized electrons, which in general lowers the overall energy of the molecule and increases stability -> **alternating multiple/single bond.**



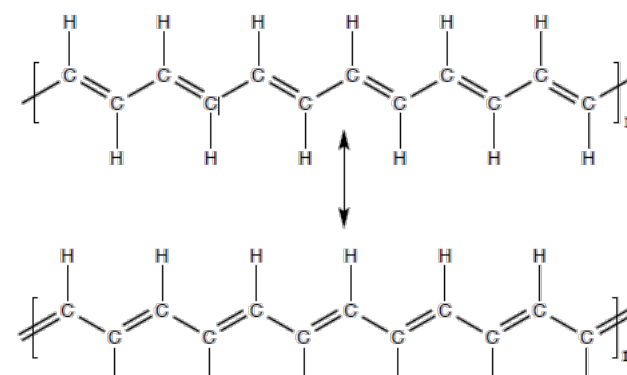
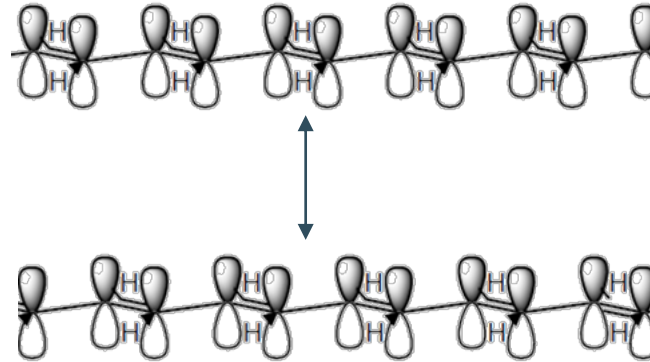
- In most polyatomic molecules, bonding can be described in terms of MOs that are essentially localized on individual bonds (built from AOs of two neighboring atoms). This approach breaks down for conjugated compounds.

# Electronic structure of conjugated molecules

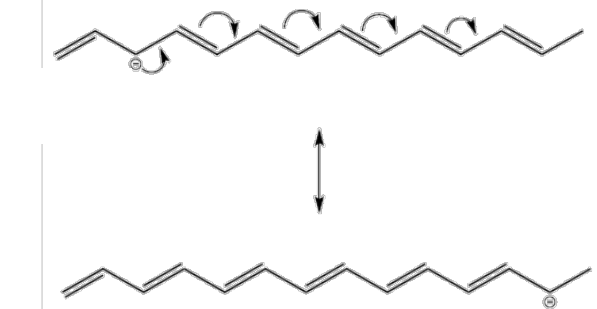
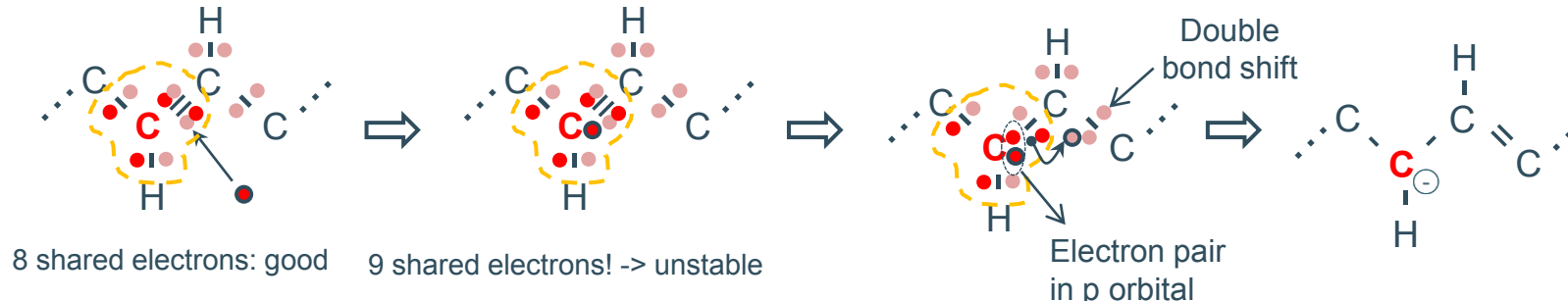
- Conjugated molecules: delocalization

- $\pi$ - bonding between  $sp^2$  C atoms results in delocalized MOs.

Two resonance structures  
(polyacetylene):



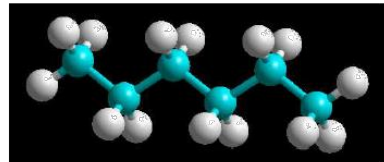
- Charges can be delocalized due to resonance structures -> Charge transport in plastics!!



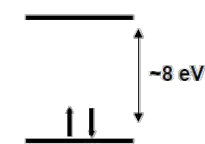
# Electronic structure of conjugated molecules

- Conjugated molecules: delocalization
  - Orbitals extend to the whole molecule

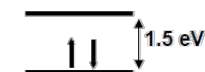
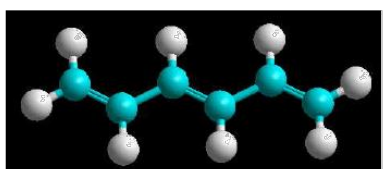
Polyethylene: insulator



Energy Gap



Polyacetylene: semiconductor



- Nobel Prize in chemistry 2000 "for the discovery and development of conductive polymers"

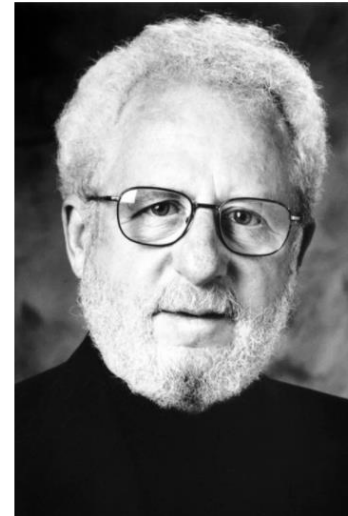


Photo from the Nobel Foundation archive.

Alan J. Heeger

Prize share: 1/3

UC Santa Barbara



Photo from the Nobel Foundation archive.

Alan G. MacDiarmid

Prize share: 1/3

University of Pennsylvania



Photo from the Nobel Foundation archive.

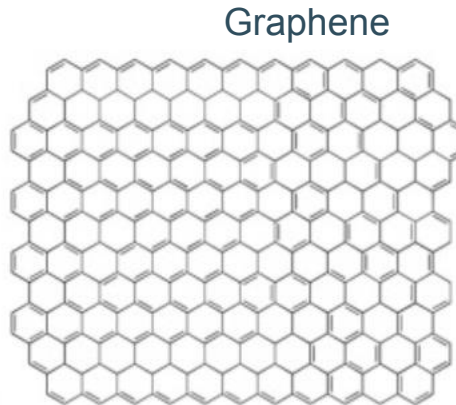
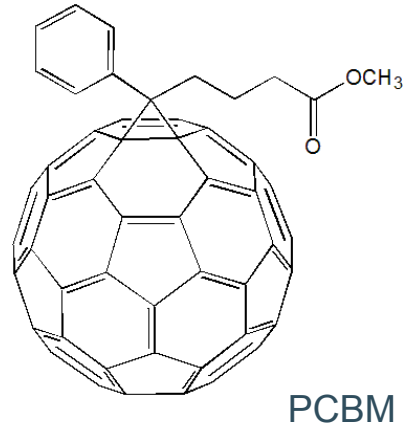
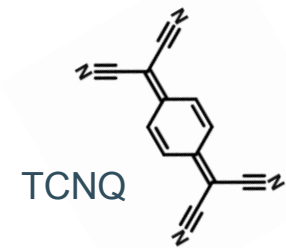
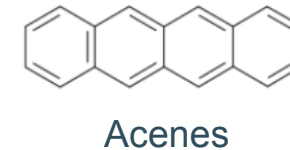
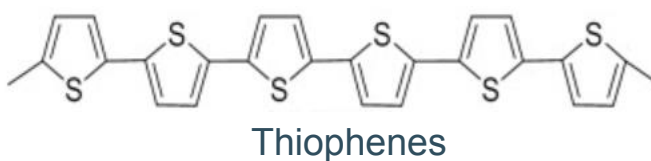
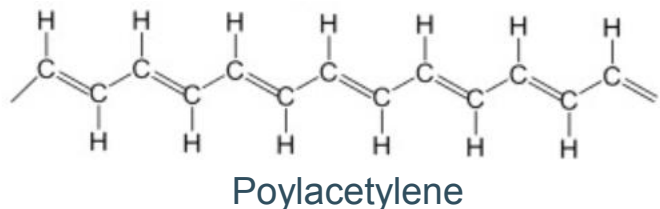
Hideki Shirakawa

Prize share: 1/3

University of Tsukuba

# Electronic structure of conjugated molecules

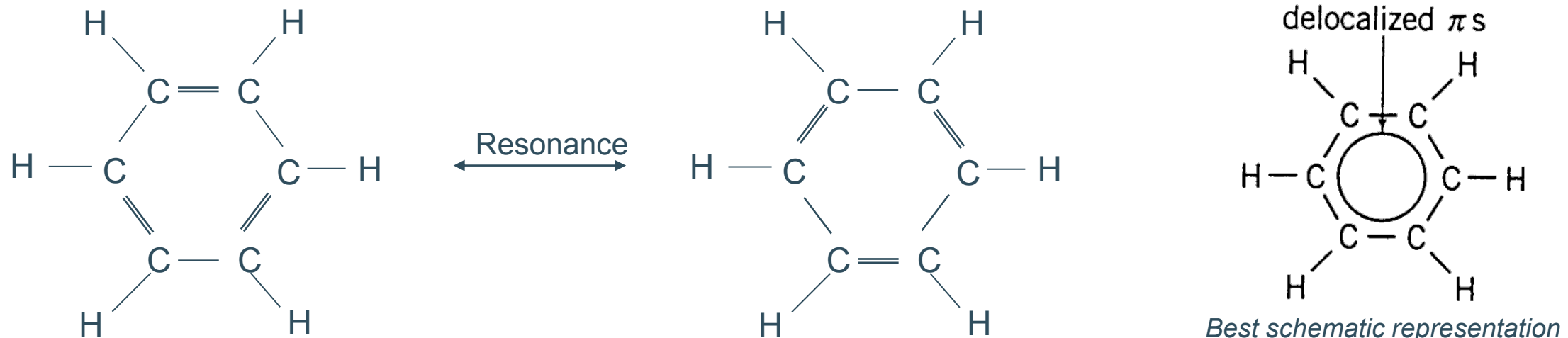
- Conjugated molecules: examples



# Electronic structure of conjugated molecules

- Conjugated molecules: Benzene

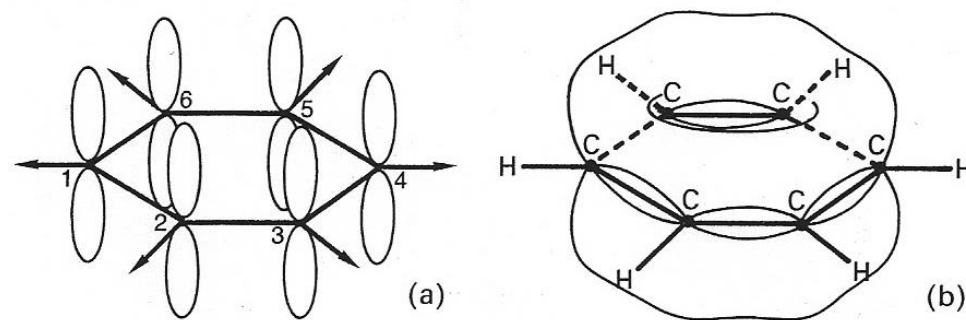
- Each of the C atoms are in a  $sp^2$  hybridized state, forming a  $\sigma$  bond with H, a single  $\sigma$  bond with one neighbor C atom, and a double ( $\sigma$  and  $\pi$ ) bond with its other C neighbor. The  $\pi$  bonds results from the overlap between two adjacent  $2p_z$  orbitals, considering the molecule lies in the (x, y) plane (planar molecule).



Benzene rings are often drawn with alternating single and double bonds. However, experiments make it clear that **all C-C bonds in benzene are equivalent**, and the strengths and lengths of the C-C bonds are intermediate between single and double bonds.

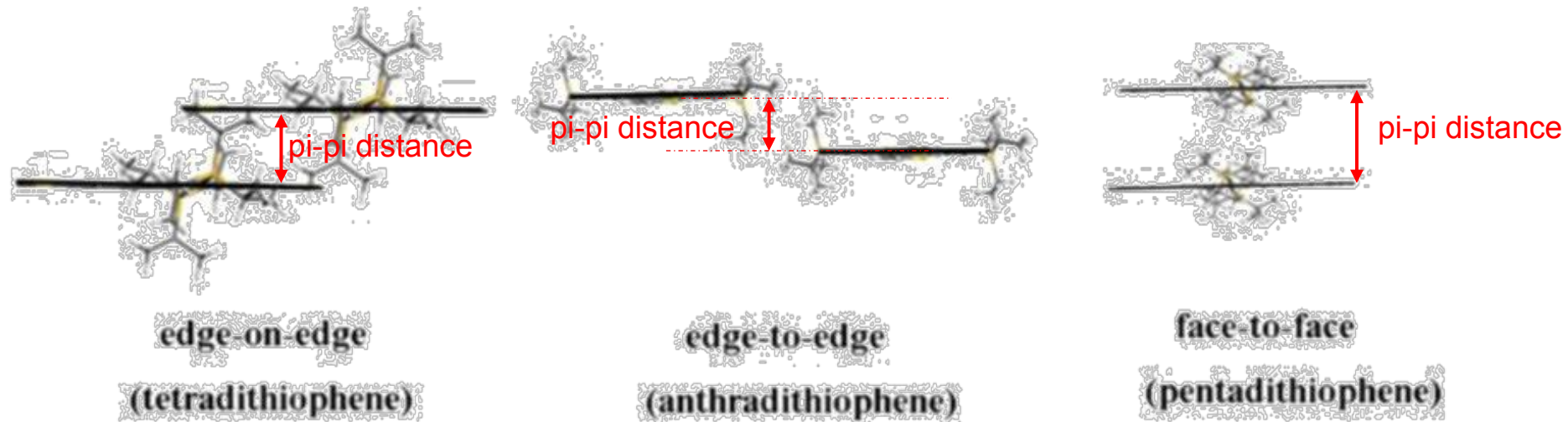
# Electronic structure of conjugated molecules

- Conjugated molecules: Benzene
  - The  $\pi$  bonds results from the overlap between two adjacent  $2p_z$  orbitals, considering the molecule lies in the  $(x, y)$  plane.



# Electronic structure of conjugated molecules

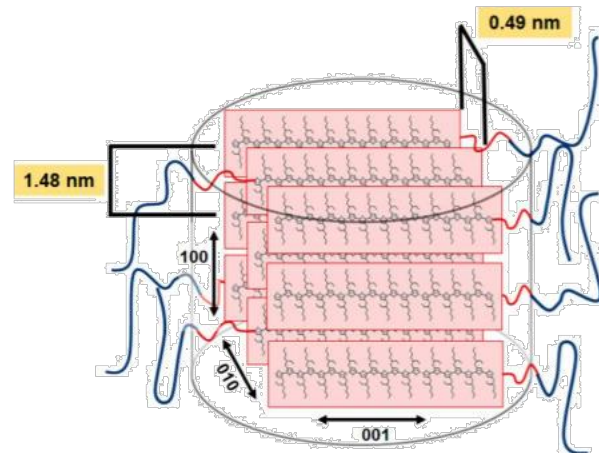
- Conjugated molecules:  $\pi$ - $\pi$  stacking
  - Noncovalent interactions between aromatic rings.



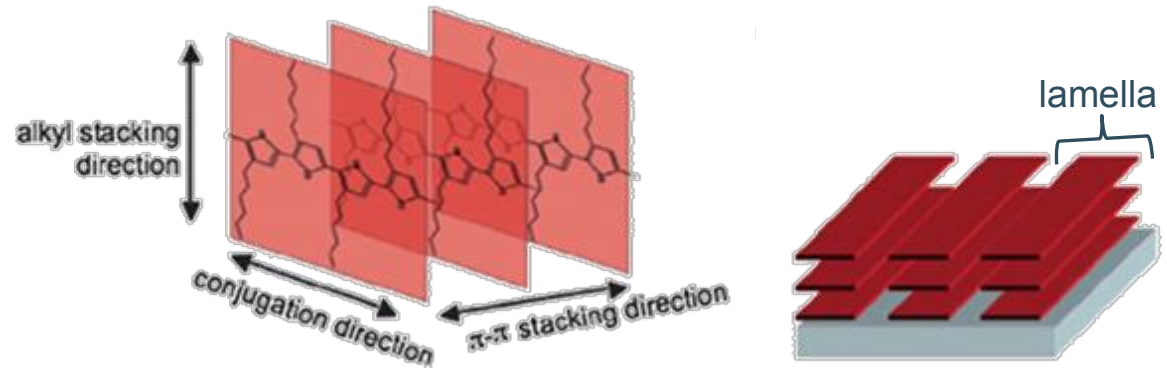
Configurations of three typical lamellar  $\pi$ - $\pi$  stacking  
(Journal of Materials Science 53(46), DOI: 10.1007/s10853-018-2719-0)

# Electronic structure of conjugated molecules

- Conjugated molecules:  $\pi$ - $\pi$  stacking
  - Responsible of the lamella formation in electronic polymers.
  - Leads to the crystallinity of electronic polymers. Electronic polymers are semicrystalline (amorphous and crystalline domains coexist).
  - Conduction is best intramolecular (along conjugation direction) and along pi-pi stacking direction.



(Macromolecules 2017, 50, 6128–6136, DOI: 10.1021/acs.macromol.7b01323)

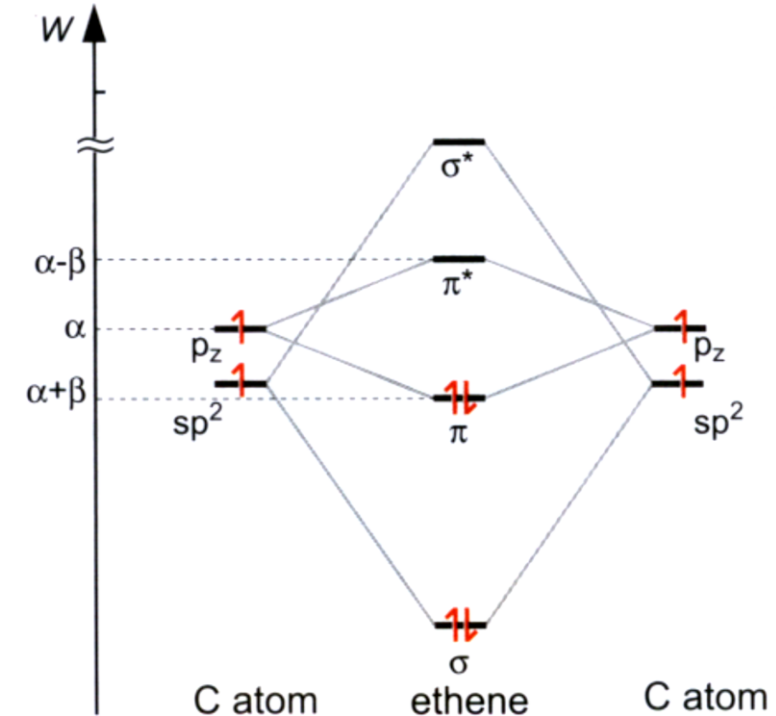


Formation of polymer lamella  
(Polym. Chem., 2013, 4, 5197-5205, <https://doi.org/10.1039/C3PY00131H>)

# Electronic structure of conjugated molecules

- Conjugated molecules: Energy structure
  - The delocalization of the  $\pi$  electrons gives rises to a stable and strong bonding between the C atoms.
  - When considering the electronic properties of conjugated systems, one need only to consider the delocalized  $\pi$  electrons (treated as valence electrons), usually lying at a higher energy level rather than the  $\sigma$  electrons (treated as core electrons).

Schematic energy diagram typical of a C=C bond



# Electronic structure of conjugated molecules

- Conjugated molecules: Energy structure. The Hückel method.
  - Applying the LCAO method to conjugated planar systems (called Hückel method when applied to  $\pi$  electrons) allows to understand their electronic properties. We can illustrate this with benzene. With LCAO-MO theory, we can understand the benzene molecule by constructing delocalized  $\pi$  MOs that extend around the entire molecule:  $\psi = c_1\phi_1 + c_2\phi_2 + c_3\phi_3 + c_4\phi_4 + c_5\phi_5 + c_6\phi_6$
  - Each of the  $\phi_i$  are  $2p$  AOs, centered on each of the six carbon atoms and directed out of the molecular plane. The ring nature of benzene requires that  $\phi_6$  bonds with  $\phi_1$ , as well as with  $\phi_5$ .
  - In the Hückel approximation the following simplifying assumptions are made:
    1. The Coulomb integrals  $H_{ii}$  for each  $\phi_i$  are all the same (call them  $\alpha$ ).
    2. The bond integrals  $H_{jj}$  for each  $\phi_i$  from adjacent carbon atoms are all the same (call them  $\beta < 0$ ) and the bond integrals from nonadjacent AOs are all zero.  $\beta$  is also called the transfer integral.
    3. The overlap integrals  $S_{ij} = \int \phi_i \phi_j dV$  are all zero. This assumption can be made legitimate with modest adjustments in the AOs. It is a severe approximation that makes the physics less realistic but the maths easier.

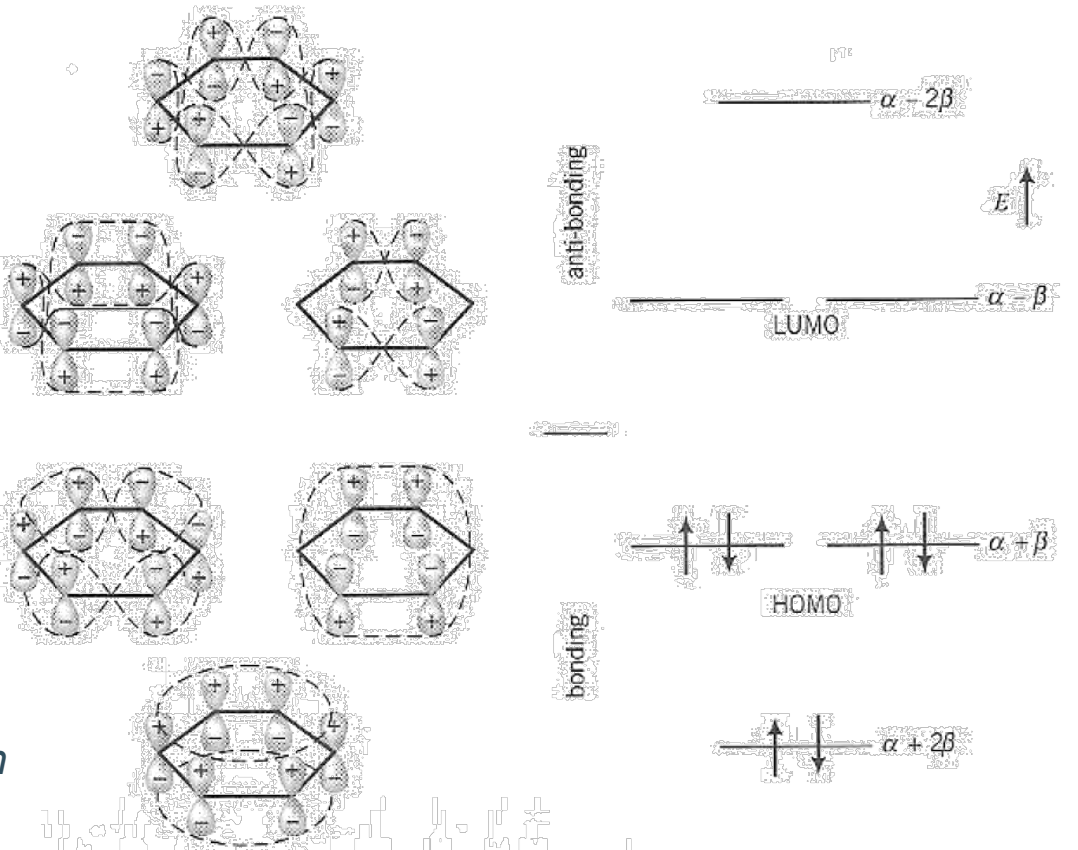
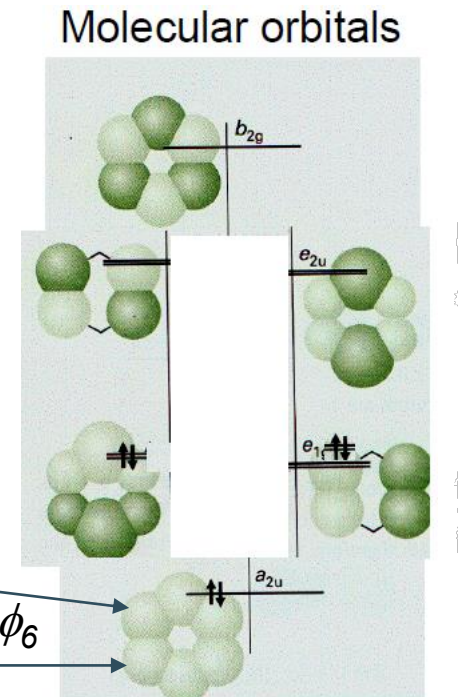
# Electronic structure of conjugated molecules

- Conjugated molecules: Energy structure. The Hückel method.

- Applying the Hückel method to benzene results in the electronic structure schematically illustrated below.

$$\psi = c_1\phi_1 + c_2\phi_2 + c_3\phi_3 + c_4\phi_4 + c_5\phi_5 + c_6\phi_6$$

Schematic MOs and energy levels for delocalized  $\pi$  electrons in benzene molecule from Hückel model.



# Electronic structure of conjugated molecules

- Conjugated molecules: Energy structure. The Hückel method.
  - Applying the Hückel method to benzene...

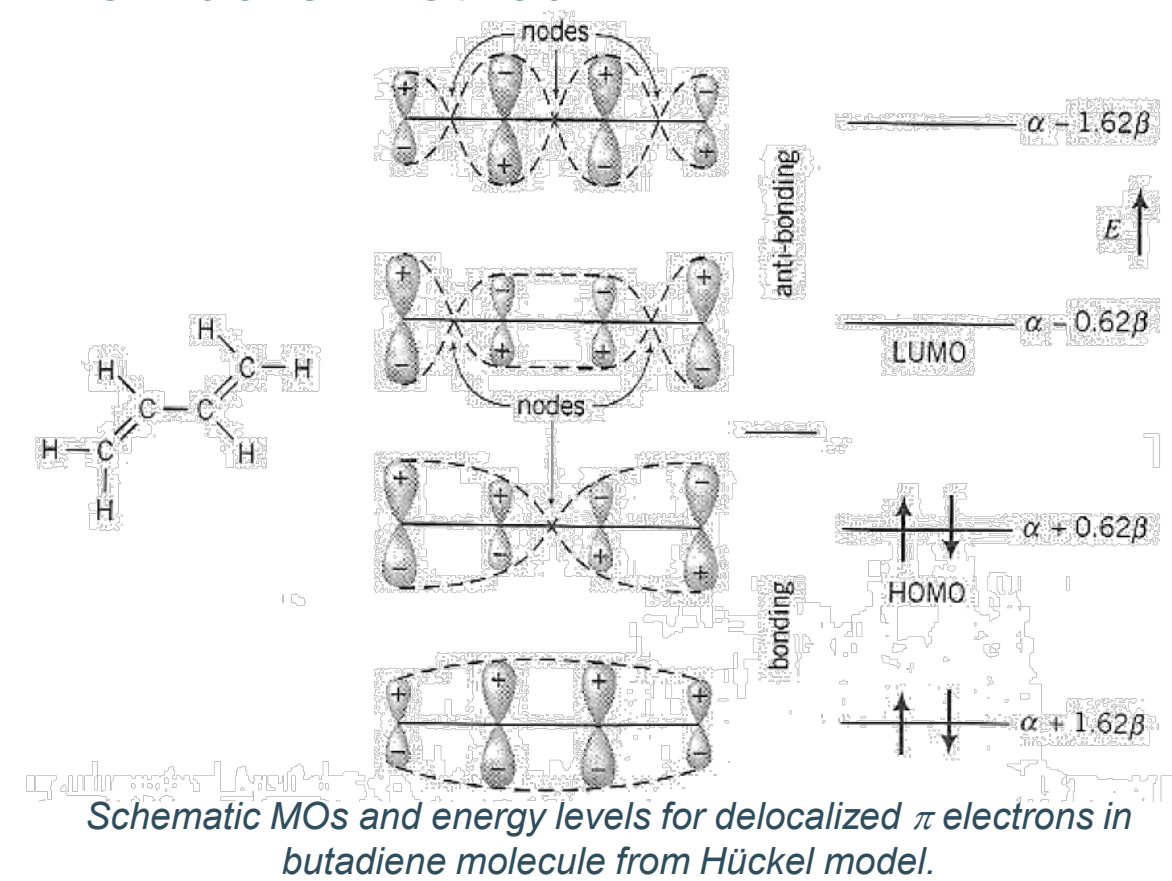
1. Yields 6 MOs (three bonding and three antibonding). The lowest energy MO corresponds to all  $c_i$  being equal. The highest energy MO corresponds to  $c_i$  with alternating signs, with nodal planes between each atom pair.
2. Also shown are the corresponding energy levels, which include two pairs of degenerate levels. The energy of the bottom level is found to be  $\alpha + 2\beta$  (the bond integral  $\beta$  is negative).
3. There are two degenerate bonding MOs with  $E = \alpha + \beta$  (these are the Highest Occupied MOs, the '**HOMO**' levels), two degenerate antibonding MOs with  $E = \alpha - \beta$  (these are the Lowest Unoccupied MOs, the '**LUMO**' levels), and the highest antibonding MO level with  $E = \alpha - 2\beta$ .
4. The Coulomb energy  $\alpha$  represents the reference state for the  $2p$  electrons, and the difference in energy between the highest and lowest level is four times the bond integral  $\beta$ .
5. In the ground state of the benzene molecule, the three bonding levels are occupied, and the three antibonding levels are unoccupied.

# Electronic structure of conjugated molecules

- Conjugated molecules: Energy structure. The Hückel method.
  - Applying the Hückel method to butadiene...

\*Notice that the amplitude of the molecular MO is modulated by a sinusoid with wavelength ( $\lambda$ )

->Higher energy bands have more nodes which means larger values of the wavenumber  $k = 2\pi/\lambda$



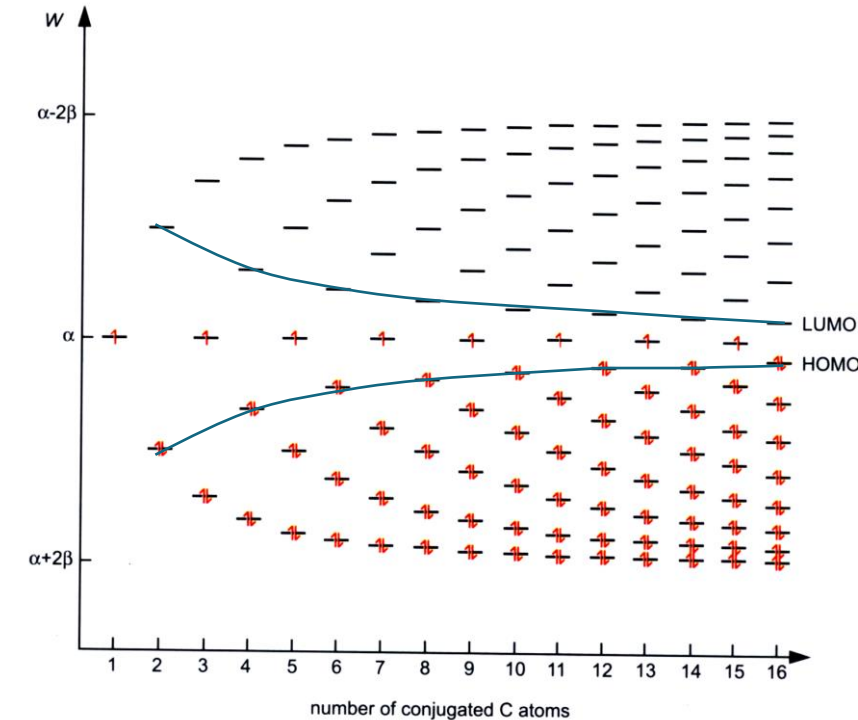
# Electronic structure of conjugated molecules

- Conjugated molecules: Energy structure. The Hückel method.
    - Applying the Hückel method to butadiene...
1. Each of the carbon atoms in butadiene ( $C_4H_6$ ) has three neighbors and  $sp^2$  hybrids form  $\sigma$  bonds. The remaining  $2p$  AOs, directed out of the molecular plane, form delocalized  $\pi$  MOs that extend along the carbon chain, and can be treated in the Hückel approximation.
  2. The figure shows the relative orientation of the  $p$  AOs in each of the four MOs (two bonding, two antibonding), with dashed lines suggesting the outline of the various MOs. The four energy levels are  $\alpha + 1.62\beta$ ,  $\alpha + 0.62\beta$ ,  $\alpha - 0.62\beta$ , and  $\alpha - 1.62\beta$ .

# Electronic structure of conjugated molecules

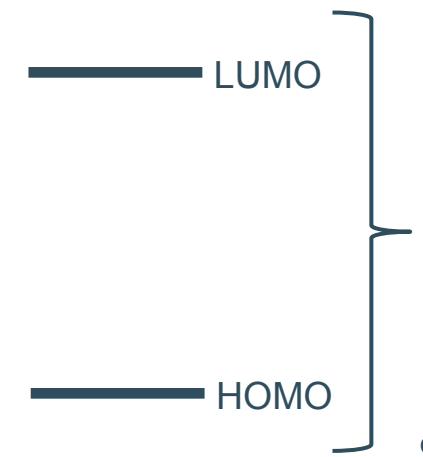
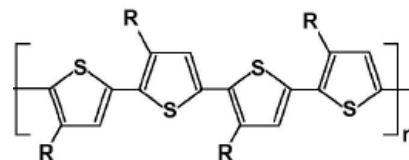
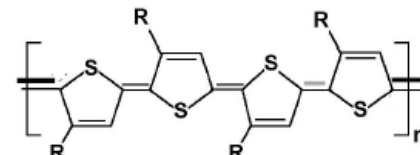
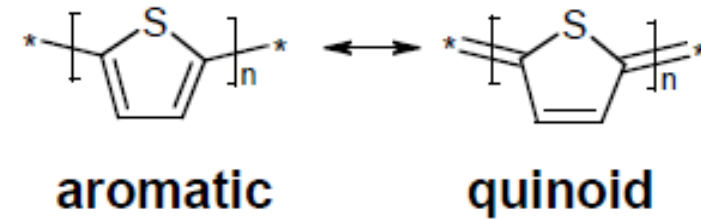
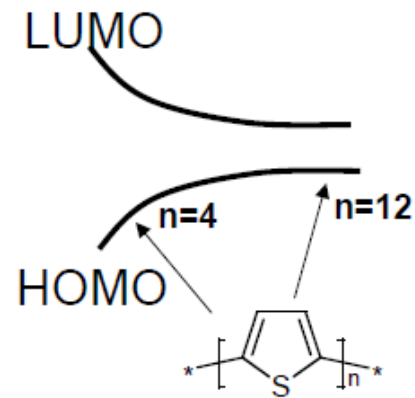
- Conjugated molecules: Energy structure. HOMO and LUMO shifting.
  - The highest occupied orbital (HOMO) corresponds to the valence band edge of a semiconductor, while the lowest unoccupied orbital (LUMO) corresponds to the conduction band edge. The band-gap thus corresponds to the difference between HOMO and LUMO energy levels.
  - All the levels are confined in between an energy interval of  $4\beta$ .

*Energy levels and electron occupation for conjugated hydrocarbon with unbranched chain structures of one to 16 C atoms as calculated by the HMO theory. The system with one C atom represents a  $sp^2$  hybridized  $CH_3$  radical.*



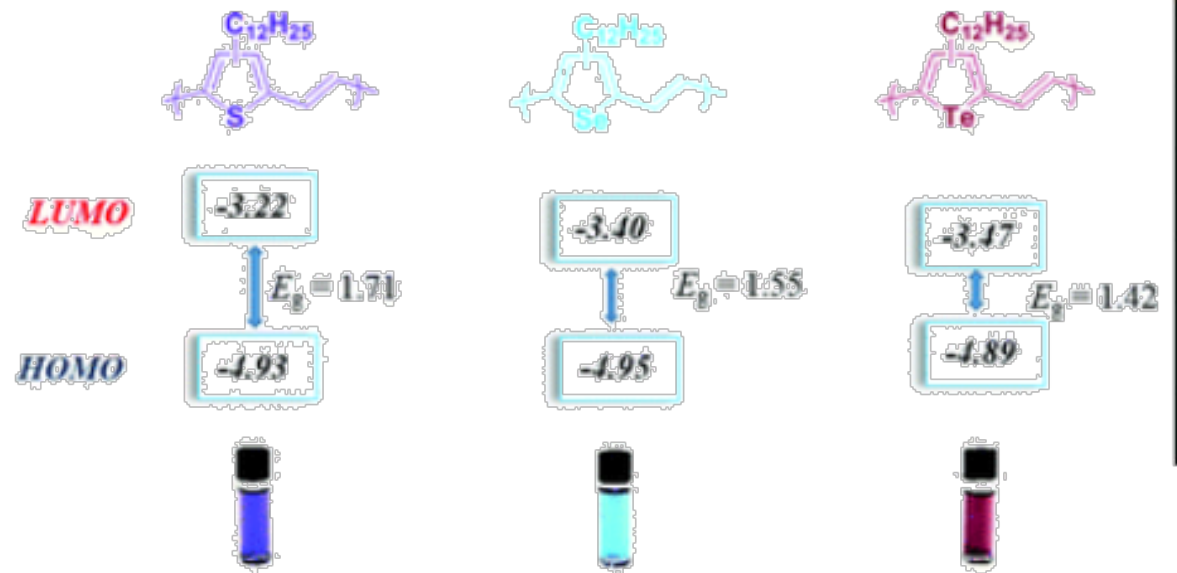
# Electronic structure of conjugated molecules

- Conjugated molecules: Energy structure. HOMO and LUMO shifting.
  - Example for polythiophene.



# Electronic structure of conjugated molecules

- Conjugated molecules: Energy structure. HOMO and LUMO shifting.
  - Heteroatoms with different electronegativity modify band gap



<sup>1</sup> H 2.20
<sup>3</sup> Li 0.98
<sup>4</sup> Be 1.57
<sup>11</sup> Na 0.93
<sup>12</sup> Mg 1.31
<sup>19</sup> K 0.82
<sup>20</sup> Ca 1.00
<sup>21</sup> Sc 1.36
<sup>22</sup> Ti 1.54
<sup>23</sup> V 1.63
<sup>24</sup> Cr 1.66
<sup>25</sup> Mn 1.55
<sup>26</sup> Fe 1.83
<sup>27</sup> Co 1.88
<sup>28</sup> Ni 1.91
<sup>29</sup> Cu 1.90
<sup>30</sup> Zn 1.65
<sup>31</sup> Ga 1.81
<sup>32</sup> Ge 2.01
<sup>33</sup> As 2.18
<sup>34</sup> Se 2.55
<sup>35</sup> Br 2.96
<sup>36</sup> Kr 3.00
<sup>5</sup> B 2.04
<sup>6</sup> C 2.55
<sup>7</sup> N 3.04
<sup>8</sup> O 3.44
<sup>9</sup> F 3.98
<sup>10</sup> Ne no data
<sup>13</sup> Al 1.61
<sup>14</sup> Si 1.90
<sup>15</sup> P 2.19
<sup>17</sup> Cl 3.16
<sup>18</sup> Ar no data
<sup>37</sup> Rb 0.82
<sup>38</sup> Sr 0.95
<sup>39</sup> Y 1.22
<sup>40</sup> Zr 1.33
<sup>41</sup> Nb 1.6
<sup>42</sup> Mo 2.16
<sup>43</sup> Tc 1.9
<sup>44</sup> Ru 2.2
<sup>45</sup> Rh 2.28
<sup>46</sup> Pd 2.20
<sup>47</sup> Ag 1.93
<sup>48</sup> Cd 1.69
<sup>49</sup> In 1.78
<sup>50</sup> Sn 1.96
<sup>51</sup> Sb 2.05
<sup>52</sup> Te 2.1
<sup>53</sup> I 2.66
<sup>54</sup> Xe 2.6
<sup>55</sup> Cs 0.79
<sup>56</sup> Ba 0.89
<sup>57</sup> - <sup>71</sup> no data
<sup>72</sup> Hf 1.3
<sup>73</sup> Ta 1.5
<sup>74</sup> W 2.36
<sup>75</sup> Re 1.9
<sup>76</sup> Os 2.2
<sup>77</sup> Ir 2.2
<sup>78</sup> Pt 2.28
<sup>79</sup> Au 2.54
<sup>80</sup> Hg 2.00
<sup>81</sup> Tl 1.62
<sup>82</sup> Pb 2.33
<sup>83</sup> Bi 2.02
<sup>84</sup> Po 2.0
<sup>85</sup> At 2.2
<sup>86</sup> Rn no data
<sup>87</sup> Fr 0.7
<sup>88</sup> Ra 0.89
<sup>89</sup> - <sup>103</sup> no data
<sup>104</sup> Rf no data
<sup>105</sup> Db no data
<sup>106</sup> Sg no data
<sup>107</sup> Bh no data
<sup>108</sup> Hs no data
<sup>109</sup> Mt no data
<sup>110</sup> Ds no data
<sup>111</sup> Rg no data
<sup>112</sup> Cn no data
<sup>113</sup> Nh no data
<sup>114</sup> Fl no data
<sup>115</sup> Mc no data
<sup>116</sup> Lv no data
<sup>117</sup> Ts no data
<sup>118</sup> Og no data

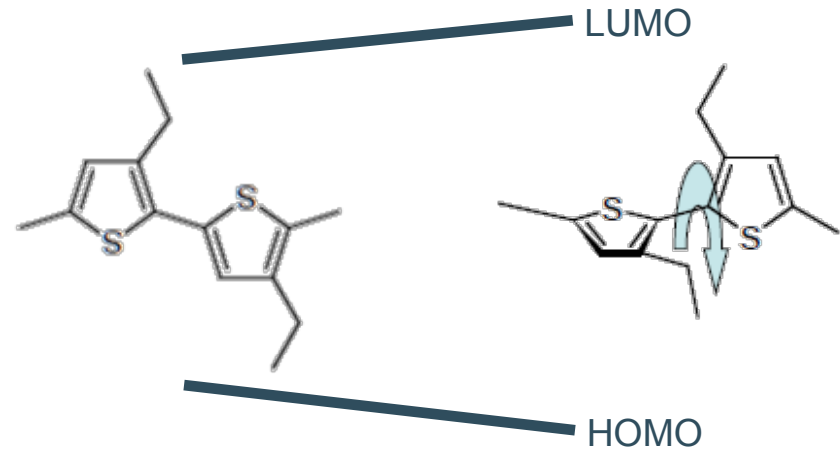
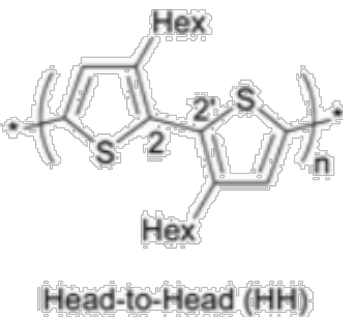
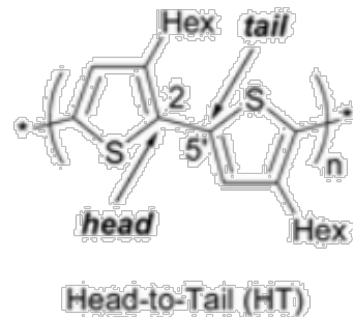
Electronegativity of elements

<sup>57</sup> La 1.10	<sup>58</sup> Ce 1.12	<sup>59</sup> Pr 1.13	<sup>60</sup> Nd 1.14	<sup>61</sup> Pm 1.13	<sup>62</sup> Sm 1.17	<sup>63</sup> Eu 1.2	<sup>64</sup> Gd 1.2	<sup>65</sup> Tb 1.22	<sup>66</sup> Dy 1.23	<sup>67</sup> Ho 1.24	<sup>68</sup> Er 1.24	<sup>69</sup> Tm 1.25	<sup>70</sup> Yb 1.1	<sup>71</sup> Lu 1.27
<sup>89</sup> Ac 1.1	<sup>90</sup> Th 1.3	<sup>91</sup> Pa 1.5	<sup>92</sup> U 1.38	<sup>93</sup> Np 1.36	<sup>94</sup> Pu 1.28	<sup>95</sup> Am 1.3	<sup>96</sup> Cm 1.3	<sup>97</sup> Bk 1.3	<sup>98</sup> Cf 1.3	<sup>99</sup> Es 1.3	<sup>100</sup> Fm 1.3	<sup>101</sup> Md 1.3	<sup>102</sup> No 1.3	<sup>103</sup> Lr no data

<https://doi.org/10.1039/C5SC03501E>

# Electronic structure of conjugated molecules

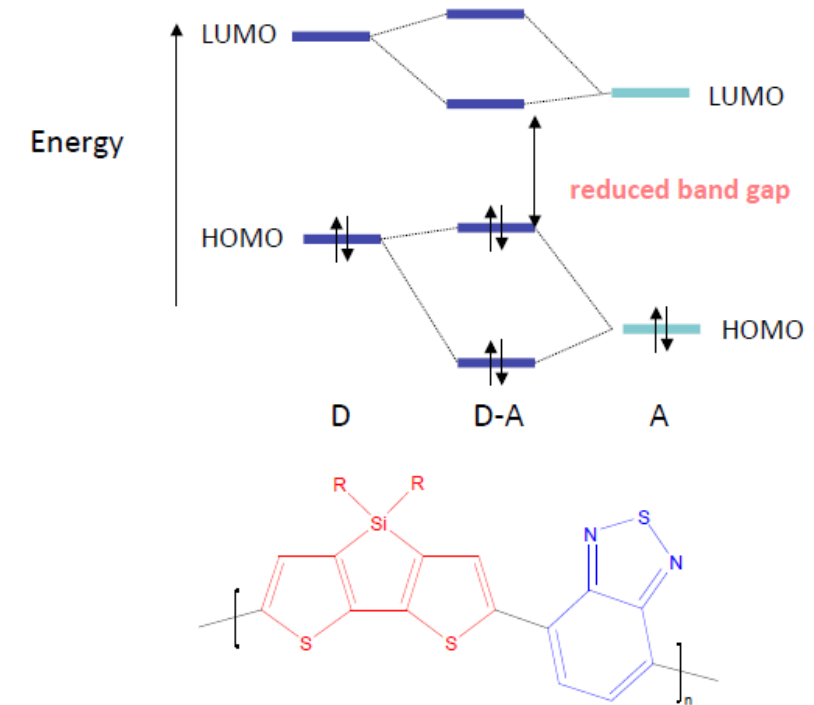
- Conjugated molecules: Energy structure. HOMO and LUMO shifting
  - Backbone twist



Twist reduce pi-orbital overlap -> bandgap increases

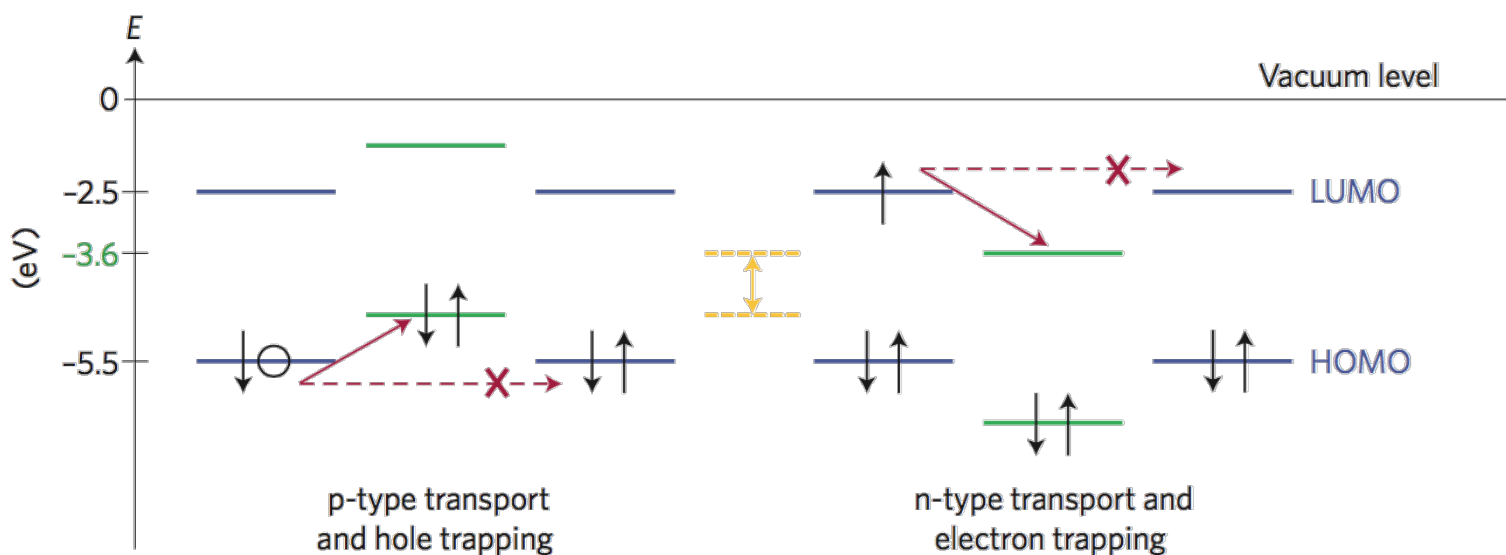
# Electronic structure of conjugated molecules

- Conjugated molecules: Energy structure. HOMO and LUMO shifting
  - Donor-acceptor polymers. The push-pull approach.
  - Molecular orbital hybridization reduces the bandgap
  - Why is small bandgap convenient...?



# Electronic structure of conjugated molecules

- Conjugated molecules: Energy structure. HOMO and LUMO. Why it matters?
  - Charge trapping: Electrons and holes differ strongly in their sensitivity to trapping at defects or impurities. The different susceptibility of electrons and holes to trapping results from the dissimilar energies of the HOMO and LUMO. For most organic semiconductors, the HOMO is located around  $-5$  to  $-6$  eV versus vacuum, whereas the LUMO ranges from about  $-2$  to  $-3$  eV.

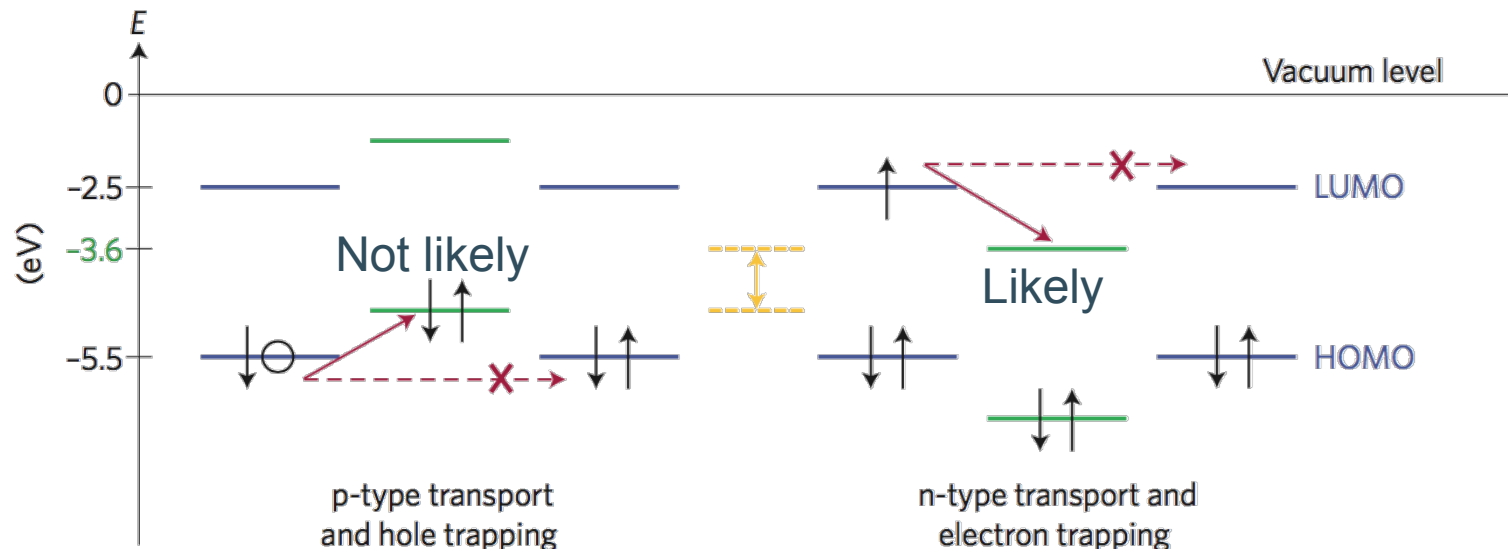


Energy level diagram illustrating hole and electron trapping in organic semiconductor films.

*In the case of p-type transport (left), a hole (black circle) can be localized by a higher-lying filled defect level (shown in green) instead of being transferred between the HOMOs of two adjacent molecules (shown in blue). n-type transport (right) requires the transfer of an excess electron (black arrow) between the LUMOs of two molecules (shown in blue). An empty lower-lying defect level (shown in green) can trap the electron for some time until it is released by thermal activation. Trap-free high-mobility transport of both electrons and holes may therefore require materials with a small HOMO–LUMO gap (shown in yellow).*

# Electronic structure of conjugated molecules

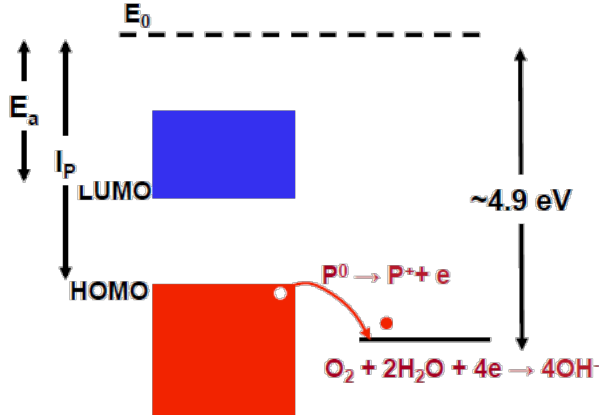
- Conjugated molecules: Energy structure. HOMO and LUMO. Why it matters?
  - Charge trapping: Defects or impurities frequently have empty orbitals between  $-3$  eV and  $-5$  eV that can take up an electron. Filled orbitals above  $-5$  eV (suitable for accepting holes) are more elusive.



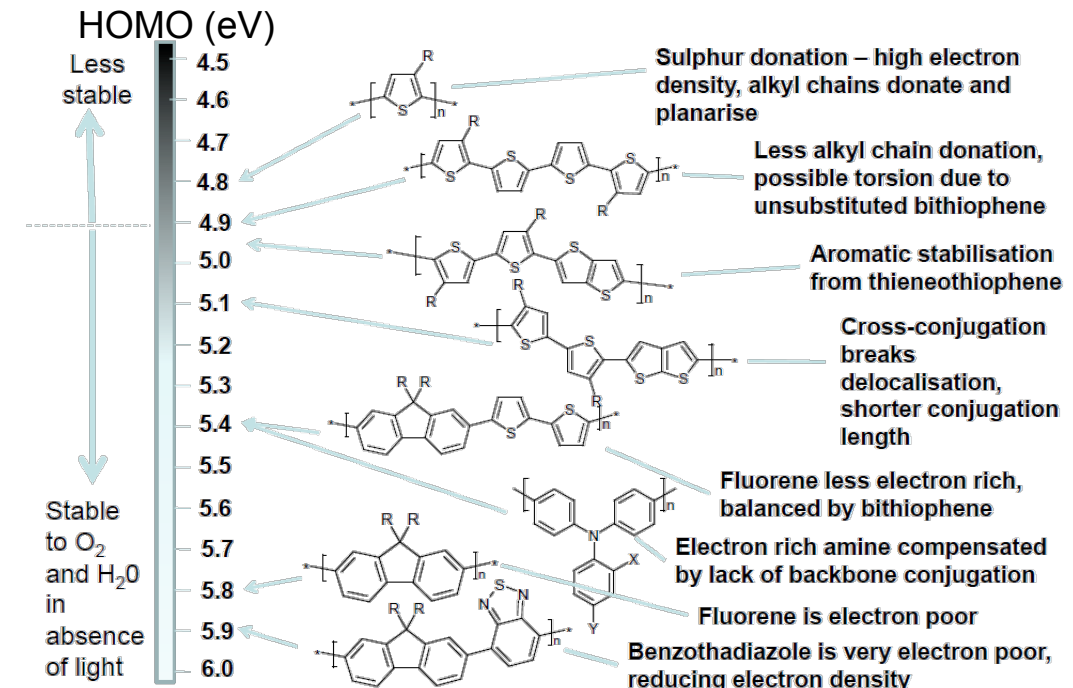
*Energy level diagram illustrating hole and electron trapping in organic semiconductor films.*

# Electronic structure of conjugated molecules

- Conjugated molecules: Energy structure. HOMO and LUMO. Why it matters?
  - Ambient stability: Polymers with ionization potential  $I_p < 4.9$  eV get oxidized by wet oxygen. Hence they are unstable in air.
    - In most n-type materials: oxidation traps electrons from the LUMO reducing electron mobility -> **Lack of n-type materials!!**
    - In some p-type materials, oxidation can act as a dopant. P-type materials with low HOMO are more stable. The HOMO can be lowered by making electron poor materials -> Electron withdrawing groups, backbone twist, conjugation break, etc..



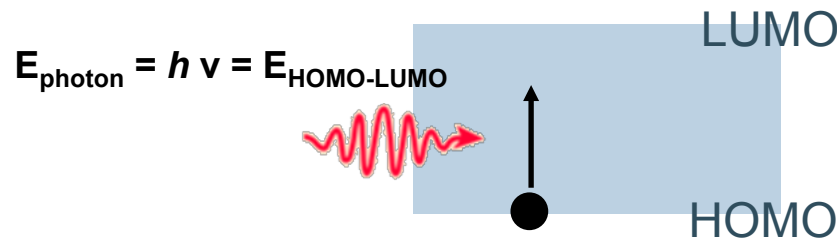
Polymers with  $I_p < 4.9$  eV tend to be unstable with respect to oxidation (=doping) by wet oxygen.



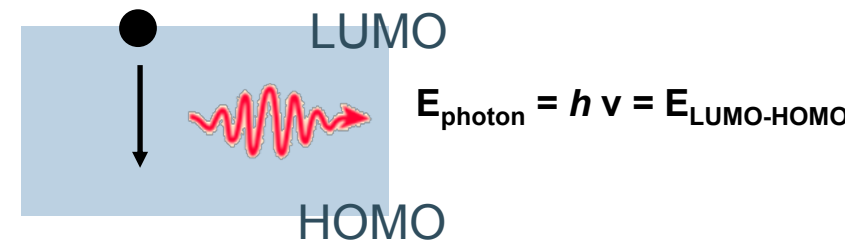
# Electronic structure of conjugated molecules

- Conjugated molecules: Energy structure. HOMO and LUMO. Why it matters?
  - Tuning performance of devices

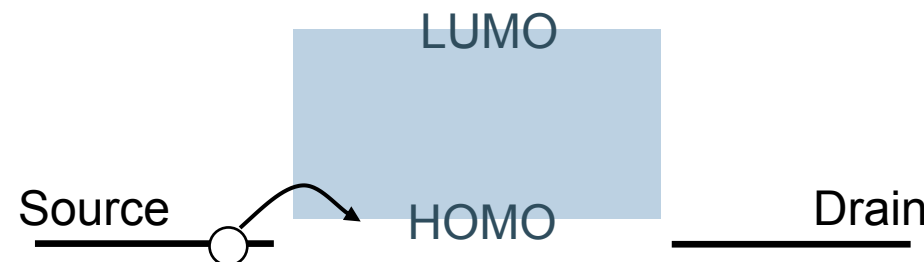
Light absorption:  
Solar cells/photodetectors



Light emission:  
LEDs



Charge injection:  
Transistors



(See Chapter 4)

# Transport in organic electronic materials

# Transport in organic electronic materials

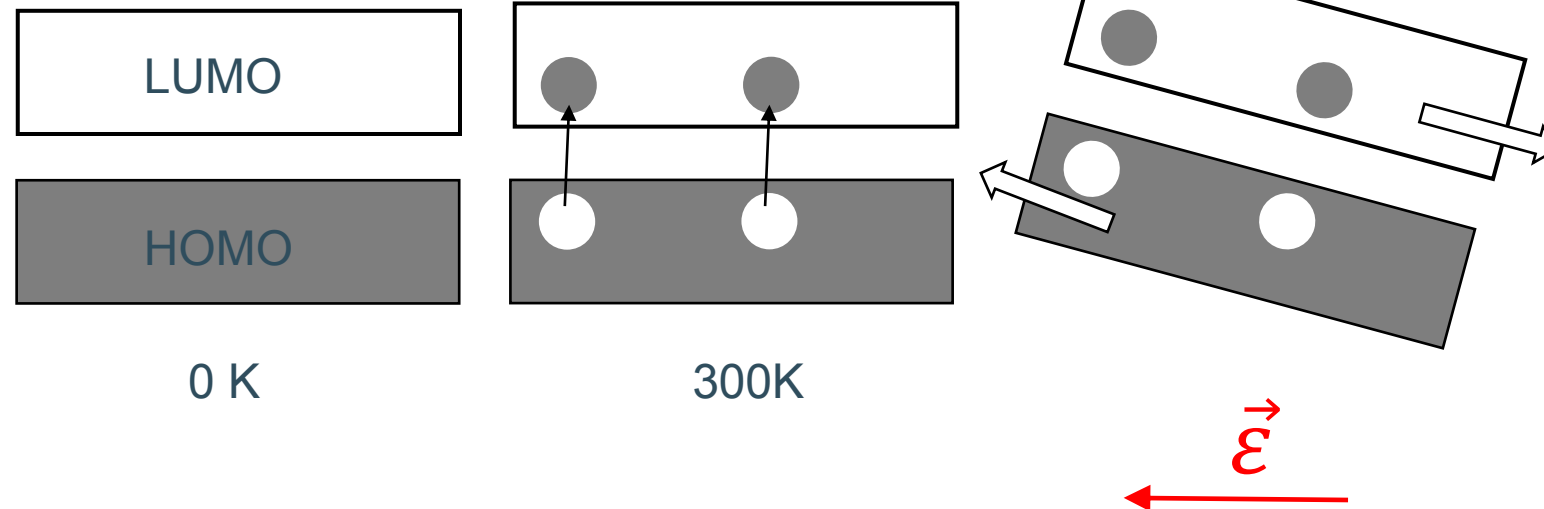
- Conductivity and mobility

- Current density:  $J = \sigma \epsilon = [n q \mu] \epsilon;$

$$\mu = \frac{v}{\epsilon}$$

Charge carrier density  
Elementary charge  
Mobility  
Conductivity      Electric field

velocity



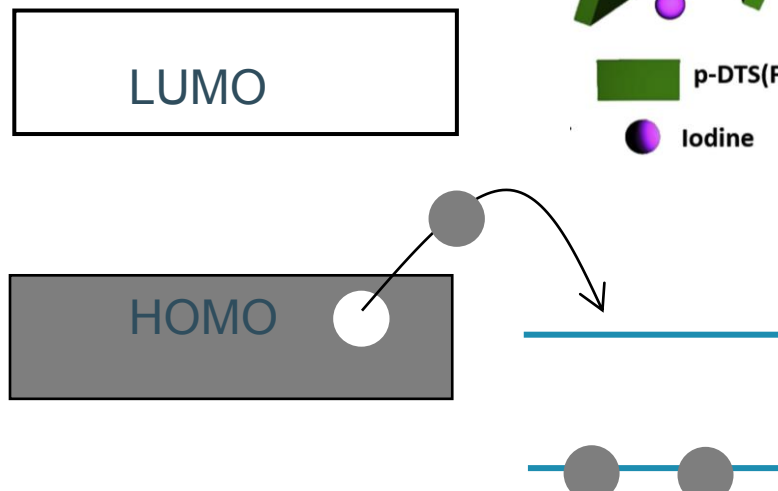
Free charges in OSC induced by:

- Chemical doping
- Photoexcitation
- Injection from electrodes
- Field effect

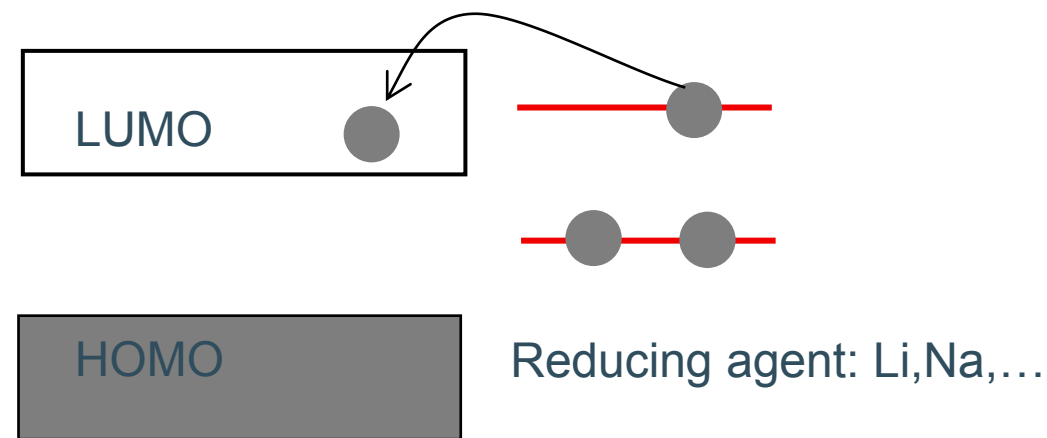
# Transport in organic electronic materials

- Doping

p-type doping

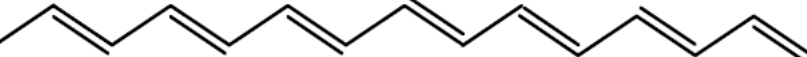


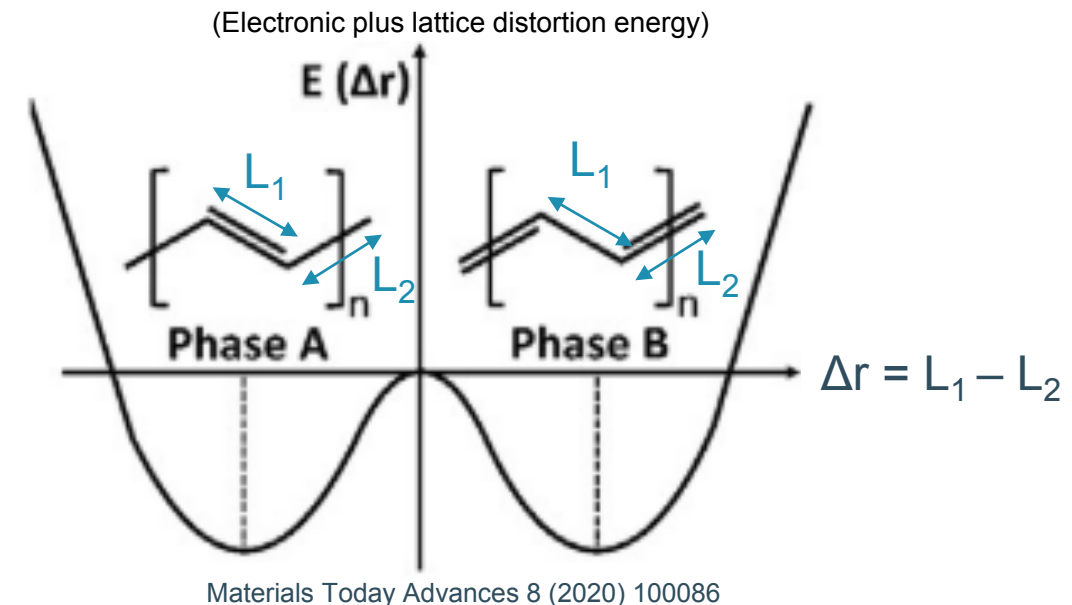
n-type doping



# Transport in organic electronic materials

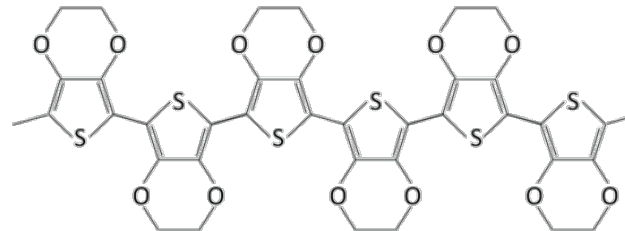
- Degenerated vs non-degenerated conjugated molecules

- In a polymer such as polyacetylene,  the energy of phase A and phase B configurations is the same. The polymer ground state is **degenerate**: all monomers are energetically equivalent with no change in energy of possible alternation of single and double bonds.
- The charge carriers created by doping in degenerated conjugated polymers are called **solitons**.



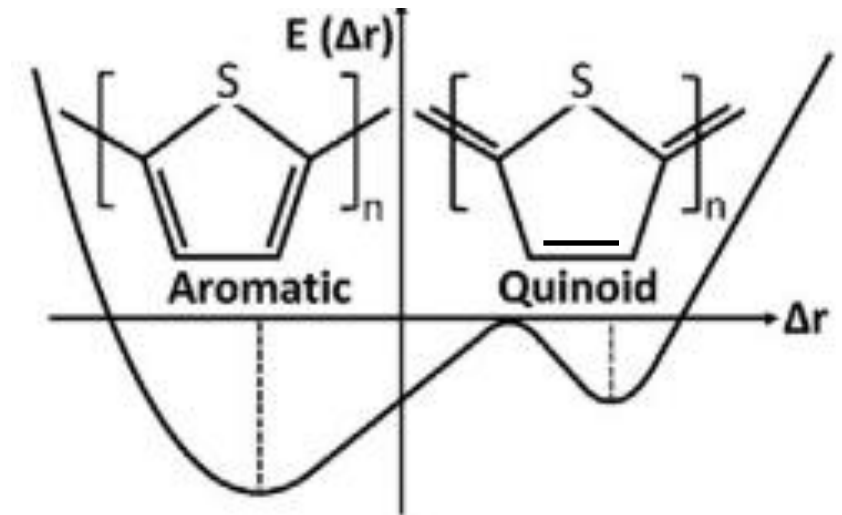
# Transport in organic electronic materials

- Degenerated vs non-degenerated conjugated molecules
  - In a polymer such as PEDOT,



a **non-degenerate** ground-state is present due to the differences in energy between the aromatic (or benzenoid) and quinoid structures.

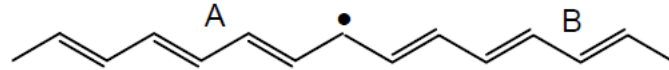
- The charge carriers created by doping in non-degenerated conjugated polymers are called **polarons and bipolarons**.



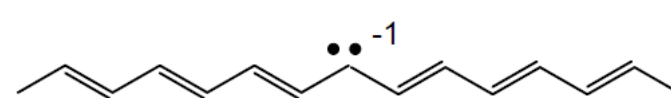
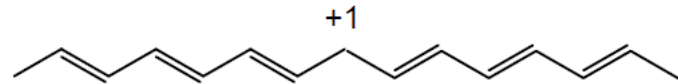
Materials Today Advances 8 (2020) 100086

# Transport in organic electronic materials

- Charges moving in organic semiconductors create changes in the bond-length alternation pattern. Charge transport comes along chain distortion forming quasiparticles.
- Quasi particles: Solitons
  - Solitons: domain boundary between the A and B phases.
  - A soliton can be ionized and transport charge



- A soliton can be ionized and transport charge



The soliton presents an unpaired  $e^-$  in between HOMO-LUMO (non-bonding level)

LUMO

HOMO

LUMO

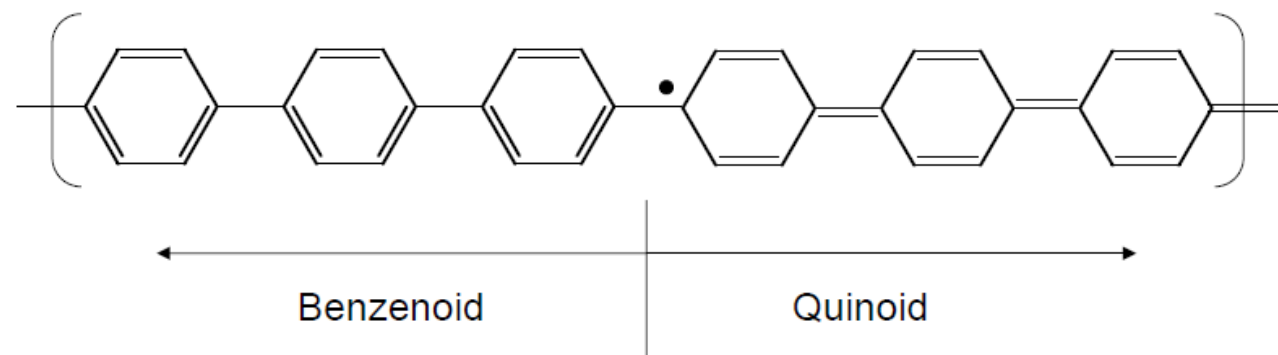


HOMO



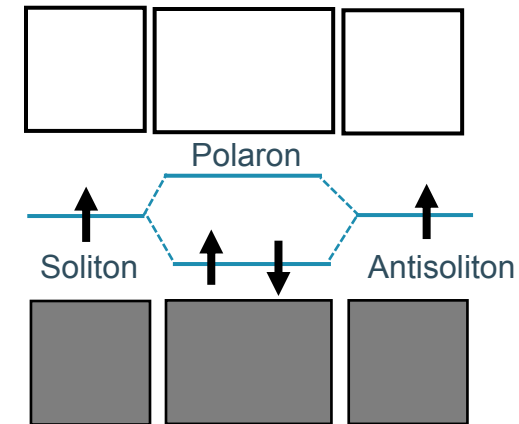
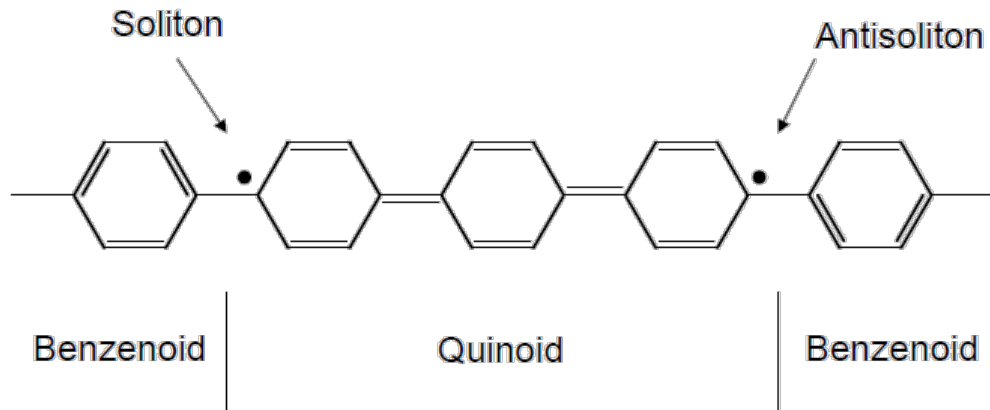
# Transport in organic electronic materials

- Charges moving in organic semiconductors create changes in the bond-length alternation pattern.
- Quasi particles: Solitons
  - Solitons: A soliton in a non-degenerate ground-state conjugated polymer costs energy because the quinoid part has more energy than the benzenoid part. Therefore, **solitons are not stable in this kind of structures**.



# Transport in organic electronic materials

- Charges moving in organic semiconductors create changes in the bond-length alternation pattern.
- Quasi particles: Polarons
  - Polaron: a bound soliton – antisoliton. **The neutral polaron is not stable** since soliton and antisoliton will annihilate.

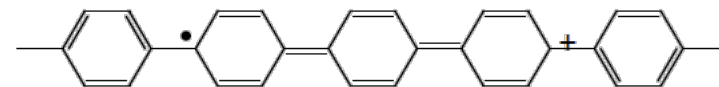


# Transport in organic electronic materials

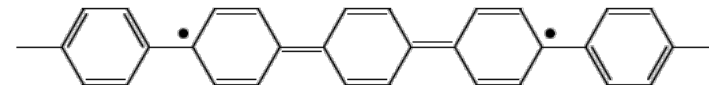
- Quasi particles :
  - Charged polarons: The charge and associated deformation act like a quasi-particle that transport charge across the molecule.

Charge    Spin

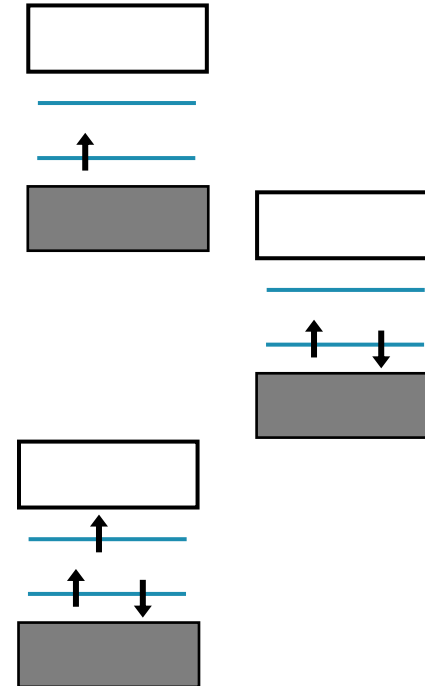
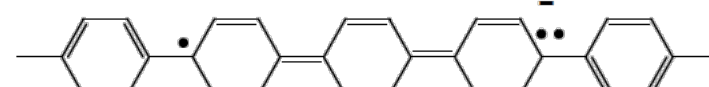
+1             $\frac{1}{2}$



0            0

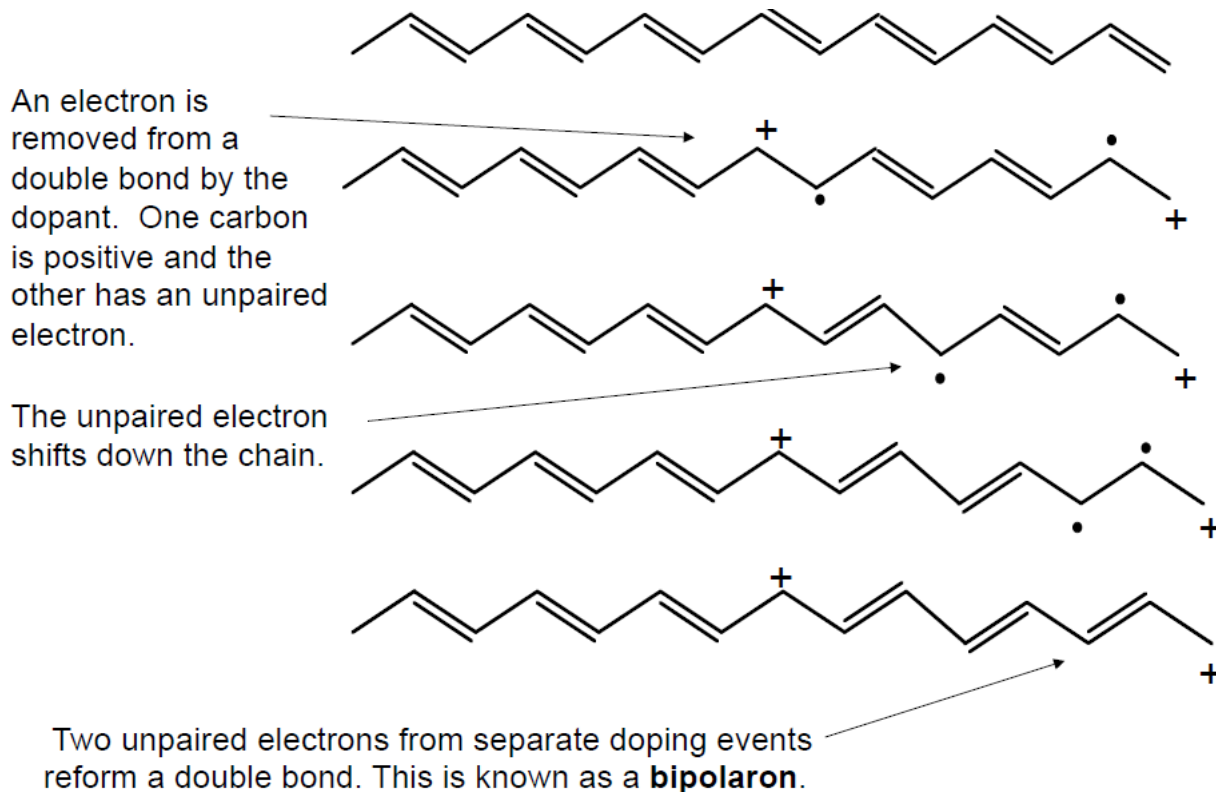


-1             $\frac{1}{2}$



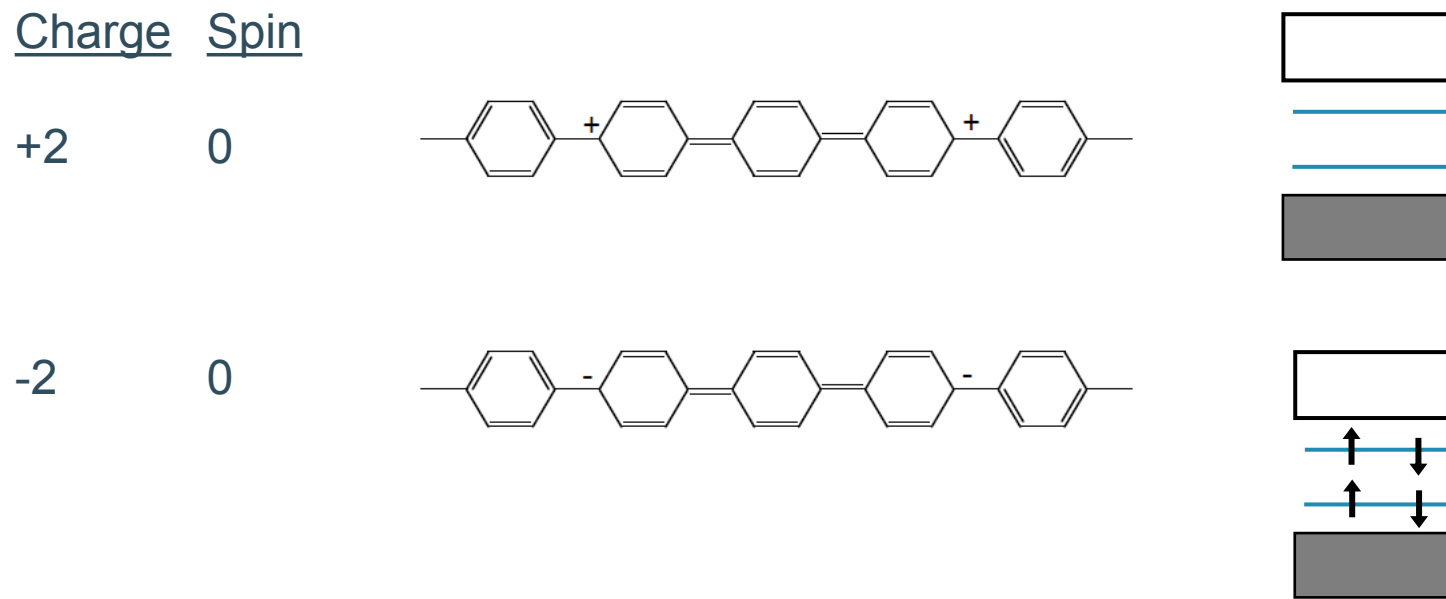
# Transport in organic electronic materials

- Quasi particles:
  - Bipolarons: Are introduced via doping.



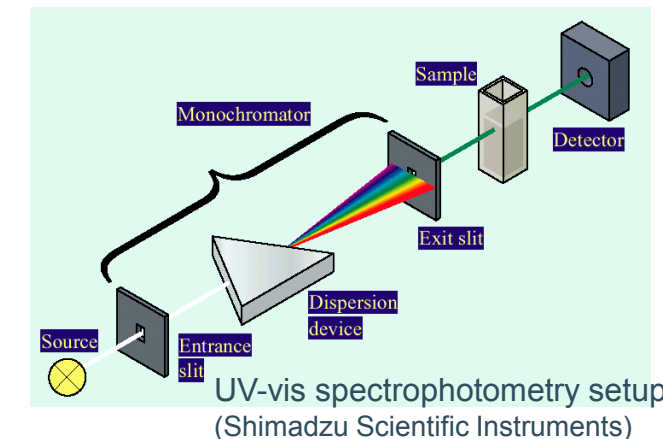
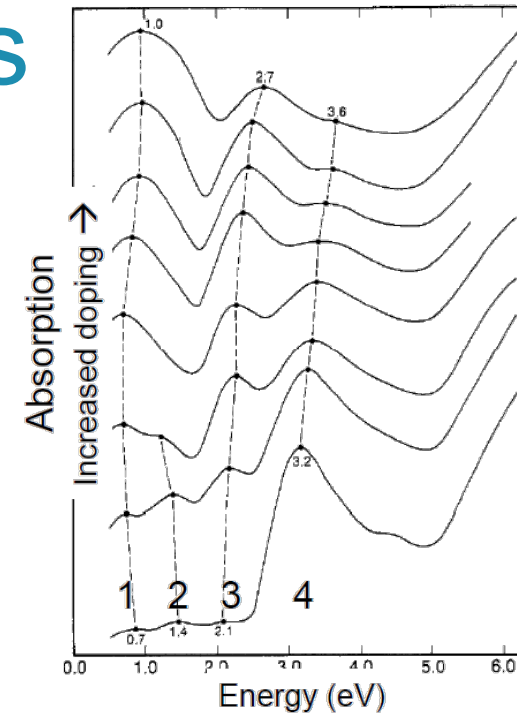
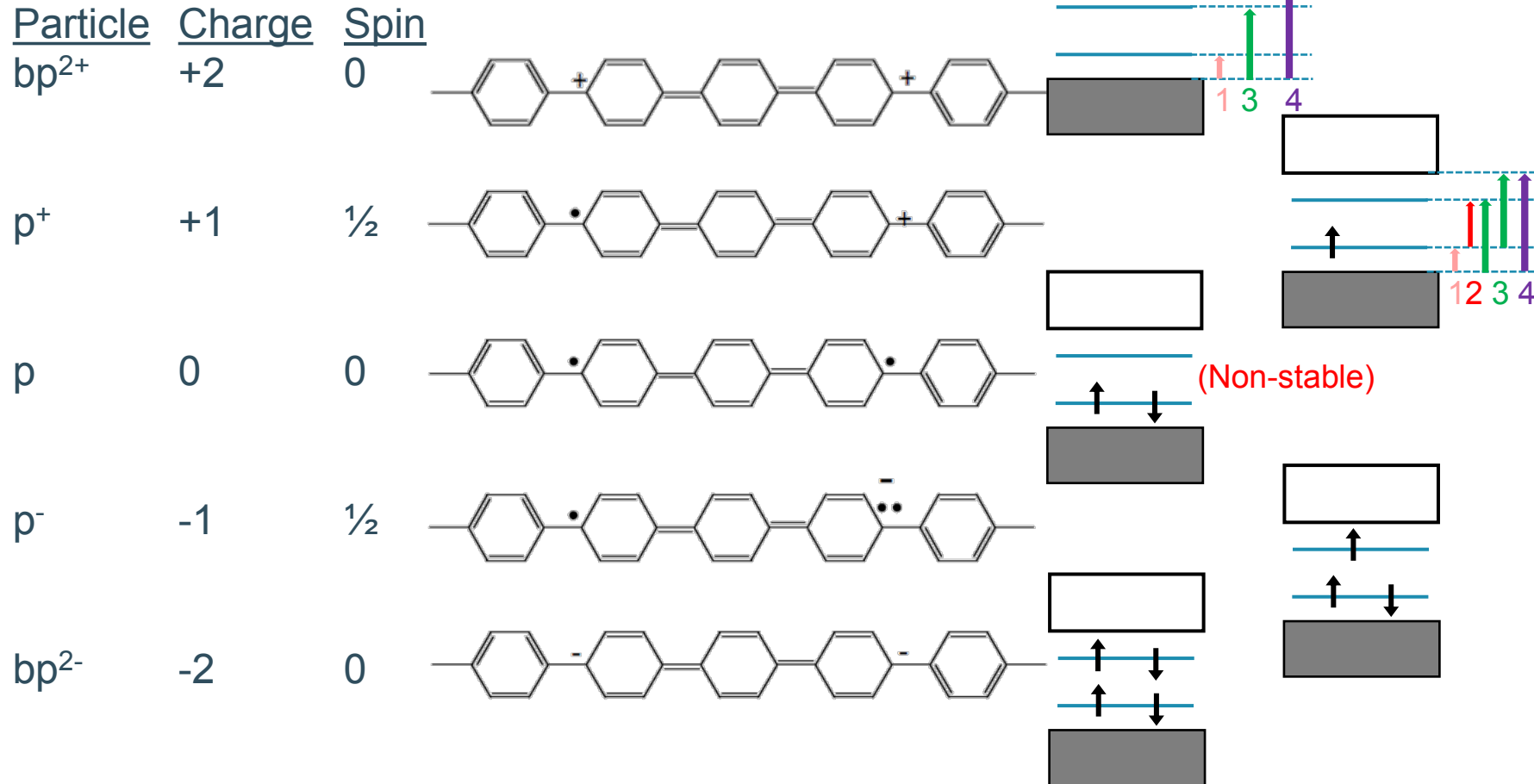
# Transport in organic electronic materials

- Quasi particles :
  - Positively- and negatively-charged bipolarons: they also act as a quasi-particle that transport charge and lattice deformation throughout the molecule.



# Transport in organic electronic materials

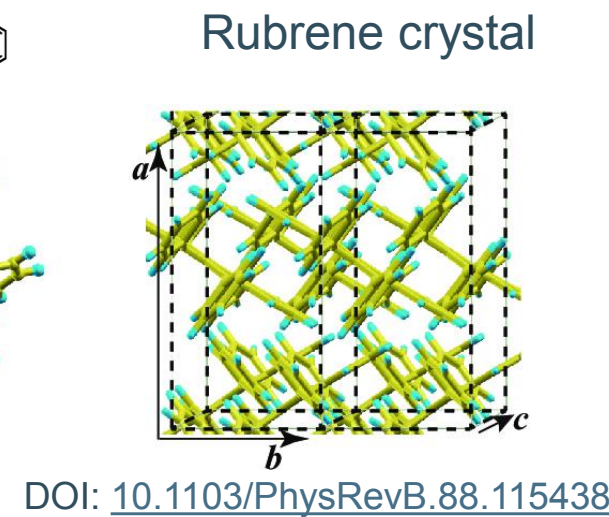
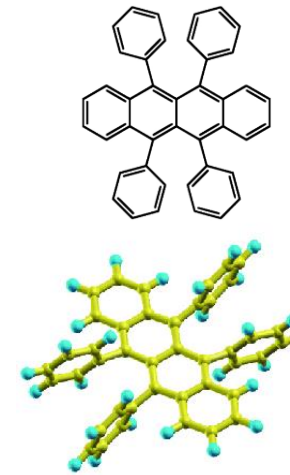
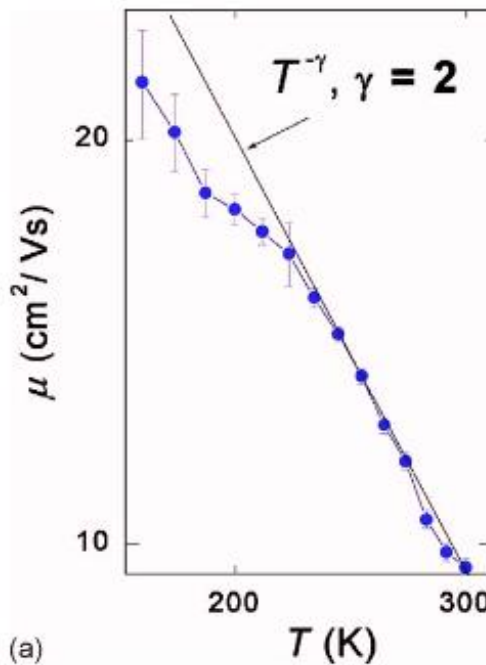
- Quasi particles :



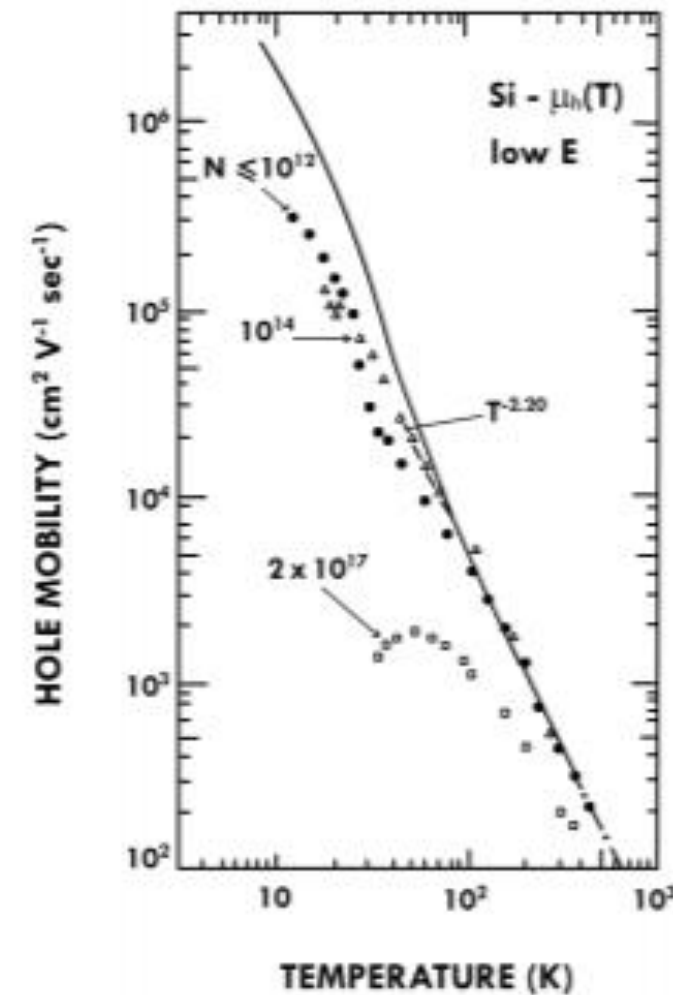
# Transport in organic electronic materials

- Mobility vs temperature: Band-like transport

Reviews of Modern Physics, Volume 78, 2006



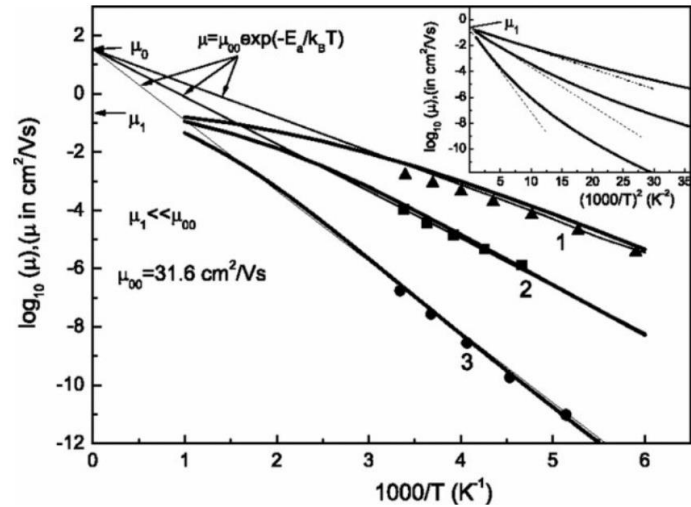
For Si →



Band transport-like behavior observed in highly purified and crystalline organic semiconductors (OSC)

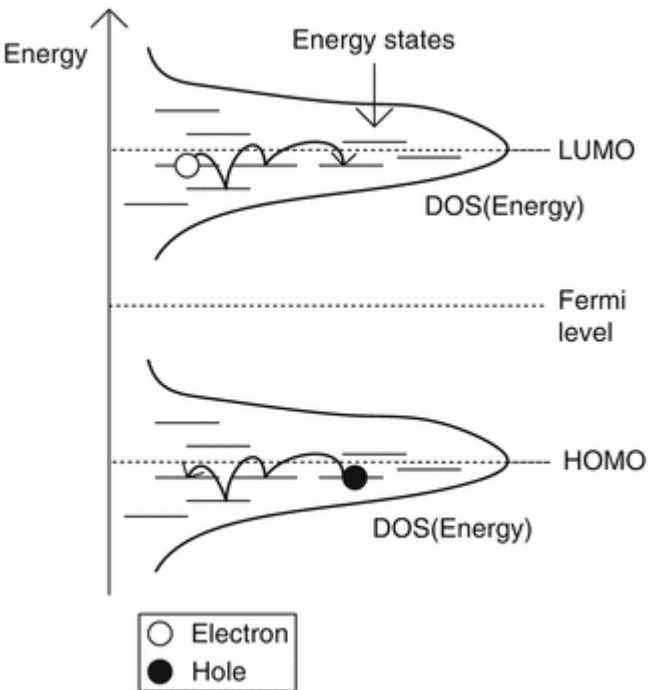
# Transport in organic electronic materials

- Mobility vs temperature: Variable Range Hopping (VRH) Transport
  - But most of the times OSC are too disordered to exhibit band transport behavior.
  - Instead, charge carriers move by hopping from molecule to molecule. The hopping process is thermally activated:



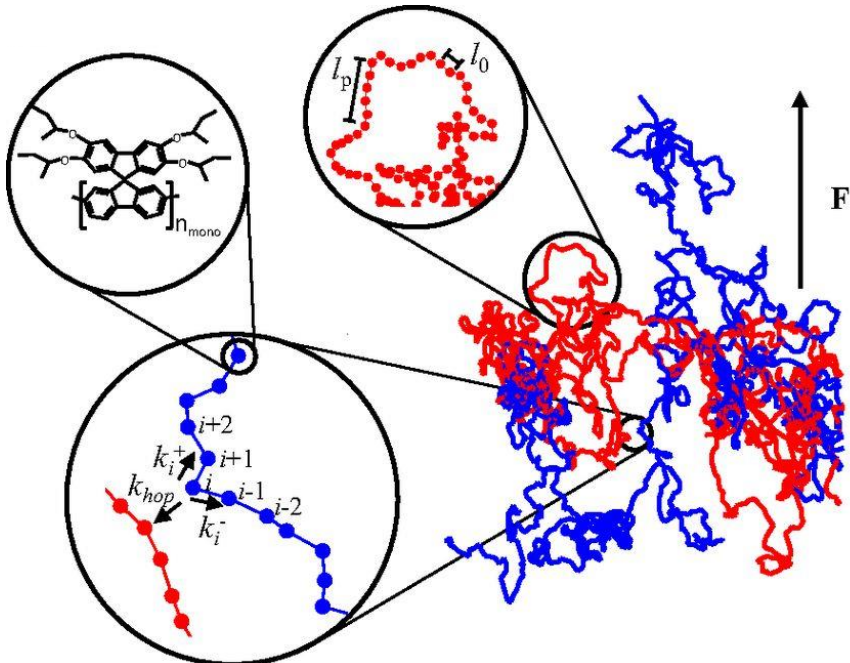
$$\mu \propto \mu_0 e^{-\frac{\Delta E}{k_B T}}$$

Mobility vs  $1/T$  for (1) PCBM, (2) region-regular P3HT, and (3) OC1C11-PPV  
(DOI: 10.1103/PhysRevB.81.045202)

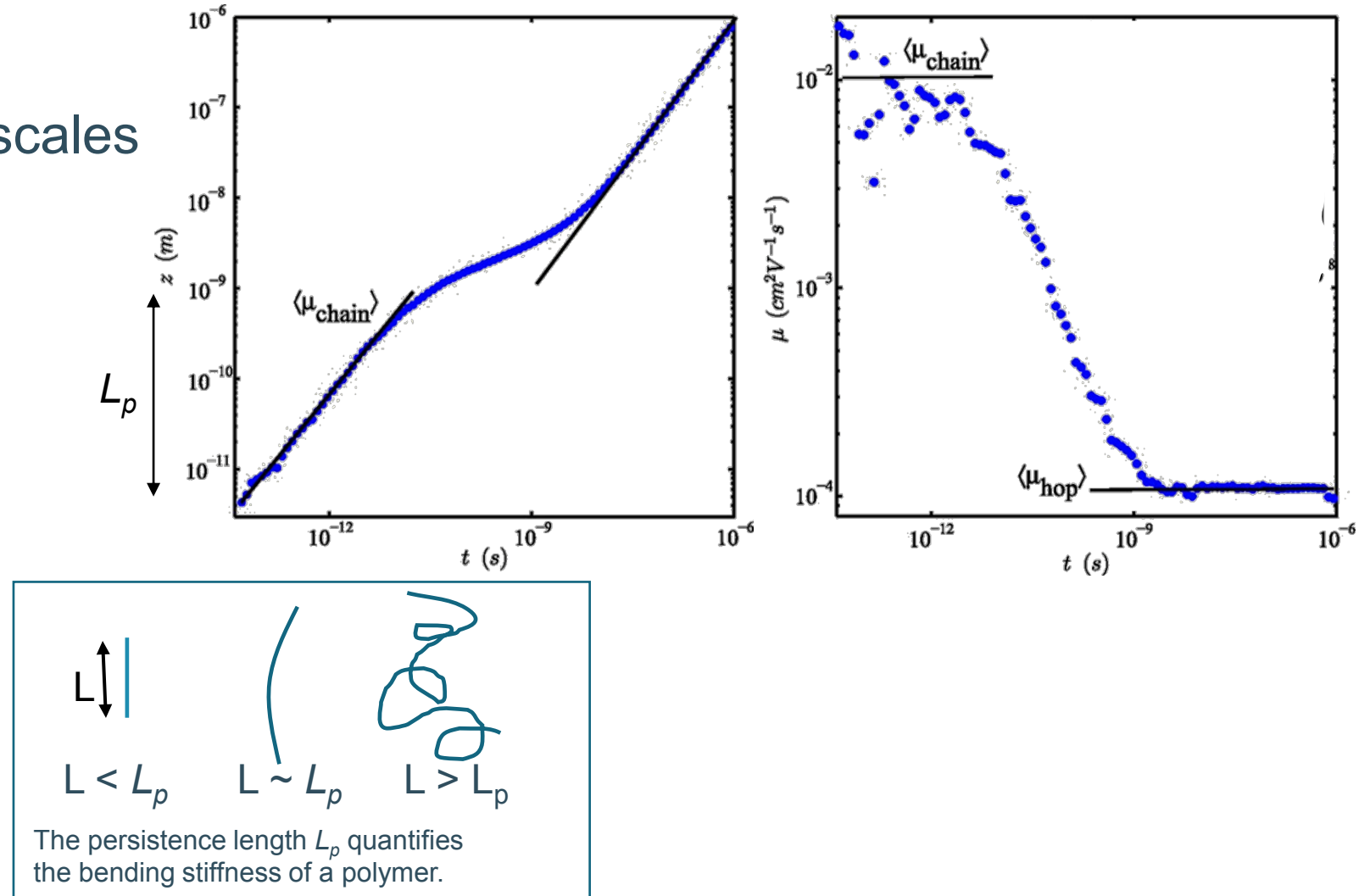


# Transport in organic electronic materials

- Mobility: time and length scales

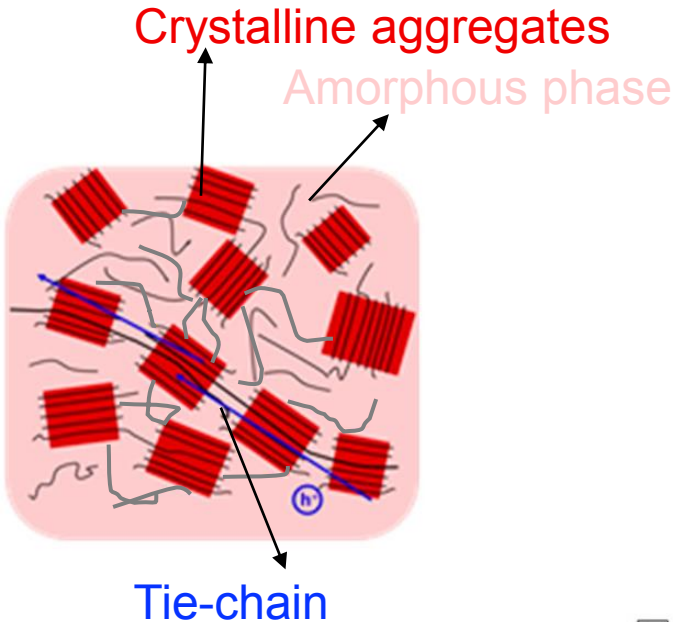


<https://doi.org/10.1073/pnas.1307158110>

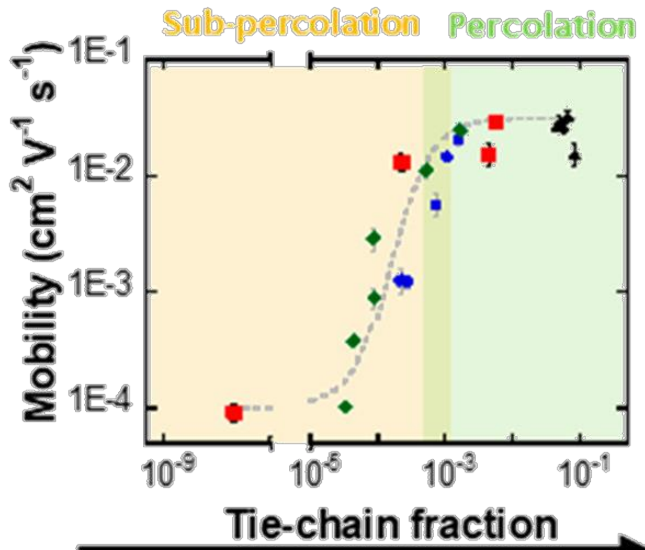


# Transport in organic electronic materials

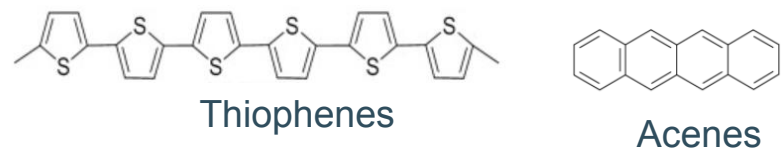
- Mobility: connectivity



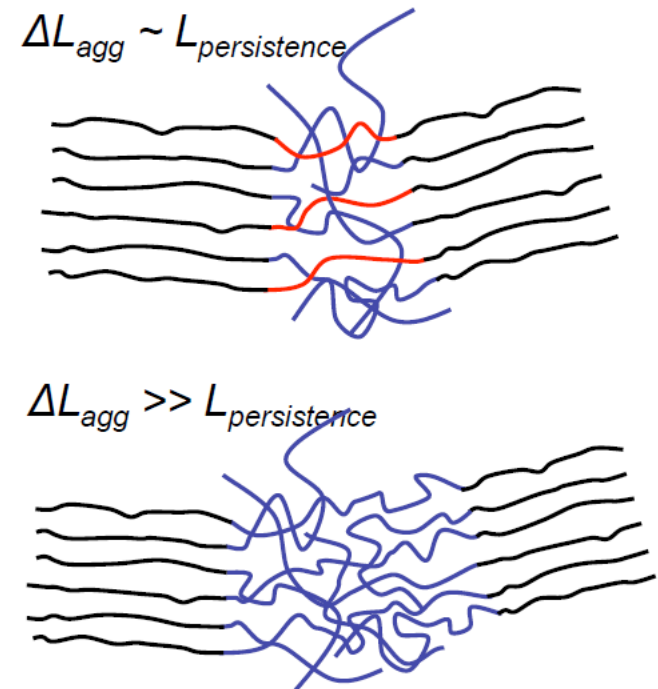
<https://doi.org/10.1021/acsmacrolett.8b00626>



Which molecule would have larger  $L_p$ ?



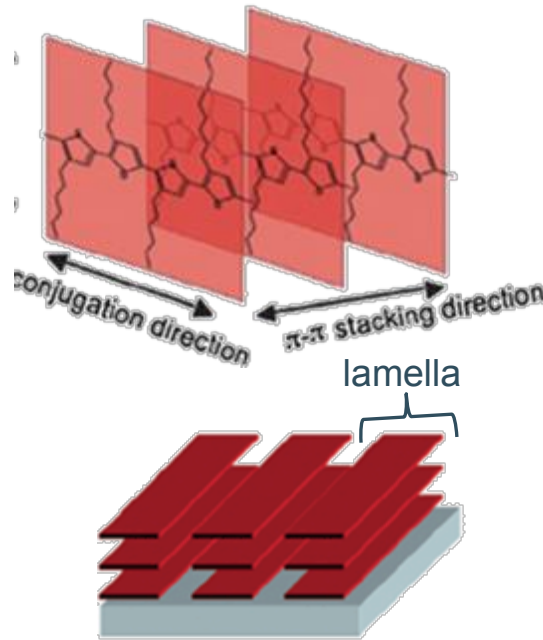
Acenes because fused rings are rigid



If the distance between aggregates  $\Delta L_{agg} \leq L_p \rightarrow$   
Tie-chain can bridge efficiently → **High mobility**

# Transport in organic electronic materials

- How to measure crystallinity: Grazing incidence wide angle X-ray diffraction (GIWAXD patterns).

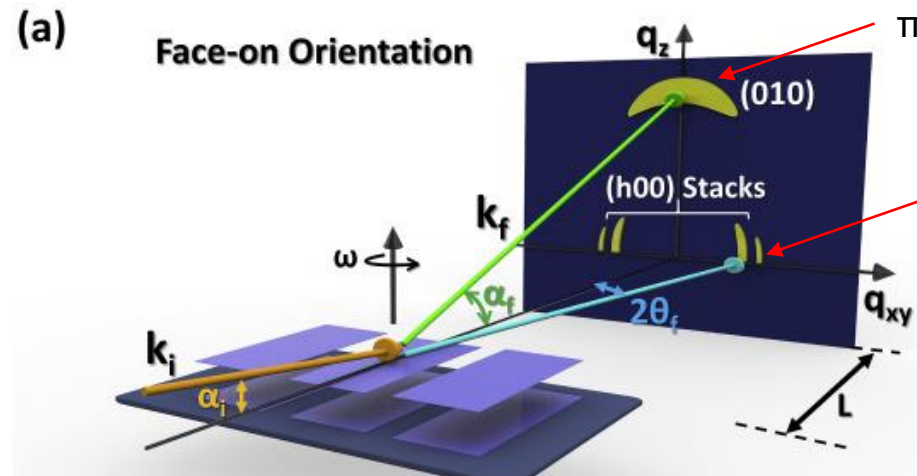


Formation of polymer lamella

(Polym. Chem., 2013, 4, 5197-5205,  
<https://doi.org/10.1039/C3PY00131H>)

(a)

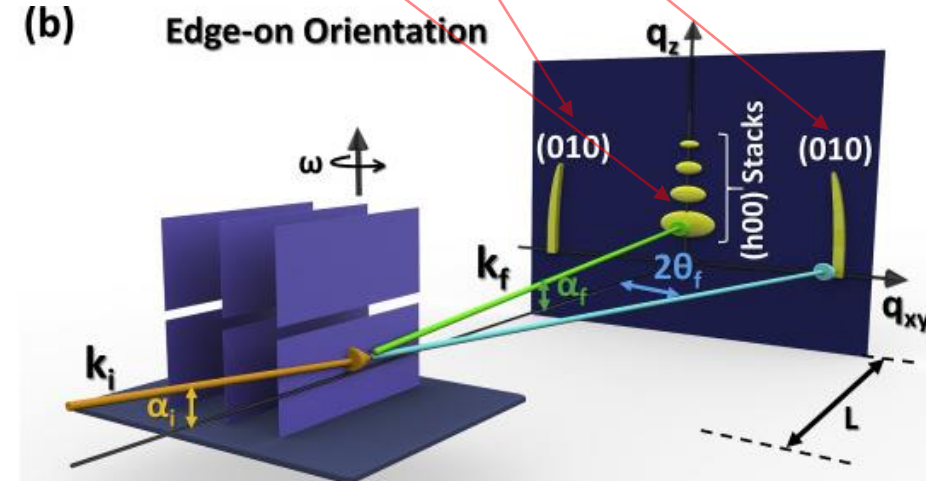
Face-on Orientation



Materials Today Advances 8 (2020) 100086 Contents

(b)

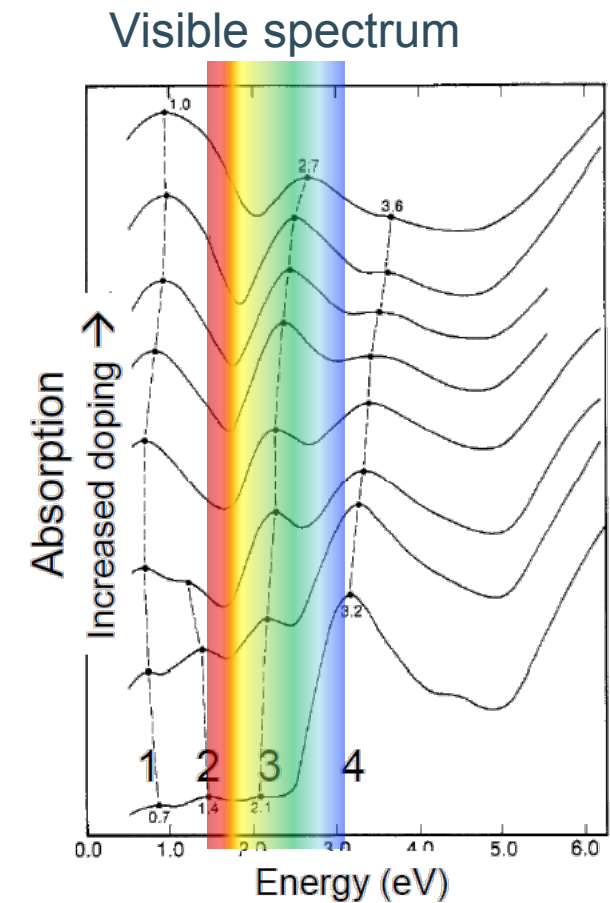
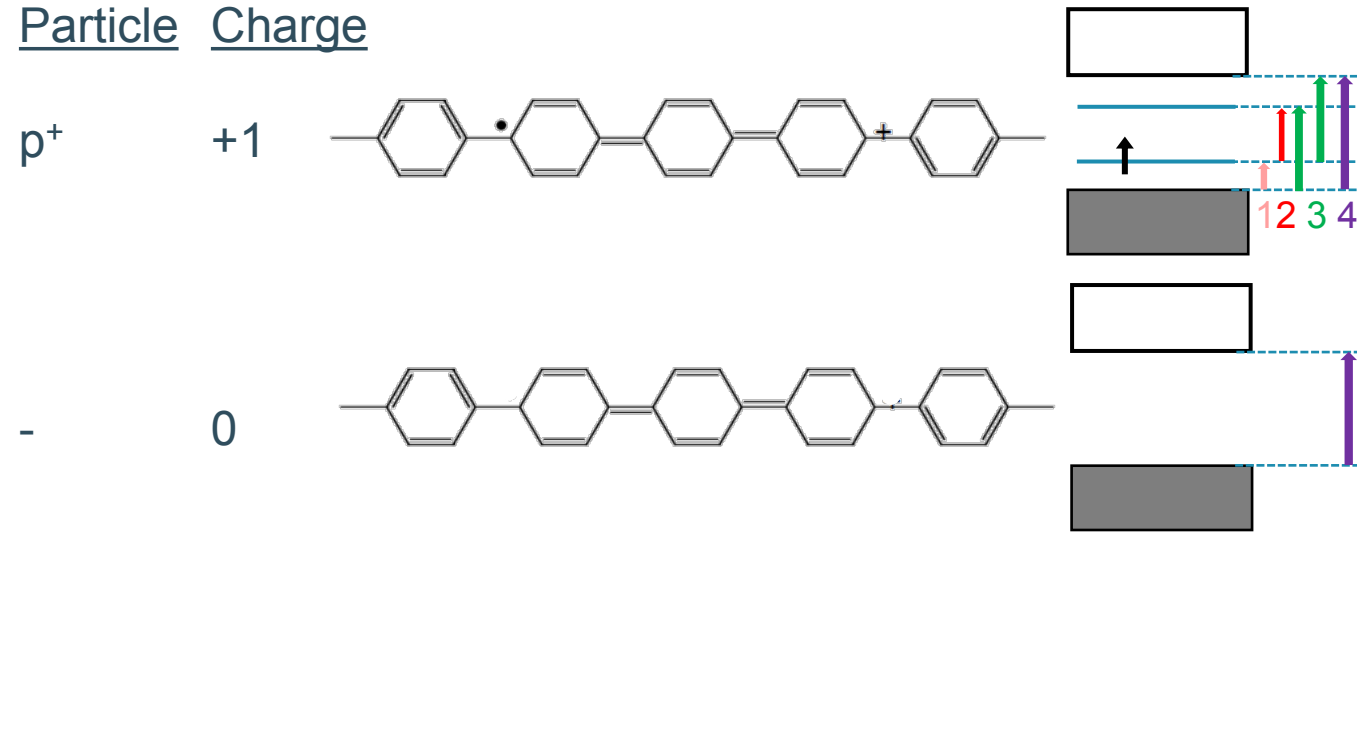
Edge-on Orientation



# Applications of organic electronic materials

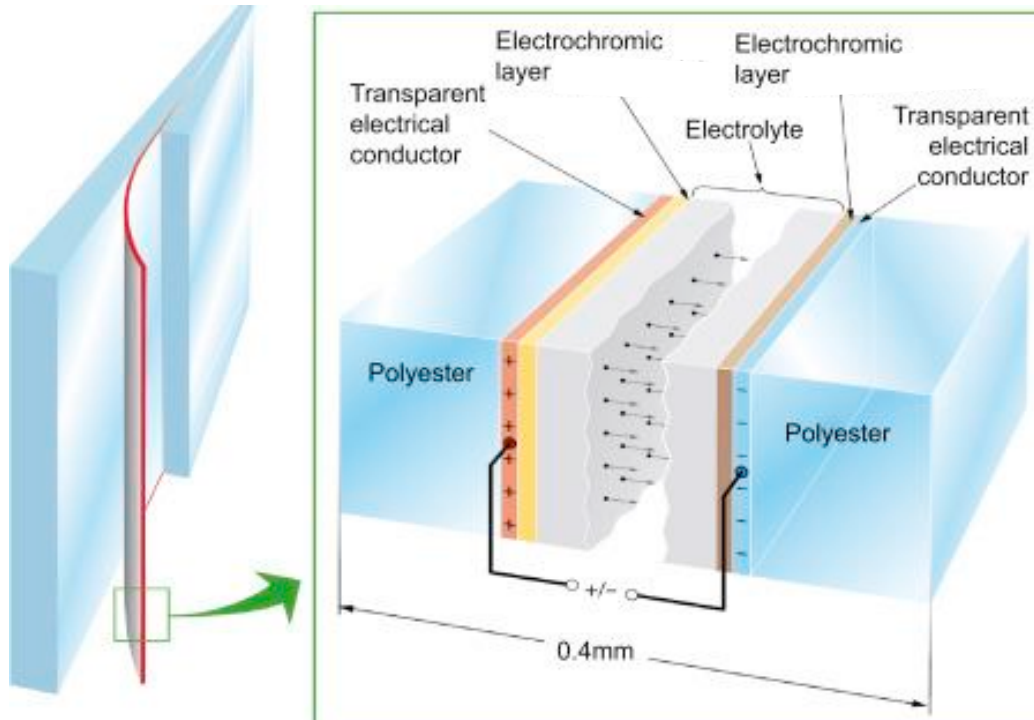
# Transport in organic electronic materials

- Electrochromic devices (ECs): Controlled doping of the material introduce visible light absorption by polarons

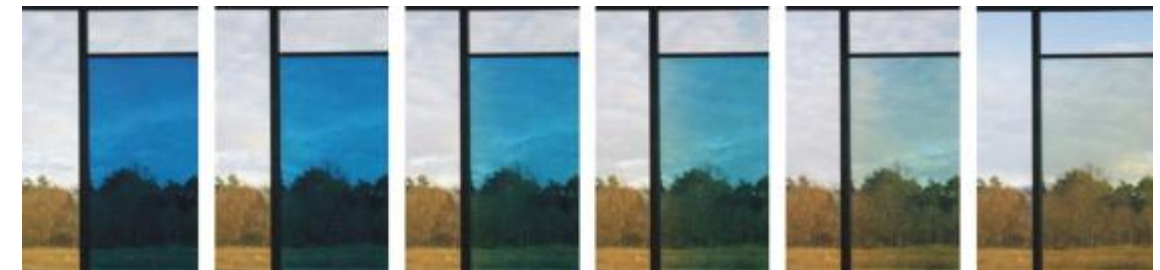


# Transport in organic electronic materials

- Electrochromic devices (ECs): More visible light absorption by polarons -> “darker glasses” activated electrically



<https://doi.org/10.1016/B978-0-12-811091-1.00008-2>

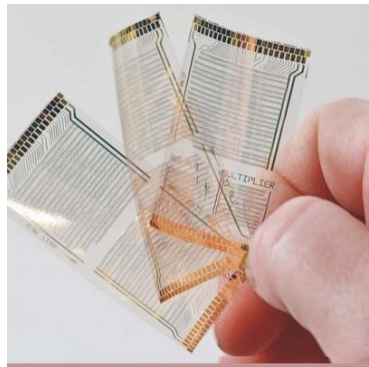


Gesimat, 2009, retrieved April 14, 2009

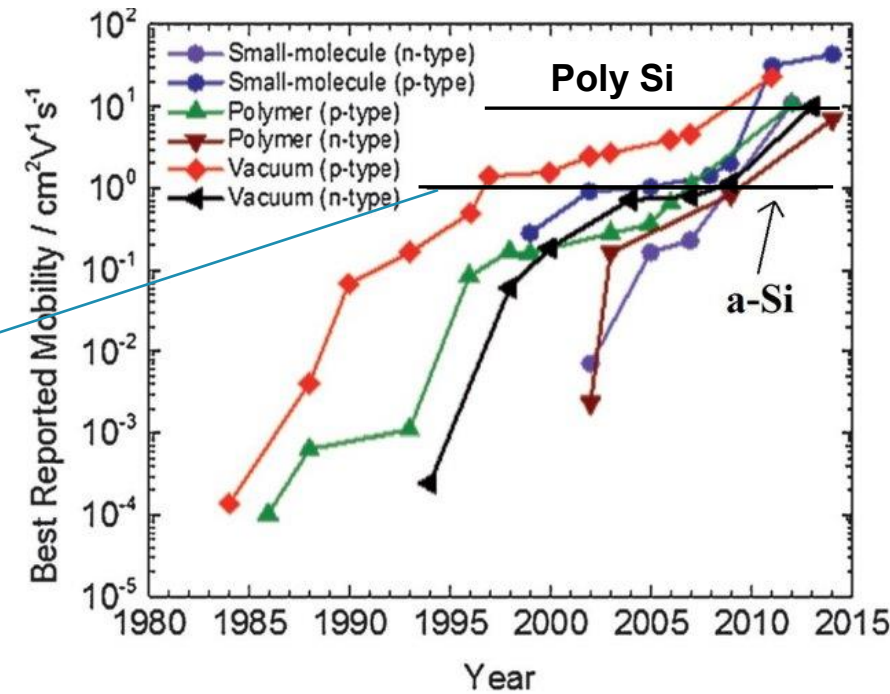
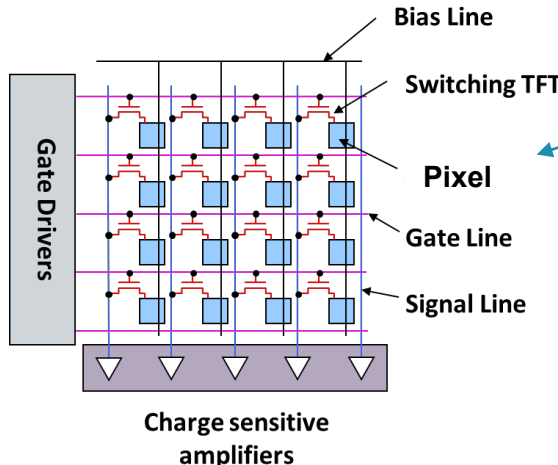
# Applications of organic electronic materials

- Organic field effect transistors (OFETs)
  - Historical evolution

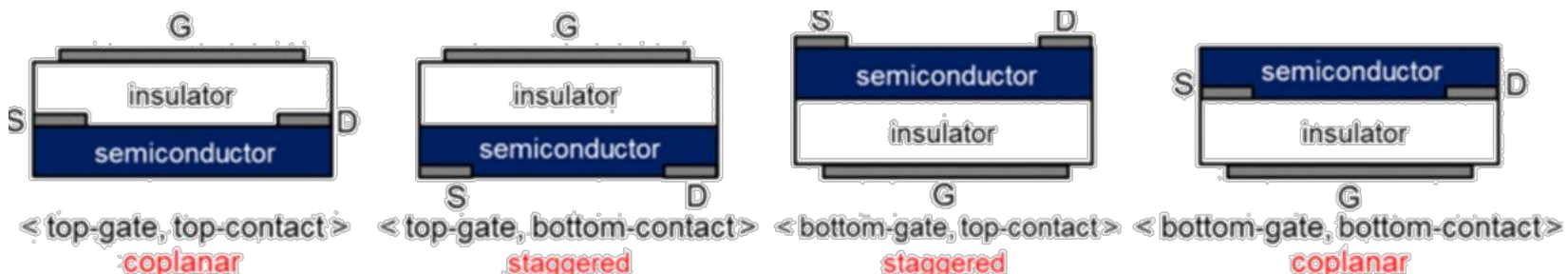
Active-matrix displays are possible with OFETs  
Frequency  $\propto \mu$



K. Myny, et al., *IEEE J. Solid State Circ.* 2012, **47**, 284.



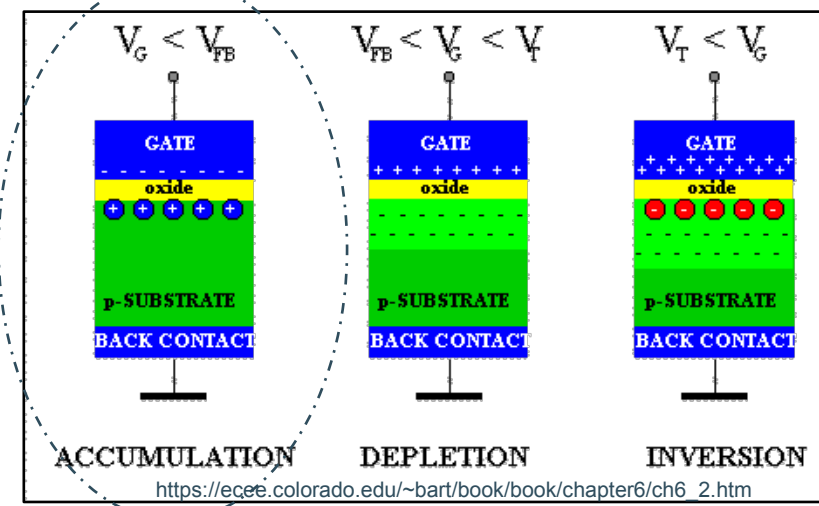
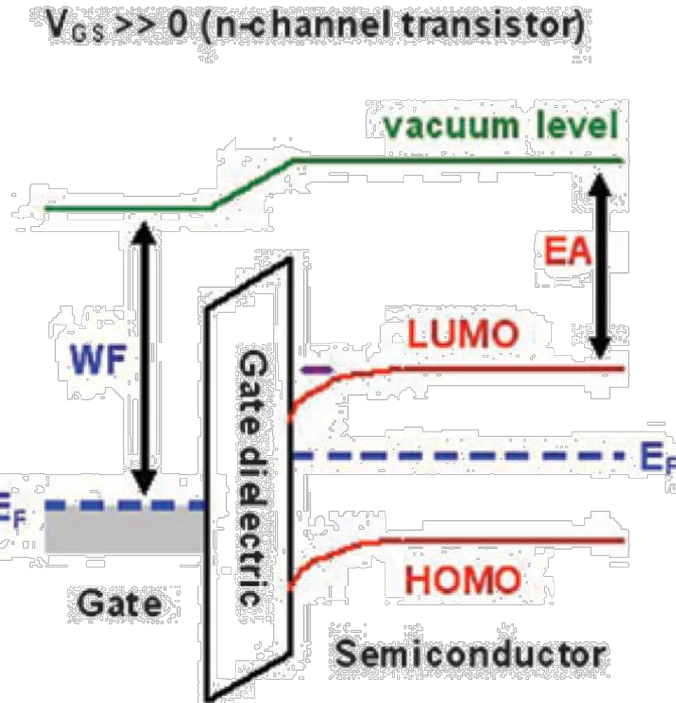
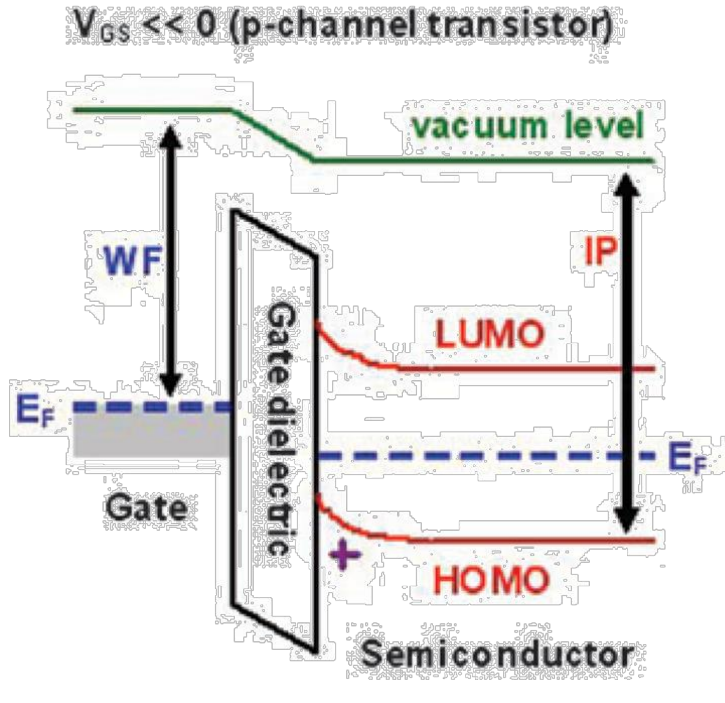
<https://doi.org/10.1002/cphc.201402757>



DOI: 10.1109/TED.2012.2226887

# Applications of organic electronic materials

- Organic field effect transistors (OFETs)
  - P-type vs n-type: contrary to inorganic FETs, OFETs work in accumulation bias regime.

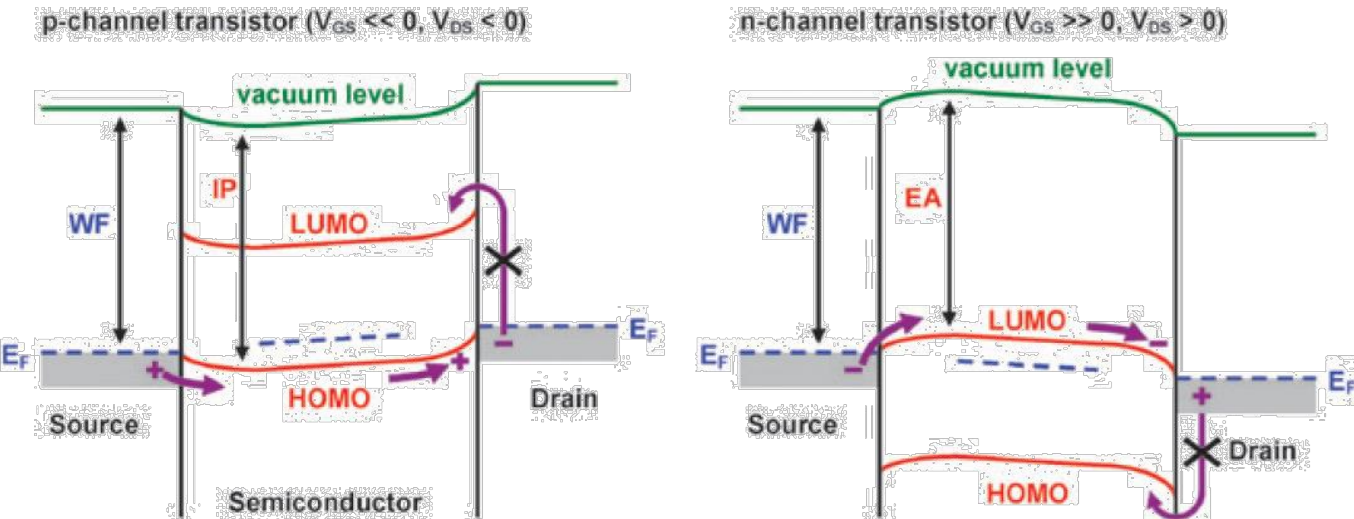


WF: Work function  
EA: Electron affinity  
IP: Ionization potential

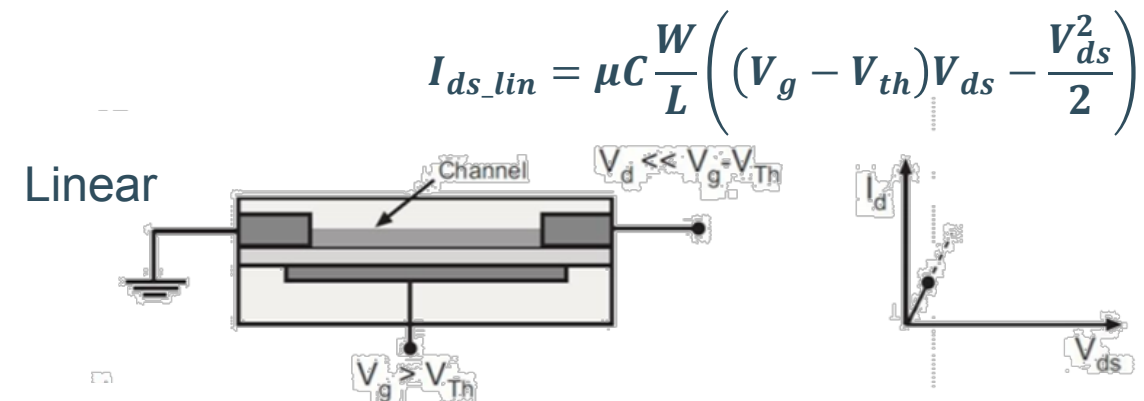
Chem. Soc. Rev., 2010, 39, 2643–2666

# Applications of organic electronic materials

- Organic field effect transistors (OFETs)
  - Operation regimes



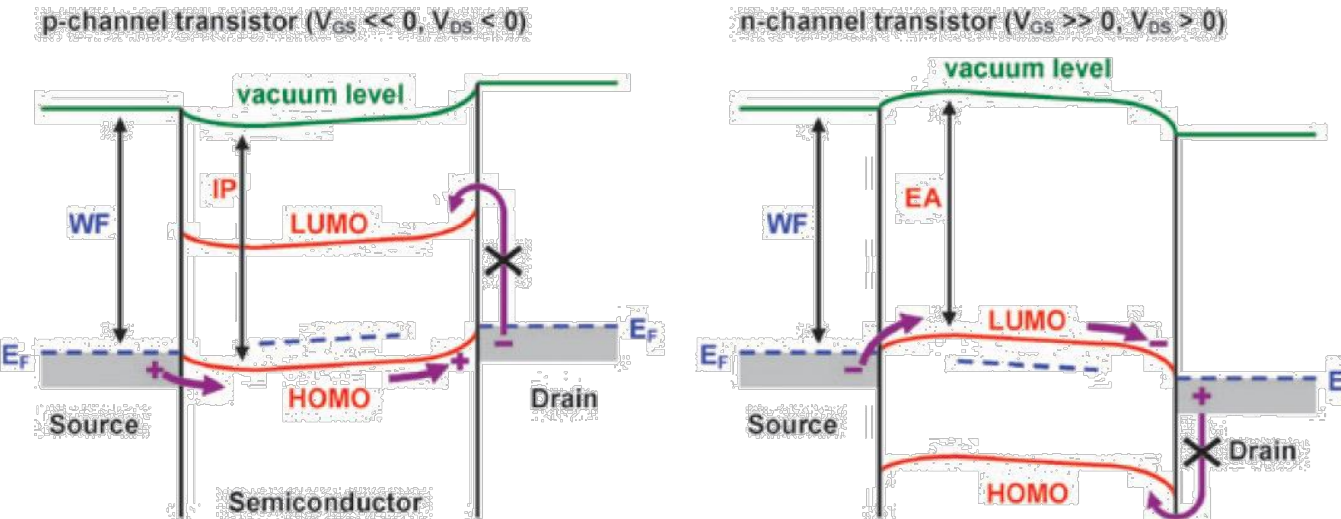
Chem. Soc. Rev., 2010, 39, 2643–2666



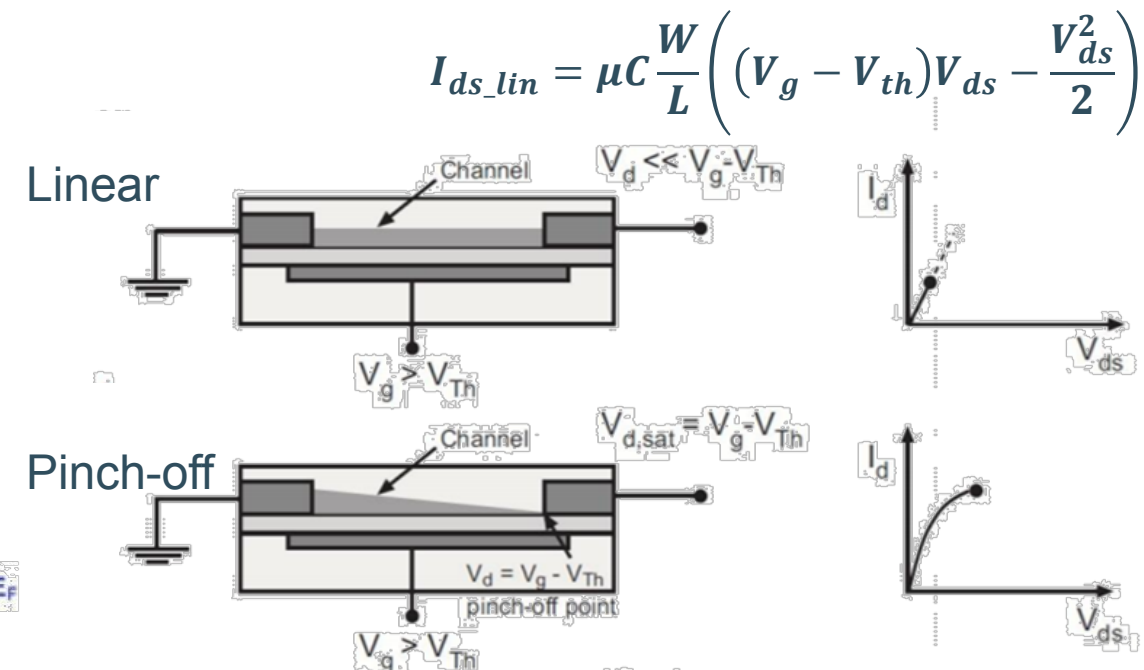
Unravelling Structure-Function Relationships in High Mobility  
Donor-Acceptor Co-Polymers, Thesis 2017, Monash University

# Applications of organic electronic materials

- Organic field effect transistors (OFETs)
  - Operation regimes



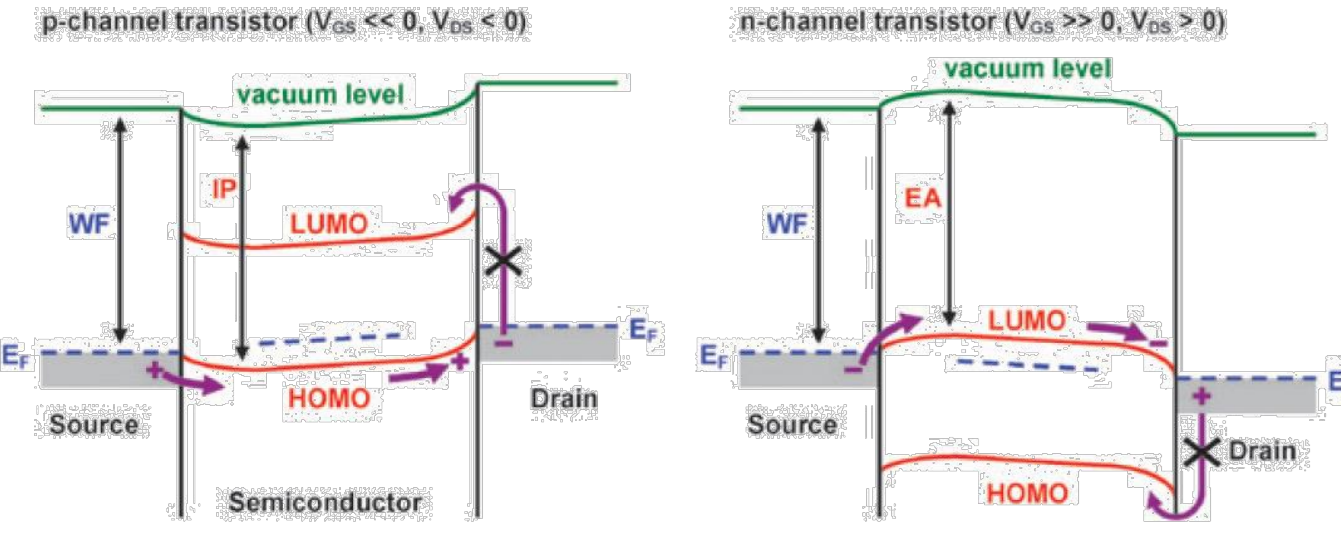
Chem. Soc. Rev., 2010, 39, 2643–2666



Unravelling Structure-Function Relationships in High Mobility  
Donor-Acceptor Co-Polymers, Thesis 2017, Monash University

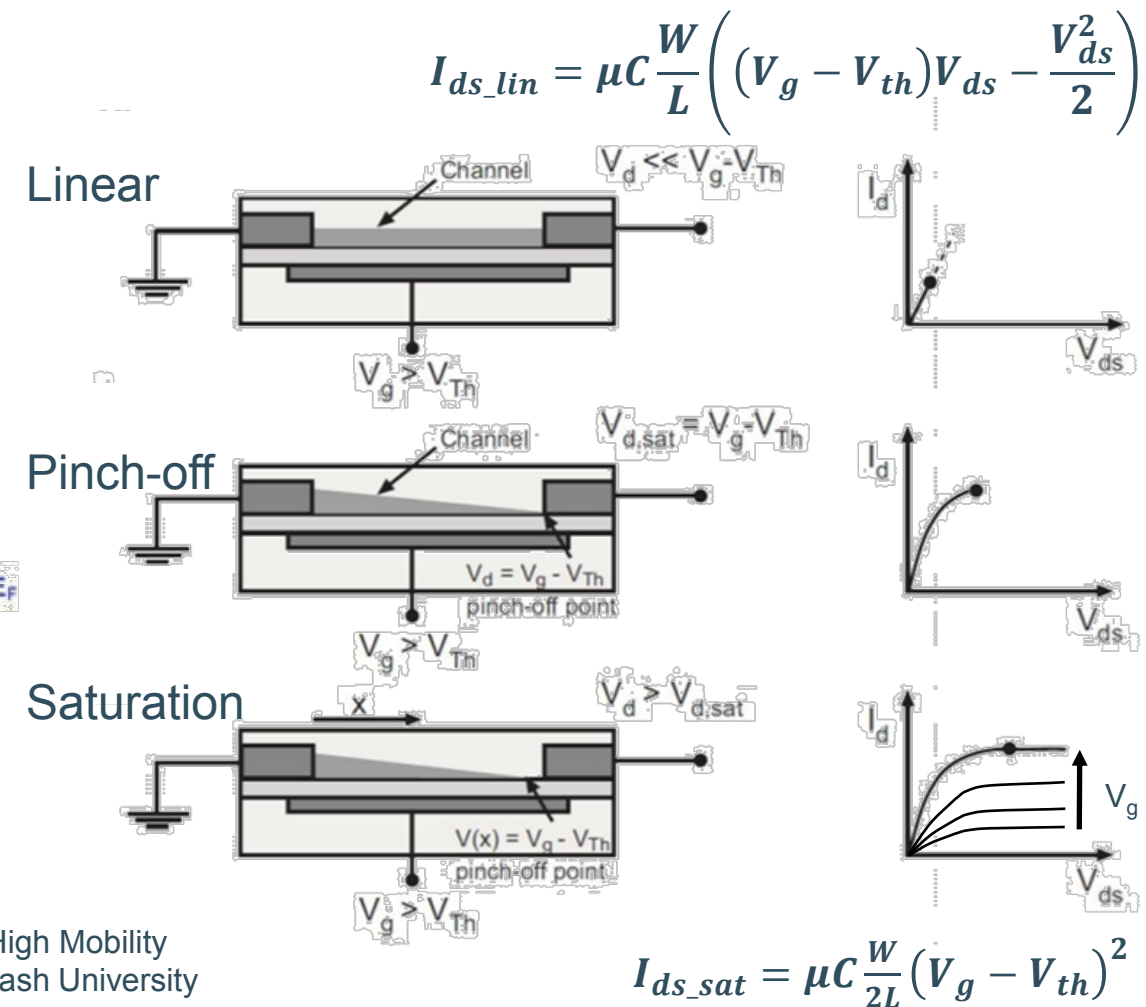
# Applications of organic electronic materials

- Organic field effect transistors (OFETs)
  - Operation regimes



Chem. Soc. Rev., 2010, 39, 2643–2666

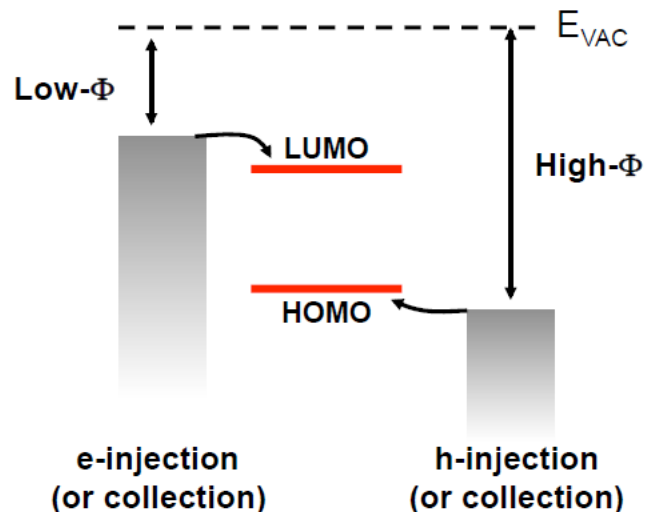
Unravelling Structure-Function Relationships in High Mobility  
Donor-Acceptor Co-Polymers, Thesis 2017, Monash University



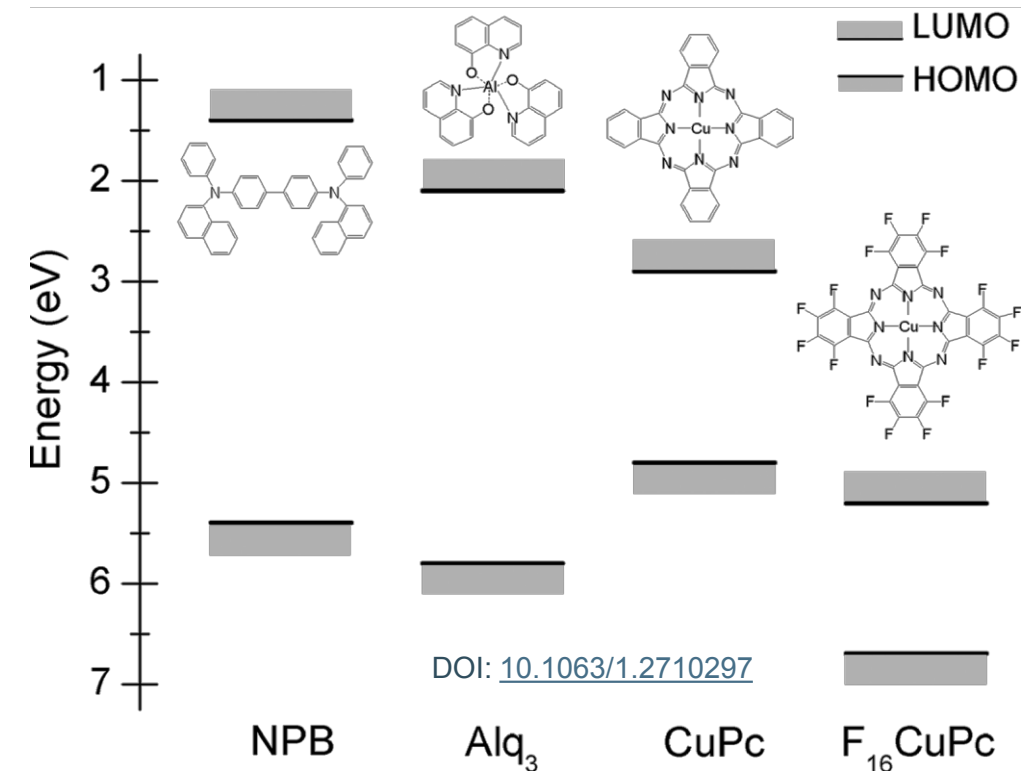
# Applications of organic electronic materials

- Organic field effect transistors (OFETs)
    - Contacts. Material is defined by the HOMO LUMO level to avoid energy barriers

<b>Element</b>	<b>Work function <math>\Phi</math></b>	<b>Char depe</b>
Cs	2.14	
K	2.30	
<b>Ba</b>	<b>2.70</b>	
Na	2.75	
<b>Ca</b>	<b>2.87</b>	
Li	2.90	
Mg	3.66	
In	4.12	
Ag	4.26	
Al	4.28	
Nb	4.30	
Cr	4.50	
Cu	4.65	
Si	4.85	
Au	5.10	
Pt	5.60	



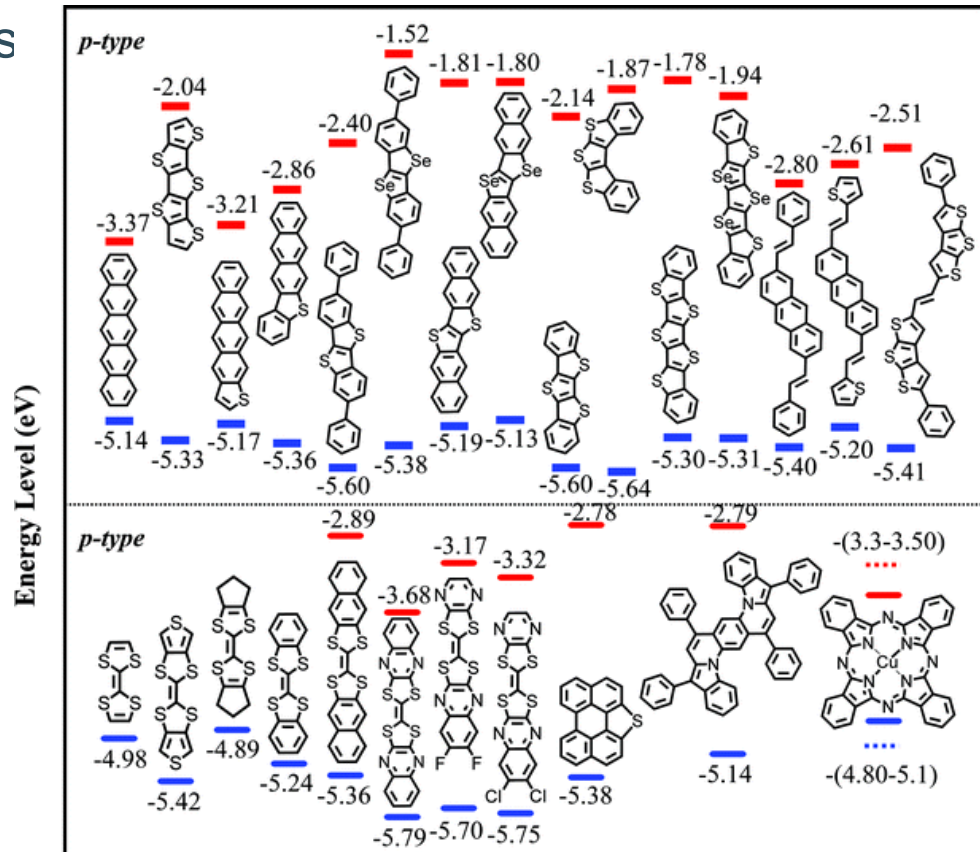
**Charge injection or collection in all devices depends on the relative band alignment of the semiconductor and the electrode materials**



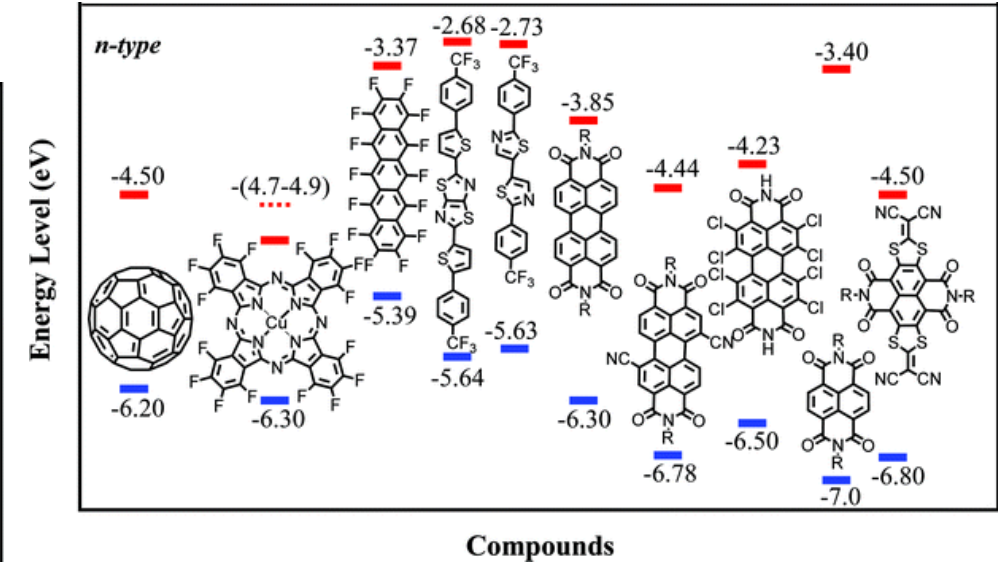
# Applications of organic electronic materials

- Organic field effect transistors (OFETs)

- Contacts



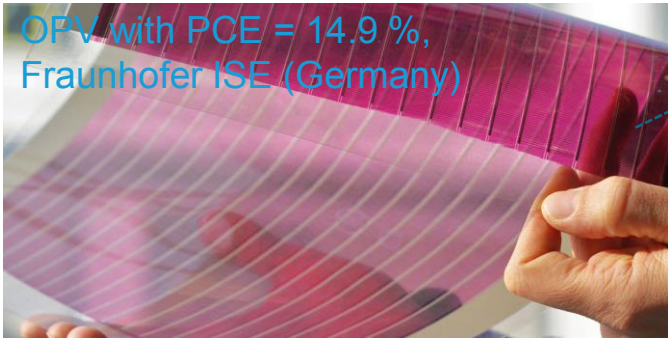
DOI: 10.1039/c0cc00947d



There are not so many good-performing n-type materials that aligned well with stable metals -> **Most OFETs performing well are p-type!**

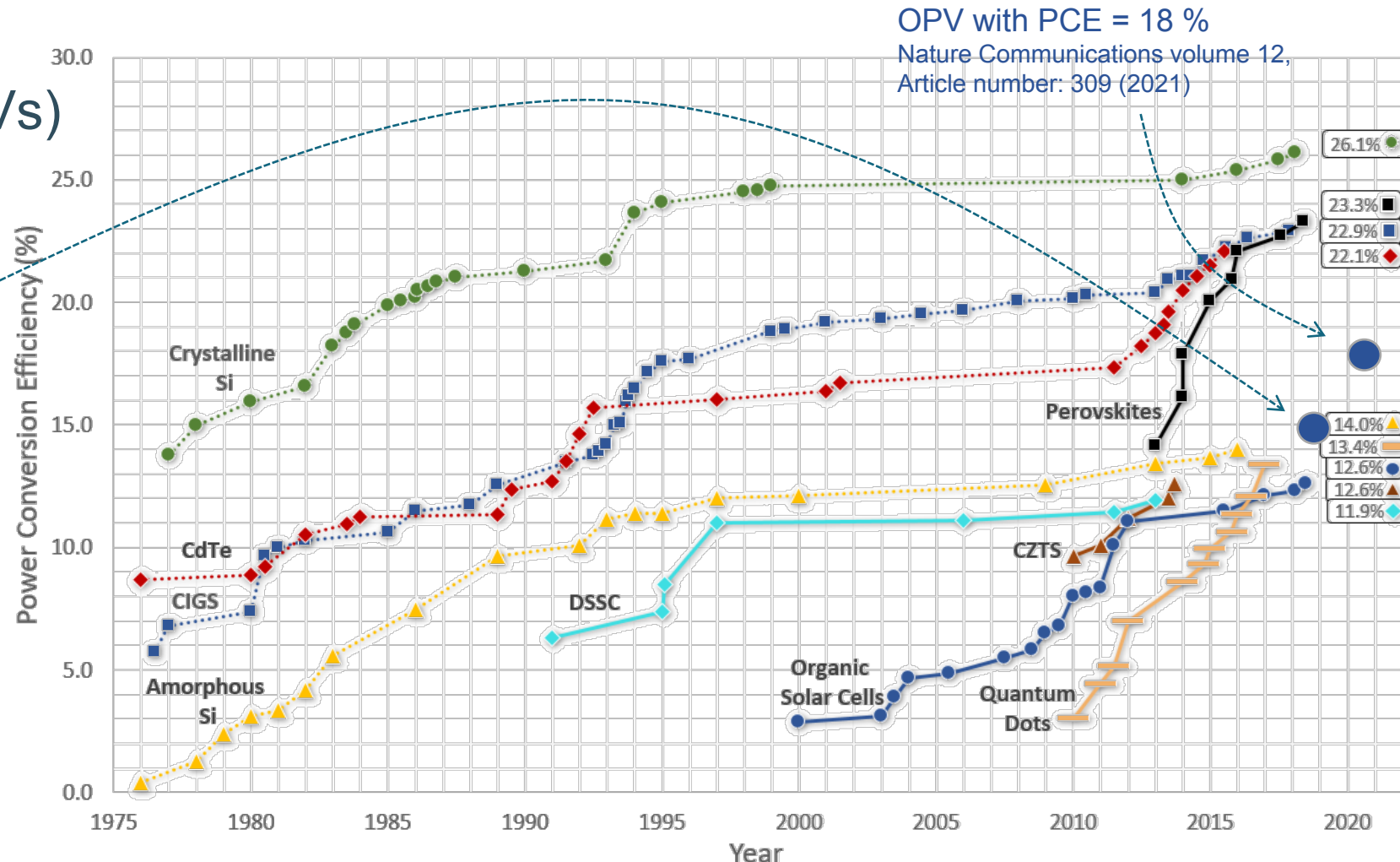
# Applications of organic electronic materials

- Organic solar cells (OPVs)
  - Historical evolution



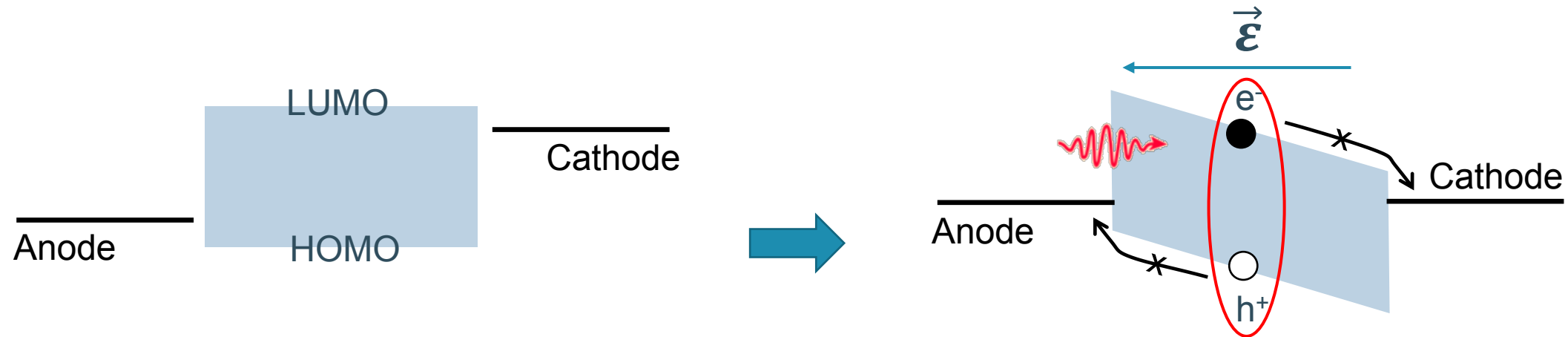
A fair comparison for all scenarios?

- Cells are rated at 1 sun, normal incidence and 25 °C.
- OPV holds performance better than Si at **low light and low angles** (opportunity indoors)
- OPVs performance degrades less than Si performance at **high temperature**



# Applications of organic electronic materials

- Organic solar cells (OPVs): They convert optical energy into electrical energy



**Exciton:** quasi particle composed of a bound electron-hole pair

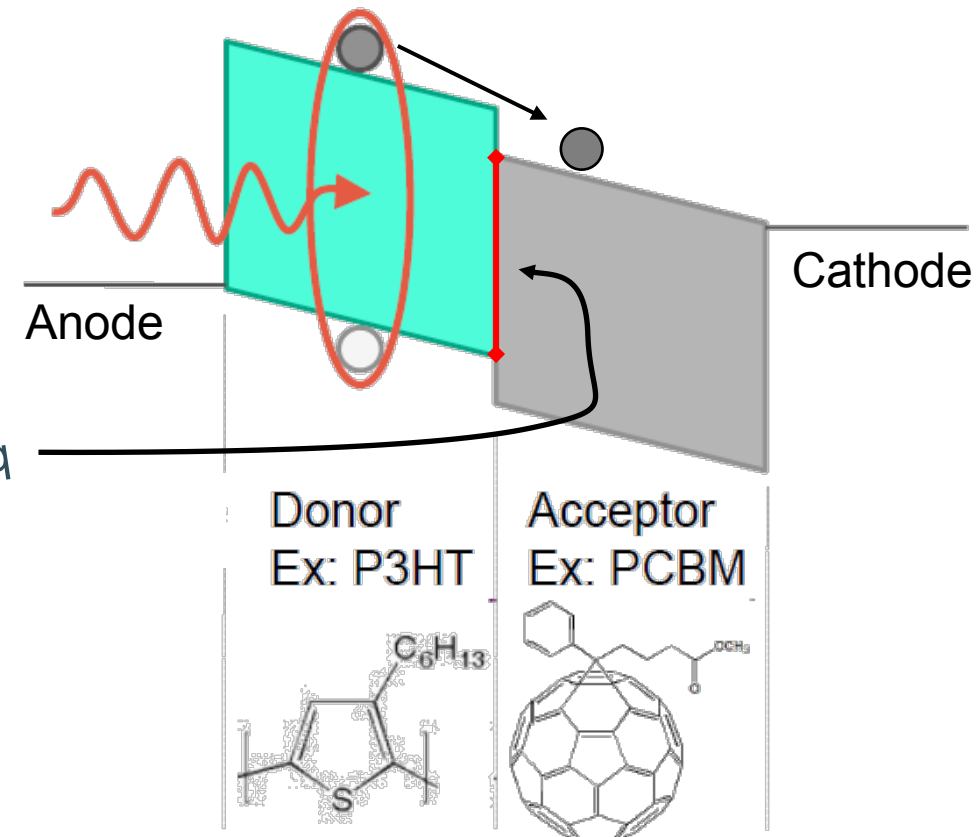
The exciton binding energy in inorganic semiconductors is only  $\sim$  meV, but in organic is up to 0.5 eV. The exciton does not split and the charges don't get collected at the electrodes.

A donor/acceptor heterojunction is needed to provide the internal electrochemical driving force for exciton dissociation.

# Applications of organic electronic materials

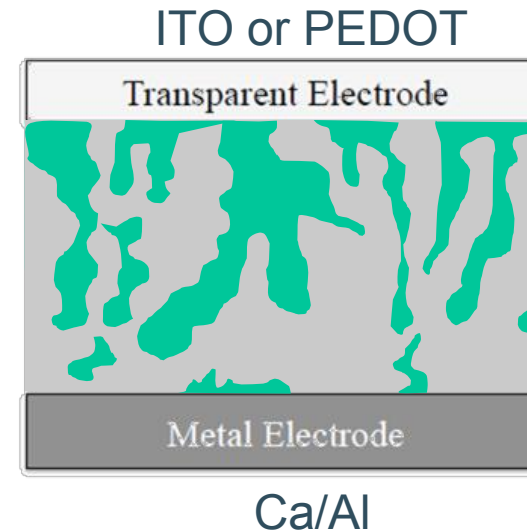
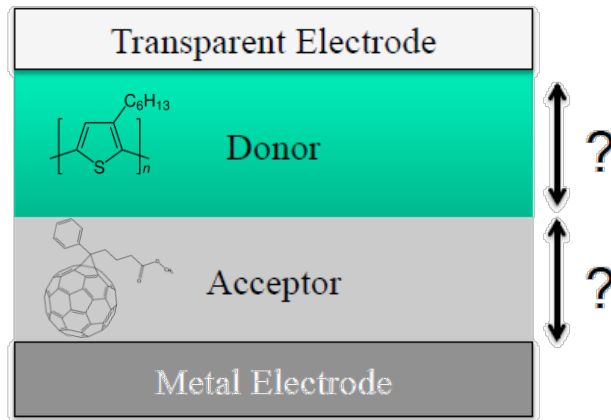
- Organic solar cells (OPVs): Structure
  1. Light absorption
  2. Exciton formation
  3. Exciton splitting
  4. Charge extraction

$$V_{\text{out, max}} \sim (E_{\text{LUMO, acceptor}} - E_{\text{HOMO, donor}})/q$$



# Applications of organic electronic materials

- Organic solar cells (OPVs): Structure

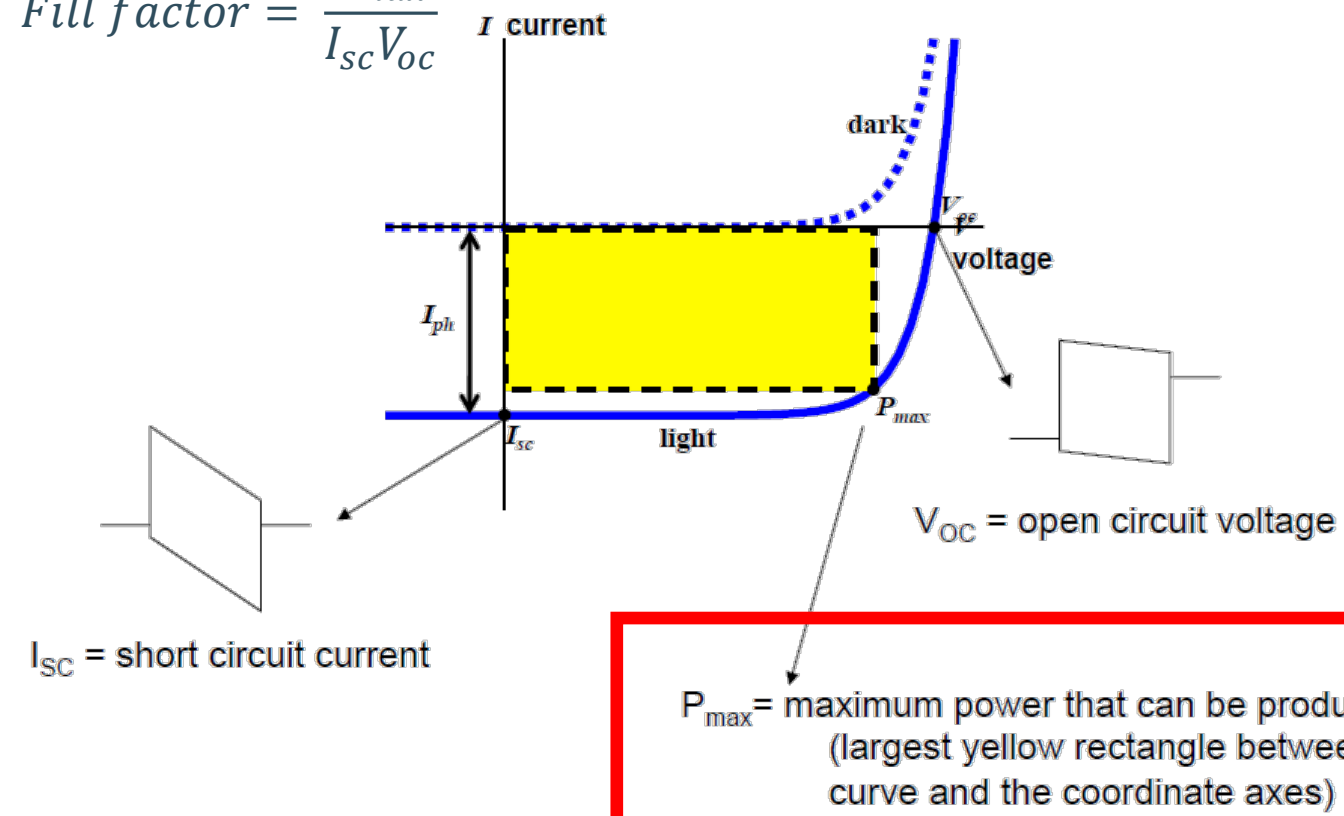


- The thickness of the material should be at least 100 nm to absorb most of the light
- However, the exciton mean free path (before recombination) is only 10 nm
- It is necessary to split the exciton (reach a D/A interface) before it recombines!  
-> Bulk heterojunction morphology: allow thick layers with many interfaces everywhere

# Applications of organic electronic materials

- Organic solar cells (OPVs): Performance

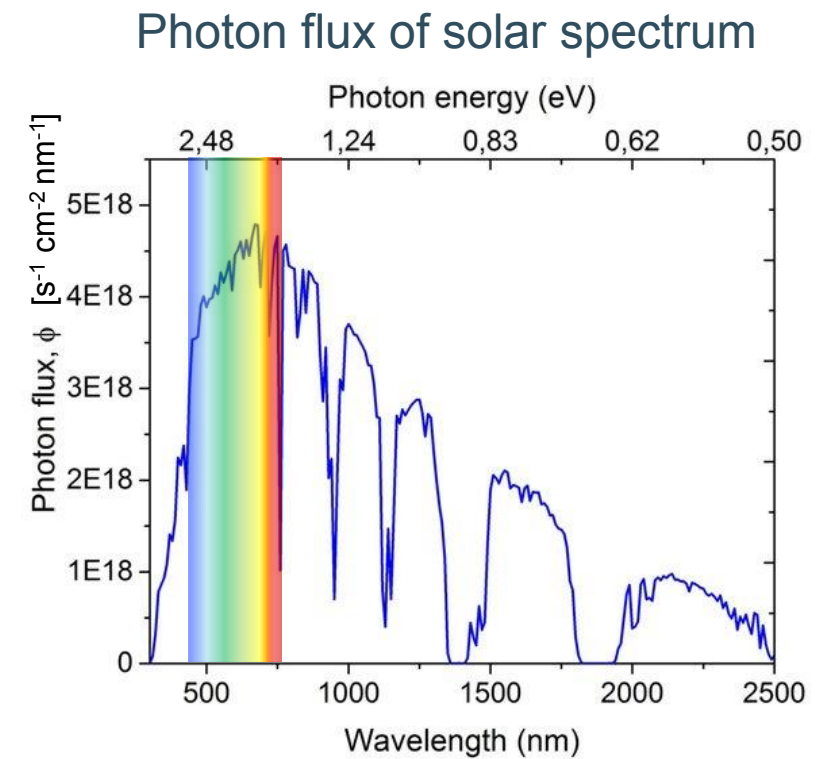
$$\text{Fill factor} = \frac{P_{max}}{I_{sc}V_{oc}}$$



# Applications of organic electronic materials

- Organic solar cells (OPVs): Efficiency
  - Internal quantum efficiency (IQE)  
(Photons ABSORBED / electrons out)
  - External quantum efficiency (EQE)  
(Rate of photons arriving to the device / rate of electrons out)  
Or incident photon to converted electron (IPCE)
- $J_{sc} = q \int EQE(\lambda) PhotonFlux(\lambda) d\lambda$
- IQE & EQI <1, IQE>EQI
- Power conversion efficiency (PCE)

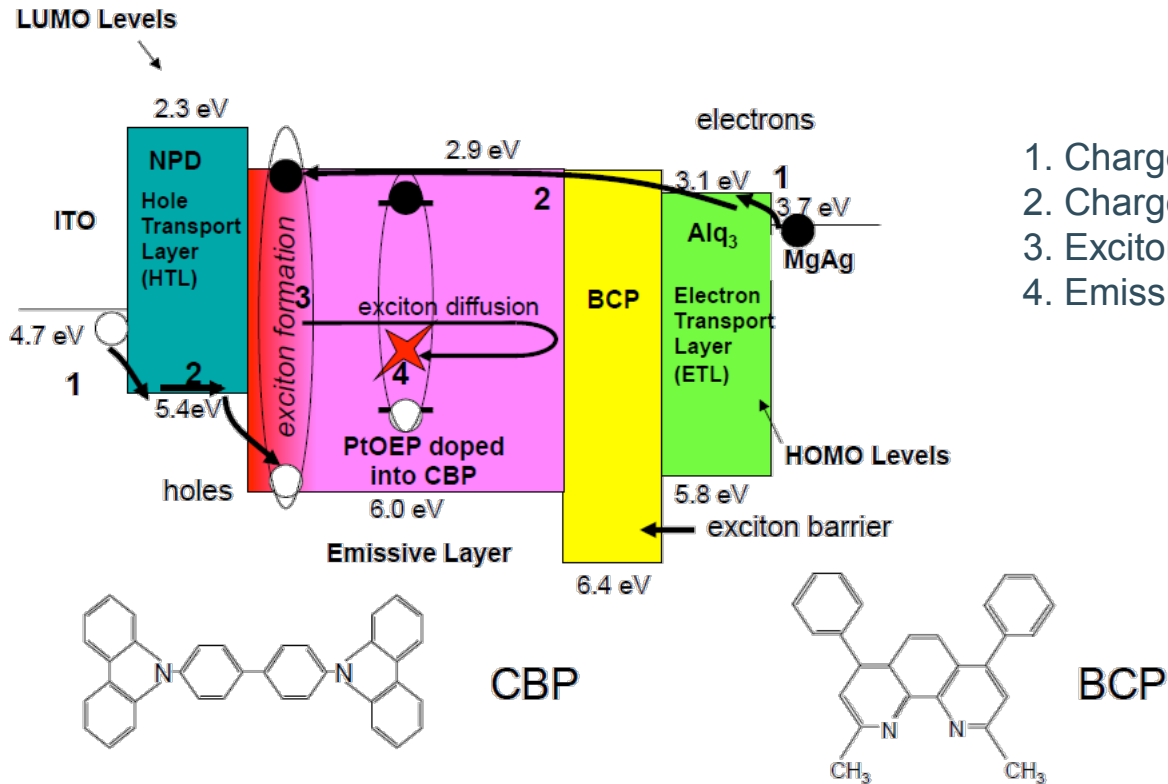
$$PCE = \frac{\text{Electrical power generated}}{\text{Incident optical power}} = \frac{P_{max}}{P_{in}}$$



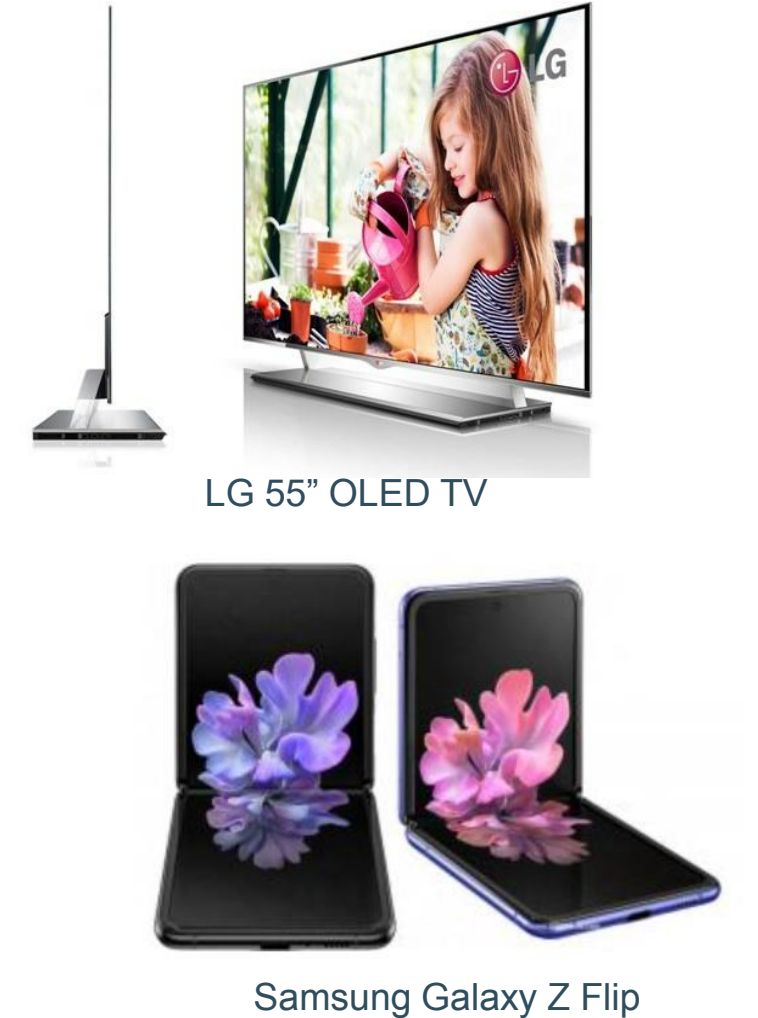
DOI: [10.13140/RG.2.2.33851.67364](https://doi.org/10.13140/RG.2.2.33851.67364)

# Applications of organic electronic materials

- Organic light emitting diodes (OLEDs)
  - The most successful case of organic electronics



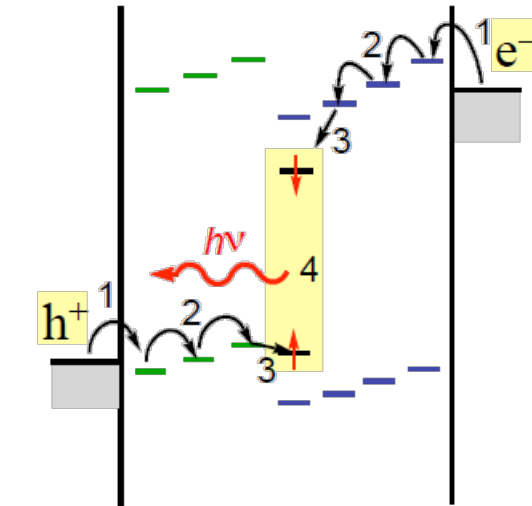
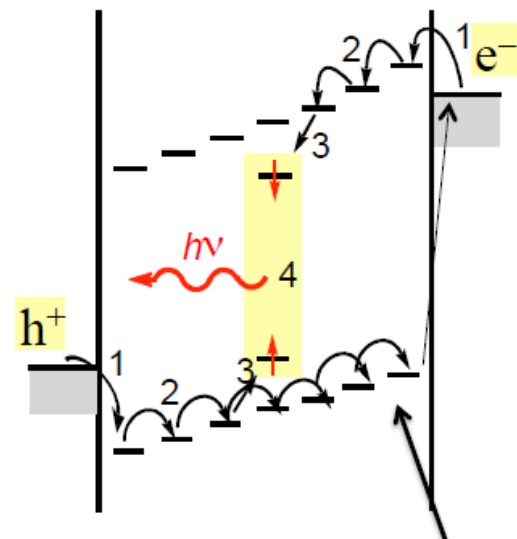
1. Charge injection
2. Charge transport
3. Exciton formation and diffusion
4. Emission



# Applications of organic electronic materials

- Organic light emitting diodes (OLEDs)
  - Structure: Multilayer

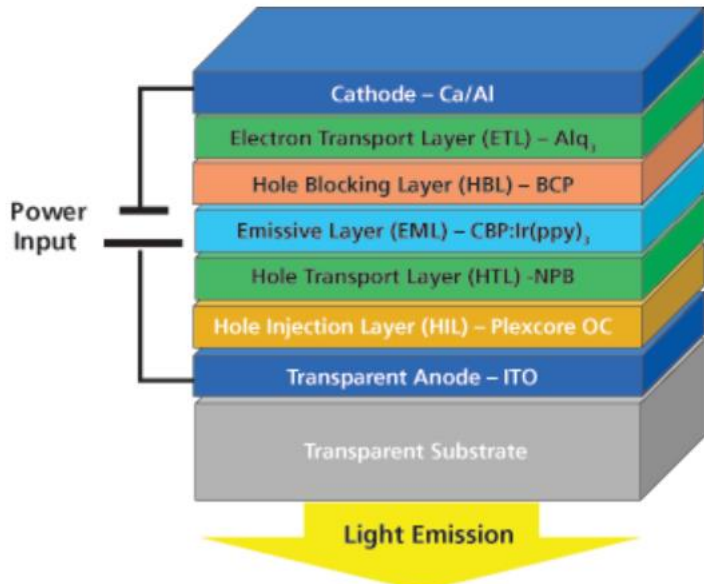
Multimaterial allows tuning charge transport balance



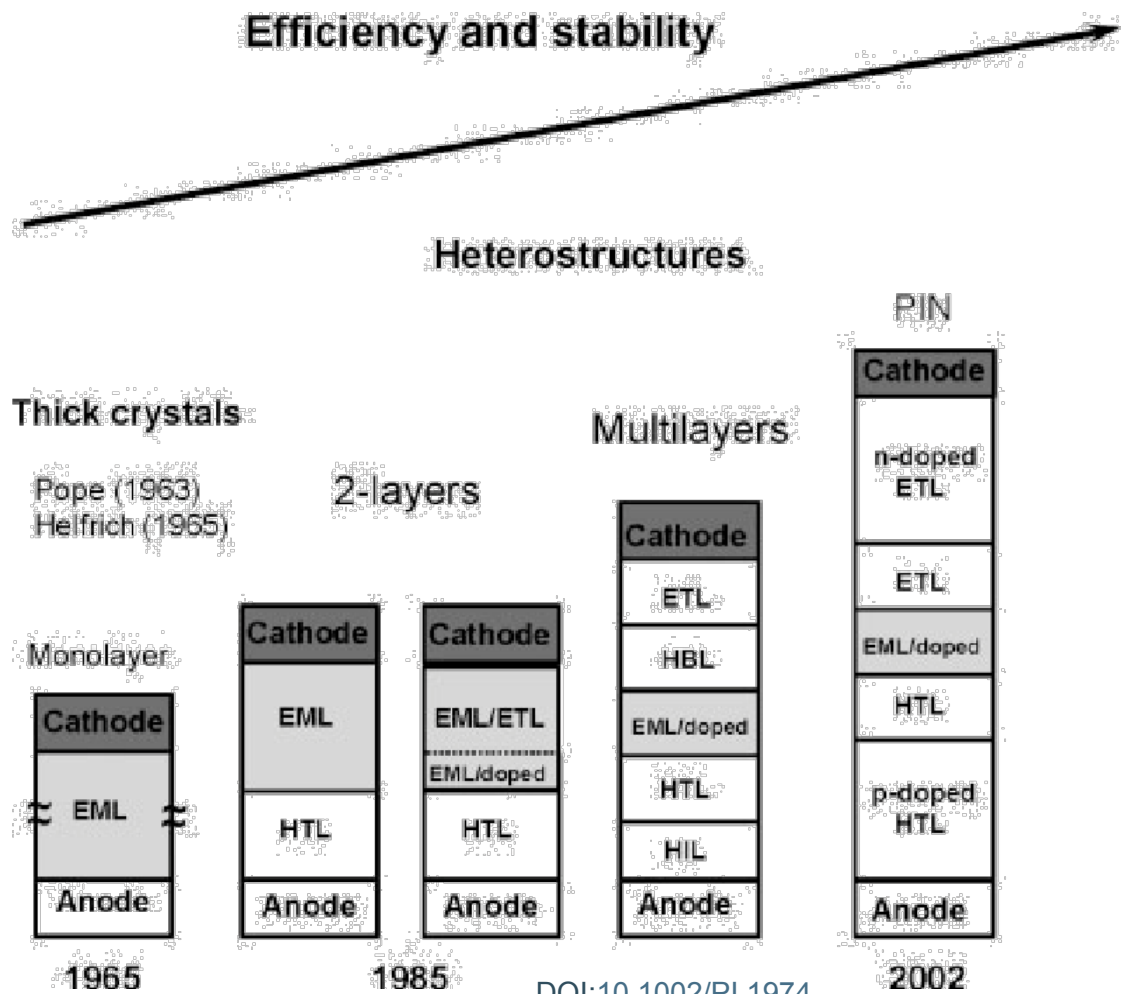
One layer makes it difficult to have balanced charge transport needed for high efficiency, specially considering the different mobility of  $h^+$  and  $e^-$  (hole mobility is larger than electron mobility in organics)

# Applications of organic electronic materials

- Organic light emitting diodes (OLEDs)
  - Structure: Multilayer



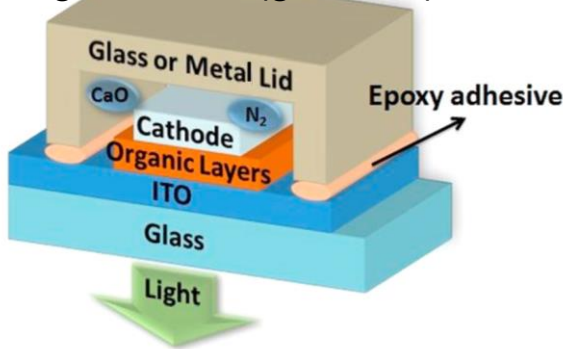
<https://www.sigmaaldrich.com/technical-documents/articles/materials-science/organic-electronics/plexcore-organic-conductive-inks.html>



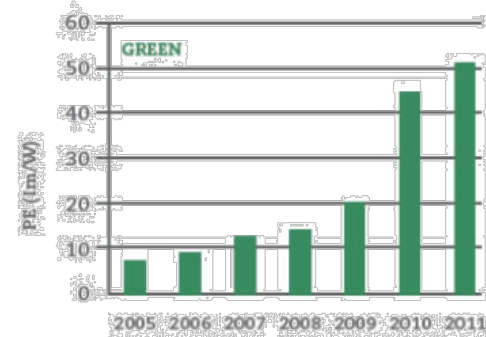
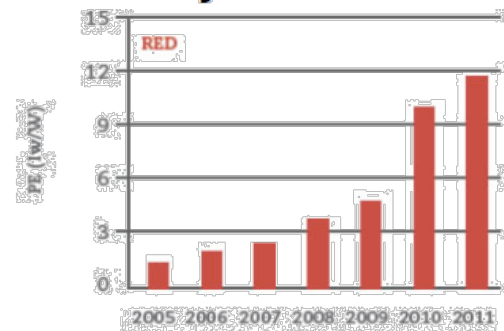
# Applications of organic electronic materials

- Organic light emitting diodes (OLEDs)
  - Problem of stability solved though material design and encapsulation

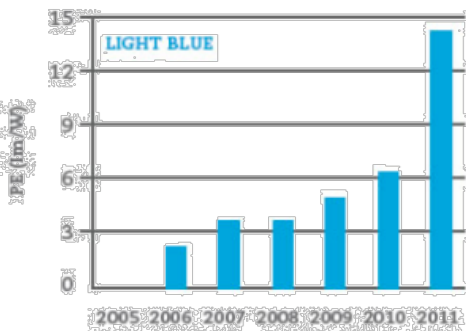
Encapsulation rigid device (glass lid)



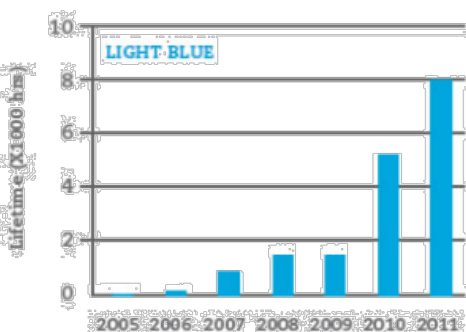
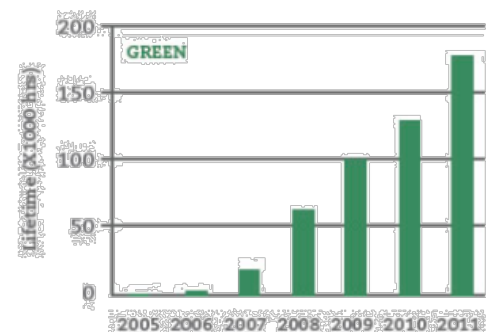
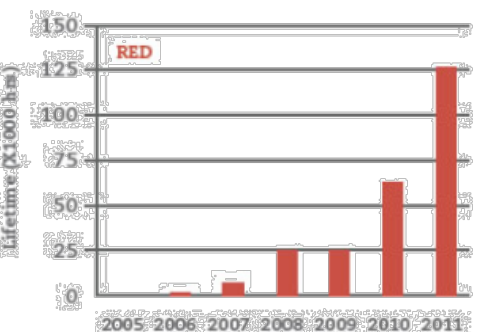
## Efficiency:



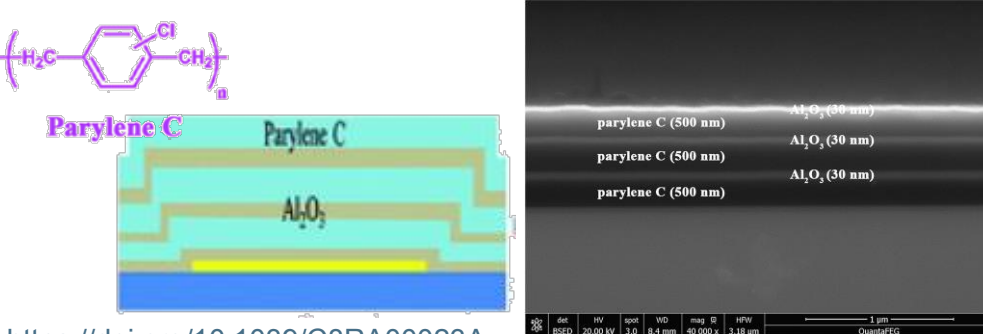
<https://www.oled-info.com/udc-pholed-material-performance-update-green-now-reaches-14-million-hours>



## Lifetime:



Encapsulation flexible device (multilayer think film)



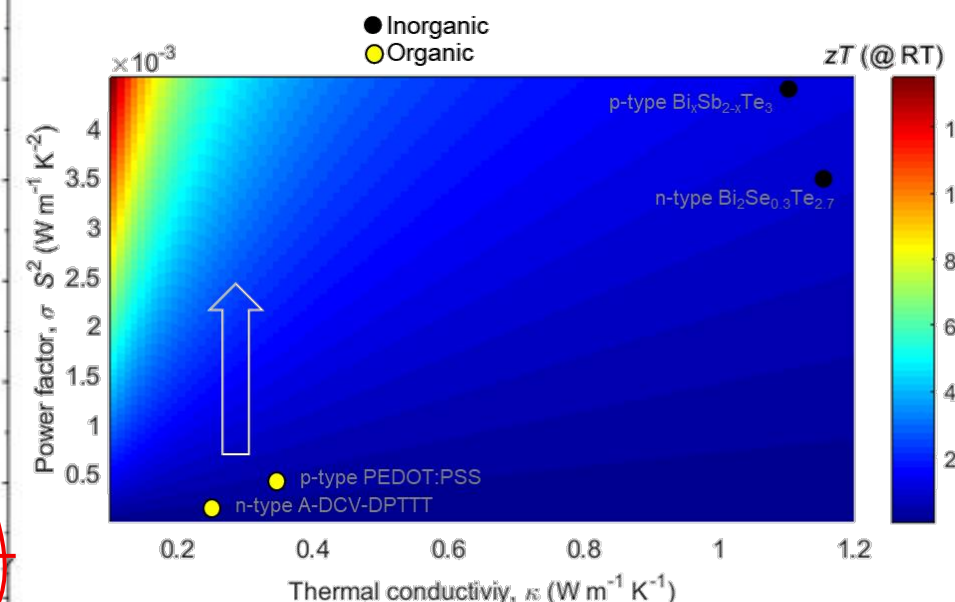
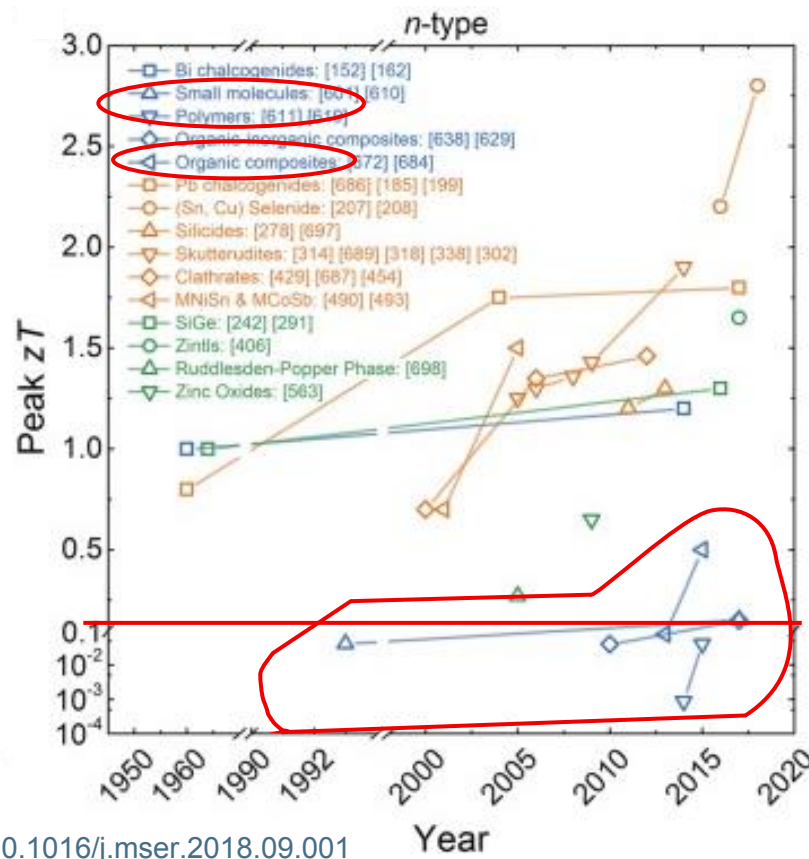
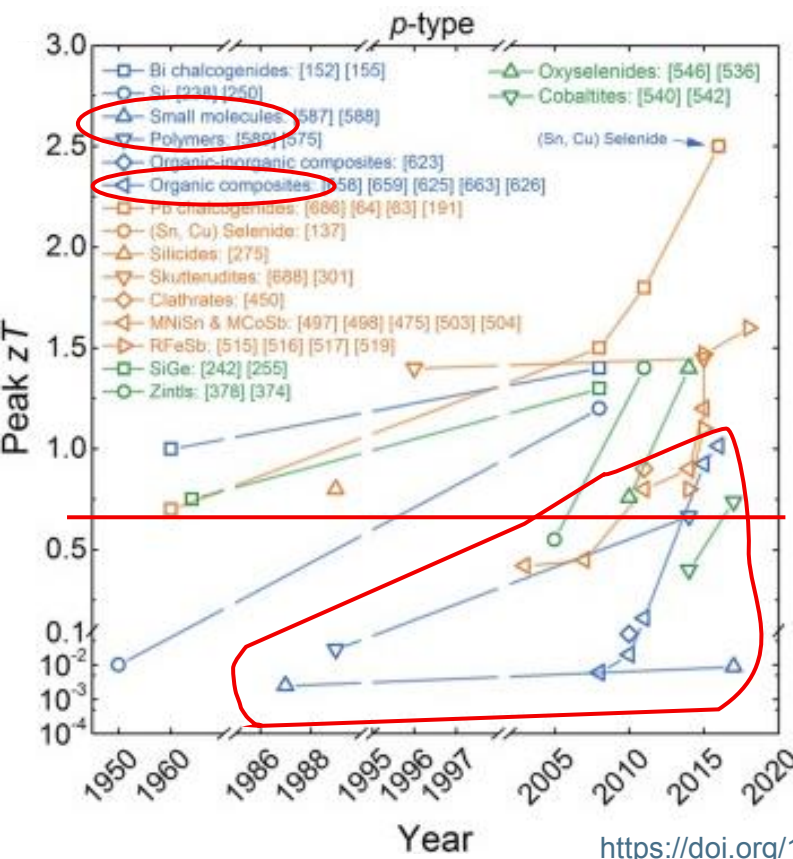
<https://doi.org/10.1039/C8RA00023A>

# Applications of organic electronic materials

- Organic light emitting diodes (OLEDs)
  - Why?
    - Compared to competing LCD technologies, OLEDs emit light and does not require backlight. It allows thinner devices.
    - Deep black is possible -> unparalleled  $10^6$  : 1 contrast because the device totally switches off. That permits also low power consumption (paramount for portable devices relying on a battery).
    - More vivid colors, better view at large angles.
    - AMOLED (active matrix organic LED) makes up 15% of mobile device displays in 2016 (LG, Samsung, etc.).

# Applications of organic electronic materials

- Organic thermoelectrics (OTEs): transform heat into electrical energy
  - Historical evolution



# Applications of organic electronic materials

- Organic thermoelectrics (OTEs):

- Efficiency:

Carnot efficiency

$$\eta = \frac{\Delta T}{T_{hot}} \frac{\sqrt{1 + zT_{avg}} - 1}{\sqrt{1 + zT_{avg}} + \frac{T_{cold}}{T_{hot}}} ;$$

- Figure of merit

Power factor

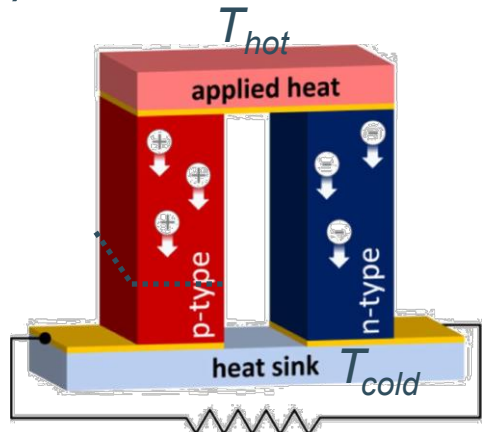
$$zT = \frac{S^2 \sigma T}{\kappa} ;$$

$S$  = Seebeck coefficient [ $\mu\text{V K}^{-1}$ ];

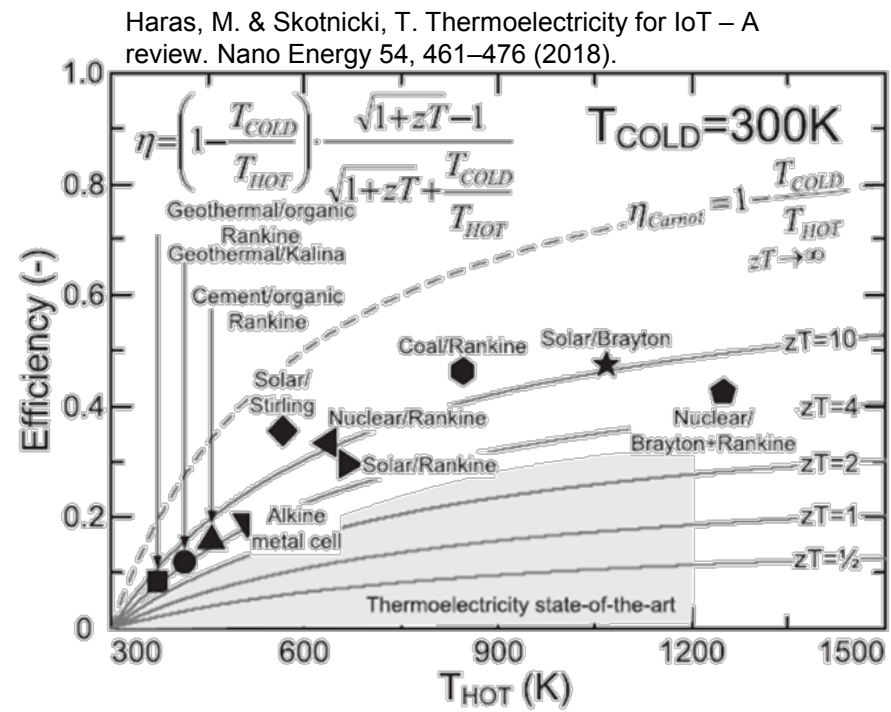
$\sigma$  = Electrical conductivity [ $\text{S cm}^{-1}$ ];

$\kappa = \kappa^{el} + \kappa^{ph}$  = thermal conduct. [ $\text{W m}^{-1} \text{K}^{-1}$ ];

$T$  = absolute temperature [K]



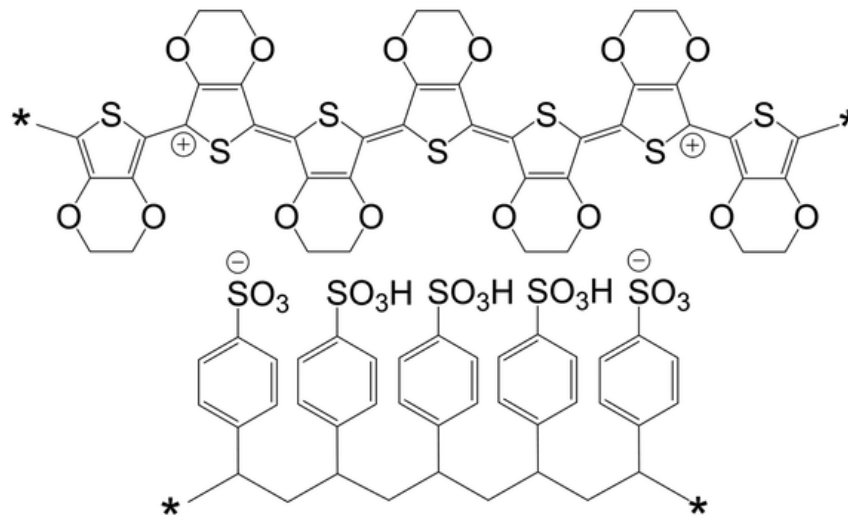
L. Cowen et al., ECS Journal of Solid State Science and Technology, 6 (3), 2017



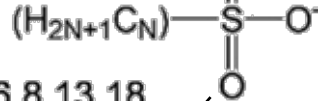
# Applications of organic electronic materials

- Organic thermoelectrics (OTEs): PEDOT and the importance of doping
  - PEDOT-derived polymers are so far **the most performing (p-type) organic thermoelectric materials**. PEDOT is doped during synthesis and the doping is stabilized by PSS.
  - They can be treated with small polar molecules (secondary dopants, SD) to improve morphology and performance.

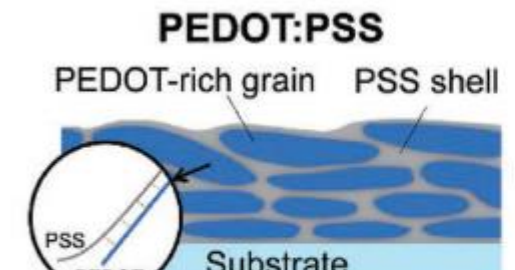
PEDOT:PSS



Sodium alkyl sulfonates

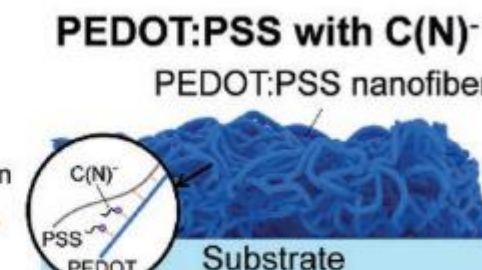


$N=1,3,6,8,13,18$



Pancake-like morphology

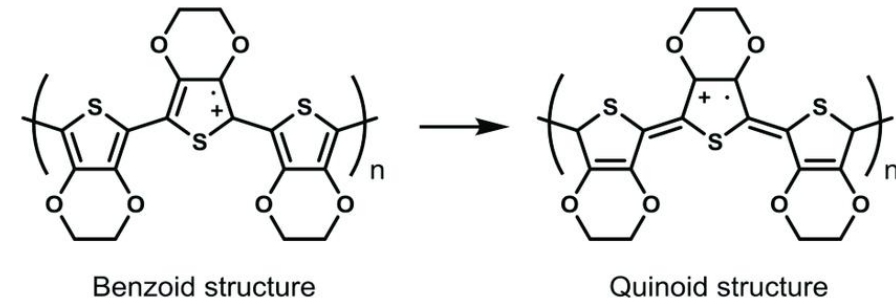
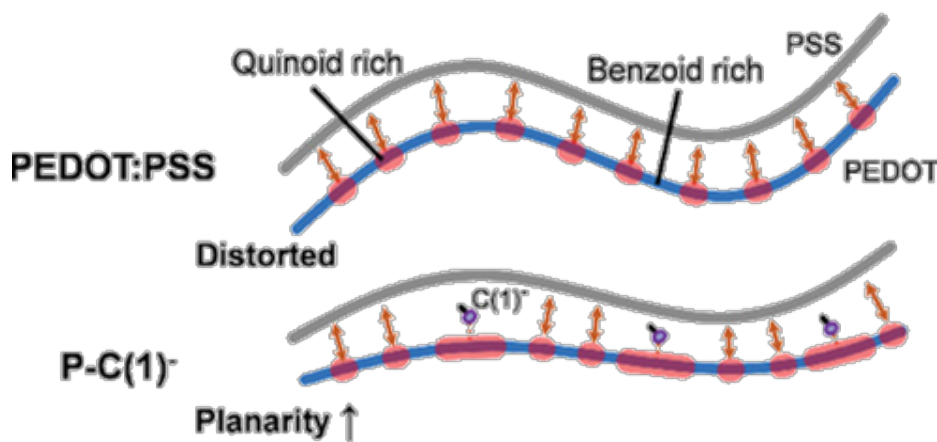
$C(N)^-$  addition



Nanofibrous morphology

# Applications of organic electronic materials

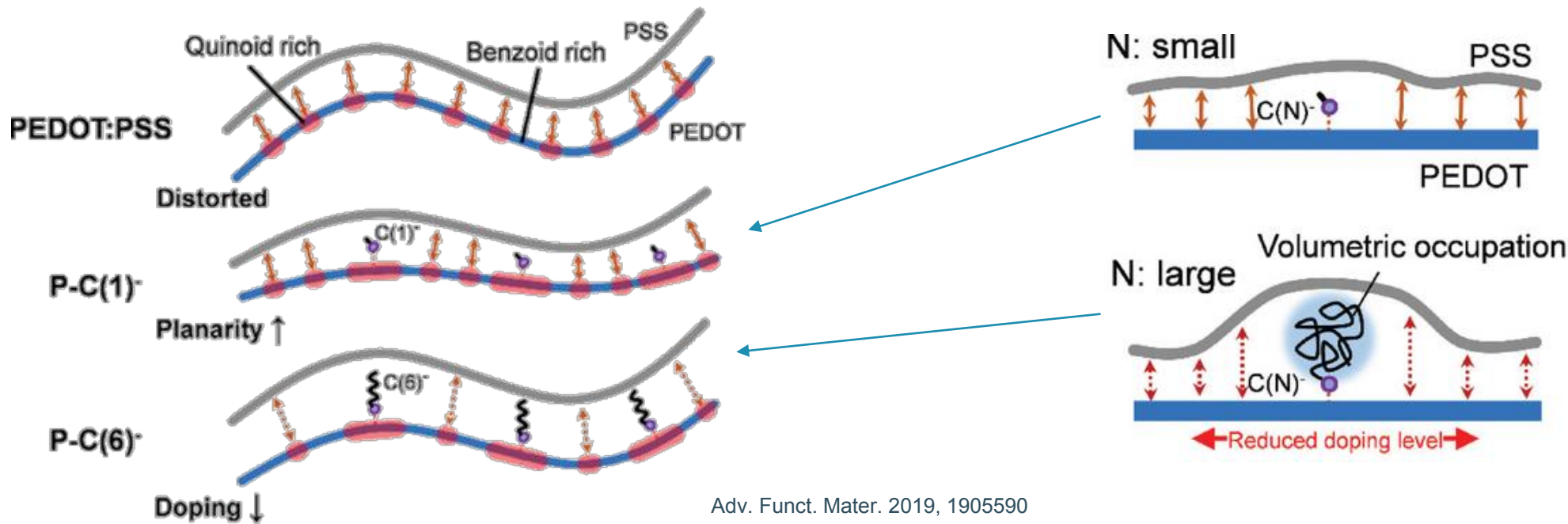
- Organic thermoelectrics (OTEs): PEDOT and the importance of doping
  - Effect of the SD on morphology and transport: SD compete with PSS for the binding sites. If the SD molecule is small, it will induce more quinoid segments in the PEDOT chains than PSS without significant dedoping.
  - Quinoid segments are more rigid and planar, promoting better  $\pi$ - $\pi$  stacking. This can be observed in GIWAXS (see next slides).



Funct. Mater. 2019, 1905590

# Applications of organic electronic materials

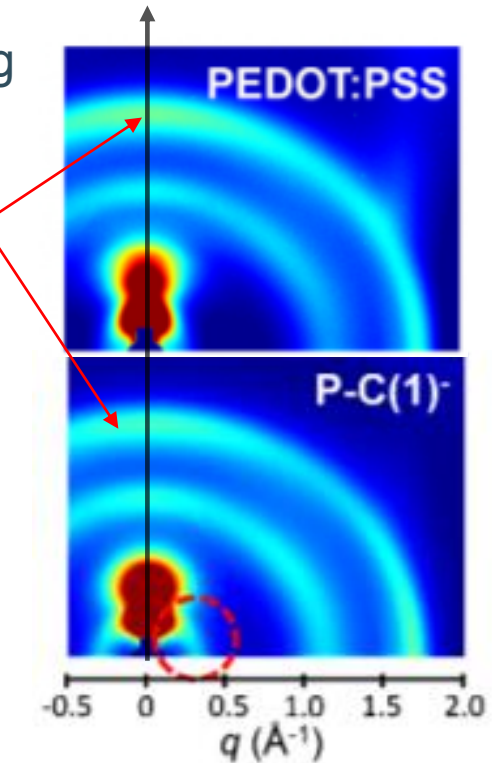
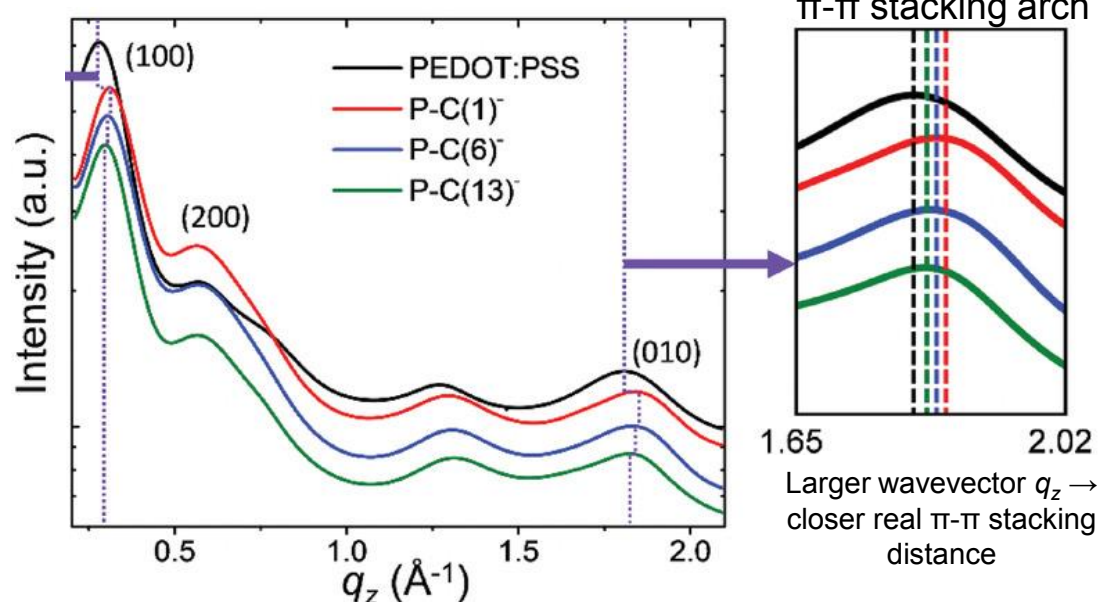
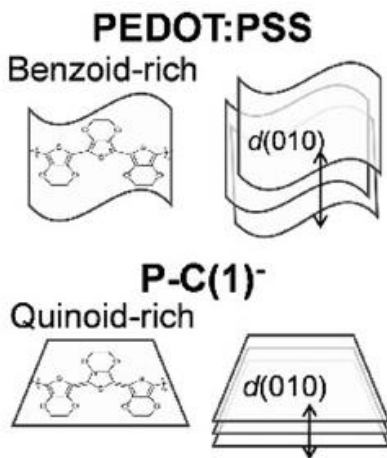
- Organic thermoelectrics (OTEs): PEDOT and the importance of doping
  - Effect of the SC on morphology and transport: On the other hand, if the SD is a large molecule (large volumetric occupation), it will separate a large segment of PSS away from PEDOT, producing dedoping and a reduction of quinoid segments (less planar molecule).



# Applications of organic electronic materials

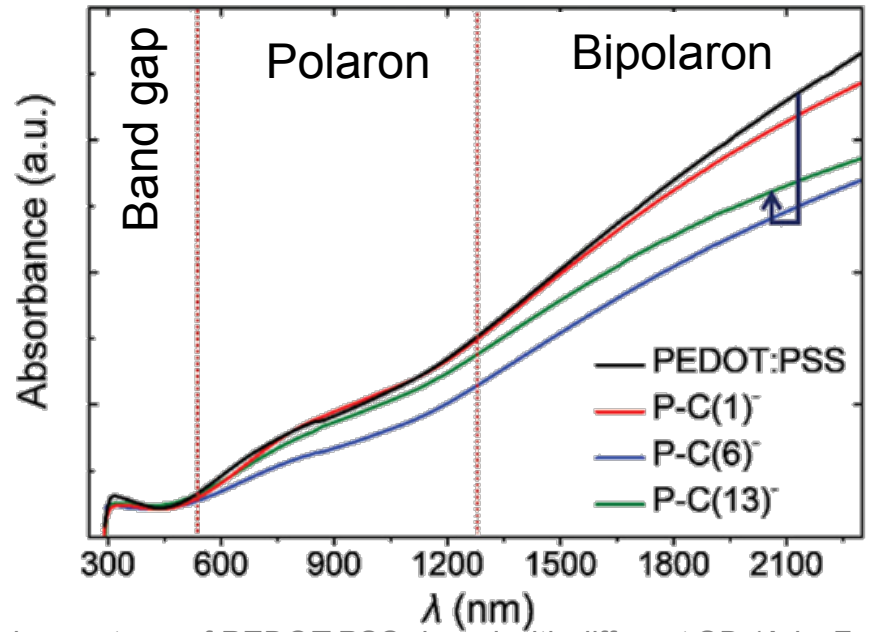
- Organic thermoelectrics (OTEs): PEDOT and the importance of doping

- Effect of the SC on morphology and transport : Quinoid segments are more rigid and planar, promoting better  $\pi$ - $\pi$  stacking. This translates in a shorter  $\pi$ - $\pi$  stacking distance that is beneficial for charge carrier transport for PEDOT:PSS doped with small molecules. The  $\pi$ - $\pi$  stacking distance can be observed in GIWAXS.



# Applications of organic electronic materials

- Organic thermoelectrics (OTEs): PEDOT and the importance of doping



UV-vis spectrum of PEDOT:PSS doped with different SD (Adv. Funct. Mater. 2019, 1905590).

- Effect of the SC on morphology and transport :  
Despite modifying the morphology, small SD do not change the oxidation level of PEDOT:PSS significantly, i.e. no dedoping is observed for C(1)<sup>-</sup>. Larger SD molecules such as C(6)<sup>-</sup> and C(13)<sup>-</sup> are more efficient for dedoping.

# Applications of organic electronic materials

- Organic thermoelectrics (OTEs): PEDOT and the importance of doping
  - Effect of the SC on morphology and transport : The effect of morphology and doping can be seen in TE performances.
  - Remember from Chapter #3 & 8 that:

$$\sigma = qn\mu,$$

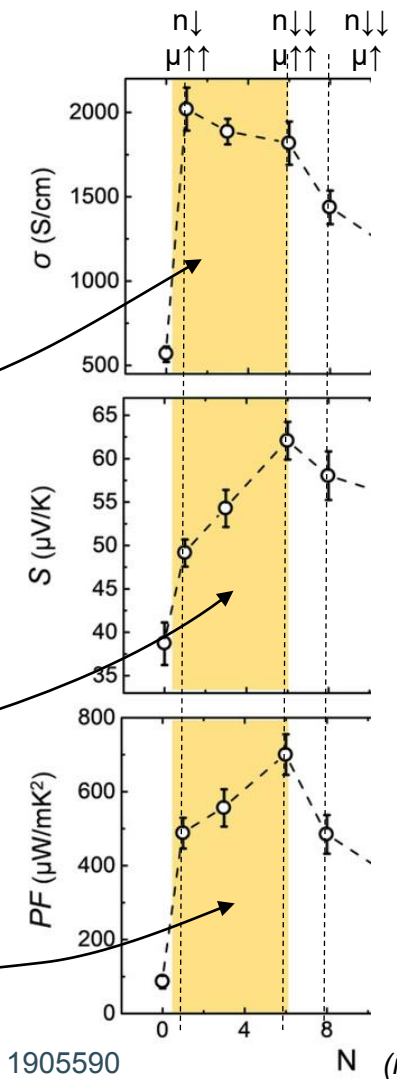
$\sigma$  increases owing to a higher  $\mu$  resulting from molecular arrangement when using C(1)- C(6)-. As larger SD molecules are used, there is a dedoping effect, which decreases  $n$  but the increase of  $\mu$  is still more relevant.

$$S = \frac{8\pi^2 k_B^2}{3qh^2} m^* T \left(\frac{\pi}{3n}\right)^{2/3}$$

The dedoping effect, very visible for C(6)-, results in lower  $n$  and a higher Seebeck coefficient.

$$PF = \sigma S^2$$

There is a “sweet spot” where the power factor gets a maximum.

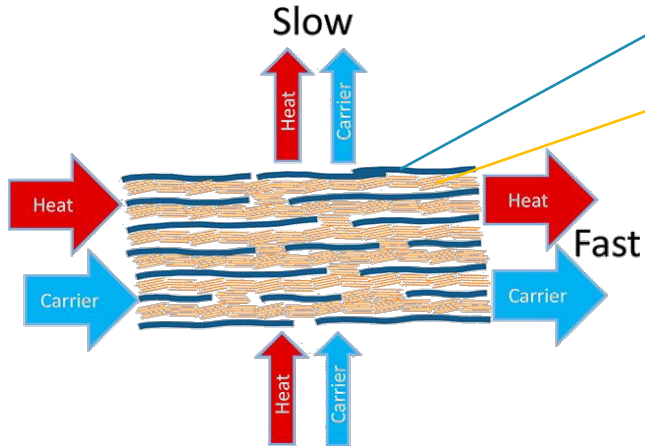


Adv. Funct. Mater. 2019, 1905590

# Applications of organic electronic materials

- Organic thermoelectrics (OTEs): Importance of morphology
  - Chain orientation and crystallinity

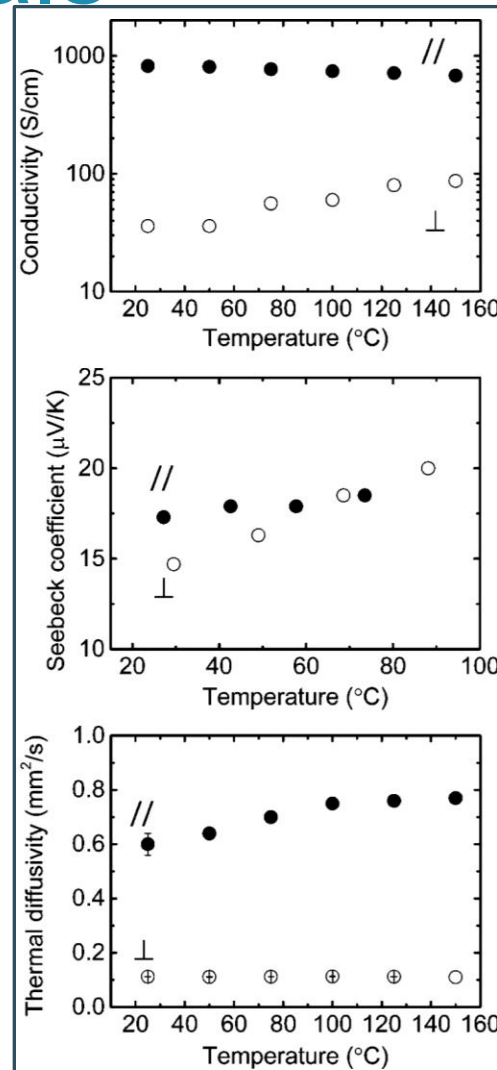
Sketch showing the directions of preferential and non-preferential transport in PEDOT:PSS. The blue and yellow lines represent PEDOT chains (oriented in plane) and PSS, respectively.



TE parameters vs temperature measured in plane (II) and through plane (L) (note that thermal diffusivity and thermal conductivity,  $\kappa$ , are linearly related by the equation  $\kappa = \text{density} \times \text{specific heat capacity} \times \text{diffusivity}$ ).

The electrical conductivity is enhanced more than the thermal conductivity along the molecule backbone.  $S$  does not change much. Therefore **alignment seems beneficial for  $zT$ !**

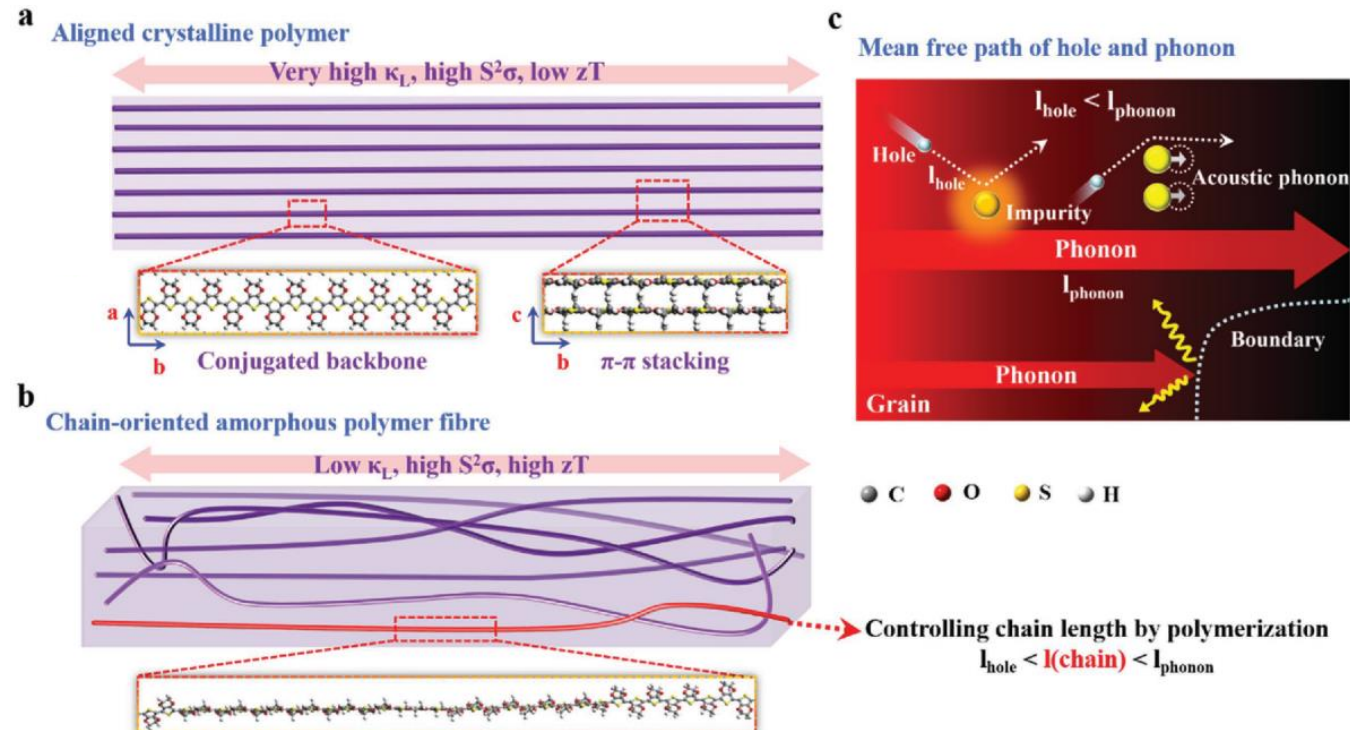
[dx.doi.org/10.1021/mz500446z](https://dx.doi.org/10.1021/mz500446z) |



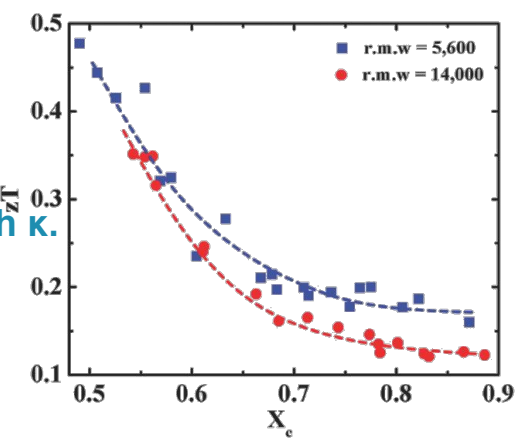
# Applications of organic electronic materials

- Organic thermoelectrics (OTEs): Importance of morphology
  - Chain orientation, crystallinity and polymer length

Simulated figure of merit,  $zT$ , versus crystallinity,  $X_c$ , for uniaxial-aligned PEDOT fibres with two different values of molecular weight. **High crystallinity is not desirable since it leads to a high  $\kappa$ .**



DOI: 10.1002/adfm.201702847

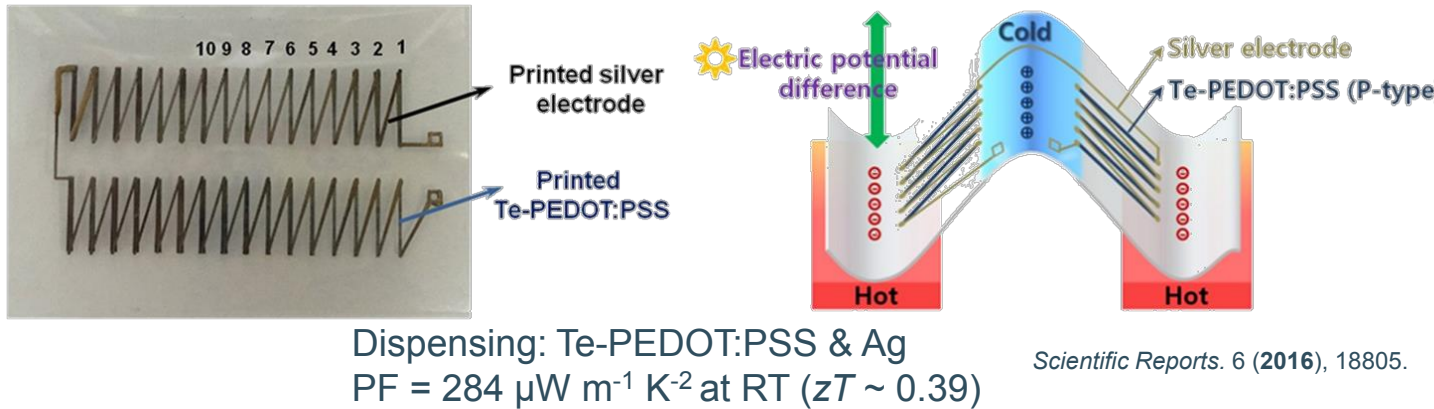


Graphical representation of the effect of uniaxial alignment and crystallinity in the transport and sketch representing the typical scattering events for phonons and charge carriers in a crystallite.

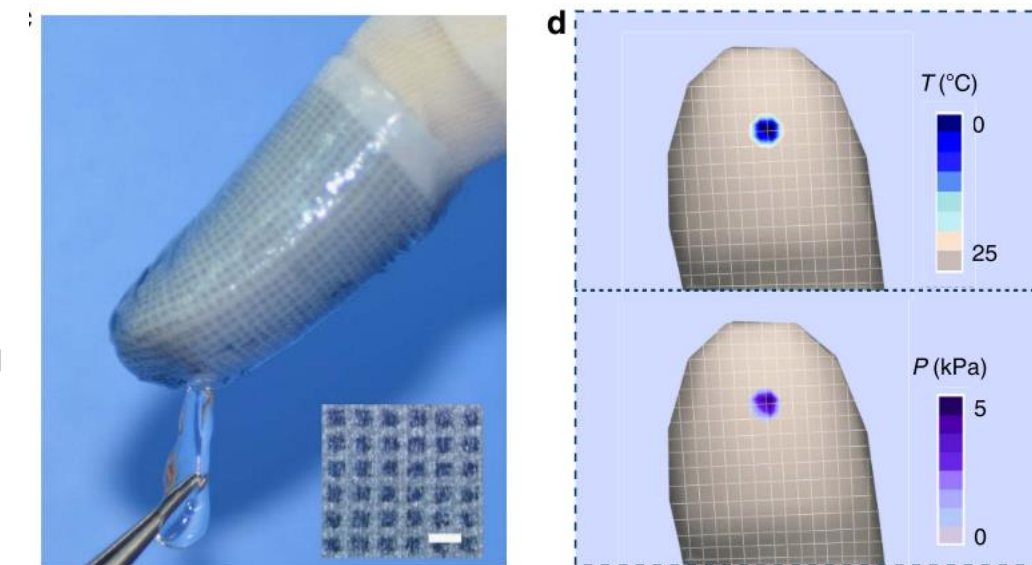
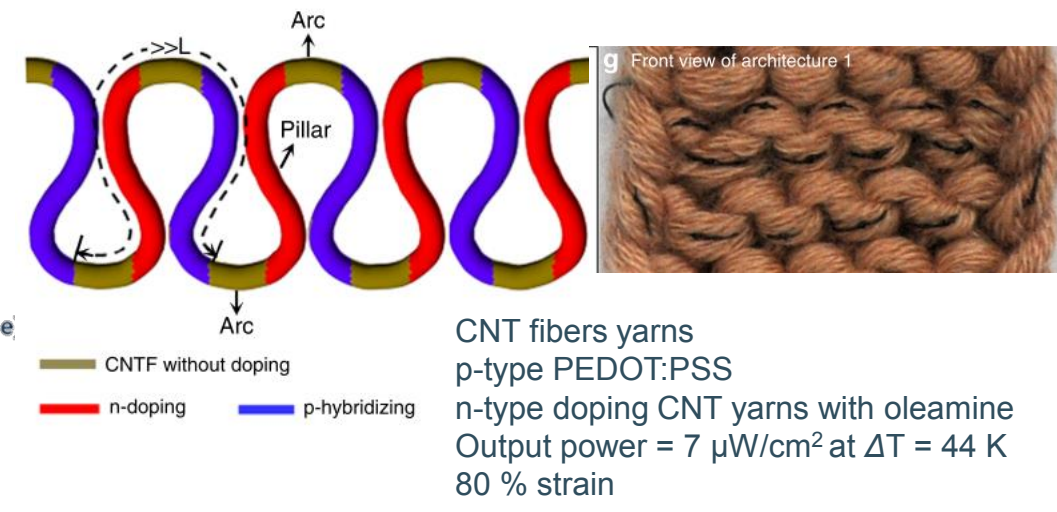
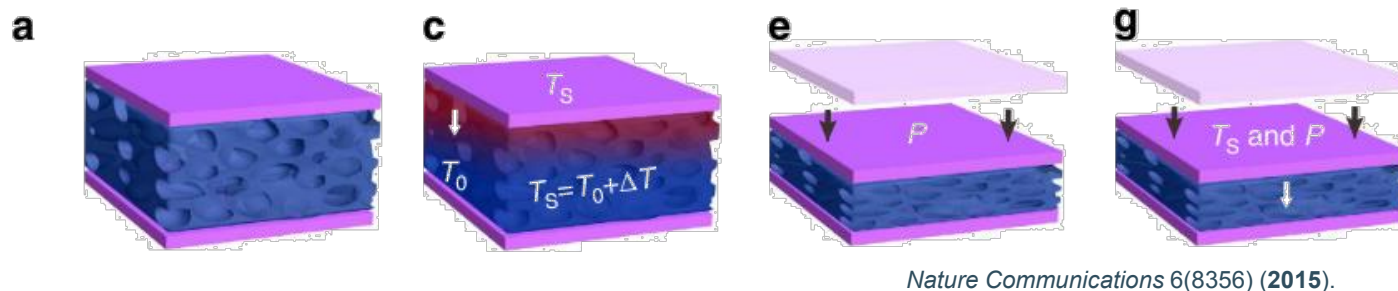
The mean free path (MFP) of phonons is longer than that of charge carriers. Therefore, by tailoring the length of the oriented molecules (or the size of the crystallites) to be longer than the charge carriers MFP but shorter than the phonons MFP, higher boundary scattering will occur for phonons. Thus, thermal transport will be suppressed more efficiently than charge carrier transport.

# Applications of organic electronic materials

- Organic thermoelectrics (OTEs): Applications
  - Printed and flexible energy harvesters



- Flexible self-powered sensors for e-skin: PEDOT:PSS TE used as dual (temp and pressure) sensor.



# Acknowledgements

- Mentioned references
- Course Organic Semiconductors for Electronic and Photonic Devices (SMATSCI 343). Prof. Alberto Salleo, Stanford University



# Materials Physics and Technology for Nanoelectronics

KU LEUVEN

imec

KU LEUVEN

MATERIAALKUNDE

**Clement Merckling**

clement.merckling@imec.be

IMEC IV, room 2.36

Kapeldreef 75, B-3001 Leuven

**Francisco Molina-Lopez**

francisco.molinalopez@kuleuven.be

Dept. Materials Engineering, room 01.51

Kasteelpark Arenberg 44, B-3001 Leuven

# Materials Physics and Technology for Nanoelectronics

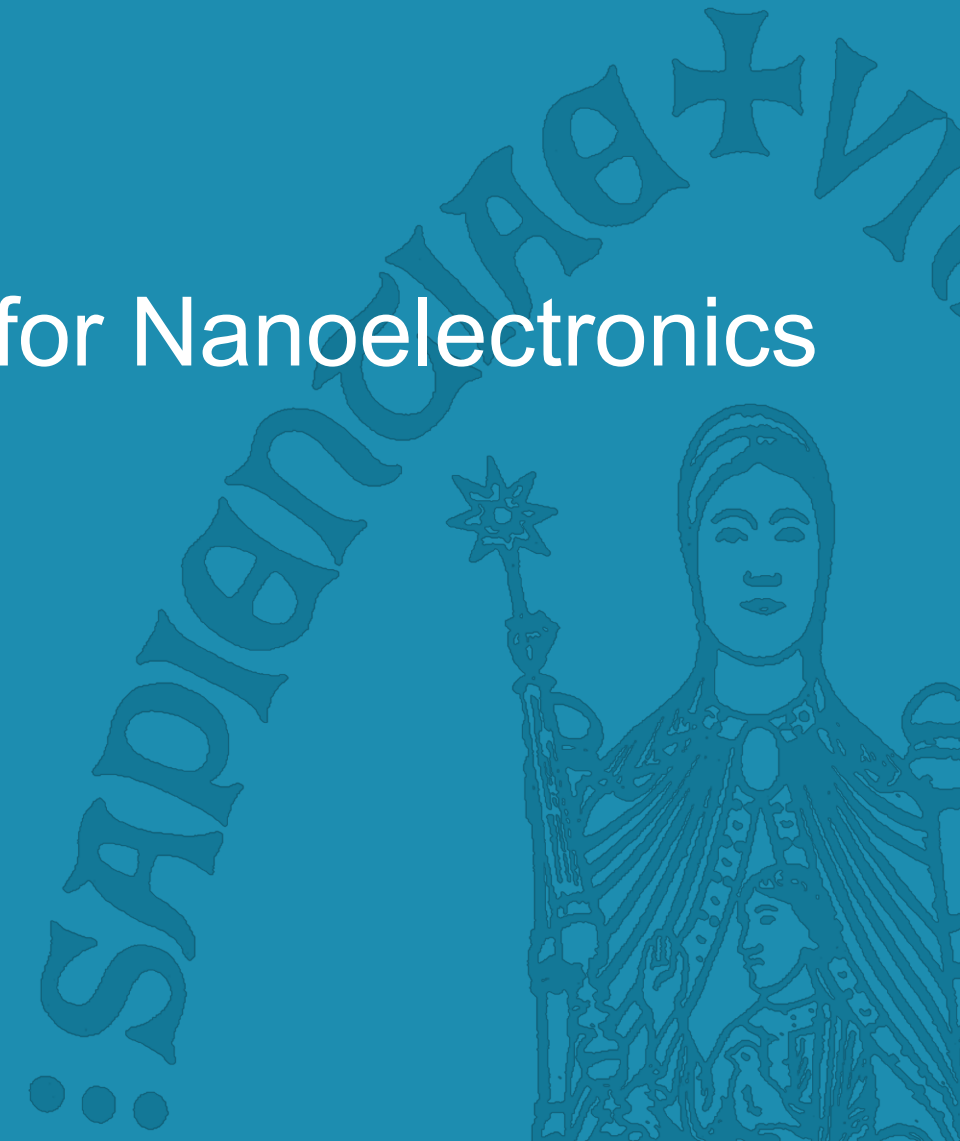
## Photonics



Clement Merckling  
[clement.merckling@imec.be](mailto:clement.merckling@imec.be)  
IMEC IV, room 2.36  
Kapeldreef 75, B-3001 Leuven

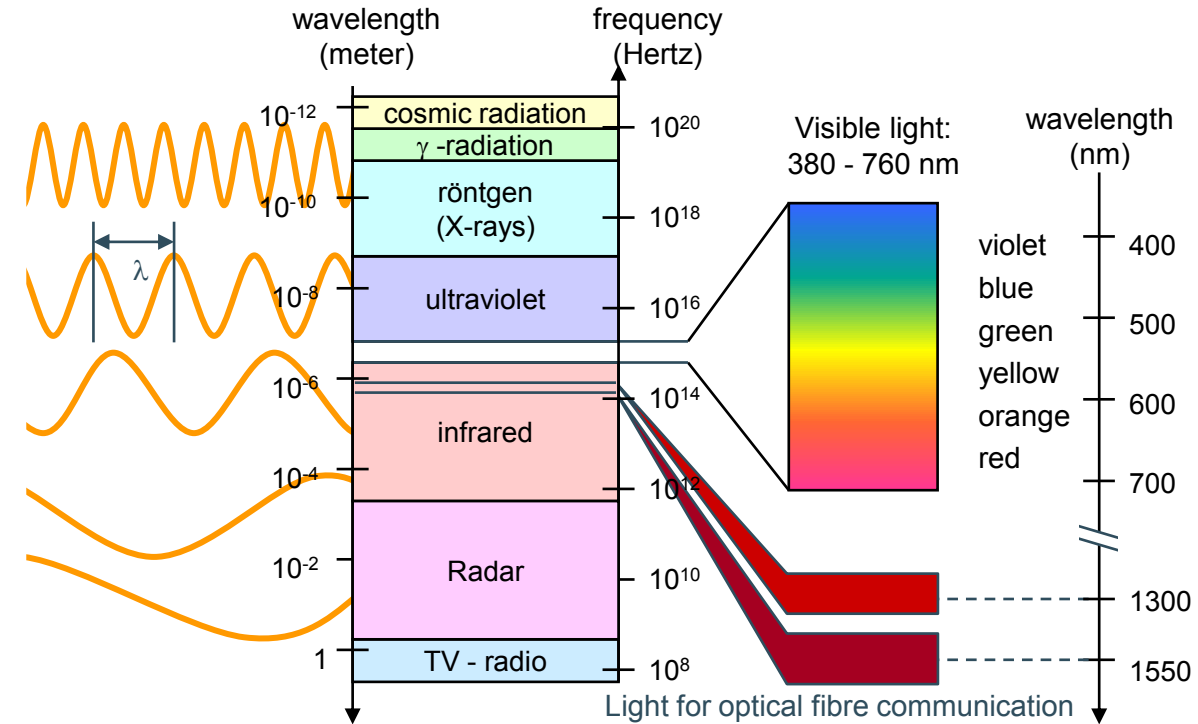


Francisco Molina Lopez  
[francisco.molinalopez@kuleuven.be](mailto:francisco.molinalopez@kuleuven.be)  
MTM Functional Materials  
Kasteelpark Arenberg 44, B-3001 Leuven



# Electromagnetic spectrum

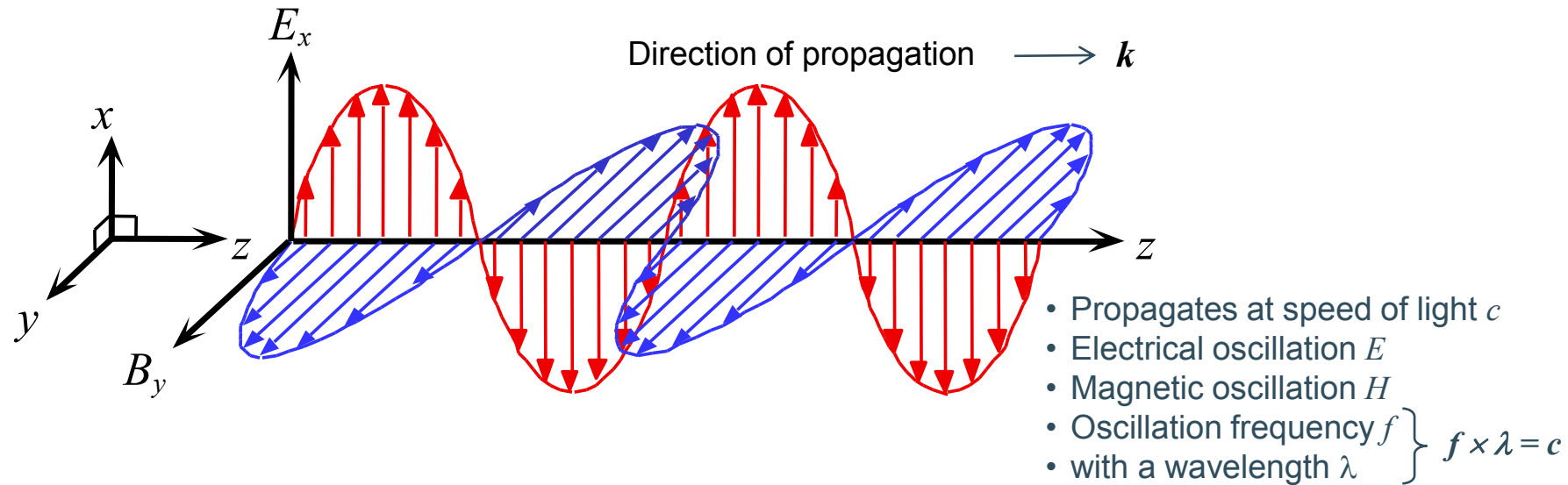
The theoretical description of light as electromagnetic waves has had an enormous impact on physics in the past two centuries.



The entire electromagnetic spectrum, from the lowest to the highest frequency (longest to shortest wavelength), includes all radio waves (e.g., commercial radio and television, microwaves, radar), infrared radiation, visible light, ultraviolet radiation, X-rays, and gamma rays.

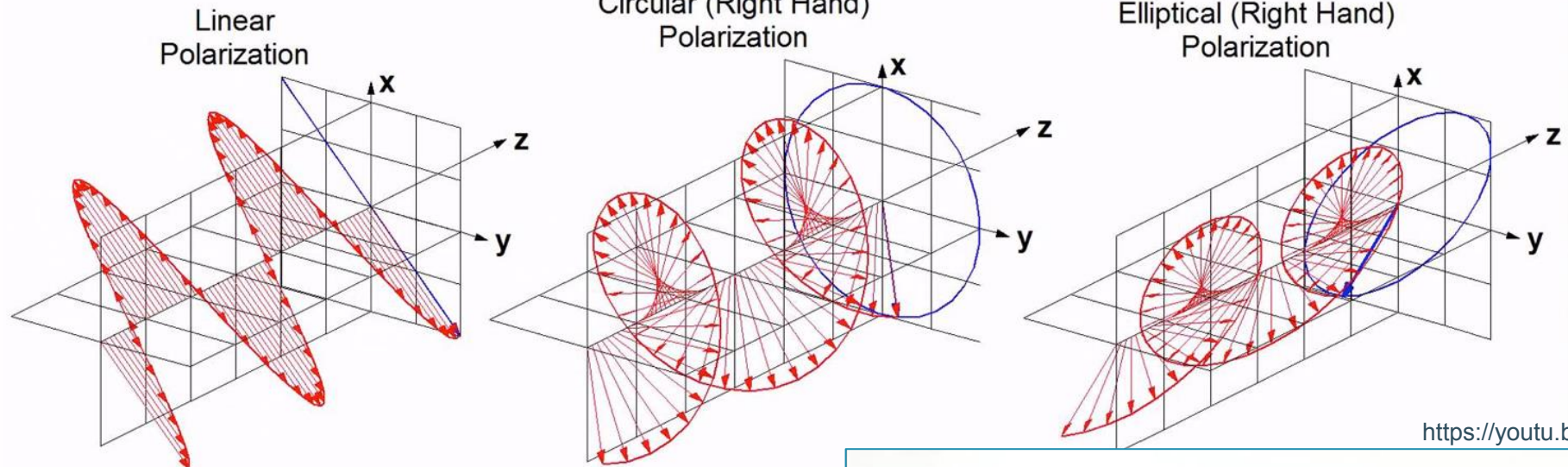
# Electromagnetic wave in free space

An electromagnetic wave is a travelling wave which has time varying electric and magnetic fields which are perpendicular to each other and the direction of propagation,  $z$ .



Light is called unpolarized if the direction of this electric field fluctuates randomly in time. Many common light sources such as sunlight, halogen lighting, LED spotlights, and incandescent bulbs produce unpolarized light. If the direction of the electric field of light is well defined, it is called polarized light. The most common source of polarized light is a laser.

# Light polarization

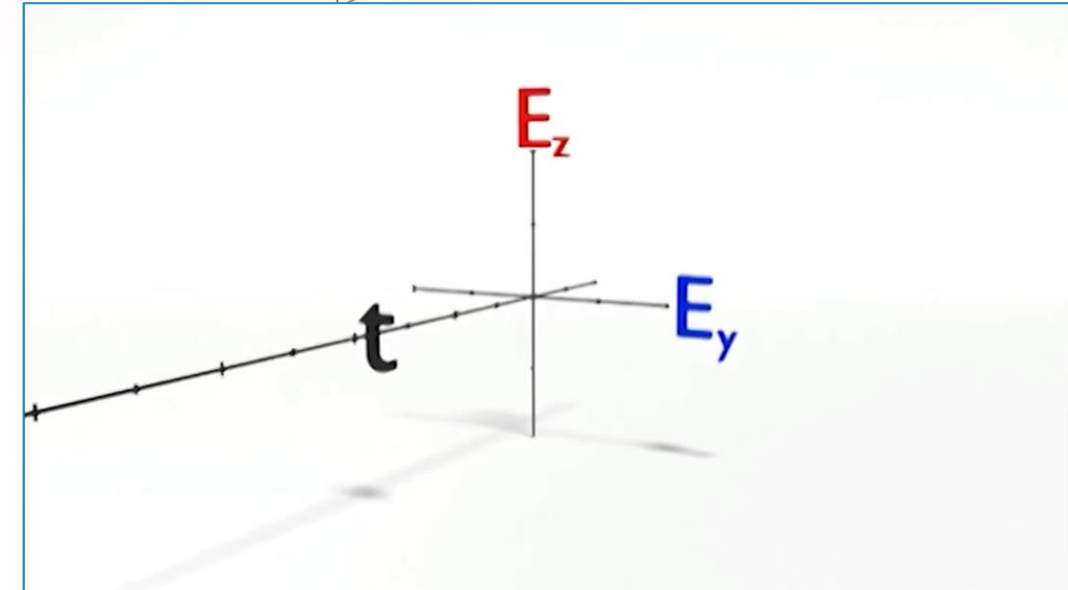


<https://youtu.be/Fu-aYnRkUgg>

The electric field (note that we will ignore magnetic field now) of **linearly polarized light** is confined to a single plane along the direction of propagation.

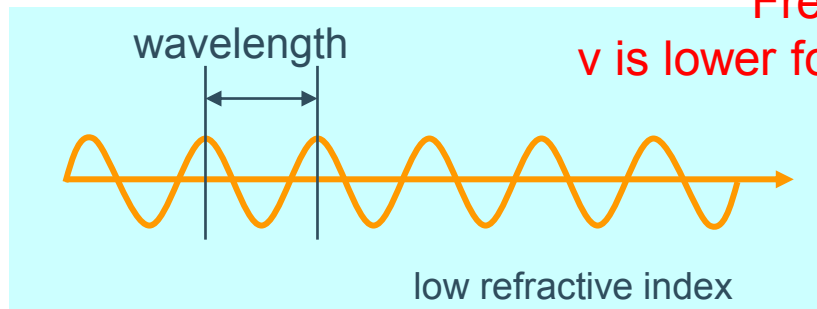
The electric field of **circularly polarized light** consists of two perpendicular, equal in amplitude, linear components that have a phase of difference of  $\pi/2$ . The resulting electric field describes a circle.

The electric field of **elliptically polarized light** consists of two perpendicular linear components with any amplitude and any phase difference. The resulting electric field describes an ellipse.

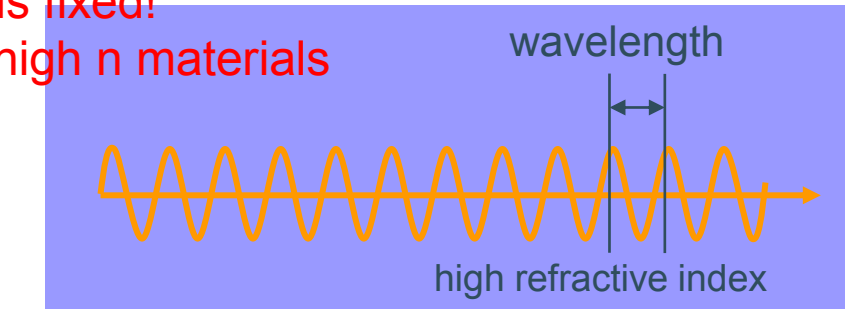


# Refractive index

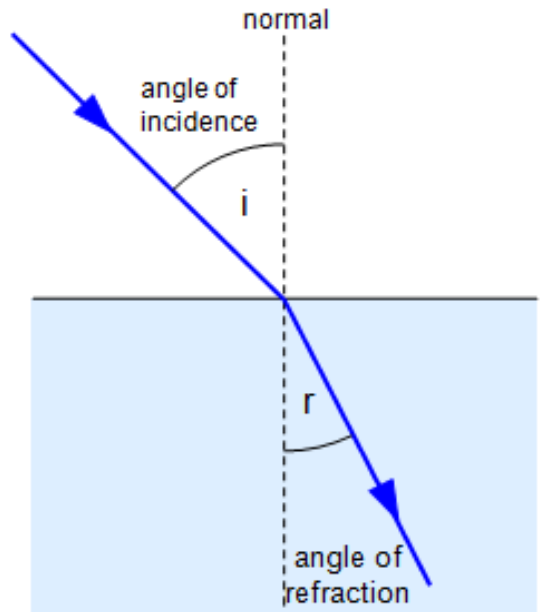
The refractive index of a material  $n$  is a dimensionless number that describes how light propagates through that medium. It is defined as:  $n = c/v$  where  $c$  is the speed of light in vacuum and  $v$  is the phase velocity of light in the medium.



Freq is fixed!



$v$  is lower for high  $n$  materials

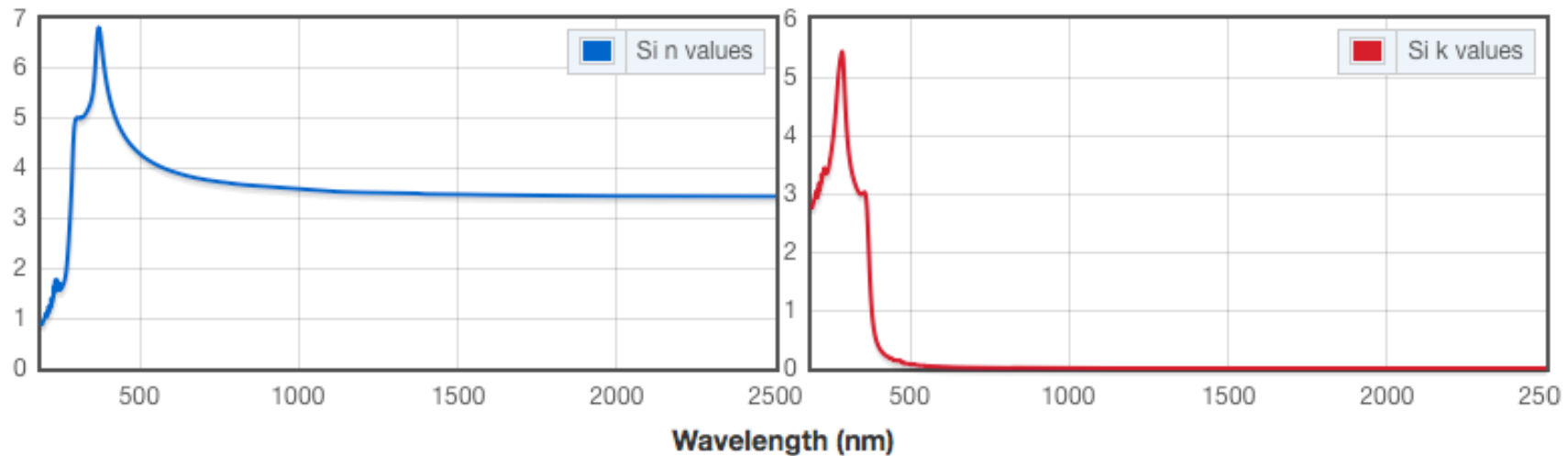
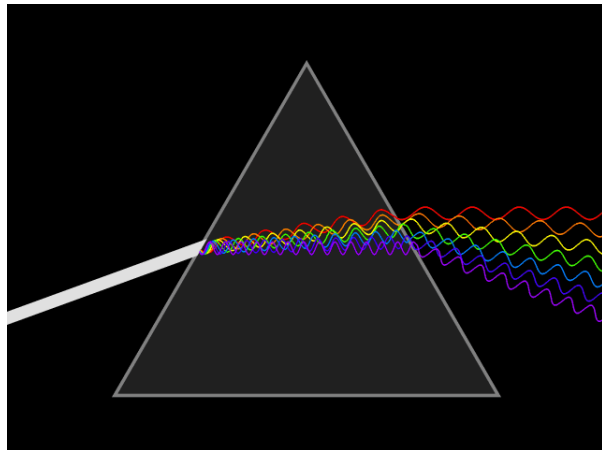


The refractive index is also measure of the bending of a ray of light when passing from one medium into another. If  $i$  is the angle of incidence of a ray in vacuum (angle between the incoming ray and the perpendicular to the surface of a medium, called the normal; see figure) and  $r$  is the angle of refraction (angle between the ray in the medium and the normal), the refractive index  $n$  is defined as the ratio of the sine of the angle of incidence to the sine of the angle of refraction; i.e.,  $n = \sin(i)/\sin(r)$ .

Rays get closer to the normal for high  $n$  materials

# Refractive index

Many materials have a well-characterized refractive index, but these indices depend strongly upon the frequency of light. This is called (chromatic) dispersion and causes the splitting of white light into its constituent colors in prisms and rainbows, and chromatic aberration in lenses.

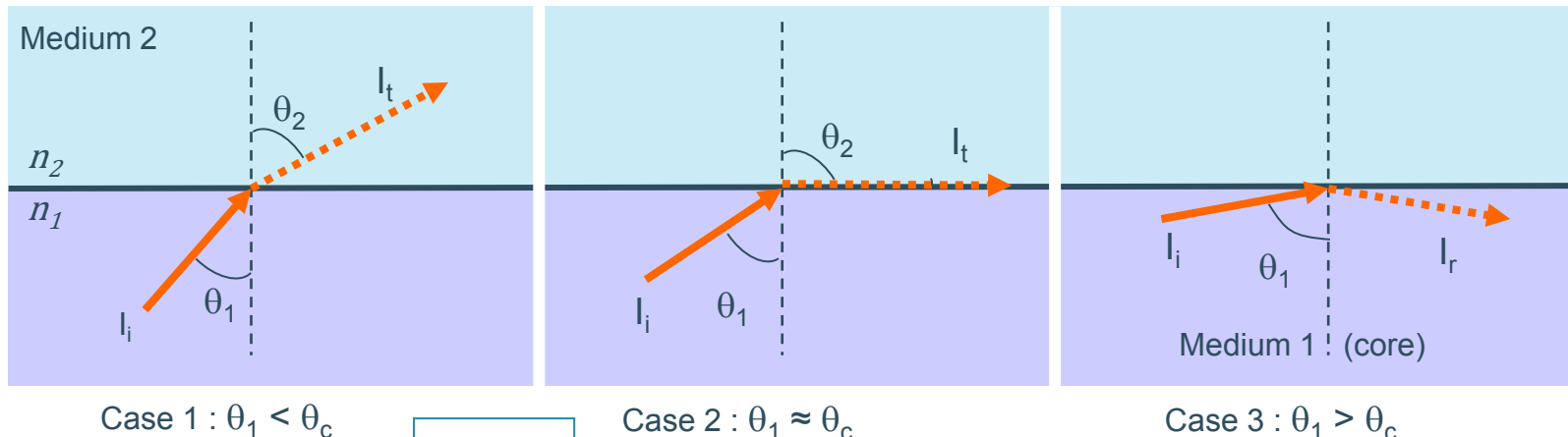


*The refractive indices for various wavelengths for Si.*

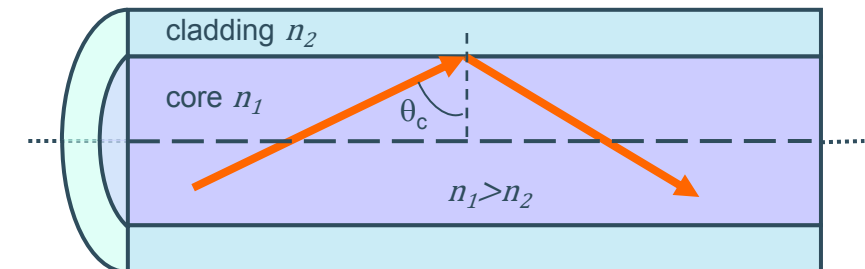
In general, an index of refraction is a complex number  $n'=n+ik$  with both a real and imaginary part.  $k$  indicates the strength of absorption loss at a particular wavelength - thus, the imaginary part is sometimes called the extinction coefficient. Such losses become particularly significant, for example, in metals at short (e.g. visible) wavelengths.

# Light propagation in optical fibers

According to the ray theory of light propagation, a light beam incident at the interface between two transparent materials with refractive indexes  $n_1 > n_2$  behaves as follows (*Snell's Law*) :  $n_1 \sin(\theta_1) = n_2 \sin(\theta_2)$



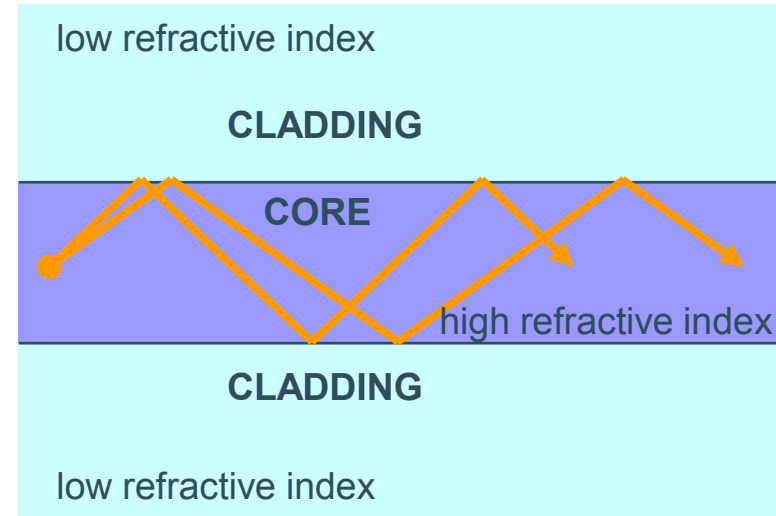
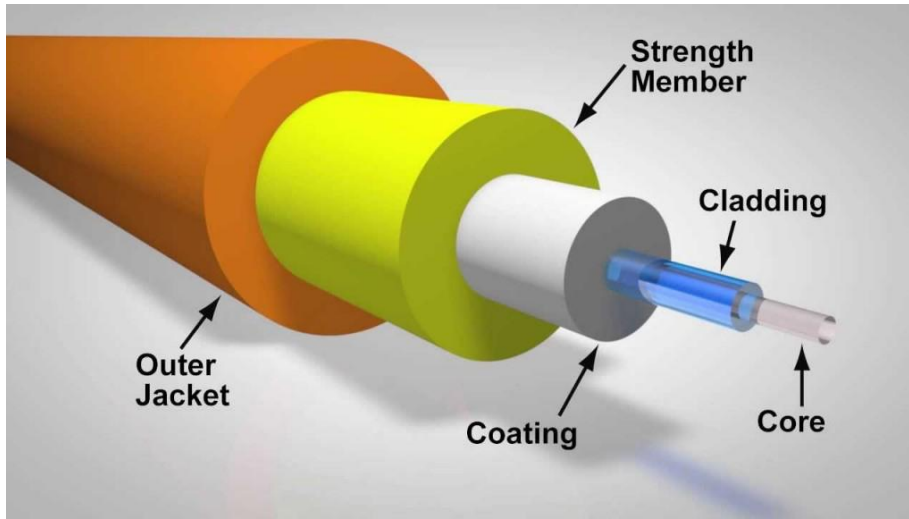
Total reflection:  $\theta_c = \arcsin(n_2/n_1)$   
 $\theta_c$ : critical angle



Above a critical angle,  $\theta_c = \arcsin(n_2/n_1)$ , total reflection occurs. This property can be used to confine light into an optical fiber.

# Optical fibers

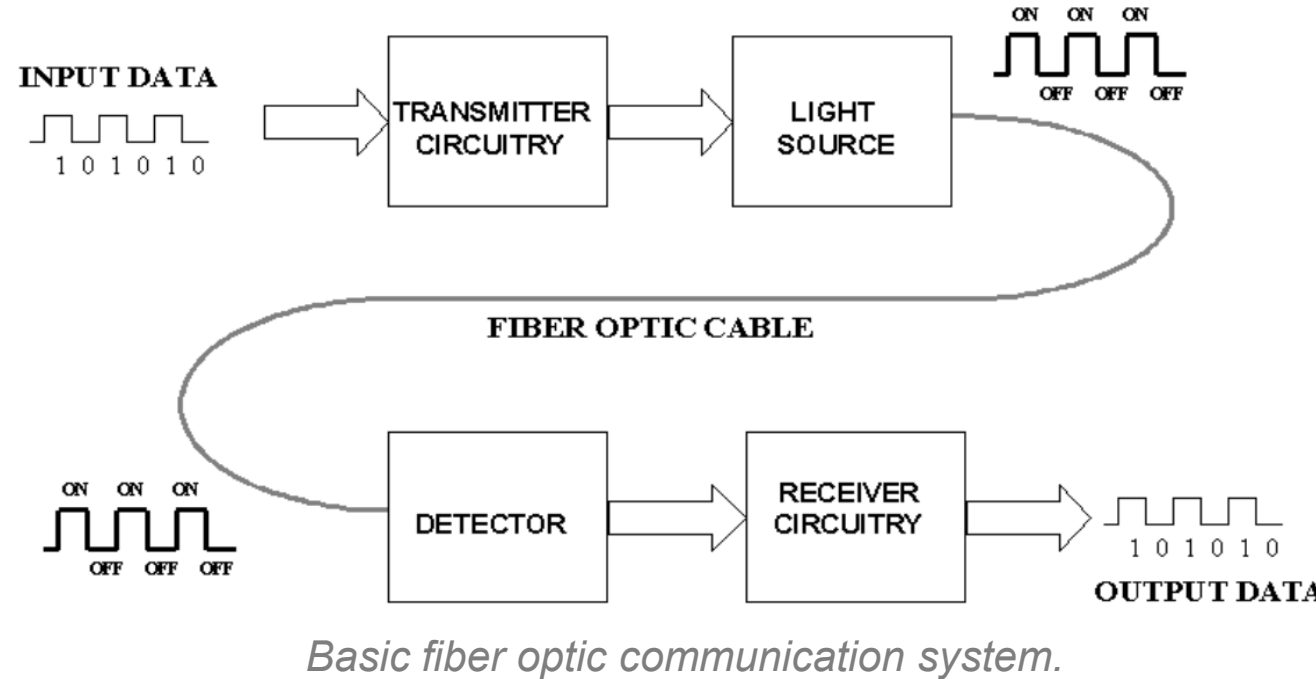
Optical fibers are made from a ‘sandwich’ of material with a high refractive index between material with a low refractive index. Light is guided by total internal reflection in a core of high refractive index surrounded by a cladding of low refractive index. The total internal reflection takes place at the cladding – core interface.



Optical fibers use total internal reflection to keep a light ray trapped within the denser glass of the center of a composite cylindrical glass fiber, the *core*. It is as if light rays are guided down the core of the fiber in a zigzag path by a succession of total internal reflections at the boundary between the core glass and the less dense glass surrounding it – the *cladding*.

# Fiber optics

Fiber optics is a major building block in the telecommunication infrastructure. Its high bandwidth capabilities and low attenuation characteristics make it ideal for gigabit transmission and beyond.

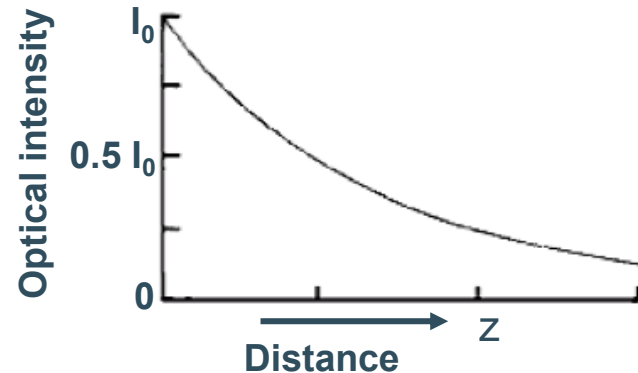


*Basic fiber optic communication system.*

A basic fiber optic system consists of a transmitting device that converts an electrical signal into a light signal, an optical fiber cable that carries the light, and a receiver that accepts the light signal and converts it back into an electrical signal.

# Light attenuation

Attenuation is loss of power. Light travelling through an optical fiber loses its power over distance. This phenomenon is mainly dependent on the wavelength of the light and the properties of the propagating medium.



*For example: in a fiber with attenuation of -10 dB/km, the intensity of light falls by a factor 10 after travelling 1 km (90% attenuation)*

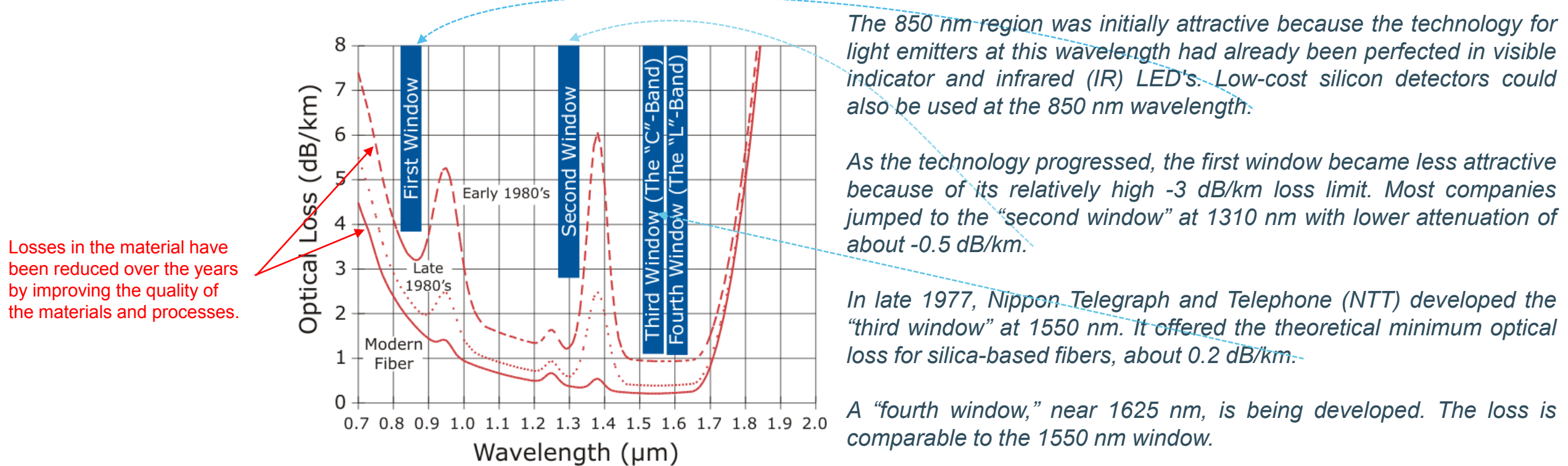
The output intensity decreases with increasing  $z$ :  $I(z) = I_0 e^{-\alpha z}$ . The attenuation is expressed in decibels per kilometer (dB/km).  $dB = -10 \log_{10} I(z)/I_0$

There are several reasons for this including absorption by the core and cladding (caused by the presence of impurities) and the leaking of light from the cladding. When light reflects off the cladding /core interface it actually travels for a short distance within the cladding before being reflected back. Today fibers have typical attenuation rates of -0.2 to -1 dB/km (5 to 20% attenuation) -> Example of 5% attenuation:  $-10 \log_{10} (0.95) \sim -0.2 \text{ dB/km}$

# Optical fibers

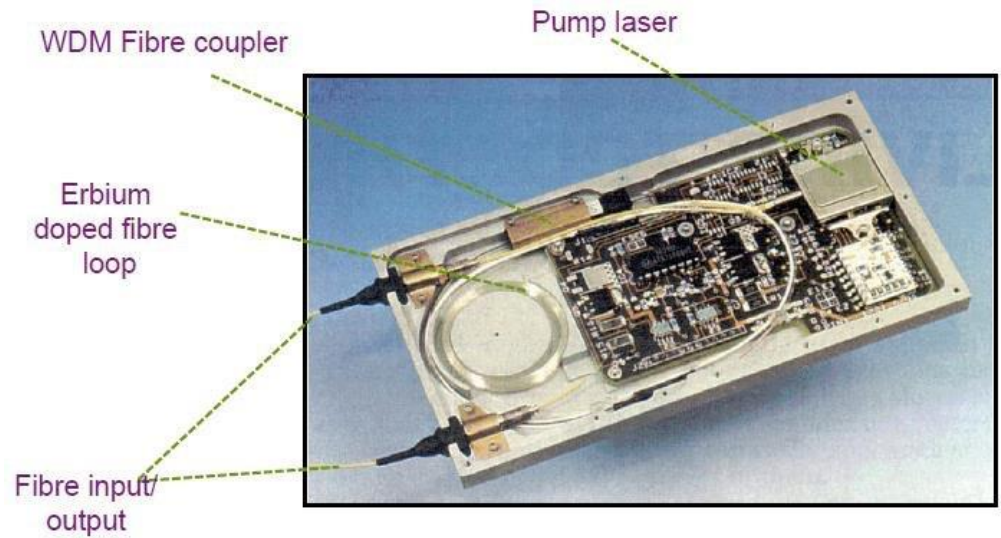
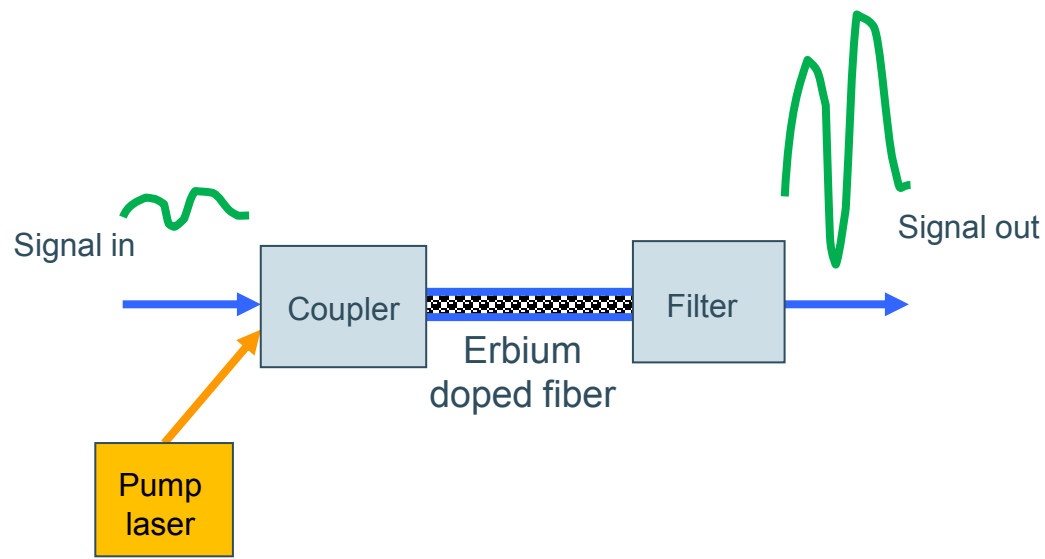
The basic material used in optical fibers is vitreous silica dioxide ( $\text{SiO}_2$ ). Various dopants are also used, ( $\text{Al}_2\text{O}_3$ ,  $\text{B}_2\text{O}_3$ ,  $\text{GeO}_2$ ,  $\text{P}_2\text{O}_5$ ). Their task is to fine-tune the refractive index of pure silica ( $\text{SiO}_2$ ).

There are two parameters of glass that have a substantial impact on its performance: the **losses** (lead to attenuation) and the changes of refractive index with wavelength (dispersion).



# Fiber amplifiers

For some applications, the attenuation of light in an optical fiber must be compensated. This is realized with a fiber amplifier. Modern fiber amplifiers are based on the **emission of stimulated light** (laser effect – light amplification by stimulated emission of radiation) in the fiber.



In a fiber amplifier, a portion of the fiber is doped with some active impurities. The most common impurity used in  $\text{SiO}_2$  is Erbium (Er); so called Erbium-doped fiber amplifiers. The laser effect is used in this portion of the fiber to amplify the signal. The inversion population is obtained with the help of a pump laser at another wavelength.

# Fiber amplifiers

## Erbium

From Wikipedia, the free encyclopedia

**Erbium** is a chemical element with the symbol **Er** and atomic number 68. A silvery-white solid metal when artificially isolated, natural erbium is always found in chemical combination with other elements. It is a **lanthanide**, a **rare-earth element**, originally found in the **gadolinite** mine in **Ytterby, Sweden**, which is the source of the element's name.

Erbium's principal uses involve its pink-colored  $\text{Er}^{3+}$  ions, which have optical fluorescent properties particularly useful in certain laser applications. Erbium-doped glasses or crystals can be used as optical amplification media, where  $\text{Er}^{3+}$  ions are optically pumped at around 980 or 1480 nm and then radiate light at 1530 nm in stimulated emission. This process results in an unusually mechanically simple **laser optical amplifier** for signals transmitted by fiber optics. The 1550 nm wavelength is especially important for **optical communications** because standard single mode **optical fibers** have minimal loss at this particular wavelength.

In addition to optical fiber amplifier-lasers, a large variety of medical applications (i.e. dermatology, dentistry) rely on the erbium ion's 2940 nm emission (see **Er:YAG laser**) when lit at another wavelength, which is highly absorbed in water in tissues, making its effect very superficial. Such shallow tissue deposition of laser energy is helpful in **laser surgery**, and for the efficient production of steam which produces enamel ablation by common types of **dental laser**.

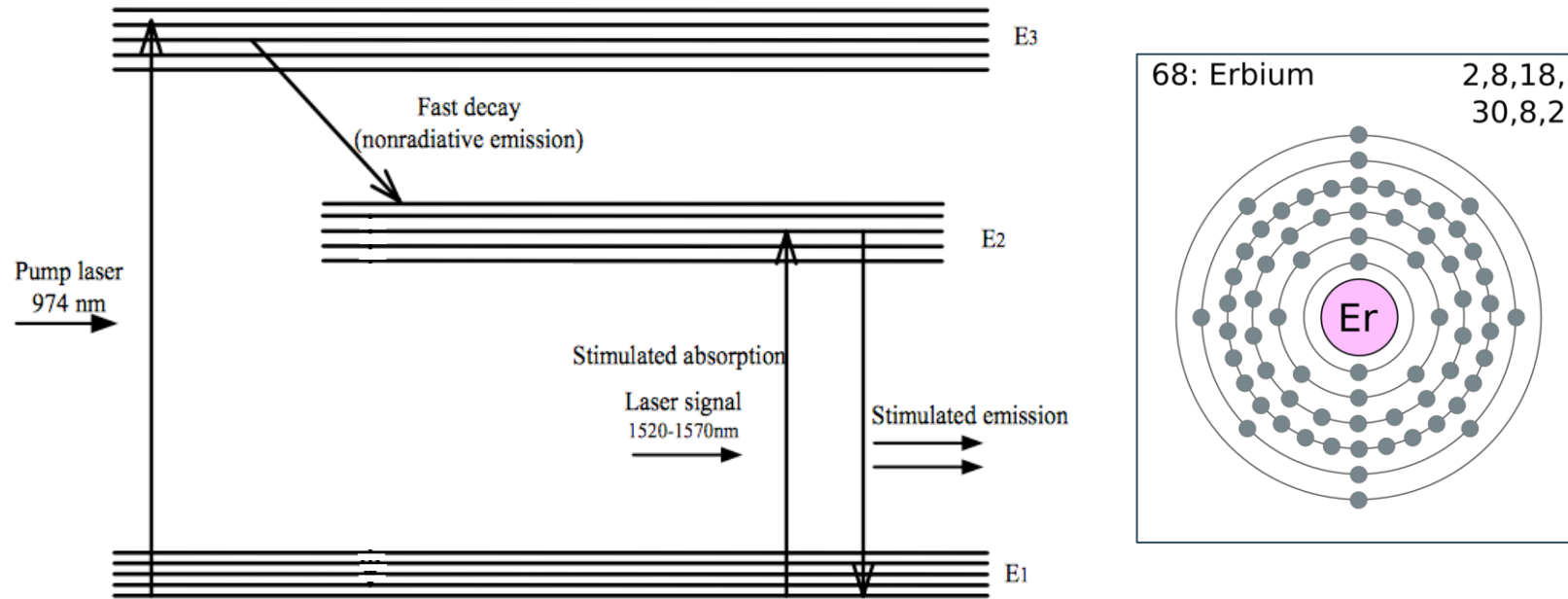


### Contents [hide]

- 1 Characteristics
  - 1.1 Physical properties
  - 1.2 Chemical properties
  - 1.3 Isotopes
- 2 History

# Er-based optical amplifier

An erbium-doped fiber is an optical fiber of which the core is doped with rare-earth element erbium ions  $\text{Er}^{3+}$ . A simplified energy level diagram of the  $\text{Er}^{3+}$  ion is shown below.

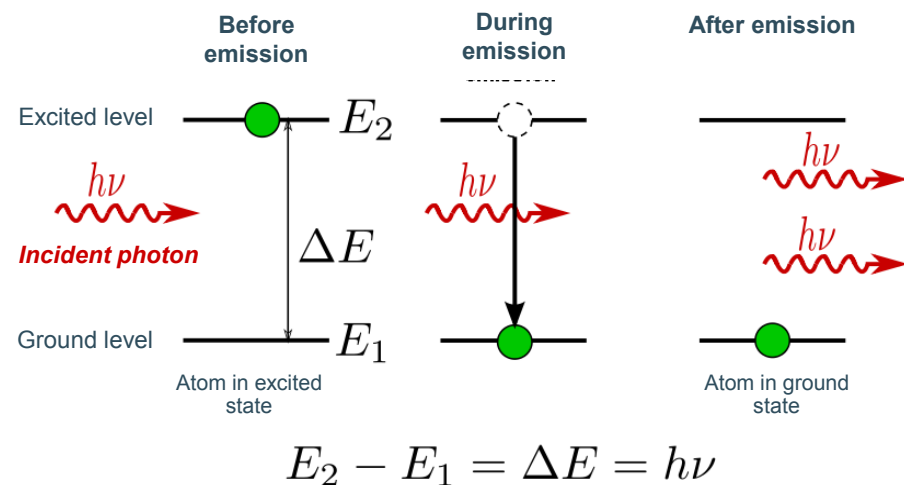


*Simplified energy levels of  $\text{Er}^{3+}$  ions in Erbium-doped fiber. The energy levels are broadening due to the dc-Stark effect, which leads to a relatively broad emission bandwidth. The Stark effect is the shifting and splitting of spectral lines of atoms and molecules due to presence of an external electric field. The Stark effect is the electric analogue of the Zeeman effect where a spectral line is split into several components due to the presence of a magnetic field.*

# Er-based optical amplifier

If a laser signal with a wavelength between 1520 and 1570 nm, and a 974 nm pump laser are fed into an erbium-doped fiber simultaneously, there are three possible outcomes for the signal photon:

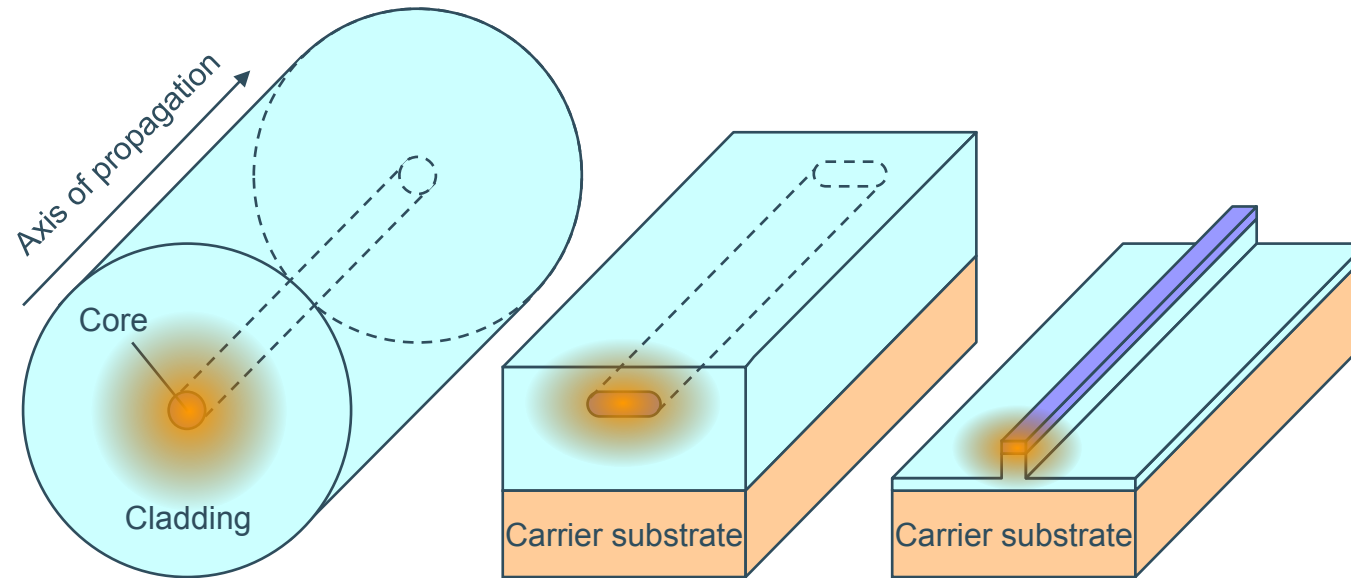
- i) The signal photon can propagate unaffected through the fiber.
- ii) Absorption: the signal photon excites an erbium ion from the state  $E_1$  to a higher level  $E_2$  and become annihilated in the process.
- iii) Stimulated emission: the signal photon stimulates an Erbium ion at state  $E_2$  to decay to  $E_1$ , producing another identical photon. This process amplifies the incoming signal. In order to achieve this we need to obtain population inversion between the energy level  $E_2$  and  $E_1$  of the Erbium-doped fiber. For this to occur the pump laser power must be sufficiently high.



Schematic illustration of the stimulated emission process. The stimulated photons are in phase with the incident photon, have the same wavelength and travel in the same direction. In this way the incoming light signal can be amplified.

# From optical fibers to waveguides

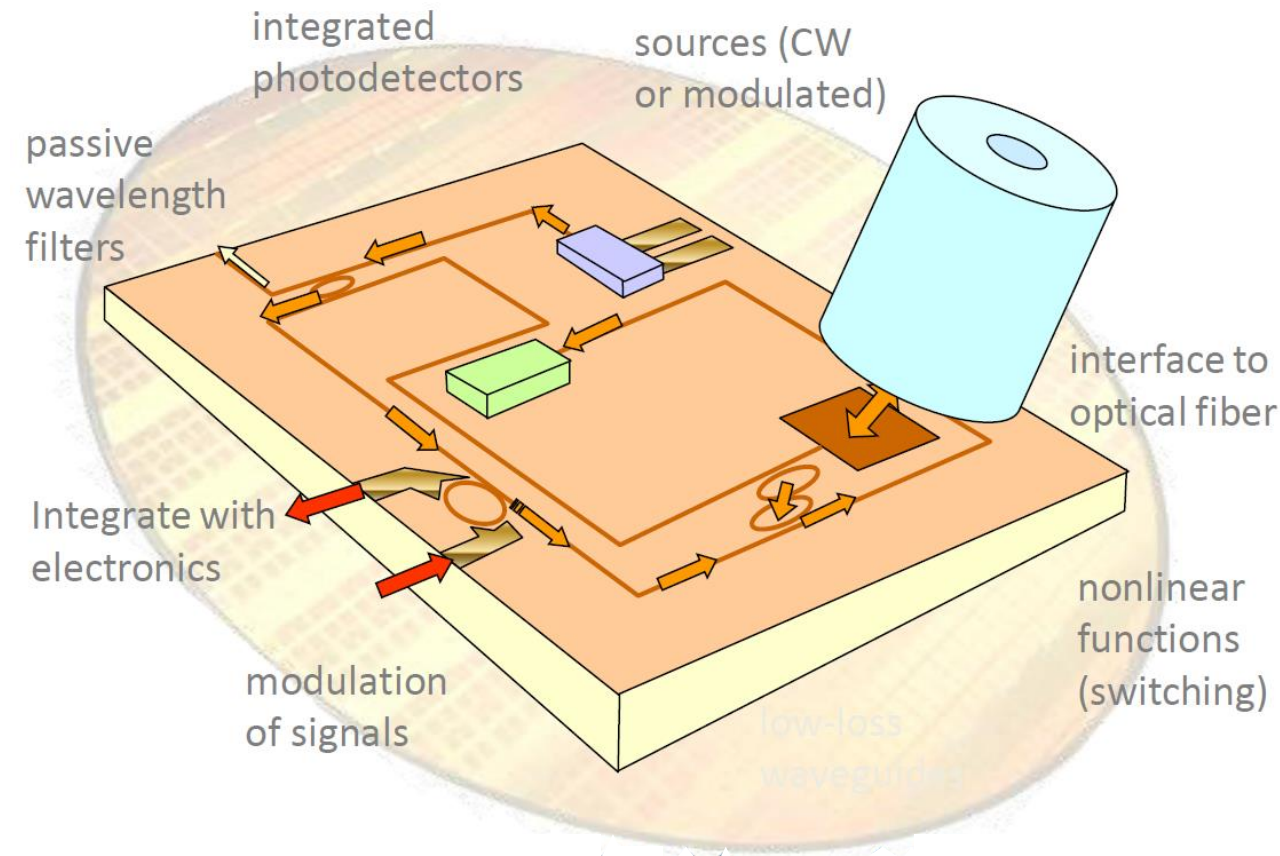
Optical fibers are rather large and usually have a relatively small refractive index contrast between the core and the cladding. When the refractive index contrast  $\frac{\Delta n}{n}$  is increased in all directions, the light can be confined in a smaller core according the expression  $D \sqrt{\frac{\Delta n}{n}} \approx \frac{\lambda}{n}$ , (with  $D$  being a typical dimension of confinement). This allows to fabricate photonic wires, the first step towards integrated optics.



- Optical fibers (low refractive index contrast, typically  $\sim 1.46\text{-to-}1.44$ ): core diameter  $\sim 10\mu\text{m}$
- Waveguides in semiconductor and air (high index contrast, 3.45-to-1): core  $\sim 0.2 \times 0.5\mu\text{m} \rightarrow$  photonic wires

# Photonic Integrated Circuits (PICs)

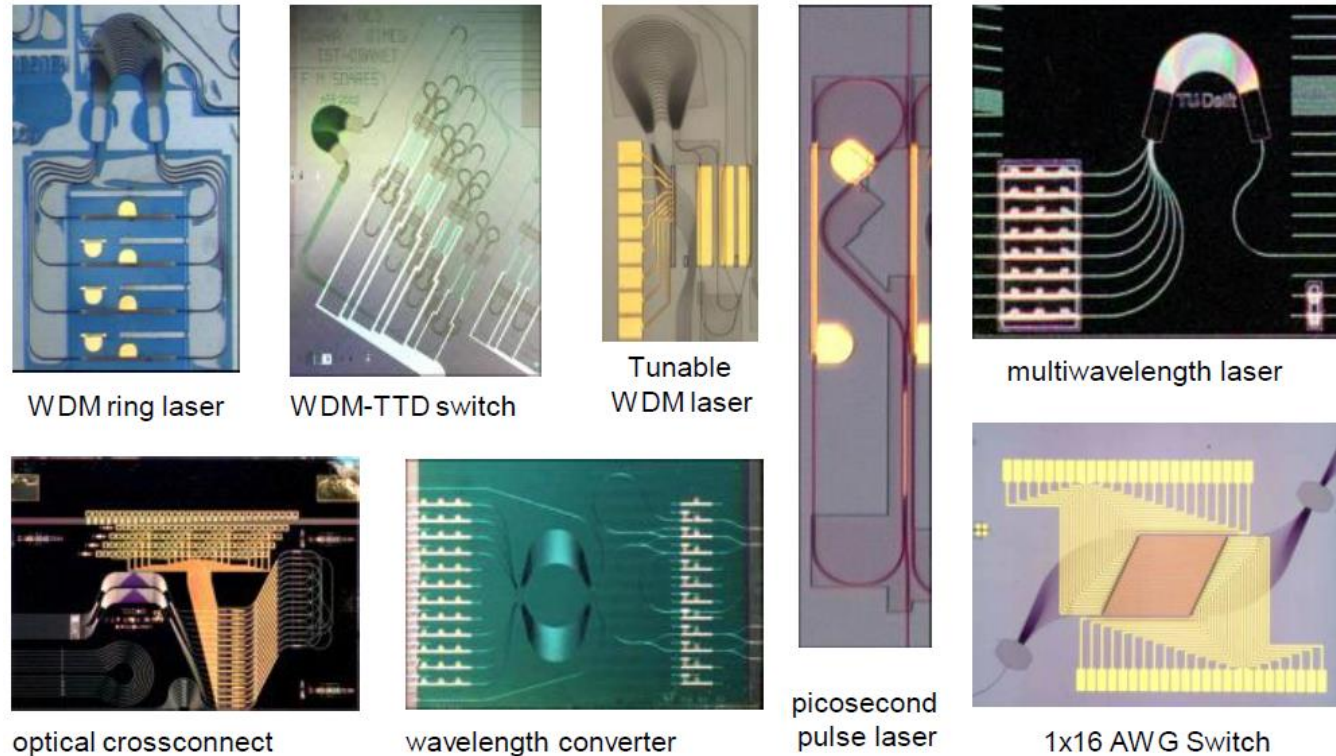
Photonic circuits require often interconnections with waveguides to communicate with the outer world.



# Materials for photonic integrated circuits

## InGaAsP / InP

- allows monolithic integration (integration of active and passive components)
- relatively high index contrast allows to make compact waveguides ( $\sim 1 \mu\text{m}$ )
- coupling to fiber is difficult

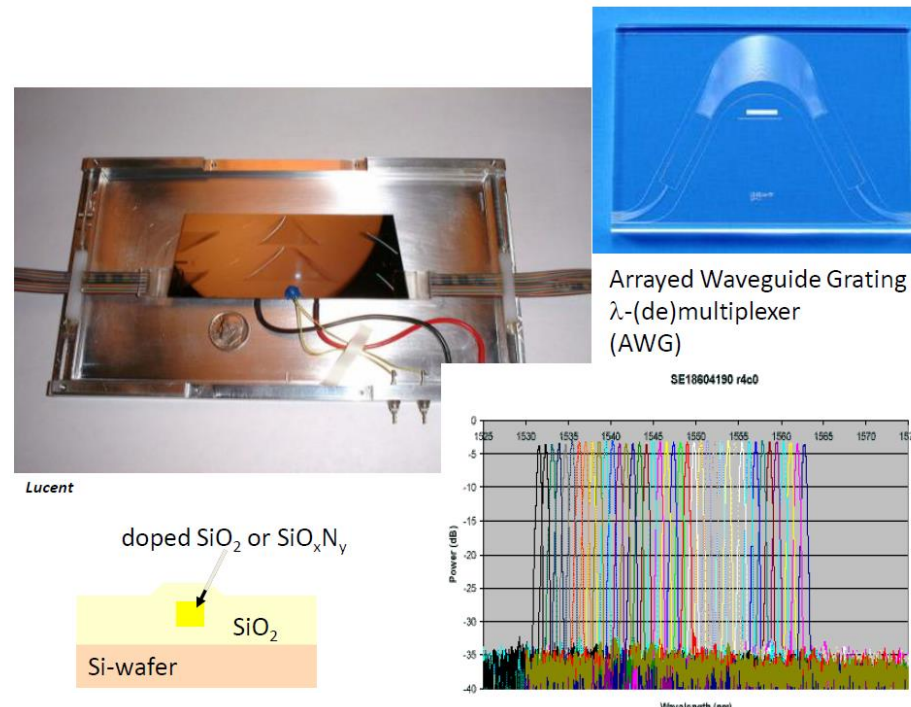


*Examples of InGaAs/InP PICs*

# Materials for photonic integrated circuits

## Glass-like materials ( $\text{SiO}_x$ , $\text{SiO}_x\text{N}_y$ )

- very low losses
- optimized for fiber coupling
- most common implementation consist of Silica on Silicon ( $\text{SiO}_x$  on Si)
- low index contrast, hence large waveguide (as in optical fiber)



Examples of silica on silicon waveguides

# Materials for photonic integrated circuits

## SOI (Silicon-on-insulator)

- Silicon layer bonded onto Silica ( $\text{SiO}_2$ )
- Silicon is transparent at telecom wavelengths (1550nm and 1300nm)
- High index contrast  
3.45 (Silicon) to 1.0 (air) / 1.45 (silica)
- CMOS compatibility

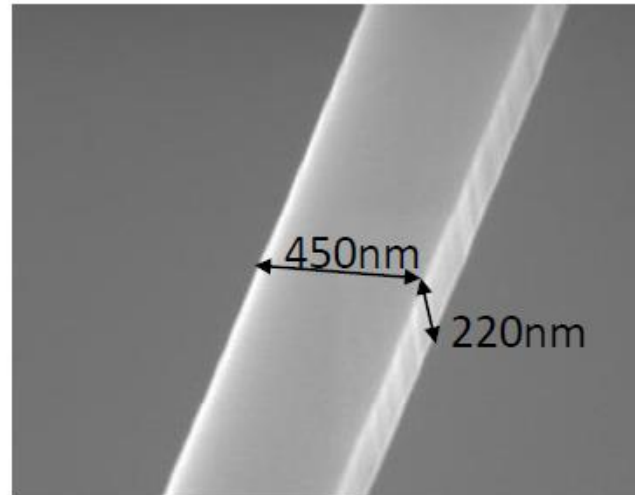
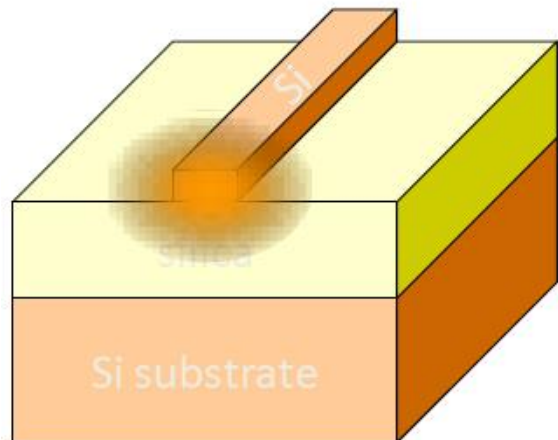
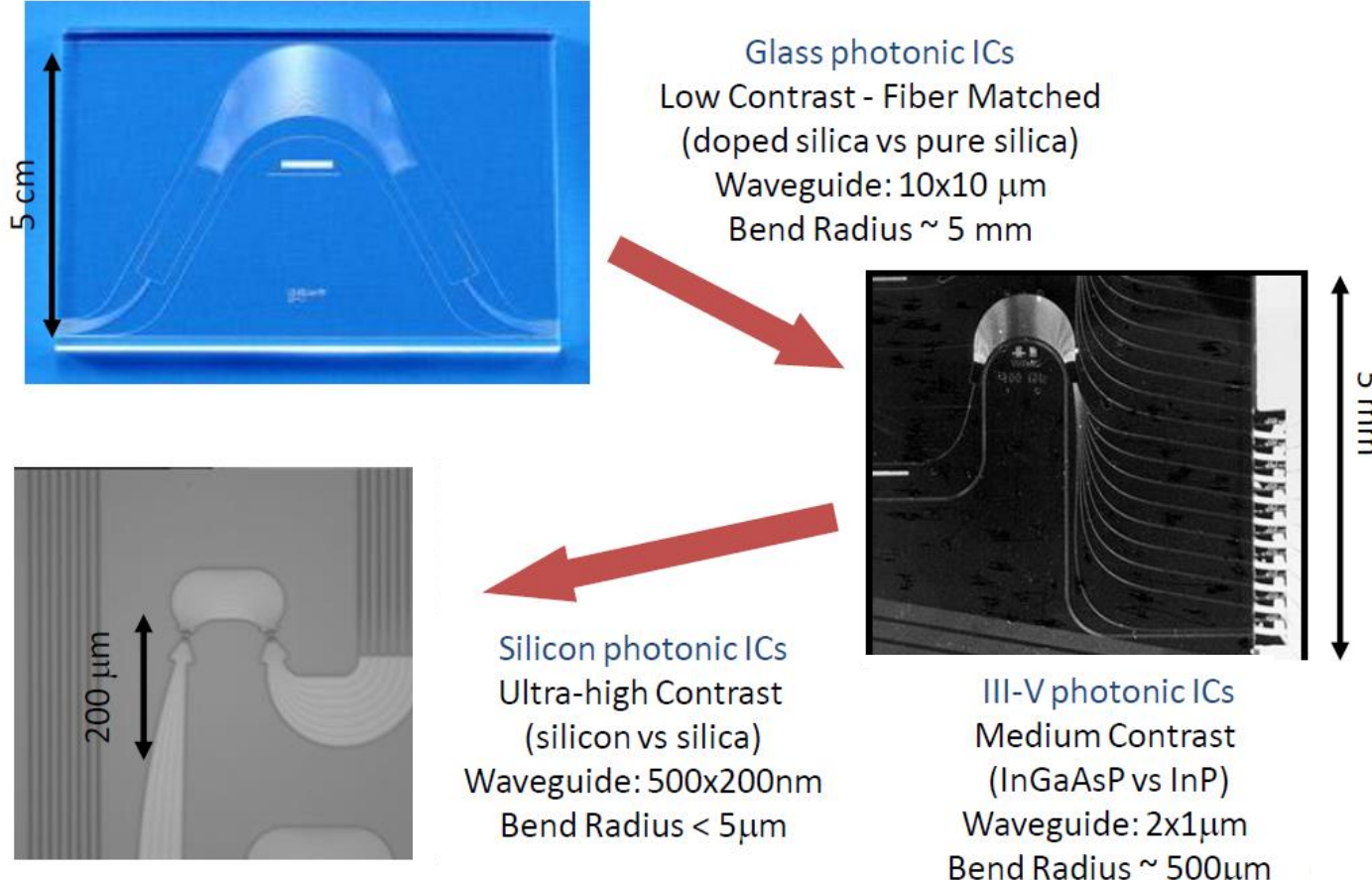


*Illustration of an SOI waveguide*

# Silicon nanophotonics

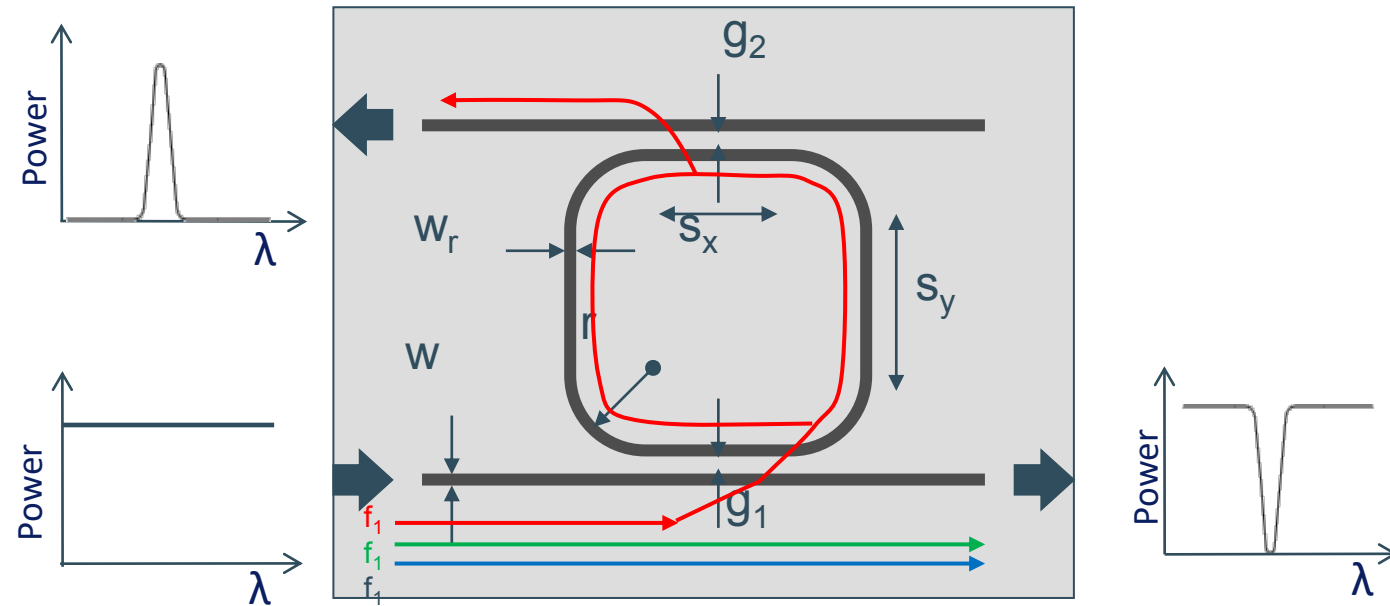
Silicon nanophotonic waveguides (or photonic wires) can strongly confine light in a submicron waveguide core, allowing sharp bends and compact components.



*Impact of increasing index contrast on typical size of photonic integrated circuits.*

# Ring and racetrack resonators

An interesting application of waveguides are ring resonators. They allow to separate a well-defined wavelength band from a broadband spectrum.



Schematic illustration and typical dimensions of a ring resonator.

In a ring resonator, light resonates if the wavelength fits a whole or multiple times in the circumference of the ring. Incoming light from the bus waveguide is coupled to the ring via a directional coupler:

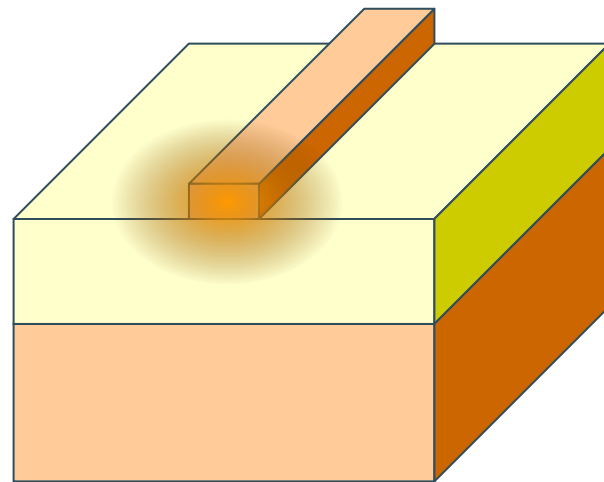
**On resonance:** light is transferred by the ring to the drop waveguide.

**Off resonance:** light stays in the bus waveguide.

Typical dimensions:	
$w$	= 450nm
$w_r$	= 500nm
$r$	= 4.5μm
$s_x$	= 6μm
$s_y$	= 6μm
$g_1$	= 180nm
$g_2$	= 190nm

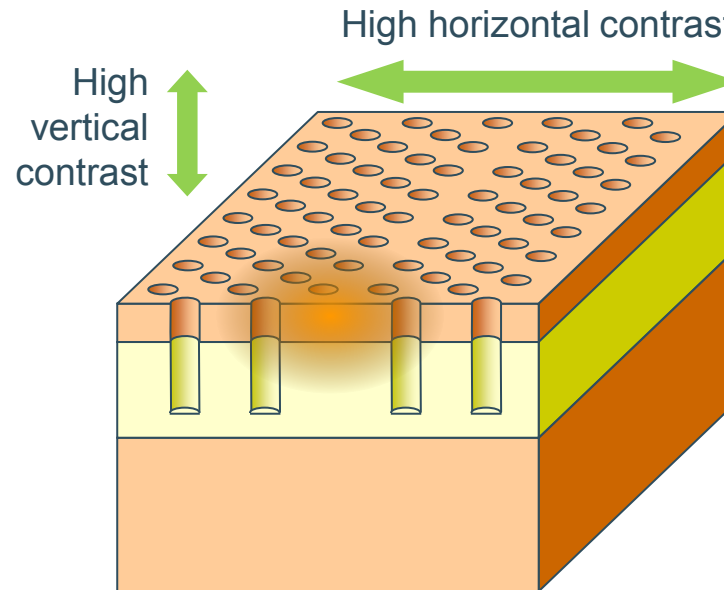
# Photonic crystals

Photonic wires are like ‘*conductors*’ for light. The next step is to make structures that are the equivalent of ‘*semiconductors*’, i.e. photonic crystals.



## Photonic Wires:

- In-plane: guiding by total internal reflection
- Vertical: total internal reflection



## Photonic Crystals:

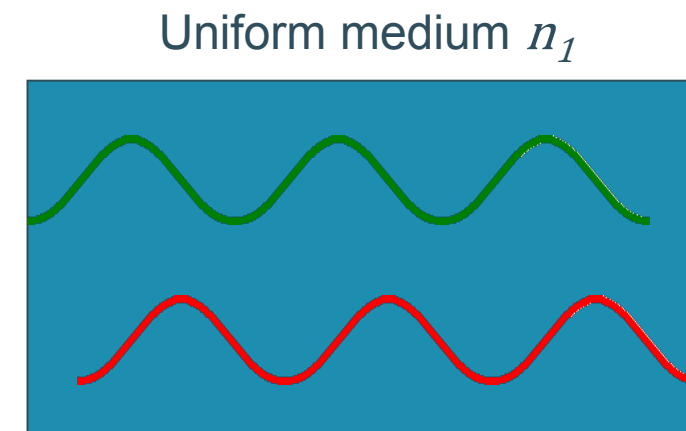
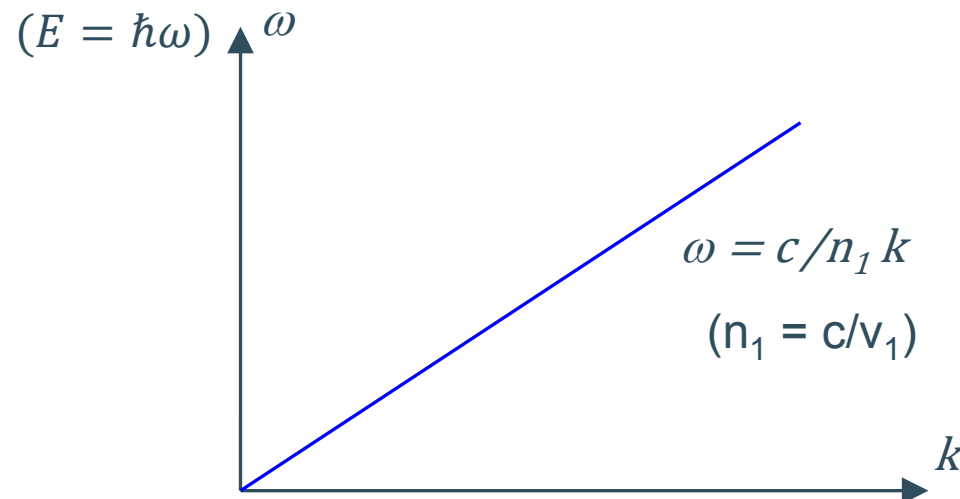
- In-plane: guiding by the photonic band gap
- Vertical: total internal reflection

The special properties of photonic crystals enables a completely new class of optical functions...

W. Bogaerts, IMEC

# Formation of an optical bandgap

The dispersion relation defines the relationship between angular frequency  $\omega$  of the photon and its wavevector  $k = 2\pi/\lambda$ . This dispersion relation describes the optical properties of a material, and a plot of  $\omega$  against  $k$  will indicate the allowed energies (bands) or states at given  $k$ -vectors.



For a one-dimensional, homogeneous material with a uniform dielectric function, the band structure or dispersion relation, is simply:  $\omega = ck/n$  where  $n$  is the refractive index of the material.

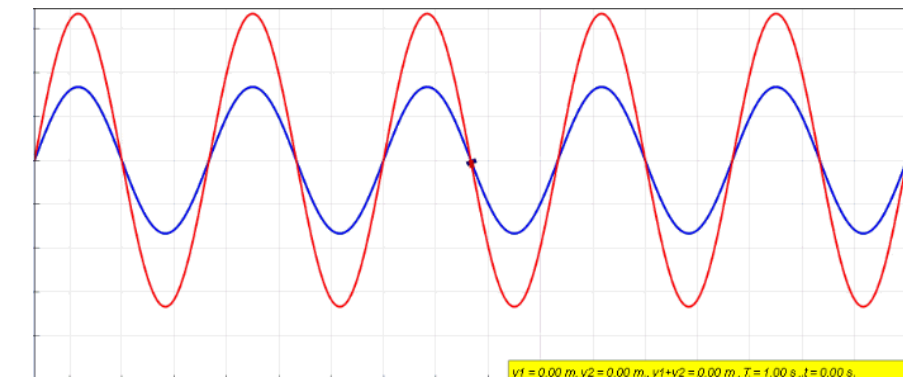
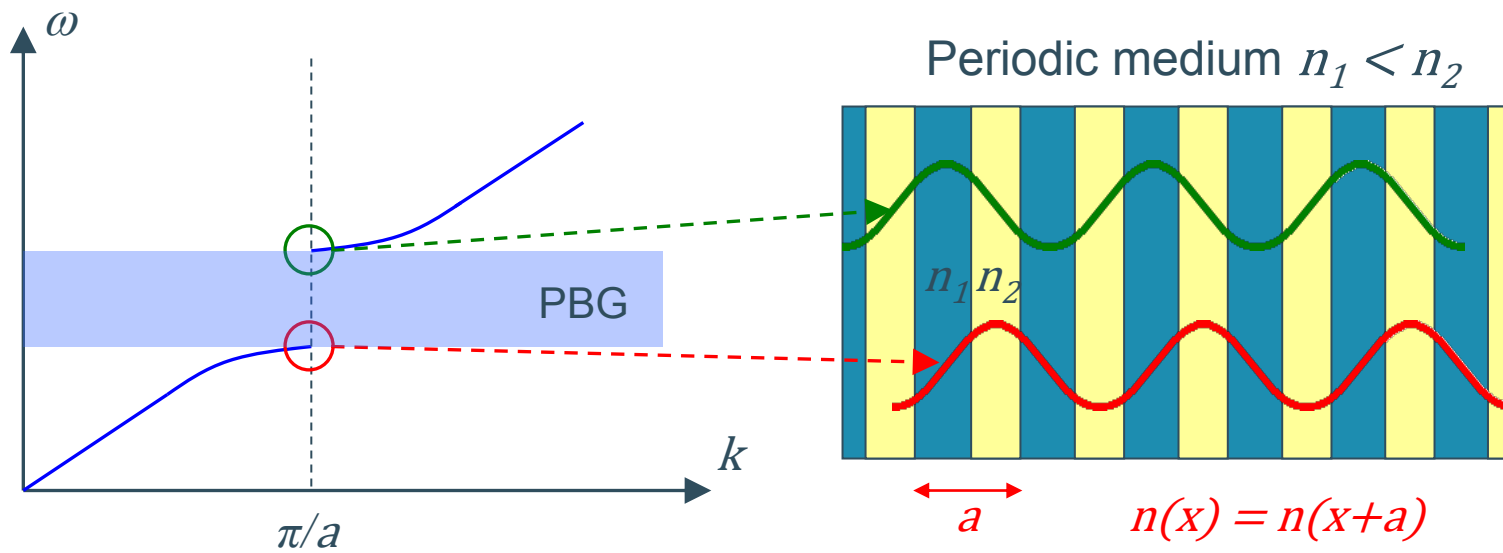
# Formation of an optical bandgap

However for a periodic material, the periodic function causes forward moving waves to be partially reflected at every interface. For frequencies that fulfill the Bragg condition ( $a/2=\lambda/4$ ), there will be total reflection conditions in the material and the interference of the forward and backward waves creates a standing wave at the edge of the Brillouin zone ( $\pi/a$ ).

$\omega(k)$  flattens out, i.e. the group velocity of the propagating waves  $d\omega/dk$  vanishes.

Light with frequencies within the photonic band gap cannot propagate in the photonic crystal.

Note that the reflected waves have a phase shift of  $180^\circ$  only if the incident light goes from low-index medium in a high-index medium.

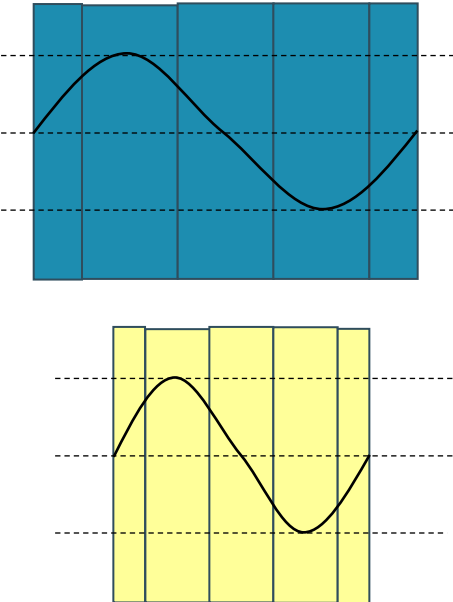


Animation of a standing wave (red) created by the superposition of a left traveling (blue) and right traveling (green) wave.  
<https://commons.wikimedia.org/wiki/File:Waventerference.gif>

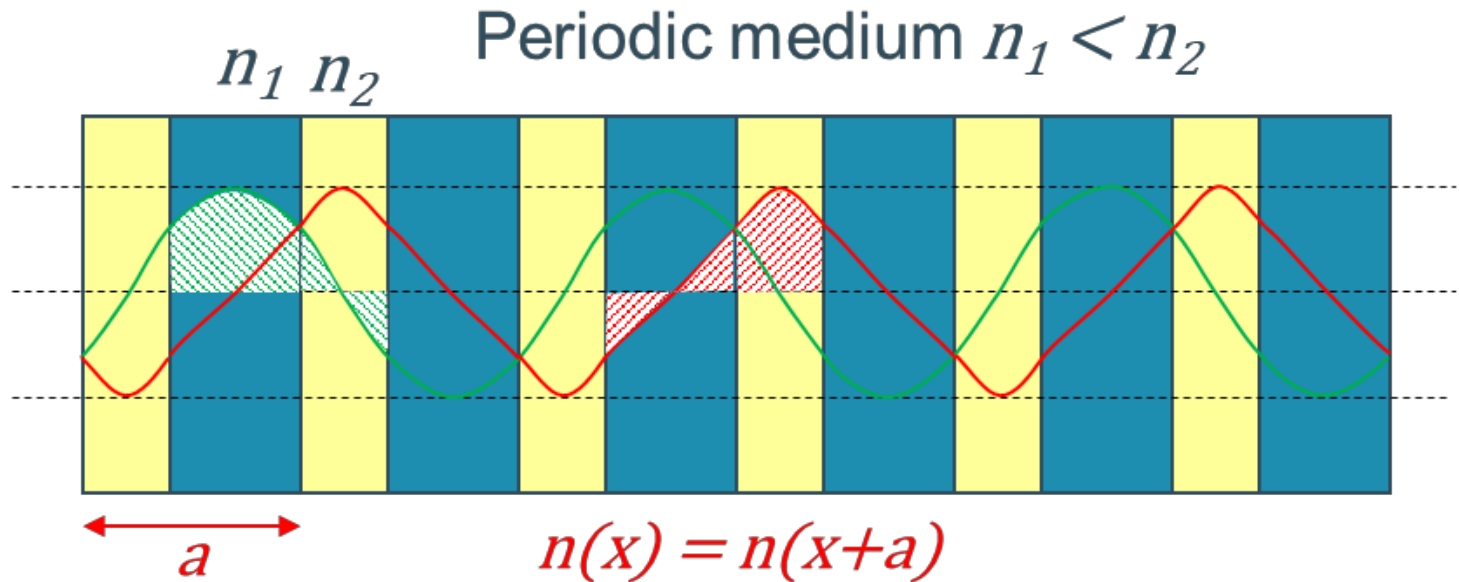
# Photonic crystals

- 1-d photonic crystal: distributed Bragg reflector. A visual description

The condition  $a/2=\lambda/4$  imposes a different “ $a$ ” distance for each  $n$  because  $\lambda$  depends on  $n$  (for a fixed frequency).



Representation of the wavelength in media with refractive index  $n_1$  (top) and  $n_2$  (bottom) for the same frequency. The wavelength is larger in regions with lower  $n$ .

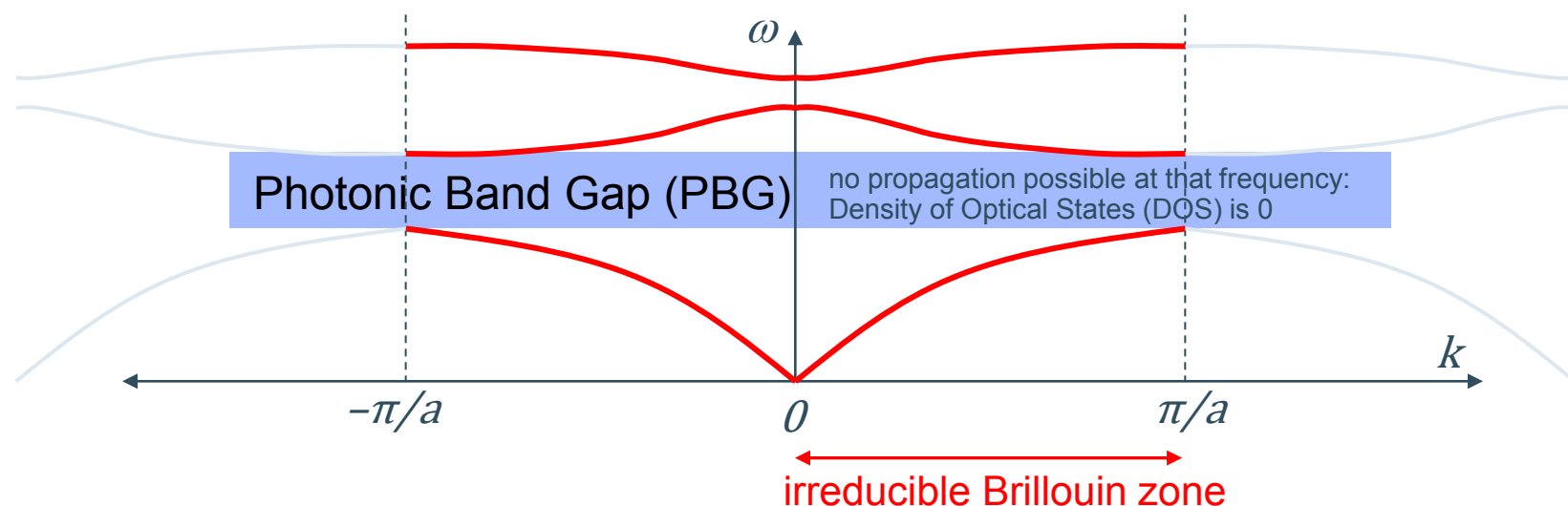
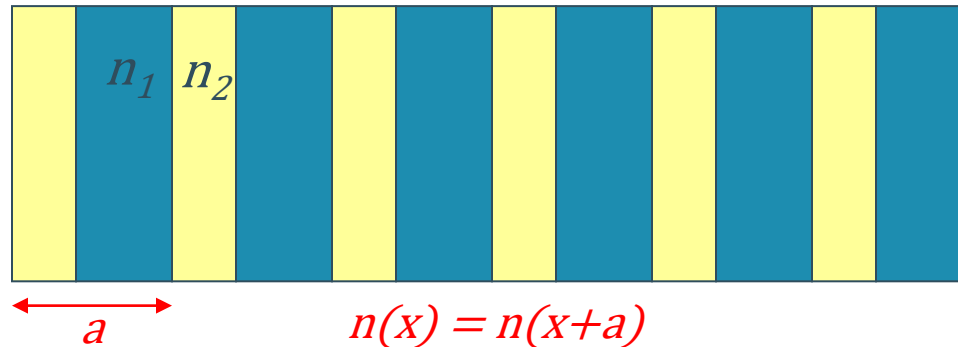


If  $Energy \sim \int E dx$ , the green wave should have higher energy

# Photonic crystals

1-d photonic crystal: distributed Bragg reflector

Periodic medium  $n_1 < n_2$



# Photonic crystals

A photonic crystal is a material whose dielectric function varies periodically. This periodicity requires the solution of the wave equations to satisfy the Floquet–Bloch theorem, which states that the solutions to the equations for periodic media are plane waves modulated by a periodic function with lattice periodicity.

Let's consider a 1D homogenous medium. The wave equation (Maxwell equations, see slide #48 chapter 3, but without damping term):

$\nabla^2 E - \mu\epsilon \frac{\partial^2 E}{\partial t^2} = 0$ , for the electric field  $E(z,t)$  of an electromagnetic wave is given by :

$$\frac{c^2}{n^2(z)} \frac{\partial^2 E(z,t)}{\partial z^2} - \frac{\partial^2 E(z,t)}{\partial t^2} = 0 \quad (c^2 = \frac{1}{\mu_0 \epsilon_0}, n = \sqrt{\mu_r \epsilon_r})$$

# Photonic crystals

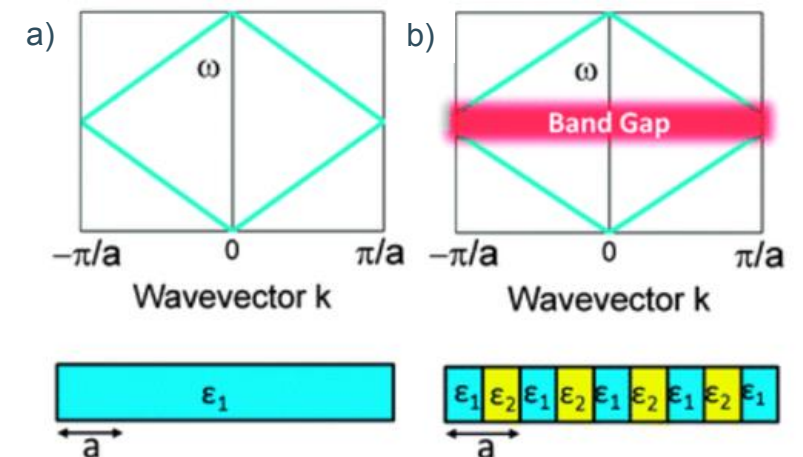
- In a homogeneous medium,  $n(z)$  is constant and the solution of the wave equation is a plane wave:

$$E(z,t) = E_0 e^{ikz} e^{-i\omega t} \text{ where } k = 2\pi / \lambda \text{ and } \omega = (c/n)k$$

Now consider a 1D crystal with a periodic refractive index  $n(z)=n(z+a)$ . According to the Floquet-Bloch theorem, the solution of the wave equation then becomes:

$$E(z,t) = u_k(z) e^{ikz} e^{-i\omega t} \text{ where } u_k(z) \text{ has the same periodicity than } n(z).$$

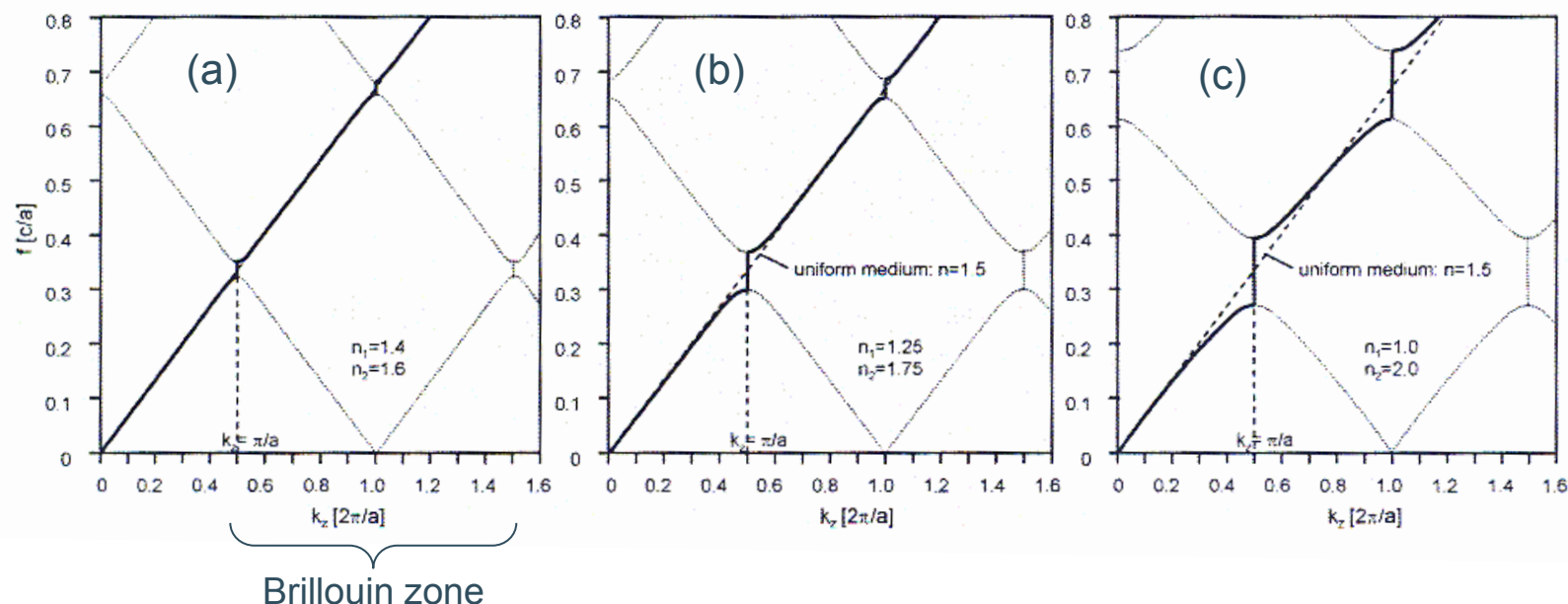
Like in a periodic crystal, the periodicity of  $n(z)$  in a photonic crystal leads to discontinuities in the dispersion relation  $\omega(k)$ . There are forbidden values of  $\omega$  in the photonic crystal.



Schematic illustrating: (a) the dispersion relation for a homogeneous material demonstrating the ‘folding effect’ of Blochs theorem and (b) a periodic material with a varying dielectric function and real lattice periodicity  $a$ .

# Photonic crystals

Like in a periodic crystal, the periodicity of  $n(z)$  in photonic crystal leads to discontinuities in the dispersion relation  $\omega(k)$ . There are forbidden values of  $\omega$ . The bigger the diffraction index contrast, the larger the bandgap.



The dispersion relation for a 1-D periodic medium with a)  $n_1 = 1.4$  and  $n_2 = 1.6$ , b)  $n_1 = 1.25$  and  $n_2 = 1.75$ , c)  $n_1 = 1$  and  $n_2 = 2$  with  $n_1 d_1 = n_2 d_2$ . The linear dispersion relation of a uniform medium with  $n = 1.5$  is also plotted.

# Photonic crystals versus electronic crystals

Photonic crystal can be seen as equivalent to a periodic solid for electrons. Both have a periodic structure and, therefore, in both cases Bloch's theorem can be used resulting in a band structure.

## Periodic crystal

- Particles = electrons
  - Schrödinger equation
  - Periodic potential
- 
- Band structure
    - Allowed energy states
    - Forbidden energy states (Band Gaps)

## Photonic crystal

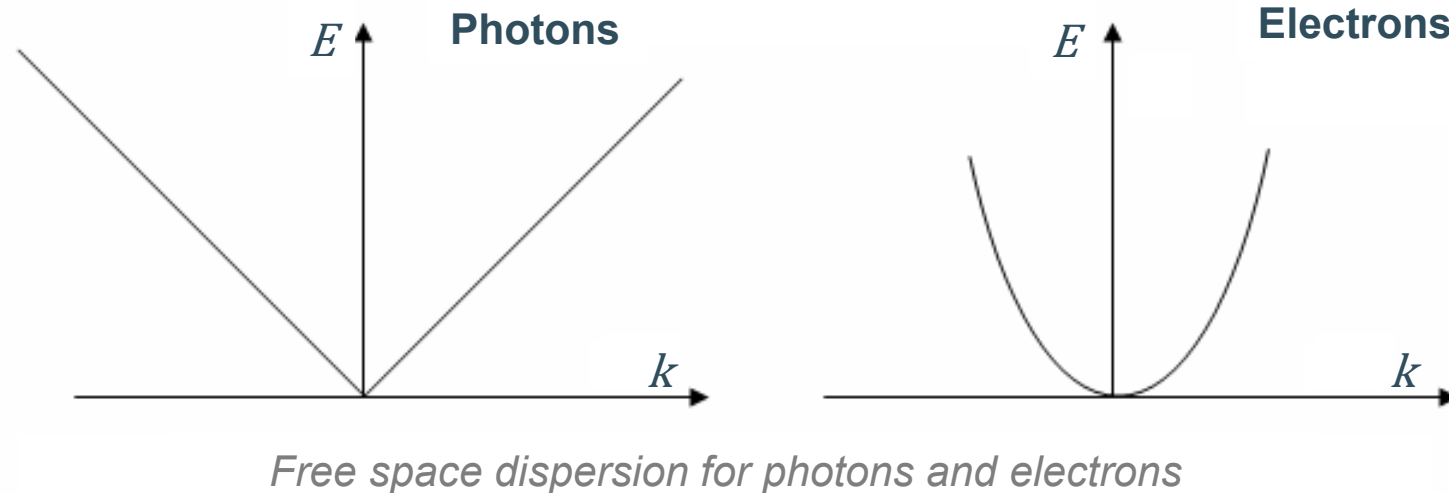
- Electromagnetic waves
  - Maxwell equations
  - Periodic refractive index
- 
- Band structure
    - Allowed “energy” states (frequencies)
    - Forbidden “energy” states (frequencies)
- Photonic Band Gap

# Photons and electrons

The free space propagation of both electrons and photons can be described by plane waves.

The momentum for both electrons and photons:  $p = \hbar k$

- For photons  $k$  is given by  $k = (2\pi/\lambda)$  and the energy by  $E = \hbar(c/n)k$
- For electrons  $k = mv/\hbar$  and the energy  $E = p^2/2m = \hbar^2k^2/2m$

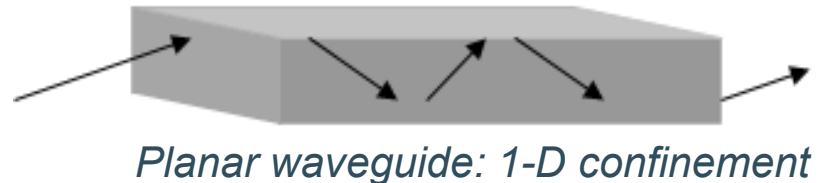


Other important differences between electrons and photons are:

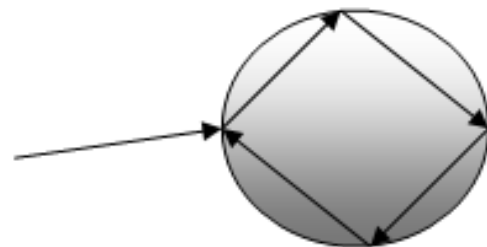
- The electron momentum is generally bigger than the photon momentum.
- Light waves are described by a vector field while the electron wavefunction is scalar.
- Photons satisfy Bose-Einstein statistics while electrons are Fermions.

# Confinement of light and electrons

## *Microscale confinement of light*



*Optical fiber: 2-D confinement*



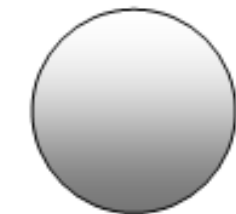
*Microsphere: 3-D confinement*

## *Nanoscale confinement of electrons*

*Thin film quantum well:  
1-D confinement*



*Quantum wire: 2-D confinement*

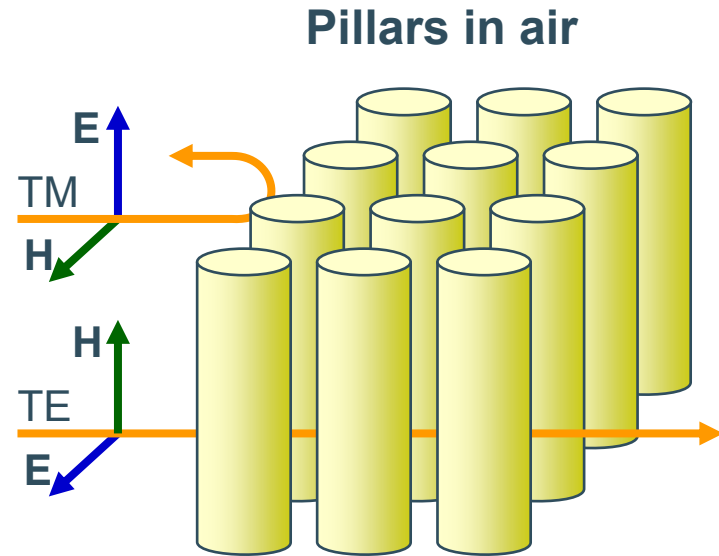


*Quantum dot: 3-D confinement*

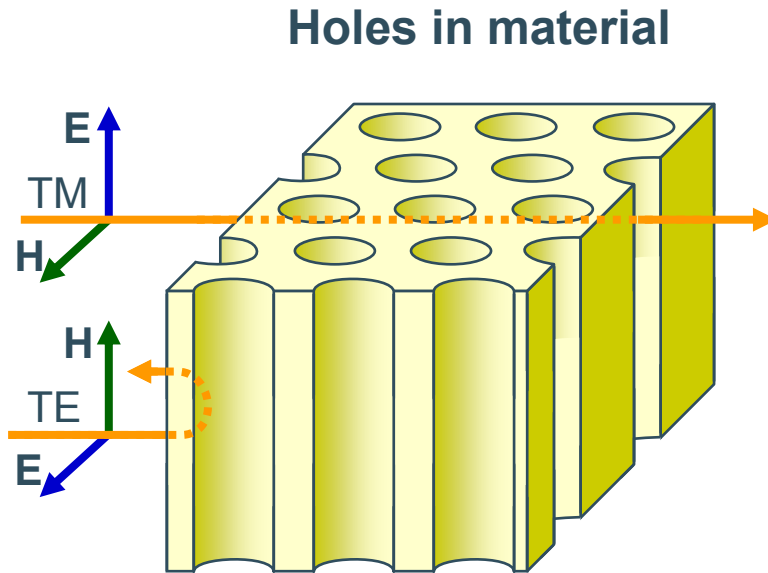
Confinement of light results in field variations similar to the confinement of electrons in a potential well. For light, the analogue of a potential well is a region of high refractive-index bounded by a region of lower refractive-index.

# Polarization in 2D photonic crystals

2D photonic crystals can be realized making two-dimensional periodic structures. The dispersion and the bandgap depends on the light polarization.



Only photonic bandgap for light with the electric field parallel to the pillar axis (= TM-polarisation)



Only photonic bandgap for light with the electric field perpendicular to the pillar axis (= TE-polarisation)

TE polarization (transverse electric field):  $E$  in the plane of the structure

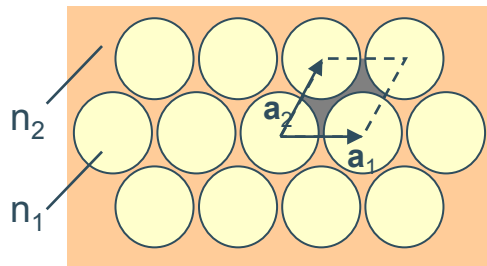
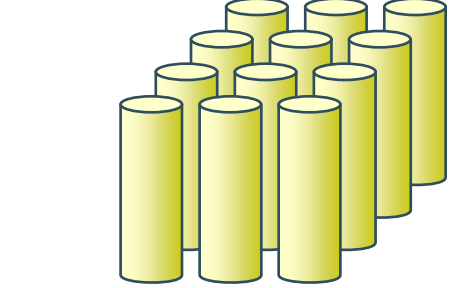
TM polarization (transverse magnetic field):  $E$  perpendicular to the structure

Note: A high refractive index contrast is needed in both cases

W. Bogaerts, IMEC

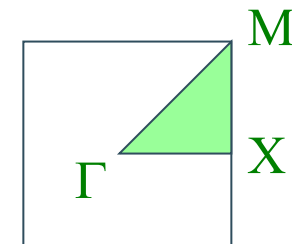
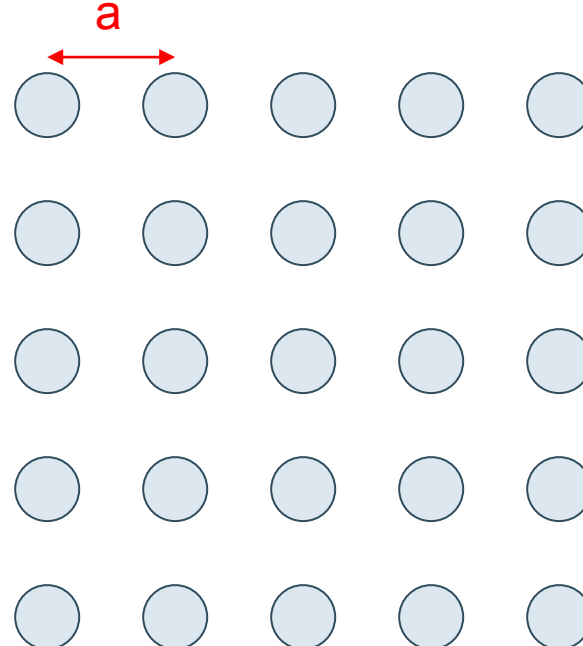
# 2D photonic crystals with pillars in air

In this structure a photonic bandgap exists for TM polarization.

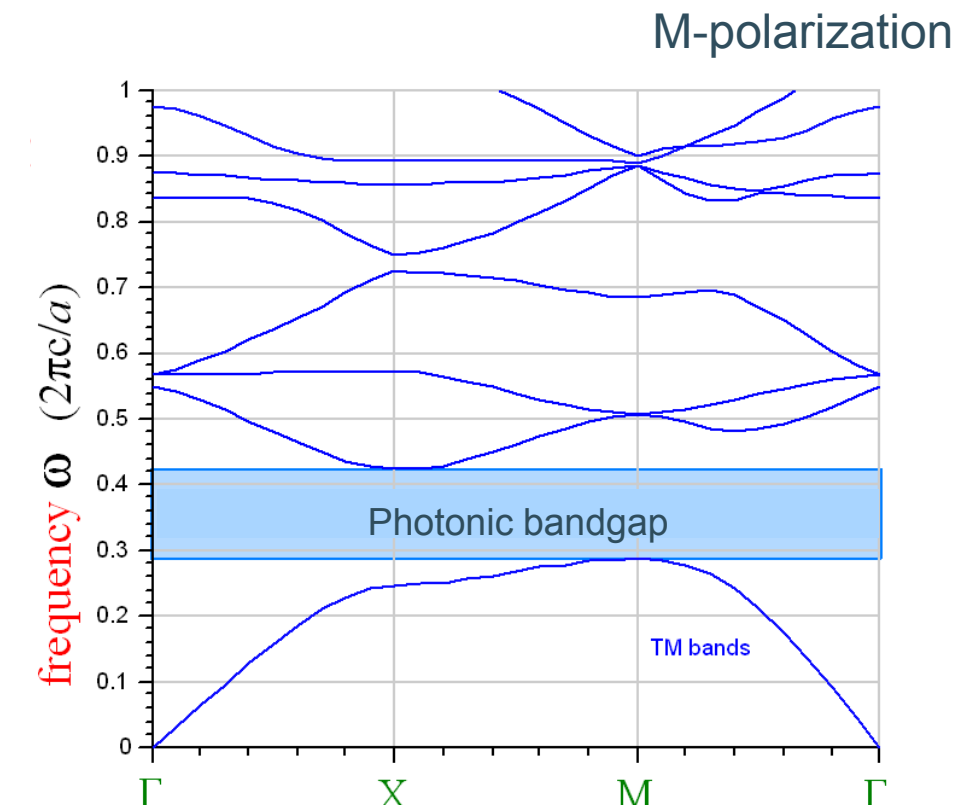


$$|\mathbf{a}_1| = |\mathbf{a}_2| = a$$

irreducible  
Brillouin zone

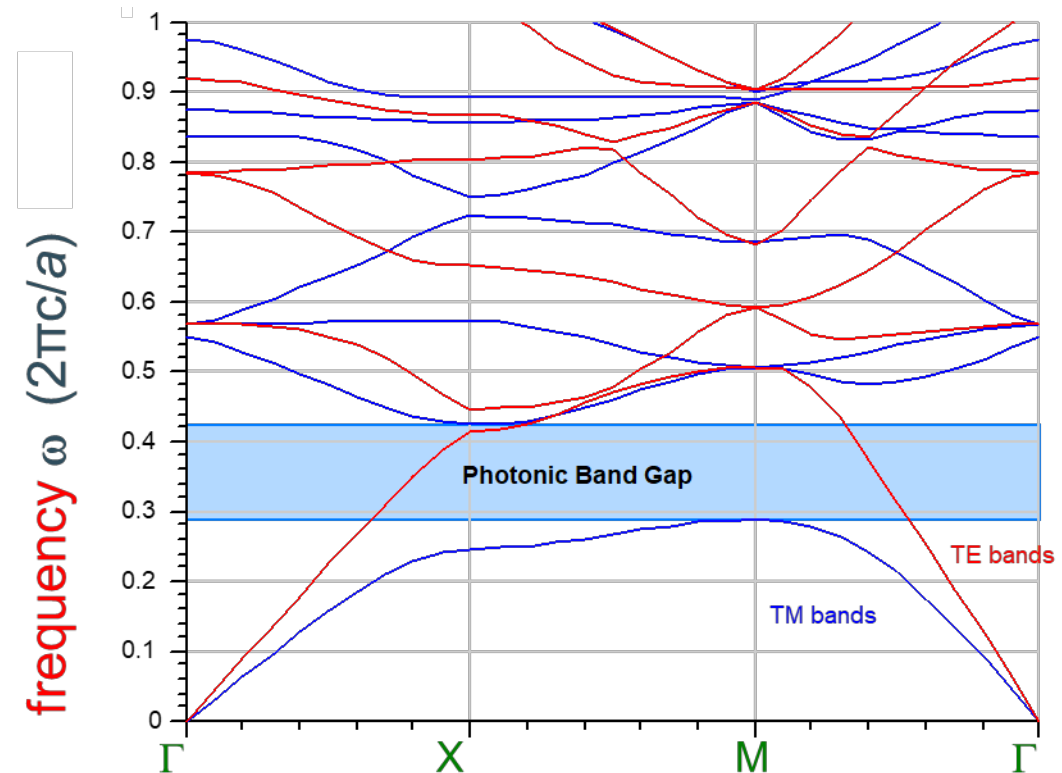
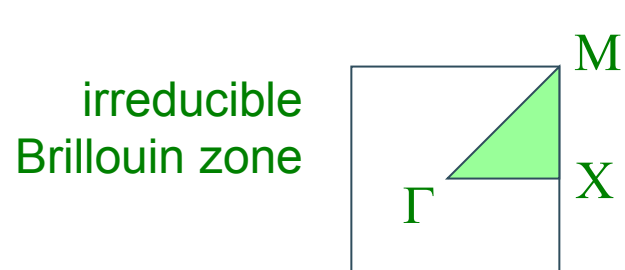
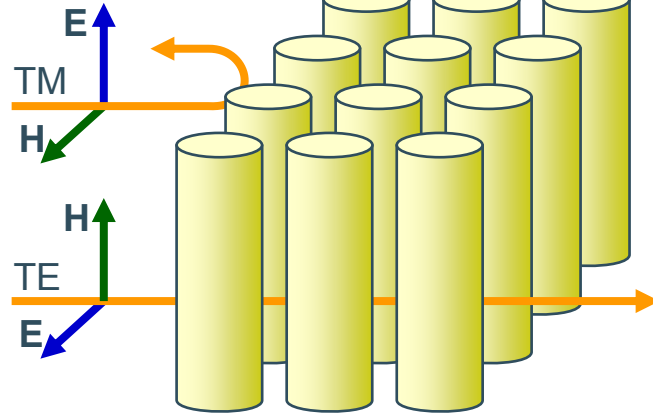


- Different  $k$ -directions correspond to different band gap frequencies
- An omni-directional PBG may not exist for small index contrast



# 2D photonic crystals with pillars in air

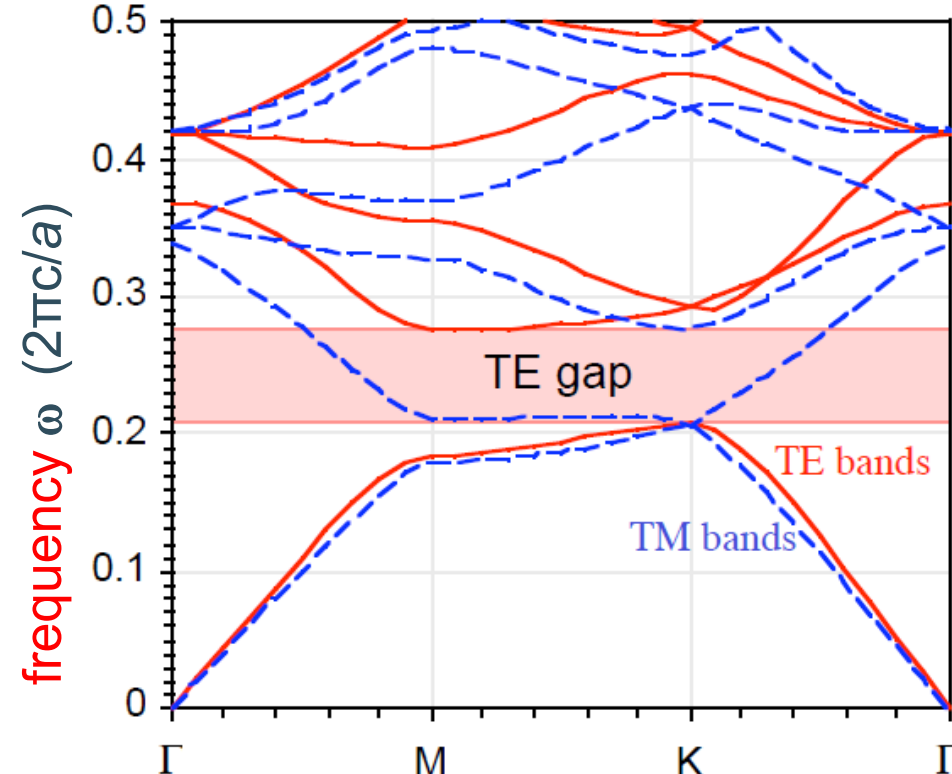
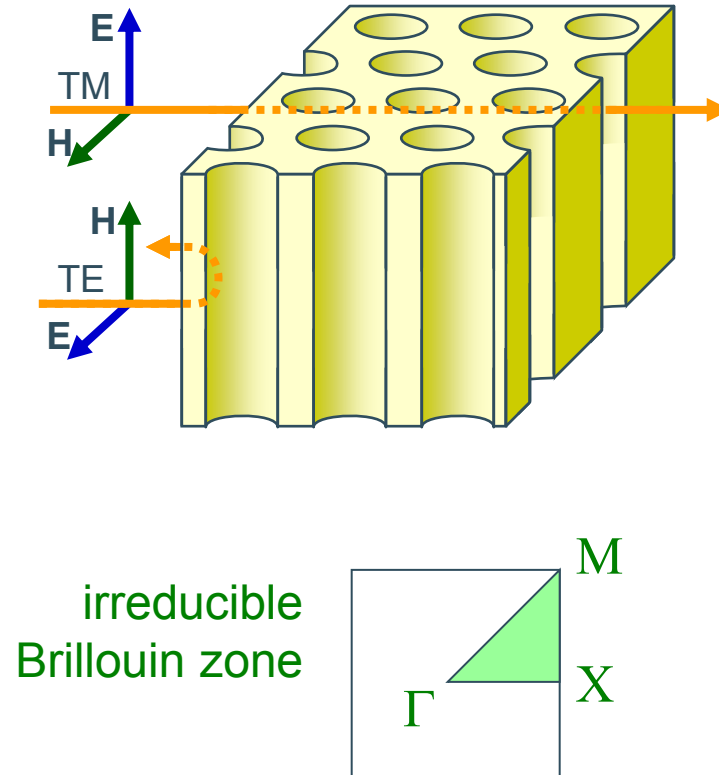
No photonic bandgap is observed for the TE bands.



- Photonic bandgap for 2D system with pillars in air only occurs for TM polarization

# 2D photonic crystals with holes in material

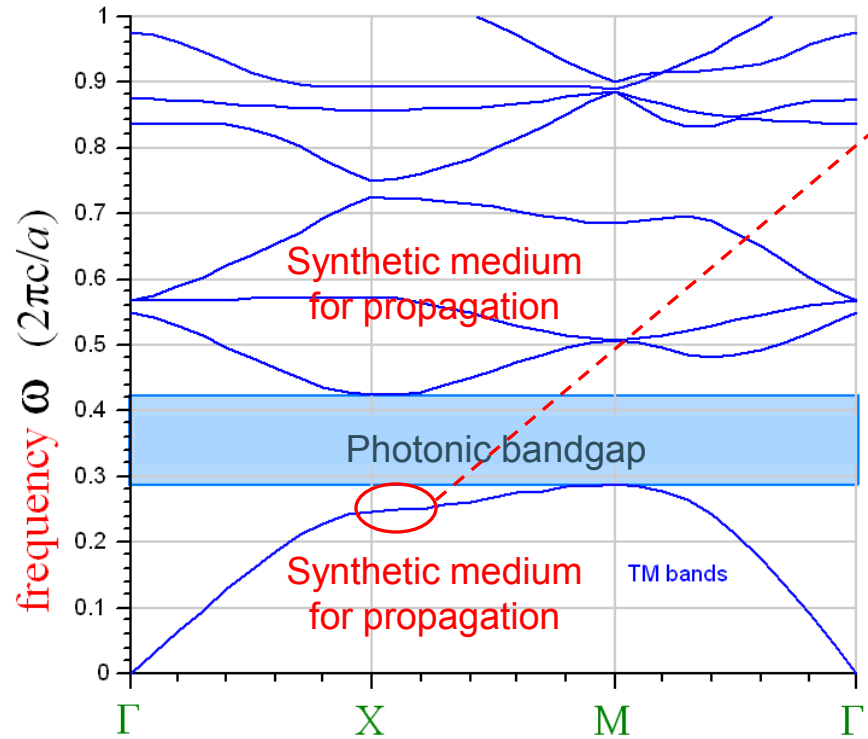
In this structure no photonic bandgap is observed for TM bands, only for TE bands.



- Photonic bandgap for 2D system with holes in material only occurs for TE polarization

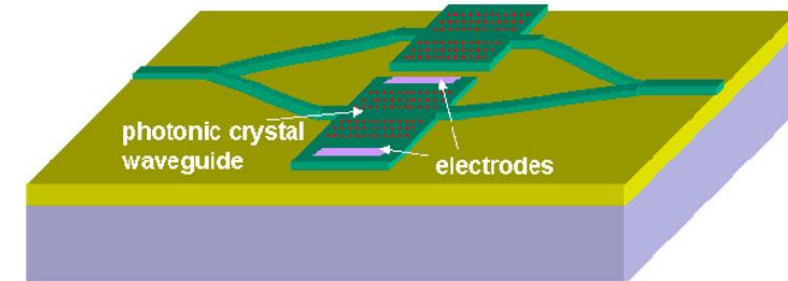
# Slow light in photonic crystals

At certain parts of the diagram some special observations are made.



$d\omega/dk = v_g \sim 0$ : large group index, **slow light**

Slow light leads to enhanced optical linear and nonlinear effects: spatial compression of light energy



Interferometer with reduced arm length using slow light in photonic crystal waveguide

In a photonic crystal the phenomenon of slow light is created by the resonant interaction of the guided mode with the periodic lattice, resulting in the formation of a slow moving interference pattern (the '*slow mode*'). Slow light might be interesting for sensing, to enhance the interaction between light and the sample under test.

A review paper: T. Baba, "Slow light in photonic crystals," Nat. Photonics 2, 465-473 (2008).

# Negative refraction in photonic crystals

Another interesting effect is the occurrence of a negative refractive index. This results in some remarkable optical properties and allows to make 'superlenses'.

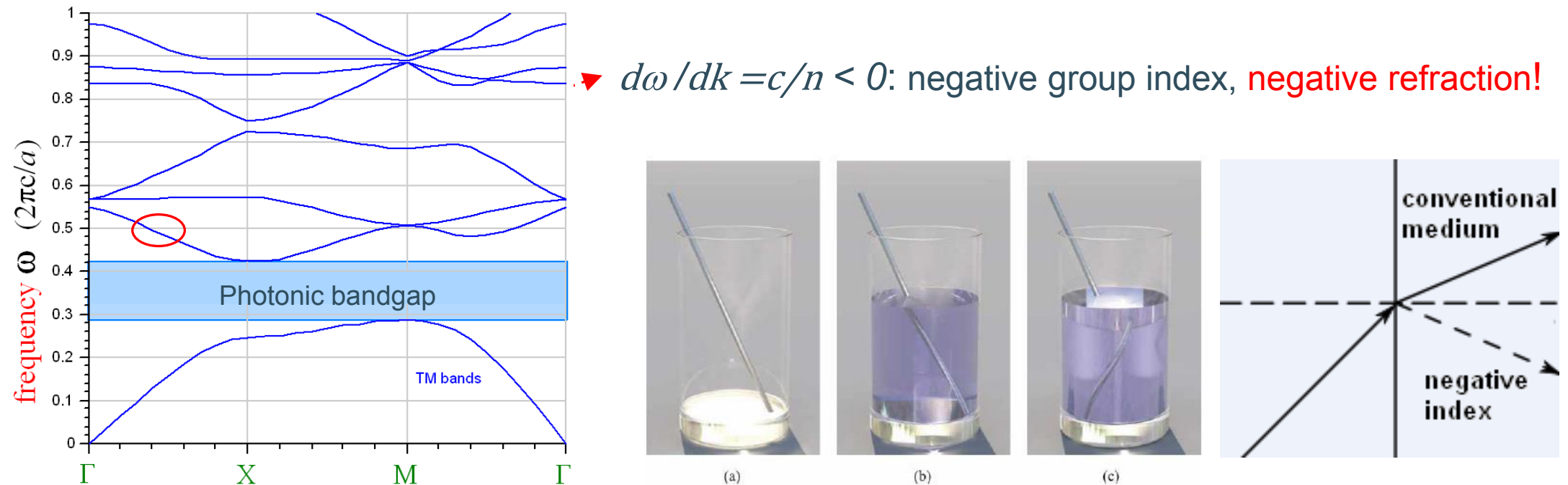
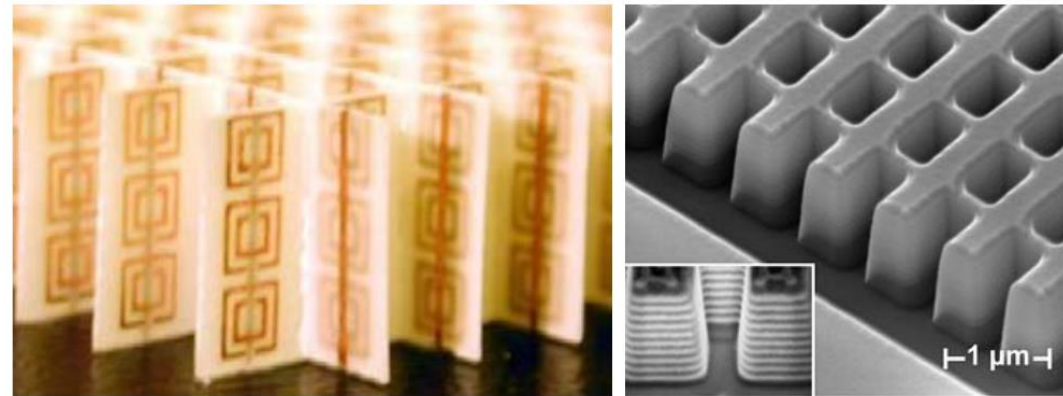
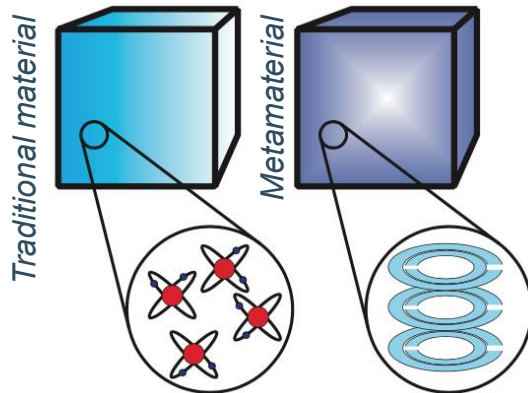


Illustration of the optical effect of negative refractive index. (a) Calculated ray-tracing image of a metal rod in an empty drinking glass. (b) Same scenery, but the glass is filled with normal water,  $n = 1.3$ , leading to ordinary refraction. (c) The water is replaced by "water" with a fictitious refractive index of  $n = -1.3$ .

C. Luo et al., "All-angle negative refraction in a three-dimensionally periodic photonic crystal," *Appl. Phys. Lett.* **81**, 2352 (2002).

# Metamaterials

Even though natural materials provide substantial means to control electromagnetic waves, they exhibit important shortcomings.



(left) A traditional material is composed of atoms and it derives its optical properties from the interaction of electromagnetic waves with its atoms. A metamaterial is composed of electric circuits that take over the role of atoms as basic constituents for the interaction with electromagnetic waves. (middle) One of the first microwave metamaterials. (right) Micrograph of an optical metamaterial with negative index of refraction.

We can devise artificial materials (*metamaterials*), in which atoms are replaced by small electric or plasmonic resonators as the basic constituents for the interaction with electromagnetic waves. The large freedom in their design allows for materials with electromagnetic and optical properties that are not accessible or much weaker in conventional materials, e.g., negative refractive index.

# Metamaterials

Permittivity and permeability of conventional materials derive from the response of constituent atoms to applied fields and  $\epsilon, \mu$  represent an average response of the system. On a length scale much greater than the separation between atoms all we need to know about the system is given by  $\epsilon, \mu$ .

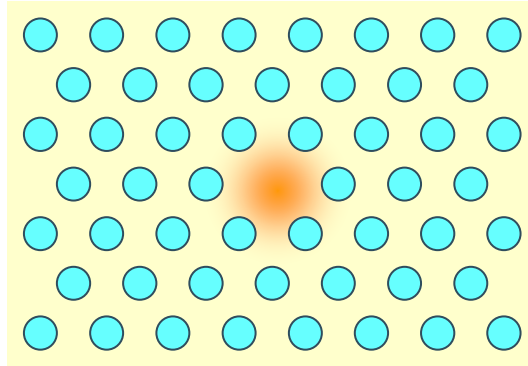
Metamaterials carry this idea one step further: the constituent material is structured into sub-units, and on a length scale much greater than that of the sub-units, properties are again determined by an effective permeability and permittivity valid on a length scale greater than the size of the constituent units. In the case of electromagnetic radiation this usually means that the sub-units must be much smaller than the wavelength of radiation (this is why nanotechnology could enable them).

In this way the properties of a complex structure can be summarized by  $\epsilon_{\text{eff}}, \mu_{\text{eff}}$  which is a great simplification in our thinking. So the concept is a familiar one but with the difference that the sub-units can take very many different forms. This flexibility in design enables metamaterials to have values for  $\epsilon_{\text{eff}}, \mu_{\text{eff}}$  which are not encountered in nature and in the present context that will mean one or both of these parameters being negative. Furthermore these materials can give magnetic activity at frequencies where previously materials have been thought of as magnetically inert.

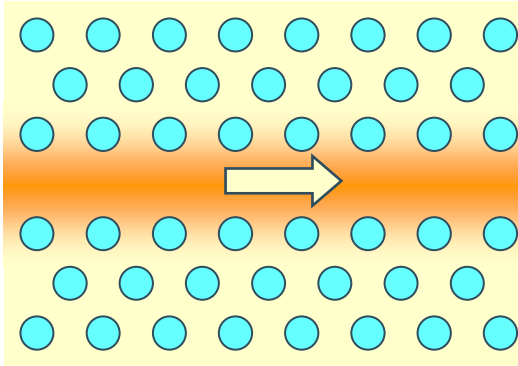
JB Pendry, Contemporary Physics 45:3, 191 (2004)

# A cage for light

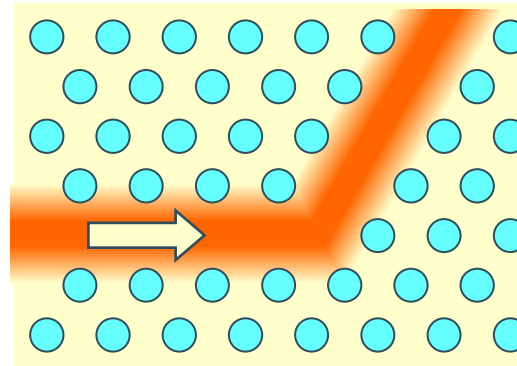
Photonic crystals can be used to confine light in small areas. In a perfect photonic crystal (e.g. with holes in a material) no light can exist with a frequency in the photonic bandgap. Defects can be formed in this structure by anything that breaks the periodicity. Around the defect light can exist with freqs in the photonic bandgap. The light is ‘trapped’ in these defects as it can not propagate away due to the properties of the photonic crystal.



*Light trapped in a missing hole.*



*Waveguide made by removing a row of holes.*



*Sharp bend in an optical waveguide.*

W. Bogaerts, IMEC

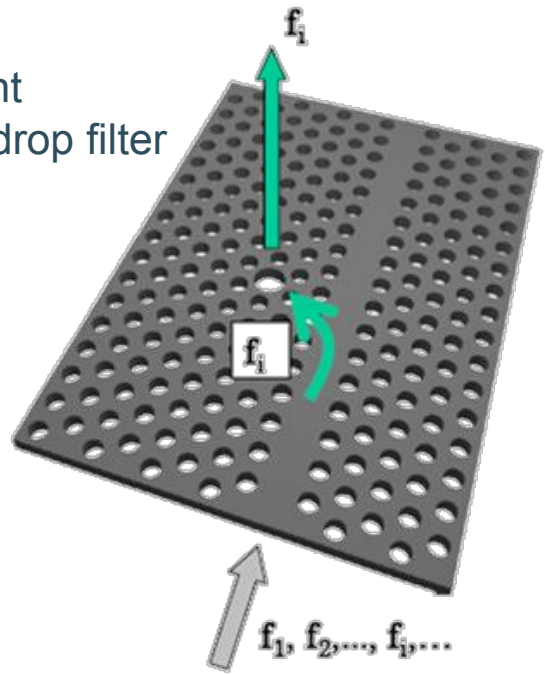
In this way waveguides can be made that confine the light in a narrow region. The waveguides can make sharp bends as the light can not get out of the waveguide into the photonic crystal, i.e. the light can not ‘miss the bend’. Light can be much more confined and follow much sharper bends than in optical fibres.

# Photonic crystal cavities

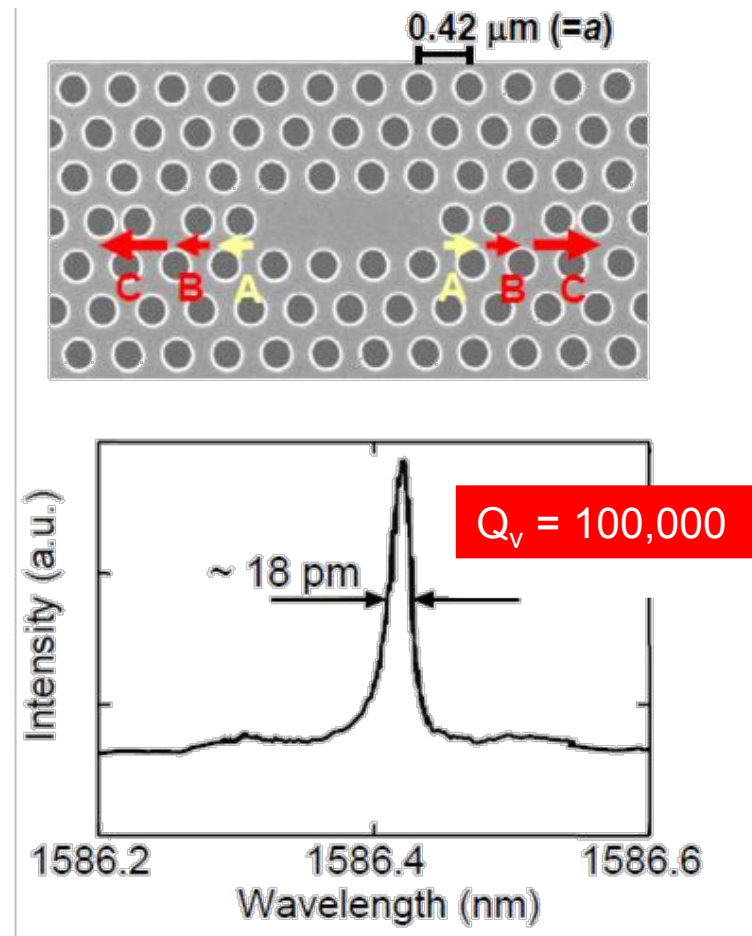
High quality optical filters can be produced using photonic crystals. Small changes in the local structure create a nano-cavity corresponding to a well-defined defect. These defects allow specific wavelengths to 'escape' from the waveguide.

Photonic crystals:

- Very good cavities
- Strong confinement
- Example: vertical drop filter



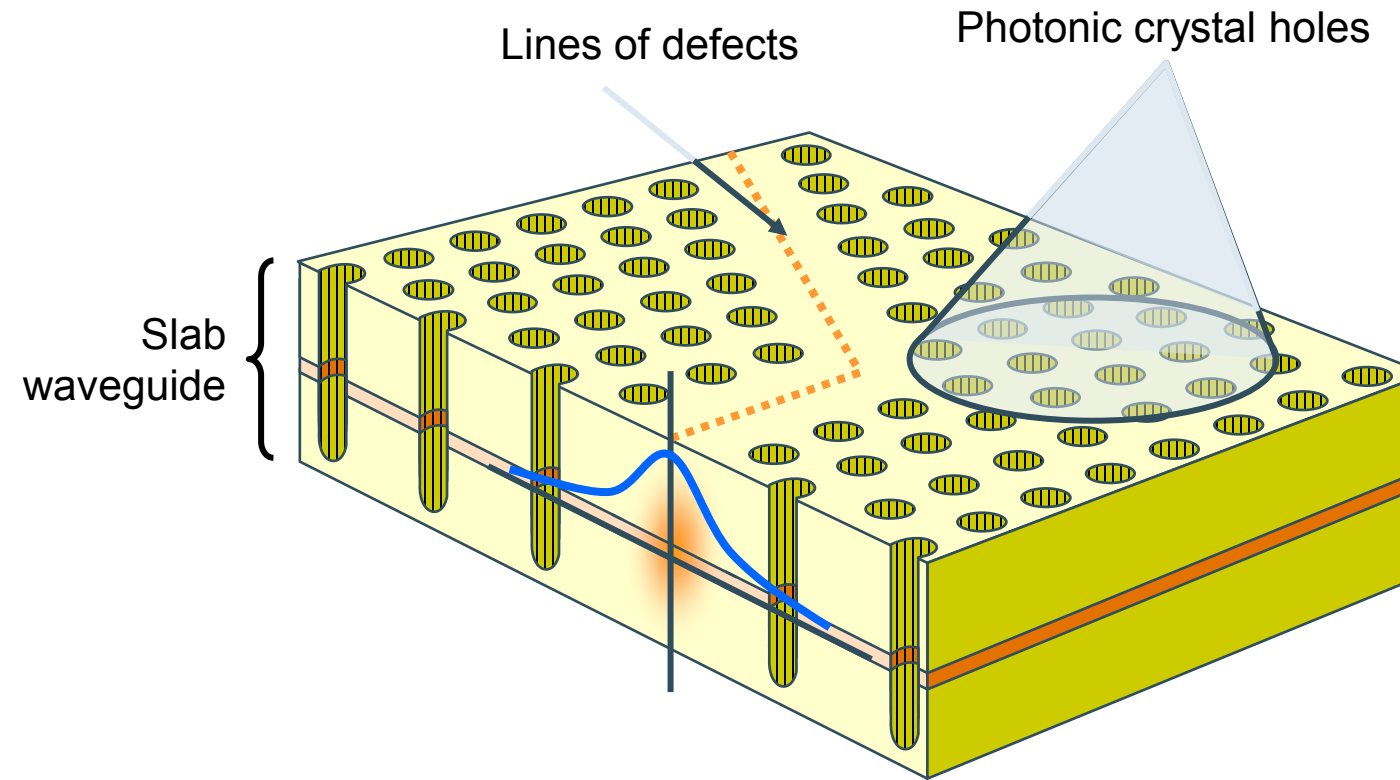
S. Noda, Nature 407, p.608 (2000)



W. Bogaerts, IMEC

# Photonic crystal slab

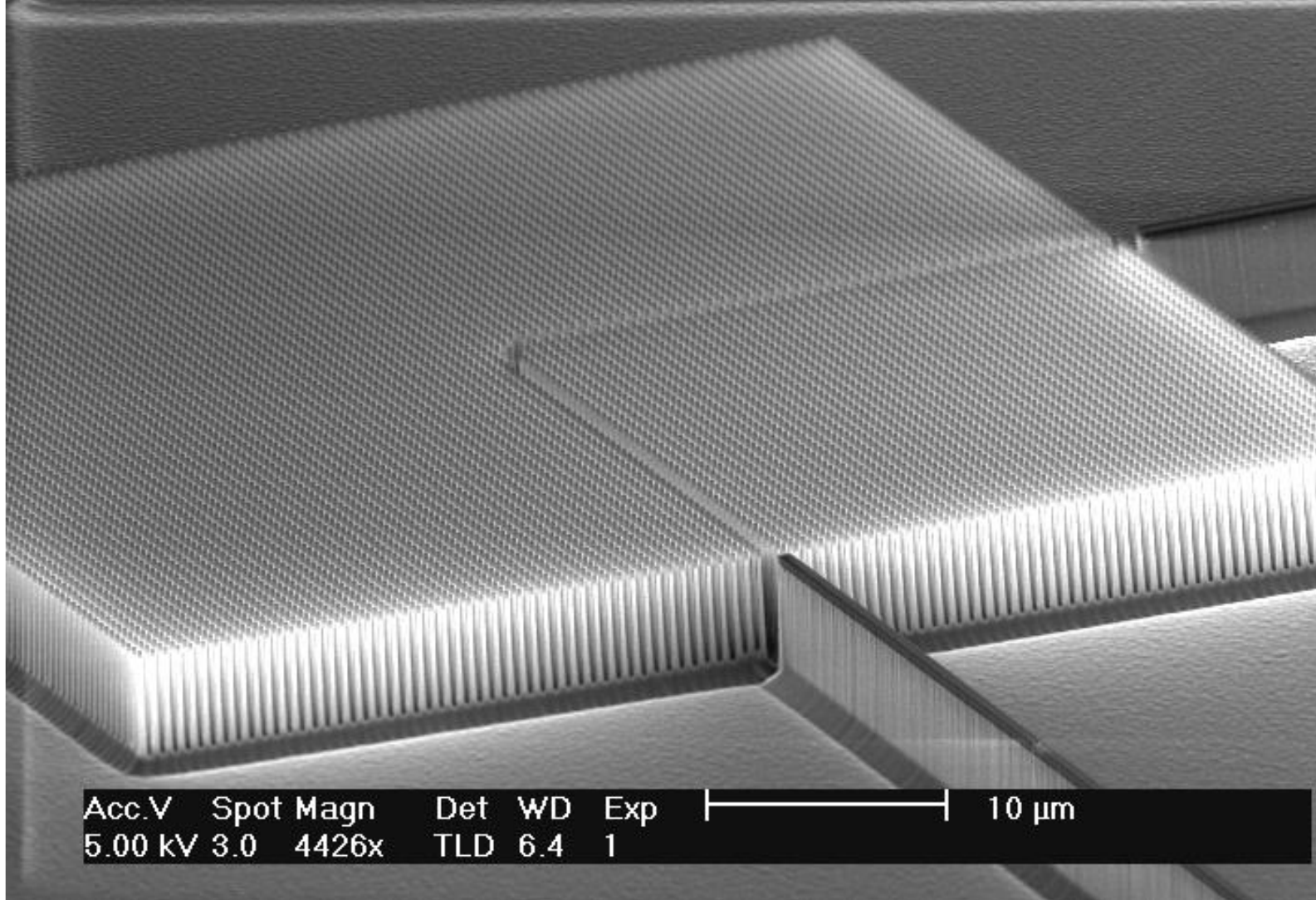
In real applications 2D crystals are usually combined with slab waveguides to confine the light vertically as well.



The vertical confinement is obtained by a layered waveguide. The horizontal confinement is formed by the photonic crystal (with a high index contrast).

W. Bogaerts, IMEC

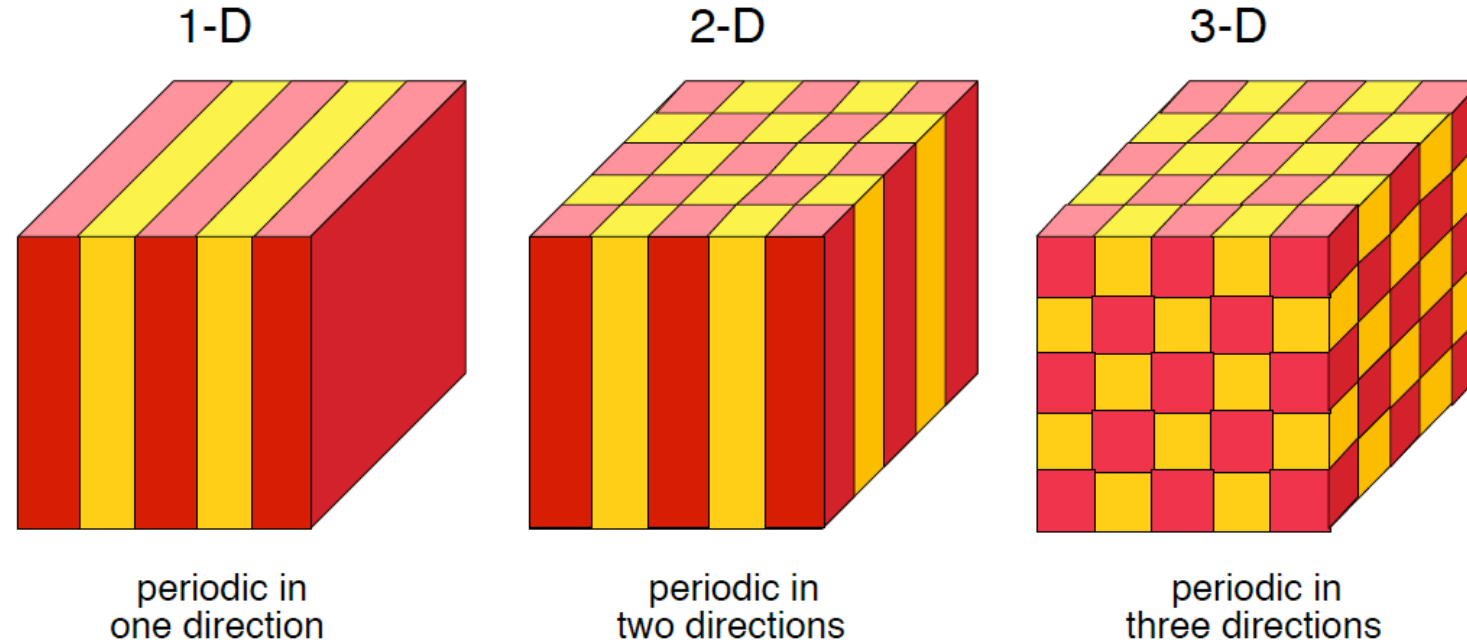
# Photonic crystals



*Silicon-based photonic crystal  
with a line of defects.*

# 3D photonic crystals

In order to make a 3D photonic crystal a three-dimensional periodic structure is needed.

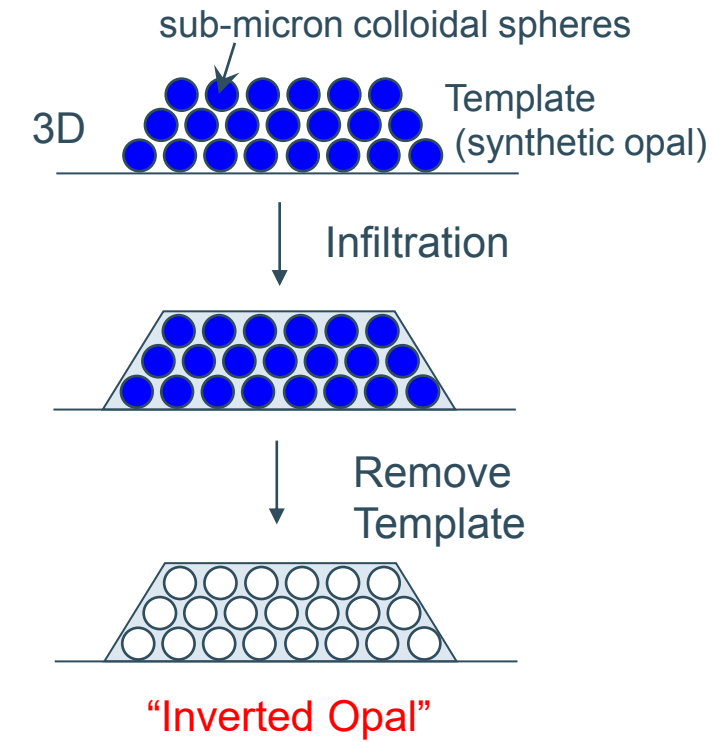
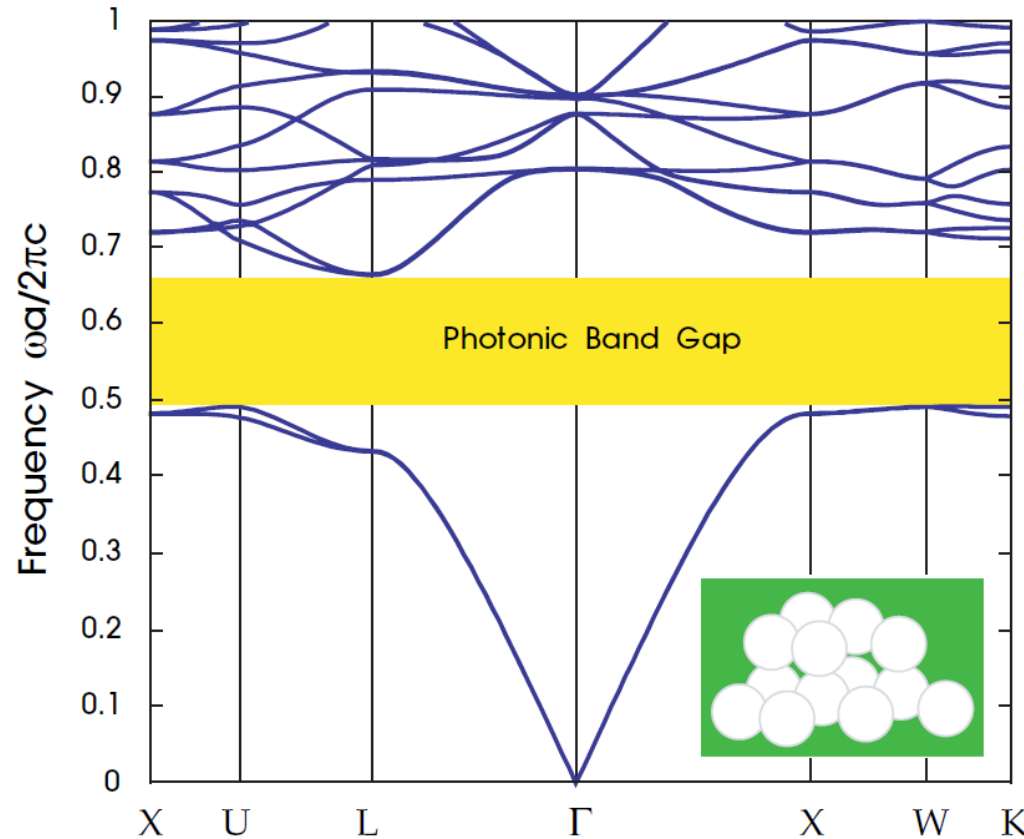


*Schematic depiction of photonic crystals periodic in one, two, and three directions, where the periodicity is in the material structure of the crystal.*

Only a 3D periodicity, with a more complex topology than is shown here, can support an omnidirectional photonic bandgap.

# 3D photonic crystals

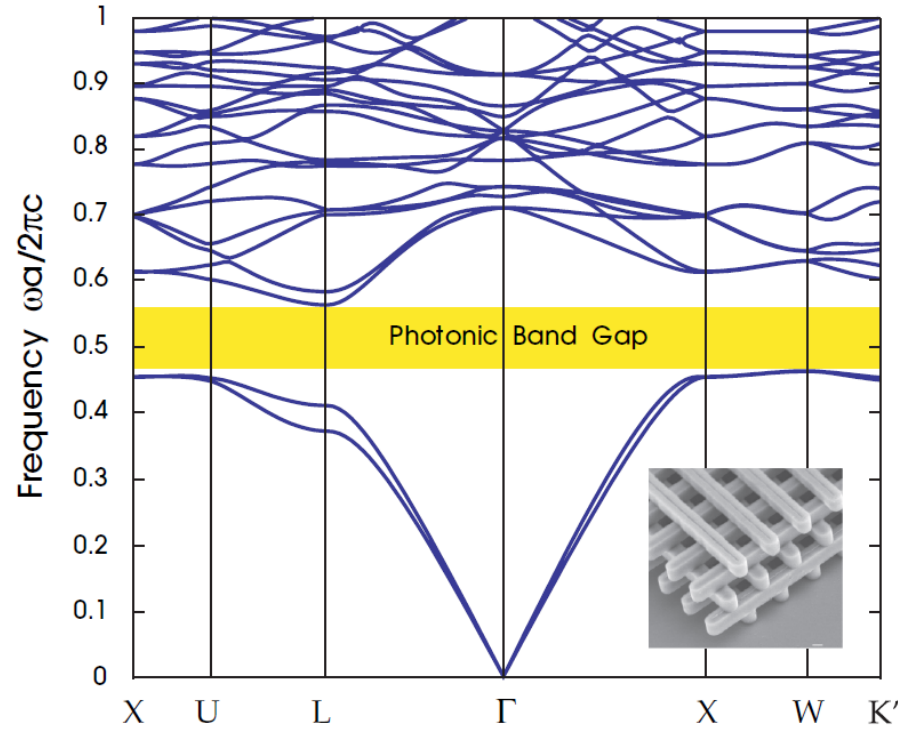
3D photonic bandgap in diamond lattice of air spheres in a dielectric material.



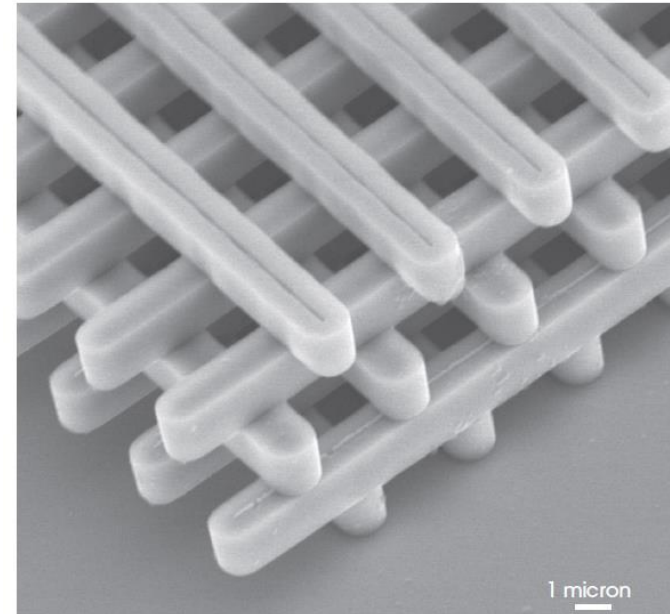
The photonic band structure for the lowest bands of a diamond lattice of air spheres in a high dielectric material ( $\epsilon=13$ ). A complete photonic band gap is shown. The wave vector varies across the irreducible Brillouin zone between the labeled high-symmetry points.

# 3D photonic crystals

3D “Woodpile” photonic crystal.

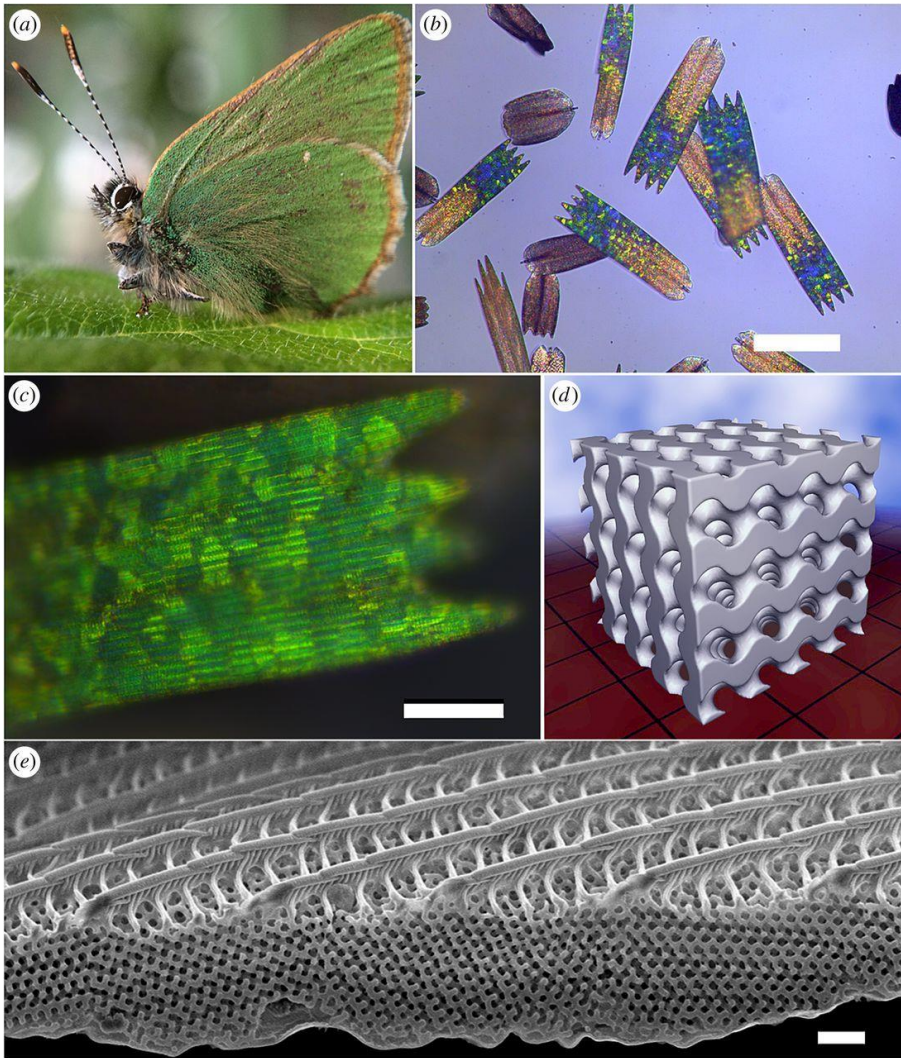


Electron-microscope image of a “woodpile” photonic crystal. The crystal is made of silicon and has a complete band gap centered at a wavelength of approximately 12 microns (Lin et al., 1998b). The dielectric “logs” form an fcc (or fct) lattice stacked in the [001] direction. (Image courtesy S.-Y. Lin.)



The photonic band structure for the lowest bands of the woodpile structure with  $\epsilon=13$  logs in air. The irreducible Brillouin zone is larger than that of the fcc lattice described earlier, because of reduced symmetry – only a portion is shown, including the edges of the complete photonic band gap.

# Photonic crystals in nature



**On the colour of wing scales in butterflies: iridescence and preferred orientation of single gyroid photonic crystals**

Robert W. Corkery and Eric C. Tyrode

Published: 16 June 2017 <https://doi.org/10.1098/rsfs.2016.0154>

(a) *Callophrys rubi* (Linnaeus, 1758) also known as the green hairstreak; (b) optical microscope image of both coloured and brown cover scales from *C. rubi* taken at low NA; (c) high NA (high magnification) optical micrograph of a coloured wing scale showing that the characteristic green–yellow colour arises from many individual photonic crystal domains. Note that the longitudinal ribs are also visible; (d) computer-generated single gyroid model -  $4 \times 4 \times 4$  unit cells; (e) SEM image of a coloured wing scale showing the ribbed upper surface, an undulating lower plate and five porous, single gyroid domains in different orientations. Note the continuous network spanning crystal grain boundaries suggestive of twinning planes, yet with some lattice defects such as dislocation planes and holes. Scale bars: (b, c and e) 100, 20 and 1  $\mu\text{m}$ , respectively.

# Materials Physics and Technology for Nanoelectronics



# Materials Physics and Technology for Nanoelectronics

## Carbon Materials



**Clement Merckling**  
[clement.merckling@kuleuven.be](mailto:clement.merckling@kuleuven.be)  
imec & KU Leuven (MTM)  
Kapeldreef 75, B-3001 Leuven



**Francisco Molina Lopez**  
[francisco.molinalopez@kuleuven.be](mailto:francisco.molinalopez@kuleuven.be)  
MTM Functional Materials  
Kasteelpark Arenberg 44, B-3001 Leuven

# The Carbon cosmos

## Diamond

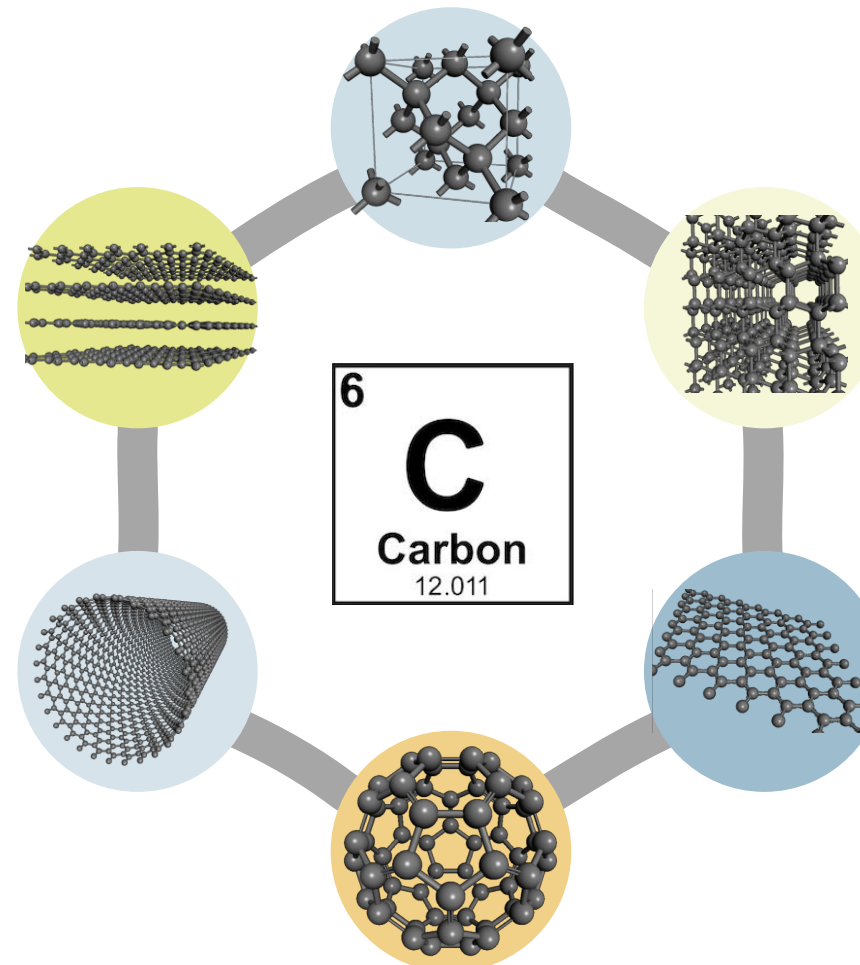
Carbon atoms in diamond have tetragonal bounds (i.e. in four spatial directions) and do not have any free electrons to each other.  $sp^3$  configuration

## Graphite

Natural graphite consists of layers of carbon atoms lying on top of each others arranged in the form of a hexagonal honeycomb structure.  $sp^2$  configuration

## Nanotubes (CNTs)

Carbon nanotube shave similar properties than graphene, again in  $sp^2$  configuration and can be pictured as a graphene layer rolled into a cylinder



## Lonsdaleite

Very rare mineral form of Carbon, occurs during the transformation of graphite into diamond where the original hexagonal crystal lattice is preserved. Also named hexagonal diamond.  $sp^3$  configuration

## Graphene

Single isolated graphite monolayer is referred to as graphene. Carbon atoms are in  $sp^2$  configuration. “Zero bandgap” semiconductor with high carrier mobility

## Fullerenes

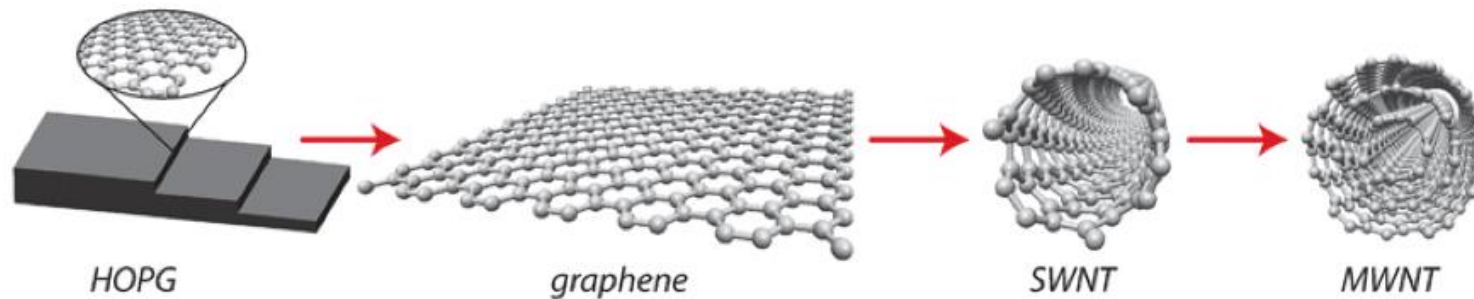
Prototypical fullerene  $C_{60}$  resembles to a football (“Buckyball”).  $sp^2$  configuration

# The versatile bonding of Carbon

The best-known carbon crystal is **diamond**, whose hardness and high dispersion of light make it useful for industrial applications and jewelry.

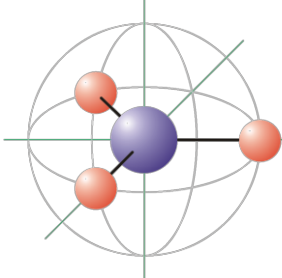
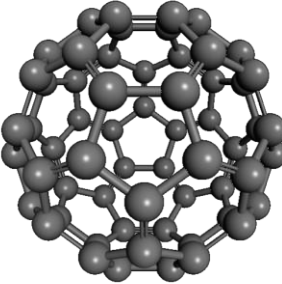
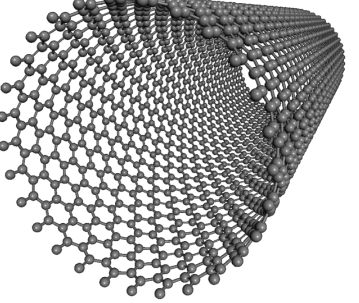
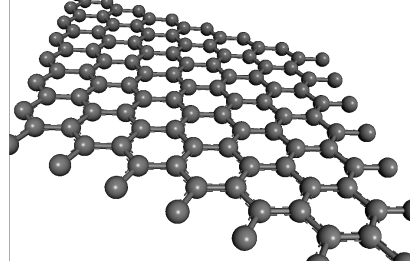
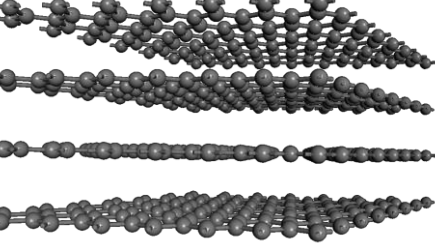
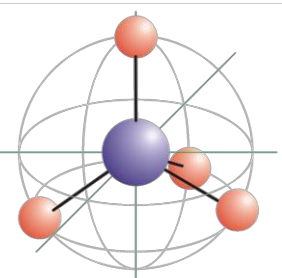
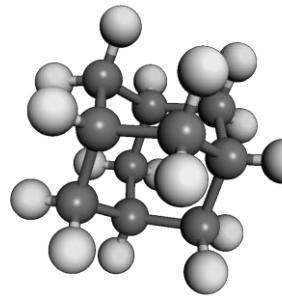
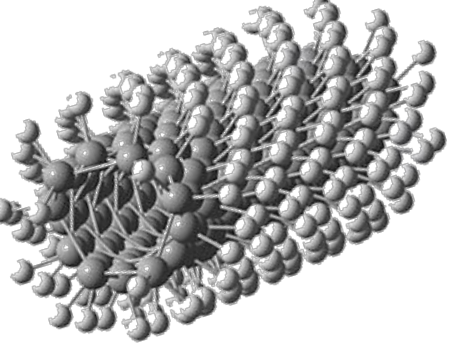
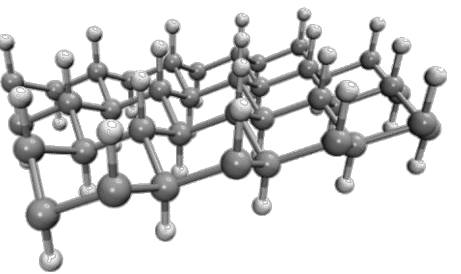
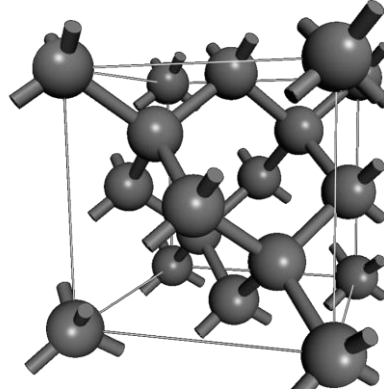
Under ambient pressures and at room temperature, however, the most stable form of carbon is **graphite**, which is used as an industrial lubricant and as the 'lead' in pencils. Graphite is a layered material in which each layer consists of a sheet of carbon atoms forming hexagonal structures (similar to benzene rings).

A monolayer of graphite is called **graphene**, and a **carbon nanotube** is a cylinder made of graphene.



Carbon nanotubes were discovered by Sumio Iijima during the synthesis of fullerene  $C_{60}$  in 1991. A nanotube exhibits **extraordinary mechanical properties** that make it ideal for **reinforced composites**: it has a huge Young modulus, is as stiff as diamond and the estimated tensile strength is more than ten times that of steel wire with the same weight.

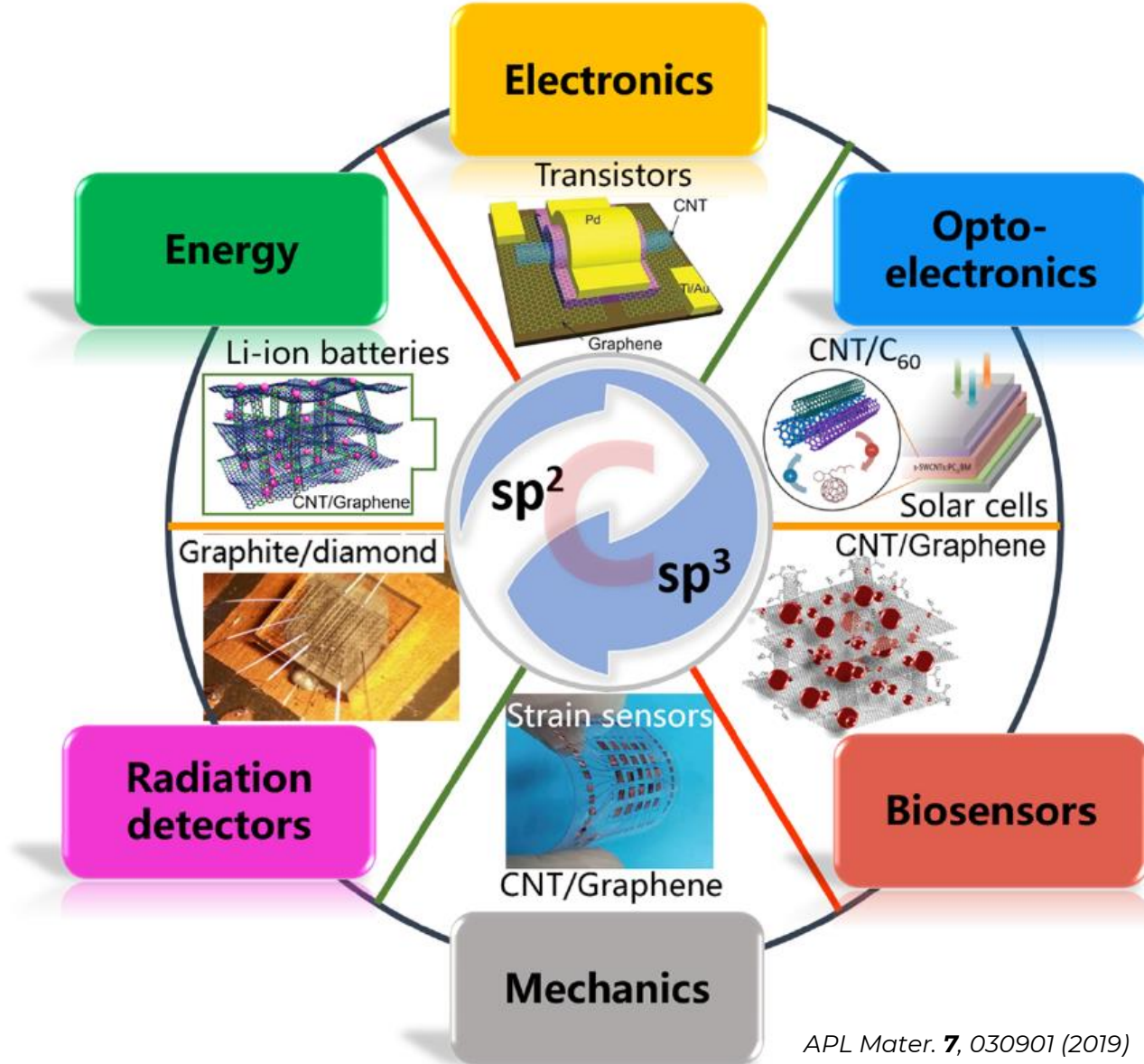
# Carbon allotropes

Bonds config.	0D	1D	2D	3D
				
$sp^2$	Fullerene	Nanotubes	Graphene	Graphite
				
$sp^3$	Diamondoids	Nanowires	Graphane	Diamond

# Applications

Various fields of all-carbon device applications:

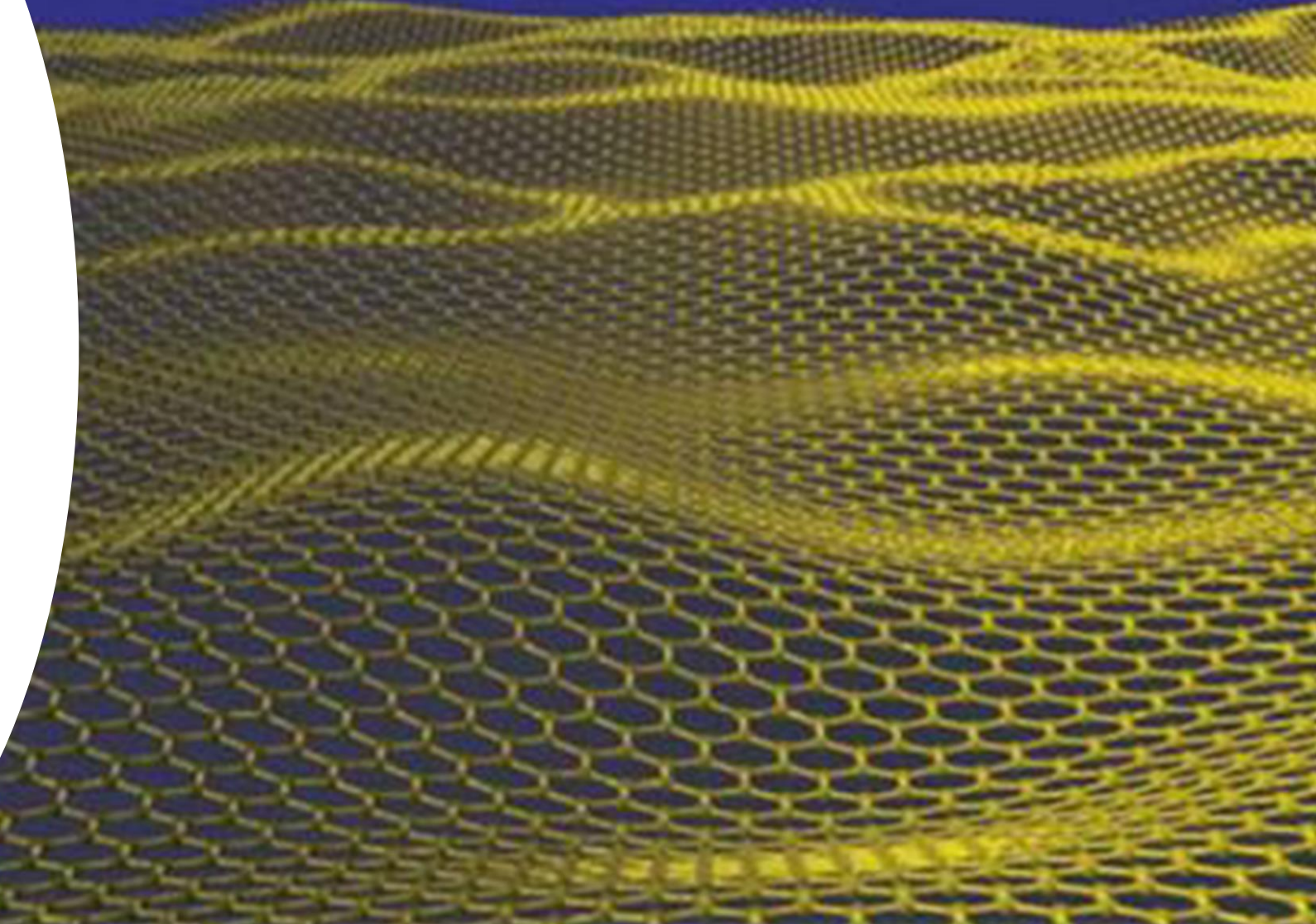
- Electronics
- Opto-electronics / Photonic
- Energy
- Biosensors
- Mechanics
- Radiation detectors
- ...



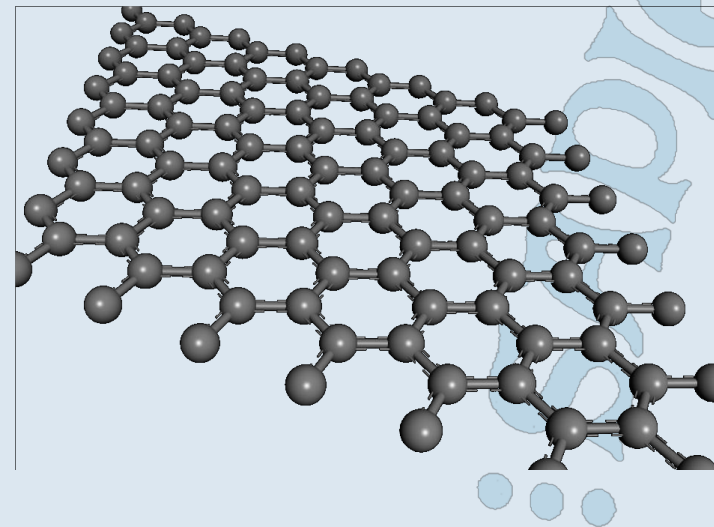
APL Mater. **7**, 030901 (2019)

# Outline

- Carbon based materials
- Graphene
  - Fundamentals & properties
  - Synthesis
  - Devices & applications
- CNTs
  - Fundamentals & properties
  - Synthesis
  - Devices & applications

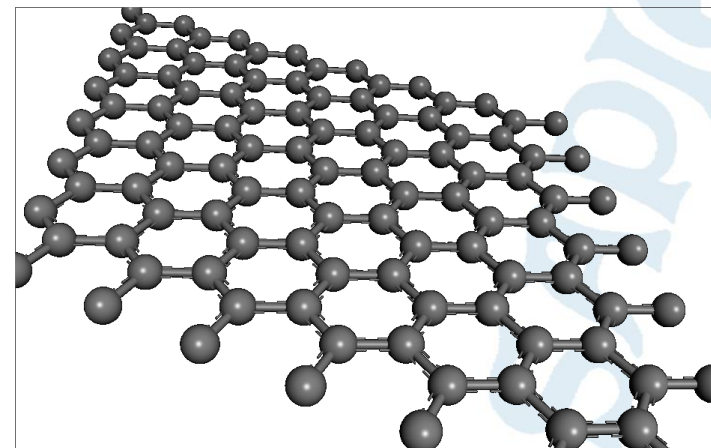


# Graphene



# Graphene

Fundamentals & properties



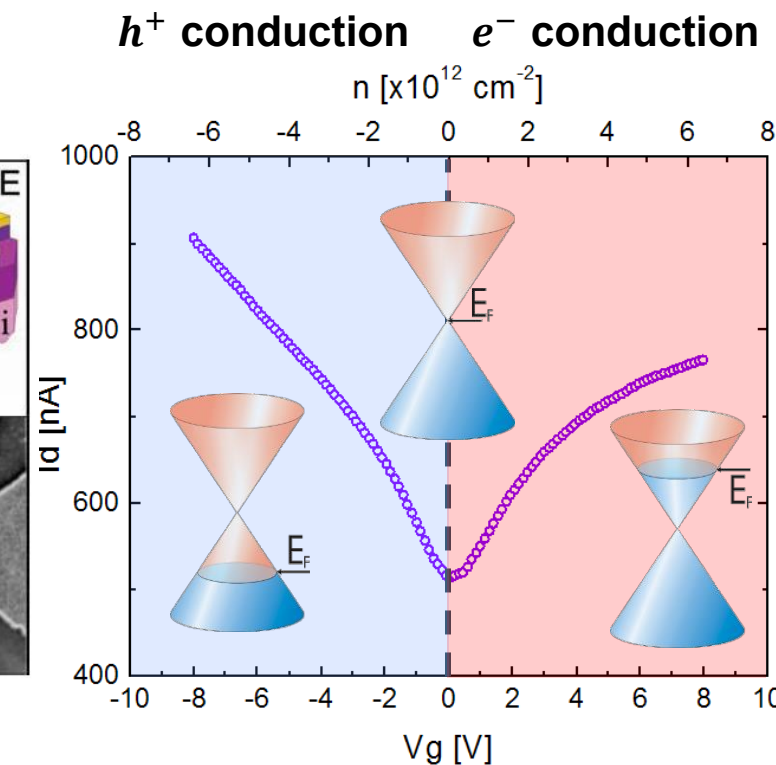
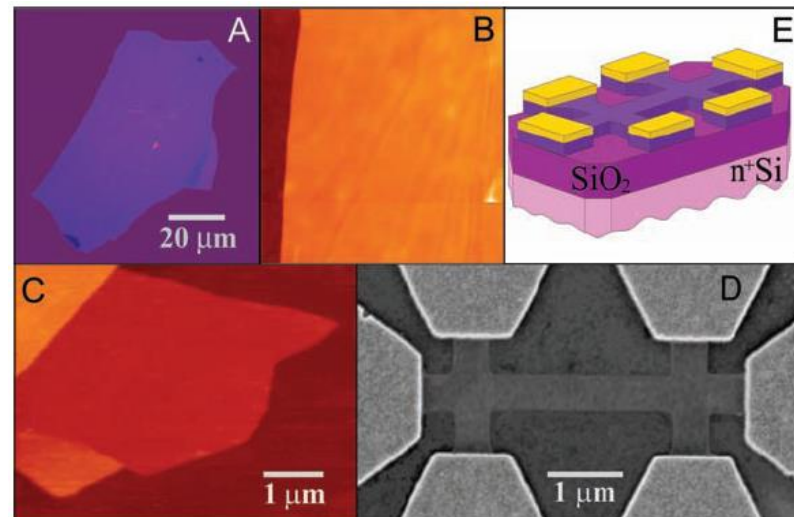
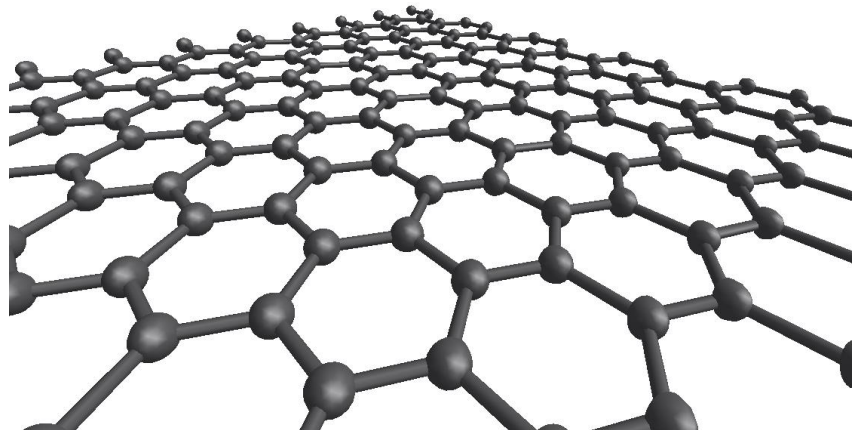
# Graphene ‘discovery’

## Electric Field Effect in Atomically Thin Carbon Films

K. S. Novoselov,<sup>1</sup> A. K. Geim,<sup>1\*</sup> S. V. Morozov,<sup>2</sup> D. Jiang,<sup>1</sup>  
Y. Zhang,<sup>1</sup> S. V. Dubonos,<sup>2</sup> I. V. Grigorieva,<sup>1</sup> A. A. Firsov<sup>2</sup>

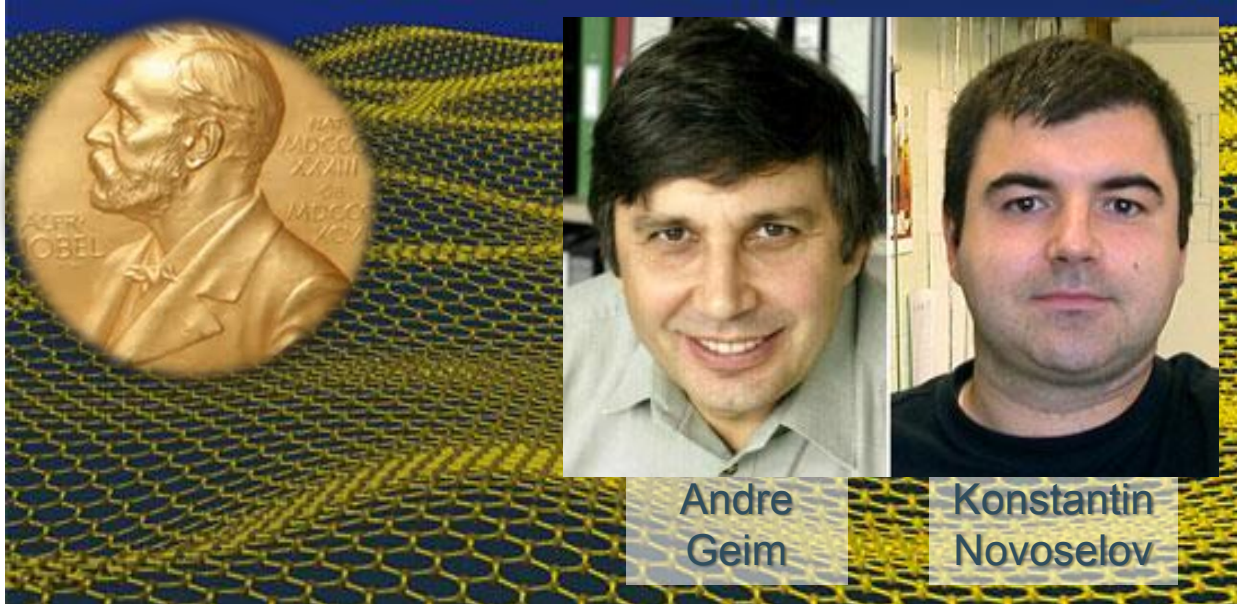
We describe monocrystalline graphitic films, which are a few atoms thick but are nonetheless stable under ambient conditions, metallic, and of remarkably high quality. The films are found to be a two-dimensional semimetal with a tiny overlap between valence and conductance bands, and they exhibit a strong ambipolar electric field effect such that electrons and holes in concentrations up to  $10^{13}$  per square centimeter and with room-temperature mobilities of  $\sim 10,000$  square centimeters per volt-second can be induced by applying gate voltage.

22 OCTOBER 2004 VOL 306 SCIENCE www.sciencemag.org



The great achievement by Geim et al. is not only in having isolated graphene; it is in the possibility to produce extrinsic behavior in it, i.e. **in changing its Fermi level**  
→ *without it, graphene would be useless...*

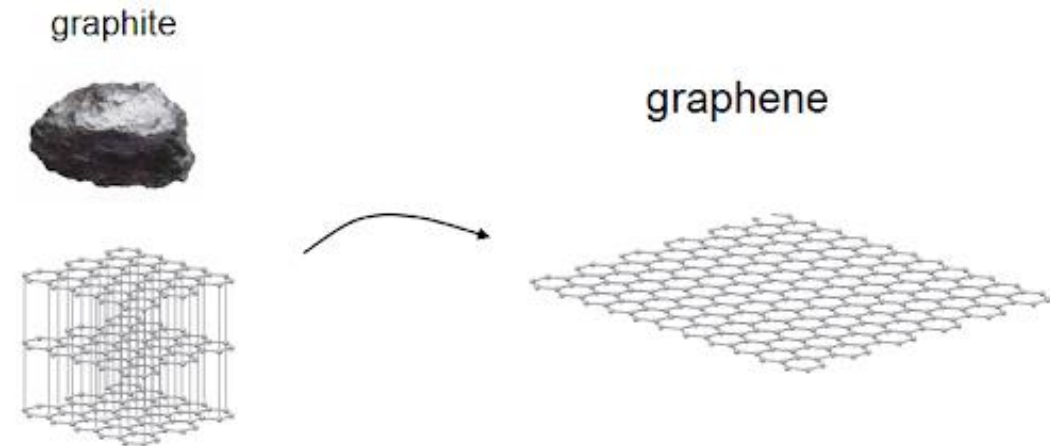
# Nobel Prize in Physics 2010



The Nobel Prize in Physics 2010 was awarded jointly to Andre Geim and Konstantin Novoselov  
***“for groundbreaking experiments regarding the two-dimensional material graphene”***.

Geim and Novoselov extracted the Graphene from a piece of graphite (from ordinary pencil) using regular adhesive tape

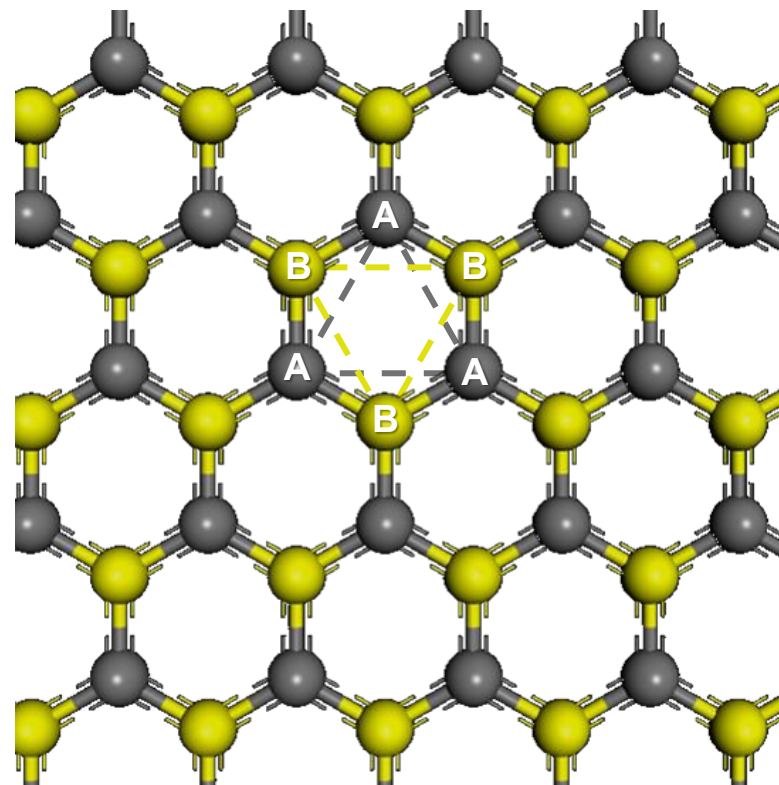
Manage to obtain an atomic scale flake of carbon



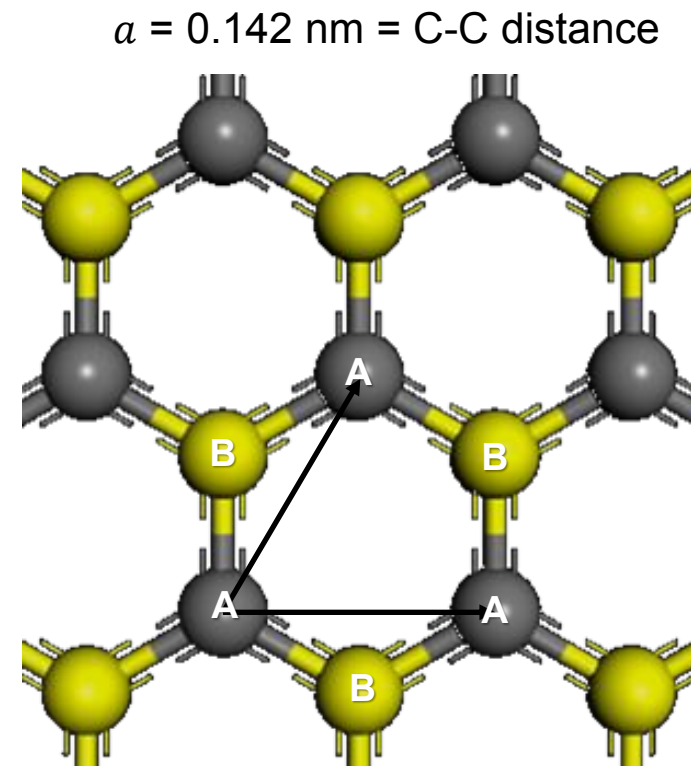
Open the way to emergence of new class of materials: **2D materials**

# Graphene lattice structure

The hexagonal lattice of graphene can be regarded as two interleaving triangular lattices. This perspective was successfully used as far back as 1947 when Wallace calculated the band structure for a single graphite layer using a tight-binding approximation.

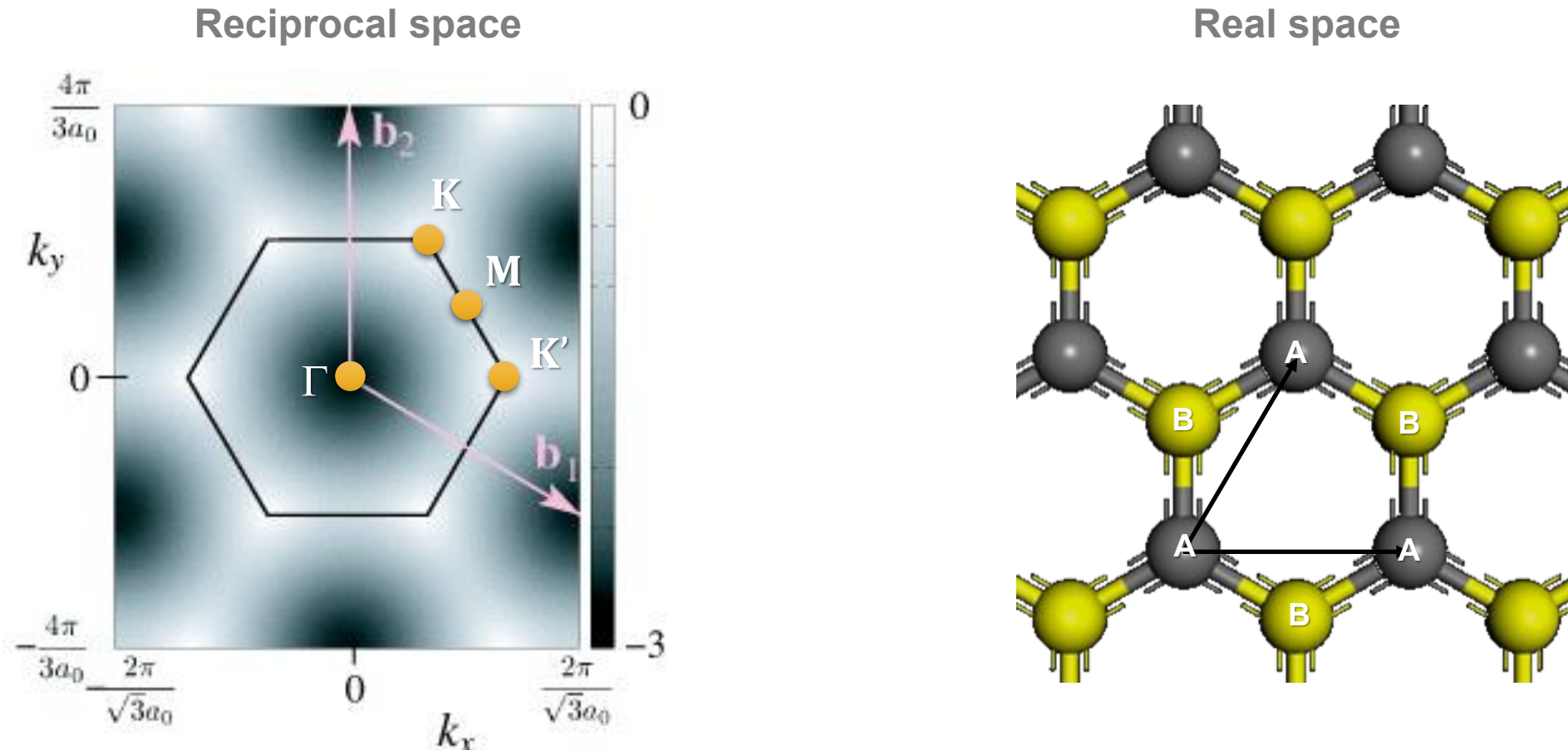


(a) Graphene structure with two equivalent sub-lattices (A, B).  
(b) Triangular Bravais lattice (2 atoms basis)



# Graphene reciprocal lattice

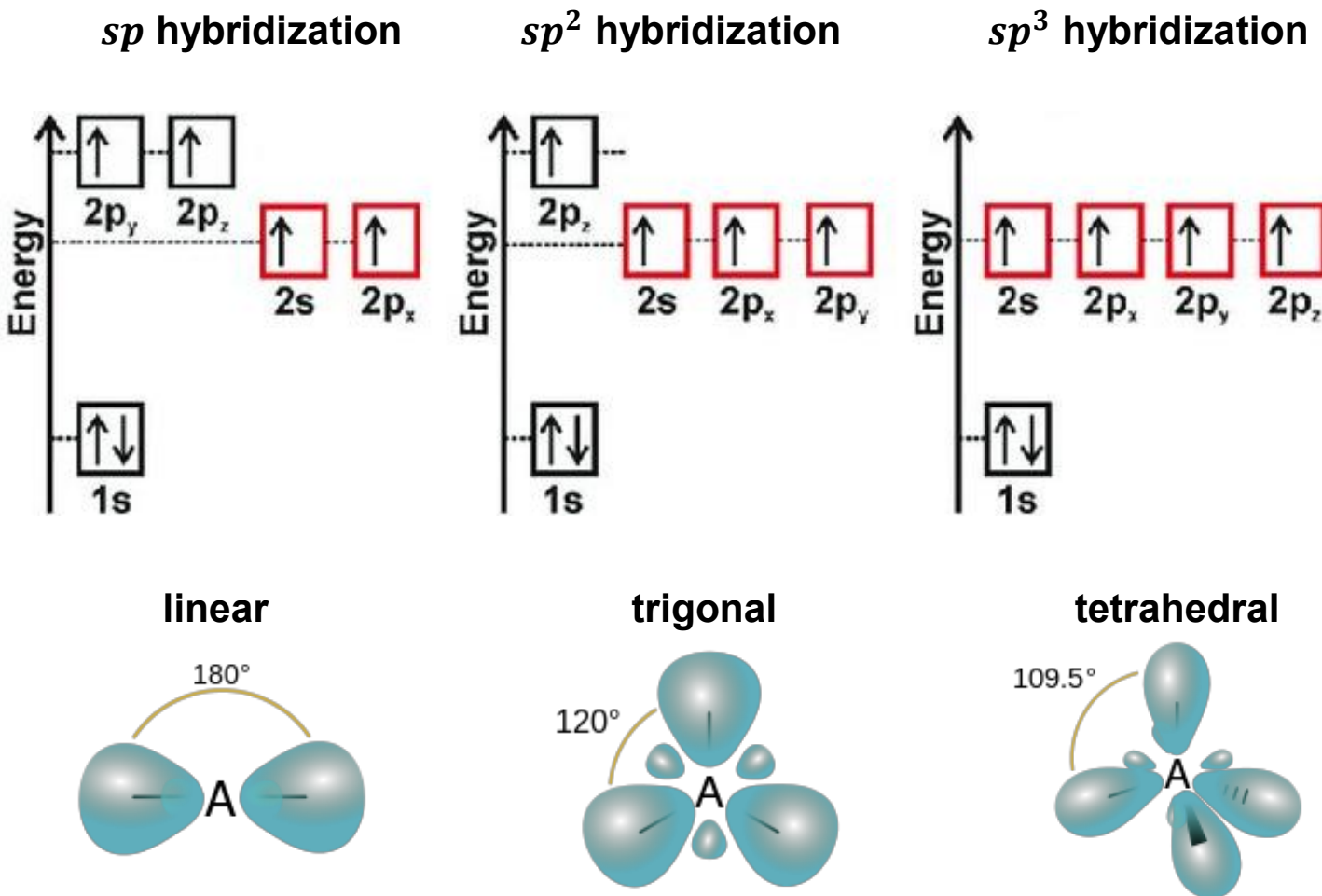
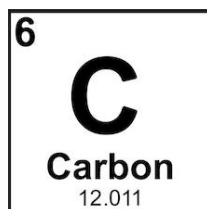
Correlation of the hexagonal graphene lattice between real and reciprocal space.



# Electronic structure of carbon

Carbon has six electrons, and its ground state configuration (orbitals) is  $1s^2 2s^2 2p^2$ .

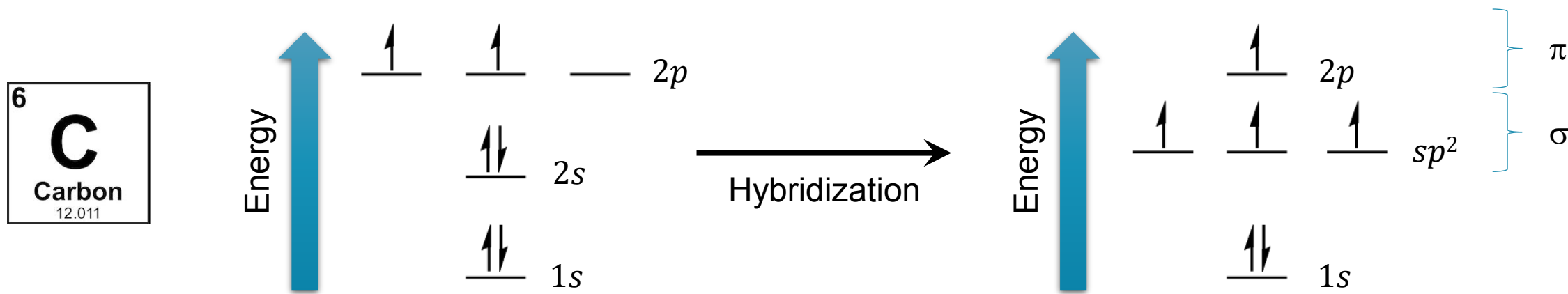
When excited, carbon presents different possible hybridization configurations  $sp$ ,  $sp^2$  and  $sp^3$ .



# Electronic structure of graphene

When arranged in the *honeycomb* crystal (ie. graphene), two electrons remain in the core  $1s$  orbital, while the other orbitals hybridize, forming three  $sp^2$  bonds and leave one  $p_z$  orbital.

The  $sp^2$  orbitals form the  $\sigma$ -band, which contains three localized electrons. The bonding configuration among the  $p_z$  orbitals of different lattice sites generates a valence band, or  $\pi$ -band, containing one electron, whereas the antibonding configuration generates the conduction band ( $\pi^*$ ), which is empty.

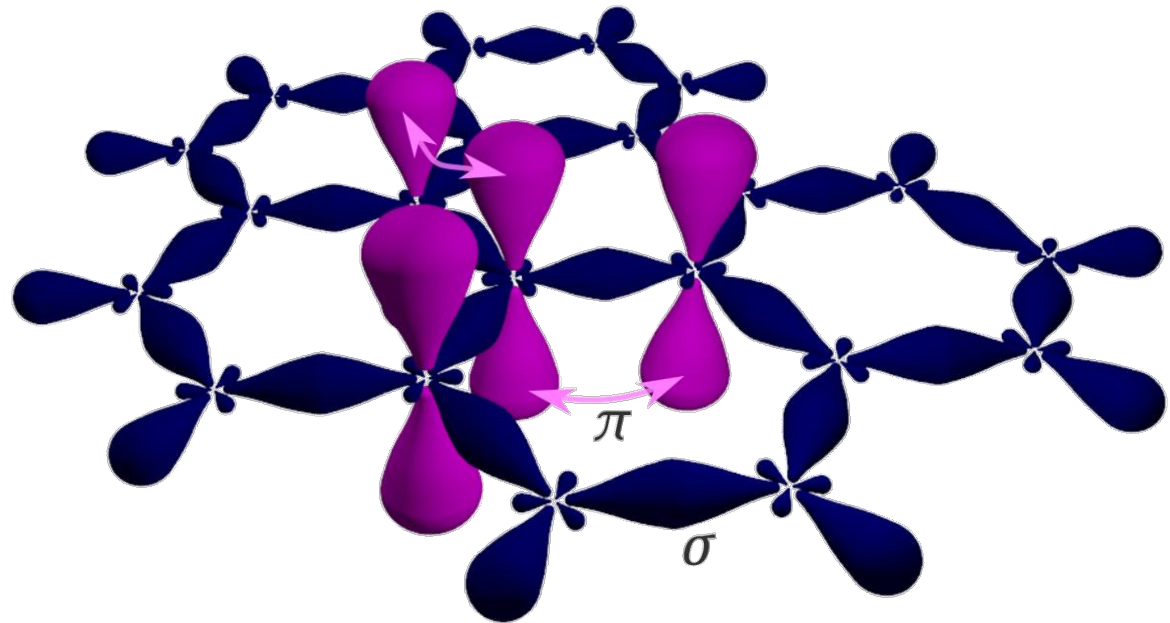


# Graphene electronic structure

Each carbon atom is about  $a = 1.42 \text{ \AA}$  from its three neighbors, with each of which it shares one  **$\sigma$ -bond**. The fourth bond is a  **$\pi$ -bond**, which is oriented in the  $z$ -direction (out of the plane).

Due to the  $sp^2$  bonding, the carbon atoms in graphene form a hexagonal lattice on a two-dimensional plane with ultra-thin atomic thickness ( $t_{1ML} = 3.45 \text{ \AA}$ ).

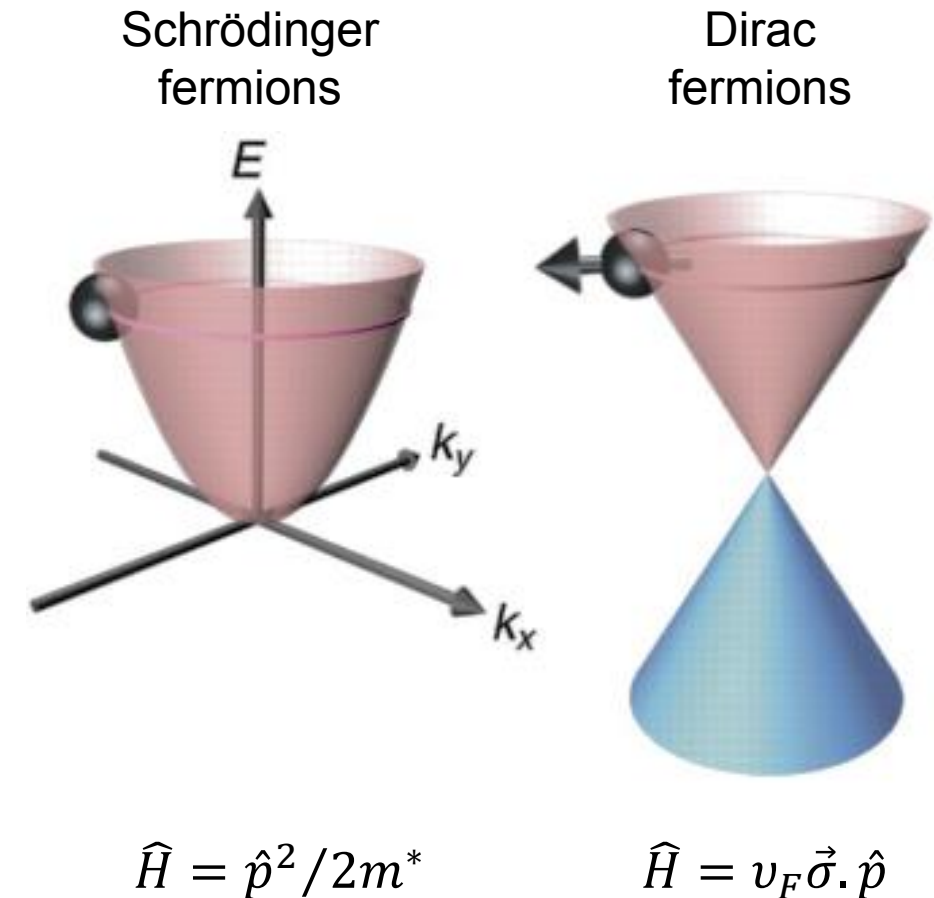
One can visualize the  $\pi$ -orbital as a pair of symmetric lobes oriented along the  $z$  axis and centered on the nucleus. Each atom has one of these  $\pi$ -bonds, which are then hybridized together to form what are referred to as the  $\pi$ -band and  $\pi^*$ -bands. These bands are responsible for most of the **peculiar electronic properties of graphene**.



# Dirac matter

Conventionally, in condensed matter physics nearly free charge carriers are effectively described using the **Schrödinger Hamiltonian** with quadratic dispersion where  $m^*$  is the carrier effective mass (being different from the free electron mass) and  $\hat{p}$  being the momentum operator.

Contrary to that Dirac matter is any material where relativistic particles in the **zero-mass limit** can be described in the low-energy excitation spectrum by the **Dirac Hamiltonian**, where  $v_F$  is the Fermi velocity and  $\vec{\sigma}$  is the Pauli matrix.



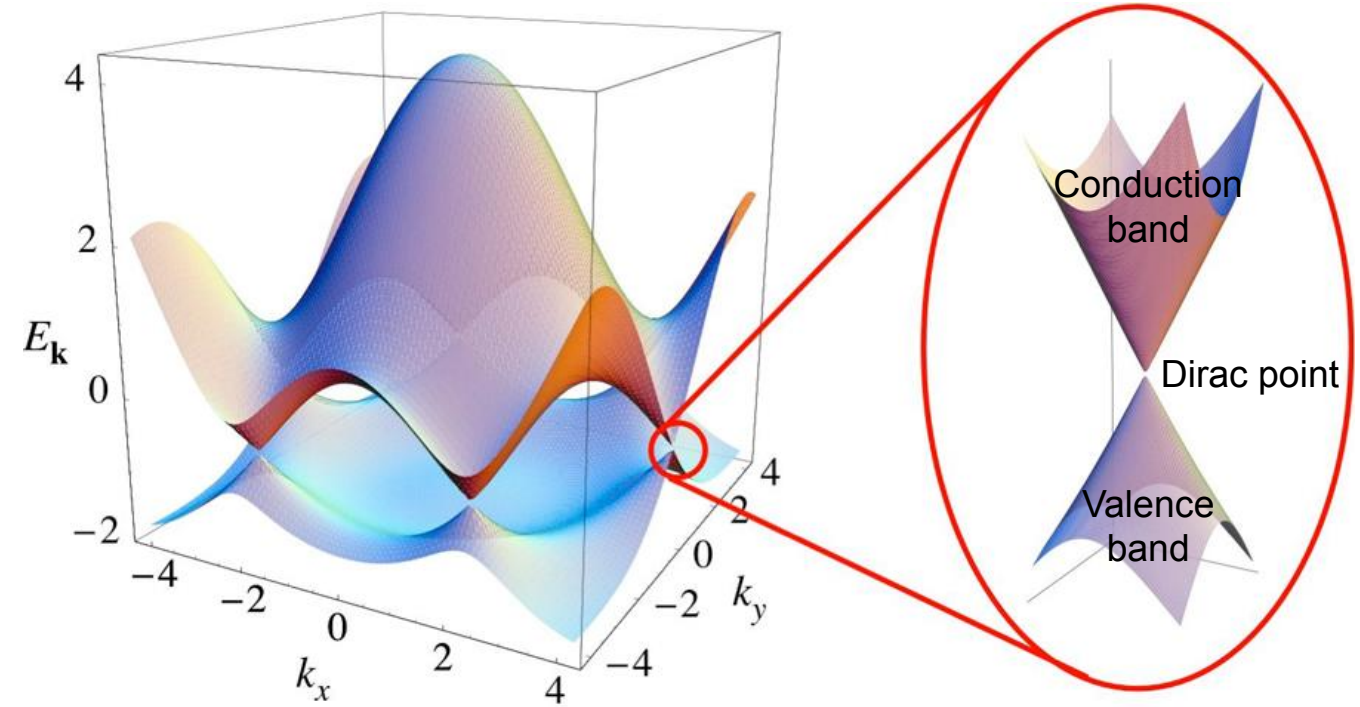
*Comparison between Schrödinger and Dirac fermions in condensed matter physics.*

# Graphene electronic structure

Graphene has two atoms per unit cell, which results in two ‘conical’ points per Brillouin zone where band crossing occurs,  $K$  and  $K'$ . Near these crossing points, the electron energy is linearly dependent on the wave vector.

Graphene is a **zero-gap** semiconductor because the conduction and valence bands meet at the **Dirac points**.

The Dirac points are locations in momentum space on the edge of the Brillouin zone.



*First Brillouin zone and band structure of graphene. The vertical axis is energy, while the horizontal axes are momentum space on the graphene lattice. Graphene has a zero bandgap at 6 K points (semimetal) and a linear energy dispersion near the Fermi level.*

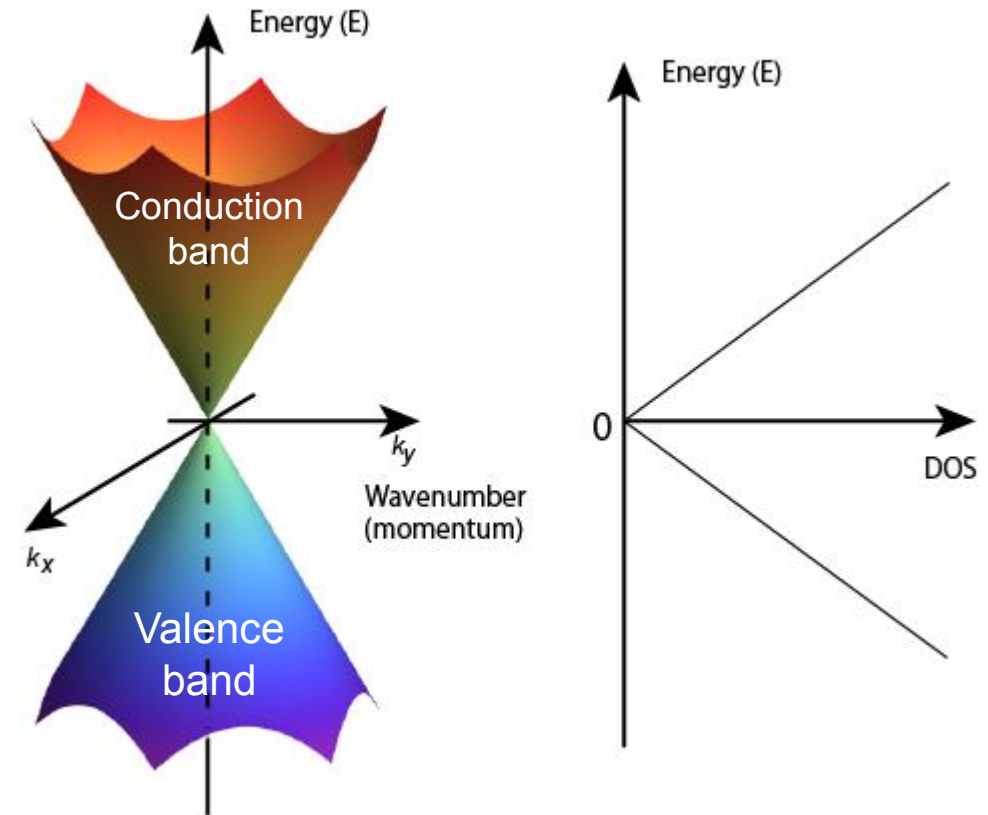
# Electronic structure of graphene

Because of the **linear spectrum**, one can expect that quasi-particles in graphene behave *differently* from those in conventional metals and semiconductors, where the energy spectrum can be approximated by a parabolic (free electron-like) dispersion relation.

Quasi-particles in graphene exhibit a linear dispersion relation  $E(\mathbf{k}) = \pm \hbar v_F |\mathbf{k} - \mathbf{K}|$ , as if they were massless relativistic particles (for example, photons) but the role of the speed of light ( $c$ ) is played here by the Fermi velocity:

$$v_F \approx \frac{c}{300} = 10^6 \text{ m/s}$$

Due to the **zero density of states at the Dirac points**, electronic conductivity is quite low.



$$E(\mathbf{k}) = \pm \hbar v_F |\mathbf{k} - \mathbf{K}|$$

for  $E \ll \sim 1 \text{ eV}$

# Graphene electronic conductivity

It is said that graphene electrons act very much like photons in their mobility due to their lack of mass. These charge carriers are able to travel sub-micrometer distances without scattering; a phenomenon known as ballistic transport.

The electronic mobility of graphene is very high, with theoretical potential limits of  $200\ 000\ \text{cm}^2.\text{V}^{-1}.\text{s}^{-1}$  (limited by the scattering of graphene's acoustic photons). However, the quality of the graphene and the substrate that is used will be the limiting factors. With silicon dioxide as the substrate, for example, mobility is potentially limited to  $40\ 000\ \text{cm}^2.\text{V}^{-1}.\text{s}^{-1}$ .

Given an appropriate doping enables an in-plane conductivity of 100 MS/m for the graphene flakes with a flake size in the tens of micrometers, the macroscopic graphene can reach an electrical conductivity of up to 80 MS/m. Graphene semimetal is potentially better at conducting electricity than, for example, copper at room temperature (58 MS/m).

A graphene-based conductor with 80 MS/m in electrical conductivity allows enormous efficiency gains, weight as well as volume savings and enables new designs for the powertrain in e-mobility.

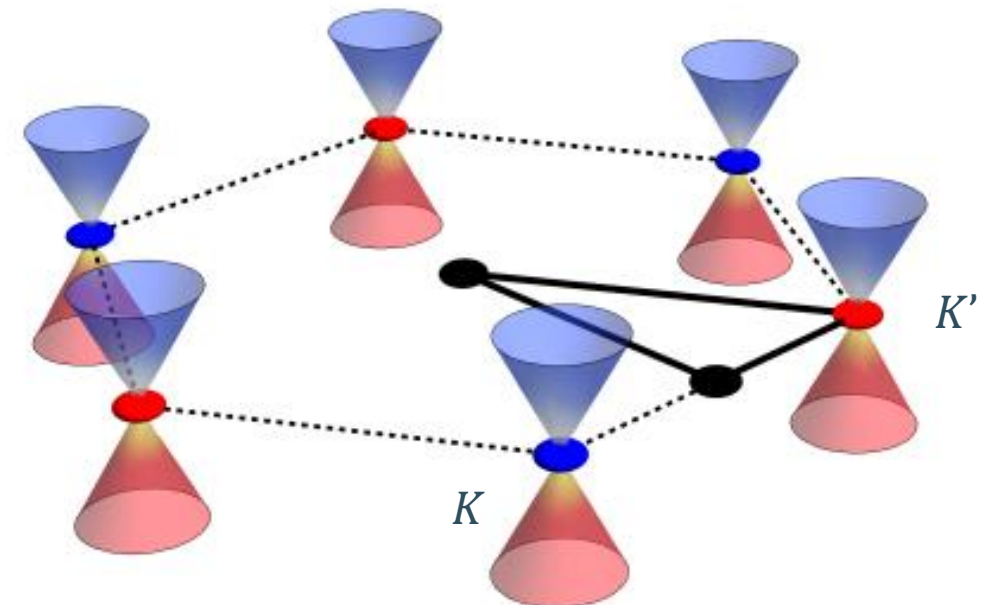


# Electronic structure of graphene

The hexagonal lattice of graphene can be regarded as two interleaving triangular sub-lattices A and B. From a kinetic energy point of view, the electronic single particle dispersion in graphene is essentially defined by the hopping of the electrons between nearest neighbor carbon sites in the honeycomb lattice.

Unlike square or triangular lattices, the honeycomb lattice is spanned by two different sets of Bravais lattice generators, forming a two-component basis with one set for each triangular sublattice.

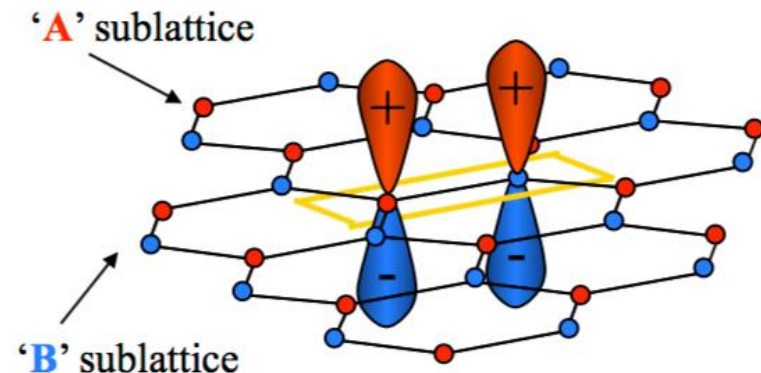
There are **two sets of three Dirac points**. Each set is not equivalent with the other set of three.



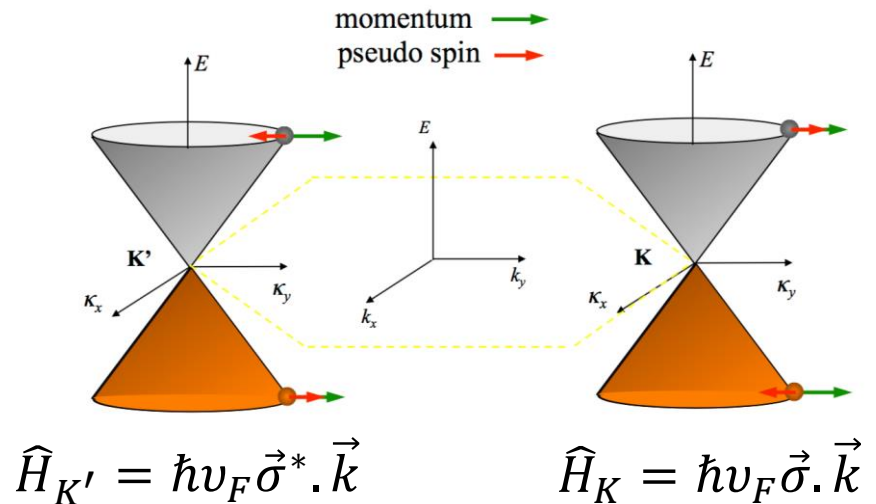
# Chirality and pseudospin in graphene

Transport in graphene exhibits a novel chirality. Each graphene sublattice can be regarded as being responsible for one branch of the dispersion. These dispersion branches interact very weakly with one another.

This chiral effect indicates the existence of a **pseudospin quantum number** for the charge carriers. This quantum number is analogous to spin but is completely *independent* of the “real” spin.



The **pseudospin** lets us differentiate between *contributions* from each of the sublattices. This independence is called **chirality** because of the inability to transform one type of dispersion into another. A *typical example of chirality is that you cannot transform a right hand into a left hand with only translations, scaling's, and rotations.*

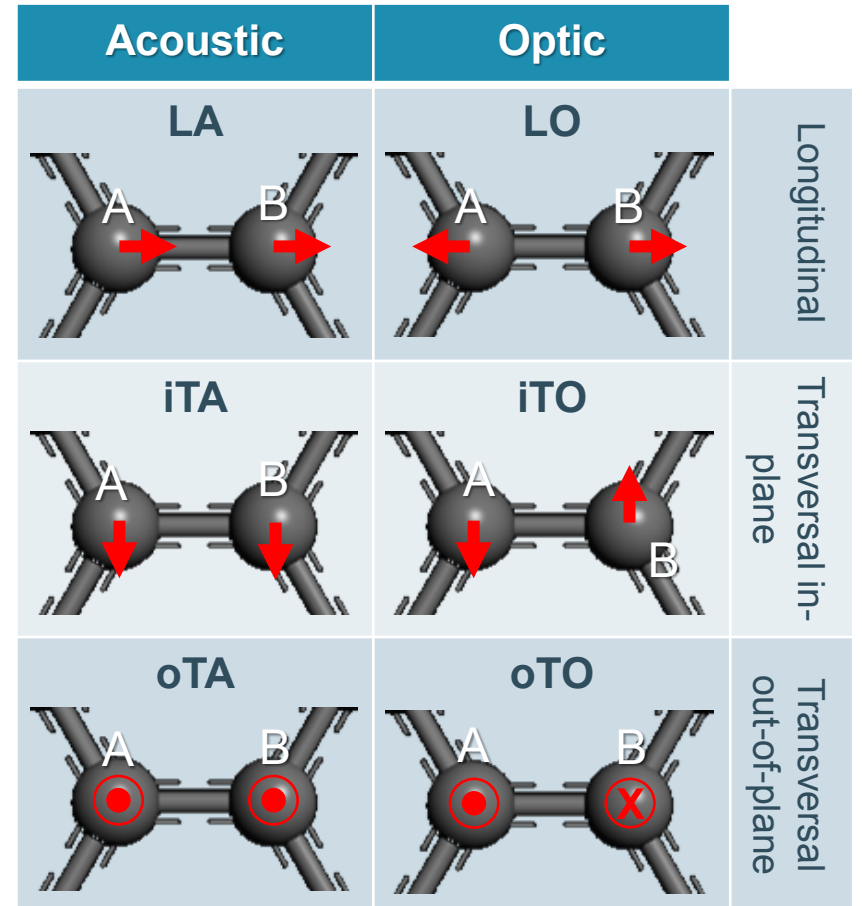


# Graphene vibrational properties

In order to obtain the phonon dispersion, it is necessary to consider the **vibrational modes** of the crystal in thermal equilibrium. This is done by considering the displacement of each atom from its equilibrium position. Each atom is effectively coupled to its neighbors by some **torsional** and **longitudinal force constants**, which only depend on the relative positions of the atoms.

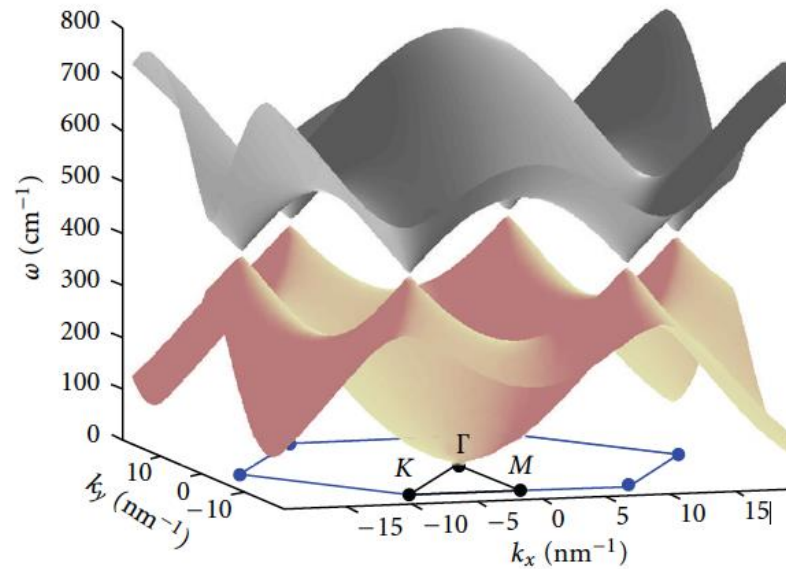
In graphene the two sublattices A and B have to be considered explicitly to solve the eigenspectrum of the **dynamical matrix**. However, the atoms can vibrate in all three dimensions, hence the dynamical matrix has to be written in terms of both the sublattices A and B as well as the 3 spatial dimensions.

Ultimately this leads to **6 eigenvalues**. Two of the eigenvalues correspond to the **out-of-plane vibrations**: oTA (acoustic) and oTO (optical), and the remaining 4 correspond to the **in-plane vibrations**: iTA (transverse acoustic), iTO (transverse optical), LA (longitudinal acoustic), and LO (longitudinal optical).

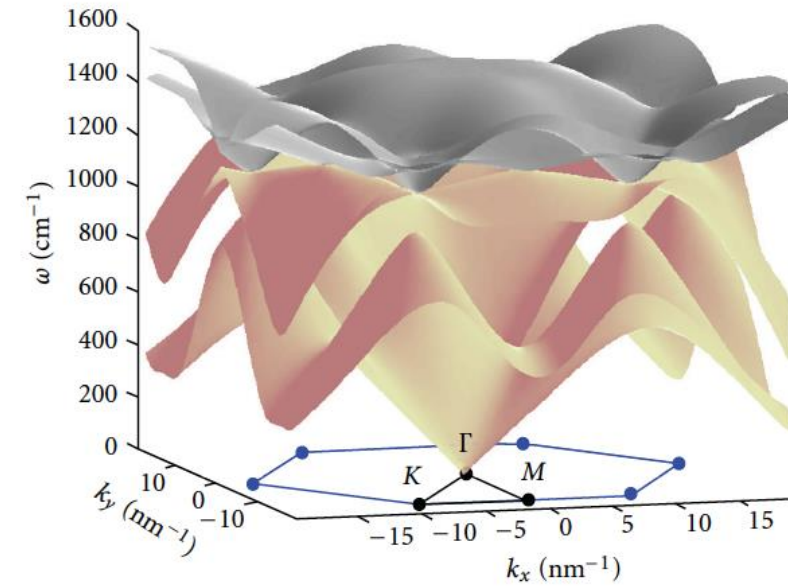


# Graphene phonon dispersion

At the  $K$  and  $K'$  points, we recover a cone structure similar to the Dirac cones in the electronic structure. However, the phonon density of states does not vanish at these points because of the presence of the in-plane modes.



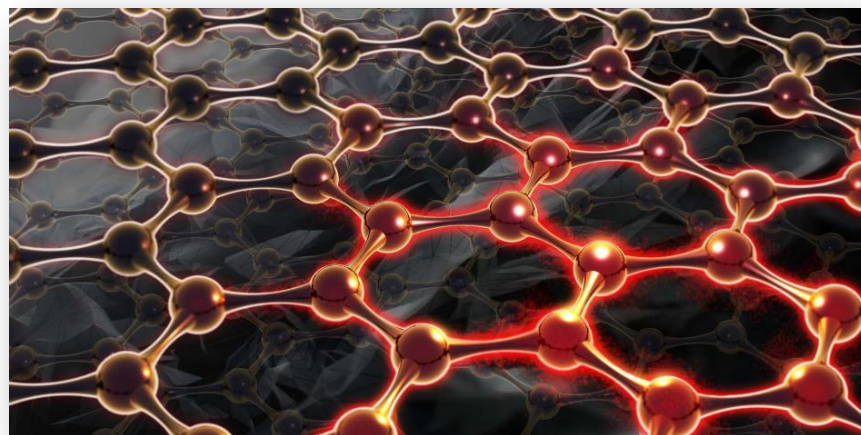
*First Brillouin zone and out-of-plane phonon modes. The vertical axis is the phonon frequency, while the horizontal axes are momentum space on the graphene lattice. The gray surface corresponds to the oTO (optical) mode, whereas the pink surface shows the oTA (acoustic) mode.*



*First Brillouin zone and in-plane phonon modes. The phonon dispersion relation of the iTO and LO modes in gray and the iTA and LA modes in pink as a function of the in-plane reciprocal vector  $k$ . The longitudinal modes are on top of the transverse modes.*

# Graphene thermal conductivity

While the electronic properties have attracted the lion's share of the interest in graphene, the vibrational properties are of great importance too. They are responsible for properties such as the **record thermal conductivities**.



From the kinetic theory of gases, the **thermal conductivity due to phonons** is given by:

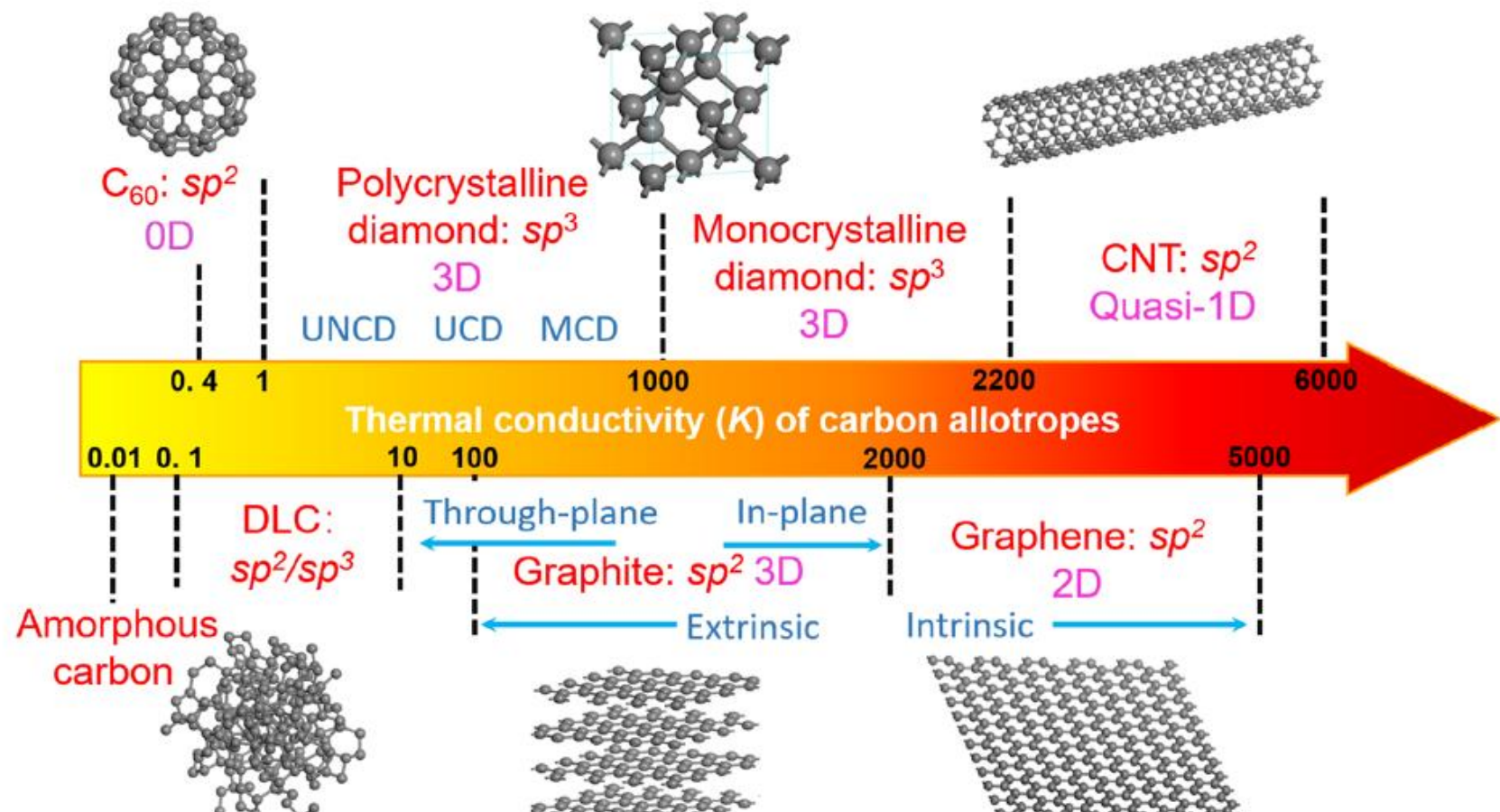
$$\kappa \sim c_{ph} C_V(T) \lambda$$

where  $C_V(T)$  is the *specific heat* per unit volume and  $\lambda$  is the *phonon mean free path*. This implies that since  $c_{ph}$  is very large in graphene, one can expect a large thermal conductivity.

Since graphene is composed of a light atom, where the in-plane bonding is very strong, graphene exhibits a very high value of the **in-plane sound velocity**, close to  $c_{ph} \approx 20$  km/s.

Indeed, experiments at near room temperature obtain  $\kappa \approx 3080\text{--}5150$  W/mK and a phonon mean free path of  $\lambda \approx 775$  nm for a set of graphene flakes.

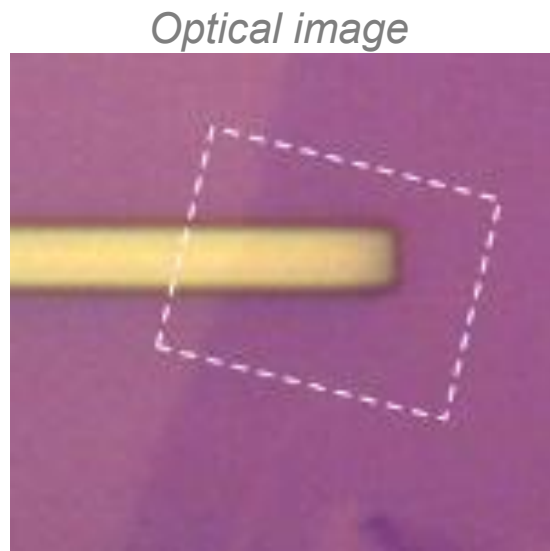
# Graphene thermal conductivity



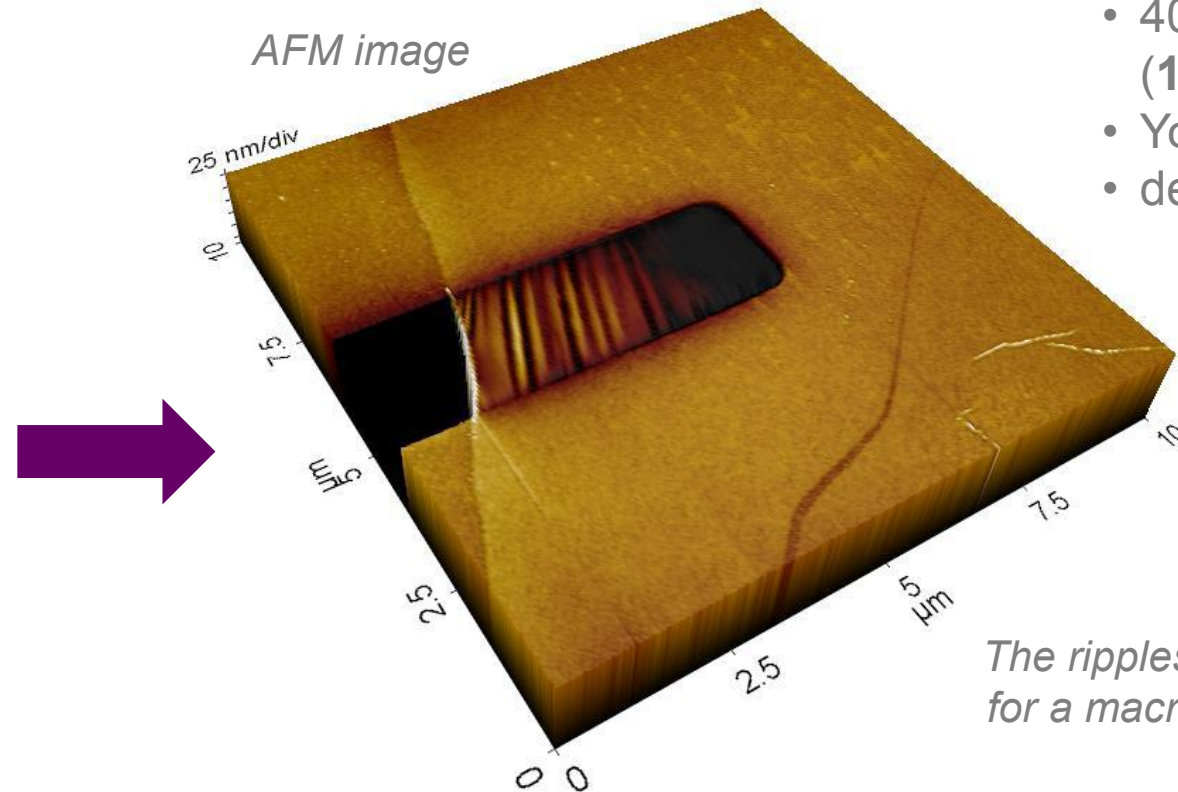
Thermal conductivities of carbon allotropes (unit:  $\text{W} \cdot \text{m}^{-1} \cdot \text{K}^{-1}$ ).

# Mechanical properties of graphene

Being only a single atom thick, and possessing an intrinsically perfect lattice, graphene is very strong and can withstand elastic deformations up to 20%.



## *Single layer graphene deposited over sharp trench*



- 40 N/m breaking strength  
**(100x steel)**
  - Young's modulus ~1 TPa
  - density: 0.77 mg/m<sup>2</sup>

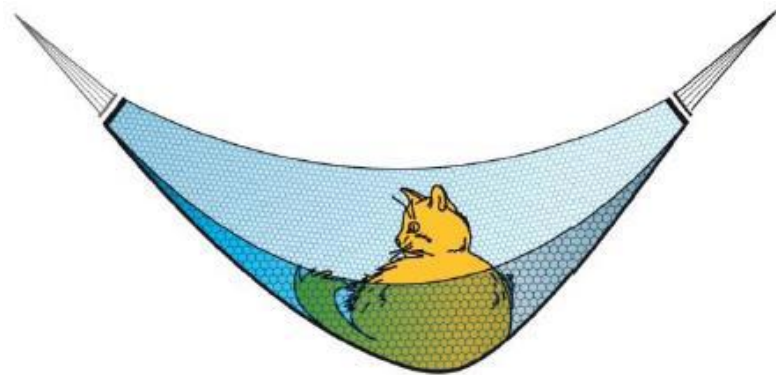
*The ripples appear just like  
for a macroscopic material*

Lee et al., Science 321, 385 (2008)

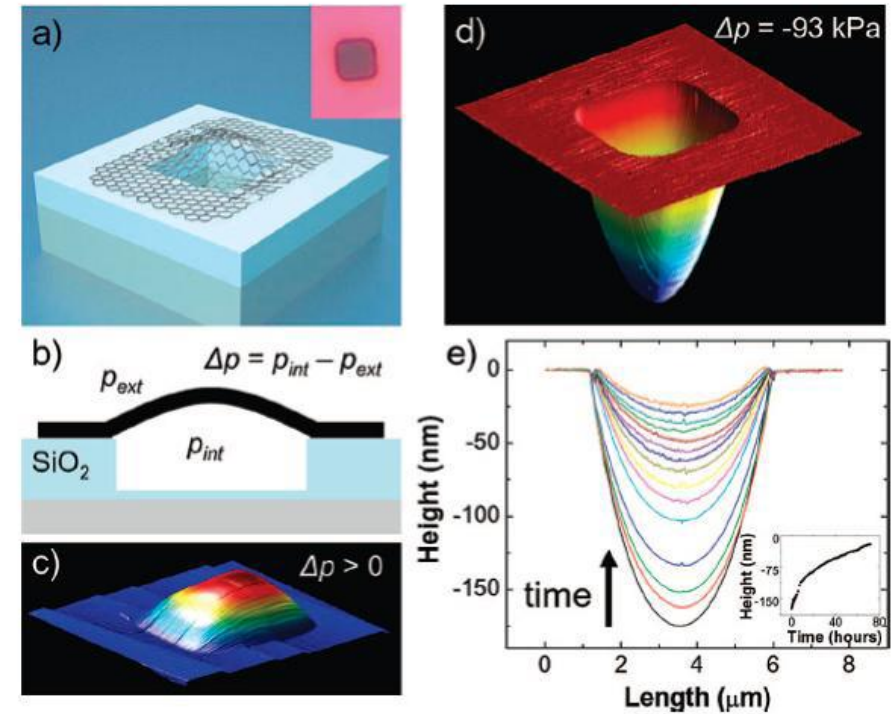
# Mechanical properties of graphene

A hypothetical 1 m<sup>2</sup> hammock would weigh only 0.77 mg (less than a cat's whisker) but:

- It would bear the weight of a cat without breaking (up to ~4 kg)
- It would be invisible!

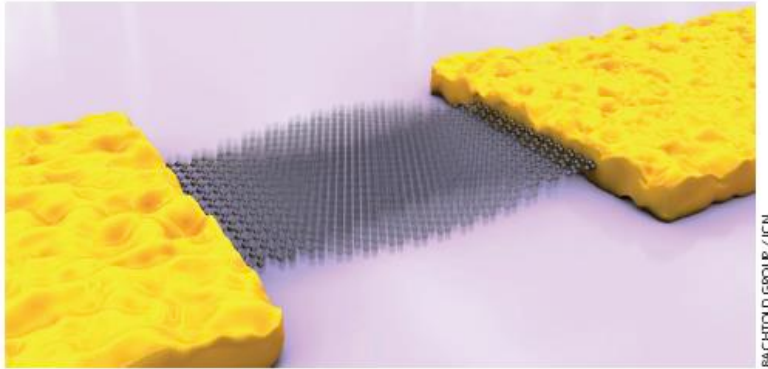


A graphene membrane is impermeable to most gases (including Helium)

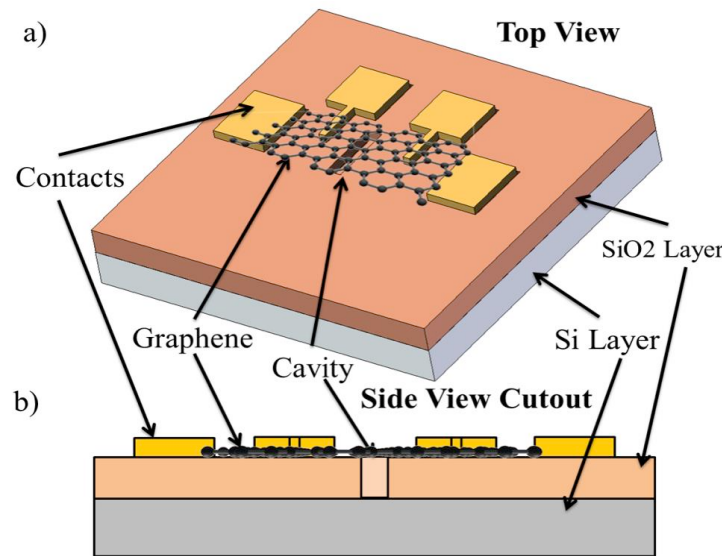


Bunch et al., Nano Lett. **8**, 2458 (2008)

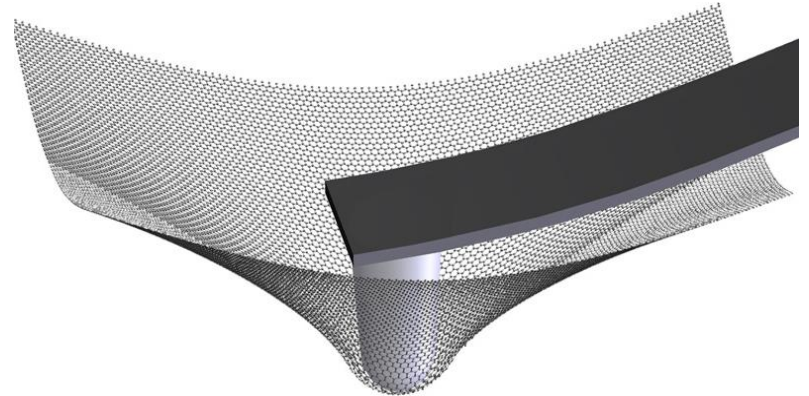
# Graphene NEMS



Source: A. Bachtold



- Young's modulus:  $\sim 1.10$  TPa ( $\text{Si} \sim 130$  GPa)
- Elastically stretchable by 20%
- High mechanical stability
- "strongest material known"
- Flexible
- Low mass



→ Graphene based mass, force, pressure sensors

# Optical properties of graphene

Graphene is very **transparent** for light over a wide range of wavelengths. The transmittance  $T$  can be expressed as:

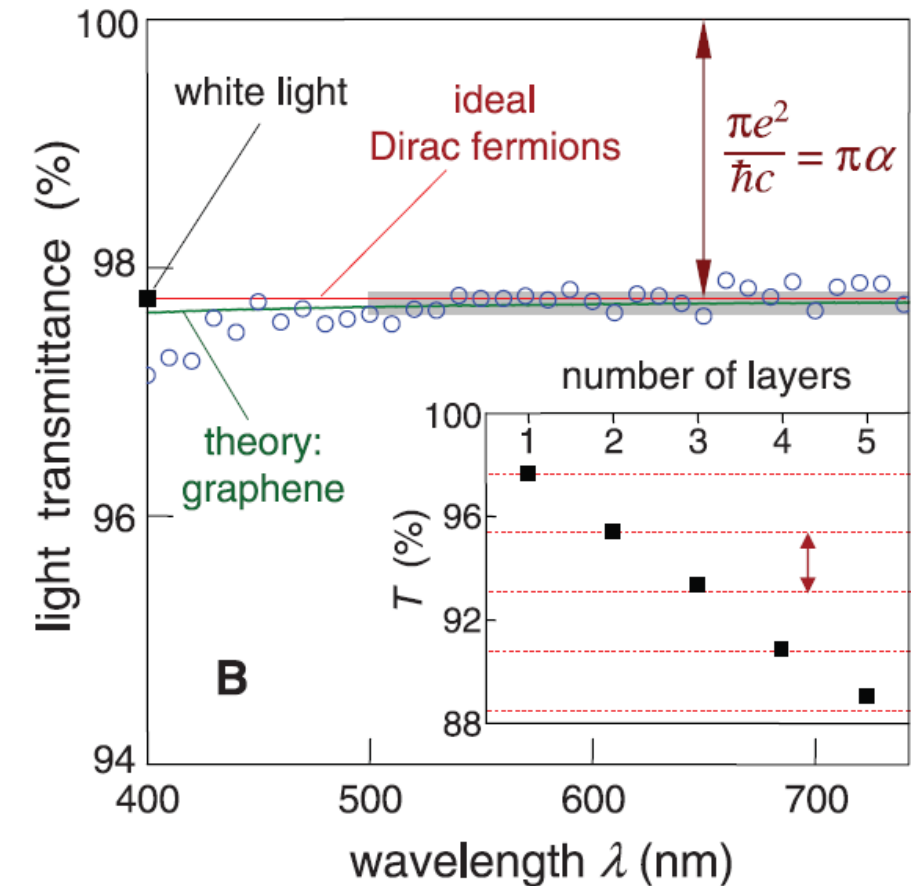
$$T = (1 + 0.5\pi\alpha)^{-2} \sim 1 - \pi\alpha \sim 97.7 \%$$

Graphene reflects < 0.1% of the incident light in the visible region (~ 2 % for 10 layers)

Few-layer graphene can be considered made up of non-interacting layers, each absorbing  $1 - T = 100 - 97.7 = 2.3 \%$

→ optical absorption linearly proportional to thickness !

The practical application of graphene as transparent conductive electrode is hampered by the relatively high resistivity of single graphene layers. Multiple graphene layers are needed to achieve resistivity low enough to be truly competitive to other materials such as ITO (Indium Tin Oxide).



Nair et al., Science 320, 1308 (2008)

# Graphene optical properties

The optical absorption of graphene arises from two distinct types of contributions, those from **intra-band** and those from **inter-band** optical transitions.

The relative importance of the two contributions depends largely on the spectral range of interest:

- In the far-infrared region, the optical response is dominated by the free-carrier (or intra-band) response. By fabricating sub-wavelength structures in graphene, one can create a tunable far-infrared response that is dominated by **plasmonic excitations** associated with these free carriers.
- In the mid- to near-infrared region, the optical absorbance is attributable primarily to inter-band transitions. This response is nearly frequency independent and is equal to a universal value determined by the **fine-structure constant**  $e^2/\hbar c$  in pristine graphene. However, this optical absorption in graphene can be controlled through **electrostatic gating**, which shifts the Fermi energy and induces Pauli blocking of the optical transitions.
- In the ultraviolet spectral range (with the transitions approaching the saddle-point singularity), the inter-band optical absorption increases well beyond the “universal” value and exhibits signatures of **excitonic effects**.

Kin Fai Mak et al., Solid State Communications 152 (2012)

# Interband optical absorption in graphene

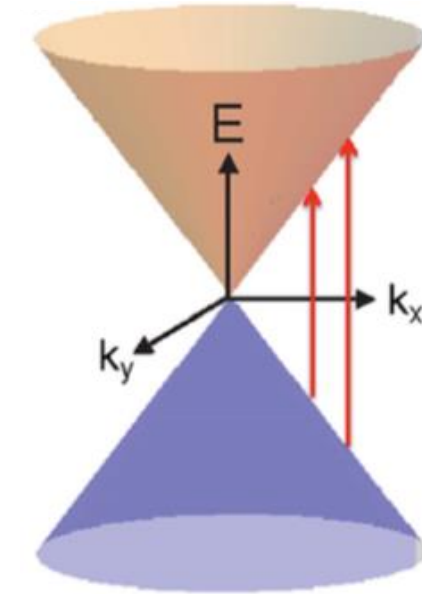
## Universal optical conductivity

- Interband absorption arises from direct optical transitions between the valence and conduction bands.

At frequencies above the far-infrared region, these interband transitions typically define the optical response of graphene.

Within the tight-binding model, the optical sheet conductivity from interband transitions can be readily calculated.

For pristine graphene at zero temperature, the optical conductivity in the linear dispersion regime of graphene is found to be independent of frequency.



*Schematic of interband optical transitions in graphene.*

Kin Fai Mak et al., Solid State Communications **152** (2012)

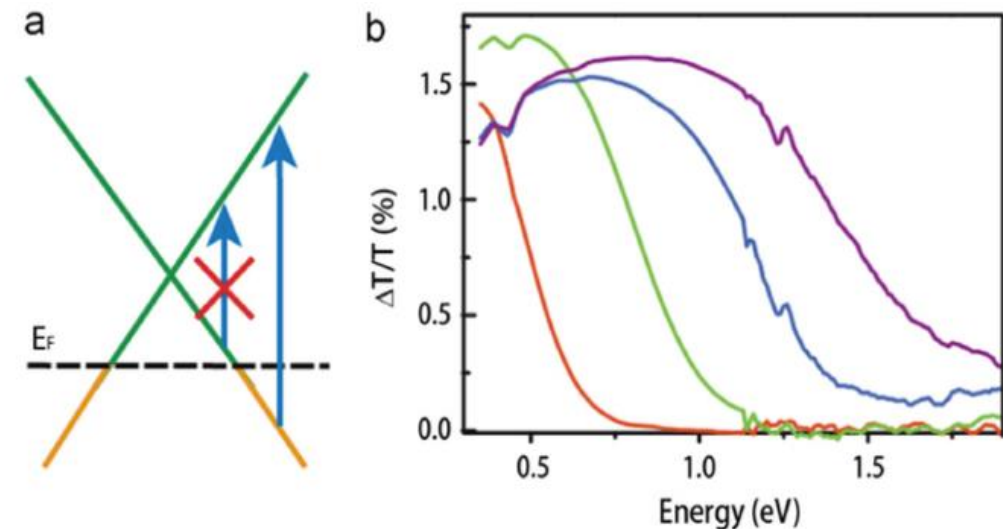
# Interband optical absorption in graphene

## Tunable interband optical transition

- Because of the single-atom thickness of graphene and its linear dispersion with a high Fermi velocity, the Fermi energy in graphene can be shifted by hundreds of meV through electrostatic gating.

Such doping leads to a strong change in the interband absorption through Pauli blocking.

The interband transitions for photon energies below  $2|E_F|$  are suppressed, while those at energies above  $2|E_F|$  are unaffected. The optical response in graphene thus becomes highly tunable.



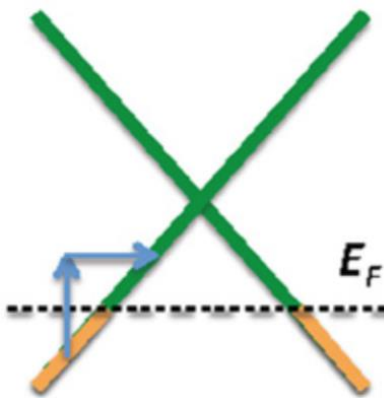
(a) an illustration of interband transitions in hole-doped graphene, (b) the gate-induced change of transmission in hole-doped graphene as a function of gate voltage  $V_g$ . The values of the gate voltage referenced to that for charge neutrality,  $V_g - VCNP$ , for the curves - 0.75, - 1.75, - 2.75 and - 3.5 V, from left to right..

Kin Fai Mak et al., Solid State Communications 152 (2012)

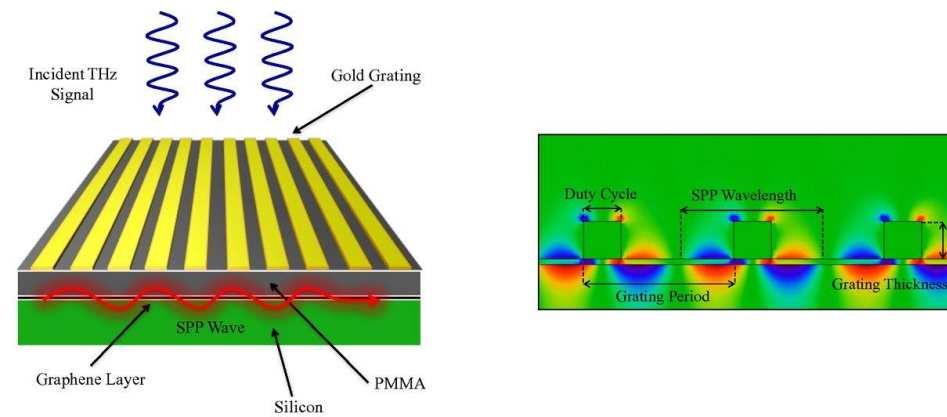
# Intraband optical absorption in graphene

Since the speed of light  $c$  is much higher than the Fermi velocity  $v_F$  of graphene ( $c/v_F \sim 300$ ), direct absorption of a photon by an intraband optical transition does not satisfy momentum conservation. To conserve momentum, **extra scattering with phonons or defects** is required.

**Plasmons** are quanta of collective oscillation of charge carriers. Direct light absorption by propagating plasmons in graphene film is not allowed due to the large momentum mismatch between photons and plasmons. However, plasmon absorption can be enabled with grating coupling, which provides an effective momentum due to the periodic grating structure.



Schematic representation of the intraband absorption process.

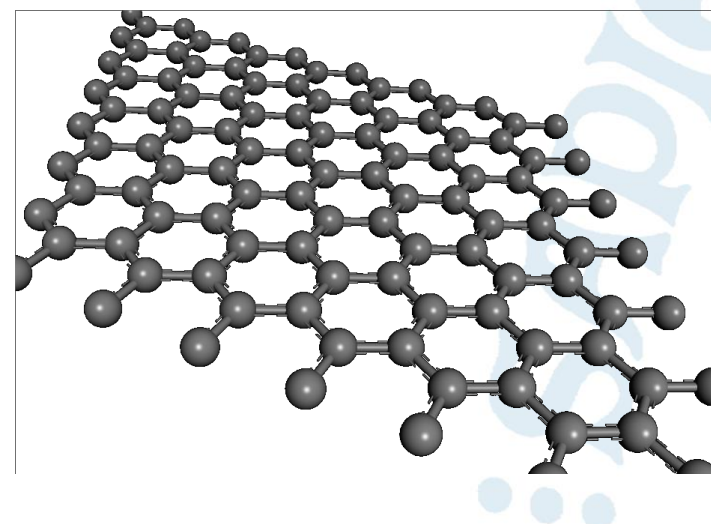


Conceptual illustration of a grating-gated graphene-based plasmonic heterostructure. In this design, the graphene layer rests on top of a dielectric (e.g.  $\text{SiO}_2$ ) and PMMA separates the graphene layer from a gold grating structure.

Kin Fai Mak et al., Solid State Communications 152 (2012)

# Graphene

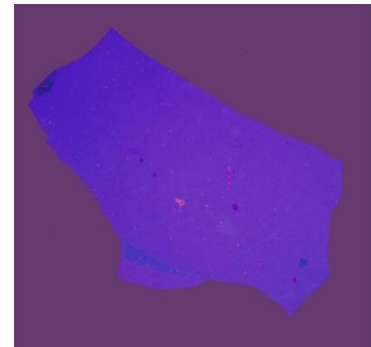
## Synthesis



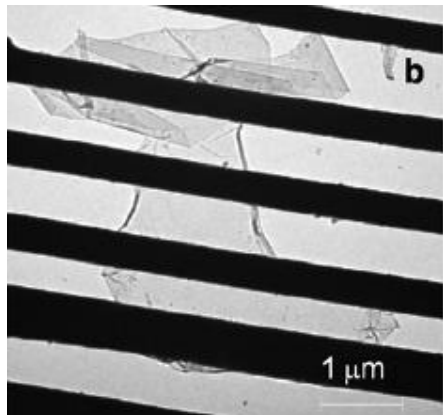
# Fabrication of graphene

Micromechanical cleavage of bulk graphite

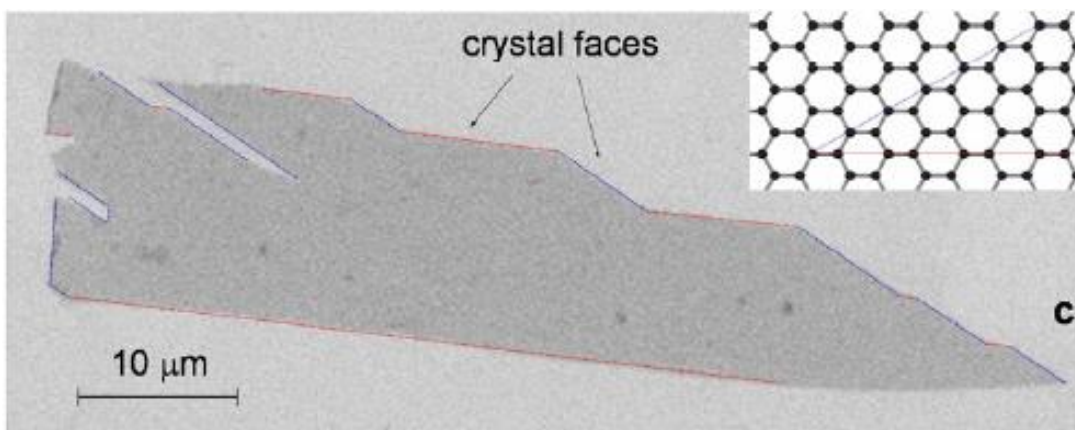
1<sup>st</sup> isolation of graphene monolayers: K.S. Novoselov et al,  
Science 306, 666 (2004)



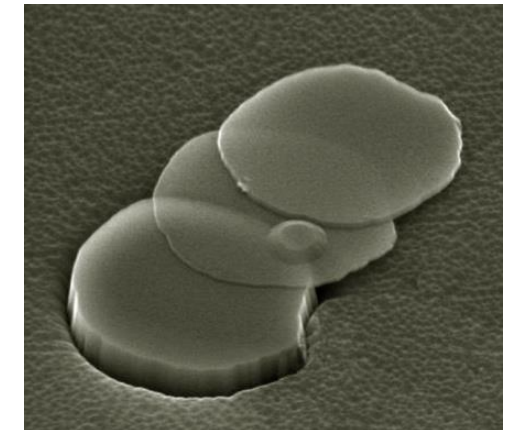
*Large graphene flake (approximately 6 layers). Optical photo in normal white light. Lateral size of the image 100 microns.*



*A TEM picture of a graphene sheet freely suspended on a micron-size metallic scaffold.*



*SEM of a relatively large graphene crystal, which shows that most of the crystal's faces are zigzag and armchair edges as indicated by blue and red lines*



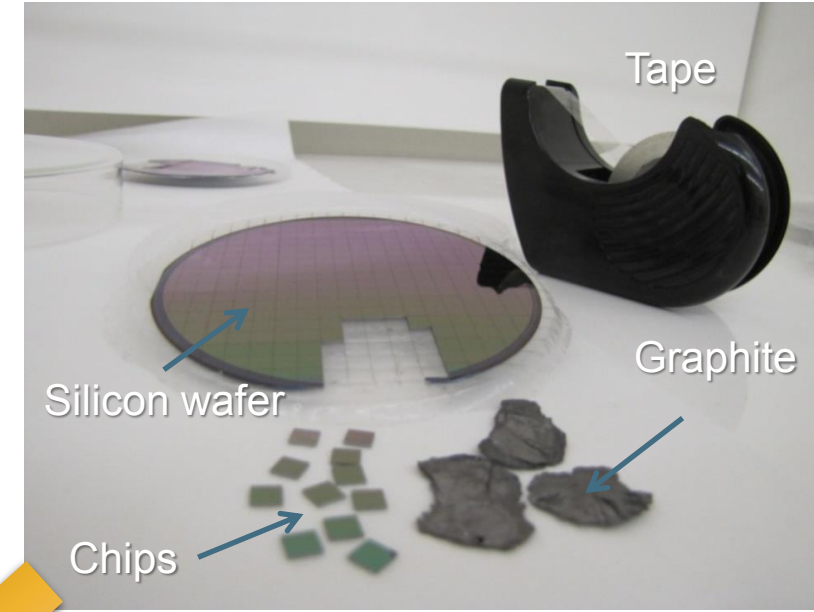
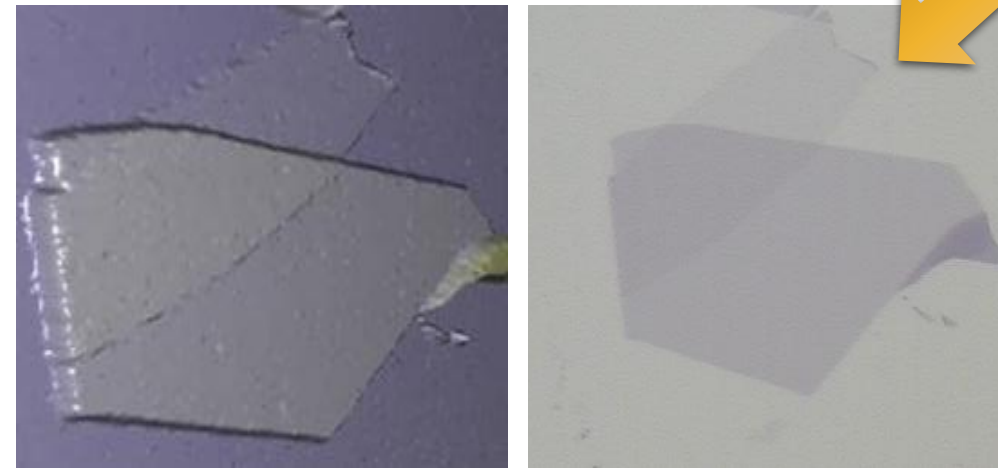
*SEM of a fallen mesa of graphite. This is the way graphene molecules were "extracted" from bulk graphite. To be reasonably visible in SEM, we show a 10 nm carbon flake (30 layer thick).*

# Graphene fabrication: exfoliation

The most common technique to fabricate graphene is by exfoliation from HOPG (Highly Ordered Pyrolytic Graphite) by using adhesive tape.

Novoselov et al., Science 306, 666 (2004)

- flake size: 5 – 100 nm
- random location
- simple process for proof-of-concept
- **no industrial relevance**



# Graphene formation by exfoliation of HOPG

1. Peel a HOPG (Highly Ordered Pyrolytic Graphite) layer with razor blade



2. Thin the HOPG piece



3. Repeatedly press and release the prepared tape



4. Find the monolayer graphite with an optical microscope

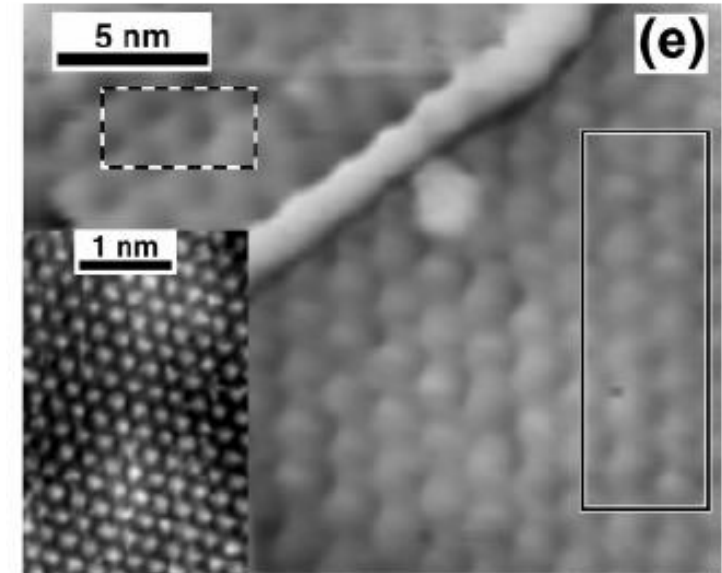
# Epitaxial graphene on c-SiC

Graphene can also be produced from silicon carbide (SiC) wafers.  
This is an old technique known since 1975.

The number of layers depends on temperature

- C-face SiC: few layers, decoupled
- Si-face SiC: mostly single layer

All quantum effects observed for exfoliated graphene have been observed in epitaxial graphene as well



Berger et al., J. Phys. Chem. B **108**, 19912 (2004)



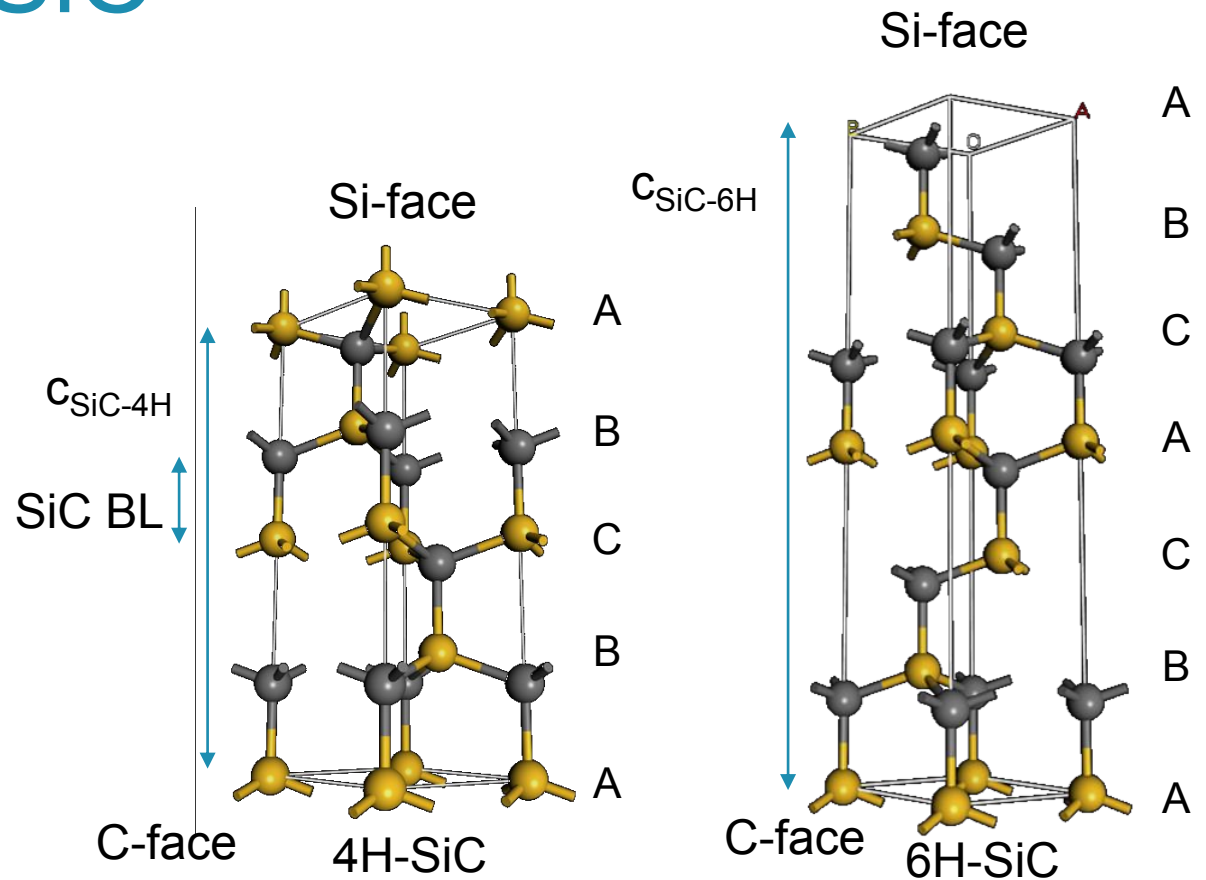
# Epitaxial graphene on c-SiC

SiC occurs in cubic form as well as several hexagonal polytypes. For graphene growth purposes, mostly hexagonal 4H and 6H SiC crystals have been used

An nH-SiC cell is made of n SiC bilayers (BL), each containing 1 Carbon and 1 Silicon plane

SiC has 2 **polar faces** perpendicular to the c axis:  
Si-terminated SiC(0001) and C-terminated  
SiC(0001)

Each face has 1 dangling bond per Si or C atom



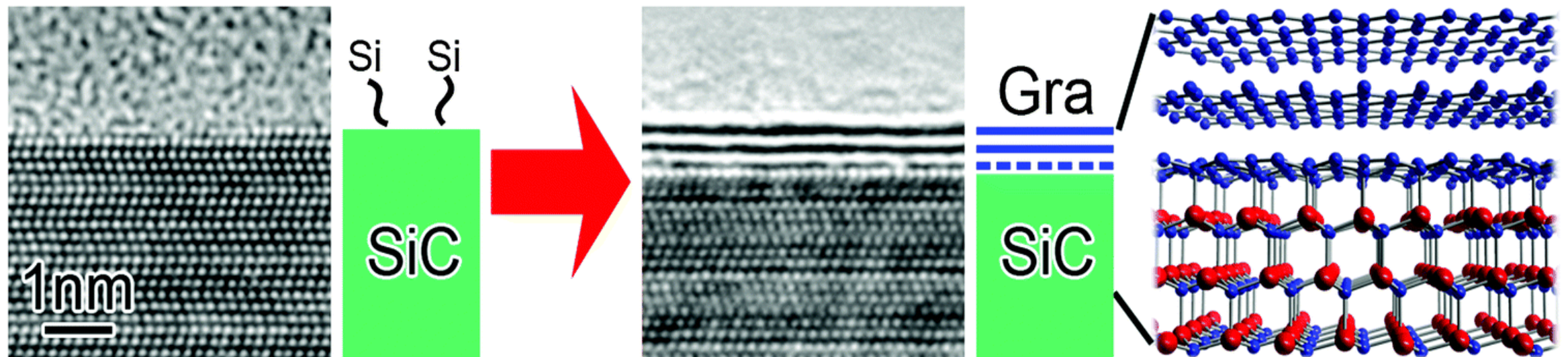
Crystal structures of 4H-SiC and 6H-SiC polytypes.

Hass et al., J. Phys. Cond. Mat. **20**, 323202 (2008)

# “Silicon sublimation” process

The **epitaxial graphene** (graphene grown via *silicon sublimation*), which is an excellent substrate for synthesis of van der Waals heterostructures.

The general process for epitaxial graphene synthesis is illustrated in the bottom figure.

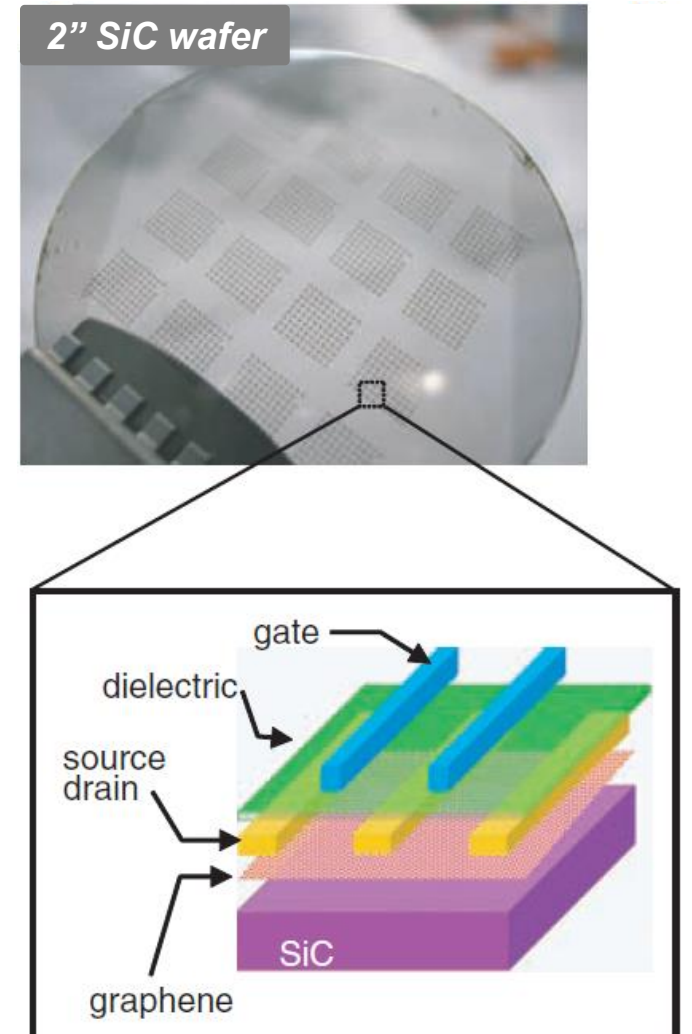
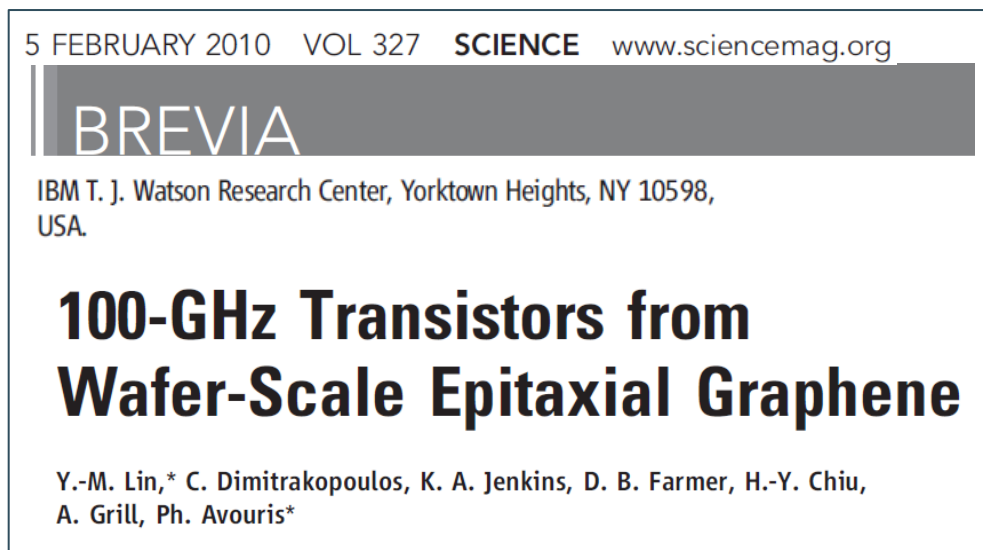


<https://sites.psu.edu/robinsonresearch/research/>

# Epitaxial graphene on c-SiC

First demonstration of ‘wafer-scale’ (2 inch) integration of graphene.

- Graphene growth carried out on a 2" SiC wafer
- Pre-cleaning @ 810 °C in 1:4 Si<sub>2</sub>H<sub>6</sub>:He
- Growth on the Si-face (1450 °C, 10<sup>-4</sup> torr, 2')



Lin et al., Science 327, 662 (2010)

# Graphene CVD

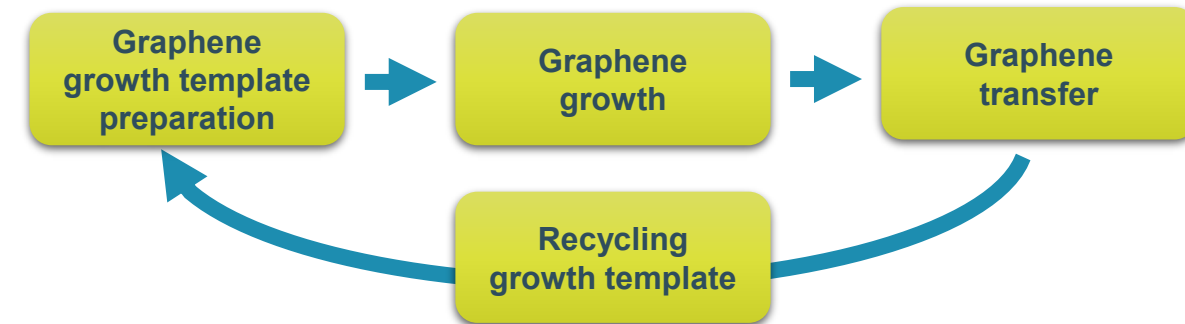
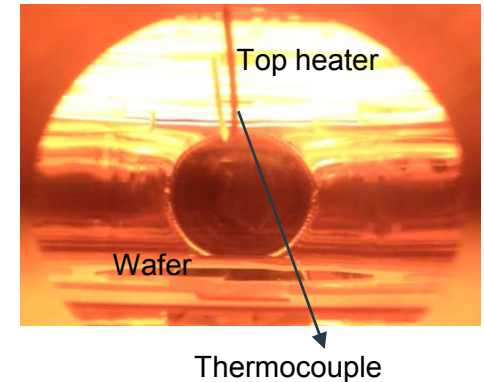
Chemical Vapor Deposition (CVD) is the most mature, cost-efficient graphene growth process that is scalable.



Requirements for the optimal (metallic) template for deposition (Pt, Cu, Ir, Pd, ...):

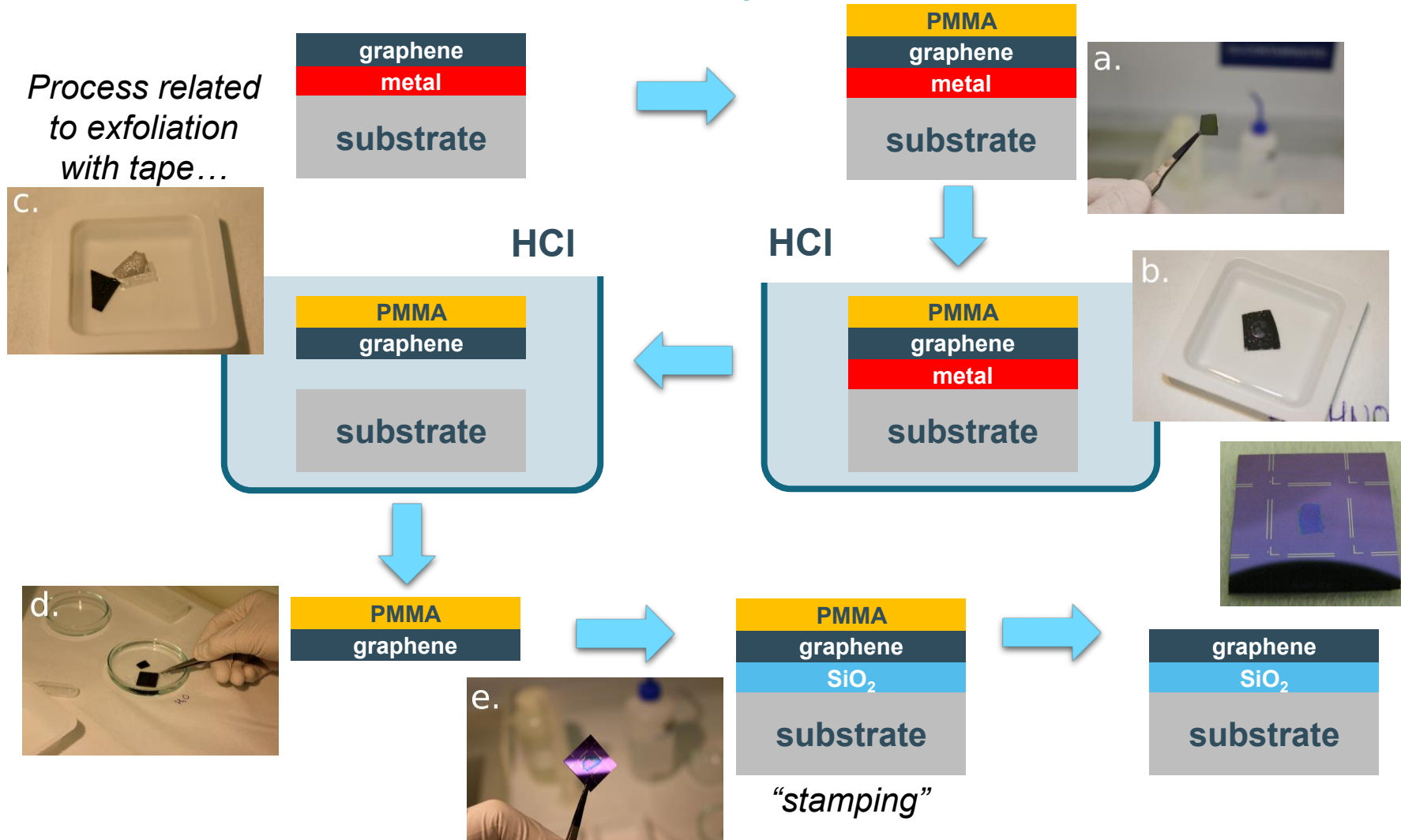
- Catalyzes dissociation
- Atomically flat and monocrystalline
- Stable thin film at high temperature
- Low carbon solubility
- Reusable (cheap)
- Capable to initiate oriented graphene growth
  - Minimize graphene grain boundaries

Graphene transfer is needed after the growth process.



# Graphene transfer step-by-step

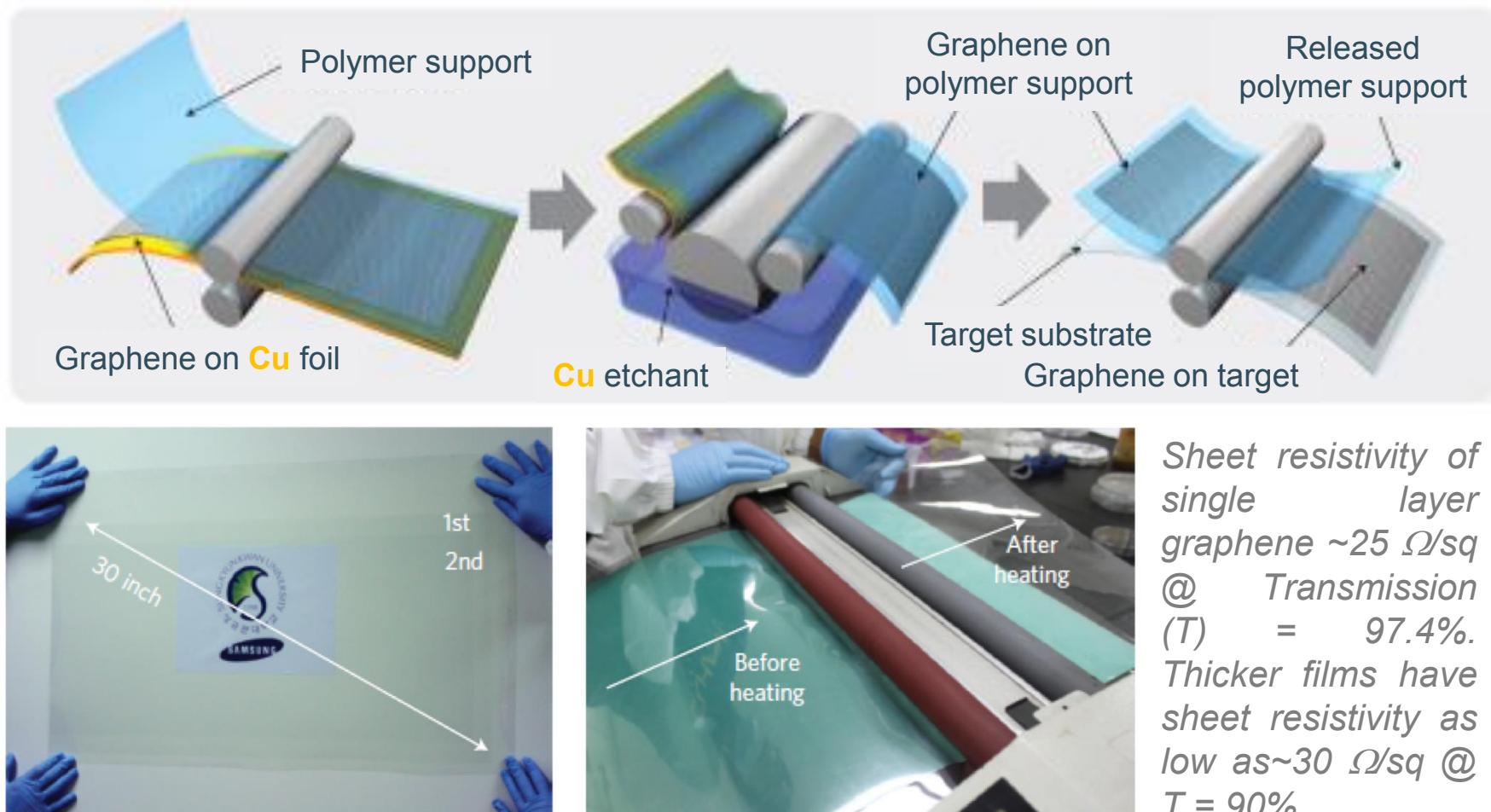
*Process related  
to exfoliation  
with tape...*



# Large sheet graphene CVD

Fabrication of large area graphene sheets by CVD on Cu foils was demonstrated.

Rollable, continuous films transferred grown on Cu foils and transferred onto a flexible display after nitric acid treatment.

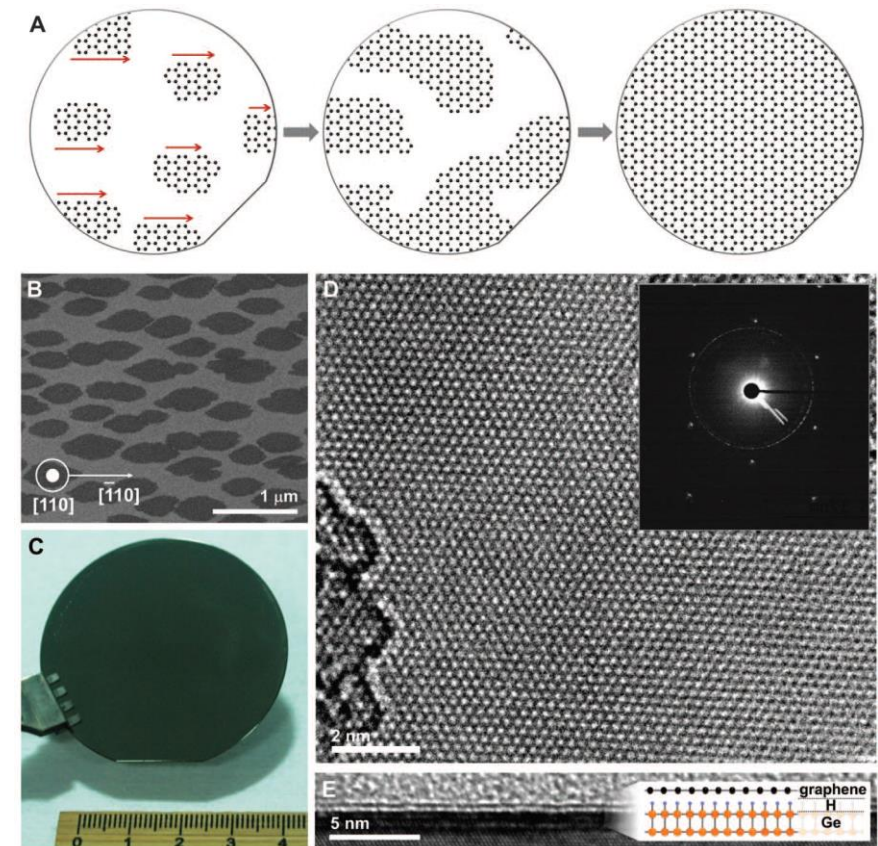


Bae et al., Nat. Nanotechnol. **5**, 574 (2010)

# High quality graphene on Ge(110) surfaces

Single-crystal monolayer graphene grown on hydrogen-terminated Ge(110) surface.

- a) A schematic illustration of catalytic growth of single-crystal monolayer graphene from uni-directionally aligned multiple seeds.
- b) A typical SEM image of graphene seeds at the early stage of growth.
- c) A photograph of graphene grown on a 2" Ge/Si (110) wafer.
- d) A HR-TEM image of the single-crystal monolayer graphene.
- e) A cross-sectional TEM image demonstrating that the as-grown graphene is monolayer.

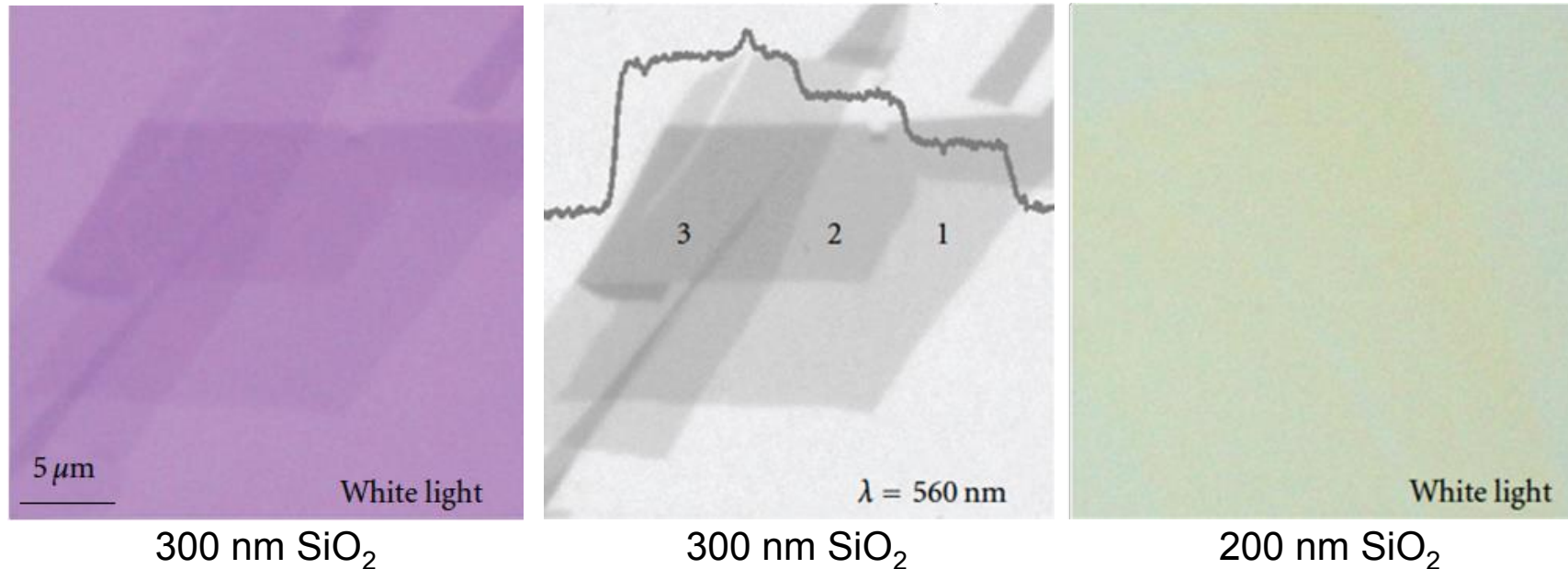


J.H. Lee et al., Science 344 (2014)

# Optical detection of graphene

Even a monolayer of graphene can become visible on  $\text{SiO}_2$  using an optical microscope. The contrast depends on the **thickness of  $\text{SiO}_2$** , the **wavelength of light** used, and the **angle of illumination**.

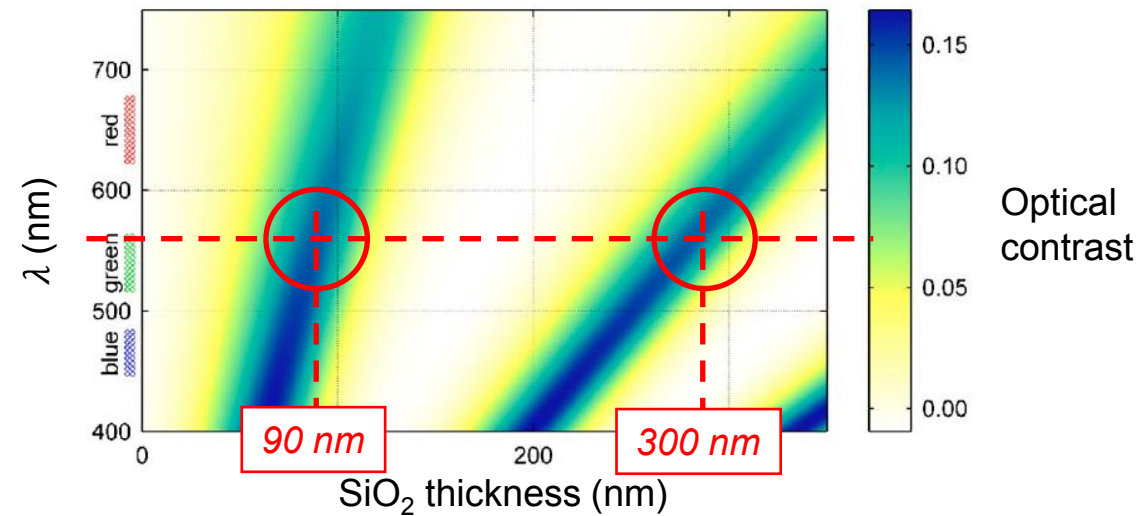
This feature of graphene is useful for the quick identification of few- to single-layer graphene sheets and is very important for mechanical exfoliation.



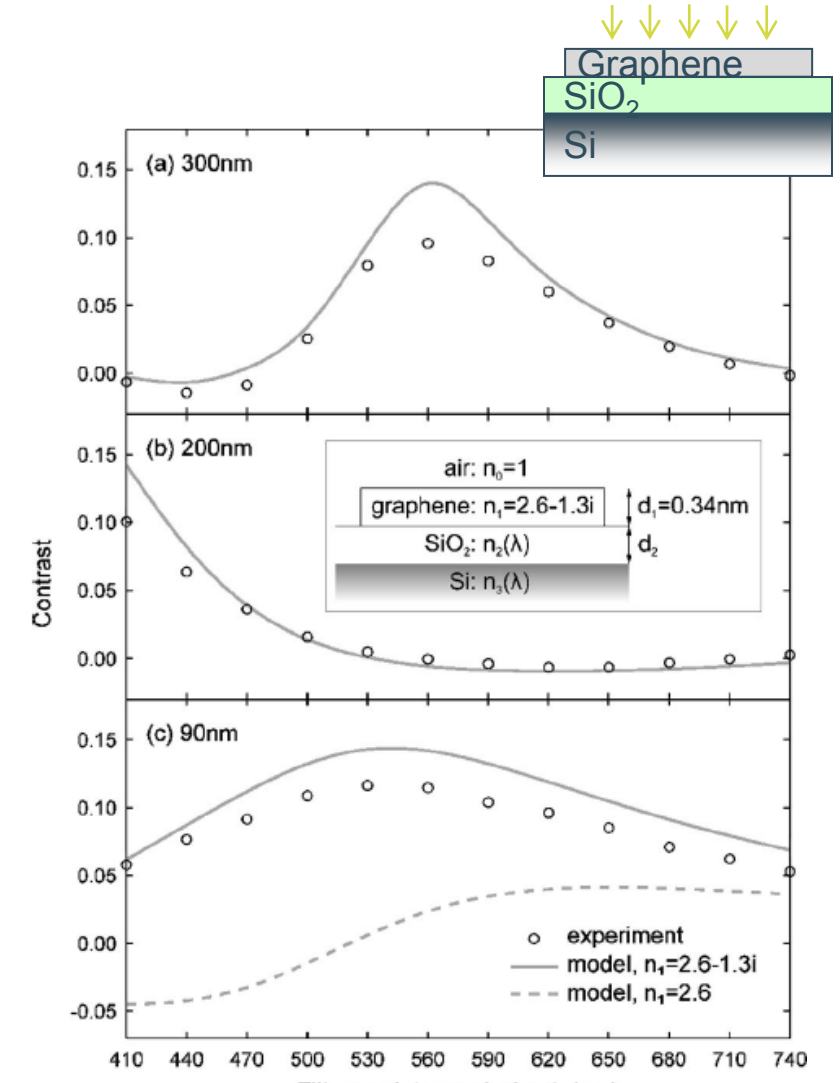
*Optical contrast of one, two, and three layers of exfoliated graphene under different wavelengths of illumination and different thicknesses of  $\text{SiO}_2$ .*

# Graphene visibility on dielectrics

Due to **optical interference** a graphene layer becomes visible on an  $\text{SiO}_2$  layer with the correct thickness (90nm, 300nm, ...)



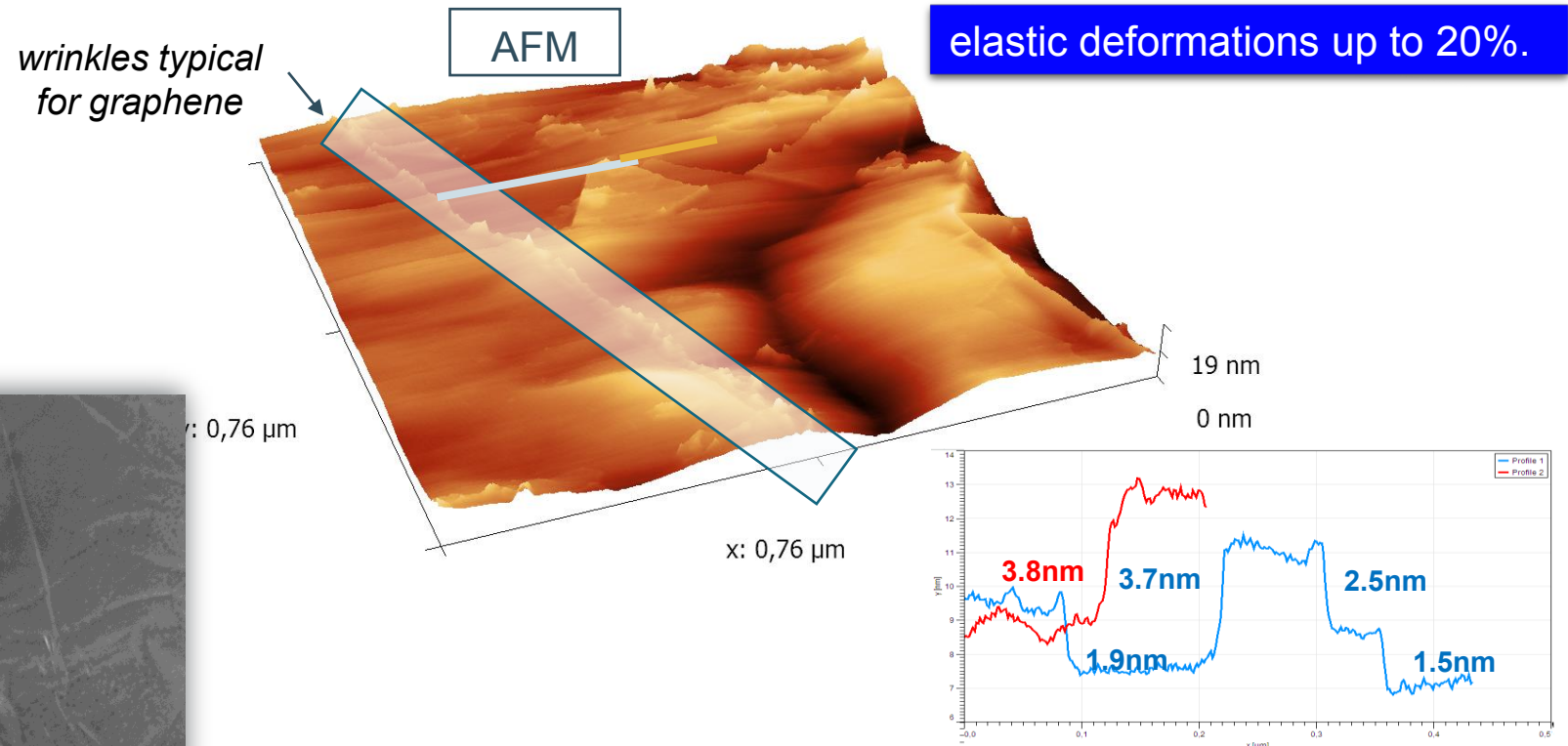
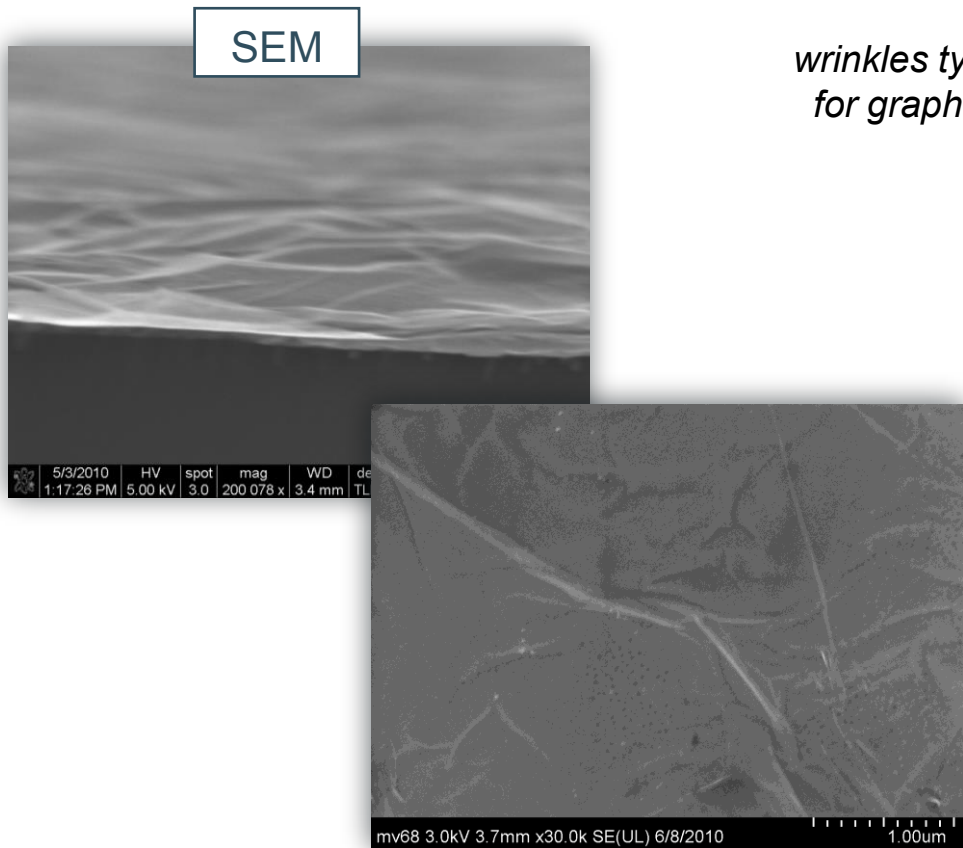
$$C = \frac{I(n_0 = 1) - I(n_1)}{I(n_0 = 1)} \quad \left\{ \begin{array}{l} \bullet \text{air: } n_0 = 1 \\ \bullet \text{graphene: } n_1 = 2.6 - 1.3i \text{ (bulk graphite)} \\ \bullet \text{SiO}_2: n_2 = n_2(\lambda) \\ \bullet \text{Si: } n_3 = n_3(\lambda) \end{array} \right.$$



Blake et al., Appl. Phys. Lett. **91**, 063124 (2007)

# Graphene morphology

When supported by a substrate graphene takes the shape of the substrate, but wrinkles can occur.

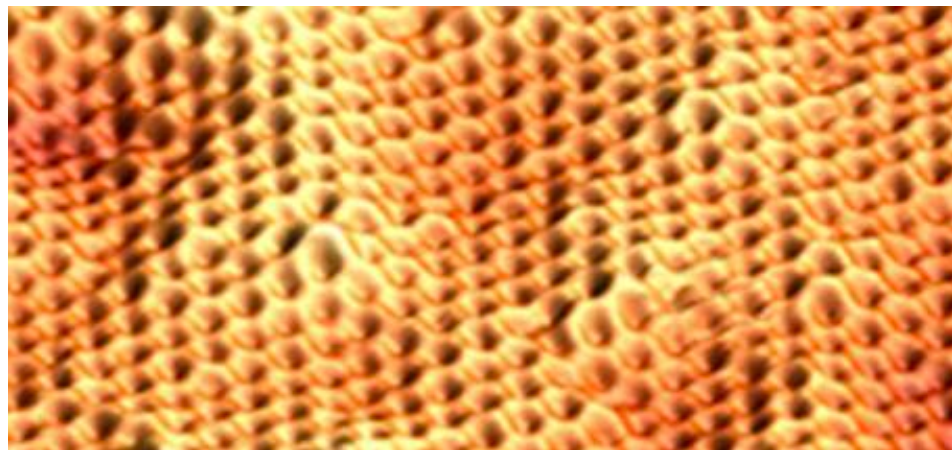


Typical smooth wrinkle-like morphology observed for graphene.

# Graphene “atomic” morphology

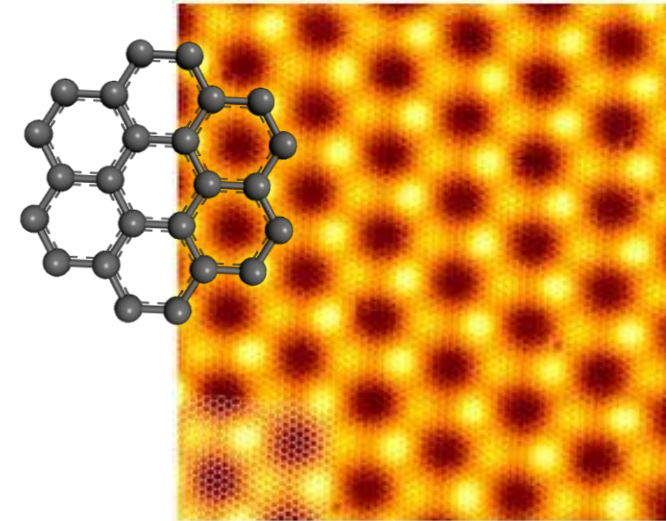
When supported by a substrate graphene takes the shape of the substrate, as shown by the STM image.

Despite the surface roughness, the honeycomb structure of the graphene is preserved.



For epitaxial graphene, extremely smooth surfaces can be achieved.

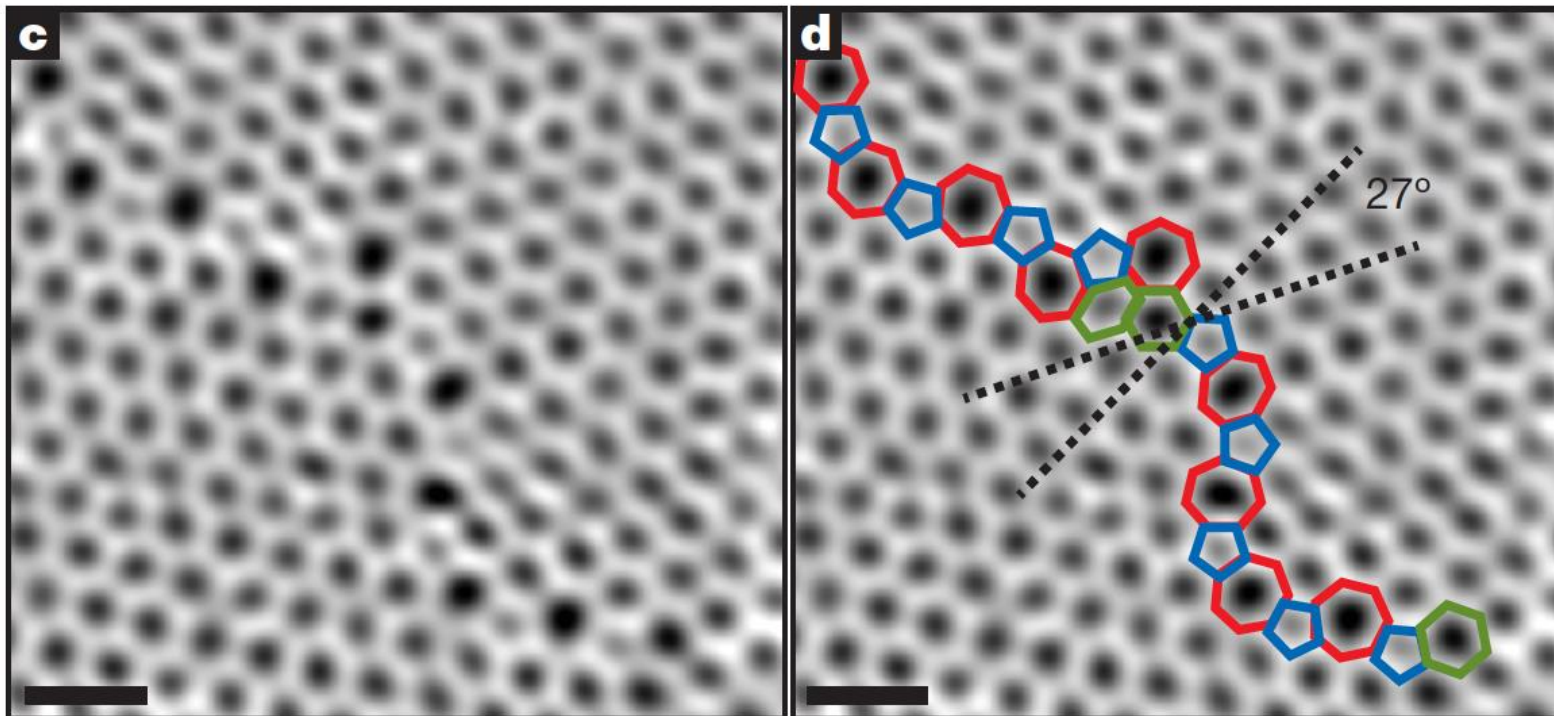
STM allows atomic characterization of the crystalline structure revealing nicely the carbon hexagonal ring.



*Graphene/Ir (0001)*

# Graphene defects

Defects in graphene can be observed by TEM.



P. Huang et al, Nature 469 (2011)

Atomic-resolution ADF-STEM image of Graphene crystal with two grains.

Left: Two grains intersect with a  $27^\circ$  relative rotation. An aperiodic line of defects stitches the two grains together.

Right: The left image with the pentagons (blue), heptagons (red) and distorted hexagons (green) of the grain boundary outlined. (scale bars, 5Å)

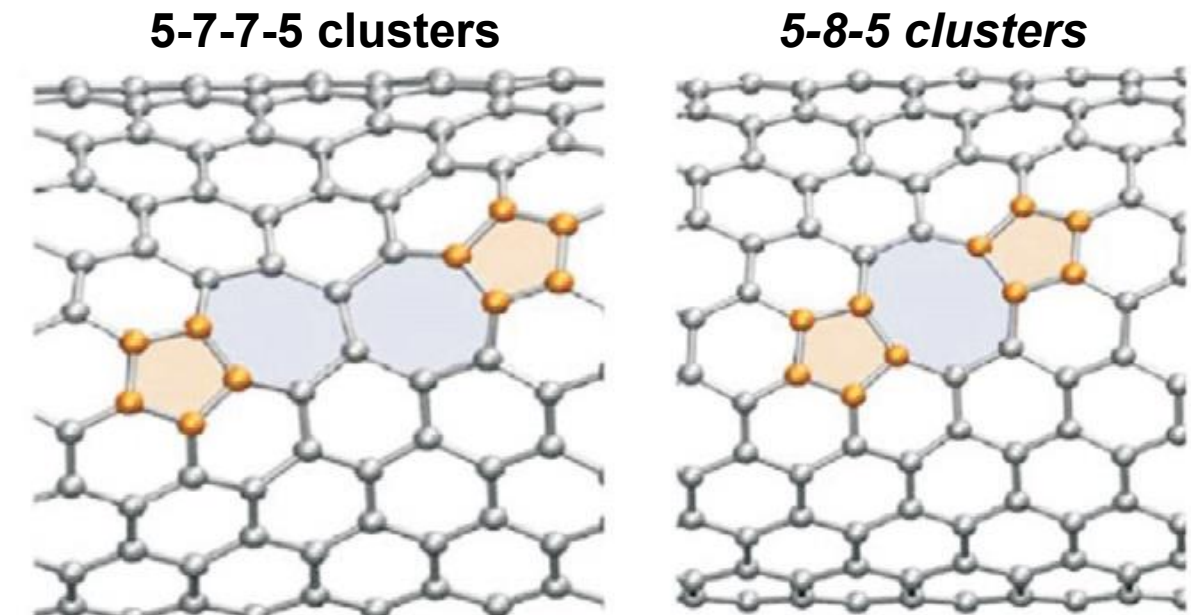
# Graphene defects

Graphene typically accommodates two common types of **carbon cluster defects** with environments locally perturbed from the perfect  $sp^2$  hybridized carbon.

The most common cluster defect is the 5-7-7-5 defect, but also frequently occurring are 5-8-5 defects, both of which maintain an average of the six carbon planar rings of Graphene.

Therefore, graphene can be annealed at sufficiently high temperatures to lower its defect concentration.

Since the 5-7-7-5 and 5-8-5 defects are symmetry-breaking, they can be observed spectroscopically in the Raman **D-band**.



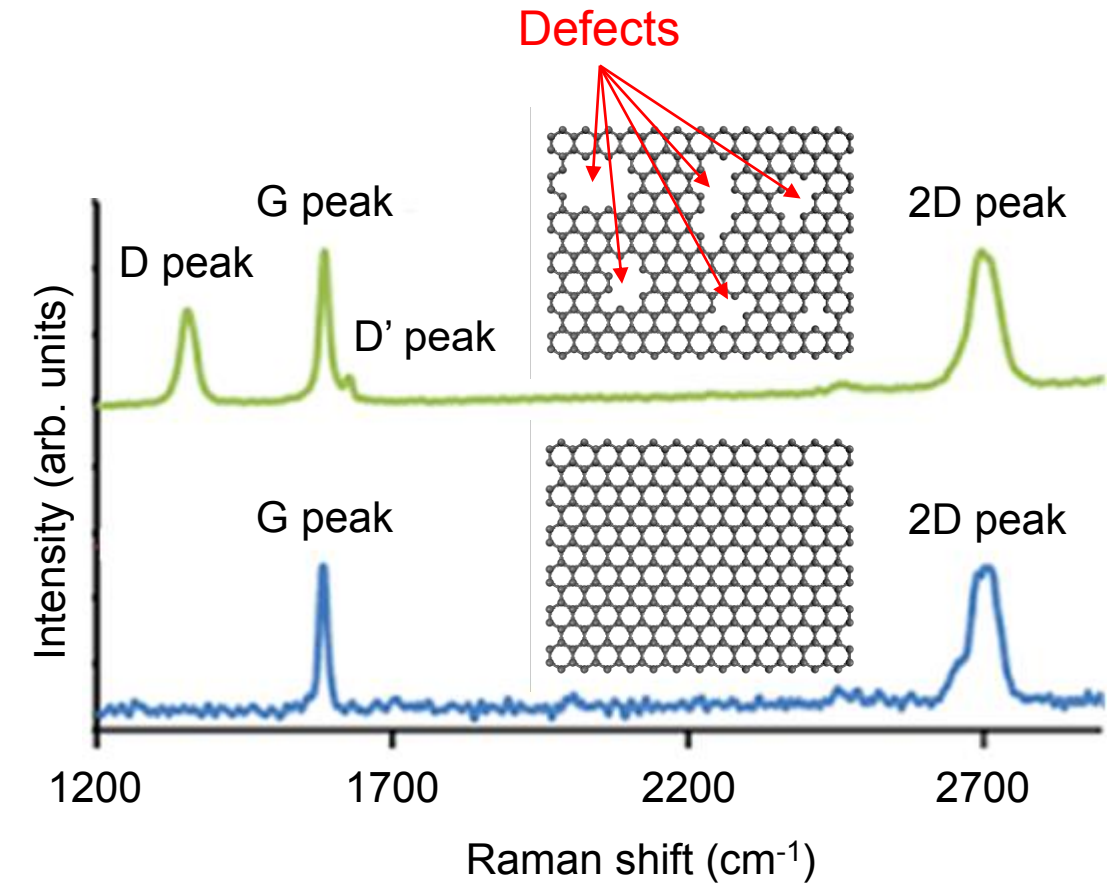
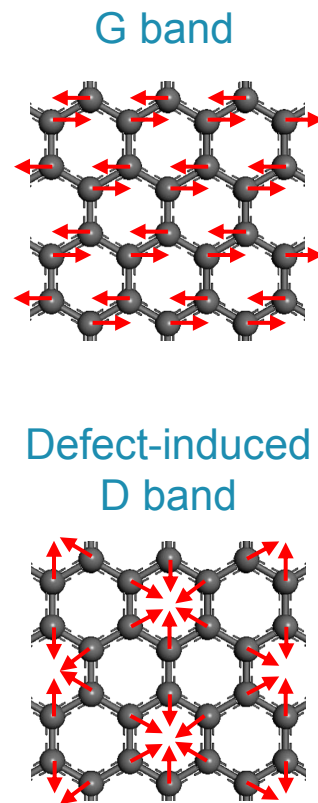
Molecular models representing: (a) the 5-7-7-5 Thrower-Stone-Wales defect and (b) the 5-8-5 vacancy-like cluster defect

P. Araujo et al, Materials Today 15(3), March 2012

# Raman – Defect peak

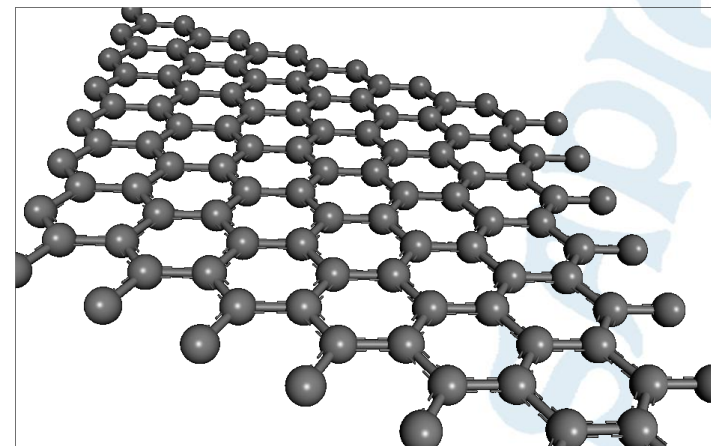
Raman spectrometry is a perfectly suitable characterization technique for the presence of defects in graphene layer.

Pristine graphene layer exhibits strong G and 2D peaks, while defective graphene will show additional D and D' peaks in the spectrum.



# Graphene

Devices & applications



# Electronic transport in graphene

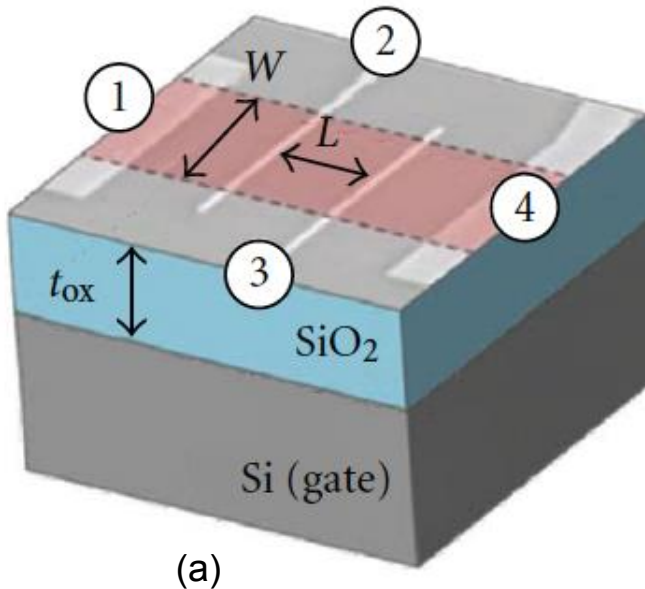
Transport properties are typically measured with a graphene device similar to those shown on the adjacent figure.

With this graphene device, one can tune the charge carrier density between holes and electrons by applying a gate voltage ( $V_g$ ) between the (doped) silicon substrate and the graphene flake. The gate voltage induces a surface charge density  $n$  as:

$$n = \frac{\varepsilon_0 \varepsilon V_g}{t q}$$

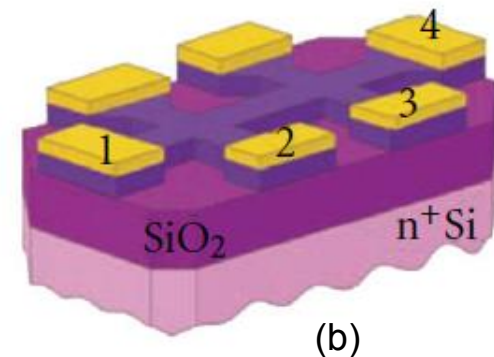
where  $\varepsilon_0 \varepsilon$  is the  $\text{SiO}_2$  permittivity,  $q$  is the electron charge, and  $t$  is the thickness of the  $\text{SiO}_2$  layer.

This charge density change shifts accordingly the Fermi level position ( $E_F$ ) in the band structure.



(a)

Schematic representation of common electronic devices.  
(a) 4-lead and (b) Hall bar.



(b)

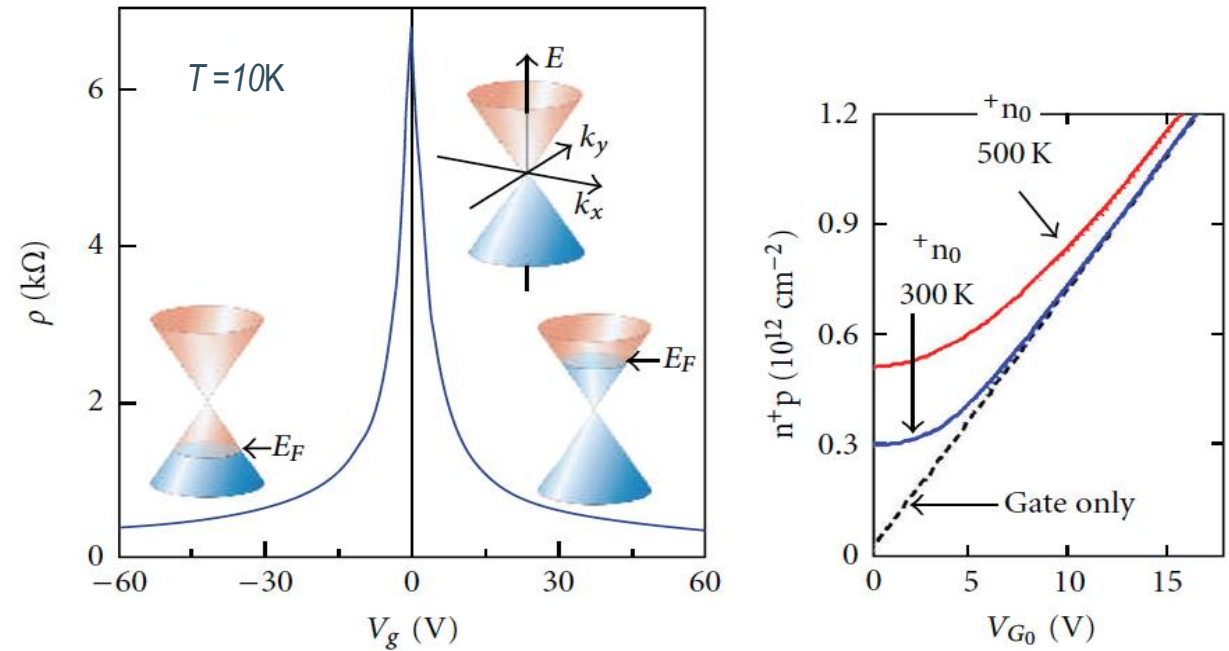
To fabricate these devices, graphene is deposited on an oxidized silicon wafer. Electrical contacts, usually made of gold, are defined using a lithographic process or a stencil mask to avoid photoresist contamination. Electrodes are generally patterned in a 4-lead or Hall bar configuration. Lastly, the device can be cleaned by annealing at ultrahigh vacuum or in  $\text{H}_2/\text{Ar}$  gas, or by applying a large current density ( $\sim 10^8 \text{ A/cm}^2$ ) through it to remove adsorbed contamination.

# Electronic transport in graphene

Due to the special shape of the band diagram, an **ambipolar** electric field effect (i.e. both electron and hole conduction) is observed in graphene.

The peak in the **resistivity** versus gate voltage curve occurs when the Fermi level is aligned with the Dirac point (i.e. where the two cones touch each other) as the density-of-states (DOS) disappears at that point.

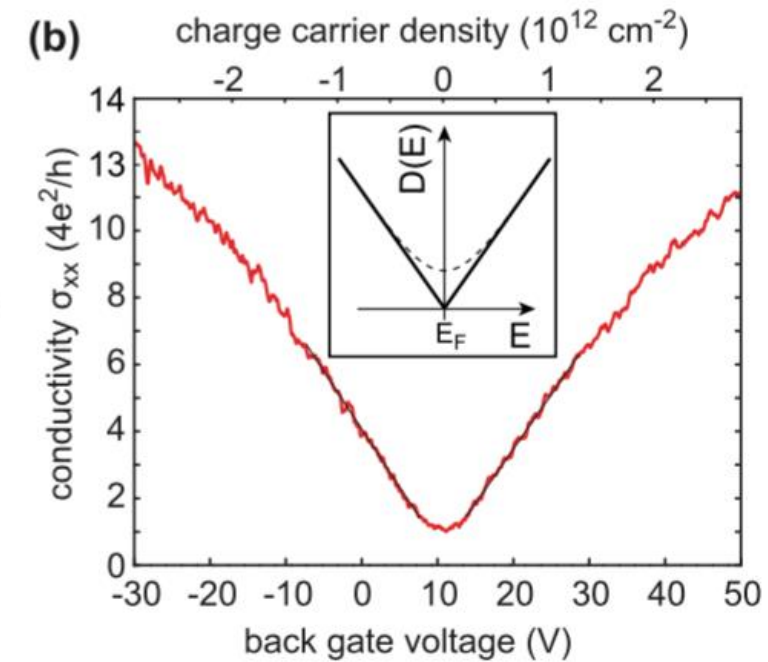
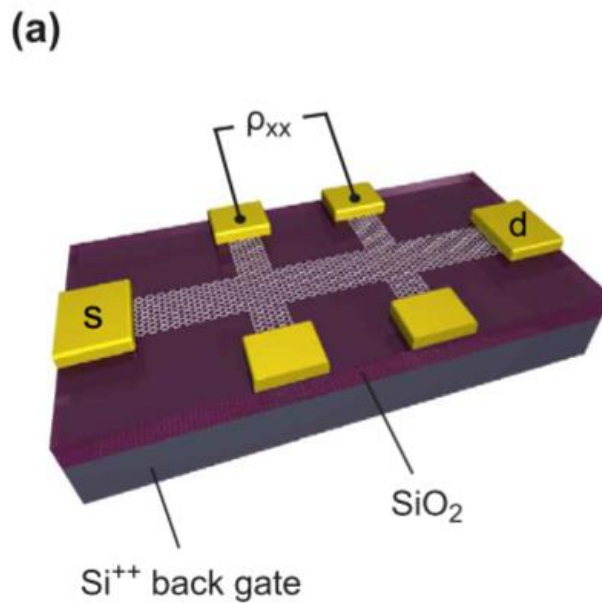
Typically, charge density can be tuned from  $10^{11}$  to  $10^{13} \text{ cm}^{-2}$  by applying a gate voltage that moves  $E_F$  from 10 to 400 meV away from the Dirac point.



Resistivity and change in the position of the Fermi level  $E_F$  as a function of gate voltage (left). Calculated charge density versus gate voltage at 300 K and 500 K (right). Solid lines include contribution from  $n^*$ ,  $n_{th}$ , and  $n_g$ . Dashed line shows only the contribution from the gating ( $n_g$ ).

# Electronic transport in graphene

At the Dirac point, the carrier density  $n$  should theoretically vanish, but thermally generated carriers ( $n_{th}$ ) and electrostatic spatial inhomogeneity ( $n^*$ ) limit the minimum charge density.



(a) Schematic of a contacted graphene Hall-bar device. (b) Conductivity as a function of back gate voltage  $V_{bg}$  at  $I_{sd} = 20 \text{ nA}$  ( $T = 2\text{K}$ ). By varying the carrier density via the back-gate charge transport is tuned from hole- to electron-like transport by passing the so-called charge-neutrality (or Dirac) point at minimum conductivity. The charge-neutrality point is offset from  $V_{bg} = 0 \text{ V}$  due to residual doping of the graphene. In the inset the smearing of the density of states around the charge-neutrality point due to electron–hole puddles is sketched.

# Mobility in suspended graphene

Concerning electronic applications, graphene has attracted considerable attention due to its high carrier mobility.

The high mobility in suspended graphene has been experimentally demonstrated.

The resistance of graphene depends strongly on the carrier density and the temperature.

nature nanotechnology | ADVANCE ONLINE PUBLICATION | www.nature.com/naturenanotechnology

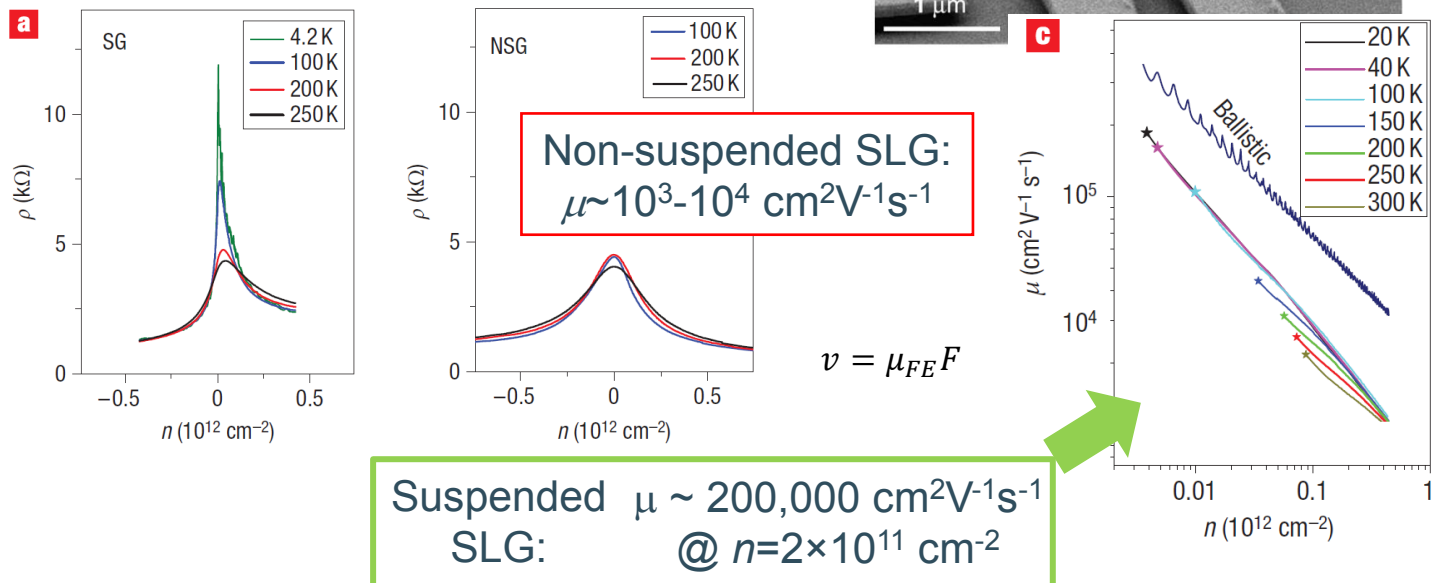
LETTERS

## Approaching ballistic transport in suspended graphene

XU DU, IVAN SKACHKO, ANTHONY BARKER AND EVA Y. ANDREI\*

Department of Physics and Astronomy, Rutgers the State University of New Jersey, 136 Frelinghuysen Rd, Piscataway, New Jersey 08854, USA

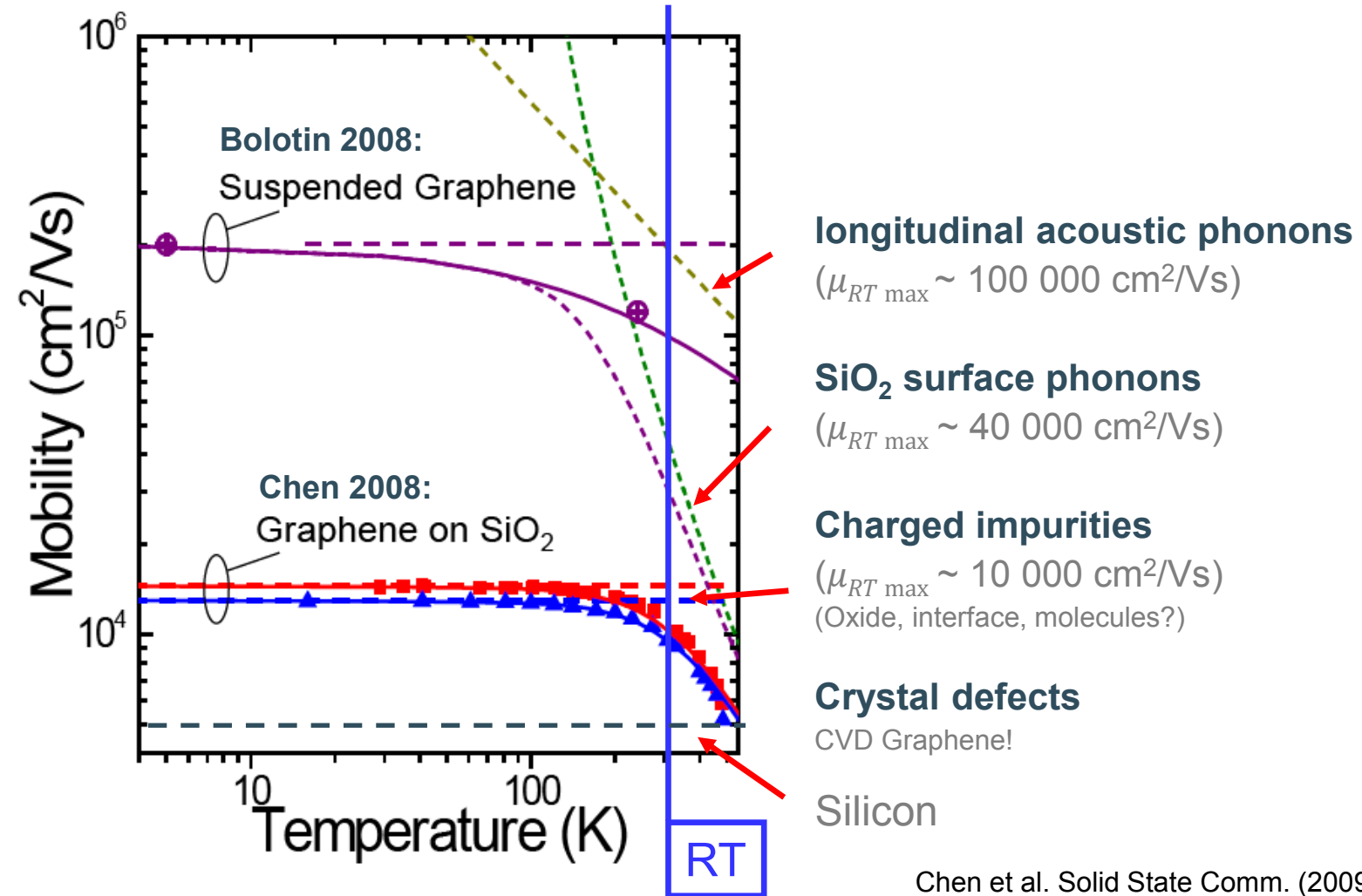
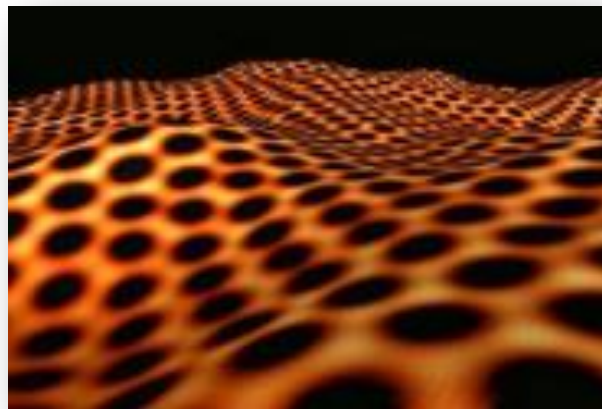
\*e-mail: eandre@physics.rutgers.edu



Du et al., Nat. Nanotechnol. **3**, 491 (2008)  
Bolotin et al., Phys. Rev. Lett. **101**, 096802 (2008)

# Graphene transistor: fundamental limits

The mobility in graphene is limited by various scattering mechanisms:



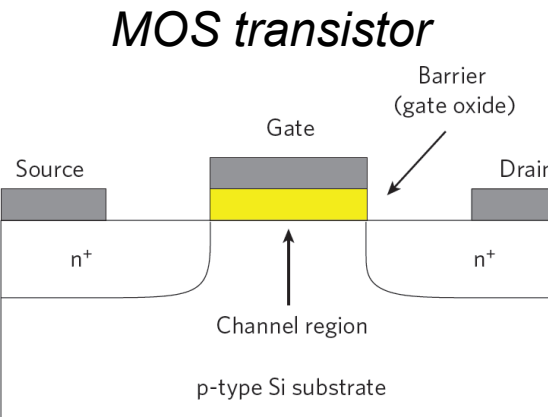
Chen et al. Solid State Comm. (2009)

# Si-based FET vs graphene-based FET

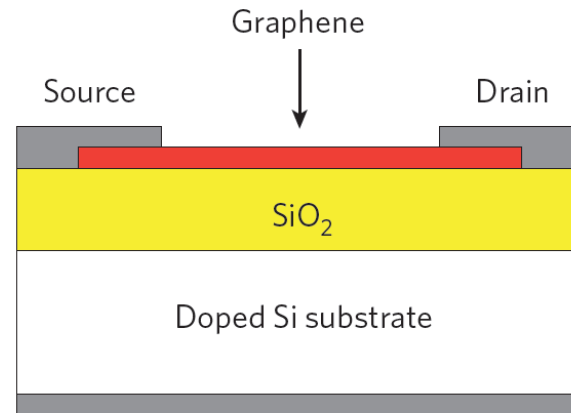
Graphene generated a lot of interest for FET devices due to its high carrier mobility and because an atomically-thick channel would allow for extreme scaling.

What else do we need?

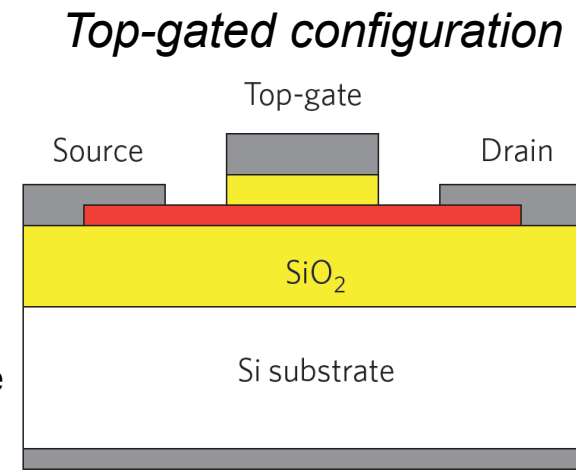
- Low  $I_{off}$  (low static power dissipation)
- $n$ - and  $p$ -doping (C-MOS)
- Gate oxide: top-gated configuration preferred over back-gate.



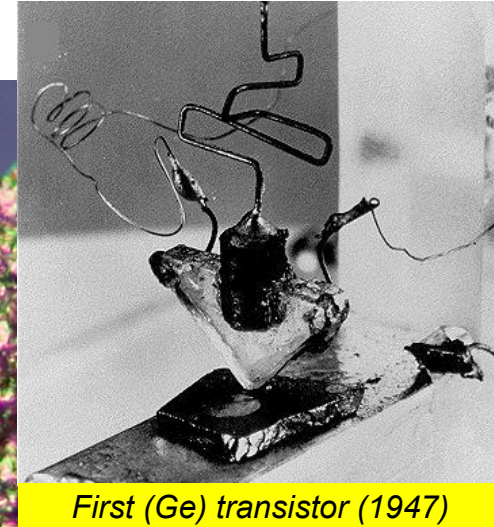
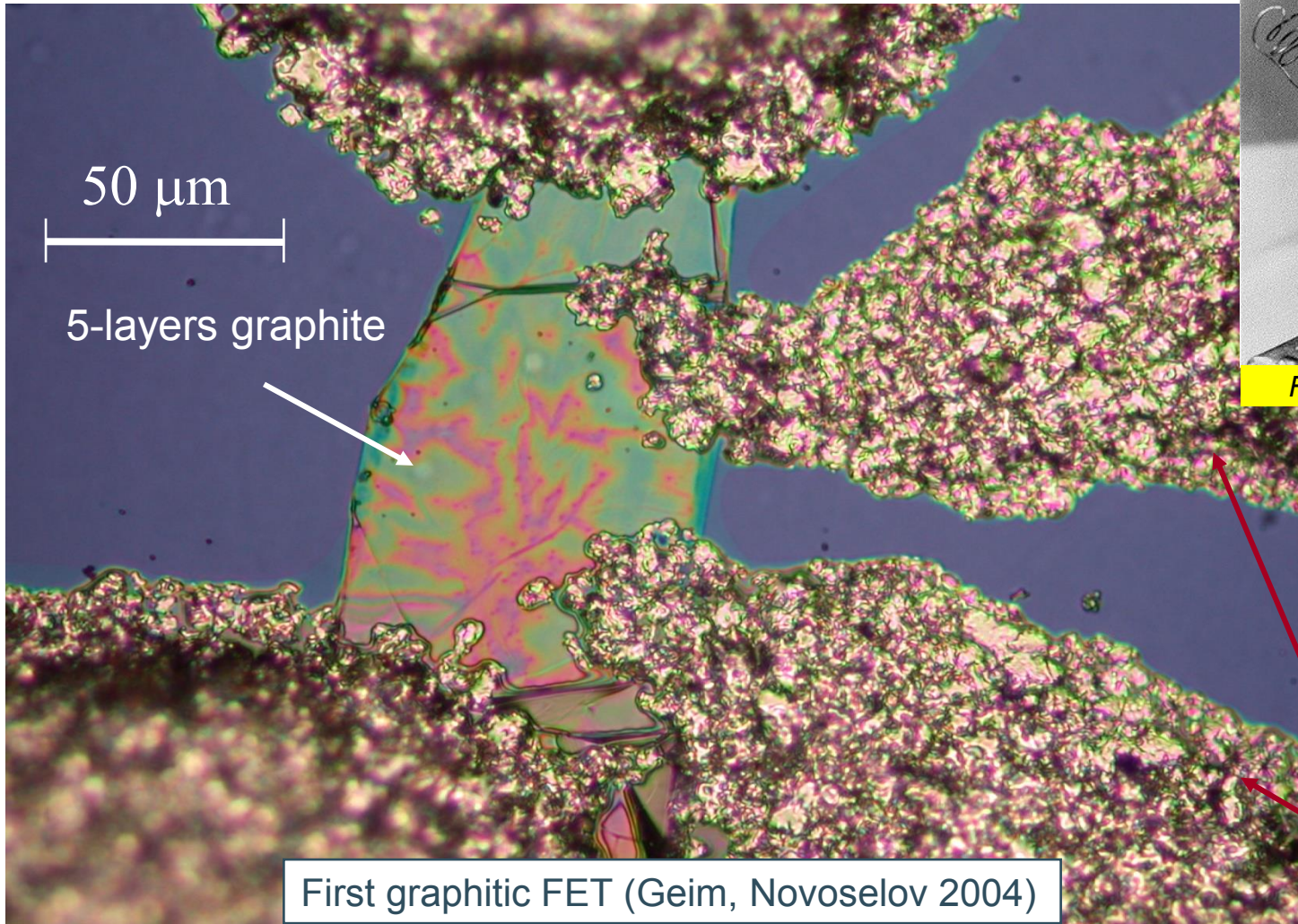
*Back-gated configuration*



Top-gate configuration involves additional concerns (graphene passivation)



# Graphene based FET



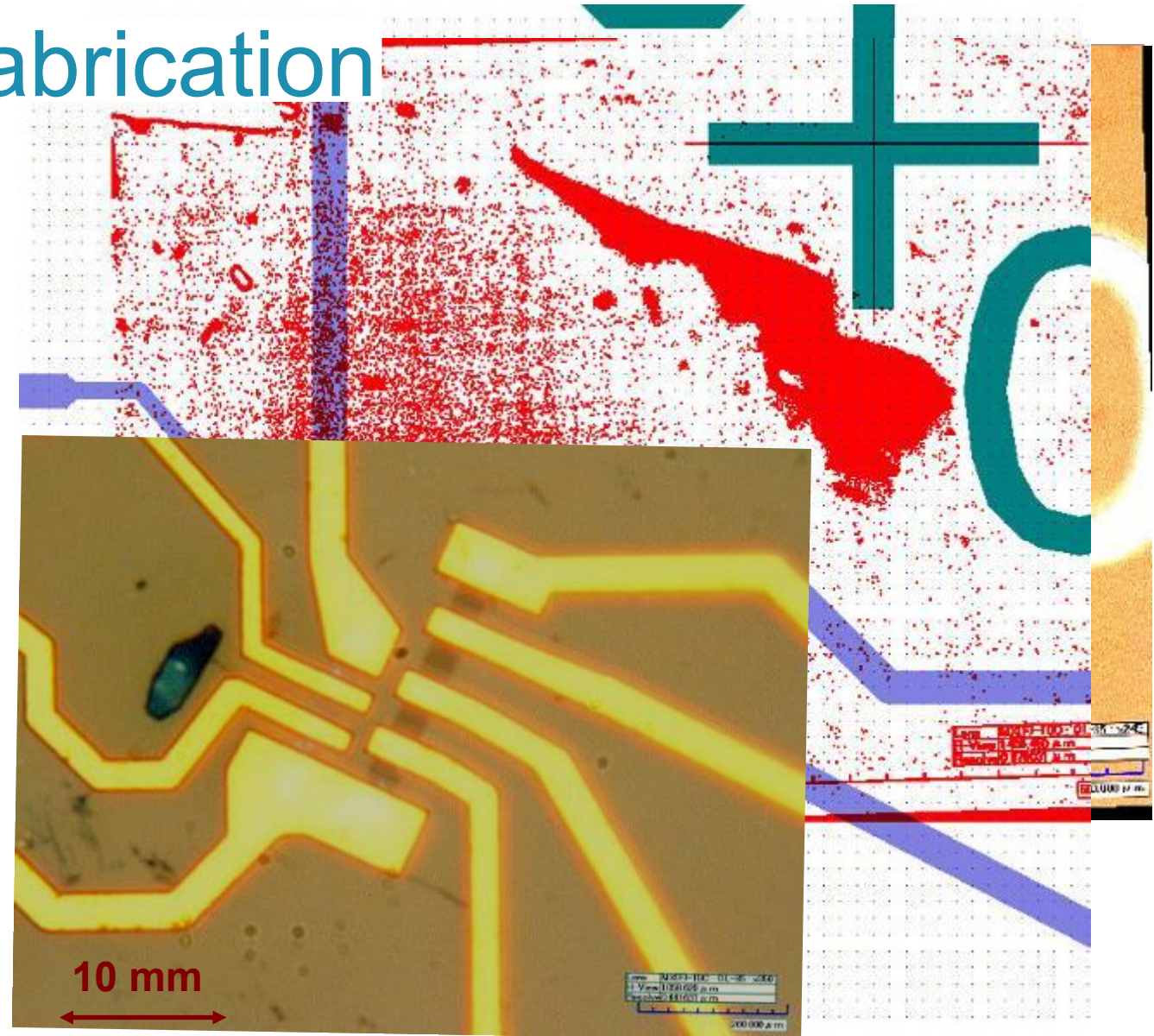
# Graphene device fabrication

## Design:

- Flake identification
- Image processing
- Import in layout design software
- Designing device shape
- Design for contacts

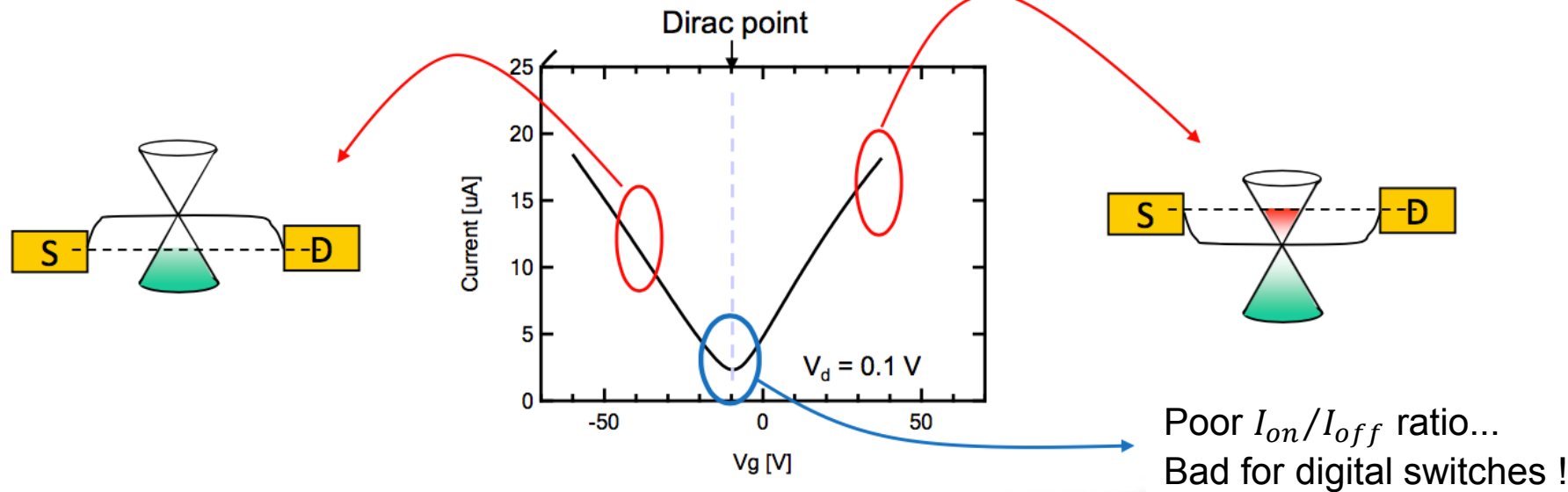
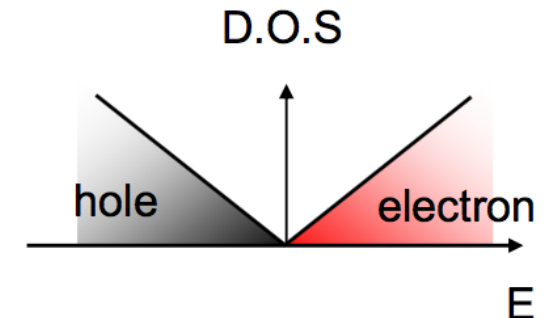
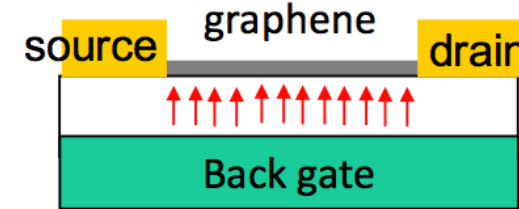
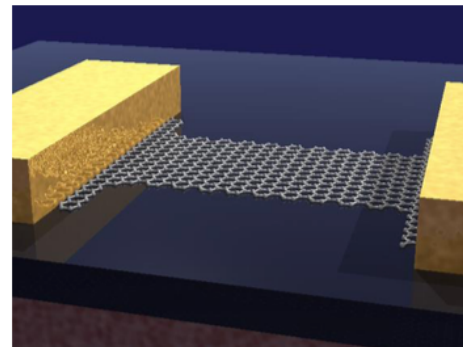
## Fabrication:

- E-beam process for shape definition, followed by O<sub>2</sub> plasma etching
- E-beam step followed by metallization and lift-off



# Graphene Field-Effect Transistor (FET)

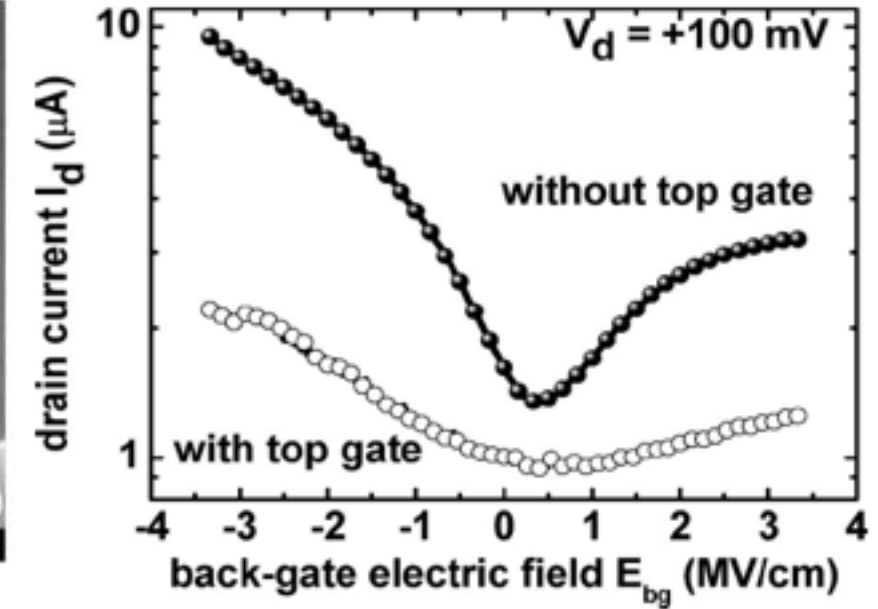
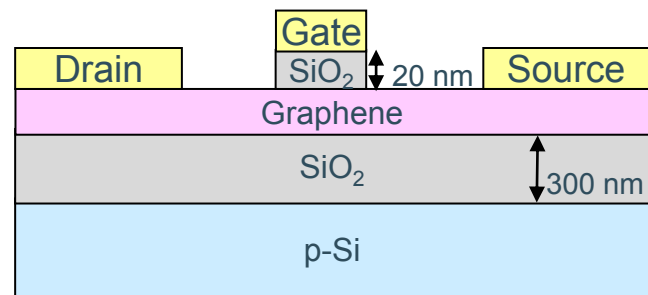
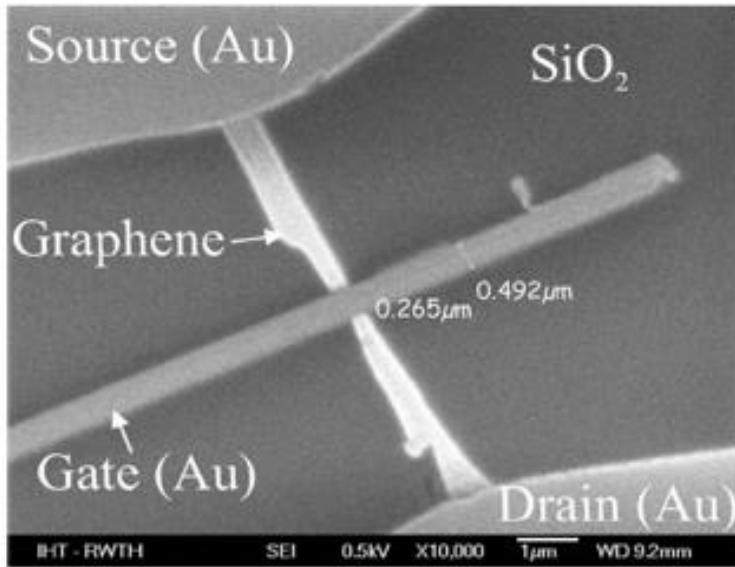
The poor  $I_{on}/I_{off}$  ratio of graphene FETs due to lack of bandgap makes them **unsuitable** for logic applications.



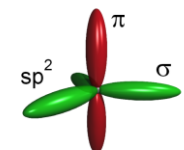
# Graphene field-effect devices

Demonstration of a “classical” field-effect devices using a top gate structure.

Notice the reduction in the drive current when a gate insulator is used. Furthermore, the device has a very low  $I_{on}/I_{off}$  ratio, limiting its applicability.



- Top-gate dielectric disturbs  $\pi$ -orbitals
- In this work evaporated  $SiO_x$  was used without annealing, leading to a poor-quality dielectric.

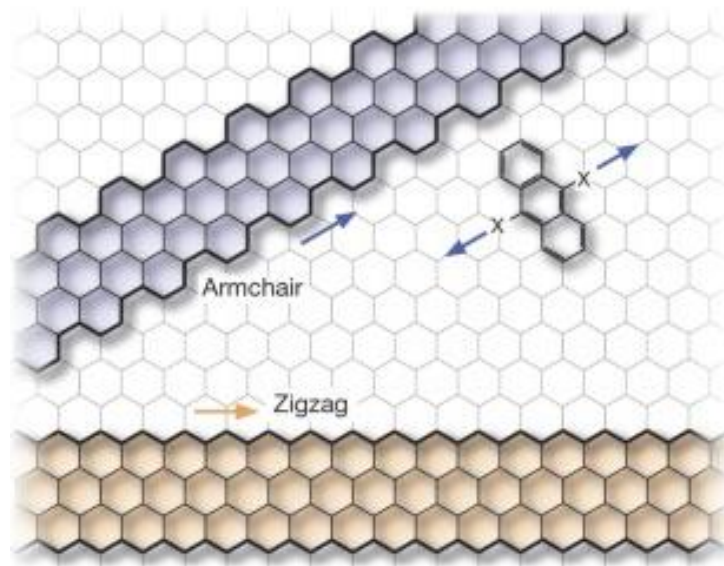


Lemme et al., IEEE Electron. Dev. Lett. **28**, 4 (2007)

# Bandgap in graphene ?

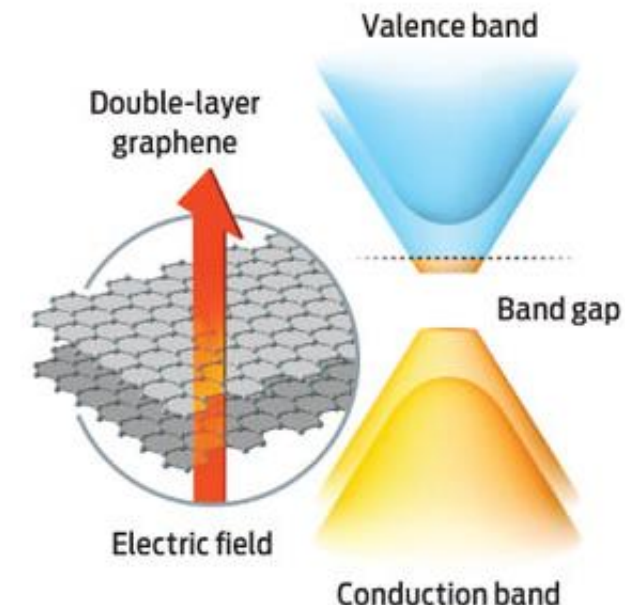
Pristine single-layer (SLG) and bilayer (BLG) graphene are semi-metallic. In order to be useful for field-effect devices, a bandgap must be created. A bandgap can be “engineered” by **symmetry-breaking** or **quantum confinement**.

**symmetry-breaking**



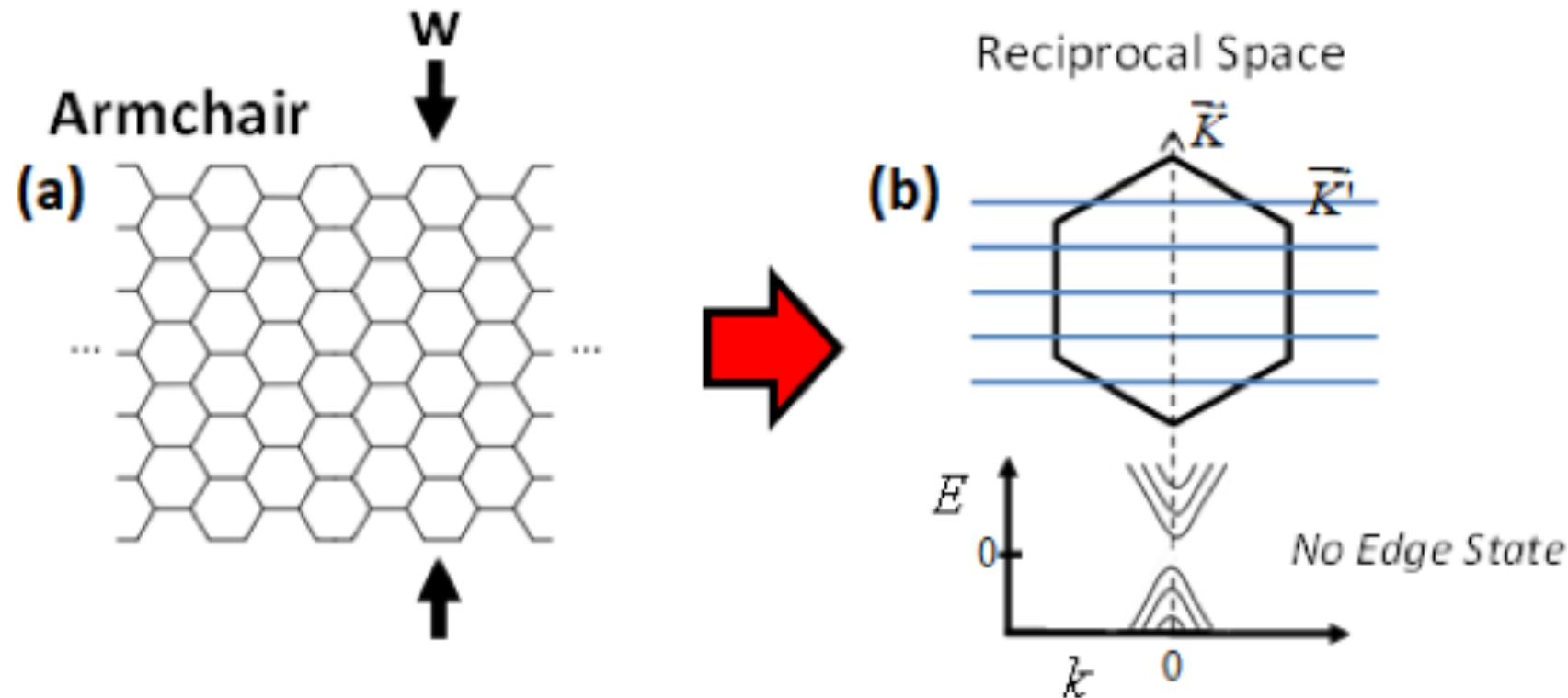
P. Ruffieux et al., Nature 531, 489-492 (2016)

**quantum confinement**



# GNR electronic structure

Due to its quasi 1D nature, electron states are **quantized** in the directions perpendicular to the GNR axis ( $k_{\perp}$ ), while the states in the direction along the GNR axis ( $k_{//}$ ) are continuous. This leads to the formation of **1D sub-bands** for electrons in the  $k_{//}$  direction.

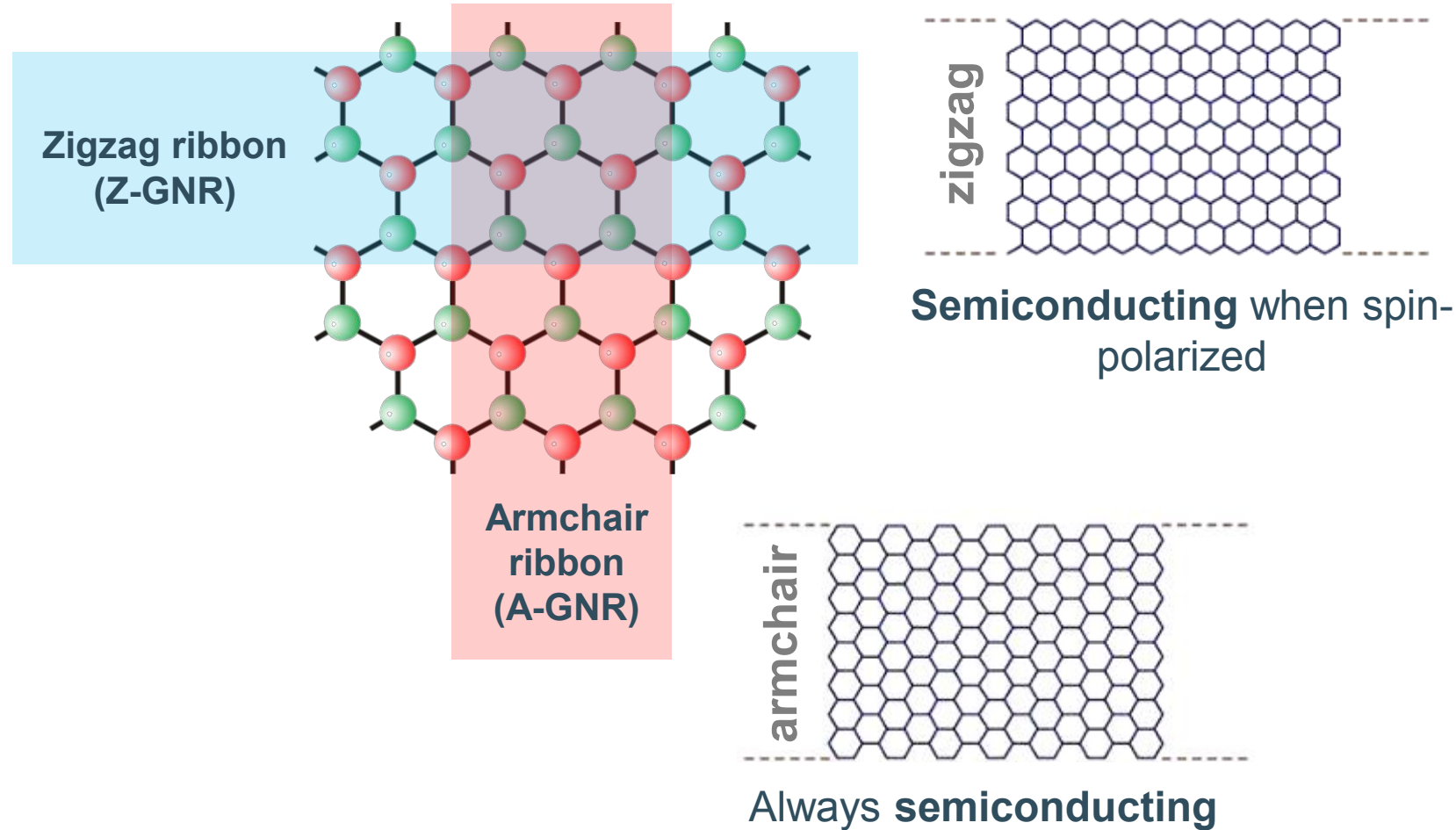


# Graphene nanoribbons

If the edge atoms belong to:

- Different sublattice : **A-GNR**
- Same sublattice : **Z-GNR**

Zigzag and armchair nanoribbons have different properties.



# Graphene nanoribbons

Some approaches have shown potential for large-scale fabrication of GNRs with controlled alignment:

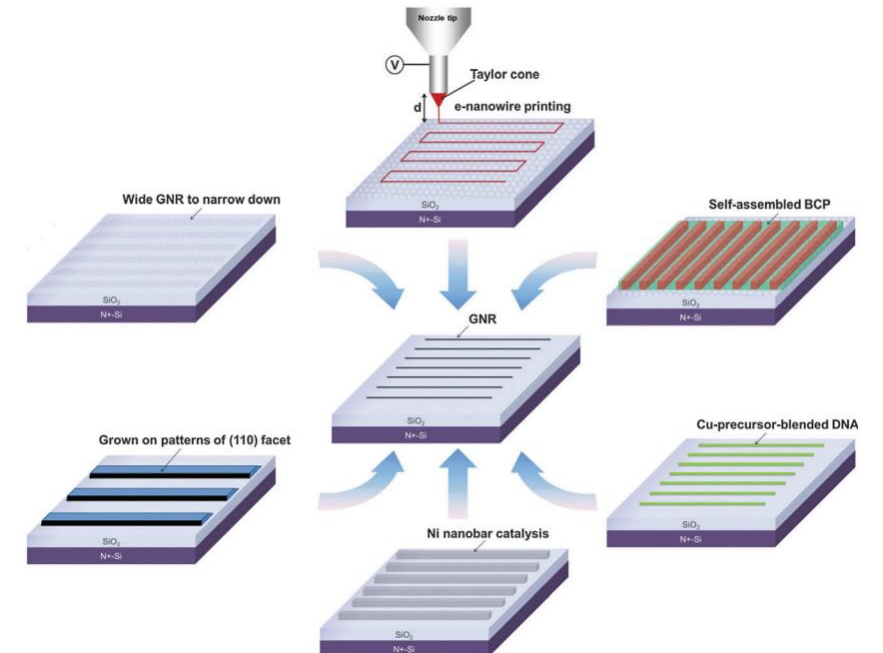
- **Bottom-up**

- organic synthesis method in solution
- Templatized or direct growth
  - Templatized growth of on SiC or on other substrates
  - Direct-growth on nickel nanostructures
  - Direct growth from a DNA template
  - Growth from catalyst composite nanofibers

- **Top-down**

- Nanowire lithography
  - Narrowing of GNRs from edges
- Block-copolymer lithography
- Unzipping carbon nanotubes

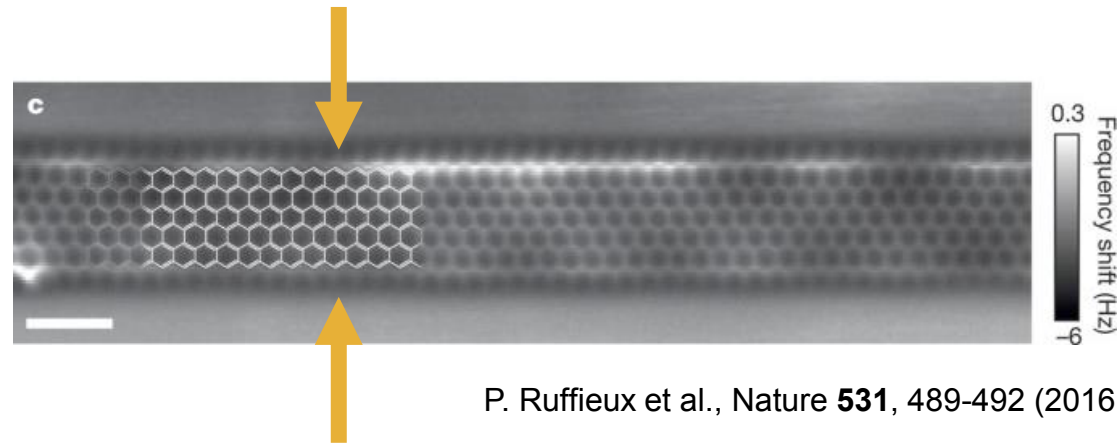
Challenges: scalable GNR, with smooth edges and controlled width



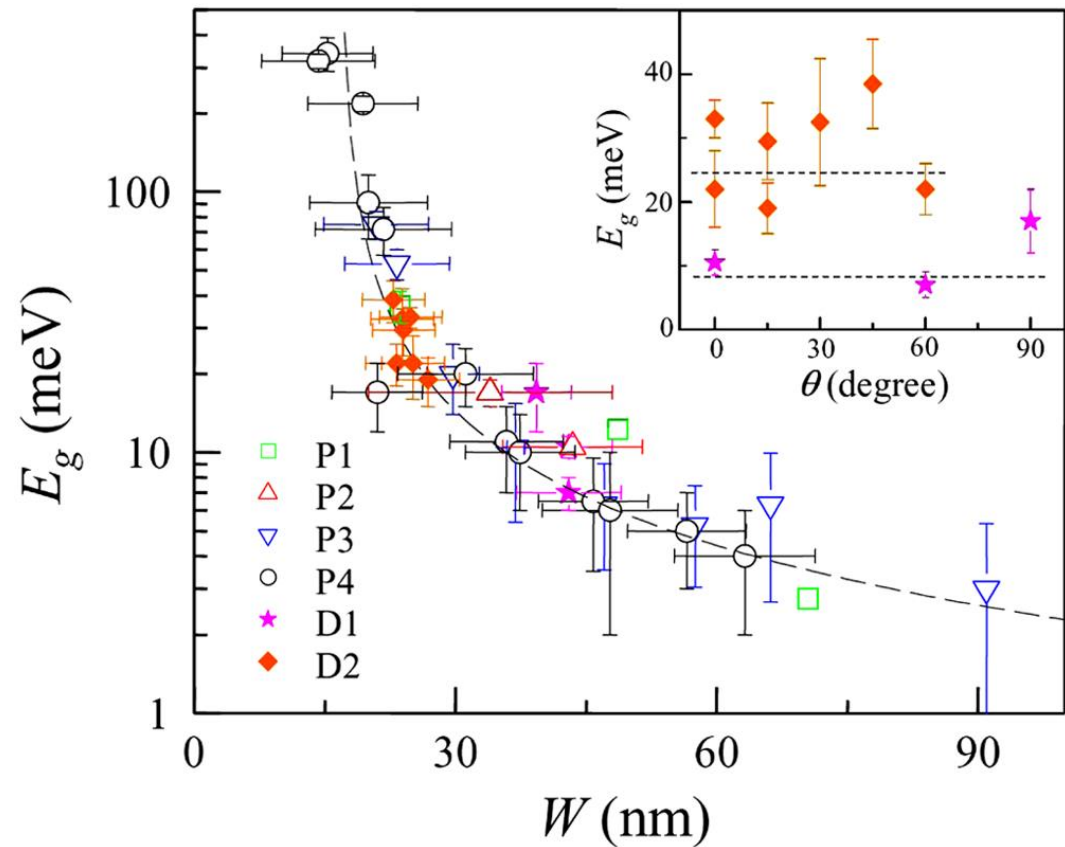
*Demonstration of various techniques for the realization of GNR arrays.*

# Bandgap in GNR

The bandgap in GNR is perfectly tunable and function of the GNR width.



Han et al, PRL 98, 206805 (2007)



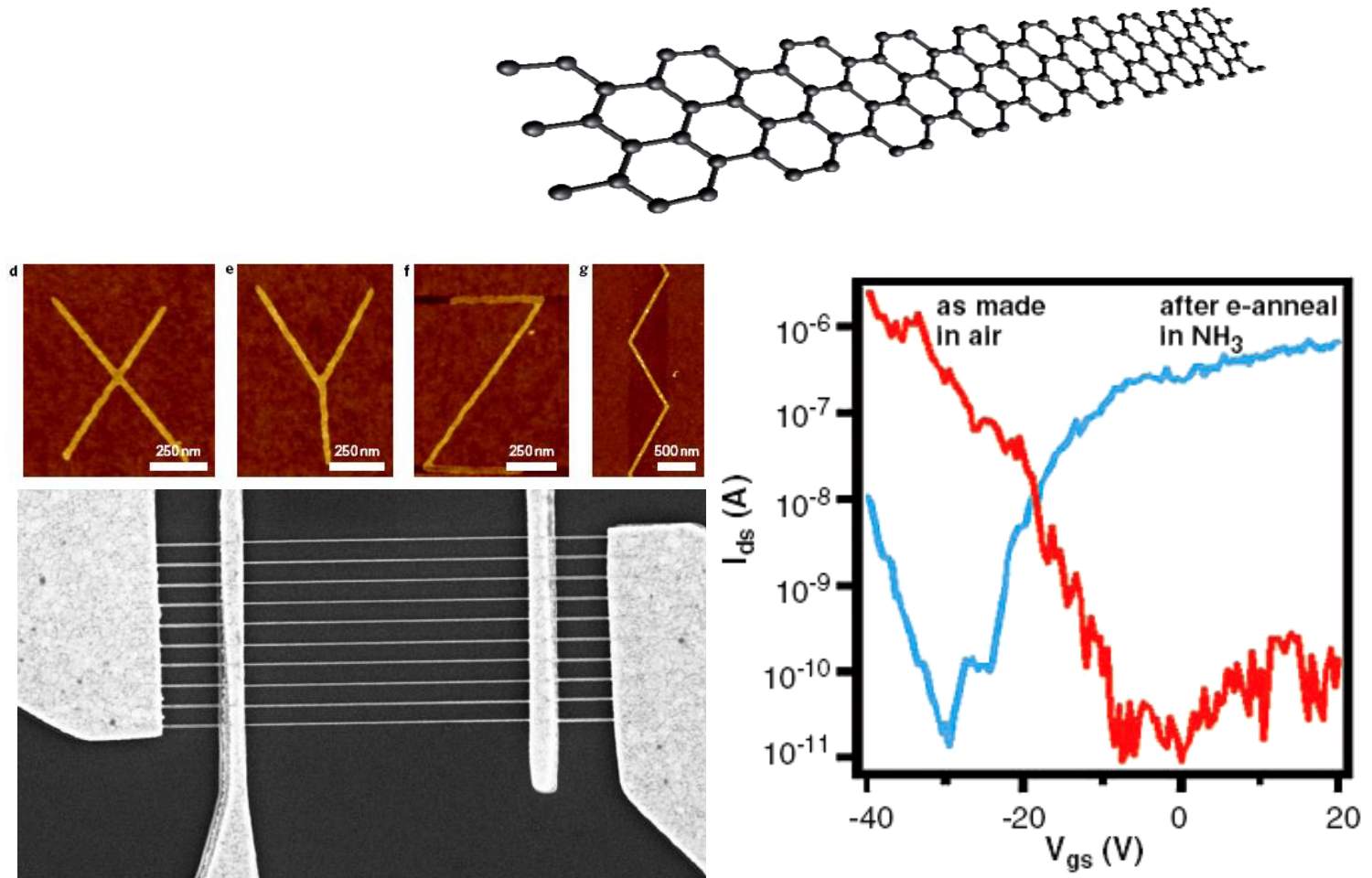
*Energy gap versus width of the graphene nanoribbon. The inset shows the bandgap versus angle of the nanoribbon. Dashed lines in the inset show the value of  $E_g$  as predicted by the empirical scaling of  $E_g$  versus width ( $W$ ).*

# Bandgap opening in graphene: nanoribbon

A bandgap can be opened in graphene by quantum confinement. Field-effect transistors less than 10nm wide have been created with  $I_{on}/I_{off}$  ratio  $> 10^6$

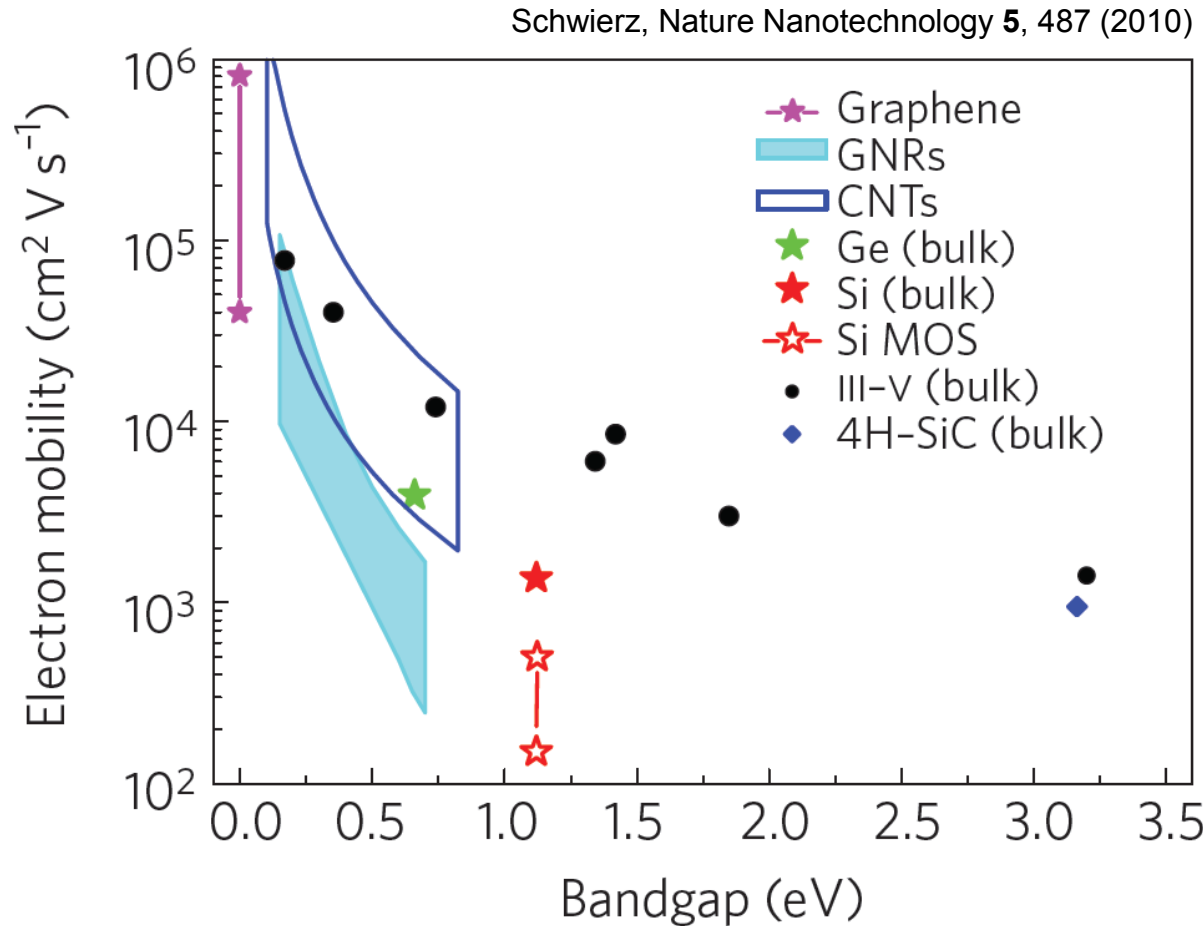
Edge disorder heavily affects the mobility.

Patterning reproducible < 5nm ribbons is unfeasible.



Wang et al., Nature chem. 2010, SCIENCE 2009

# Benchmarking of graphene nanoribbons



Graphene nanoribbons show substantial suppression of performance.

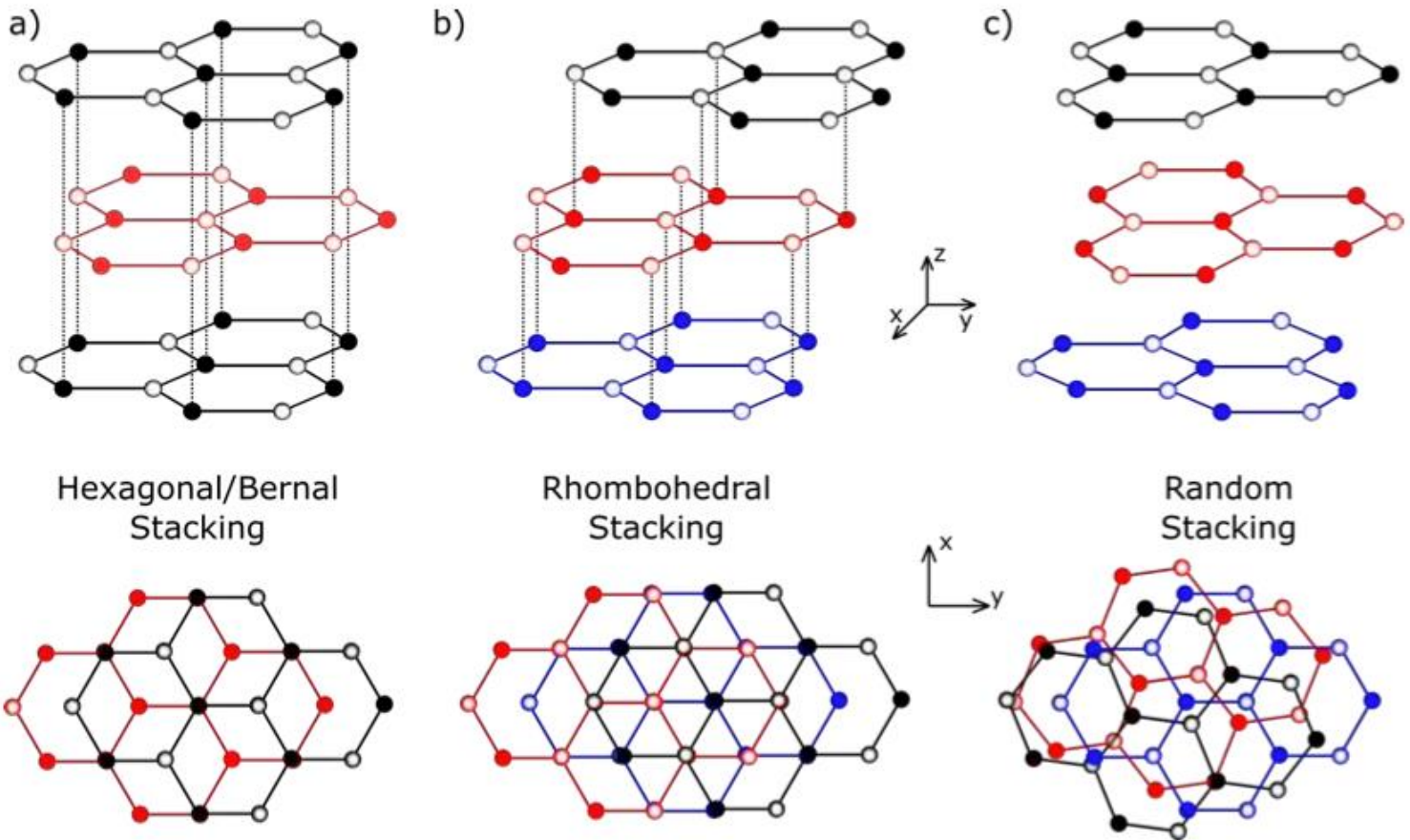
When a bandgap is opened the **electron mobility drops** considerably.

As a result, it is difficult for graphene to beat performance of more *standard technologies*.

*Mobilities (measured in the undoped case) for various materials as a function of the bandgap.*

# Multilayer graphene

Bi-layer graphene (BLG) consists of two single layer graphene layers stacked on top of each other.

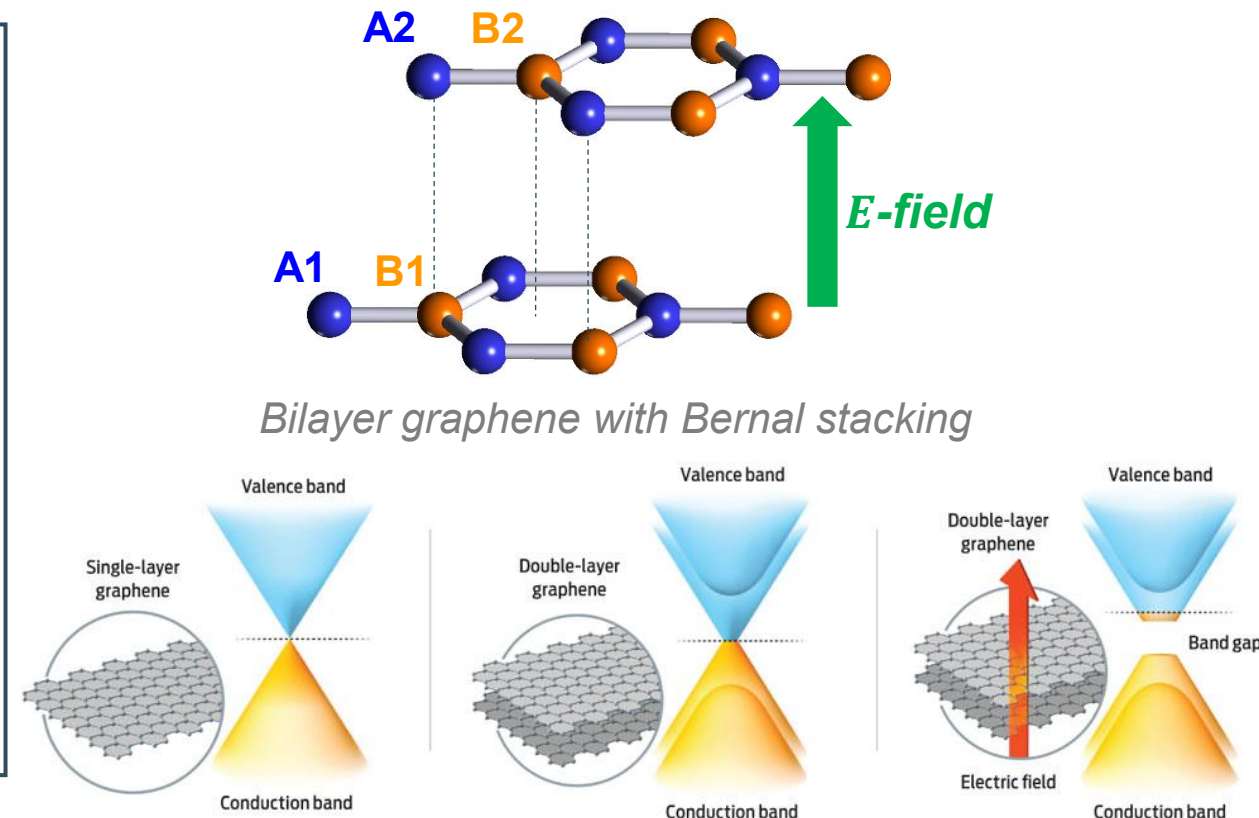
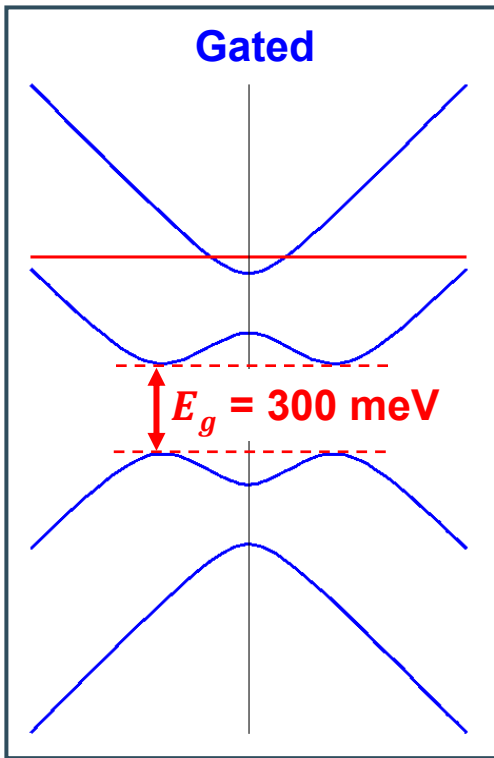


*Side and top view of different possible graphene layer stacks a) hexagonal / Bernal, b) rhombohedral and c) random stacking.*

# Bandgap opening in graphene bilayers

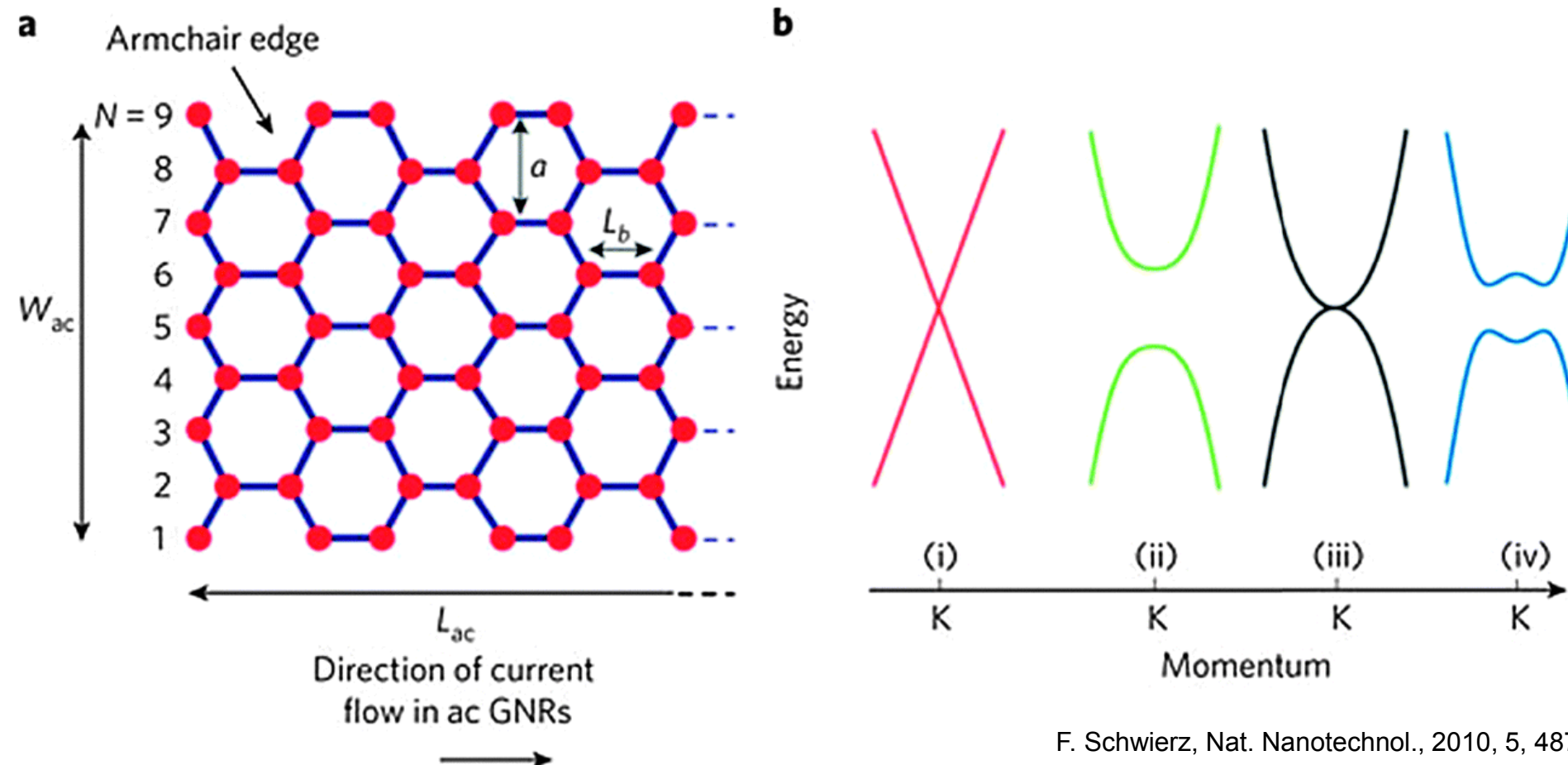
In bilayer graphene without gating, the lowest CB and highest VB in BLG touch each other at  $K$  and no bandgap is present.

In bilayer graphene with **Bernal stacking**, a bandgap occurs when an electric field is applied due to **symmetry breaking**.



Opening of a bandgap in graphene bilayers due to a perpendicular  $E$  field.

# Bandgap in graphene bi-layers

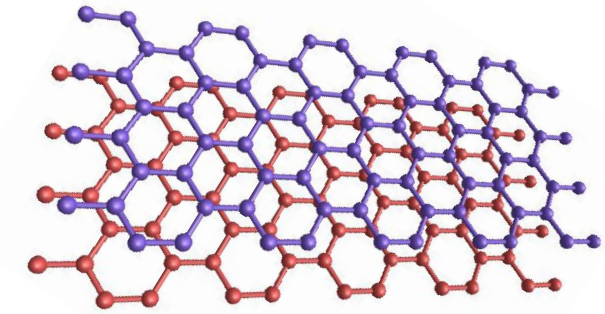
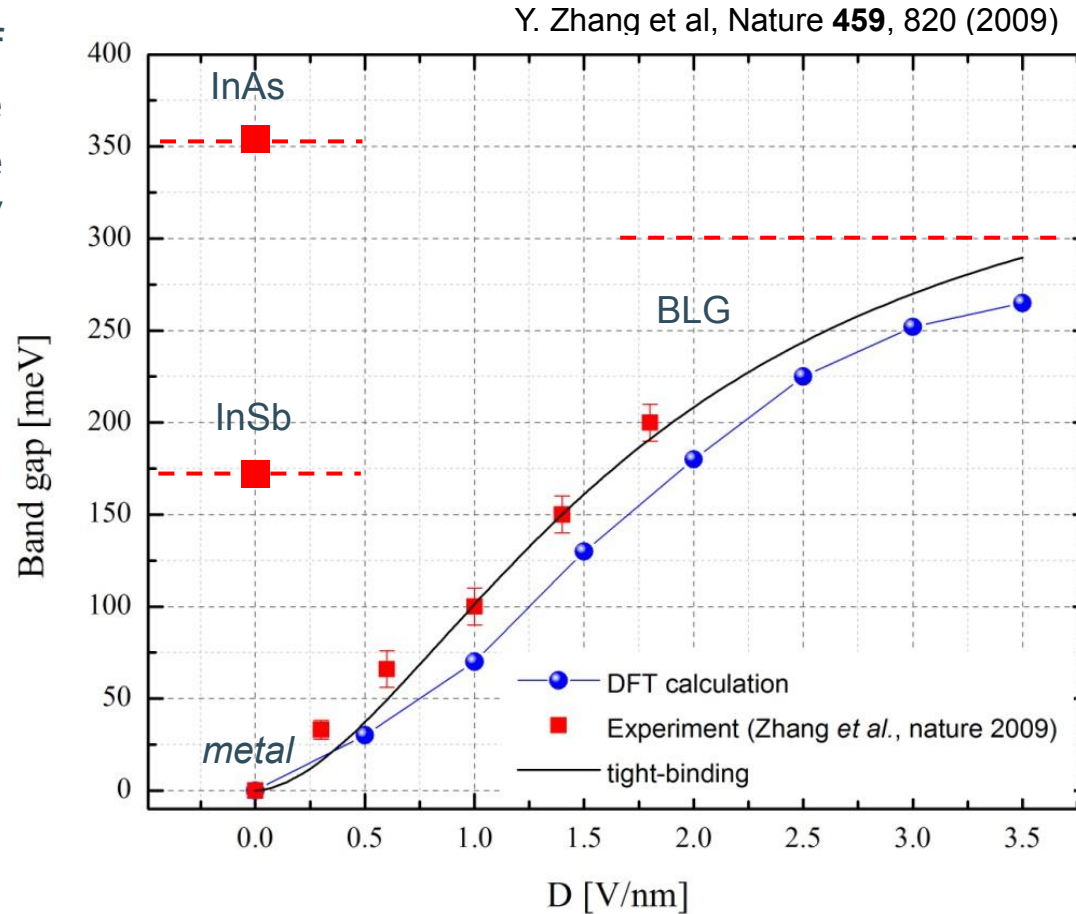


F. Schwierz, Nat. Nanotechnol., 2010, 5, 487

(a) Schematic demonstration of an armchair GNR. (b) Band structure near the  $K$  point of (i) bulk graphene, (ii) graphene nanoribbons, (iii) bilayer graphene, and (iv) bilayer graphene in an applied perpendicular electric field.

# Bandgap in graphene bi-layers

Stacking two bilayer of graphene gives the possibility of tuning the energy gap up to 300 meV by a vertical electric field.



Electric-field dependence of tunable energy bandgap in graphene bilayer. Experimental data are compared to theoretical predictions based on self-consistent tight-binding *ab initio* density functional (red trace).

# Twistronics

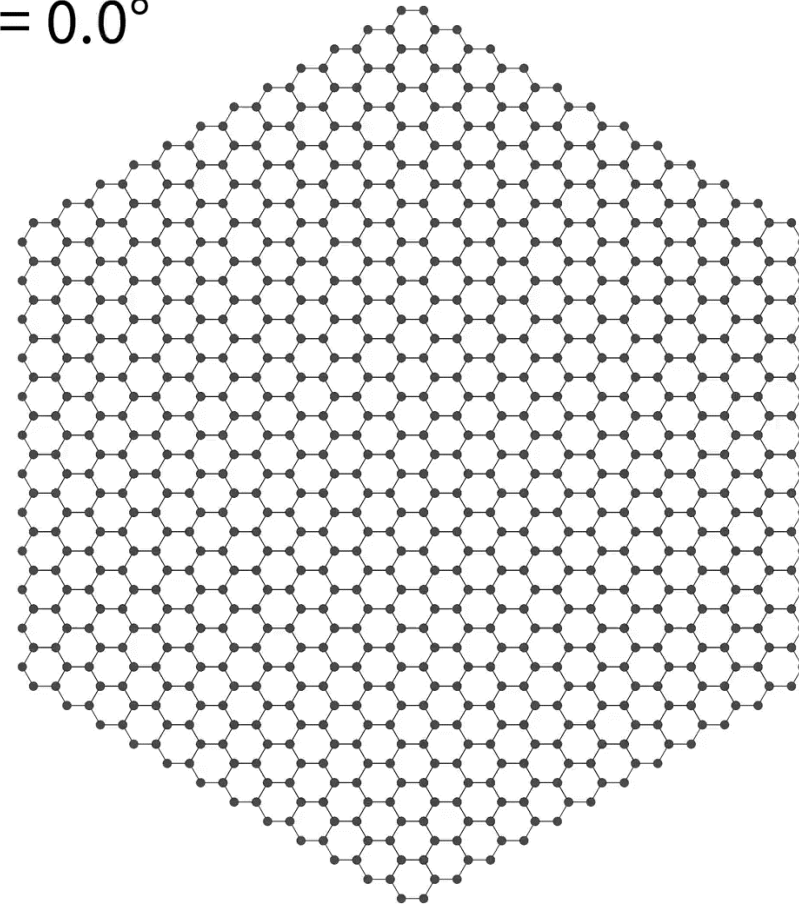
When a graphene bilayer is ‘twisted’ so that the top sheet is rotated out of alignment with the lower sheet, the unit cell (the smallest repeating unit of the material’s 2D lattice) becomes enlarged.

A ‘**moiré** pattern’ is produced in which the local stacking arrangement varies periodically.

The variation of the ‘twist’ angle between layers of graphene (or other 2D materials) affects their **electronic, optical and mechanical** properties.

This emerging field of research is called ‘**twistronics**’ which offers new approach to device engineering.

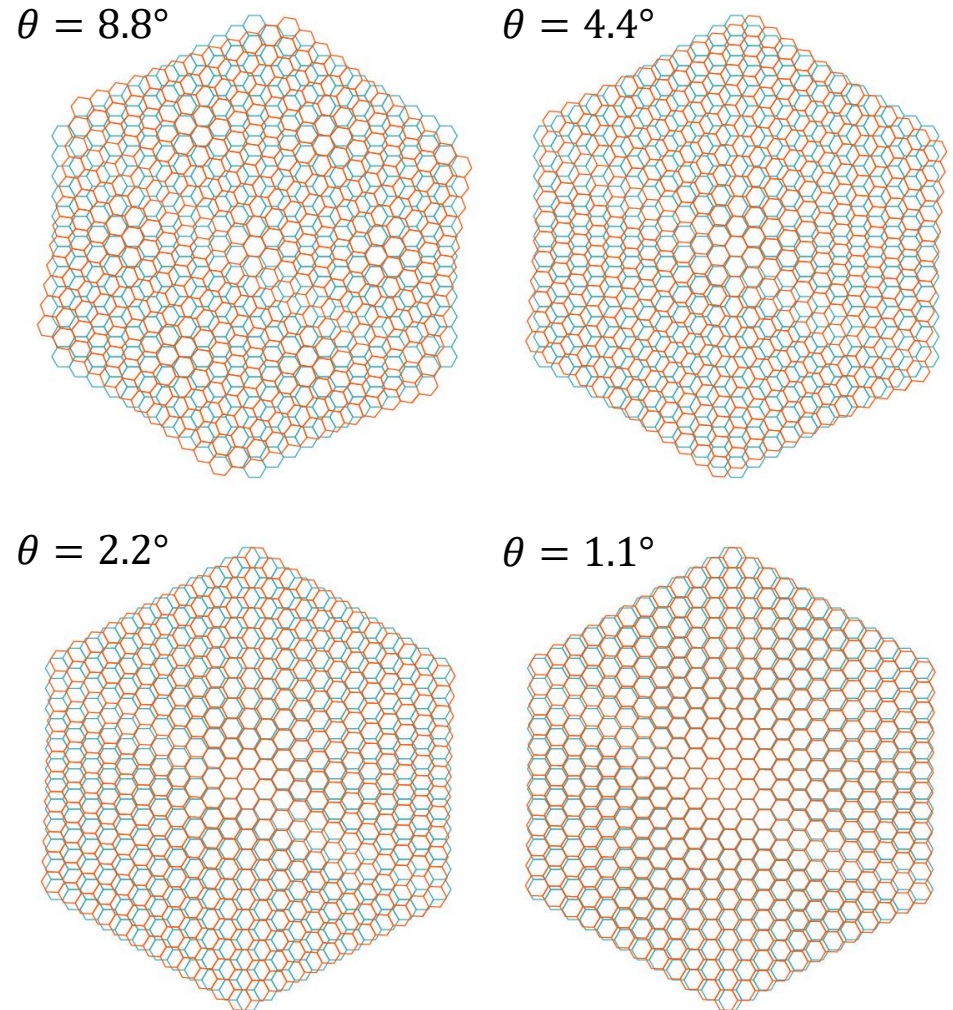
$$\theta = 0.0^\circ$$



Moiré patterns for overlapping graphene sheets rotated between 0 and 30 degrees.

# Moiré patterns in Graphene

- For  $8.8^\circ$  rotation, the moiré pattern that emerges has a central superlattice hexagon surrounded by six others of the same size. Each of these moiré hexagons occupies about a quarter to a third of the entire hexagonal field in each direction.
- At  $4.4^\circ$  rotation, the central superlattice hexagon expands to about twice its previous size, covering about one-half to two-thirds of the entire field.
- At  $2.2^\circ$  rotation, the central superlattice hexagon covers the entire original bounding hexagon.
- For  $1.1^\circ$  rotation, the angle that produces the interesting effects in graphene, the superlattice seems to have disappeared completely and the pattern looks almost like a single sheet without any moiré.

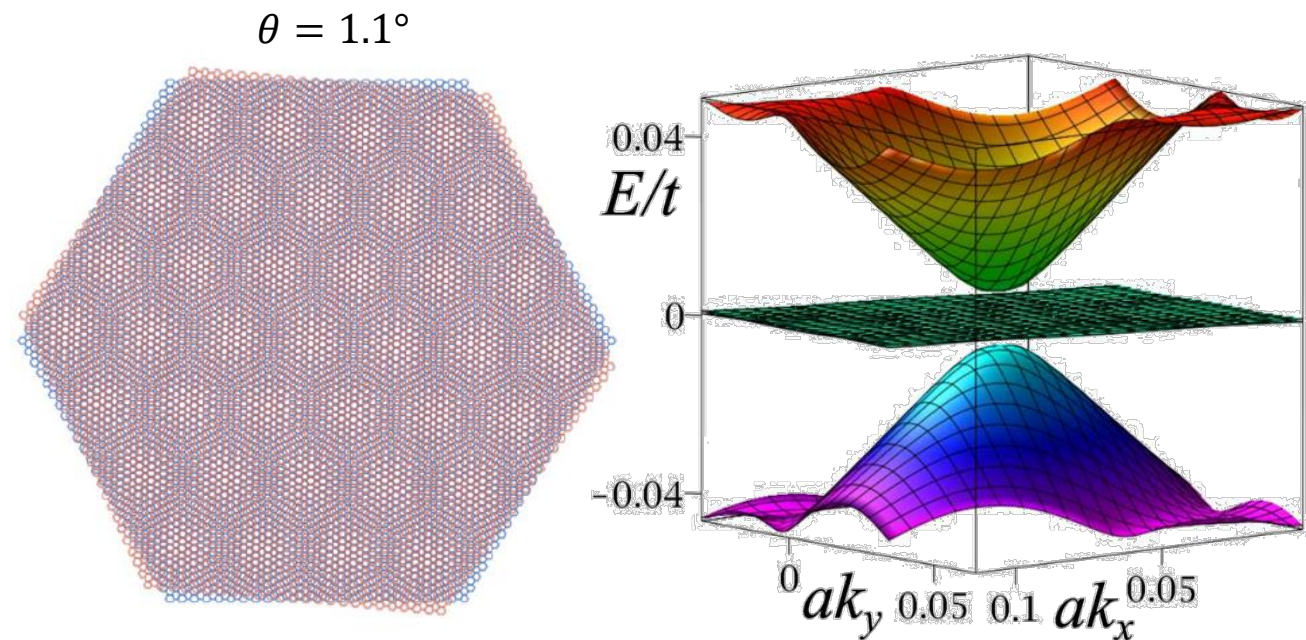


# Effects of rotation in twisted bilayer graphene

For rotation angles of  $\sim 1.1^\circ$  (**the magic angle**), regions in which the atoms are directly above each other (the lighter regions in the pattern) form narrow electron energy bands, in which electron ‘correlation’ effects are enhanced.

This results in the generation of a non-conducting state (a Mott insulator), which can be converted into a **superconducting state** if charge carriers are added to the graphene system by applying a small electrical field.

This ‘Mott’ insulator is a material that should be a metal but which, because of strong repulsion between electrons, does not conduct.



# Metal contacts to graphene

When a metal and a semiconductor come into contact, charges are transferred from higher energy states to lower energy states until the energy levels are balanced in an equilibrium state. Due to the small density of states in a semiconductor, there is energy band bending along the vertical direction known as the depletion.

In a similar manner, graphene can also be modeled as a semiconductor with a zero bandgap, and band bending is necessary if graphene has a finite thickness as a bulk semiconductor materials. Because graphene has no band gap, instead of an 'energy band,' the 'Dirac energy level' ( $E_{Dr}$ ) would be a proper term for graphene. Dirac energy level bending in graphene along the lateral direction does not occur, but there is a work function shift in graphene.

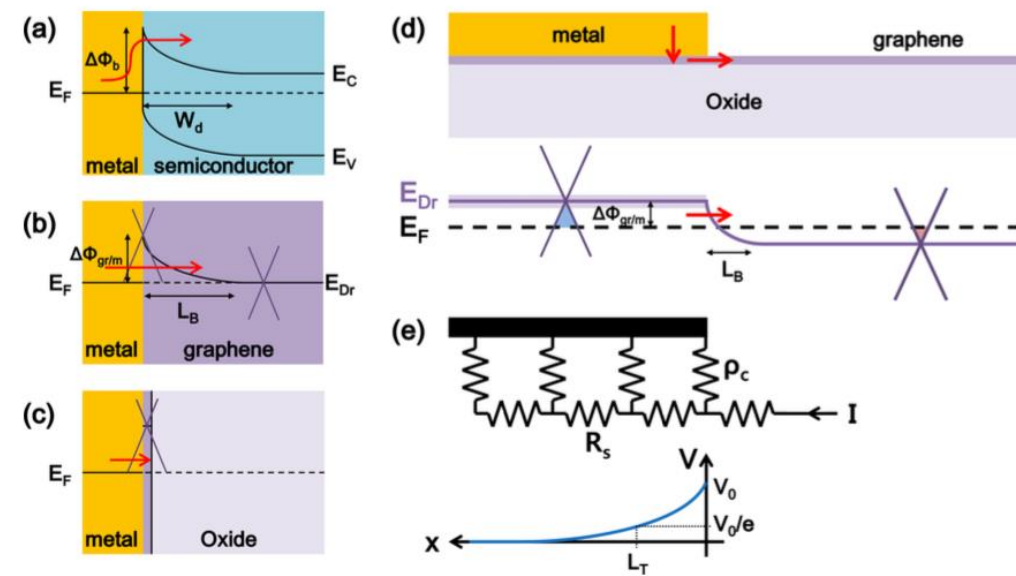
It was first theoretically estimated that graphene on various crystalline metals can be doped due to the presence of an interface dipole layer induced by the charge transfer. In addition to the shift of the work function of graphene underneath metal, there is a gradual bending of the Dirac energy level along the horizontal direction near the contact edge due to the work function difference between the exposed graphene and the graphene underneath the metal. This region is known as the charge transfer region.

# Metal contacts to graphene

The facial contact between a metal and graphene typically results in large contact resistance dominated by the contact length rather than the contact area.

Graphene underneath metal is doped in holes and the channel graphene is negatively doped by the back-gate voltage. The thicker  $E_{Dr}$  underneath the metal represents the broadening of the density of states near the Dirac energy level.

The model of the graphene-metal contact includes the contact resistivity ( $\rho_c$ ) and sheet resistance ( $R_s$ ). Transfer length ( $L_T$ ) is the effective contact length and is defined with the distance where the potential drops to  $1/e$  times from the edge.



S.M. Song et al, Carbon Letters **14** (2013)

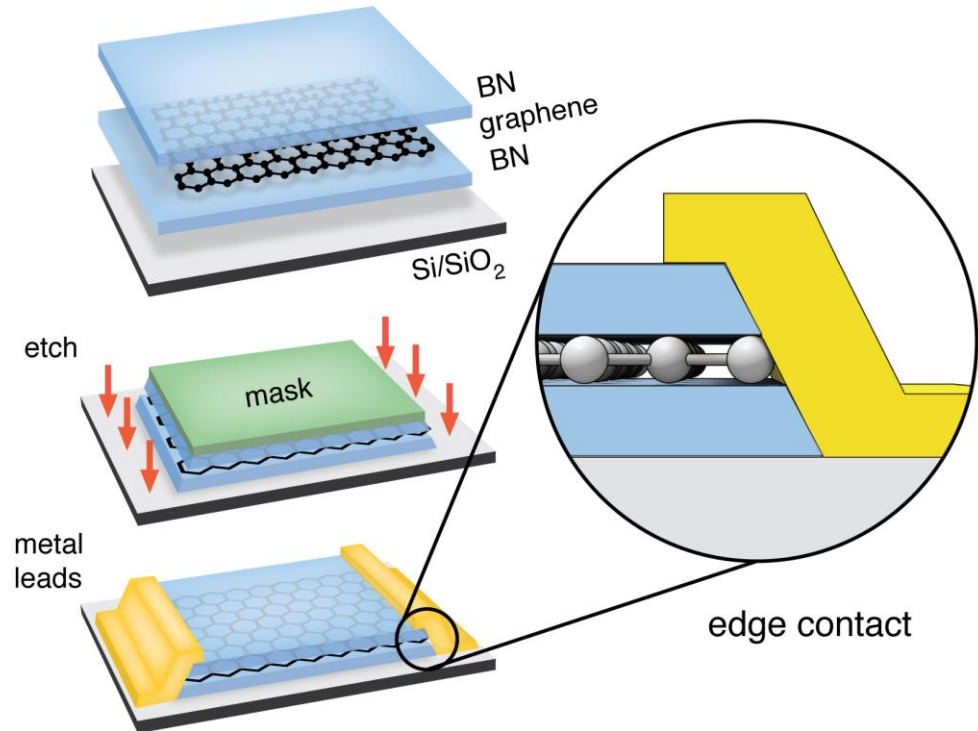
In this figure  $E_{Dr}$  is the Dirac energy level,  $\Delta\Phi_b$  is the Schottky barrier height,  $\Delta\Phi_{gr/m}$  is the work function change due to the metal-induced doping, and  $W_d$  and  $L_B$  are respectively the depletion width and the length of the charge transfer region. The red solid arrows indicate the path of the carriers.

# Metal contacts to graphene

An alternative approach to overcome the facial contact is to use the edge contact structure which is formed by a covalent bond between the metal atoms and the graphene.

This contact is expected to show significantly lower contact resistance compared to the facial contact.

Theoretical reports estimated that the contact resistivity could be as low as 10 to  $10^3$  times the facial contact based on a quantum tunneling process.



*Schematic illustration of an edge contact to a graphene layer sandwiched between two hexagonal Boron Nitride (h-BN) layers.*

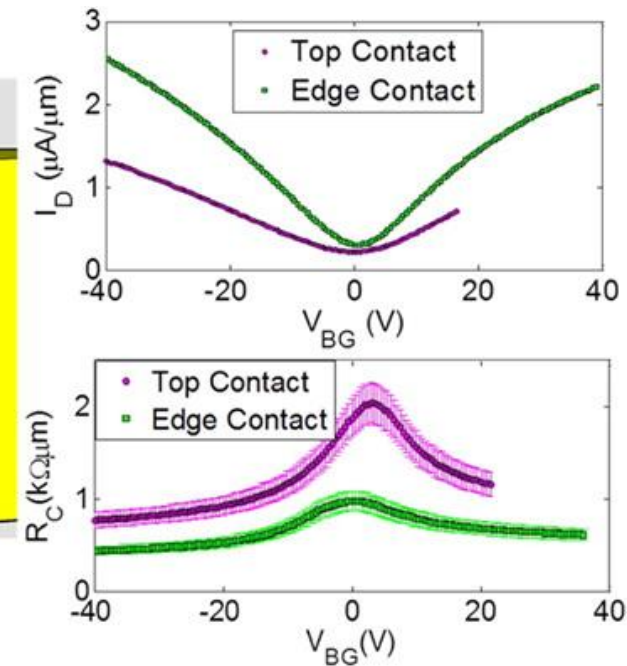
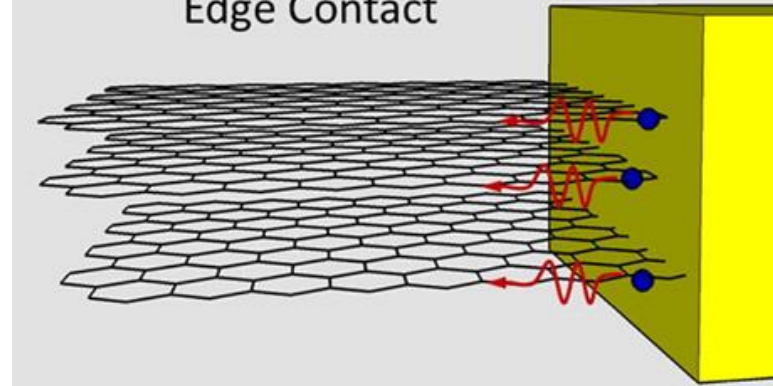
# Metal contacts to graphene

Contact modules with edge contact were developed and demonstrated.

An about 2 times lower contact resistance is observed in edge-contacted few layer graphene (FLG) devices compared to those with conventional top contacts.

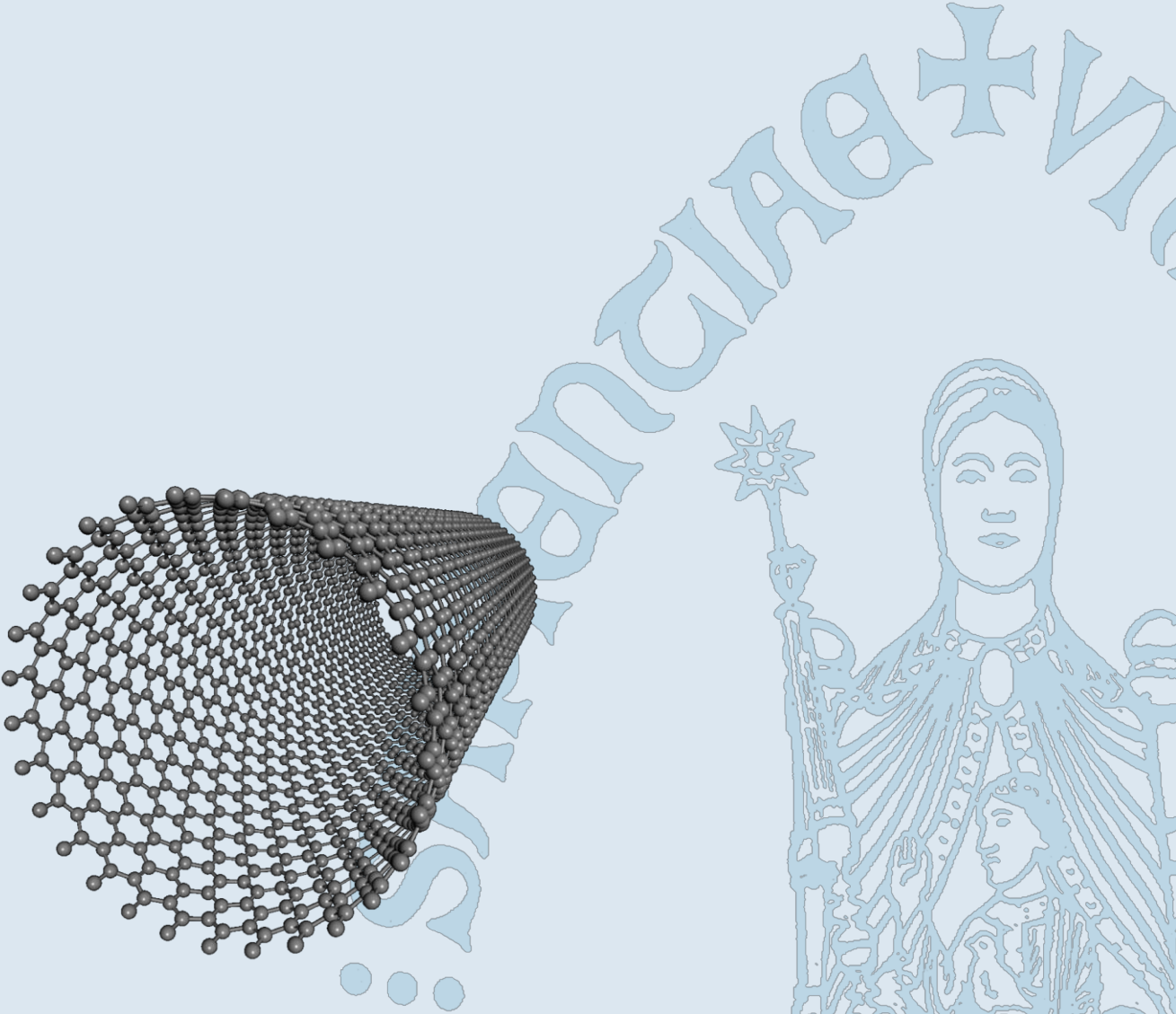
T. Chu et al, ACS Nano, 8(4), 3584-3589, (2014)

Edge Contact

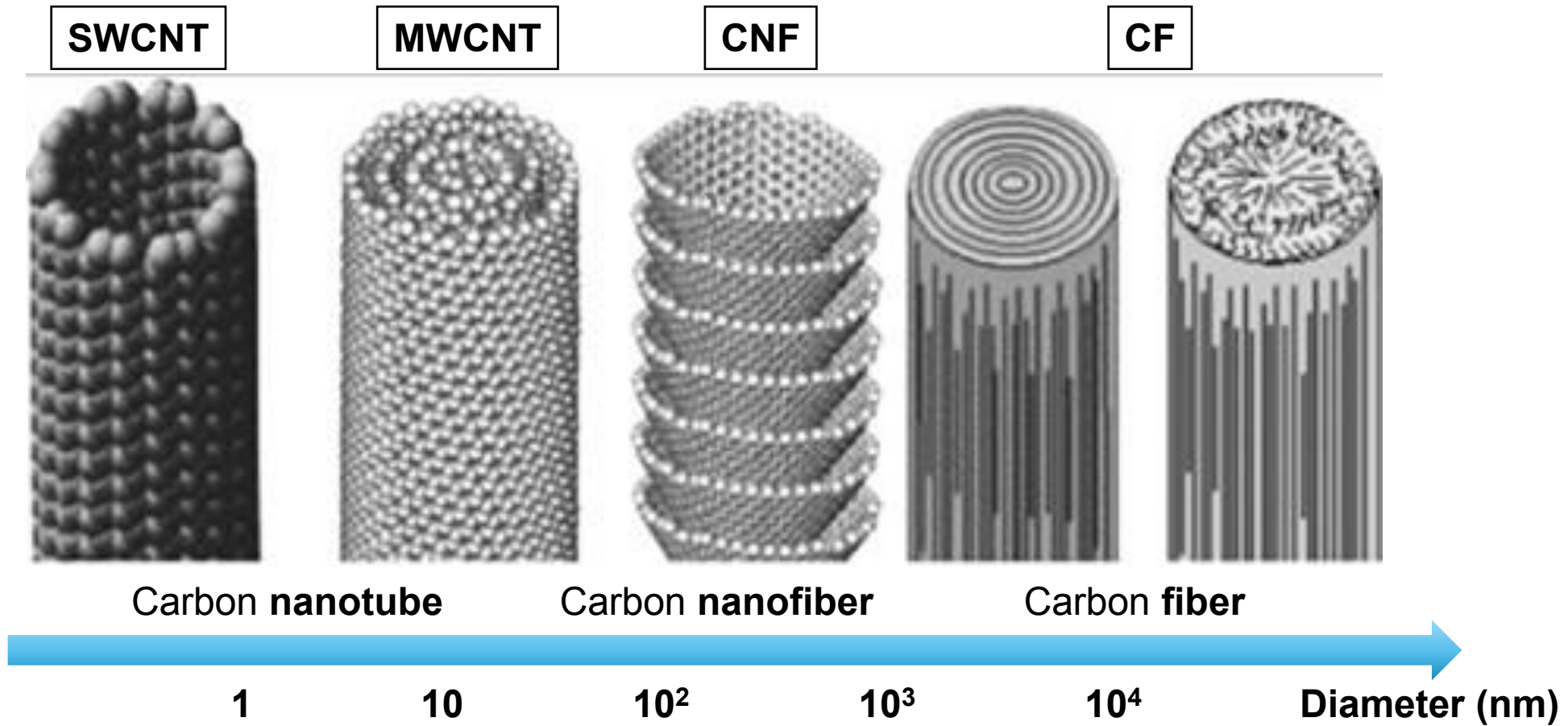


*Using a self-aligned process, graphene is etched and carbon atoms at the cut edges are directly contacted by a subsequently deposited metal layer. The covalent/ionic bonds formed between metal and carbon atoms allow for a lower contact resistivity compared to the weak van de Waals bonds under conventional top contacts. These edge contacts bypass the tunneling resistances between layers and allow direct current injection into individual graphene layers.*

# CNTs

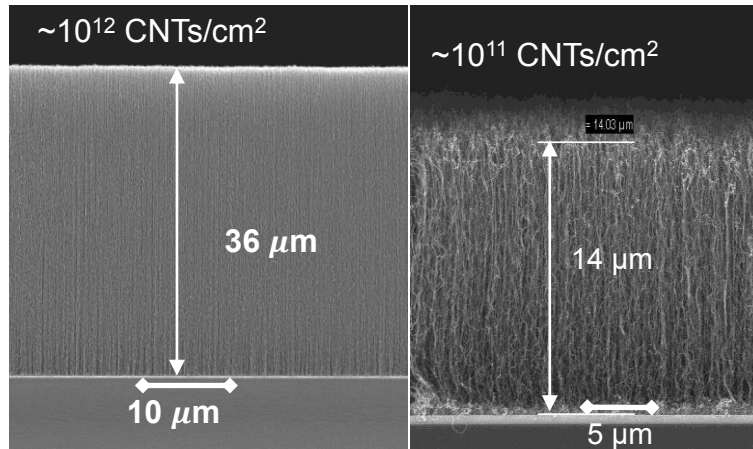
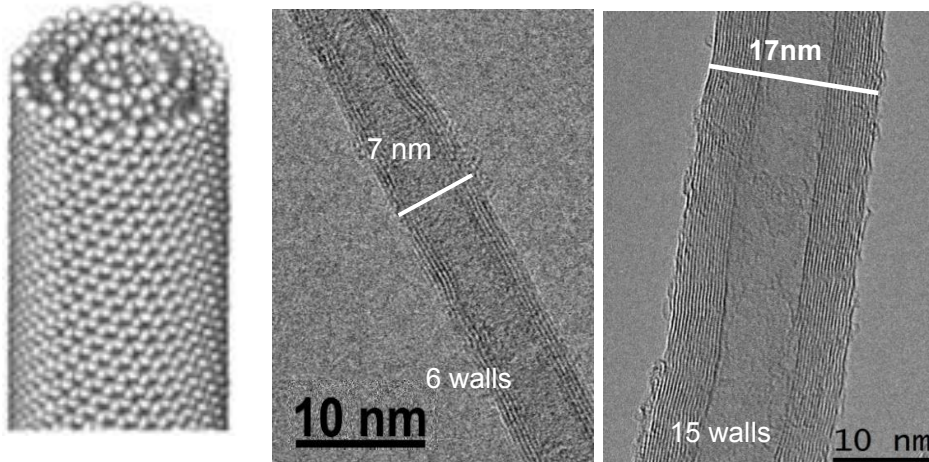


# Carbon filaments in different flavors



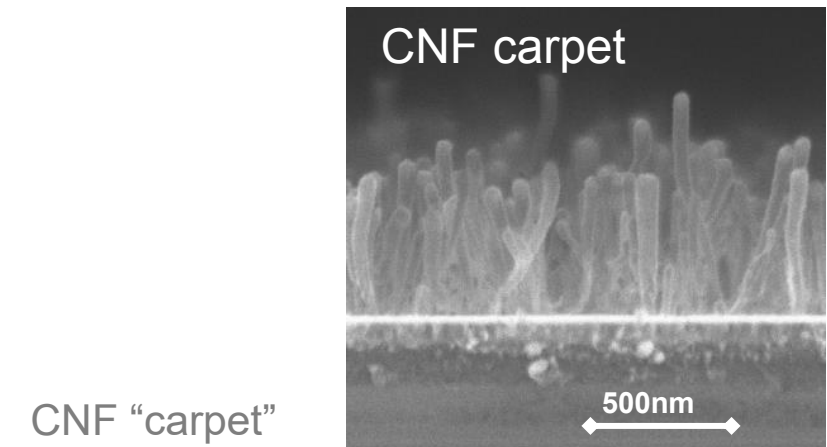
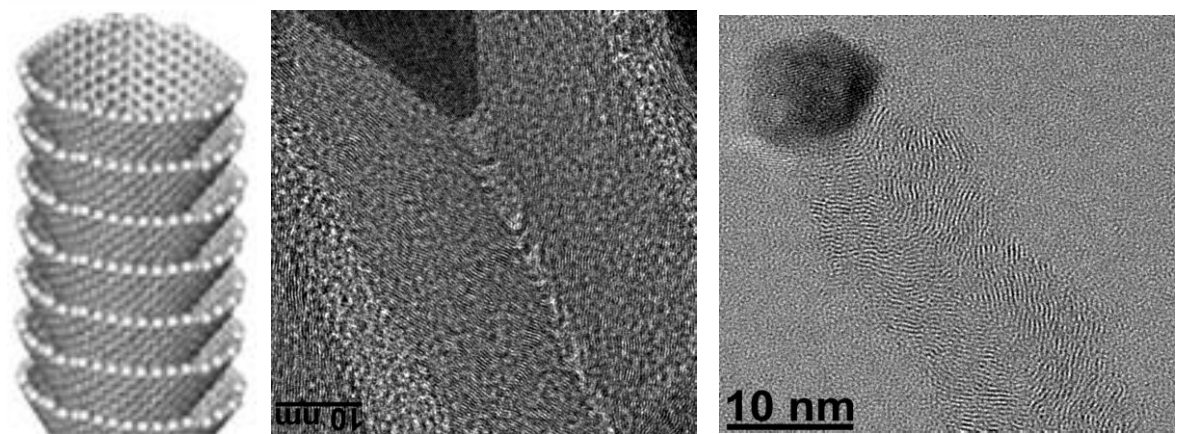
# Carbon filaments in different flavors

## Multi-Walled CNT (MWCNT)



Densely aligned CNT  
“carpets” of different  
densities

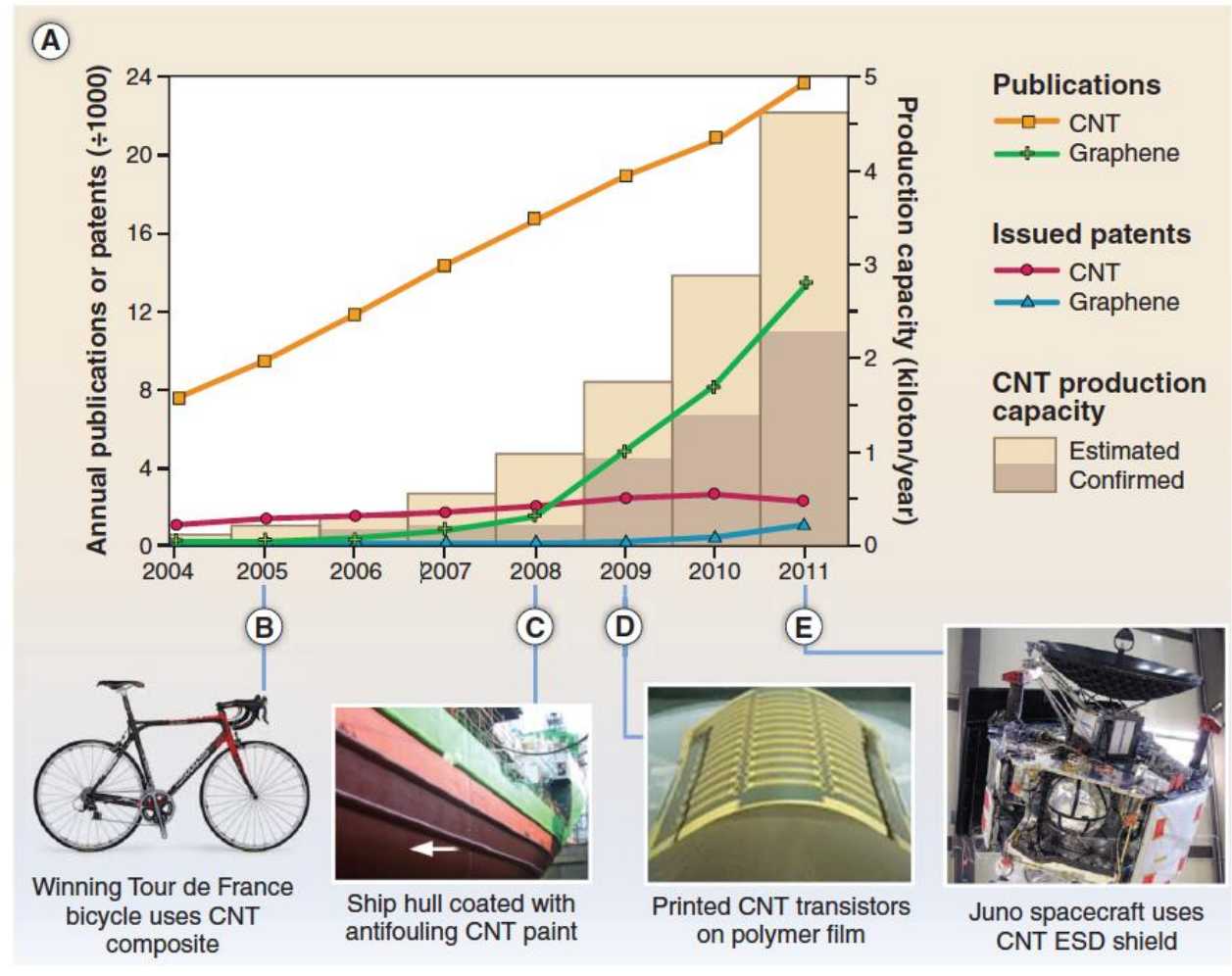
## Carbon nanofibers (CNF)



# Trends in CNT research and applications

Carbon nanotubes have found their way in many applications.

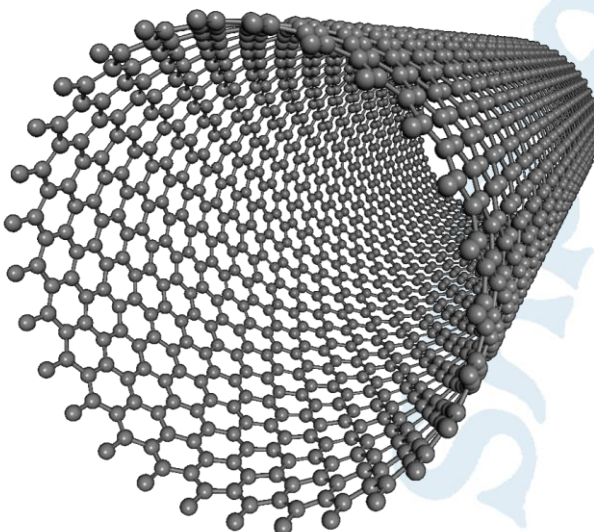
(A) *Journal publications and issued worldwide patents per year, along with estimated annual production capacity. (B to E) Selected CNT related products: composite bicycle frame, antifouling coatings, printed electronics and electrostatic discharge shielding.*



M. De Volder et al, Science 2013

# CNTs

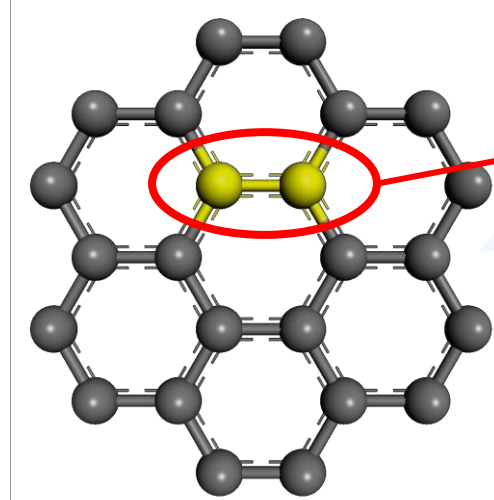
Fundamentals & properties



# Electronic properties of CNTs

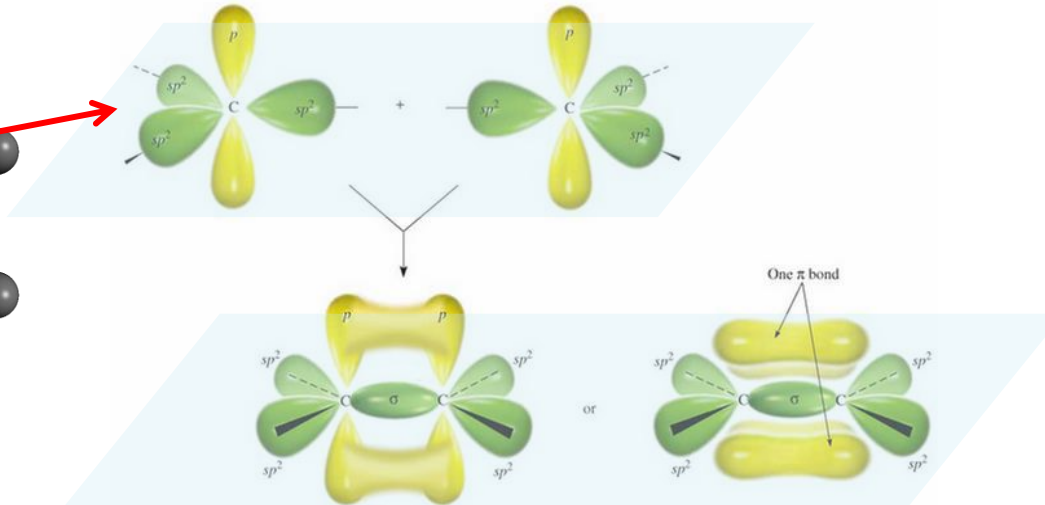
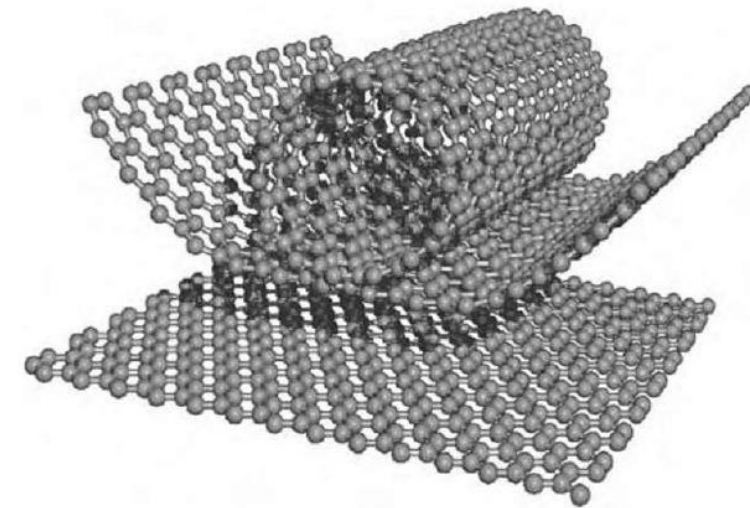
The electronic properties of CNTs can be understood by looking to the electronic properties of **graphene**. The  $sp^2$  bonded structure from a graphene plane provides some remarkable properties of the graphene band structure.

The carbon atoms in graphene form a hexagonal lattice on a two-dimensional plane. Each carbon atom is about  $a_{C-C} = 1.42 \text{ \AA}$  from its three neighbors, with each of which it shares one  **$\sigma$ -bond**. The fourth bond is a  **$\pi$ -bond**, which is oriented in the  $z$ -direction (out-of-plane).



$sp^2$  hybridisation

- single  $2s$  and two  $2p$  orbitals hybridise forming three  $\sigma$  bonds in the  $xy$  plane
- remaining  $2p_z$  orbital [ $\pi$  orbital] exists perpendicular to the  $xy$  plane

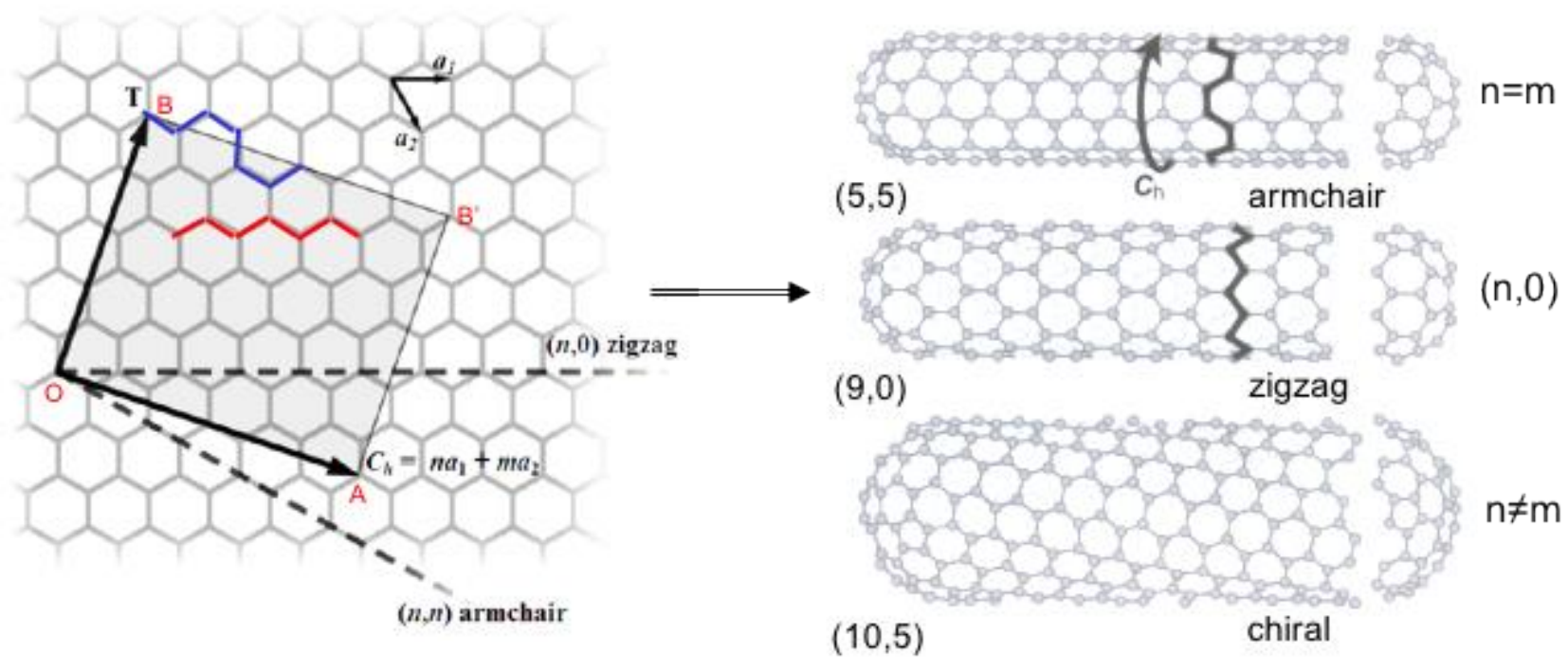


# Carbon nanotubes

Single Walled Nano Tubes (SWNTs) are obtained by wrapping a graphene sheet along **chiral directions**.

The 2 vectors  $C_h$  and  $T$  defines a **2D unit cell**. This rectangle is rolled-up in the chiral vector direction, i.e. the segment  $OB$  is put together with segment  $AB'$ .

The pair of  $(n, m)$  indices thus defines the diameter of the CNT.

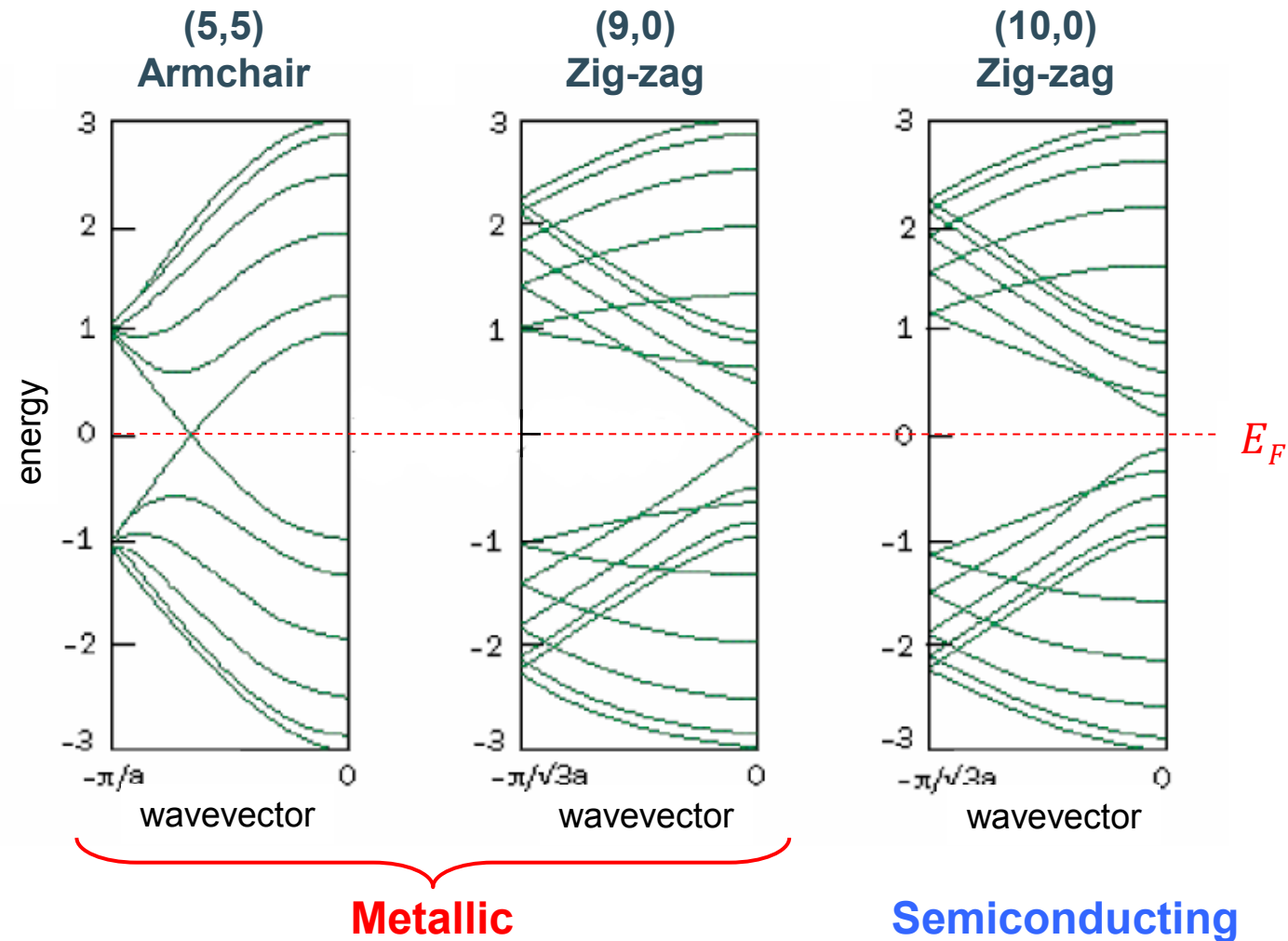
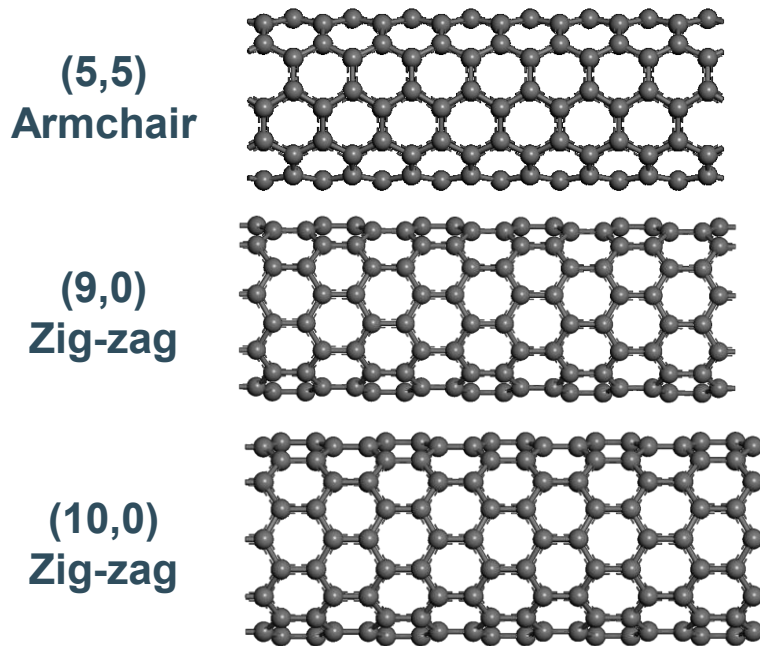


$C_h = na_1 + ma_2$ : **chiral vector**, with  $(n, m)$  the indices of the tube  
with  $a_1, a_2$ : **primitive lattice vectors** of the graphene sheet  
 $T$  : **translation vector** perpendicular to  $C_h$ .

# Band structure of SWNTs

The **band structure** of SWNTs changes dramatically with diameter and chirality.

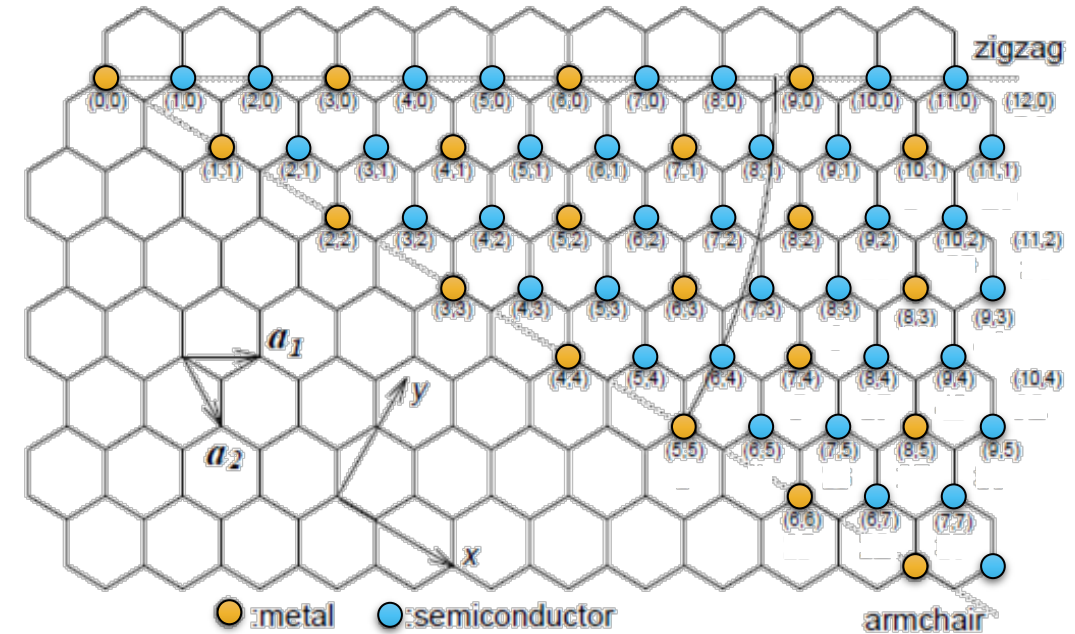
Both **metallic** and **semiconducting** nanotubes can be formed.



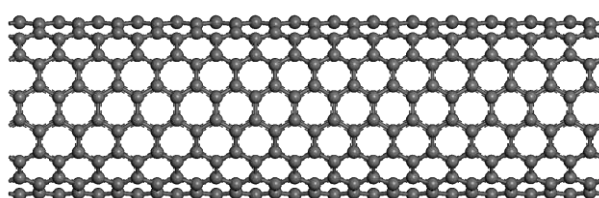
# Carbon nanotubes

Statistically, in a random SWNTs mixture, **1/3 are metallic** and **2/3 semiconducting**.

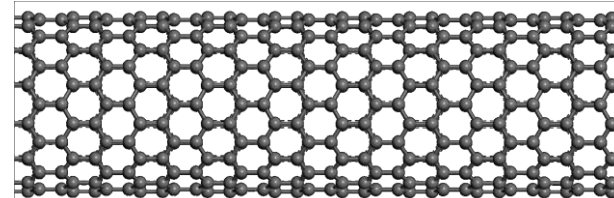
- $(n, n)$ : armchair SWNTs  $\Rightarrow$  always **metallic**
- $(n, 0)$ : zigzag SWNTs  $\Rightarrow$  **metallic** if  $n$  is multiple of 3
- $n - m = 3k$ ,  $k$  integer  $\Rightarrow$  **metallic** SWNTs
- $n - m = 3k \pm 1$ ,  $k$  integer  $\Rightarrow$  **semiconducting** SWNTs



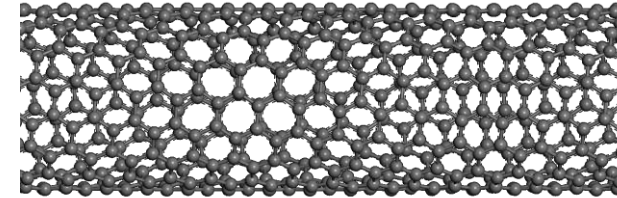
Dresselhaus et al., Top. Appl. Phys. **80**, 1 (2001)



(8,8)  
Armchair



(14,0)  
Zig-zag



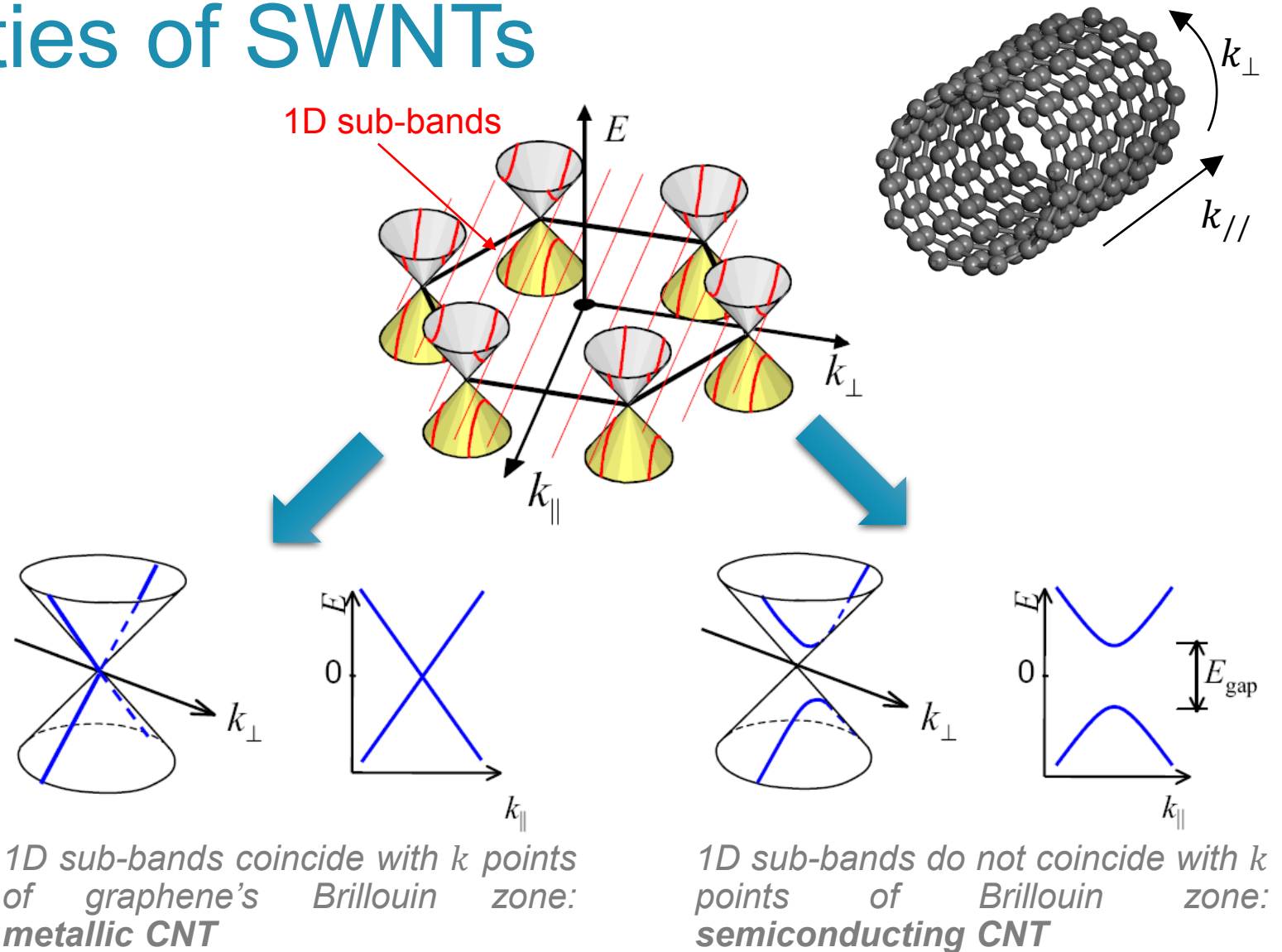
(9,7)  
Chiral

# Electronic properties of SWNTs

This rule is related to the symmetry of the CNT.

Due to its quasi 1D nature, electron states are **quantized** in the directions perpendicular to the CNT axis ( $k_{\perp}$ ), while the states in the direction along the CNT axis ( $k_{\parallel}$ ) are continuous.

This leads to the formation of **1D sub-bands** for electrons in the  $k_{\parallel}$  direction



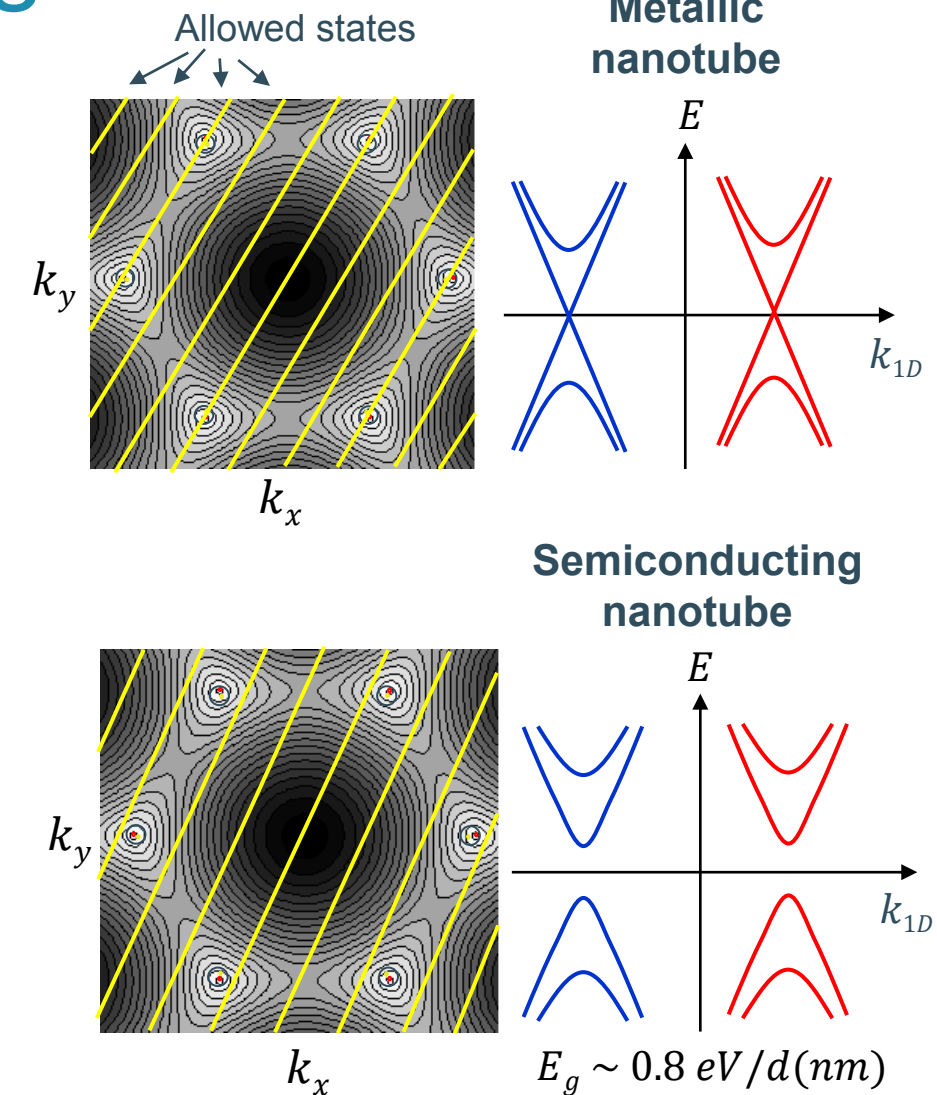
# Electronic properties of SWNTs

The band structure of SWCNTs can (approximately) be determined from that of graphene.

In graphene the wave vectors  $k_x$  and  $k_y$  can assume arbitrary (continuous) values in the reciprocal space (infinite 2D sheet).

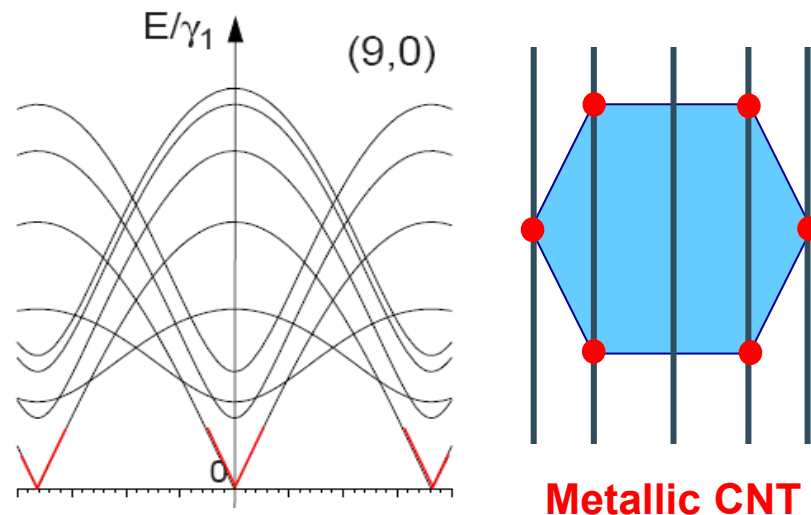
In a SWCNT the wave-vector along the circumference is fixed and the wave-vectors  $k_x$  and  $k_y$  are therefore linearly related (lines). The band structure is determined by  $m$  and  $n$  values

- Electron confinement → quantization of the wave vector along circumference.
- Each band is a “slice” through the dispersion curve of graphene

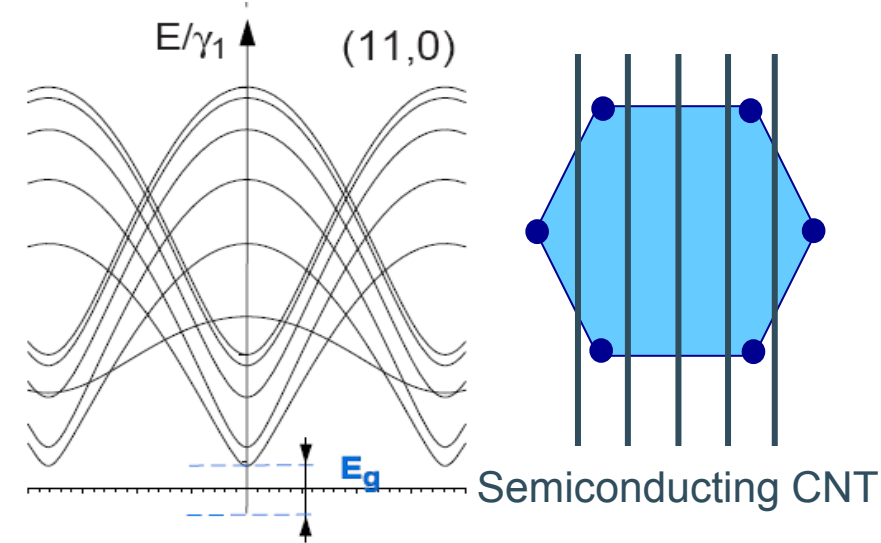


# Electronic properties of SWNTs

The SWNT band structure obtained by “slicing” the  $E - k$  dispersion of graphene along planes defined by the quantized  $k_{\perp}$  vector, depends on the chirality of the CNT. This leads to metallic and semiconducting nanotubes.



If one slice crosses a  $k$ -point:  $E_{gap} = 0$



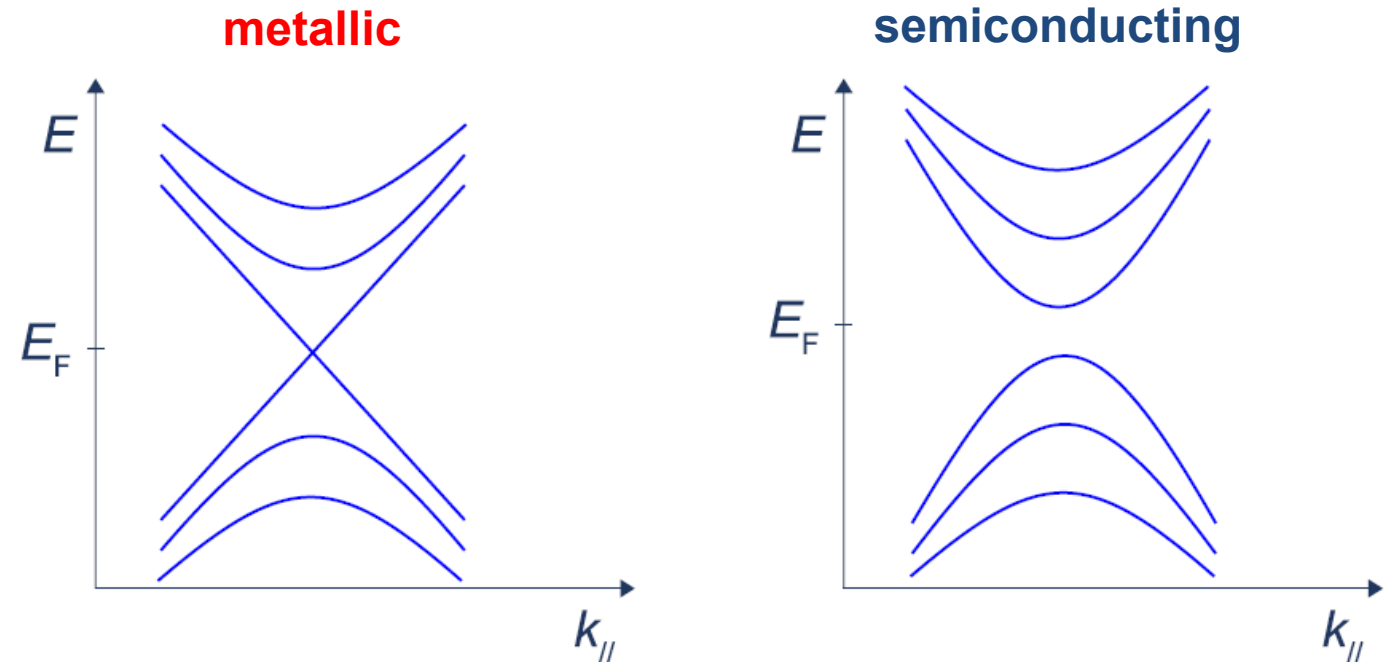
If the slice does not cross a  $k$ -point:  $E_{gap} \neq 0$  and inversely dependent on CNT diameter.

# Conduction in CNTs

The electronic band structure of a carbon nanotube is **quasi one-dimensional**: it consists of a set of one-dimensional subbands, shown schematically in the figure below.

The **larger the diameter** of the CNT, the **smaller the energy separation** between the different subbands.

Each subband can conduct **two electrons** with opposite spin.



Schematic representation of the band diagram of (a) a metallic SWCNT and (b) a semiconducting SWCNT. The symbols  $E$ ,  $E_F$  and  $k_{\parallel}$  represent respectively the energy, the Fermi energy and the  $k$ -vector in the direction parallel to the CNT axis.

# The resistance of a single walled CNT

CNTs have an intrinsic resistance. With each subband, one unit of quantum resistance is associated. The unit of **quantum resistance** is:

$$R_{quantum,unit} = \frac{h}{2e^2} = 12.9 \text{ k}\Omega$$

it includes conduction by two electrons with opposite spin.

When multiple subbands carry current, the total quantum resistance is the quantum unit resistance divided by the number of available subbands.

The quantum resistance of a single walled semiconducting CNT is:

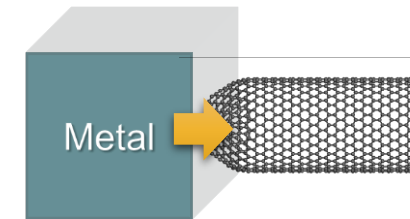
$$R_{quantum,SWCNT} = \frac{1}{2} R_{quantum,unit} = 6.5 \text{ k}\Omega$$

since there are only two channels close to the Fermi level which can carry current.

Also, metallic CNT's are expected to have the same quantum resistance (the first metallic subband is degenerate). The quantum resistance is **independent** on the length of the carbon nanotube.

Due to the inefficient coupling of the electron wavefunction from the electrode into the CNT, reflections can be expected at both electrode interfaces. This results in a contact resistance that can be represented as:

$$R_{contact} = \frac{1}{\sum \frac{T_i}{R_{quantum,i}}}$$



with  $R_{quantum,i}$  the quantum resistance associated with each sub-band  $i$  and  $T_i$  the corresponding transmission coefficient.

# The resistance of a single walled CNT

The inter-subband scattering depends on the diameter of the CNT. The energy separation between the Fermi level and higher order subbands for a metallic SWCNT is roughly proportional to  $1/d$ , with  $d$  the diameter of the CNT.

This gives rise to two counteracting effects:

- 1) the value of the quantum resistance is expected to decrease (more channels contribute)
- 2) the scattering is expected to increase due to coupling between the subbands.

Additional sources of scattering are imperfections, adsorbed molecules, effect of the surrounding material and carrier excitation into higher order subbands.

Both elastic (no energy loss) and inelastic scattering (with energy loss) generate an extra component in the resistance of CNT's.

Elastic scattering is suppressed near the Fermi level due to symmetry reasons because the electronic wavefunction is smeared out over the whole nanotube circumference. Inelastic scattering can come from acoustic phonons, optical phonons and zone boundary phonons.

# Phonon scattering in CNTs

Acoustic phonon **scattering** is always present, even at low voltages.

- Typical values for the mean free path  $l_{mfp,phon}$  in case of acoustic scattering are  $l_{mfp,phon} = 1 - 2 \mu\text{m}$ .
- Converting this to resistance per unit length according to the formula:  $\rho = \frac{h}{4e^2} \frac{1}{l_{mfp,phon}}$  results in a typical value of about:  $\rho_{ac.phon} = 4 - 7 \text{ k}\Omega/\mu\text{m}$ .

Optical phonon/zone boundary phonons **scattering** can occur when the applied voltages are sufficiently large.

- The threshold voltage for these scattering mechanisms is typically  $V_{th,opt phon} = 200 \text{ mV}$  (optical phonon) and  $V_{th,zb phon} = 160 \text{ mV}$  (zone boundary phonon).
- The mean free path is typically about  $l_{mfp,opt phon} = 200 \text{ nm}$  for optical phonon scattering and  $l_{mfp,zb phon} = 10 - 40 \text{ nm}$  for zone boundary phonon scattering. However, the total scattering length is also determined by the applied voltage  $V$ .
- The resistance due to optical phonon and/or zone boundary scattering is given by:

$$R_{opt/zb phon} = \frac{h}{4e^2} \frac{l}{l_{scattering,total}} = 6.5 \text{ k}\Omega \frac{l}{l \frac{V_{th,opt/zb phon}}{V} + l_{mfp,opt/zb phon}}$$

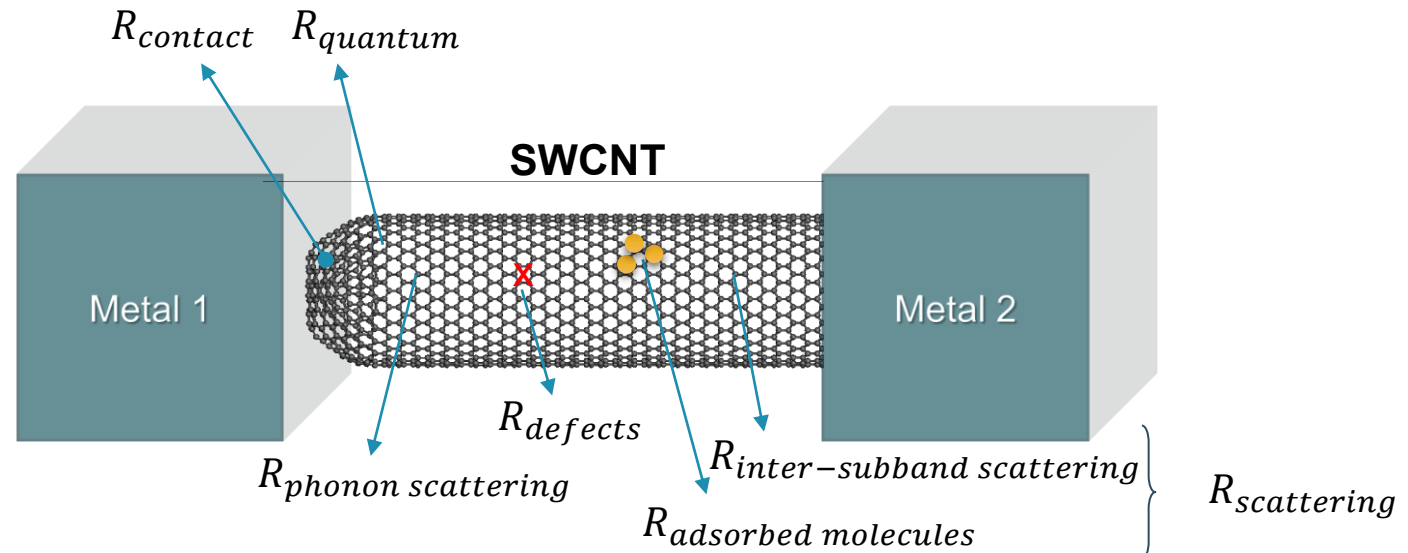
with  $V$  the applied voltage, and provided that  $V > V_{th}$ .

- For a scattering length of 30nm (dominant zone boundary scattering) the resistance per unit length is about  $\rho_{opt/zb phon} = 200 \text{ k}\Omega/\mu\text{m}$ .

# The resistance of a single walled CNT

As an overall result the externally measured resistance of a single walled CNT shows an important contribution from the contact resistance and the quantum resistance that are independent on the length of the CNT.

The scattering contribution related to phonon interactions is dependent on the **CNT length** and the **applied voltage**.



When the contact resistance is neglected the overall resistance of a high-quality single walled CNT can be approximated by:

$$R_{sCNT} = R_{quantum, metallics SWCNT} + \rho_{ac.phon} l + \rho_{opt.phon} l$$

# Inductance of a CNT

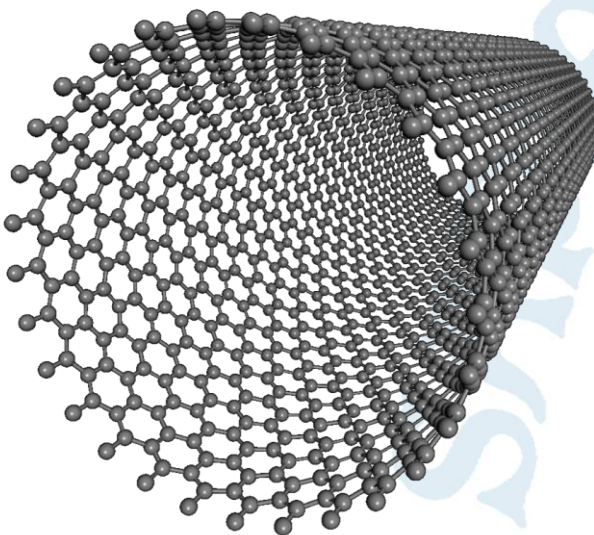
The inductance consists of magnetic and kinetic inductance:

- $L_{mag}$  corresponds to the inertia towards changes in **magnetic energy** of the carriers upon current flow.
  - The value of the magnetic inductance per unit length is of the order of  $L_{mag} \sim 1 \text{ pH}/\mu\text{m}$ .
- $L_{kin}$  corresponds to the inertia towards changes in the **kinetic energy** of the carriers upon current flow.
  - It is calculated from equating the kinetic energy per unit length in a 1D wire with the  $\frac{1}{2}LI^2$  energy of the kinetic inductance.
  - The total kinetic inductance for a metallic SWCNT is typically in the order of  $L_{kin} \sim 16 \text{ nH}/\mu\text{m}$ .

In CNTs the kinetic inductance will usually dominate the magnetic inductance. This is an important characteristic. In macroscopic circuits, long thin wires are usually considered to have relatively large (magnetic) inductances. This is **not the case** in CNTs where the **kinetic inductance dominates**.

# CNTs

## Synthesis



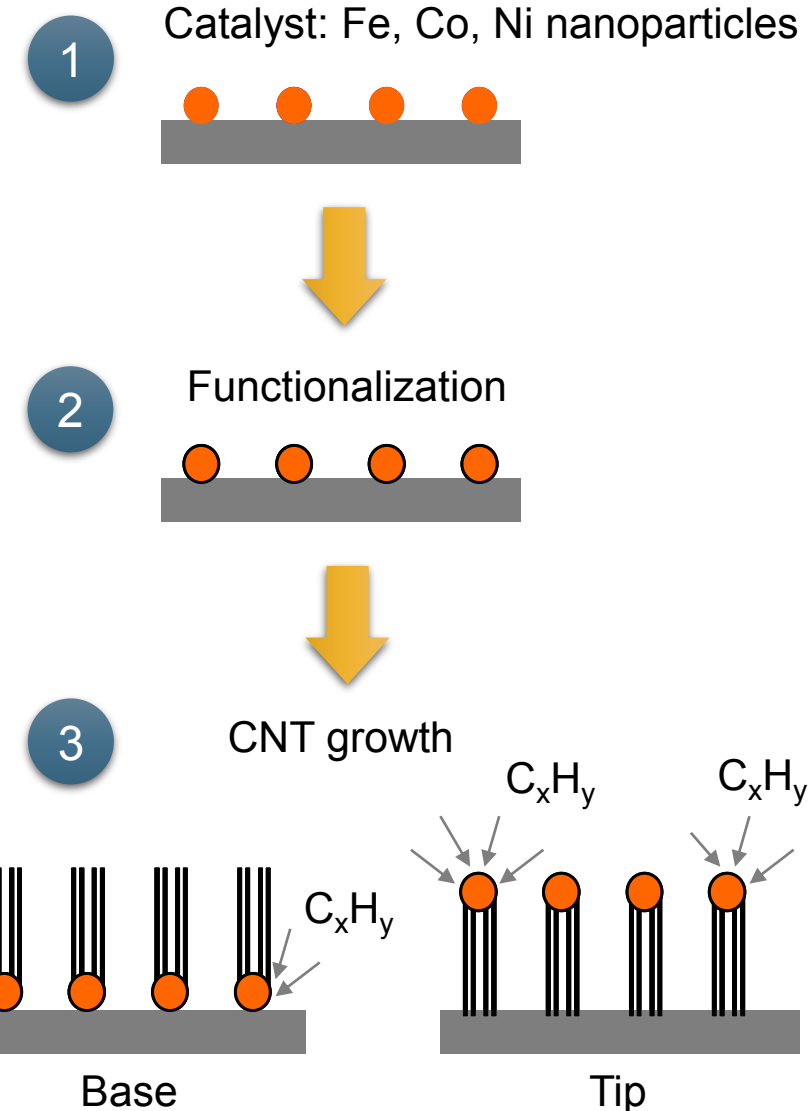
# CNT growth

The CNT growth process generally consists of 3 steps:

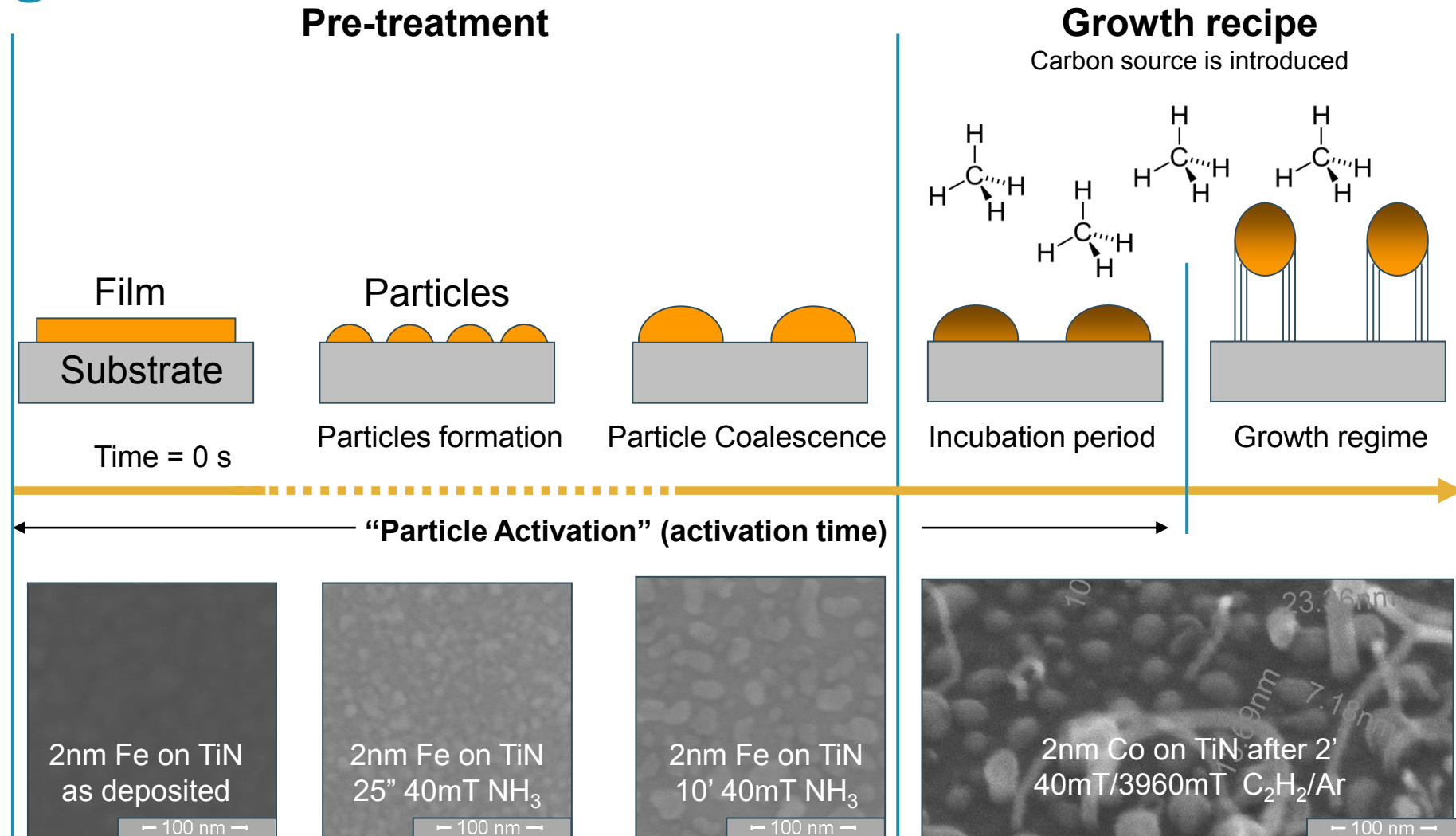
1. The **catalyst deposition**: metal (compound) nanoparticle which catalyzes thermal decomposition of carbon-containing molecule
  - determines position & diameter of CNT on substrate
  - deposition techniques:
    - electrochemical deposition (ECD)
    - sputtering + anneal
2. The (plasma-enhanced) **pretreatment**
3. The **CNT growth**: carbon source, e.g. methane

Growth techniques:

- Chemical Vapor Deposition (CVD)
- Plasma-Enhanced Chemical Vapor Deposition (PECVD)



# CNT growth



# CNT growth

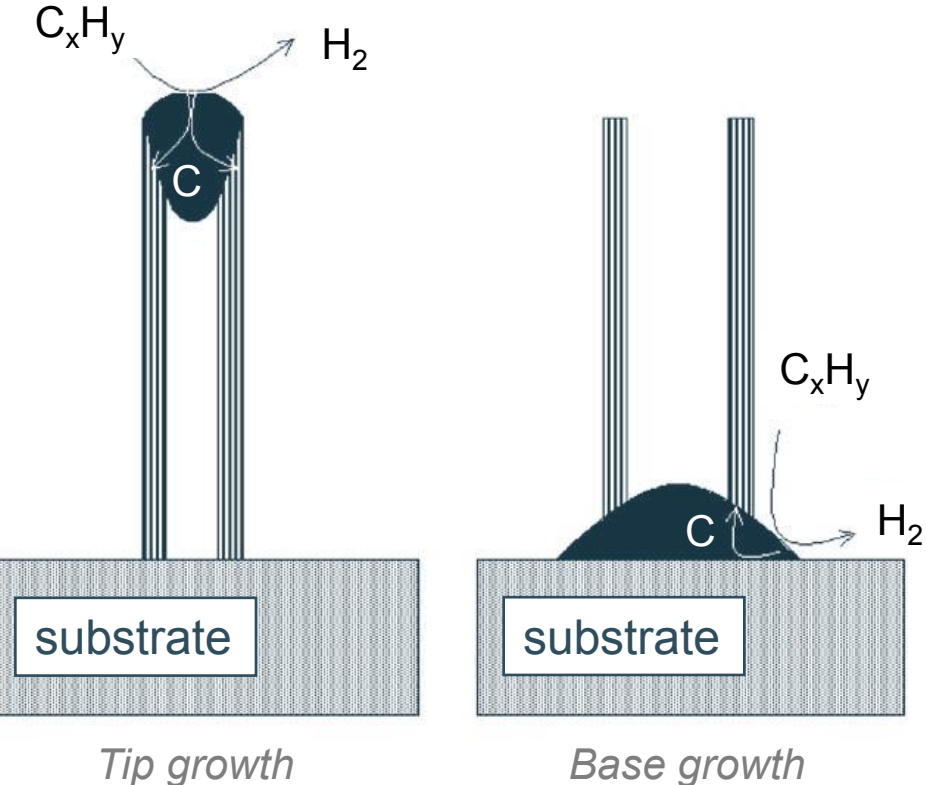
The catalyst-substrate interaction determines the **growth mode**:

- Tip-growth:

- Weak interaction between substrate and catalyst nanoparticle
  - Poor catalyst wetting on metal substrates (*i.e.* large contact angle)
  - (hemi) spherical nanoparticles

- Base-growth:

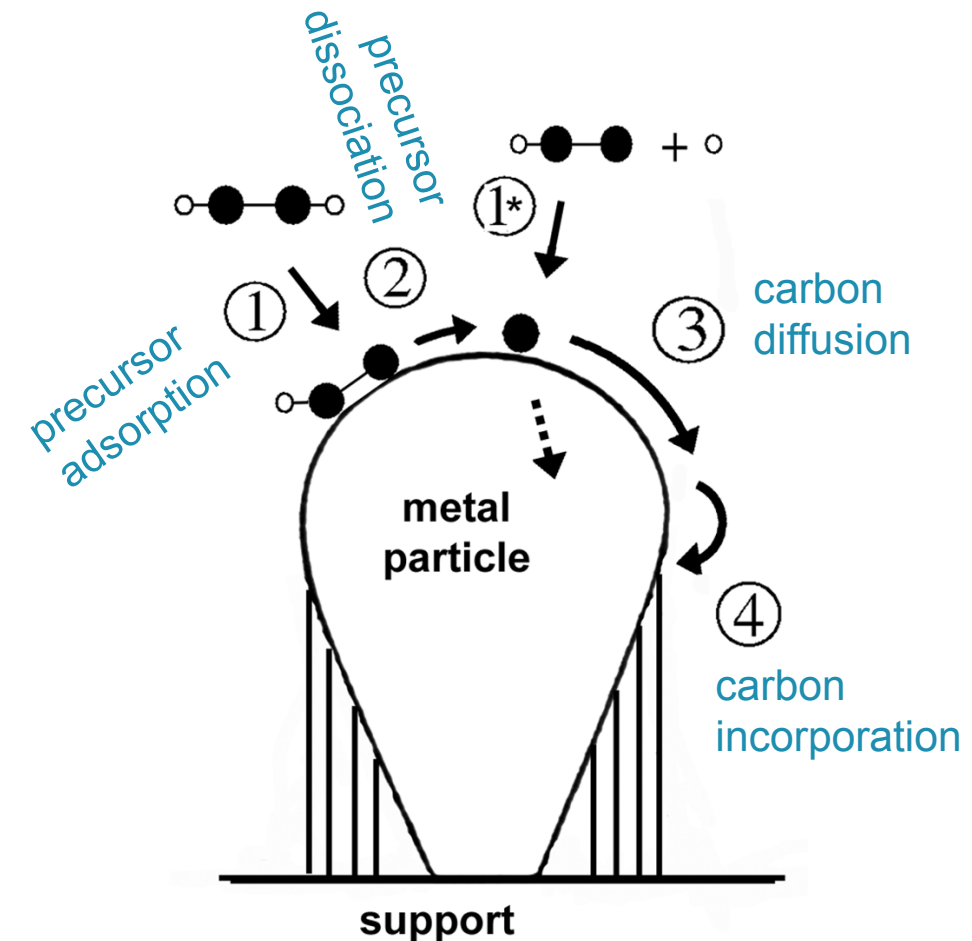
- Strong interaction between substrate and catalyst nanoparticle
  - Good wetting on oxide substrates (*i.e.* small contact angle)
  - Determined by amount of catalyst (film thickness), pretreatment and morphology
- Solid-state reactions between substrate and metal nanoparticle
  - e.g.  $\text{FeO} + \text{TiO}_2 \rightarrow \text{FeTiO}_3 (\Delta G < 0)$
  - May be facilitated in pretreatment (*e.g.* hydrogen plasma)



# CNT growth

The CNT growth involves various steps. The step with the largest energy barrier limits the growth rate.

- Carbon formation (1,2)
  - Chemical decomposition at catalyst (Fe, Ni, Co) surface
    - Adsorption + dissociation
- Carbon diffusion (3)
  - “Bulk” diffusion: dissolves into the metal catalyst and diffuses towards growth site
    - Concentration gradient: from decomposition site (high [C]) to crystallization site (low [C])
    - Enhanced by local temperature difference for exothermic decomposition and endothermic crystallization
  - Surface diffusion
    - from decomposition to crystallization sites
  - Formation of Carbide intermediates
- Crystallization (4)
  - Incorporation of carbon at step edge

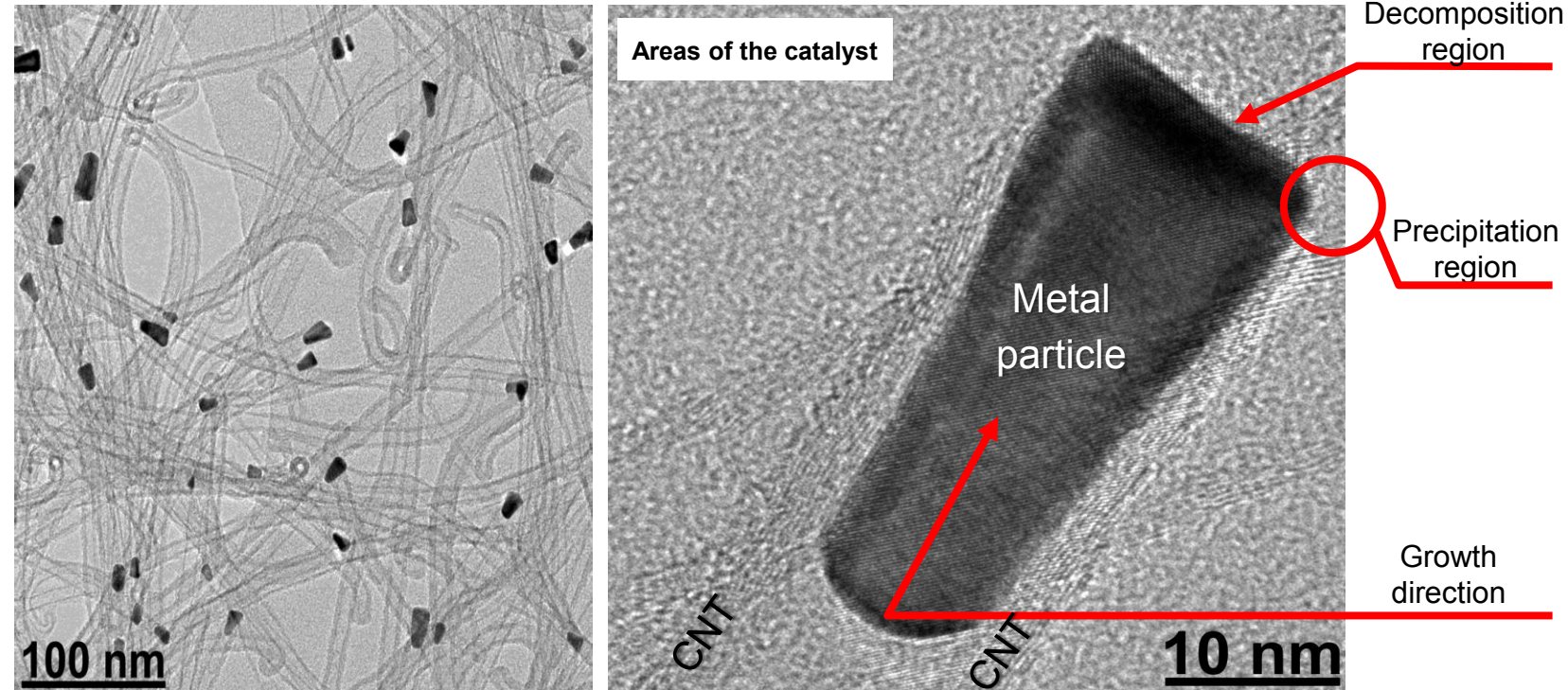


largest energy barrier (1)-(4) = rate limiting step

# CNT growth mechanism

High resolution cross-sectional TEM measurements provide more insight into the details of the CNT growth.

Predominant crystal facet reaches the steady-state growth, *i.e.* the minimum of the surface free energy and  $C_{Supplied}/C_{Released} = 1$ , the grown carbon nanostructure is a perfect CNT.

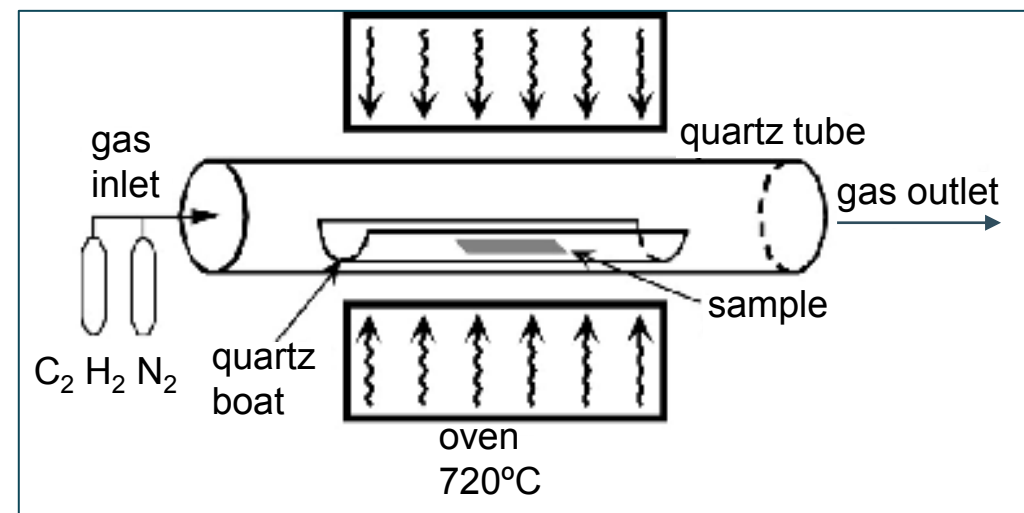
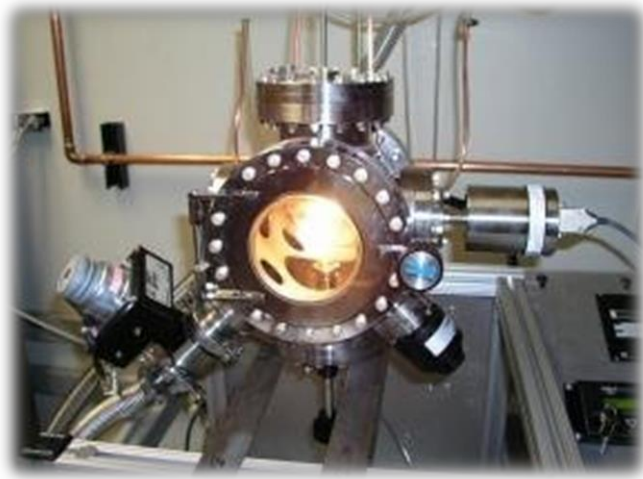


# CNT growth by Chemical Vapor Deposition

CNTs can be produced by various techniques. For high quality CNTs chemical vapor deposition (CVD) is the preferred method.

A substrate is prepared with a layer of metal catalyst particles (Ni, Co, ...) and then heated up to 700°C.

Two gases are blend into the reactor: a process gas and a carbon gas (e.g. CH<sub>4</sub>). The carbon gas is broken apart at the surface of the catalyst particle and the carbon moves to the edges to form nanotubes.



# CNT growth by Chemical Vapor Deposition

Laminar gas ( $\text{CH}_4$ ) flow in tube furnace

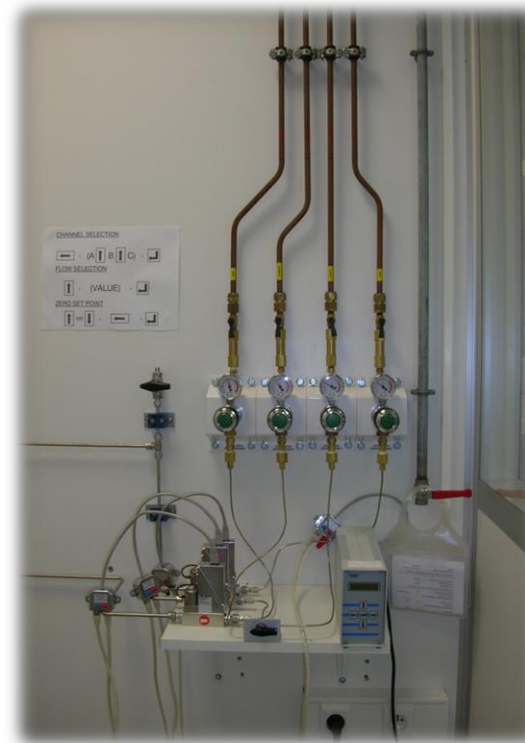
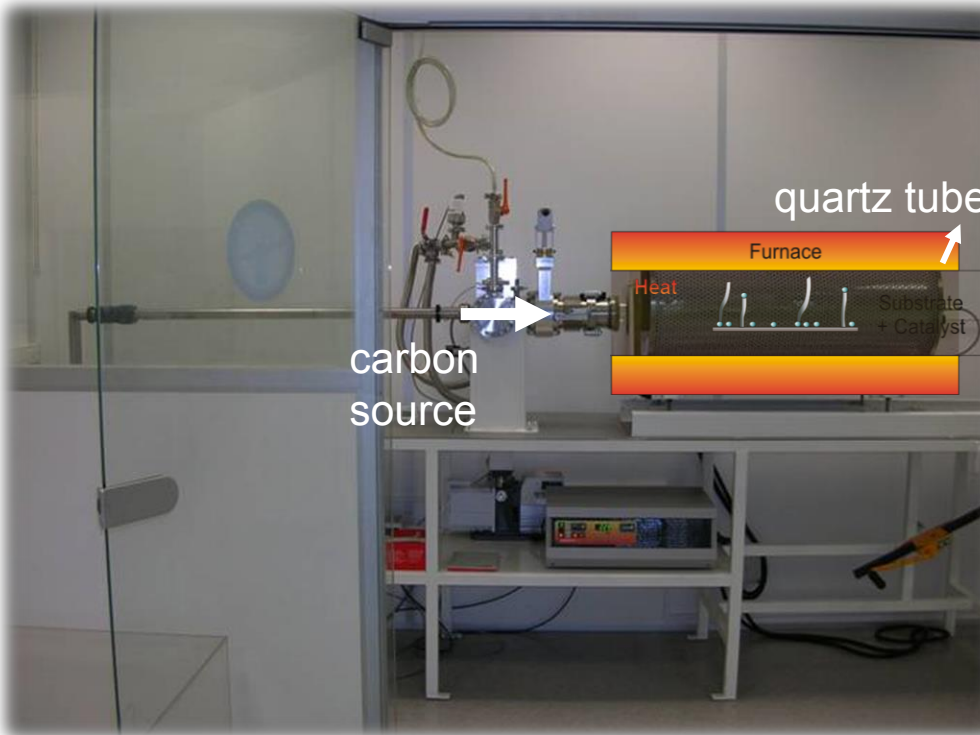
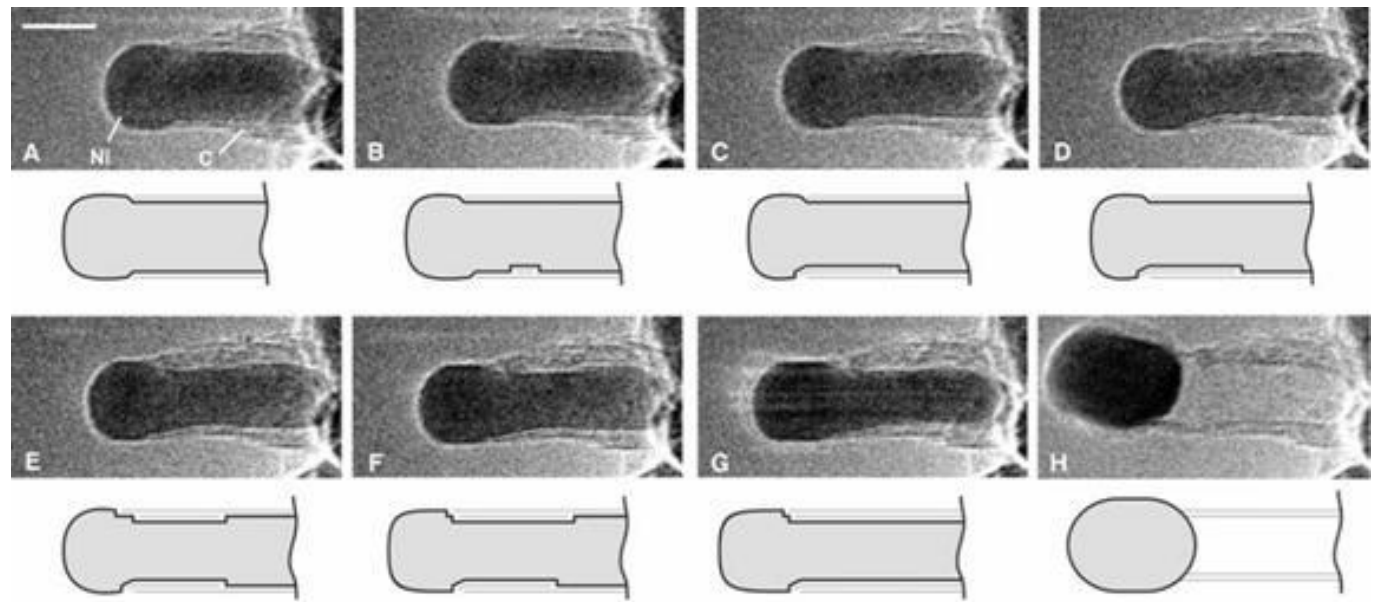


*Illustration of a thermal catalytic chemical vapor deposition tool (C-CVD) at NANOCYL, Namur.*

# in-situ TEM analysis of CNT nucleation

The nucleation and growth of CNT's can also be studied by in-situ TEM.

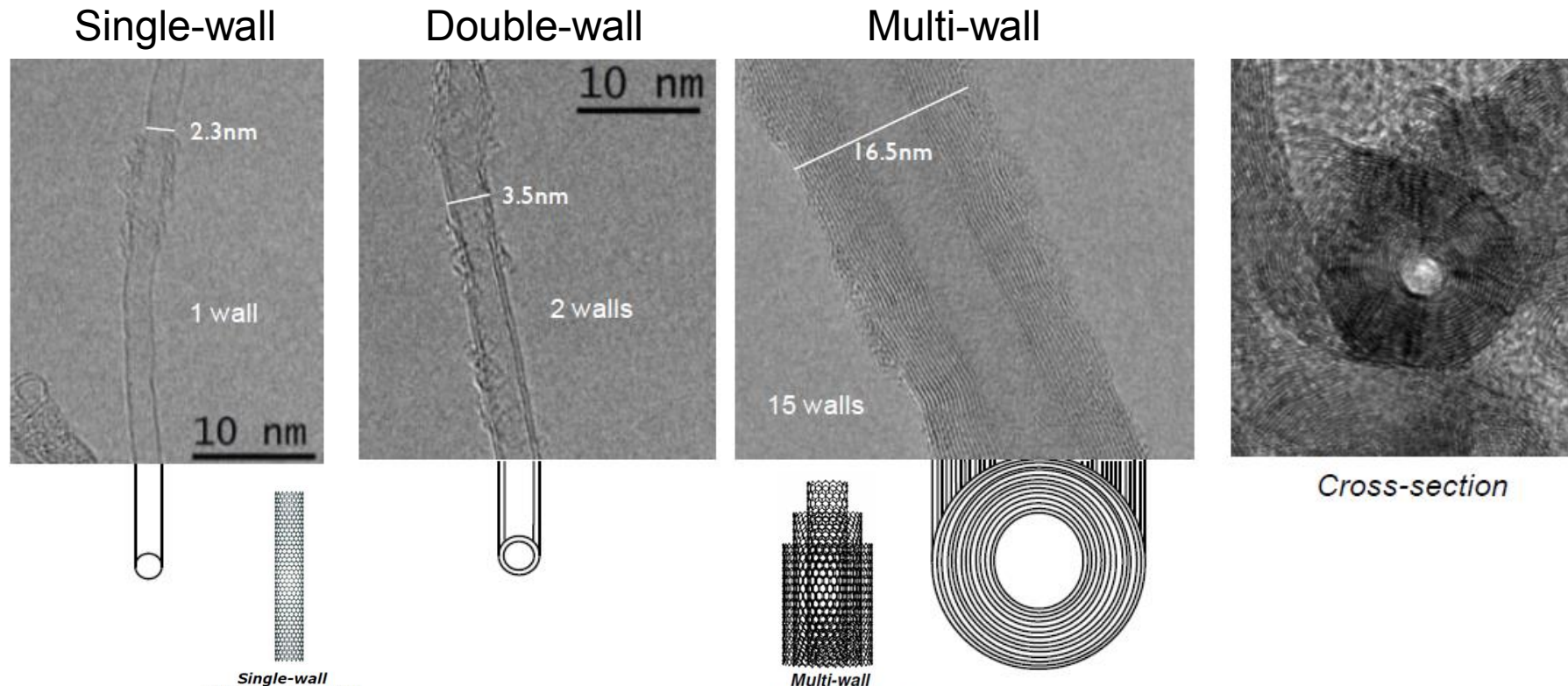
- Graphene layers are formed around the elongated catalyst particle
- Nucleation of additional graphene sheets at subsequent step edges
- Eventually particle retracts and CNT grows (tip growth)
- Note that Ni is still in crystalline form, however highly “mobile” (ductile)



*in-situ TEM image sequence of growing CNT, Hervege , Nature 427, 426 (2004)*

# Carbon nanotubes

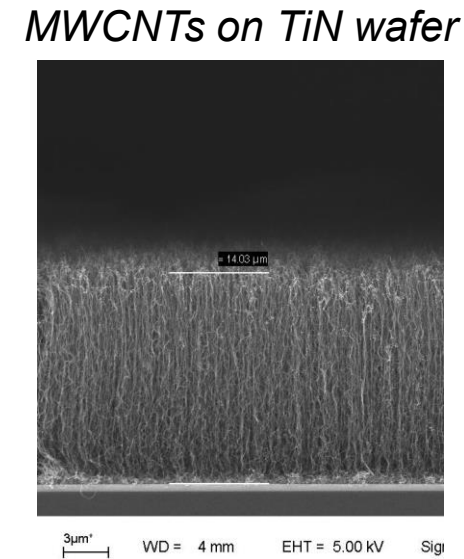
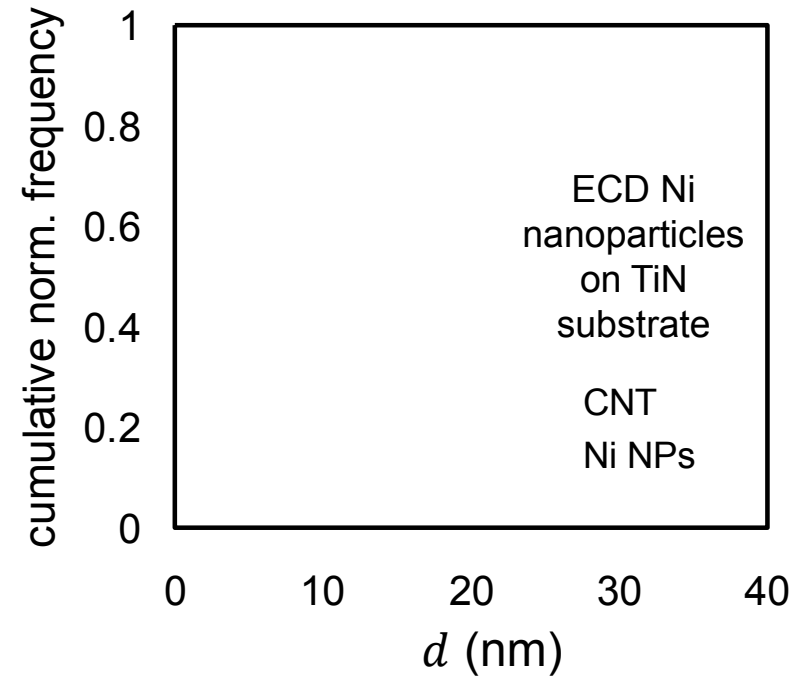
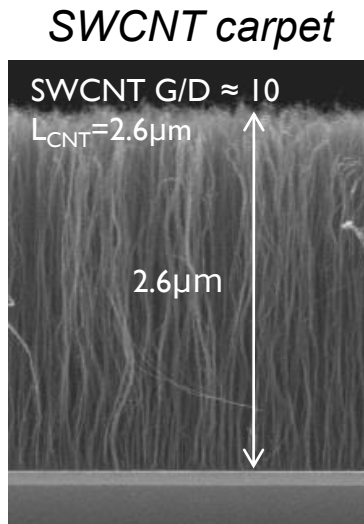
In practice single-walled and multi walled tubes will be grown in this process, dependent on the **size of the catalytic particle** and the **growth conditions**.



# Impact of nano particle size on CNT growth

The diameter of the catalyst nanoparticle  $d_{NP}$  determines the CNT diameter  $d_{CNT}$

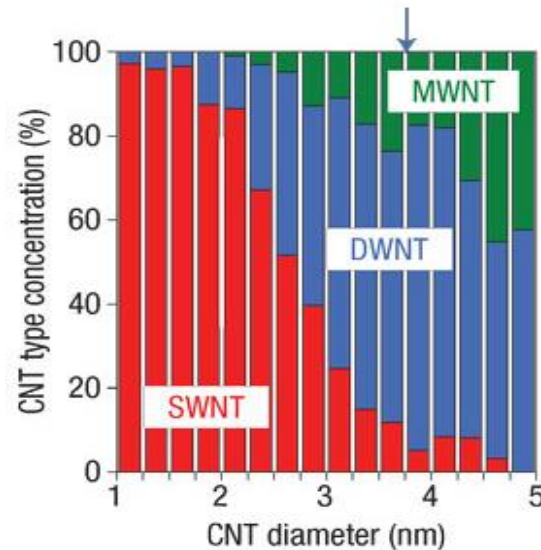
- $d_{NP} < 5 \text{ nm}$ : mostly SWCNTs (Single-Walled CNTs)
- $d_{NP} > 5 \text{ nm}$ : mostly MWCNTs (Multi-Walled CNTs)



*Correlation between particle size and CNT size ( $d_{NP}$ ,  $d_{CNT}$ )*

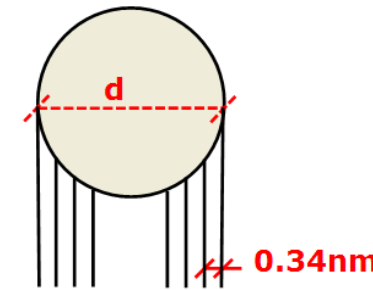
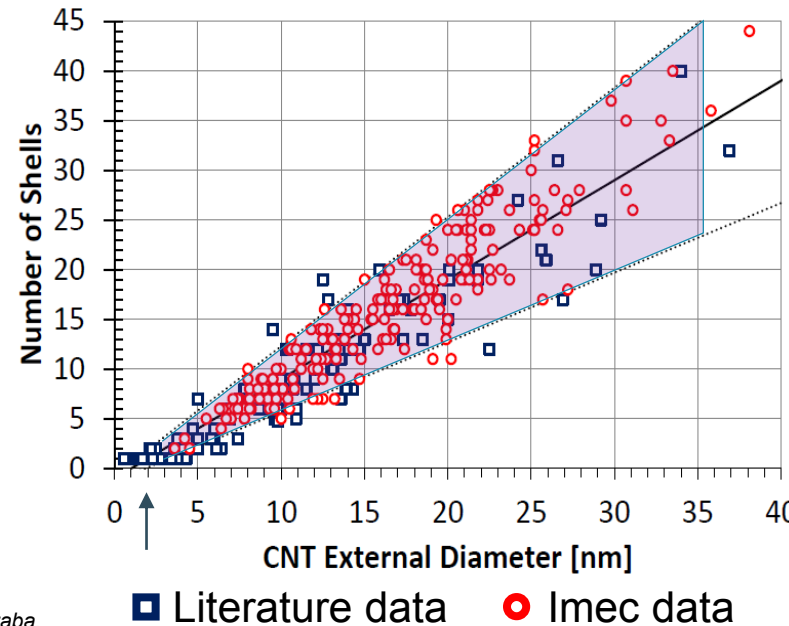
# Number of walls: “rule of thumb”

The relation between the CNT diameter ( $d_{CNT}$ ) and the number of walls ( $N$ ) is given by the empirical expression:  $N = d_{CNT} - 2$  (and  $N = 1$  for  $d_{CNT} < 2\text{ nm}$ ).



Fe nanoparticles on  $\text{SiO}_2$

Takeo Yamada, Tatsunori Namai, Kenji Hata, Don N. Futaba, Kohei Mizuno, Jing Fan, Masako Yudasaka, Motoo Yumura & Sumio Iijima *Nature Nanotechnology* 1, 131 - 136 (2006)



$$N \cong \frac{d_{CNT}}{1\text{nm}} - 2$$

*Compilation of experimental data (CVD grown CNT only) shows on average a linear relationship between number of walls ( $N$ ) and tube diameter ( $d_{CNT}$ ) for  $d_{CNT} > 2\text{nm}$ .*

# High density aligned CNTs

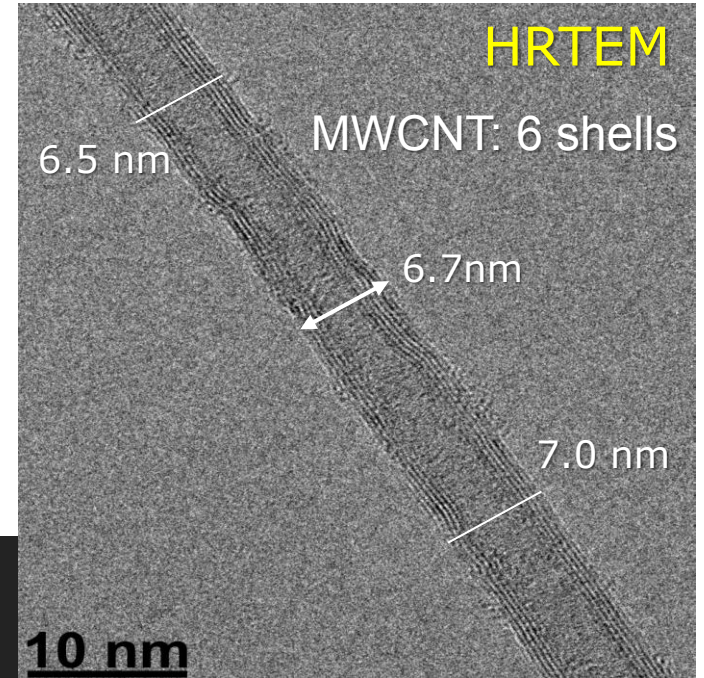
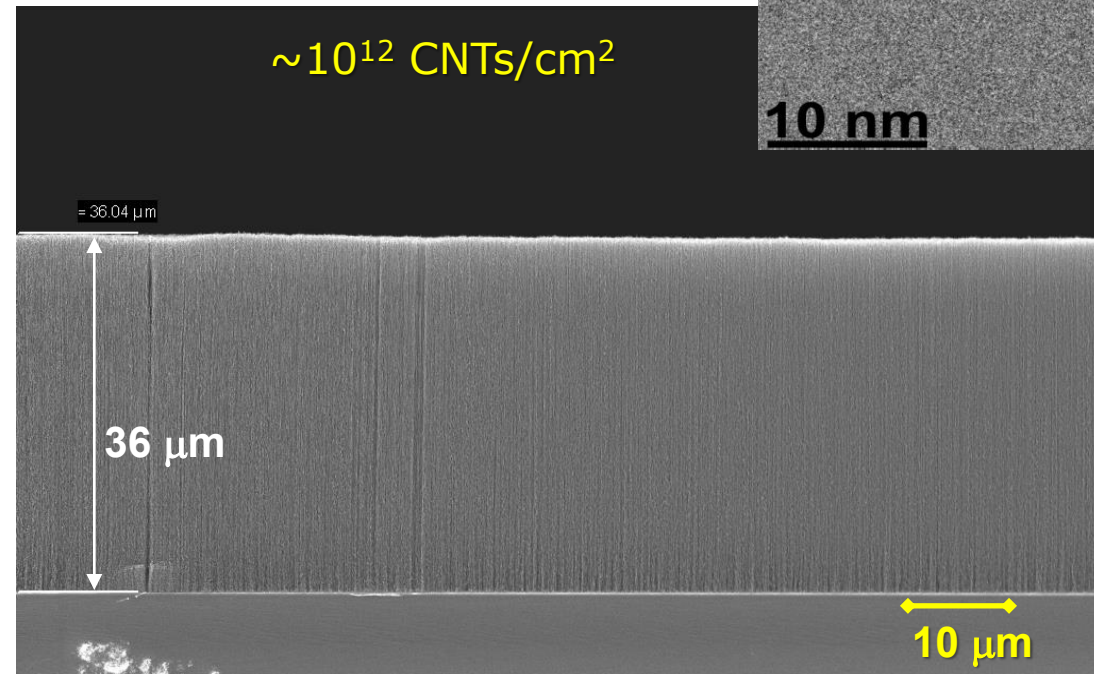
By optimizing the catalyst and growth process, **dense CNT “forests”** can be grown.

Example : high-density of MWCNTs obtained with Fe/Ti layer:

- $\sim 10^{12}$  MWCNT:
  - outer diameter of 6.5 - 8.0 nm
  - inner diameter ~ 5nm
- $\sim 10^{13} \text{ cm}^{-2}$  CNT shells

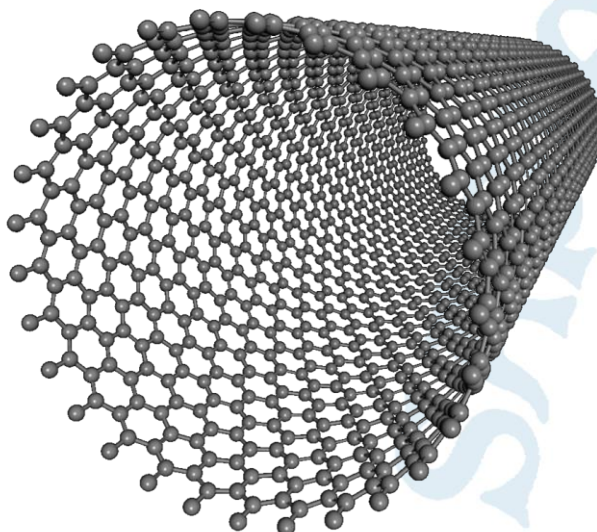


Catalyst pretreatment: 1Torr H<sub>2</sub>, 650 °C, 200W HF-plasma: 5min  
Growth: 1 Torr C<sub>2</sub>H<sub>2</sub> (200 sccm), T<sub>stage</sub> = 650 °C: 60 min



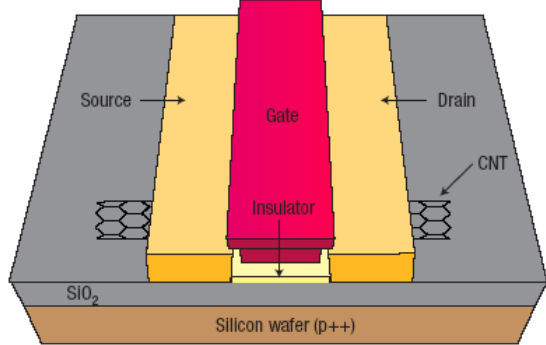
# CNTs

Devices & applications



# Nanotube FET

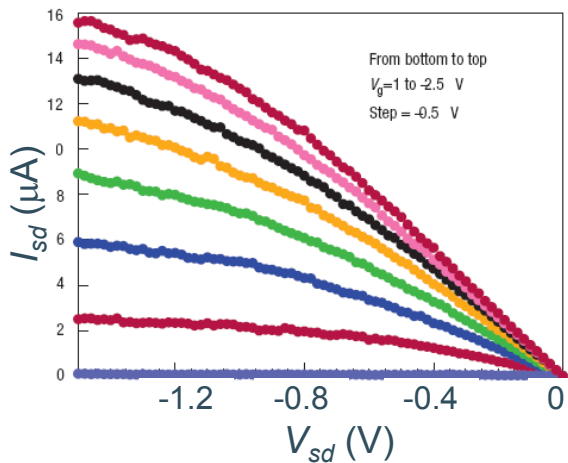
- For the fabrication of FET's with CNT's, only **semiconducting** CNT's can be used with a well-defined **bandgap**. This requires a growth process with *perfect control* on the **chirality** and **diameter** of the CNT's. This is not possible at present.
- However, with '**pick-and-place**' methods, CNT devices have been demonstrated.



Bandgap: 0.5 – 1 eV

On-off ratio:  $\sim 10^6$

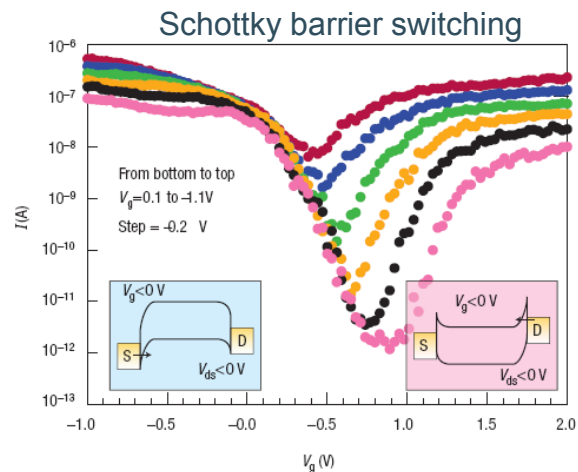
Mobility:  $\sim 100,000 \text{ cm}^2/\text{V.sec}$  @ RT



Ballistic @RT  $\sim 300\text{-}500 \text{ nm}$

Fermi velocity:  $10^6 \text{ m/sec}$

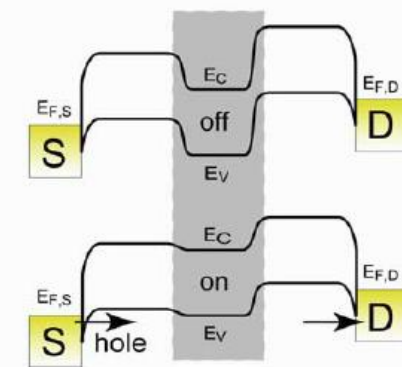
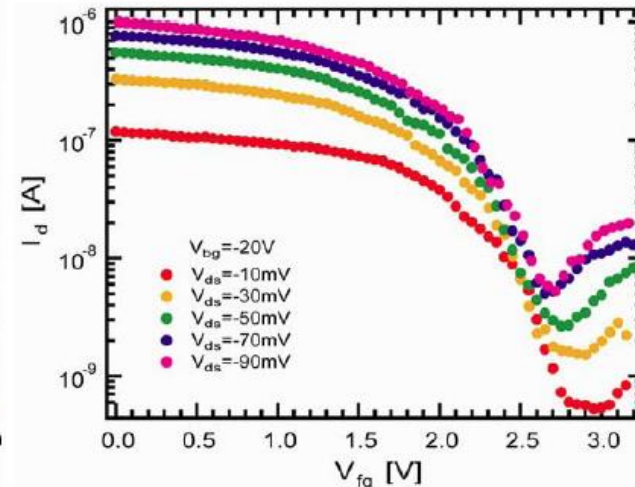
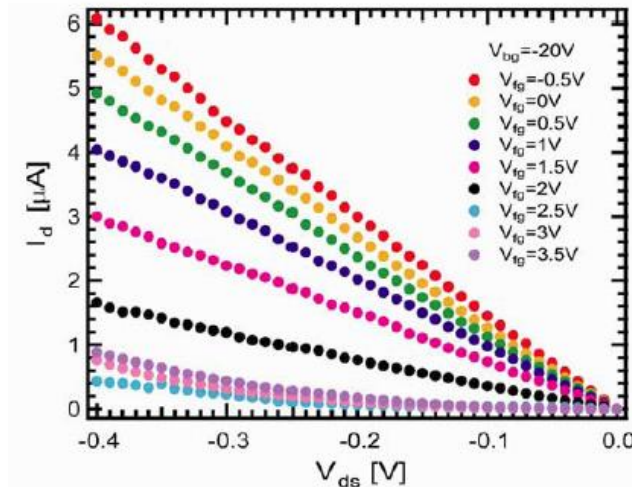
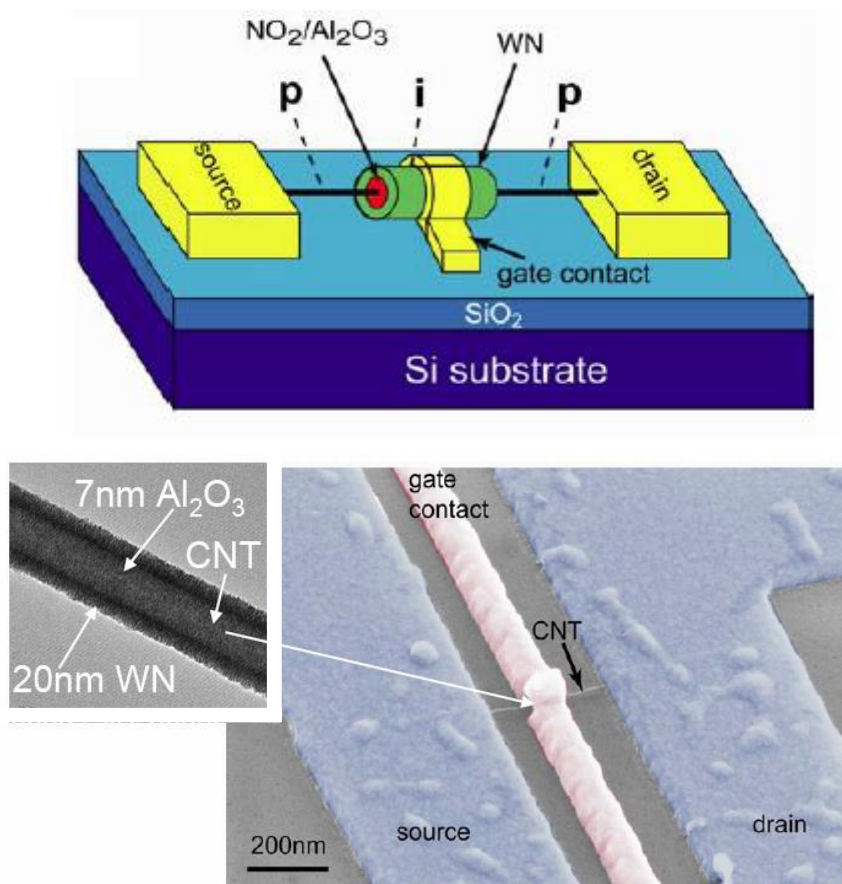
Max current density  $> 10^9 \text{ A/cm}^2$



Ph. Avouris et al, Nature Nanotechnology 2, 605 (2007)

# Gate-all-around CNT FET

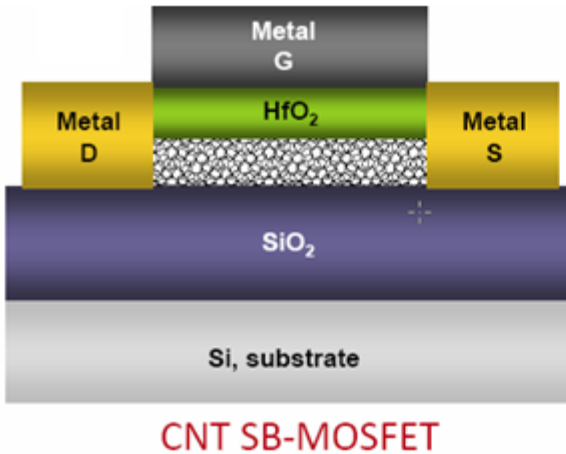
Gate-all-around CNT FET demonstrated using ‘pick-and-place’ of a CNT.



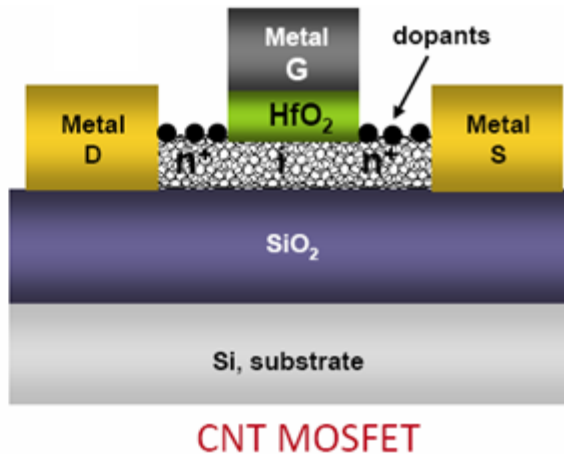
Zhihong Chen et al, APL, 2008

# CNT FET structures

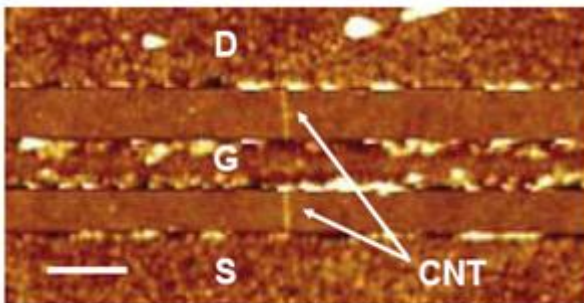
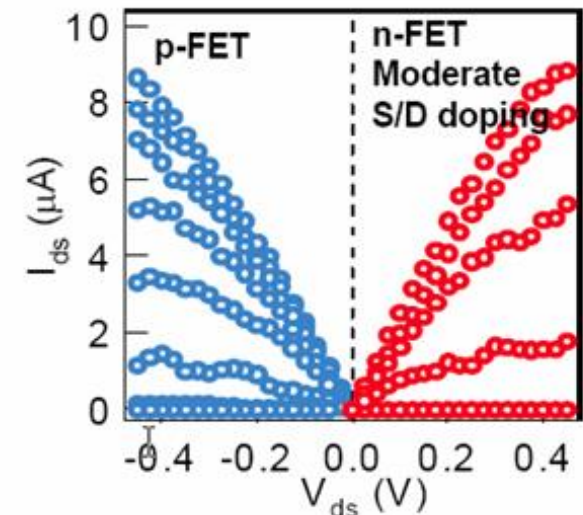
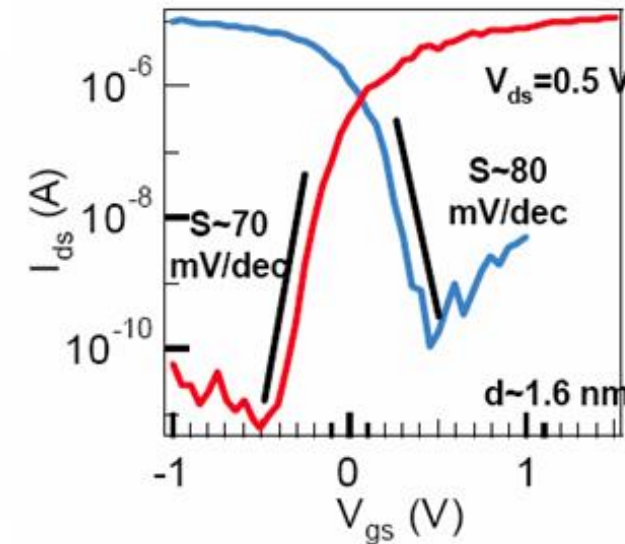
Both Schottky-barrier FETs and regular MOSFETs with 'doped' source/drain regions have been demonstrated.



CNT SB-MOSFET



CNT MOSFET



SB-MOSFET: Gate modulates the carrier injection at the S/D Schottky (metal) contacts

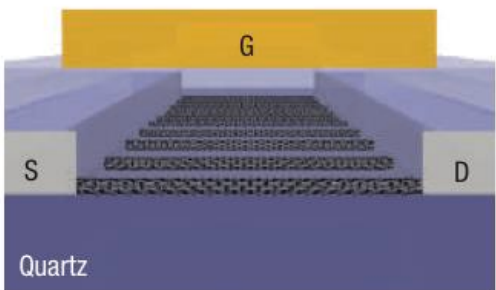
CNT-MOSFET: Gate modulates the charge density of the nanotube channel

A. Javey et al, Nano Letters, 2004, 2005

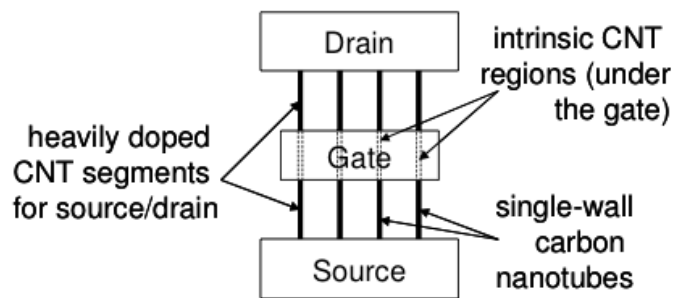
# Carbon nanotube FET

An “Ideal” MOSFET-like CNFET is formed by 1 or more semiconducting CNTs perfectly aligned and well-positioned whose section under the gate is intrinsic and the source/drain extension regions are *n/p* doped.

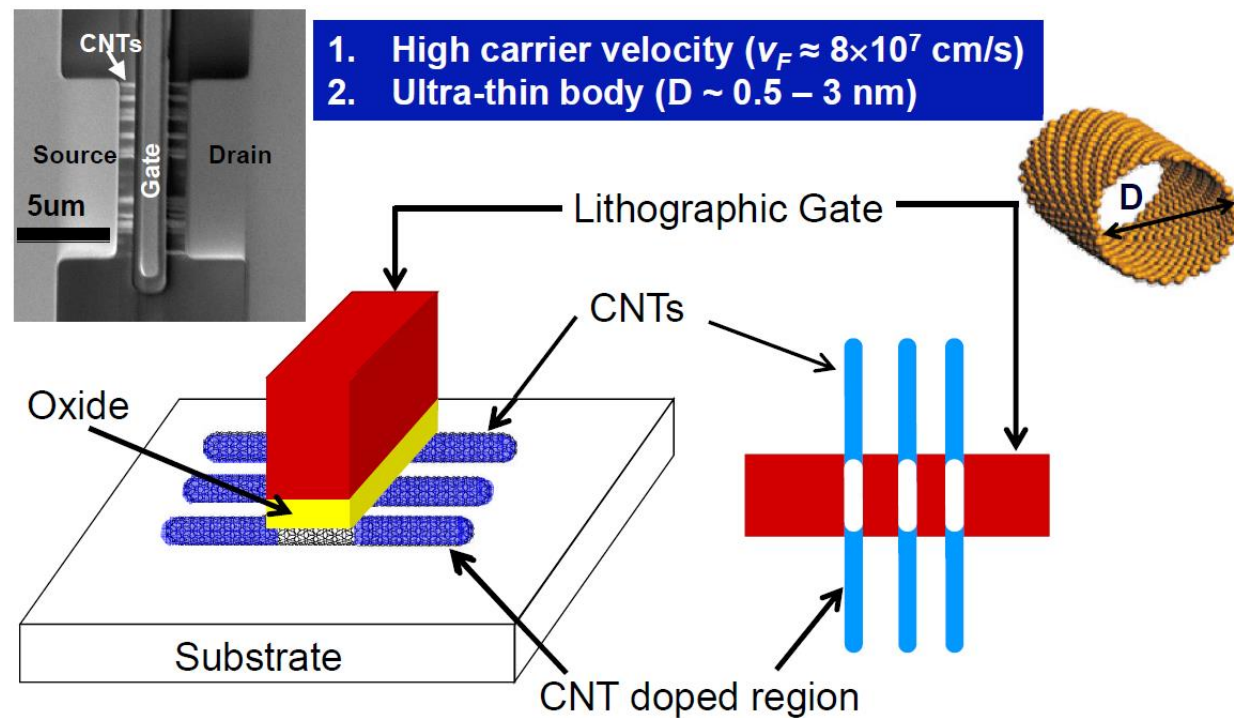
CNT FETs are promising candidates to replace silicon CMOS, assumed that we could make these ‘perfect’ CNT devices.



Horizontal

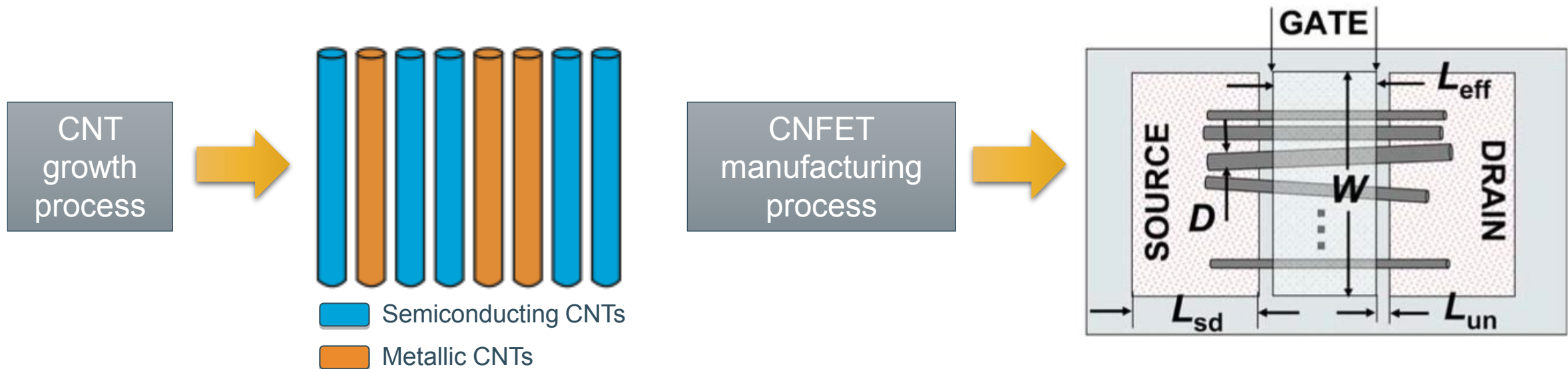


Vertical



# Carbon nanotube FET

There are some imperfections inherent to CNT synthesis and CNFET manufacturing process that may eclipse the expectations.

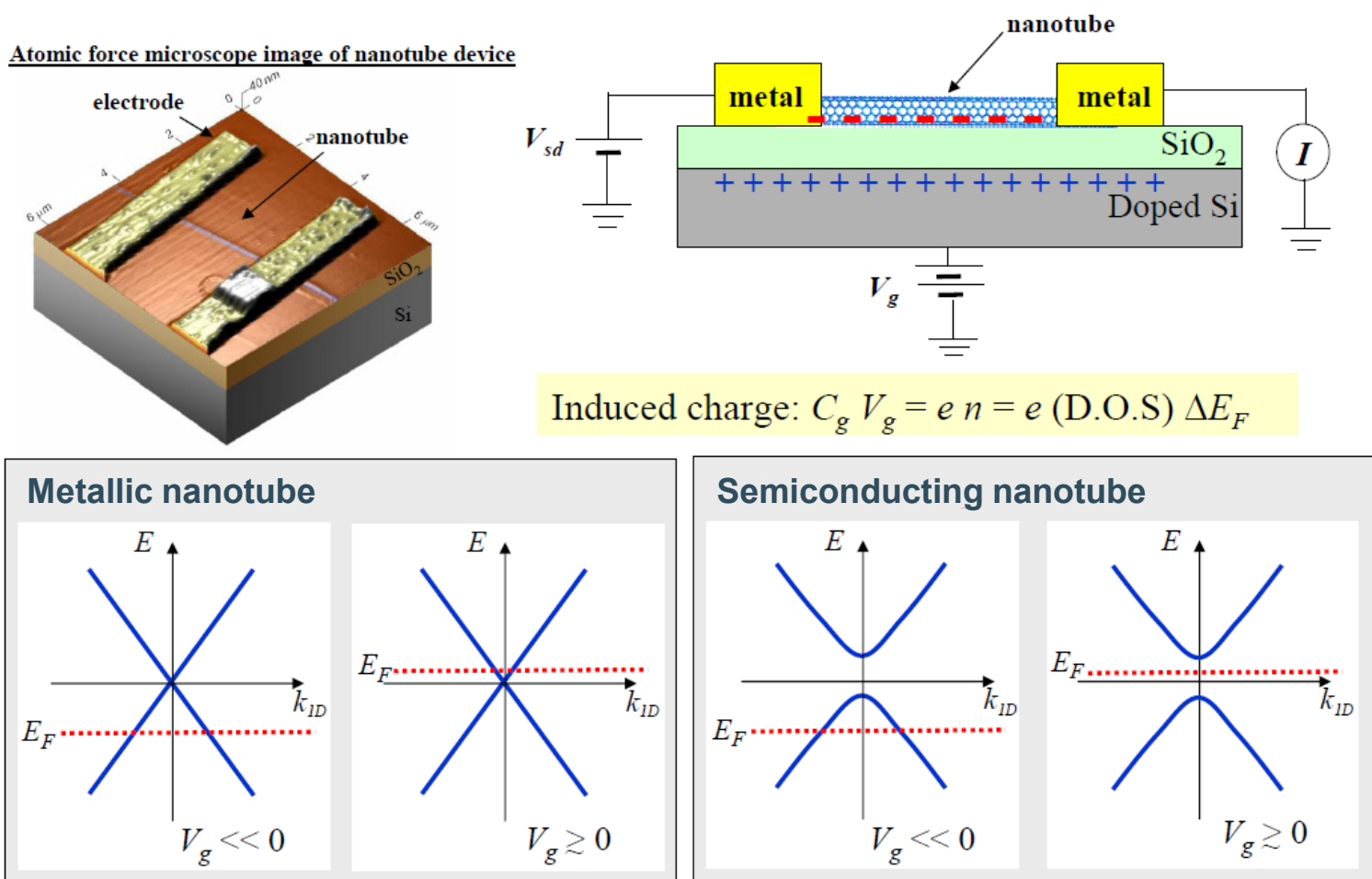


- **NO control of chirality**
  - Percentage of metallic-CNTs
- Diameter variations
- S/D doping variations
- Mispositioned and misaligned CNTs

# CNT FET

In a CNT FET (Field Effect Transistor) the carrier density is tuned by the field effect.

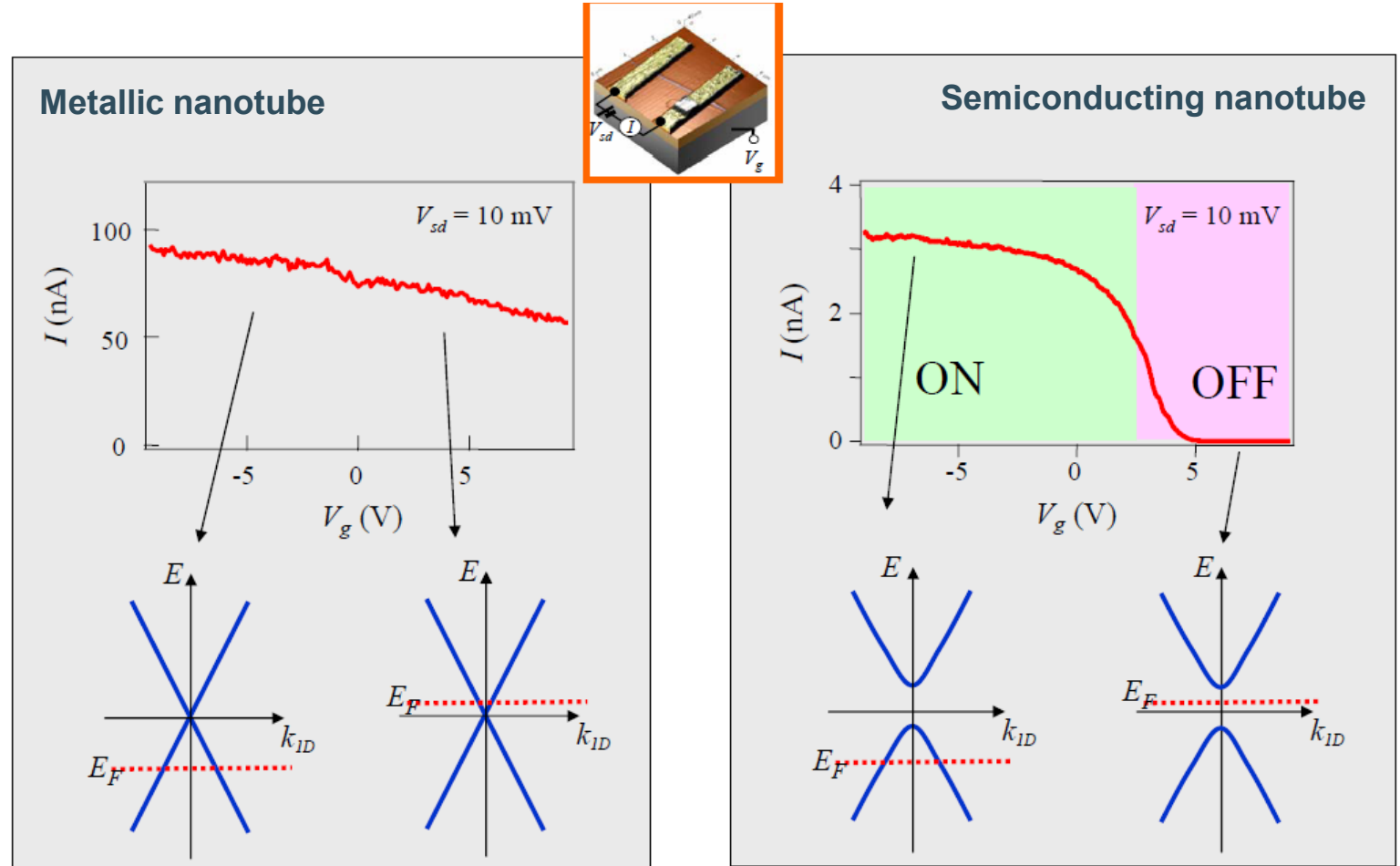
This is illustrated aside for a back-gated device where the Si substrate is used as control gate.



# Electrical transport in nanotube devices

Only in semiconducting nanotubes the current can be sufficiently modulated to obtain and acceptable ON/OFF ratio of the transistor current. Metallic nanotubes must be avoided in transistor applications.

Currently there is no method available that allows to directly produce semiconducting CNTs only in a controlled way on a substrate, necessary to fabricate CNT circuits.

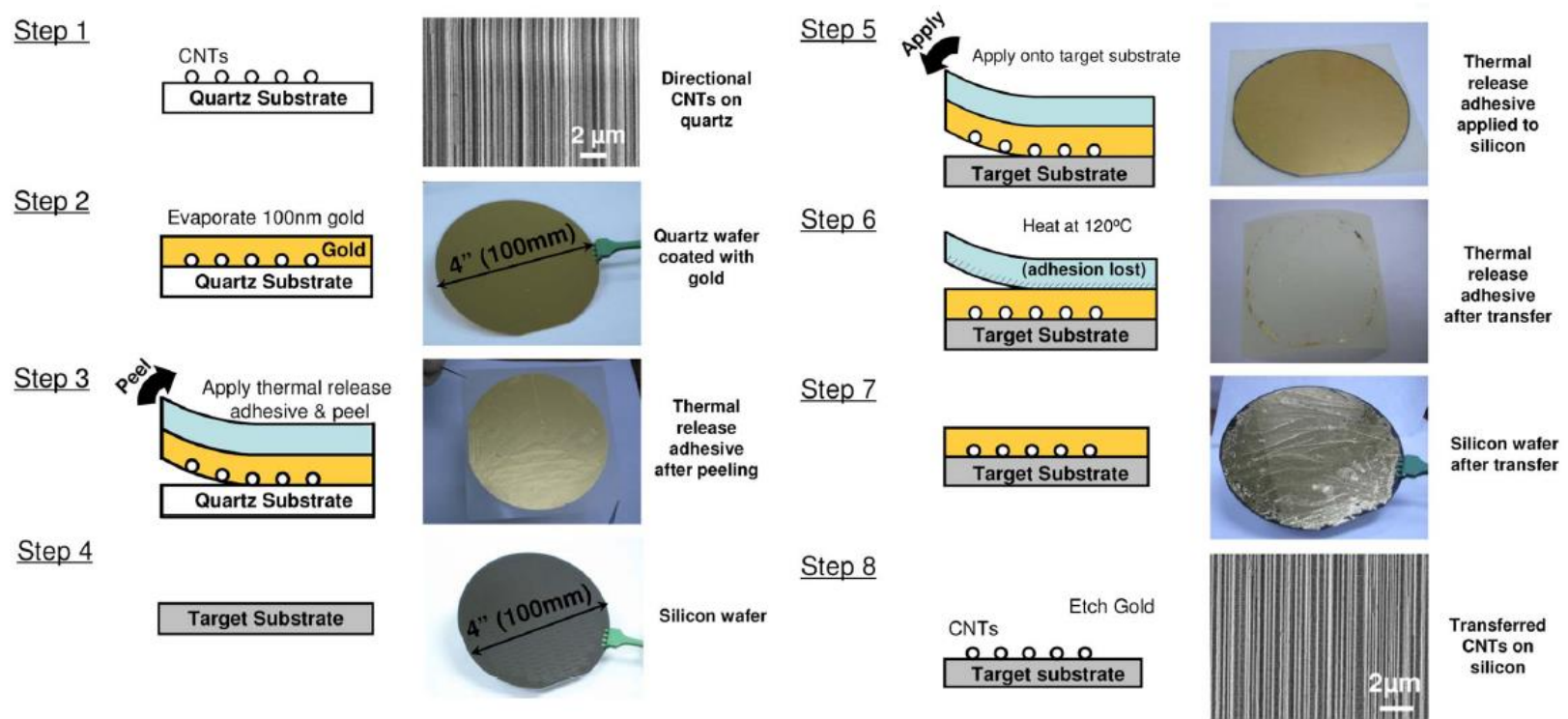


# CNT transistors on a Si substrate

CNT transistors and circuits have been fabricated from mixed semiconducting and metallic nanotubes transferred as a 'tapestry' onto a Si wafer.

A CNT transfer technique was developed which transfers CNT from as-grown on a crystalline quartz substrate (where the CNTs grow horizontally) to a target substrate.

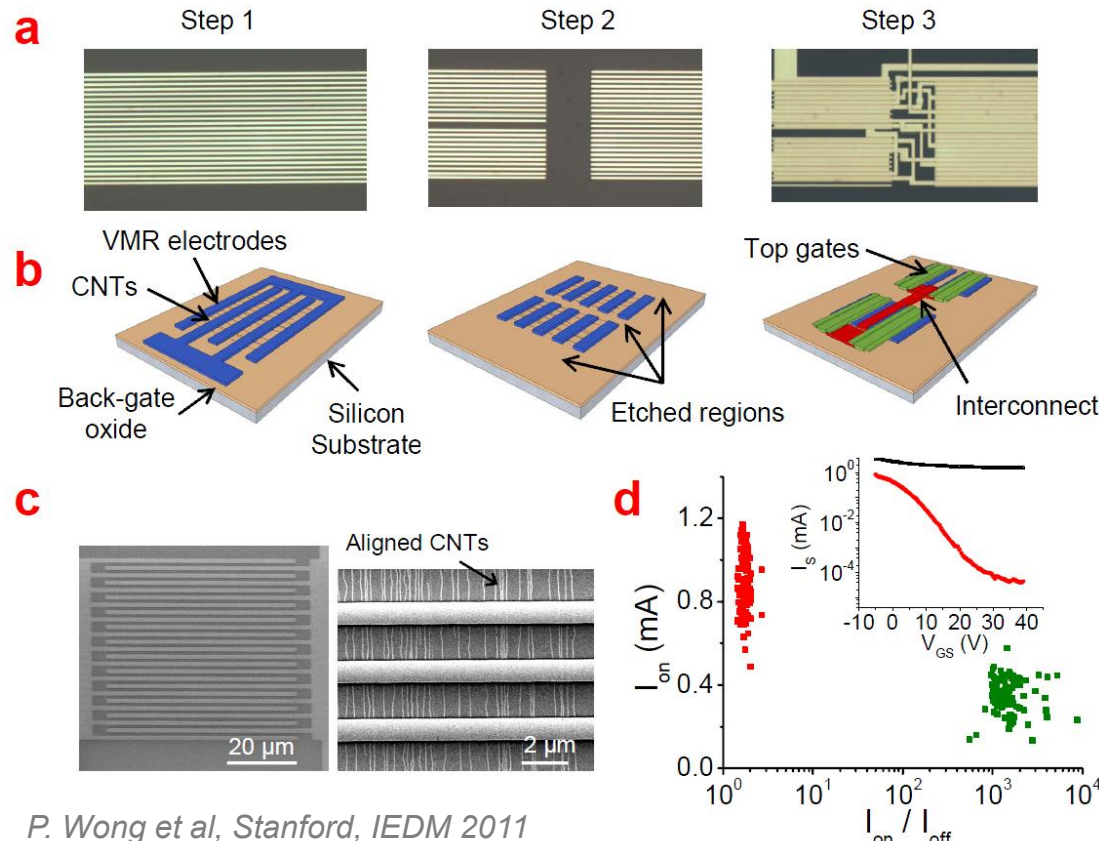
In this way a complete Si wafer can be densely covered with aligned CNTs.



P. Wong et al, Stanford, IEDM 2011

# CNT transistors on a Si substrate

After transfer metallic CNTs are removed by ‘burning’ before transistors are made. Final transistors will contain a varying number of semiconducting CNTs. This statistical variation can be handled by proper design methodologies.



P. Wong et al, Stanford, IEDM 2011

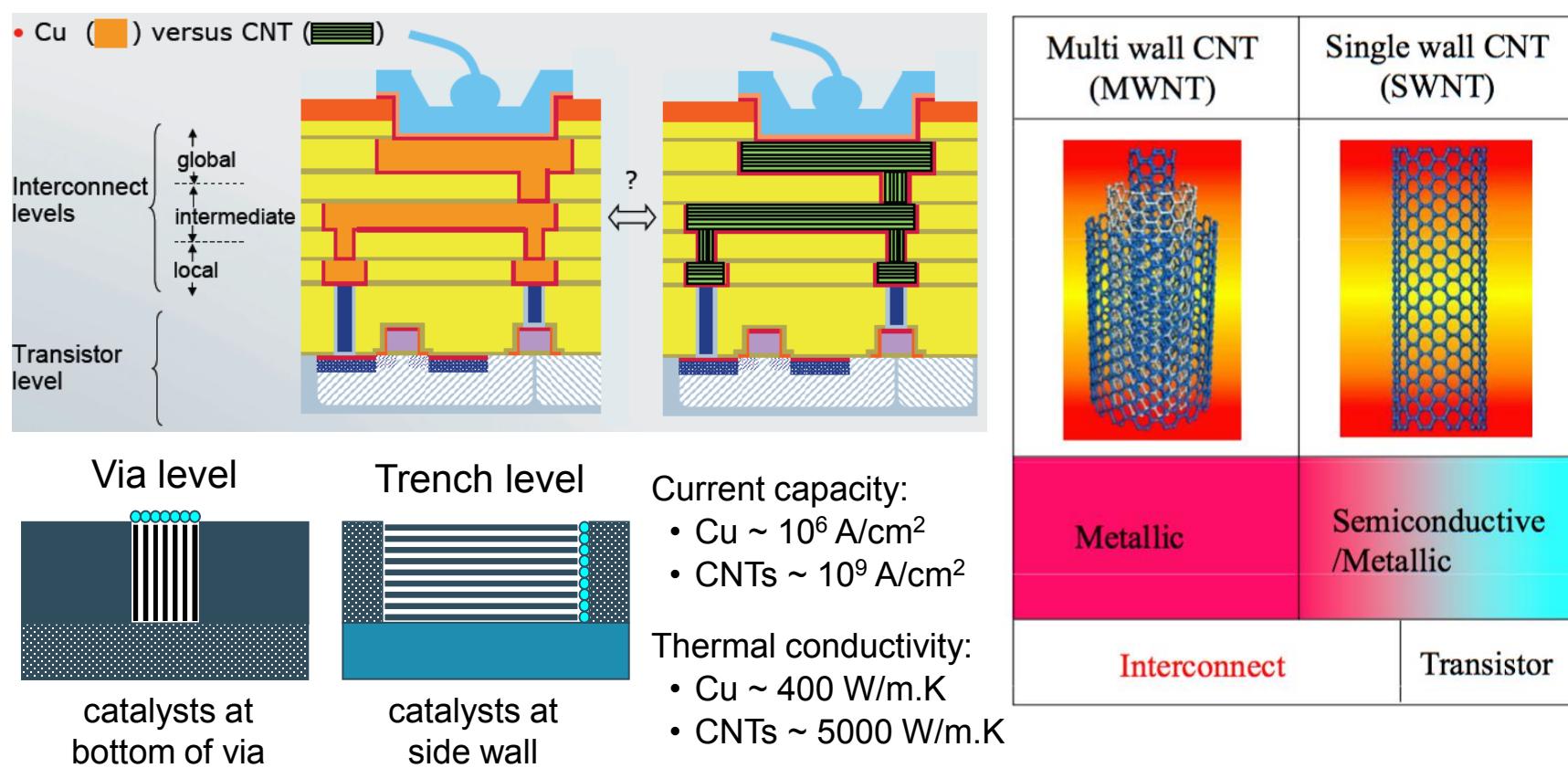
## VLSI-compatible Metallic-CNT Removal (VMR) technique.

- Top view optical photo*
- Schematic illustration: the VMR electrodes for electrically breaking down (burning) the m-CNT are retained and used as source/drain electrodes for the CNFETs. The s-CNTs are turned off by the back-gate electrode during the electrical burning process.*
- SEM photo of VMR electrodes. A large region encompassing multiple CNFETs is covered by one set of VMR electrodes. Close-up view of the VMR electrodes with aligned-CNTs underneath.*
- $I_{ON}$  vs.  $I_{ON}/I_{OFF}$  of CNFETs before (red) and after (green) VMR m-CNT removal. Inset:  $I_D$  vs.  $V_{GS}$  of a typical CNFET before (black) and after (red) VMR m-CNT removal.*

# CNT interconnects

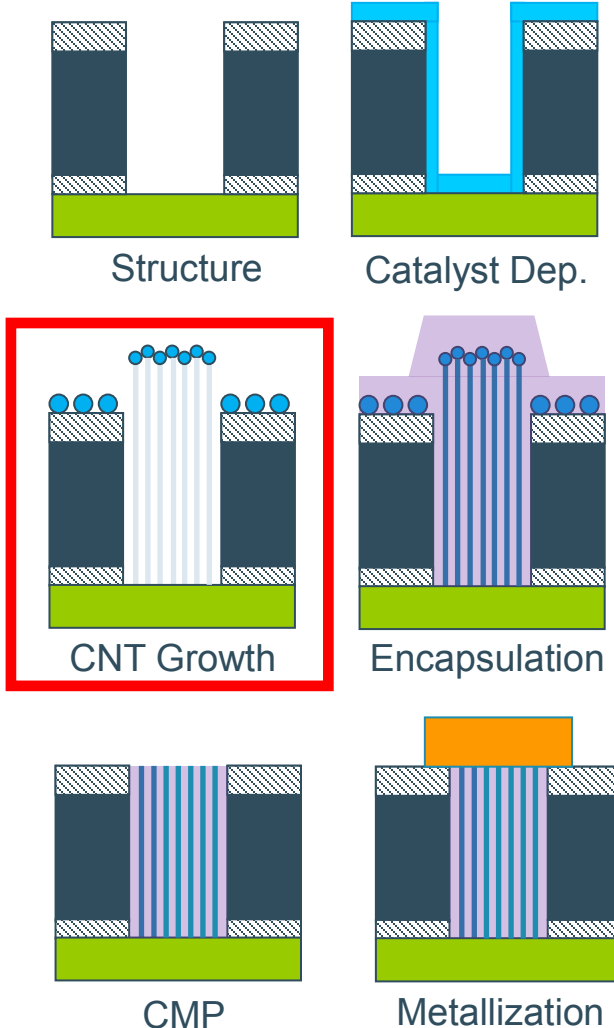
CNTs exhibit enhanced electrical and thermal properties over Cu and could probably be used for interconnects.

To replace Cu by CNT for interconnects, a high nucleation density of MWCNT or SWCNT is required to **overcome the contact and quantum resistance issues**.

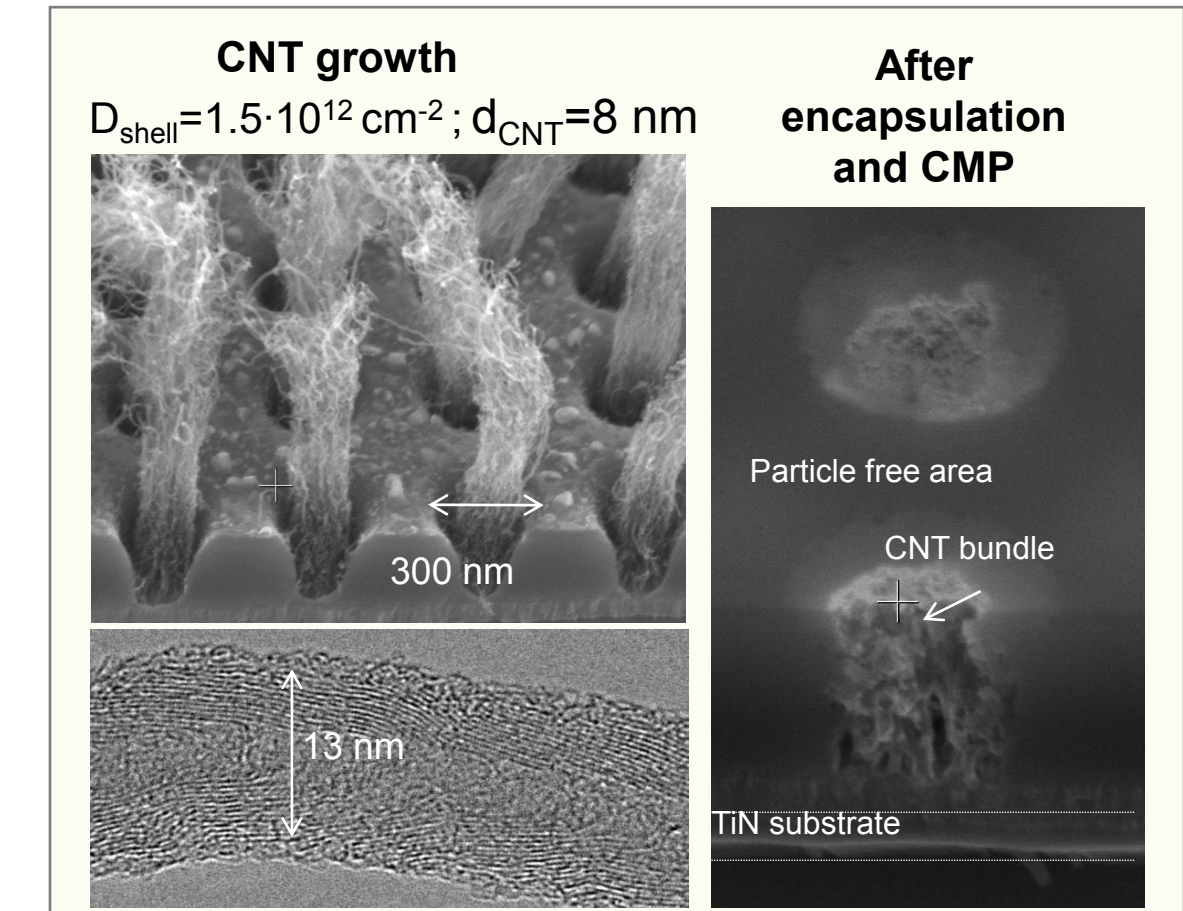


# CNT interconnects

Demonstration of vertical interconnects by CNTs.



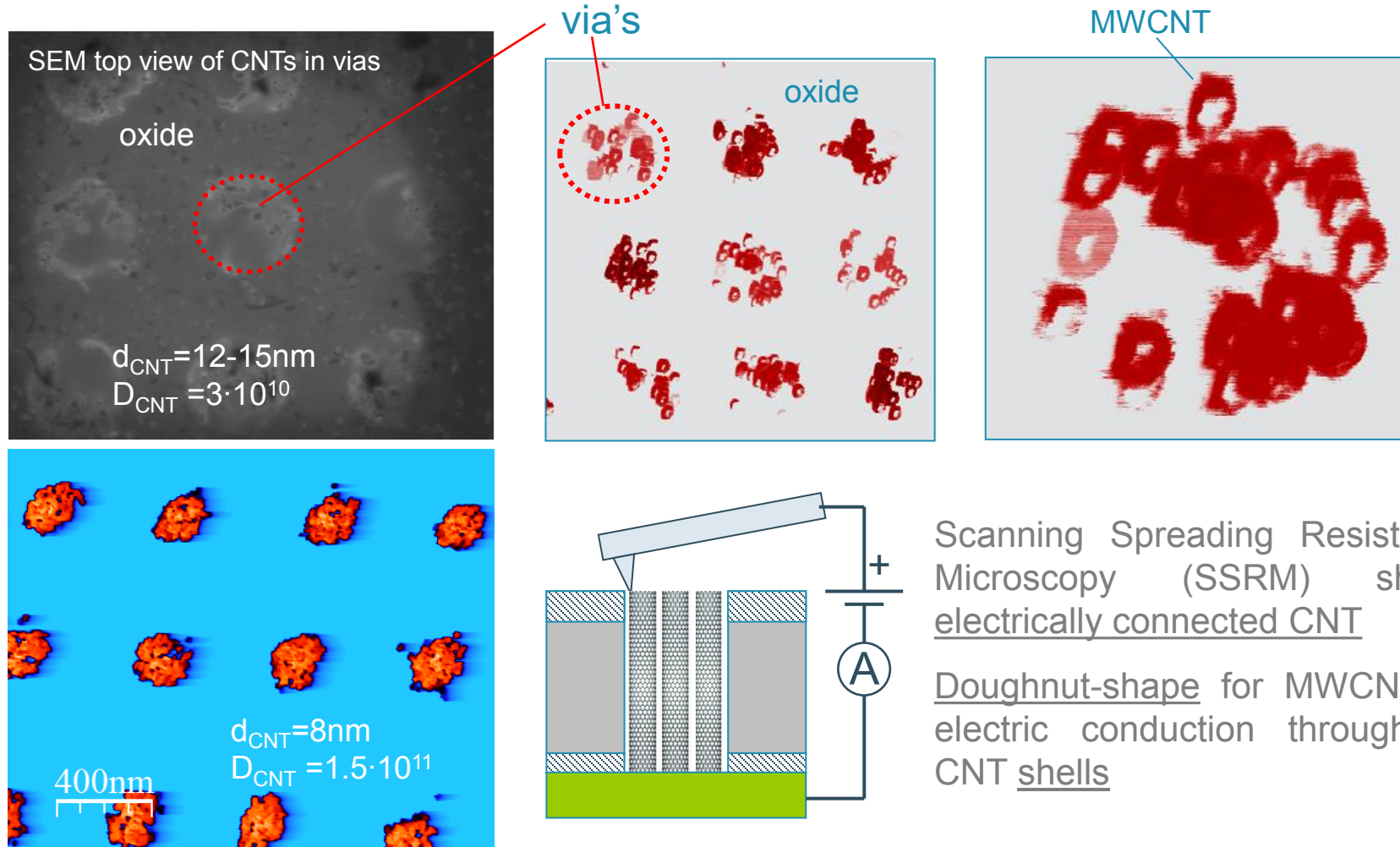
N. Chiodarelli et al., J. Electrochem Soc, 157(10) (2010)



*The CNT are grown in the Vias. After encapsulation a Chemical Mechanical Polishing (CMP) step is used to planarize the surface.*

# CNT interconnect

Demonstration of CNT growth and electrical conductivity in via's.

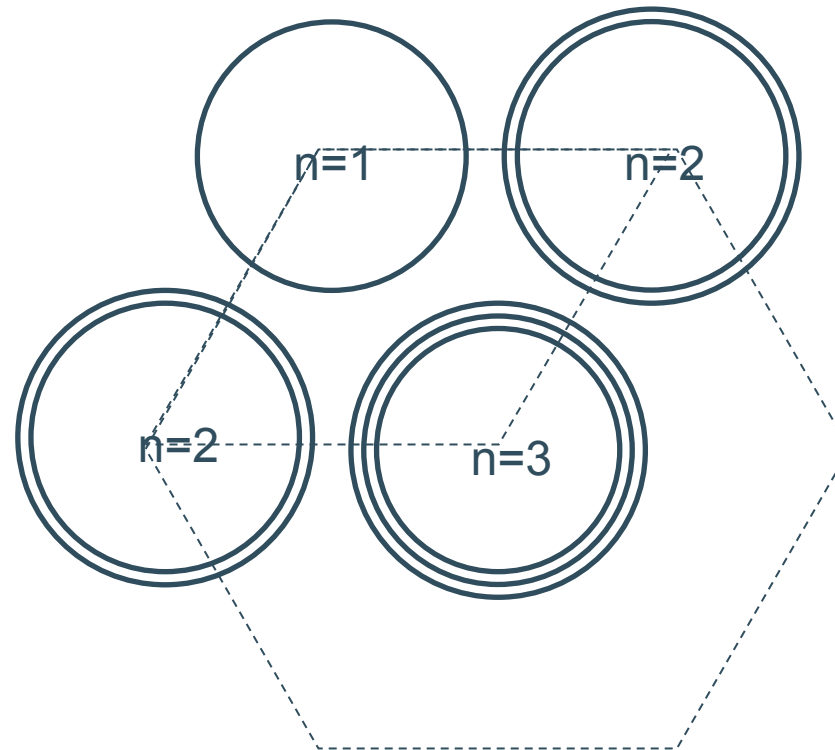


# Resistance of a CNT bundle

In a CNT bundle the **shell density** determines  $R$ , and not the number of CNTs.

The resistance of a single CNT shell,  $R_{sCNT}$ , is only a weak function of the CNT diameter ( $\sim$  SWCNT).

The lower resistance in a CNT bundle is obtained for a higher CNT shell density.



Resistance of CNT bundle:

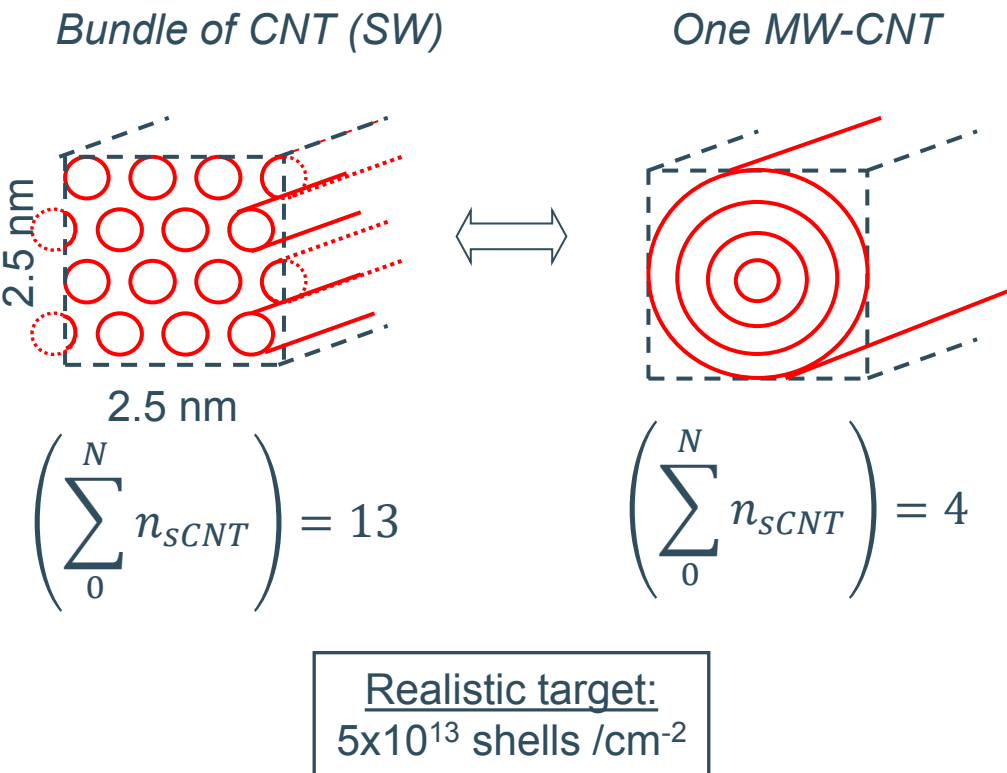
$$R_{CNT,bundle} = \frac{R_{sCNT}}{\frac{8}{\pi} n_{sCNT}}$$

number of CNT:  $N = 4$

total number  
of CNT shells:  
$$\sum_0^N n_{sCNT} = 8$$

P. Vereecken, IMEC

# Optimum packing density for low resistance



A higher stacking density can be obtained with SWCNTs than with MWCNTs.

Maximum CNT density:

$$\left( \sum_0^N n_{SCNT} \right)_{max} = 2 \times 10^{14} \text{ cm}^{-2}$$

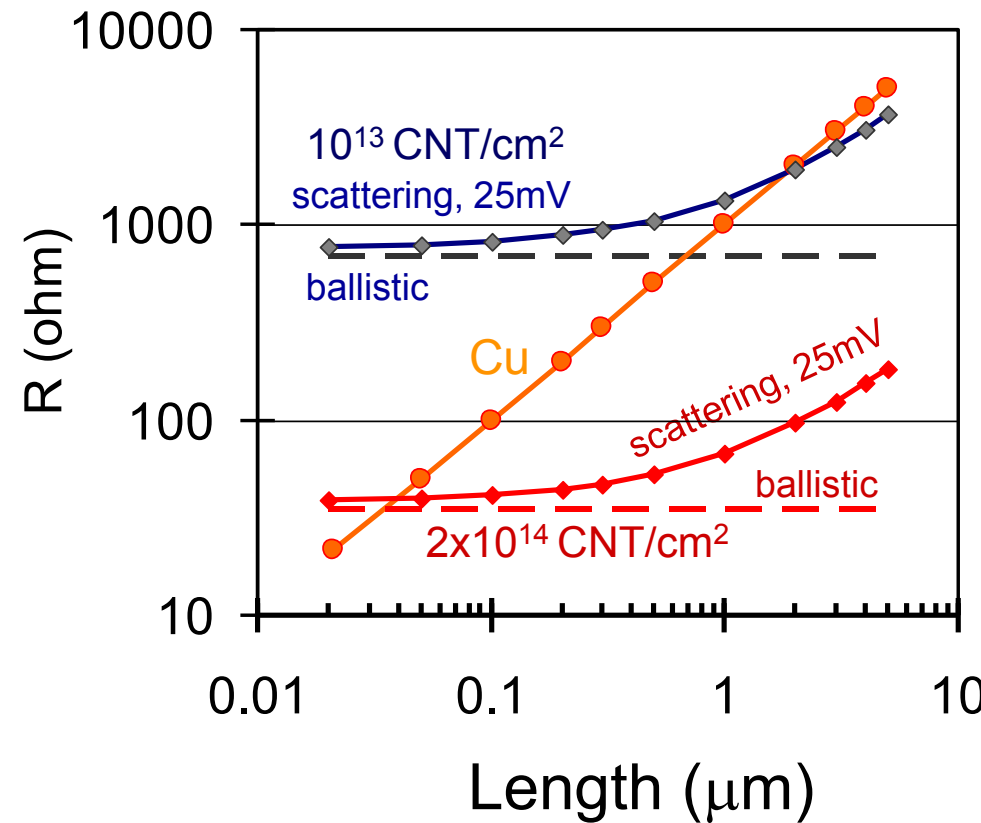
with:

- hexagonal stacking
- smallest SW-CNT with diameter of 0.4nm
- inter-tube distance of 0.34nm

# Resistance of CNT interconnects

When plotting the resistivity as a function of the interconnect length for various densities of CNT shells and for Cu, it is found that  $R_{CNT} < R_{Cu}$  only at **longer interconnect length** (dependent on CNT density and dependent on voltage)

For short interconnect lengths the **quantum resistance** dominates the resistance.



P. Vereecken, IMEC

# Materials Physics and Technology for Nanoelectronics



**Clement Merckling**

clement.merckling@kuleuven.be

imec & KU Leuven (MTM)

Kapeldreef 75, B-3001 Leuven



**Francisco Molina Lopez**

francisco.molinalopez@kuleuven.be

MTM Functional Materials

Kasteelpark Arenberg 44, B-3001 Leuven